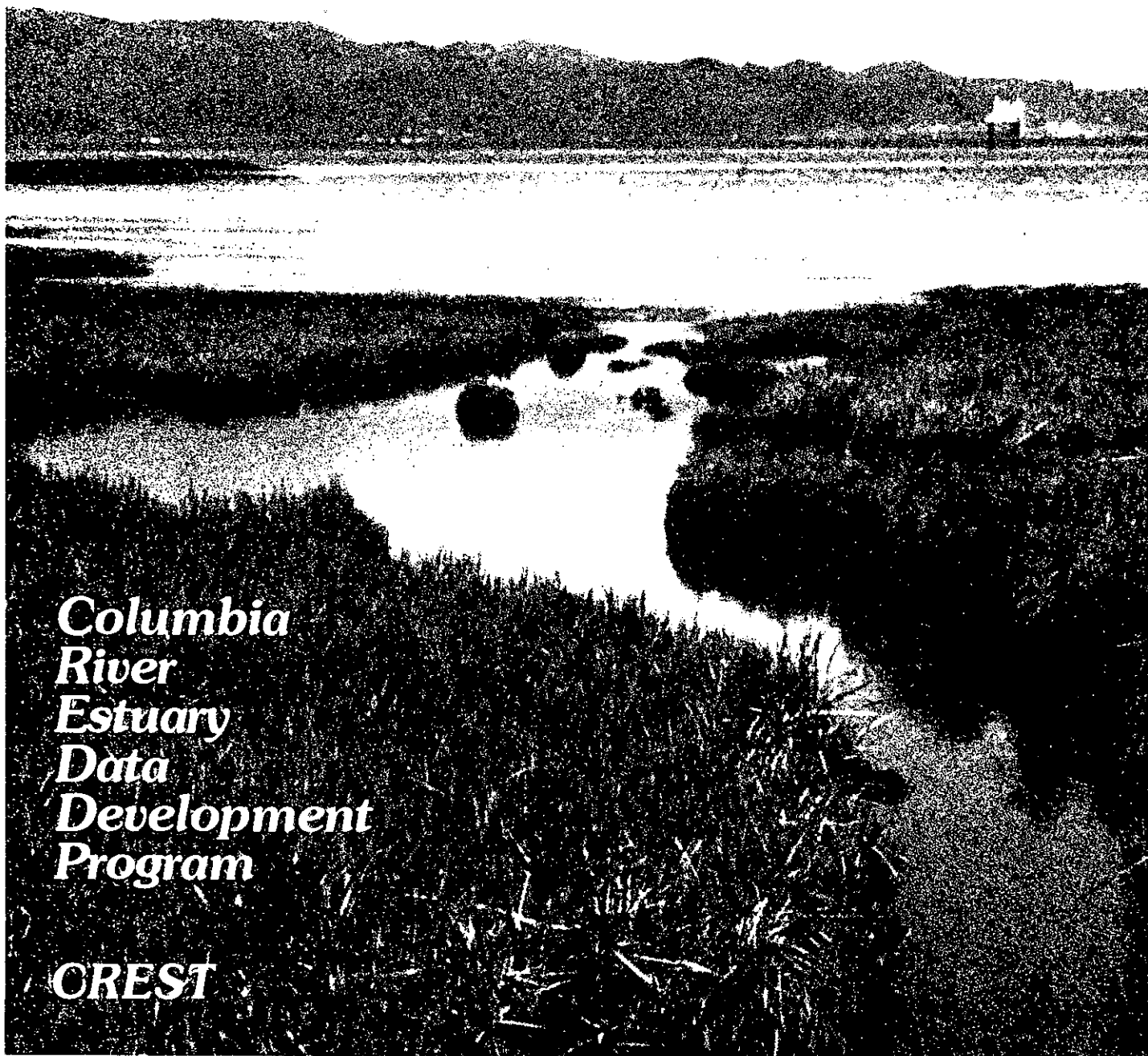


THE DYNAMICS OF THE COLUMBIA RIVER ESTUARINE ECOSYSTEM, VOLUME I



*Columbia
River
Estuary
Data
Development
Program*

CREST

Columbia River Estuary
Data Development Program
(CREDDP)

THE DYNAMICS OF THE
COLUMBIA RIVER
ESTUARINE ECOSYSTEM

VOLUME I

June 1984

THE DYNAMICS OF THE
COLUMBIA RIVER
ESTUARINE ECOSYSTEM

AUTHORS

Charles Simenstad
David Jay
C. David McIntire
Willa Nehlsen
Christopher Sherwood
Lawrence Small

WORD PROCESSING

Isabel Turner
Julie Guerrero
Elizabeth Rummell

GRAPHICS COORDINATION

Elizabeth Krebill
William Barnett

ACKNOWLEDGEMENTS

University of Washington authors (Mr. Jay, Mr. Sherwood, and Mr. Simenstad):

Dr. J. Dungan Smith and W. R. Geyer of the University of Washington contributed important insights into the physics of the estuary. Benjamin Giese carried out the one-dimensional harmonic tidal model and energy budget analyses.

Su Fagerberg and Terry Sochia performed much of the word processing.

Appreciation is extended to William Fassett at the University of Washington School of Pharmacy for the use of their word processing file transfer facility.

The Estuaries Select Program, College of Ocean and Fishery Sciences, University of Washington, also provided salary time and word processing equipment for the completion of the report.

Oregon State University authors (Dr. McIntire and Dr. Small):

We would like to thank Drs. Bruce E. Frey and Ruben Lara-Lara for their considerable efforts in the field portions of the water-column primary production program, and for their insight and discussions in data interpretation and analysis. The program could not have been completed without them. We would like to thank Mr. Sandy Moore and Ms. RaeDeane Leatham for help in the field and in data analysis.

We benefitted considerably from discussions with Drs. Keith Macdonald and Ted Winfield, on their emergent marsh plant data. Mr. David Anderson was responsible for much of the on-site work with the marsh vegetation, and he was helpful with some of the interpretive work.

Dr. Michael Amspoker was invaluable in his assistance with the field sampling, and with analysis and interpretation of benthic algal data. This portion of the primary production work could not have been accomplished without his input.

PREFACE

The Columbia River Estuary Data Development Program

This document is one of a set of publications and other materials produced by the Columbia River Estuary Data Development Program (CREDDP). CREDDP has two purposes: to increase understanding of the ecology of the Columbia River Estuary and to provide information useful in making land and water use decisions. The program was initiated by local governments and citizens who saw a need for a better information base for use in managing natural resources and in planning for development. In response to these concerns, the Governors of the states of Oregon and Washington requested in 1974 that the Pacific Northwest River Basins Commission (PNRBC) undertake an interdisciplinary ecological study of the estuary. At approximately the same time, local governments and port districts formed the Columbia River Estuary Study Taskforce (CREST) to develop a regional management plan for the estuary.

PNRBC produced a Plan of Study for a six-year, \$6.2 million program which was authorized by the U.S. Congress in October 1978. For the next three years PNRBC administered CREDDP and \$3.3 million was appropriated for the program. However, PNRBC was abolished as of October 1981, leaving CREDDP in abeyance. At that point, much of the field work had been carried out, but most of the data were not yet analyzed and few of the planned publications had been completed. To avoid wasting the effort that had already been expended, in December 1981 Congress included \$1.5 million in the U.S. Water Resources Council (WRC) budget for the orderly completion of CREDDP. The WRC contracted with CREST to evaluate the status of the program and prepare a revised Plan of Study, which was submitted to the WRC in July 1982. In September, after a hiatus of almost one year, CREDDP work was resumed when a cooperative agreement was signed by CREST and the WRC to administer the restructured program and oversee its completion by June 1984. With the dissolution of the WRC in October 1982, the National Oceanic and Atmospheric Administration (NOAA) assumed the role of the WRC as the federal representative in this cooperative agreement.

CREDDP was designed to meet the needs of those groups who were expected to be the principal users of the information being developed. One such group consists of local government officials, planning commissions, CREST, state and federal agencies, permit applicants, and others involved in planning and permitting activities. The other major anticipated user group includes research scientists and educational institutions. For planning purposes, an understanding of the ecology of the estuary is particularly important, and CREDDP has been designed with this in mind. Ecological research focuses on the linkages among different elements in the food web and the influence on the food web of such physical processes as currents, sediment transport and salinity intrusion. Such an ecosystem view of the estuary is necessary to

predict the effects of estuarine alterations on natural resources.

Research was divided into thirteen projects, called work units. Three work units, Emergent Plant Primary Production, Benthic Primary Production, and Water Column Primary Production, dealt with the plant life which, through photosynthesis and uptake of chemical nutrients, forms the base of the estuarine food web. The goals of these work units were to describe and map the productivity and biomass patterns of the estuary's primary producers and to describe the relationship of physical factors to primary producers and their productivity levels.

The higher trophic levels in the estuarine food web were the focus of seven CREDDP work units: Zooplankton and Larval Fish, Benthic Infauna, Epibenthic Organisms, Fish, Avifauna, Wildlife, and Marine Mammals. The goals of these work units were to describe and map the abundance patterns of the invertebrate and vertebrate species and to describe these species' relationships to relevant physical factors.

The other three work units, Sedimentation and Shoaling, Currents, and Simulation, dealt with physical processes. The work unit goals were to characterize and map bottom sediment distribution, to characterize sediment transport, to determine the causes of bathymetric change, and to determine and model circulation patterns, vertical mixing and salinity patterns.

Final reports on all of these thirteen work units have been published. The present work, entitled The Dynamics of the Columbia River Estuarine Ecosystem, integrates the results of the work units in a comprehensive synthesis. Its purpose is to develop a description of the estuary at the ecosystem level of organization. In this document, the physical setting and processes of the estuary are described first. Next, a conceptual model of biological processes is presented, with particular attention to the connections among the components represented by the work unit categories. This model provides the basis for a discussion of relationships between physical and biological processes and among the functional groups of organisms in the estuary. Finally, the estuary is divided into regions according to physical criteria, and selected biological and physical characteristics of the habitat types within each region are described. Historical changes in physical processes are also discussed, as are the ecological consequences of such changes.

Much of the raw data developed by the work unit researchers is collected in a magnetic tape archive established by CREDDP at the U.S. Army Corps of Engineers North Pacific Division Data Processing Center in Portland, Oregon. These data files, which are structured for convenient user access, are described in an Index to CREDDP Data. The index also describes and locates several data sets which were not adaptable to computer storage.

The work unit reports, this document, and the data archive are intended primarily for scientists and for resource managers with a scientific background. However, to fulfill its purposes, CREDDP has developed a set of related materials designed to be useful to a wide

range of people.

Guide to the Use of CREDDP Information for Environmental Assessments demonstrates how CREDDP information can be used to assess the consequences of alterations in the estuary. It is intended for citizens, local government officials, and those planners and other professionals whose training is in fields other than the estuary-related sciences. Its purpose is to help nonspecialists use CREDDP information in the planning and permitting processes.

A detailed portrait of the estuary, but one still oriented toward a general readership, is presented in The Columbia River Estuary: Atlas of Physical and Biological Characteristics, about half of which consists of text and illustrations. The other half contains color maps of the estuary interpreting the results of the work units and the ecological synthesis. A separate Bathymetric Atlas of the Columbia River Estuary contains color bathymetric contour maps of three surveys dating from 1935 to 1982 and includes differencing maps illustrating the changes between surveys. CREDDP has also produced unbound maps of the estuary designed to be useful to resource managers, planners and citizens. These black-and-white maps illustrate the most recent (1982) bathymetric data as contours and show intertidal vegetation types as well as important cultural features. They are available in two segments at a scale of 1:50,000 and in nine segments at 1:12,000.

Two historical analyses have been produced. Changes in Columbia River Estuary Habitat Types over the Past Century compares information on the extent and distribution of swamps, marshes, flats, and various water depth regimes a hundred years ago with corresponding recent information and discusses the causes and significance of the changes measured. Columbia's Gateway is a two-volume set of which the first volume is a cultural history of the estuary to 1920 in narrative form with accompanying photographs. The second volume is an unbound, boxed set of maps including 39 reproductions of maps originally published between 1792 and 1915 and six original maps illustrating aspects of the estuary's cultural history.

A two-volume Literature Survey of the Columbia River Estuary (1980) is also available. Organized according to the same categories as the work units, Volume I provides a summary overview of the literature available before CREDDP while Volume II is a complete annotated bibliography.

All of these materials are described more completely in Abstracts of Major CREDDP Publications. This document serves as a quick reference for determining whether and where any particular kind of information can be located among the program's publications and archives. In addition to the abstracts, it includes an annotated bibliography of all annual and interim CREDDP reports, certain CREST documents and maps, and other related materials.

To order any of the above documents or to obtain further information about CREDDP, its publications or its archives, write to CREST, P.O. Box 175, Astoria, Oregon 97103, or call (503) 325-0435.

FOREWORD

This report is the result of a collaborative effort by five CREDDP principal investigator/researchers and CREDDP's staff science/management coordinator. The five (Simenstad, Jay, McIntire, Sherwood, and Small) contracted with CREDDP in late 1982 to carry out the Integration work unit, described in CREDDP's Revised Plan of Study (1982) as follows:

The purpose of the Integration work unit is to synthesize the results of the various biological and physical work units and to produce a report describing the structural and functional attributes of the estuarine ecosystem. Satisfactory integration is particularly crucial for the successful completion of CREDDP, as most of the important management concerns are related to the complex interactions among the individual subsystems under examination by the work units. Most management questions cannot be answered from information generated by an individual work unit without a good knowledge of how that information couples with the results of other work units.

TABLE OF CONTENTS
(VOLUME I)

	<u>Page</u>
EXECUTIVE SUMMARY	ES-1
1. INTRODUCTION	1
2. REGIONAL SETTING AND PREVIOUS STUDIES	7
2.1 GEOLOGIC SETTING OF THE COLUMBIA RIVER ESTUARY	7
2.1.1 Plate Tectonics	7
2.1.2 Sea Level	8
2.2 COLUMBIA RIVER HYDROLOGY	8
2.2.1 Historical and Seasonal Riverflow Pattern	9
2.2.2 Variability and Extreme Flows	10
2.2.3 Estuary Tributary Inflow	21
2.2.4 Estuary Seasons	22
2.3 SEDIMENT SUPPLY	22
2.4 ATMOSPHERIC AND COASTAL OCEANIC PROCESSES	25
2.4.1 Continental Shelf Circulation	25
2.4.2 Winds, Storms, and Waves	26
2.4.3 Water Types, Water Masses, and Mixing	29
2.4.4 Ocean Tides of the Northeast Pacific	30
2.5 PREVIOUS STUDIES OF GEOLOGIC AND CIRCULATORY PROCESSES	33
2.6 PREVIOUS BIOLOGICAL STUDIES	33
2.6.1 Primary Producers	33
2.6.2 Primary Consumers	34
2.6.3 Predators	34
3. CIRCULATORY PROCESSES	37
3.1 THE RELATIONSHIP BETWEEN TIDAL FLOW, MEAN FLOW AND THE SALINITY DISTRIBUTION	38
3.1.1 Modes of Circulation	38
3.1.2 The Salinity Distribution	42
3.1.3 Residual Flow Processes	42
3.1.4 Vertical Mixing, Stratification, and Circulation	47
3.2 DATA COLLECTION	49

	<u>Page</u>
3.3 TIDAL PROCESSES	49
3.3.1 Tidal Heights	57
3.3.2 Factors Influencing the Tidal Range	67
3.3.3 Tidal Inundation Time	68
3.3.4 Currents	68
3.3.5 Tidal Effects on Residual Circulation	79
3.4 TIDAL-FLUVIAL INTERACTIONS	91
3.4.1 Observations	91
3.4.2 Model Results	92
3.5 ENERGY CONSIDERATIONS	93
3.5.1 Formulation of the Energy Budget	93
3.5.2 Neap-Spring Effects	98
3.5.3 Energy Budget Calculations	99
3.6 THE DISTRIBUTIONS OF SALINITY AND MEAN FLOW	103
3.6.1 Seasonal-average Salinity Distributions	104
3.6.2 The Variations of Salinity and Mean Flow During the Low Flow Season	107
3.6.3 The High Flow Distributions of Salinity and Mean Flow	126
3.6.4 Neap-to-Spring Transitions, Riverflow, and Tidal Range	133
3.7 TRANSPORT PROCESSES	135
3.7.1 Salt Transport Calculation Method	135
3.7.2 Transports at Clatsop Spit	135
3.7.3 Salt Transport at Astoria (RM-15): Temporal Variations	147
3.8 PERIPHERAL BAYS	149
3.8.1 Baker Bay	149
3.8.2 Youngs Bay	150
3.8.3 Grays Bay	151
3.8.4 Cathlamet Bay	151
3.9 SUMMARY	152
3.9.1 Summary of Present Knowledge	152
3.9.2 Areas for Future Work	155
4. SEDIMENTARY GEOLOGY	157
4.1 SEDIMENT TRANSPORT	158

	<u>Page</u>
4.2 APPROACHES TO THE STUDY OF SEDIMENT TRANSPORT	162
4.2.1 Bedload Transport	162
4.2.2 Suspended Sediment Transport	181
4.3 LARGE-SCALE MORPHOLOGY	192
4.4 BOTTOM SEDIMENTS	199
4.4.1 Sediment Sampling and Analysis	200
4.4.2 Sediment Size Variation	203
4.4.3 Areal and Seasonal Variation in Sediments	213
4.4.4 Factor and Cluster Analyses	220
4.4.5 Implications of Sediment Size Data	223
4.5 ENERGY CONSIDERATIONS AND SEDIMENTARY ENVIRONMENTS	230
4.5.1 Influences on Sedimentation and Erosion	230
4.5.2 Interpretation of the Energy Budget	234
4.5.3 Sedimentary Environments	237
4.6 SUMMARY	237
5. HISTORICAL CHANGES IN COLUMBIA RIVER ESTUARINE PHYSICAL PROCESSES	241
5.1 HISTORICAL CHANGES IN THE COLUMBIA RIVER ESTUARY	242
5.2 CHANGES IN THE MORPHOLOGY OF THE ESTUARY	243
5.2.1 Causes	243
5.2.2 Measurements of Structural Changes	244
5.2.3 Area Changes	253
5.2.4 Volume Changes and Sedimentation Estimates	263
5.3 ANALYSIS OF HISTORICAL CIRCULATION PATTERNS	267
5.3.1 Modeling Procedure	267
5.3.2 Changes in Transport Patterns	267
5.3.3 Changes in Tidal currents, Mean Flow, and Salinity Distribution	275
5.4 EFFECTS OF THE CHANGES IN MORPHOLOGY AND CIRCULATION	313
5.4.1 Implications for Turbidity Maximum Processes	313
5.4.2 Long-Term Shoaling Patterns and the Sediment Budget	315
5.4.3 Equilibrium	317
5.5 SUMMARY OF HISTORICAL TRENDS IN THE ESTUARY AND IMPLICATIONS FOR THE FUTURE	317
LITERATURE CITED (VOLUME I)	319

EXECUTIVE SUMMARY

The Columbia River is the second largest river in the United States; its mean discharge is about $7,280 \text{ m}^3\text{sec}^{-1}$. The Columbia River drainage basin (about $660,480 \text{ km}^2$) is divided into eastern and coastal sub-basins. Snowmelt in the eastern sub-basin is responsible for the spring freshet. Storms cause sporadic heavy runoff from the coastal basin during the winter. The natural runoff cycle has been substantially modified by flow regulation at numerous dams and by irrigation withdrawal. Historical flow data shows that the effects of flow regulation increased substantially in about 1969. This increase in flow regulation is so recent that the sediment distribution may not yet be in equilibrium with it.

Winds, pressure fluctuations, wind waves, the coastal upwelling and downwelling cycle, and the tides determine coastal sea level and the oceanic water masses that intrude into the estuary. Large winter storms can affect circulation and sediment transport at the entrance, but atmospheric processes have much less influence on circulation inside the estuary than the tides. The tide at the entrance to the estuary is of the mixed, predominantly semidiurnal type, with a diurnal range of about 1.8m.

The sedimentary geology of the Columbia River Estuary is greatly influenced by the physiographic location of the estuary. The tectonic regime, associated with the estuary's location on the western margin of the continental plate, has directly affected local sea level and indirectly affected climate and hydrology in the formation of the Coast Range and upper drainage basin of the Columbia River. The estuary occupies a drowned river valley incised into volcanic and sedimentary bedrock of Tertiary age. The valley has been partially filled by Pleistocene and Holocene sediments derived from the Columbia River basin and deposited in fluvial and estuarine settings. The river may supply 10 million tons of sediment per year to the estuary, most of it coarse silt carried in suspension. Ten percent of the river load is very fine to medium sand which is transported as bedload. The mineralogy of this sand reflects the various sources of volcanic and plutonic rock and sedimentary deposits in the eastern part of the drainage basin as well as the andesitic volcanic contribution from the active volcanoes of the Cascade Range. The other major source of sediment to the estuary is the adjacent marine environment. Because most of the marine sediment is originally derived from the Columbia River system, it is not possible to easily differentiate the two sources on the basis of mineralogy.

In addition to determining the nature of the sediments and the rate of sediment supply, the physiographic and oceanographic location of the estuary determines the energy inputs available for controlling physical and geological processes operating within the estuary. Tidal energy is the dominant energy source in most of the estuary but riverflow assumes increasing importance with distance upriver from the entrance. Sedimentary processes near the entrance are driven by tidal currents and, to a lesser extent, ocean waves. In the upper estuary and in the

fluvial reaches, river currents control the erosion, transportation, and deposition of sediments. Over most of the lower estuary, however, both major sources of energy are important, and they are greatly modified by the effects of salinity-induced stratification, tidal- and density-driven residual circulation, local wind waves, and topography.

Circulatory studies were carried out in six areas: theory of estuarine circulation, tidal circulation, density distribution, salt transport, residual flow processes, and estuarine modeling. These studies show that:

-The three most important time scales of estuarine motion are tidal daily, tidal monthly and seasonal. The tidal flow (which varies during the tidal day), the mean flow (which varies over the tidal month and seasonally) and the salinity distribution (which varies on all three time scales) are closely linked to one another. The interactions between the three are caused by non-linear processes associated with shallow topography, bottom friction, and stratification.

-Tidal range decreases more rapidly in the upriver direction on the tides of greater range; that is, an increase in tidal range at the mouth results in a less than proportional increase upriver. Freshets reduce the tidal range and greatly increase the river stage (water surface level) above RM-20. Both of these phenomena are caused by the strong friction in the system.

-Tidal exchange and salinity are greater in the north channel than in the south channel. Most of the tidal prism of the lower estuary is filled by the flow in the north channel.

-The tidal energy flux from the ocean is the dominant source of energy for estuarine circulation. The potential energy flux of the riverflow (i.e., energy released as the water flows downhill) is the dominant source of energy in the fluvial part of the system. Major freshets provide much more energy than any possible tide, but most of this energy is dissipated in the fluvial part of the system above RM-30.

-There is a distinct energy minimum, between RM-18 and RM-30, where neither tidal nor fluvial energy inputs are large. This energy minimum may explain the location of the many deposition features of Cathlamet Bay.

-There is more energy available for mixing on the ebb than on the flood, because of the strength of the riverflow. The vertical structure of the ebb current is very different from that of the flood current. The large shear on ebb, the vertical uniformity of the flood flow and the salinity intrusion combine to generate upstream bottom currents in the lower estuary.

-The vertical structure of the currents is, however, also strongly influenced by along-channel variations in depth and width. For this reason, mean upstream bottom flow usually is not continuous

from the entrance to the upstream limits of salinity intrusion. The accumulation of detritus and other suspended material in the turbidity maximum, which is dependent upon the upstream bottom flow, is thus also strongly affected by channel configuration.

-Neap-spring changes in tidal energy cause changes in vertical mixing that alter the density structure and the mean flow. The tidal monthly changes in the spatial distribution of the mean flow cause neap-spring changes in suspended sediment concentration and cycling in the turbidity maximum. These neap-to-spring changes become less important as the riverflow increases.

-Salinity intrusion length is greatest under low-flow, neap-tide conditions, when salinity intrusion may reach to about RM-30 in the navigation channel. Under the highest flow conditions, salt may be absent upriver of RM-2 for several hours at the end of ebb.

-Salt and water transport calculations also show that most of the net outflow of water is near the surface in the south channel. Upstream bottom flow is strongest in the north channel. Salt enters the estuary primarily by tidal mechanisms in a near-surface jet in the north channel. The large, surface outflow in the south channel transports salt out of the estuary. Thus, the movement of salt is in the north channel, across the mid estuary flats and out the south channel. Water in the south channel has, therefore, been in the estuary longer than water in the north channel. This causes biological and geological differences between the two channels.

Several methods were utilized in the investigations of both the processes and the resultant distributions of sediments and bedforms in the estuary. A large suite of bottom sediment samples was obtained over the entire estuary in each of the three riverflow seasons (fall, winter, and spring). These samples were analyzed to determine their grain-size distribution and some aspects of their mineralogy. Factor analysis, cluster analysis, and direct interpretations of the distribution of grain size statistics were employed in order to interpret the patterns of sedimentation in the estuary. Information on the morphology of the estuary bottom was obtained using side-scan sonar over various tidal stages during all three seasons. Larger-scale features of the estuarine morphology were addressed using data from aerial photos and modern bathymetric maps. Suspended sediment processes were monitored with both fixed transmissometers and profiling nephelometers which were calibrated with physical samples of suspended sediments. An analysis of the historical changes in the volumes and rates of sediment accumulation were performed using digitized bathymetric data from four estuary-wide surveys, the earliest of which was made in 1868.

Overall, the estuary floor is comprised of fine sand; deposits of gravel are rare and restricted to areas of extreme scour, while deposits of silt and clay are mostly confined to peripheral bays and inactive channels. Much of the sediment is of a size that is transported intermittently as suspended sediment under high tidal currents but moves regularly as bedload. As a result, the grain size distributions in the estuary depend on daily, spring-neap, seasonal, and catastrophic current

events, as well as sediment supply. In general, the sediments in the estuary show a greater variance among samples and are finer and more poorly sorted than the river sediments. Sediments on the continental shelf immediately seaward of the entrance are much better sorted than the estuary sediments and slightly finer. The variance among estuary sediments is attributable to the variety of sedimentary environments and range of active processes within the estuary.

The importance of bedload and intermittently suspended load transport in the estuary is emphasized by the ubiquitous bedforms. Although sediment transport and deposition depend on local conditions which change with time, the bedform distribution allows the integrated effect of sediment transport rates to be observed. Bedform distributions in the Columbia River Estuary indicate that tidally-reversing bedload transport occurs at depth in the entrance region, but that density-driven circulation influences the tidal transport sufficiently to cause net upstream transport as far upriver as the Port of Astoria in the major channels. Seasonal changes in the bedform distributions occur and indicate that upstream sediment transport does not extend as far upriver during high discharge as it does during low discharge. Bedform studies also indicate that fluvial processes dominate upriver from Tongue Point, and that sediment transport rates and pathways vary with neap-spring and seasonal circulation changes.

The study of suspended sediment processes and the distribution of fine sediment suggest that a turbidity maximum exists in the Columbia River Estuary; the turbidity maximum contains high concentrations of suspended sediment, it is advected with semidiurnal tidal currents, and it changes character in response to neap-spring and seasonal current changes. Much of the sediment suspended in the turbidity maximum is re-suspended bottom material. Ephemeral fine sediment deposits are the result of deposition beneath the turbidity maximum during the waning phases of a spring tide, but most of the suspended sediment in the estuary is either flushed out into the Pacific Ocean or transported to and deposited in one of the peripheral bays. As a result, silt and clay are volumetrically less important than sand in the estuary sediments, and estuarine sedimentation is most closely associated with deposition of bedload material. Thus, the long-term shoaling of the estuary is a result of horizontal accretion of bedform and point-bar deposits during channel migration, rather than vertical accretion of fine sediment deposited from suspension.

Numerical model results suggest that the circulation in the estuary prior to human intervention (e.g., in 1868) was somewhat more energetic, because the tidal prism was larger and the riverflow both larger and more variable at that time. Channel maintenance activities have simplified the channel network, shifted flow away from subsidiary channels, and changed the principal outflow of river water from the north to the south channel. The flushing time is slightly longer for the estuary as a whole but may be substantially longer for areas from which flow has been diverted. The salinity intrusion length and stratification are both greater than in 1868, because mixing has been reduced. It appears that the neap-spring transition in density structure and turbidity maximum processes was less important at low

flows, but more important at high flows in 1868.

The construction of the jetties and channel maintenance activities have had a profound effect on the sedimentology and the morphology of the estuary. Rapid accumulation of sediments (average of 0.5 cm yr^{-1} over the entire area of the estuary) has occurred in historic times. Approximately one half of these sediments are derived from the beach/spit/tidal delta complex that has been displaced by the increased tidal currents resulting from jetty construction. The remainder are derived from the river. Jetty construction has forced sediments farther offshore and northward, abundantly supplying the continental shelf and the littoral drift system along the Washington coast with sediment. Decreased rates of erosion on the outer tidal delta suggest that this transitory period of increased sediment supply may be ending as the system reaches equilibrium.

Dredging operations, the filling of wetlands, and the construction of pile dikes has changed the distribution of water in the estuary: because of area changes, more water is now contained in moderate depths and less in shallow and very deep depths than in 1868. As a result of these operations, the tidal prism has been decreased by 15-20% in the last 90 years. Although tidal energy still dominates the processes in the estuary, both tidal energy and riverflow energy have been reduced by human activities.

The sedimentary processes that occur in the estuary have a broad effect on the estuarine ecosystem. Local bottom shear stresses, sediment composition, and rates of erosion and deposition are important in determining the habits of benthic infauna, epifauna, and primary producers. The distribution of organic detritus in the water column is controlled by the same processes that form the turbidity maximum. Finally, the large-scale changes that have occurred in the estuary and are reflected in the sedimentary processes, such as the reduction in tidal prism and the increase in sedimentation rate in historic time, reflect physical changes in the environment that could have profound effects on the ecosystem.

The physical-biological synthesis of CREDDP scientific information required the development of a conceptual framework that was able to accommodate an enormous diversity of products and raw data provided by the individual research groups. For this purpose, a hierarchical model of biological processes was adopted as the structural basis for the integration of the biological research and related physical data. Although the model emphasizes biological processes relevant to data synthesis, its structure also allows for the identification of key species and functional groups of species which are involved in the processes. Therefore, the model is flexible enough to organize the presentation of the patterns of energy flow in the estuary, as well as information concerning distributional patterns of dominant taxonomic groups. Physical processes are treated as system inputs that limit, control, or regulate biological processes and their relevant coupling variables.

The conceptual model partitions Estuarine Biological Processes into

Primary Food Processes and Consumption. The Primary Food Processes subsystem represents the dynamics of variables associated with the accumulation and degradation of plant biomass and detritus, whereas the Consumption subsystem is concerned with the dynamics of the macrofauna, including zooplankton, as they function as consumers of the primary food supply, i.e., living plant biomass and detritus. The subsystems of Primary Food Processes are Primary Production, which represents the production dynamics of autotrophic organisms, and Detrital Decomposition, a process that is concerned with the breakdown of dead organic matter. The process of Consumption is partitioned into four coupled subsystems: Deposit Feeding, Suspension Feeding, Wetland Herbivory, and Predation. Deposit Feeding involves the dynamics of the sediment-associated macrofauna feeding on the primary food supply, while Suspension Feeding includes processes relating to the removal of organic material from the water column by benthic macrofauna and zooplankton. Wetland Herbivory is a process that includes the activities of animals feeding on the emergent plants in the estuarine marshlands. Predation represents macroconsumer processes responsible for the consumption of zooplankton; deposit feeders; suspension feeders; and herbivorous birds, mammals, and insects.

The scientific synthesis of CREDDP data also involves the consideration of system dynamics at different levels of temporal and spatial resolution. The behavioral characteristics of the systems and subsystems are reported in relationship to the temporal scales that are compatible with the data and the coupling structure of the conceptual model. The problem of spatial variation in the Columbia River Estuary is approached by examining the dynamics of biological processes in relationship to a set of inputs that are specific for the spatial area under consideration. These inputs can include physical and chemical driving variables as well as various biological couplings with adjacent regions.

The estuary is dominated (over 75%) by freshwater diatoms, including both planktonic and benthic taxa. Phytoplankton taxa composition, standing crop, and productivity were affected greatly at the boundary between freshwater and seawater (0 to 5 ppt salinity) in the estuary. Live cells are more abundant, and standing crop and production higher, in the freshwater region as compared to the more saline region immediately downriver. Evidence suggests that live, chlorophyll-containing cells are lysed and converted to dead, non-chlorophyllous detrital particles at this freshwater-seawater interface.

Without considering the effect of the Mount St. Helens eruption in May 1980, import and export of phytoplankton-derived carbon was estimated to be 56,000 MT C yr⁻¹ and 34,000 MT C yr⁻¹, respectively, with an estimated loss (by difference) of 22,000 MT C yr⁻¹ within the estuary. The annual production of phytoplankton carbon within the estuary was estimated to be 17,000 MT C yr⁻¹, or 68 gC m⁻² yr⁻¹. Import of phytoplankton carbon from upriver always exceeded primary production within the estuary. On an annual basis, 75% of the phytoplankton carbon was supplied from upriver, with only 25% produced in situ within the estuary.

Light appears to be the major factor limiting phytoplankton primary production in the estuary. Of the major inorganic nutrients necessary for phytoplankton growth, only nitrogen appears to become depleted to the point of limiting phytoplankton growth and production.

Microalgae, primarily diatoms, are the most abundant group of benthic plants associated with the tidal flats of the estuary. A detailed quantitative analysis of the taxonomic structure of the benthic diatom flora indicated that the taxa composition in Cathlamet Bay, Grays Bay, and the Upper Estuary region above Cathlamet Bay are similar. The Youngs Bay benthic diatom flora was more similar to the floras of these upriver regions than to the flora of Baker Bay, a pattern apparently related to freshwater input into Youngs Bay from the Lewis and Clark River, the Youngs River, and the Columbia River itself.

There was relatively little seasonal change in microalgal biomass at intensive study sites, and the biomass was usually highest in the low marsh and lowest close to the river channel. Production rates were highest from March through October and lowest during winter months. Low marsh and upper tidal flat habitats tended to have the highest production rates and lower tidal flat habitats the lowest rates.

In addition to water column turbidity and daylength, sediment properties and stability were considered to be the principal factors controlling benthic primary production. Animal activity was not conspicuous and may be minor in the Columbia River Estuary compared to other coastal and inland estuaries in the region.

Submergent vascular plants in tidal flat habitats are rare and their distribution extremely patchy. Emergent vascular plants are prominent primary producers on 5,873 ha in the estuary, 3,341 ha of which are marsh habitats dominated by herbaceous plants and 2,532 ha are swamp habitats dominated by woody plants. Using a numerical classification analysis, six emergent plant assemblages were discriminated: (1) low marsh habitats in brackish water dominated by Carex lyngbyei; (2) high marsh habitats in the estuary's estuarine mixing zone characterized by Oenanthe sarmentosa, Lotus corniculatus, Mimulus guttatus, Carex lyngbyei, and Deschampsia caespitosa; (3) low marsh Carex lyngbyei habitats in the estuarine mixing zone; (4) Typha latifolia marsh in the upriver region of the tidal-fluvial zone; (5) a low marsh habitat near Tongue Point dominated by Myosotis laxa and Equisetum sp.; and, (6) a unique marsh habitat in Trestle Bay which included primarily Lathyrus palustris, Potentilla pacifica, Carex lyngbyei, Juncus balticus, and Agrostis alba.

Excluding the effect of the fluvial detritus load generated by the eruption of Mount St. Helens in May 1980, annual import of particulate detrital carbon into the estuary was estimated from measurements of non-chlorophyllous POC_i to be 146,000 MT C yr⁻¹. Export was estimated to be 159,000 MT C yr⁻¹. Transformation of phytoplankton to detritus within the estuary was estimated to account for 39,000 MT C yr⁻¹; using a 47% conversion factor, it was estimated that 5,300 MT C yr⁻¹ of marsh vascular plant carbon becomes detritus. Assuming that most of the benthic primary production is consumed directly rather than being

converted to detritus, a total of 191,000 MT C yr⁻¹ of detrital particulate carbon enters the estuarine detrital pool. Given the 159,000 MT C yr⁻¹ exported from the estuary to the plume and ocean zone, an estimated 32,000 MT C yr⁻¹ is lost (consumed or enters a detrital "sink") within the estuary.

Prominent wetland herbivores in the estuary include avifauna (mallard and American widgeon ducks, black-capped chickadee), terrestrial mammals (Columbian white-tailed and black-tailed deer, deer mouse, Townsend's vole), and aquatic mammals (nutria, muskrat, American beaver). It was estimated that between 745 and 780 MT C of wetland herbivores occupy the estuary. Herbivory by mammals and avifauna accounts for between 380 and 3,028 MT C yr⁻¹ transferred to the primary consumer level of the estuarine food web. However, herbivory by insects is completely unassessed.

Benthic infauna (bivalves, oligochaetes, polychaetes, gammarid amphipods) and epibenthic zooplankton (harpacticoid, calanoid, and cyclopoid copepods, and gammarid amphipods) comprised the principal deposit-feeding organisms in the estuary. Reciprocal averaging ordination of the deposit-feeding benthic infauna density data defined four groups, including assemblages (1) uniquely associated with tidal-fluvial zone habitats; (2) prevalent in protected tidal flat habitats in both the plume and ocean and estuarine mixing zones; (3) channel bottoms and exposed tidal flats in the estuarine mixing zone; and, (4) exposed tidal flats and channel bottoms in the plume and ocean and estuarine mixing zones. These groups were distinguished principally by: (1) Corophium salmonis, Heleidae, Chironomidae, and Oligochaeta; (2) Hobsonia florida, Macoma balthica, and Neanthes limnicola; (3) Eohaustorius estuarius, Neanthes limnicola, and Rhynchocoela; and, (4) Rhynchocoela and Paraphoxus milleri, respectively.

The standing crop of benthic infauna was closely related to sediment structure, and in particular the fraction of fine particles and the percent organic content. As a result, the peripheral bays in the downriver regions of the estuary sustain higher standing crops than protected tidal flats in other regions of the estuary. The lowest standing crop values were found in the high-energy, coarse-grained habitats of all channel bottoms and demersal slopes in the estuarine mixing zone. Production of deposit-feeding benthic infauna was estimated to total 356.3 MT C yr⁻¹, second only to suspension feeding zooplankton though only 11% of the total production by estuarine consumers. It was estimated that 1,943.3 MT C yr⁻¹ is consumed by deposit-feeding infauna.

At least half of the standing stock of epibenthic zooplankton in the estuary were considered to be deposit feeders, and in particular the harpacticoid copepods (predominantly Scottolana canadensis, Microarthridion littorale, Tachidius triangularis, Atheyella sp.). Numerical classification analysis (clustering) indicated that epibenthic assemblages change dramatically with hydrologic season.

Densities of deposit feeding epibenthic zooplankton were estimated to range widely between about 43 and 20,000 individuals m⁻² and

standing crop values between 0.9 and about 1,932 mg m⁻². Average standing stock was highest in tidal flat habitats and lowest in channel bottom habitats. Maximum standing stock consistently occurred within the estuarine mixing zone, but shifted farther upriver between the high and low flow seasons in conjunction with the increased salinity intrusion and location of the turbidity maximum. Based on the estimated total annual production of 32.36 MT C yr⁻¹, consumption by deposit feeding epibenthic zooplankton was estimated to be 161.8 MT C yr⁻¹. The combined annual consumption rate for deposit feeders is approximately 2,105 MT C yr⁻¹.

Suspension-feeding benthic infauna were limited primarily to two bivalves, Corbicula manilensis, and Mya arenaria. Mya dominated the standing stock distribution, which peaked at 77 mgC m in the Baker and Trestle Bays tidal flats. Total annual consumption by suspension feeding benthic infauna was estimated to be about 170 MT C yr⁻¹.

Most of the suspension-feeding epibenthic zooplankton found in the estuary are calanoid and cyclopoid copepods and cladocerans, the most prominent of which is the endemic calanoid, Eurytemora affinis. Annual consumption by the suspension-feeding component of the epibenthic zooplankton was considered to be approximately equal to that of the deposit-feeders, 167 MT C yr⁻¹.

Suspension-feeding pelagic zooplankton of channel water column habitats fall into three assemblages, distributed along the longitudinal salinity gradient according to seasonal variations in river discharge: (1) a dominantly freshwater group of cladocerans; (2) endemic estuarine calanoid copepods; and, (3) a polyhaline group of calanoid and cyclopoid copepods characteristic of the plume and oceanic water masses intruding at the mouth of the estuary. The estimated annual production rate of pelagic zooplankton, 2,505 MT C yr⁻¹, was the highest of any animal groups in the estuary, suggesting an average annual consumption rate of 13,000 MT C yr⁻¹. Combined, suspension-feeding accounts for the consumption of approximately 13,337 MT C yr⁻¹ of phytoplankton and detrital carbon within the estuary.

Errantate polychaetes and amphipods constituted the benthic infauna predators. Mean standing crop of all benthic infauna predators was generally an order of magnitude higher (144 to 800 mgC m) in the Cathlamet Bay and Fluvial Regions compared to more estuarine or marine regions downriver (0 to 25 mgC m). As a result of their high standing stock and turnover rate, these infaunal predators had the highest production rate (61.2 MT C yr⁻¹) of any predator group. This high level of production implied a corresponding annual consumption rate of about 300 MT C yr⁻¹.

Motile macroinvertebrates (Dungeness crab, Cancer magister and the crangonid shrimp, Crangon franciscorum) and certain zooplankton (mysids) were prominent predators in the plume and ocean and estuarine mixing zones. Overall, this assemblage of predatory macroinvertebrates accounts for about 27 MT C yr⁻¹ annual production, approximately equal to the production rate of fish in the estuary and indicative of an annual consumption rate of about 135 MT C yr⁻¹.

Although not a diverse assemblage, larval fish (only eleven taxa, of which only Cottus asper and general osmerids are abundant) occurred in high densities (100 to 300 individuals m^{-2}) immediately prior to the low flow season. As a result of their high foraging rate during this short period, the estimated production ($44.4 \text{ MT C yr}^{-1}$) of larval fish ranked higher than that of juvenile and adult fishes and implied equally high annual consumption rate of about 220 MT C yr^{-1} .

The ten "key" fish species studied included American shad, Pacific herring, northern anchovy, coho salmon, chinook salmon, longfin smelt, shiner perch, Pacific staghorn sculpin, English sole, and starry flounder, all of which occurred predominantly as juveniles (subyearlings and early yearlings) rather than as adults. Ten to twelve fish assemblages were consistently distributed among the three zones of the estuary. Among the major factors influencing the composition and distribution of fish assemblages are: (1) seasonal cycles in migration and life history of the fishes; (2) longitudinal salinity gradient as influenced by seasonal variation in riverine discharge of freshwater and neap-spring tidal cycles; (3) the distribution of four habitats (protected embayments, pelagic channels, demersal channels, demersal slopes) within the three zones; and, (4) density and distribution of preferred invertebrate prey taxa.

Water column (pelagic) fishes occurred in densities as high as 0.3 individuals m^{-2} and standing crops as high as 3.6 g m^{-2} . Demersal slope assemblages occurred at approximately the same standing stock level, as high as 0.3 individuals m^{-2} and 4.3 g m^{-2} , respectively. The highest standing stock was typically illustrated by channel bottom fish assemblages, averaging 1.0 individuals m^{-2} and 11.7 g m^{-2} . Although sampled separately and less frequently, there were indications that tidal flats in the peripheral bays and on the mid-estuary shoals supported densities and standing crops as high as 2.3 m^{-2} and 34.5 g m^{-2} , respectively. Average annual consumption was estimated to be approximately $1,086 \text{ MT C yr}^{-1}$.

Carnivorous birds (western grebe, double-crested cormorant, hybrid gulls, and a multi-species shorebird assemblage) were seasonally abundant in the estuary. Indirect estimation of annual consumption by predatory birds suggests that it is relatively low, i.e., on the order of 0.3 to 0.6 MT C yr^{-1} .

Three terrestrial-wetland predators are important in the estuary, the Canadian river otter, raccoon, and vagrant shrew. Vagrant shrews were locally abundant and may play a major role as a prominent insectivore in the estuarine food web. Average raccoon density and standing crop were estimated to be 0.08 individual ha^{-1} and $0.32 \text{ kg wet weight } ha^{-1}$, respectively, and Canadian river otter, 0.02 ha^{-1} and $0.17 \text{ kg wet weight } ha^{-1}$. Consumption of crayfish, Corbicula manilensis, birds, Rosaceae fruit, and sculpins by raccoon was estimated to be $8.52 \text{ MT C yr}^{-1}$; consumption of crayfish, sculpins, carp, unidentified fish, and starry flounder by Canadian river otter was estimated to be between 1.37 and $1.63 \text{ MT C yr}^{-1}$.

Four marine mammals (northern sea lion, California sea lion, harbor

seal, northern elephant seal) are common to the estuary, although the elephant seal is not extremely abundant. Overall, total marine mammal densities ranged from 1.25 individuals km^{-2} during the low flow season to a maximum of 3.55 individuals km^{-2} in the high flow season; however, standing crop was higher (347.87 kg wet weight km^{-2}) during the low flow season because of the higher densities of sea lions. Motile macroinvertebrates (Dungeness crab, crangonid shrimp), bivalves, and fish (including predominantly longfin smelt, Pacific staghorn sculpin, Pacific tomcod, English sole, starry flounder, snake prickleback, Pacific herring) comprised the prey resource of sea lions and seal in the estuary. Indirect estimates of total annual consumption by sea lions in the estuary was 69.55 MT C yr^{-1} and by harbor seals was 244.21 MT C yr^{-1} , for a total of 313.76 MT C yr^{-1} for all marine mammals.

Thus, total consumption by these secondary and tertiary level carnivores annually equals approximately 2,057 MT C yr^{-1} .

Annual production (P), biomass (B), and production/biomass ratios (P/B) were calculated or estimated for each functional group of organisms in each of eight regions and six habitat types in the Columbia River Estuary. In addition, the predominant species within each region and habitat type were identified. Such an exercise allows comparisons of P, B and P/B for purposes of identifying regions and habitats of high and low mean annual production, mean biomass, and mean production efficiencies.

Annual phytoplankton production in the water column was approximately 17,115 MT of carbon, annual marsh plant production was 11,324 MT C, and annual benthic algal production on tidal flats was 1,545 MT C, for an overall annual primary production in the estuary of 29,984 MT C. The annual production of the three plant groups above was largely a function of how much estuarine area was covered by each group. Phytoplankton production beneath a unit area of water surface (to the depth of photosynthetically-active light penetration) was relatively small in the Columbia River Estuary when compared to values for estuaries on the eastern seaboard of the U.S. and Canada. Values were comparable to those measured in the Fraser River Estuary, British Columbia, however.

Total annual production of all consumer groups in the Columbia River Estuary was estimated at 3,134 MT C, which was 10.45% of total estuarine primary production. The suspension-feeding organisms (principally zooplankton) represented the bulk of the consumer production (82%), although zooplankton estimates were not very precise. Suspension-feeder production was about 15% of the phytoplankton production in the water column, as a yearly average. Deposit-feeding organisms represented about 12% of total consumer production, predators represented about 5%, and wetland herbivores accounted for only about 0.2% of the total consumer production.

Plant biomass concentration in terms of carbon per square meter of surface was very high in the marshes, where emergent marsh plants dominated. Concentrations up to 702 gC m^{-2} were recorded in the low marsh areas of Youngs Bay. Plant biomass was lowest in the water

column, where the highest phytoplankton concentrations were only about 2.9 gC m⁻² in the Fluvial Region. Benthic algal biomass was intermediate, with the highest concentration (29.6 gC m⁻²) on the low marsh sediments in the Youngs Bay Region.

Animal biomass concentrations varied widely as a result of the diversity of animal species in the estuary, and their diverse distributions. Total biomasses of top-level predators such as seals and predatory fish were usually very low compared to estimated biomasses of zooplankton or benthic infauna, although the larger animals are more visually obvious than the myriad smaller forms in the water or bottom sediments. Mean biomass of deposit-feeding infauna in the tidal flats of Baker and Trestle Bays was estimated at about 3.5 gC m⁻², for example, whereas mean biomass of predatory fish in all suitable habitat types in Baker and Trestle Bays was about 23 times less.

Of the calculated annual P/B ratios in the plant groups, phytoplankton had the highest by a large measure (about 25 to 84), while emergent vascular plants had the lowest (near 1). Benthic algal P/B ratios ranged from approximately 1.6 to 2.6. P/B ratios for most animal groups were estimated from the literature.

Comparisons of total annual production by region or by habitat were not attempted because there were too many instances in which no data were taken for potentially significant groups of organisms.

Future research needs include:

- Field experiments and modeling to further evaluate the fluxes of water, salt, and sediment across the mid-estuary flats.
- Measurement, analysis and modeling of flow and transport through the estuary entrance.
- Measurement and modeling of circulation in the peripheral bays.
- Development of a sediment budget for the estuary.
- Estimates of fluxes of suspended sediments, especially related to the turbidity maximum.
- Numerical modelling of sediment transport.
- Study of the formation, transport, and decomposition of detritus.
- Research on the role of the turbidity maximum in secondary productivity.
- Synoptic sampling and multivariate analyses to delineate phytoplankton, benthic algal, and emergent plant assemblages and habitat structure.

- Determination of factors affecting primary productivity of major plant groups.
- Understanding of import and export of fluvial phytoplankton and zooplankton.
- Development of grazing rate estimates for primary consumers.

1. INTRODUCTION

This report presents an ecological synthesis of the physical and biological studies carried out by the Columbia River Estuary Data Development Program (CREDDP). It is written primarily for estuarine scientists and resource managers with training in the physical and biological sciences. However, some sections may be of interest to resource managers, planners, and others whose training is in other fields.

There have been few comprehensive ecological studies of the Columbia River Estuary (Figure 1.1). Most studies have been site-specific and/or focused on target organisms. Although there is considerable data on physical and biological characteristics of the estuary, little information is available on relationships among biological processes and physical processes. This report, which focuses on physical-biological relationships and other ecological processes, provides a major advance in our understanding of the Columbia River estuarine ecosystem.

Related CREDDP publications are described in the Preface to this report. Materials are available that describe CREDDP findings in nontechnical terms and discuss their management applications. Reviews of literature related to the Columbia River Estuary are also available.

APPROACH AND ORGANIZATION OF THIS REPORT

Chapter 2 provides the background and regional setting for the more detailed discussions of physical processes presented in Chapters 3 through 5. Chapter 2 includes a review of the tectonic setting of the estuary and long-term sea-level trends. An extensive discussion of the hydrography of the Columbia River is included and the river "seasons" used in this report are defined. The sources of sediment input into the estuary are discussed, and the local atmospheric and oceanic conditions which affect the estuary are summarized. A brief review of previous studies of the physical aspects of the estuary is presented, followed by a review of biological studies.

Chapter 3 uses as a framework a definition of estuarine flow modes based on an analysis of the equations of motion. This analysis is designed to determine the importance of tides, riverflow, topography, bottom friction, and density structure. The effects of channel curvature and changes in channel cross-sectional area are not of major importance in most parts of the estuary. In contrast, bottom friction, horizontal salinity gradients, and stratification are part of tidal circulation, which is the primary circulation mode. Tidal circulation is modified by secondary modes, which occur at different frequencies, and which account for riverflow, topographic effects, steady gravitational circulation, distortion of the tidal wave in shallow water, etc. The same analysis is extended to the salinity distribution equation, in order to define the processes that maintain salinity in the

estuary. Salt is maintained in the estuary, in the face of strong outward riverflow, primarily by the tides acting on the horizontal salinity gradient. The topics considered within the framework of this analysis are: tidal circulation and its interaction with riverflow; system energetics; salinity distribution and the transport of salt and water; the response of the system to storms; and changes in riverflow and tidal range. These problems are analyzed using time series and vertical profile data, and three different circulation models.

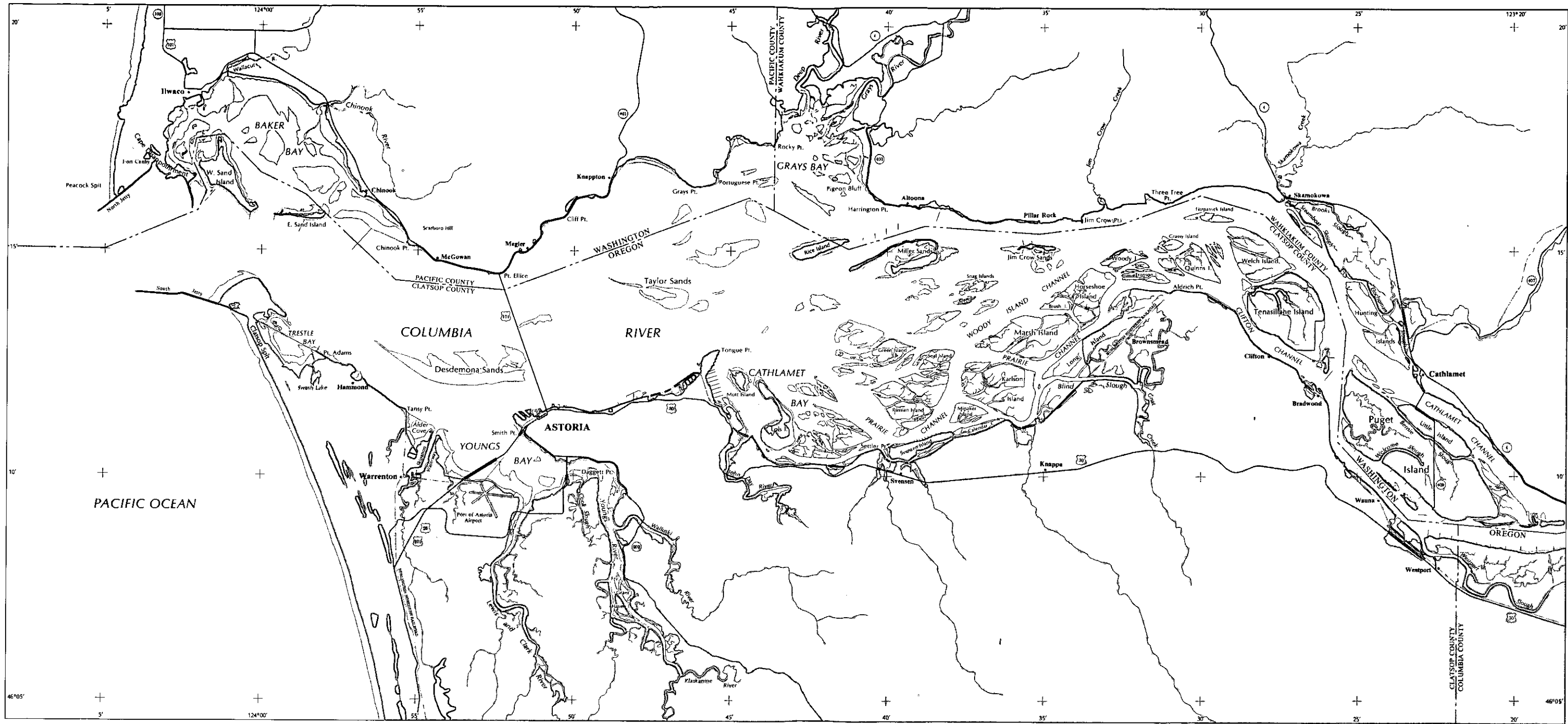
Chapter 4 continues the discussion of the physical environment of the estuary with an analysis of the CREDDP sedimentology data. Research into the processes of erosion, transportation, and deposition of sediment is presented, along with an interpretation of the morphologic characteristics of the estuary. Chapter 4 draws on the results presented in Chapter 3, and the sedimentation research to complete the physical description of the estuary and its subtidal and intertidal habitats.

In Chapter 5, a chronology of the physical changes in the estuary that have occurred in historic time is listed, and the results of two approaches to an historical analysis of the evolution of the modern estuary are presented. Modeling results are interpreted in light of the knowledge gained in the studies of currents and sedimentation, and historical bathymetric charts and area/volume calculations are discussed. Trends which appear as the estuary and the river have developed are evaluated in terms of the changes in the physical environment and the habitats of the estuary. Collectively, Chapters 2 through 5 present the physical backdrop for the ecosystem approach taken in Chapters 6 through 8.

Chapter 6 presents a conceptual model of the complex interrelationships among biological processes in the Columbia River Estuary. This model has a hierarchical structure which identifies the coupling variables, state variables, and system inputs and outputs that provide the framework for Chapter 7. The conceptual model also provides an organizational structure for the synthesis of physical and biological data obtained at many different levels of temporal and spatial resolution. In the chapter, the theoretical basis for the synthesis of CREDDP scientific information is stated, and the systems and subsystems corresponding to the theory are diagrammed and described in detail.

In Chapter 7, biological processes and associated state variables are discussed in relation to the physical processes that influence their dynamics. First, the taxonomic structure of the assemblages of organisms involved in each process is described, and in some cases, the physical and biological variables that determine the distribution of these organisms are identified. Next, mechanisms that control process rates are explored relative to systems inputs and outputs, and within the coupling structure of the hierarchical conceptual model introduced in Chapter 6.

Chapter 8 provides a regional and habitat summary of information presented in Chapter 7. The estuary was divided into eight regions on the basis of physical properties. Some or all of six identified habitat



Columbia River Estuary

Scale 1:160,000



Map produced in 1983 by Northwest Cartography, Inc.
 for the Columbia River Estuary Data Development Program

-  Shoreline (limit of non-aquatic vegetation)
-  Major highways
-  Intertidal vegetation
-  Cities, towns
-  Shoals and flats
-  Railroads
-  Lakes, rivers, other non-tidal water features
-  Other cultural features

Figure 1.1 Columbia River Estuary

types occur in each region. Tables are presented showing, as far as the data allow, the dominant taxa associated with the biological producers (phytoplankton, benthic algae, and vascular plants) and consumers (wetland herbivores, deposit feeders, suspension feeders, and predators) found in each region/habitat combination. In addition, the biomasses, numbers of organisms, and production of the producers and consumers found in each region/habitat combination are tabulated.

Conclusions resulting from this synthesis of the CREDDP data are presented in Chapter 9. Major conclusions resulting from the physical and biological research are described. The implications of the research results on understanding of the river-estuary-plume continuum is discussed. Ramifications of anthropogenic changes to the estuarine community and processes are suggested. These conclusions end with an analysis of the adequacy of our understanding of the Columbia River estuarine ecosystem after the CREDDP research, focusing on data gaps and recommending directions for the next generation of research. Chapters 8 and 9 may be of special interest to planners and resource managers.

2. REGIONAL SETTING AND PREVIOUS STUDIES

Estuaries are transitional environments between the land and sea. The particular geologic, oceanographic, meteorologic, and hydrographic characteristics of the region surrounding an estuary in large part determine the physical processes occurring in that estuary. Physical processes in turn constrain biological processes. Since regional characteristics differ, so do estuaries. The purposes of this chapter are, then, to explain the regional setting that renders the Columbia River Estuary different from other North American estuaries and to briefly summarize previous physical and biological work in the system.

2.1 GEOLOGIC SETTING OF THE COLUMBIA RIVER ESTUARY

The physiographic setting of the Columbia River Estuary is unique among North American estuaries and contributes to several aspects of the physical, geological, and biological processes that occur in the estuarine system. The Columbia River drains a vast expanse of western North America and a variety of terrains. The lower reaches flow through the Cascade Mountains, a rugged and youthful range that includes active volcanoes. The mountains trap moisture and force precipitation which, in combination with the contributions from the upper drainage basin, provides the estuary with large volumes of freshwater and an abundant sediment supply. The estuary itself occupies a valley incised into Tertiary marine sediments and volcanic rocks. Much of the bedrock valley has been subsequently filled with Pleistocene and Holocene fluvial sediments, and it continues to fill with estuarine sediments. These sedimentary deposits dominate the morphology of the estuary and exert important influences on the patterns of tidal circulation and the nature of the bottom habitats.

The following sections generally describe the tectonic setting of the estuary, the historical and longer term trends in the sea level at Astoria, and the nature and volume of sediment supplied to the estuary by the Columbia River. A discussion of the important physical oceanographic parameters at work in the estuary in Chapter 3 is followed by a detailed discussion of the modern sedimentology of the estuary.

2.1.1 Plate Tectonics

The Pacific coast of the northwestern United States is located on an active continental margin. The North American plate of continental crust overrides the Juan de Fuca plate, a portion of relatively young ocean floor that is currently forming along the Gorda and Juan de Fuca ocean ridges (Atwater 1970; McKee 1972). The subduction of the seafloor is associated with the eruptions of the andesite volcanoes of the Cascade Range and with a tilting of the continental crust. The result is an uplift of the continental shelf and coastal regions of Oregon and Washington and a downwarp of interior regions along a linear lowland trough, which includes Puget Sound, parts of the Chehalis Valley, and the Willamette Valley. Minor, deep-focus earthquakes occur along the subduction zone, but these are notably less severe than those found

along similar structures elsewhere in the world (Ando and Balazas 1979).

The tectonic regime exerts both direct and indirect effects on the physical processes within the estuary, and exerts ultimate control over estuarine sedimentation on a geological time scale. Indirectly, plate tectonics have determined the large-scale topography of the surrounding ocean basin, continental shelf, and uplands. This topography influences oceanographic, atmospheric, and hydrographic processes. More directly, tectonic control of uplift and volcanism regulates sediment supply, and crustal movements determine, in part, changes in local sea level.

2.1.2 Sea Level

Average sea level around the United States, as measured from tide gauges, has been rising at a rate of approximately 1.5 mm yr^{-1} since 1940 (Hicks 1978). Apparently this is a continuation of a trend associated with the melting of glaciers following the last Pleistocene glaciation which ended about 9,000 years ago. Geological evidence suggests that initially sea level rose world-wide at a relatively rapid rate of $5 \text{ to } 7 \text{ mm yr}^{-1}$ but the rise subsequently slowed to the present rate of $1 \text{ to } 2 \text{ mm yr}^{-1}$ about 5,000 years ago (Kraft 1971). Glenn (1978) reports radiocarbon dates in a core from Tillamook Bay that suggest similar rates for coastal Oregon. However, sea level has not continued to rise along the Oregon-Washington coast adjacent to the estuary in recent (historic) times. The tectonic uplift of the coastal regions is resulting in a lowering of relative sea level along the western United States north of Cape Mendocino (Hicks 1972). Geodetic leveling data from 1904 to 1974 and tide gauge data from 1946 to 1974 both suggest that sea level in Astoria has been falling since the turn of the century at rates of $2 \text{ to } 5 \text{ mm yr}^{-1}$ (Ando and Balazas 1979; Chelton and Davis 1982).

2.2 COLUMBIA RIVER HYDROLOGY

The Columbia River is one of the major rivers of North America and the largest river that enters the northeastern Pacific Ocean. Its average flow of about 257 kcfs (thousand cubic feet per second) $7,280 \text{ m}^3 \text{ sec}^{-1}$, cubic meters per second) contributes some 60% (winter) to 90% (summer) of the freshwater input to the ocean between San Francisco Bay and the Straits of Juan de Fuca and plays a major part in definition of the regional water properties of the northeast Pacific Ocean (Barnes et al. 1972). Effluent from the Columbia River moves in response to prevailing coastal winds and currents. This movement is generally south and offshore during the summer and north along the coast in the winter (Figure 2.1).

The Columbia River drainage basin is divided by the Cascade Range into eastern and coastal sub-basins, each with different climatic, hydrologic, and geologic characteristics (Figure 2.1). The coastal sub-basin contains only about 8% of the total area of $660,480 \text{ km}^2$ but contributes about 24% of the total riverflow (Good and Jay 1978). The high runoff intensity (runoff per unit area) of the coastal sub-basin results from the large excess of precipitation over evaporation and the mild, wet winters. Lifting of warm air masses by the Coast and Cascade

Mountains is in large part responsible for the wet climate. The major coastal tributaries (the Willamette, Lewis, and Cowlitz rivers) have winter flows that are five to ten times greater than those during other months (Figure 2.2). Winter freshets are brief and are caused by warm winter storms that bring heavy rains and significant snowmelt.

The Eastern sub-basin has about 92% of the total drainage basin area. It has a drier, more continental climate and a lower runoff intensity, because the Cascades separate cold interior air masses from the warmer marine air masses to the west. Most of the runoff occurs as the snow melts in the months of April to July, during which period virtually the entire riverflow comes from the east side of the Cascades (Figure 2.2).

2.2.1 Historical and Seasonal Riverflow Pattern

Definition of the seasonal cycle of Columbia River freshwater flow is essential to the understanding of biological, geological, and circulatory processes. Separate definition of the historical and modern riverflow patterns is essential, because flow regulation by dams and irrigation withdrawal have significantly altered the seasonal flow cycle. The effects of this alteration of flow are considered in Chapter 5. The best available estimate of the unregulated riverflow is given by the monthly average, "estimated adjusted" flows defined in Orem (1968), and calculated by the United States Geological Survey (USGS) (Figure 2.3). A major shortcoming of the adjusted flow data is the lack of any correction for irrigation withdrawal and return flow. Irrigation in the Columbia River Basin began in about 1840 (Depletions Task Force 1983). The amount of land irrigated was about 2,000 km² in 1900, about 9,300 km² in 1910, about 14,600 km² in 1928, and about 31,600 km² in 1980. Available data do not allow correction of the adjusted riverflow data to flows that would have occurred in the absence of both dam regulation and irrigation. The relative acreages under irrigation and the difference between the 1928 and 1980 level of development (Depletions Task Force 1983) suggest that the annual mean irrigation depletion presently amounts to about 10 to 15 kcfs (280 to 425 m³sec⁻¹) and was about half that amount in 1928. There is also an annual cycle of irrigation withdrawal and return flow. Irrigation withdrawal is greatest in June and July; return flows are greatest in winter months. It is possible that irrigation may reduce the spring freshet by about 40 to 60 kcfs (or 1,130 to 1,700 m³sec⁻¹) in some years.

In order to define "present day" conditions it was necessary to divide the 1928-82 observations into "pre-regulation" and "modern" periods. The division is somewhat artificial in that some regulation and irrigation have occurred during the entire period of observation. Examination of the difference between the "estimated observed" (that flow calculated to have actually occurred at the mouth; Orem 1968) and "estimated adjusted" flows shows that the standard deviation of the flow difference greatly increased in about 1968 (Figure 2.4), that the magnitude of the maximum monthly flow difference increased radically (Figures 2.5 and 2.6), and that year-to-year transfers of flow became significant for the first time in about 1968 (the yearly mean curve in Figure 2.4). Present-day conditions are therefore defined on the basis

of the 1969-82 observations (Figure 2.7). Figures 2.3 and 2.5 to 2.7 indicate the magnitude of the changes in flow cycle that have occurred as a result of the construction of dams. The magnitude of the average spring freshet has been curtailed by at least 140 kcfs ($3,900 \text{ m}^3\text{sec}^{-1}$), and the probability of large freshets having important sedimentological effects has been greatly reduced. The true decrease in freshets is somewhat larger than indicated by Figures 2.3 and 2.7; the years 1969 to 1982 included an unusual number of strong freshets. Comparison of 1969-82 adjusted (Figure 2.2) and observed (Figure 2.7) flows suggests that the difference may be closer to 185 kcfs ($5,240 \text{ m}^3\text{sec}^{-1}$). Average observed flows throughout the rest of the year have been increased by regulation, and minimum monthly average flows in the fall have increased from about 65 kcfs ($1,840 \text{ m}^3\text{sec}^{-1}$) to about 105 kcfs ($2,970 \text{ m}^3\text{sec}^{-1}$).

2.2.2 Variability and Extreme Flows

Physical and biological processes respond to extreme flows as well as to the average flow. Furthermore, climatic changes with time scales of 10 to 40 years are evident in the flow data. The variability of the riverflow is the subject of this section.

The climatic changes are best defined by examining the yearly average flows. The adjusted yearly average flows (Orem 1968) from 1928 to 1982 varied by about a factor of 2.7 between about 140 kcfs ($3,960 \text{ m}^3\text{sec}^{-1}$; 1977) and about 382 kcfs ($10,800 \text{ m}^3\text{sec}^{-1}$; 1974). The yearly observed flows ranged from about 153 ($4,330 \text{ m}^3\text{sec}^{-1}$; 1977) to about 347 kcfs ($9,830 \text{ m}^3\text{sec}^{-1}$; 1974). Three years between 1880 and 1894 were probably wetter than 1974, but flows at the mouth prior to 1928 are not available. Flow data for the entire eastern sub-basin are available (1878 to date) from a gauging station at The Dalles, Oregon (RM-189; USGS 1958, 1963, and subsequent Water Supply Papers). These data (Figure 2.8) indicate an approximately 25% decline in average flow from the late nineteenth century to the 1920-42 period, some recovery during 1943-60, and a slight decline since then. The decrease in mean annual flow between 1881-1900 (about 219 kcfs; $6,200 \text{ m}^3\text{sec}^{-1}$) and 1961-80 (about 182 kcfs; $5,150 \text{ m}^3\text{sec}^{-1}$) is several times the irrigation depletion and is probably due to a change in climate. That climatic fluctuations are the primary factor involved is also suggested by the fact that flows are greater now than during the 1920-42 period, despite the present higher level of irrigation.

Monthly average flows show stronger variations than the yearly flows. Monthly average adjusted flows at the mouth range from about 65 kcfs ($1,840 \text{ m}^3\text{sec}^{-1}$; January 1937) to about 921 kcfs ($26,100 \text{ m}^3\text{sec}^{-1}$; June 1974); the monthly average flow for June 1894 at The Dalles alone (without the coastal sub-basin) was about 1,002 kcfs ($28,400 \text{ m}^3\text{sec}^{-1}$). Daily average flows are yet more variable. Daily flows at the mouth are not available but USGS has published daily flows from 1878 to date and yearly maximum flows from 1858 to date (USGS 1958, 1963, and subsequent Water Supply Papers). The highest recorded daily flow was during June 1894 (by far the wettest year in the last century); it was about 1,240 kcfs ($35,100 \text{ m}^3\text{sec}^{-1}$; USGS, 1958). The freshet of spring 1849 is believed to have been almost this large (Henshaw and Dean 1915). Daily flows in excess of 1,000 kcfs ($28,300 \text{ m}^3\text{sec}^{-1}$) at The Dalles are known

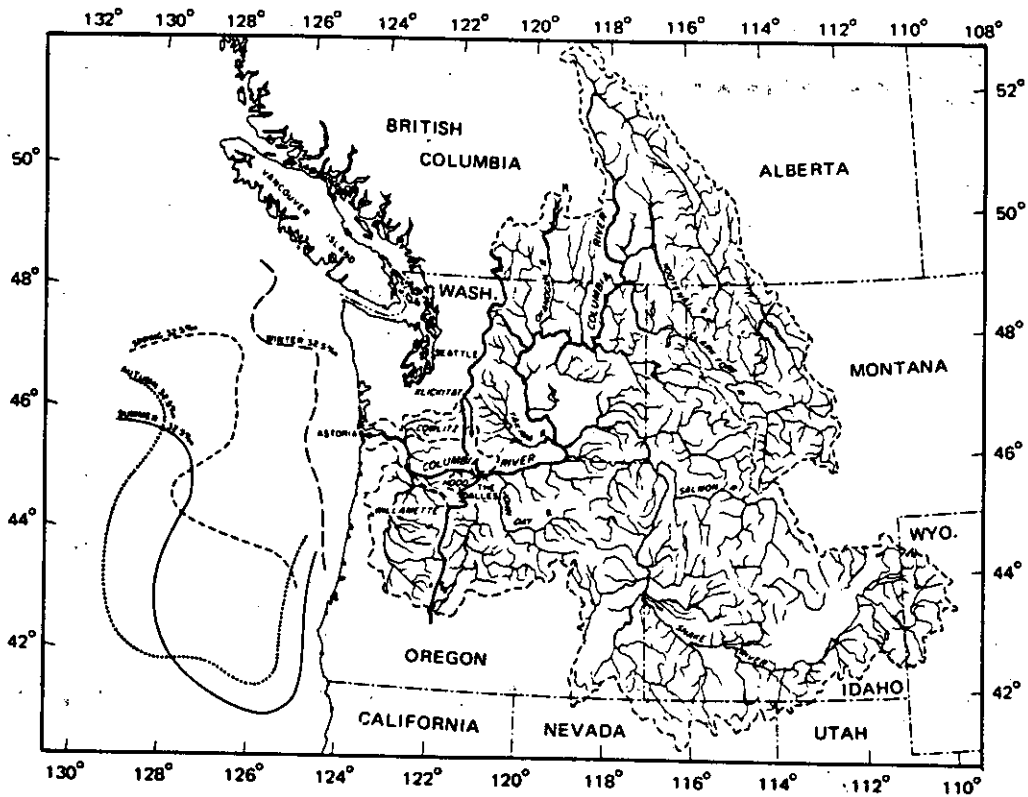


Figure 2.1. Map of the Columbia River drainage basin and average seasonal extent of the Columbia River effluent shown by the 32.5 ppt salinity isopleth. The crest line of the Cascade Mountains is shown by a solid line. (Pruter and Alverson, 1972)

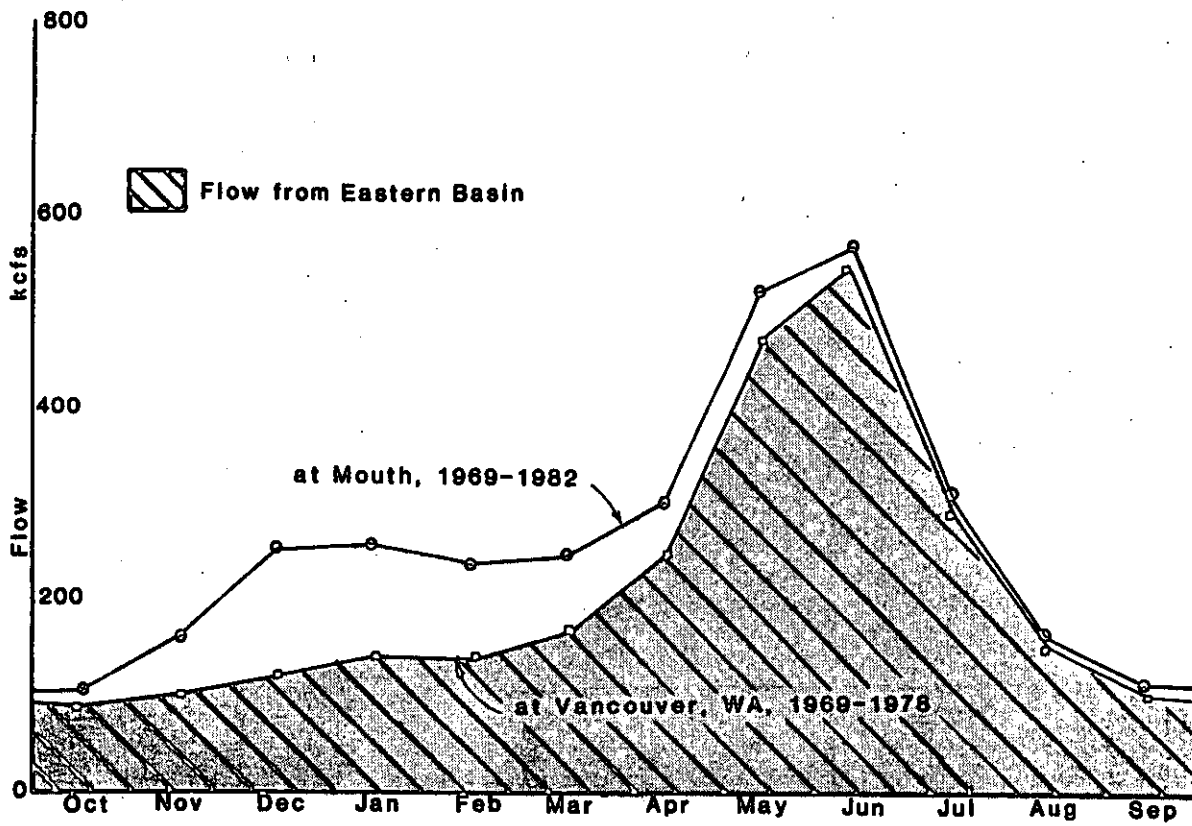


Figure 2.2. Monthly average estimated adjusted flow, Columbia River at Vancouver (Eastern Basin) and the mouth (Eastern and Coast Basins).

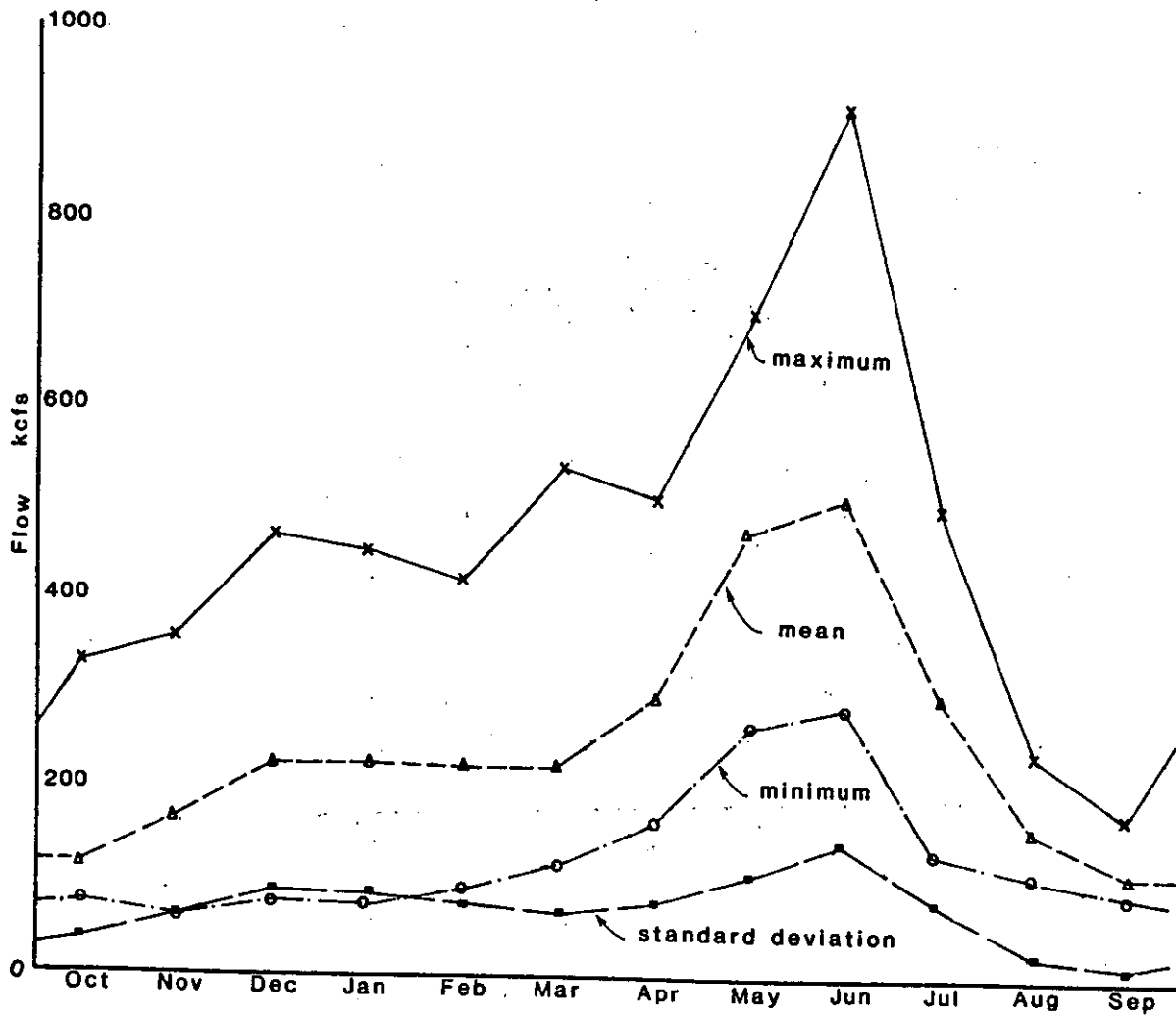


Figure 2.3. Monthly estimated adjusted flows, averages for 1928-1982, mouth of Columbia River.

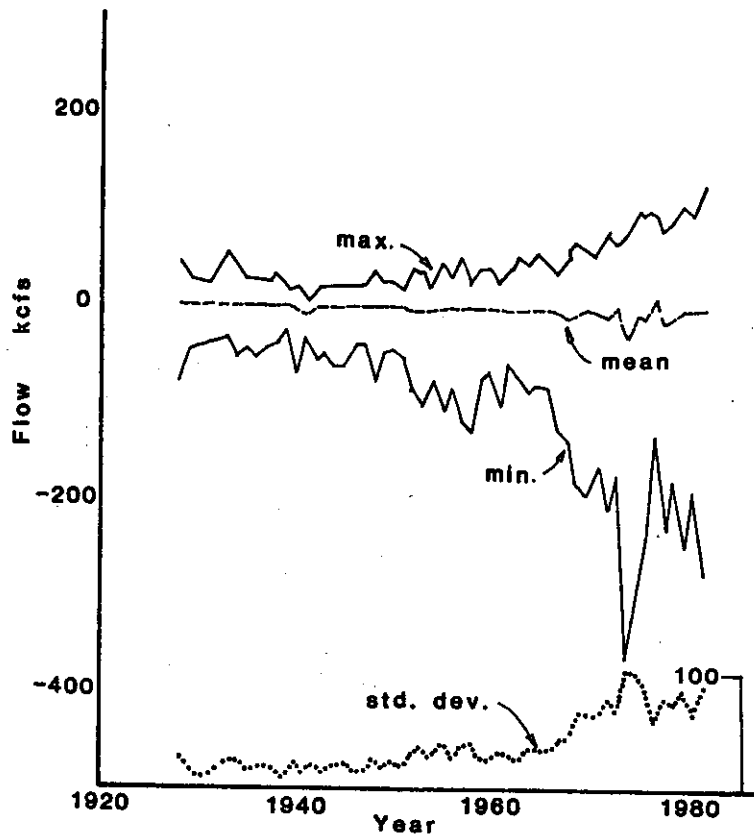


Figure 2.4. Monthly estimated observed-estimated adjusted flows, by year, 1928-1982.

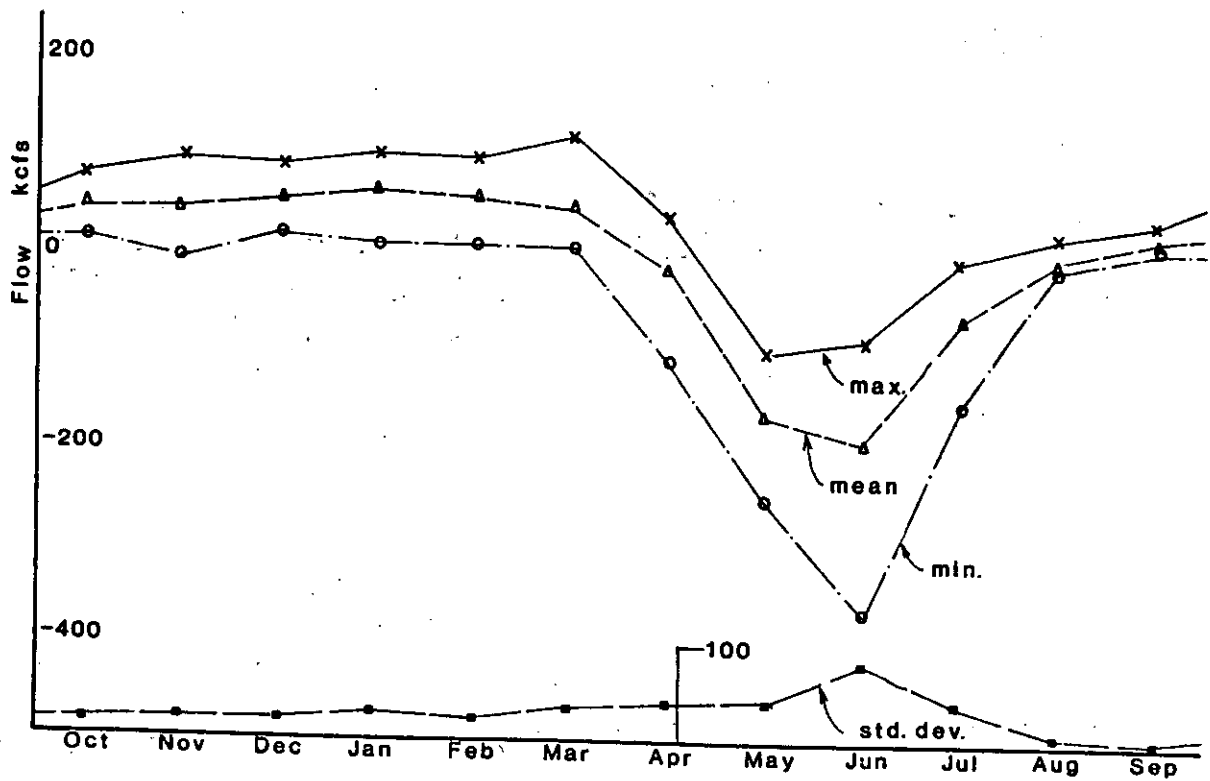


Figure 2.5. Monthly estimated observed-monthly estimated adjusted flows, averages for 1969-1982.

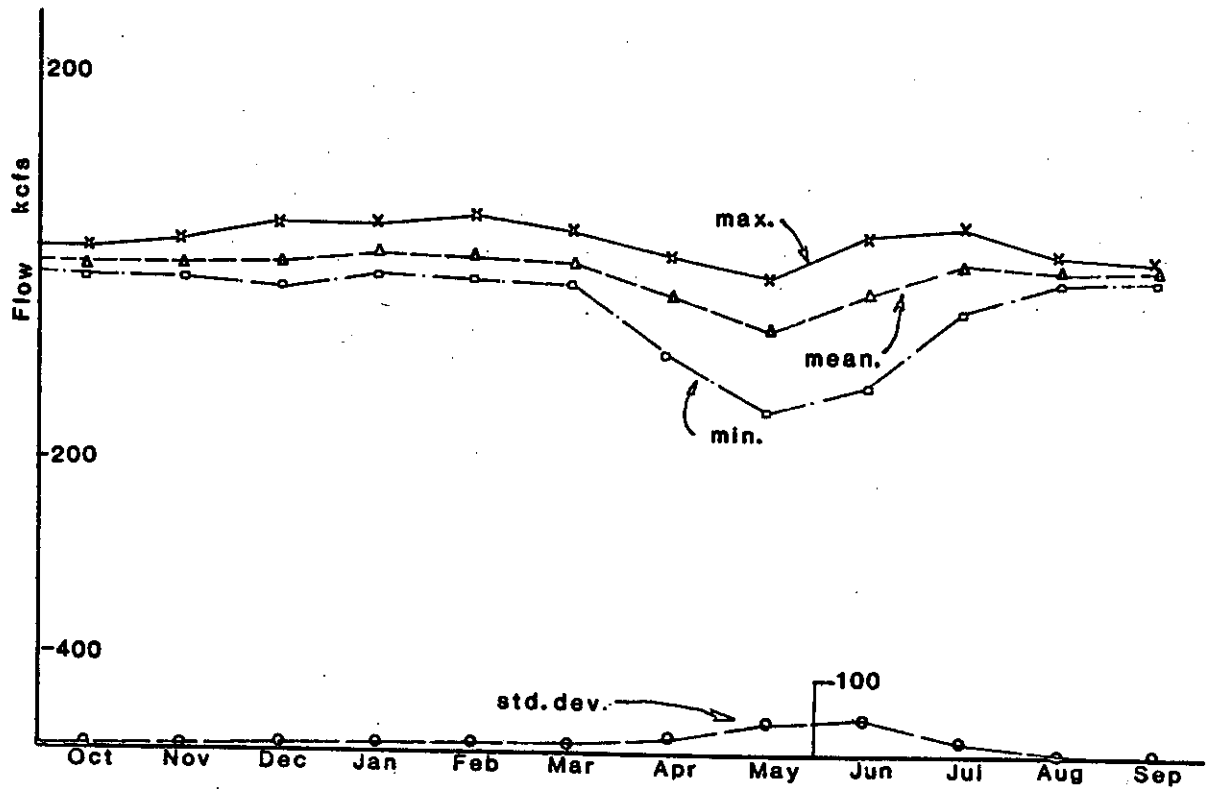


Figure 2.6. Monthly estimated observed-monthly estimated adjusted flows, monthly averages for 1928-1968.

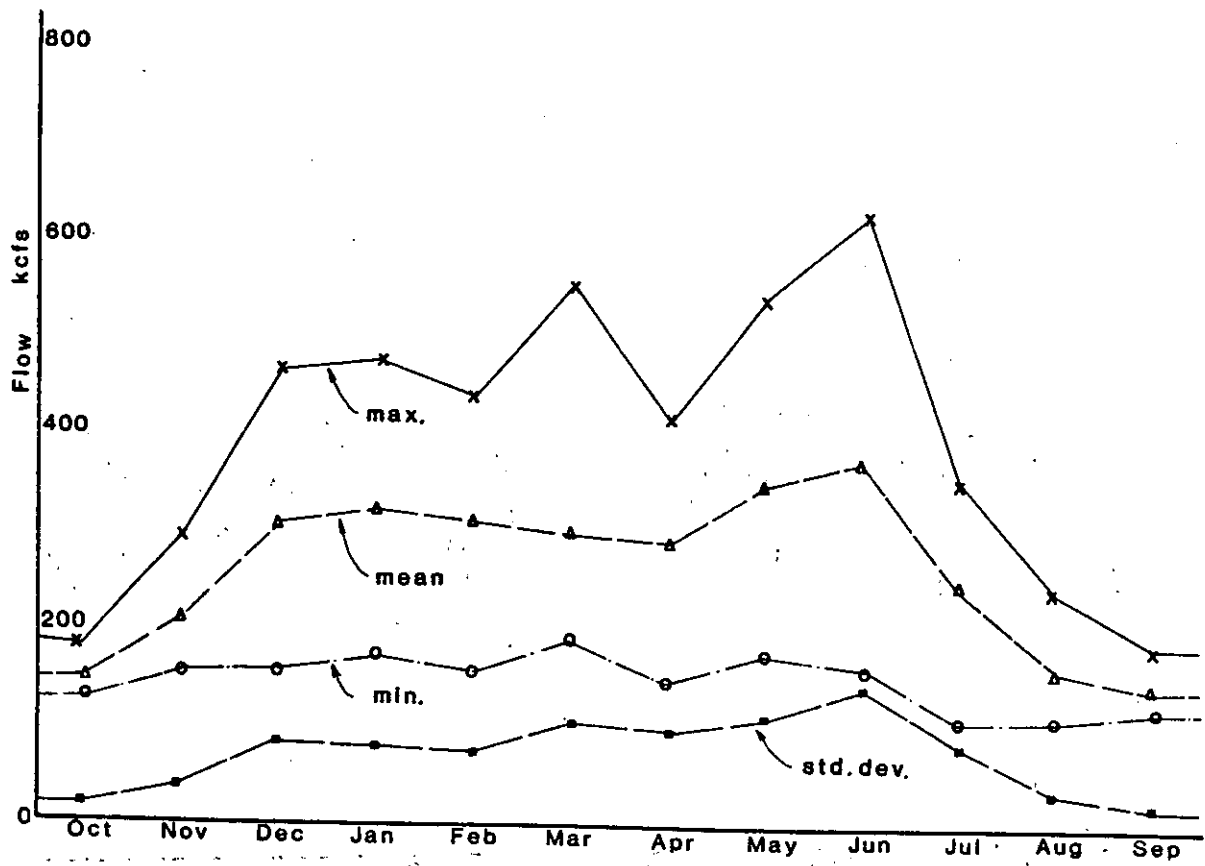


Figure 2.7. Monthly estimated observed flows, averages for 1969-1982.

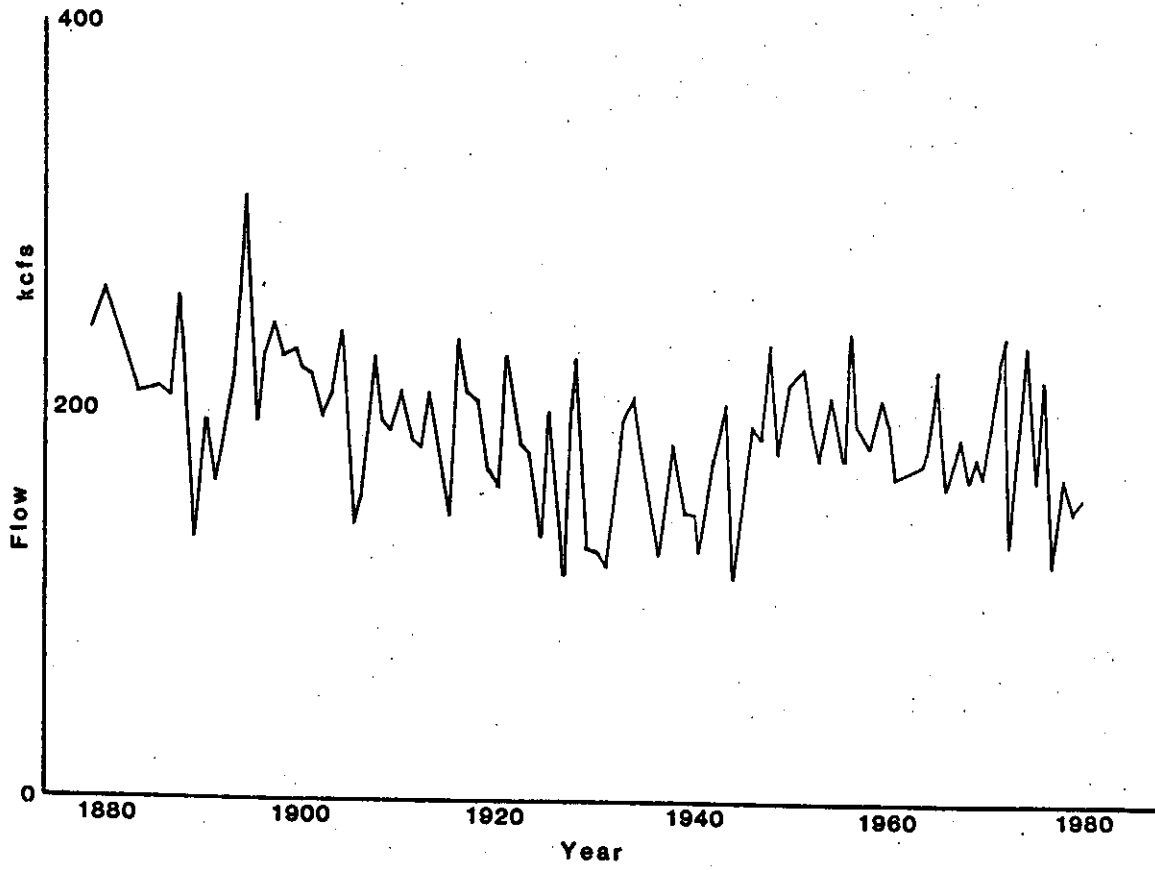


Figure 2.8. Mean observed flow at The Dalles, 1879-1980, by year.

ESTIMATED COLUMBIA RIVER FRESH WATER FLOW
AT ASTORIA

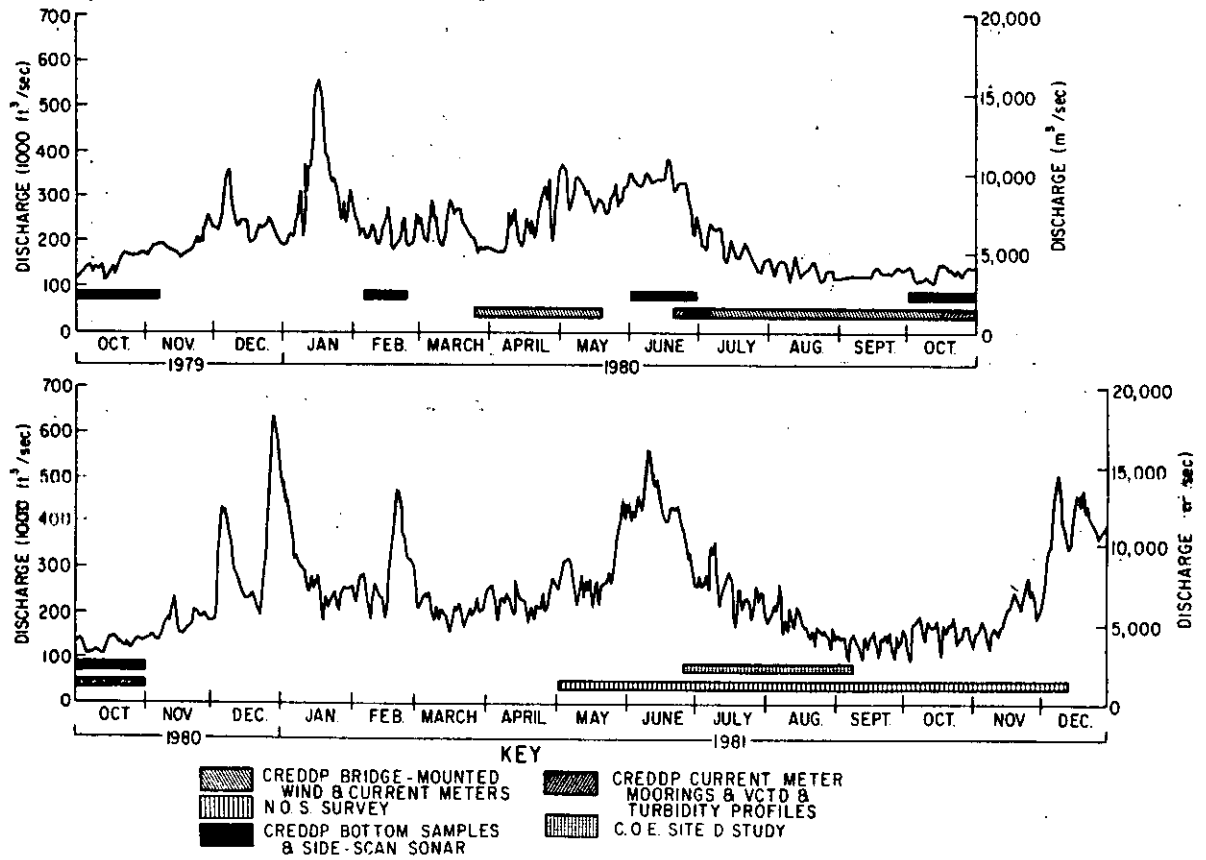


Figure 2.9. Columbia River Estuary discharge, and study periods.

Table 2.1. Seasonal cycle of riverflow 1969-82 and 1980-81.

	Riverflow 1969-82	Riverflow 1980-81	
	<u>Average, $\text{m}^3\text{s}^{-1} \times 10^3$</u>	<u>Average, $\text{m}^3\text{s}^{-1} \times 10^3$</u>	<u>Std. dev., $\text{m}^3\text{s}^{-1} \times 10^3$</u>
Jan.	9.17	8.61	2.41
Feb.	8.31	7.10	1.84
Mar.	8.45	6.09	0.84
Apr.	8.29	6.57	1.06
May	10.03	8.39	1.34
Jun.	10.53	10.43	2.13
Jul.	6.87	6.12	1.40
Aug.	4.65	4.45	0.84
Sep.	4.07	3.77	0.38
Oct.	4.33	4.16	0.68
Nov.	5.97	5.34	0.96
Dec.	8.80	10.45	2.97
Mean	7.46	6.76	2.68

to have occurred on only one other occasion (1948; 1,010 kcfs or 28,600 $\text{m}^3\text{sec}^{-1}$). Daily flows at The Dalles in excess of 850 kcfs (24,100 $\text{m}^3\text{sec}^{-1}$) occurred on seven occasions between 1858 and 1900 but only once in the twentieth century; they might have occurred in 1972 and 1974 in the absence of regulation. The present flow regulation system prevents floods of the magnitude of those of June 1849; according to the Corps of Engineers, the 100-year flood (assuming 1973 storage conditions) is in the 700 to 750 kcfs (19,000 to 21,200 $\text{m}^3\text{sec}^{-1}$) range. The lowest flows at The Dalles occur during periods of prolonged winter cold in the interior (Henshaw and Dean 1915); the minimum recorded daily average flow was about 35 kcfs (990 $\text{m}^3\text{sec}^{-1}$) in January 1937 (the driest single month on record; USGS 1958).

The daily and monthly flows at The Dalles give a good idea of the magnitude of the spring snowmelt freshet. Spring freshets were, before regulation, the largest freshets in the system, both in terms of instantaneous flow and total flow. They have been described by Paulsen (1949). The largest spring freshets occur after wet, snowy winters with cold springs, when the weather warms suddenly and melting is accompanied by heavy rains throughout the basin. Winter freshets are not well-measured, but it appears that winter freshets achieve instantaneous flows as large as most regulated spring freshets, but of much shorter duration. In years with small spring freshets, the winter freshet may exceed the regulated spring freshet (e.g., 1979-80).

For purposes of this report, daily flows were calculated from daily Bonneville Dam and mouth of the Willamette River flows for late 1979 to 1981 (Figure 2.9). The method used in the calculations minimizes the difference between the monthly average calculated flow at the mouth and the USGS monthly average estimated observed flow at the mouth (Jay 1984). Table 2.1 compares seasonal cycles for 1980-1981 (both notable for strong winter freshets) with the seasonal means of the recent period (1969-82). December flows for 1980-81 are above the long-term average; all other months are at or below average. The standard deviation of the daily flows is greatest in December, January, and June. This occurs because of sharp, sporadic freshets in all three months and because of differences in the size of the 1980 (weak) and 1981 (strong) June freshets. While all major freshets occur in June, large freshets do not occur every June, and in some years (e.g., 1980) the average flow is greater in May.

2.2.3 Estuary Tributary Inflow

The climate in the vicinity of Astoria is moderate and maritime, with a large excess of precipitation over evaporation. Annual rainfall averages about 198 cm (78 in) and has varied from about 135 to 290 cm (OSU Ocean Engineering Programs 1975). Annual evaporation amounts to about 51 cm (OSU Ocean Engineering Programs 1975).

Despite the maritime climate, the relatively small drainage basins of tributaries emptying directly into the estuary (below RM-47) prevents local runoff from being important in the circulation, except in the peripheral bays and the rivers and perhaps briefly throughout the estuary during winter storms. On an annual basis local tributary inflow

amounts to about 9 kcfs ($290 \text{ m}^3 \text{ sec}^{-1}$), or 3.5% of the total (Good and Jay 1978). About two-thirds of this inflow occurs during the December to March period, and less than 5% occurs during July to September on the average (OSU Ocean Engineering Programs 1975). The largest local tributaries are the Lewis and Clark, Youngs, Grays, and Elochoman rivers. It appears that local tributary flow might contribute as much as 10-20% of the total inflow at the beginning of a winter freshet before runoff from other west-side tributaries reaches the estuary.

2.2.4 Estuary Seasons

It is convenient for many purposes to divide the present annual flow cycle into three seasons: winter or fluctuating flow (November to March), spring or high flow (April to June), and summer-fall or low flow (July to October). The winter and spring seasons are distinguished less by the average level of riverflow than by the source and variability of flow. Winter freshets come from the coastal sub-basin and bring very high flows of a few days' duration. Winter flows during non-freshet periods may be quite low. The spring freshet comes from snowmelt in the eastern sub-basin and brings moderate to high flows for several months. Flows in the summer-fall season are reliably low except for July which, because regulation prolongs and moderates the spring freshet, is transitional.

2.3 SEDIMENT SUPPLY

The Columbia River is responsible for almost all of the sediment supplied to the estuarine system. The river drains approximately $660,480 \text{ km}^2$ of geologically varied terrain (Figure 2.2) which includes igneous, sedimentary, and metamorphic rocks and extensive alluvial and eolian surficial deposits (Whetten et al. 1969). Estimates of the total suspended load of the river vary from 7 to 30 million tons per year (Van Winkle 1914a,b; Judson and Ritter 1964; Haushild et al. 1966; Jay and Good 1978) and a generally accepted mean value is 10 million tons per year. Bedload supply is estimated at about 10% of this value, or one million tons per year (Whetten et al. 1969).

The sediments trapped behind upriver reservoirs reflect the plutonic, volcanic and metamorphic source rocks and the extensive loess deposits found in eastern Washington and the drainage basin of the Snake River (eastern sub-basin). The dominant minerals in these sediments are quartz and feldspars; the dominant heavy mineral is hornblende. Metamorphic and plutonic rock fragments are common. The sediments in the lower reaches of the Columbia River reflect the contribution of andesite volcanic materials from the tributaries draining the western slopes of the Cascades (western sub-basin). Downriver, the sediments contain increasing amounts of plagioclase and volcanic rock fragments and decreasing percentages of quartz and potassium. Hypersthene becomes the dominant heavy mineral in the lower reaches (Kelley and Whetten 1969; Whetten et al. 1969). The overall composition of the sediment in the lower Columbia River resembles graywacke and may provide a modern example of the source of ancient graywackes (Whetten 1966).

Volcanism in the Cascade Range may be responsible for an important

fraction of the sediment input. The 1980 eruption of Mt. St. Helens and the subsequent debris flow down the Toutle-Cowlitz Rivers and into the Columbia River at Longview provide models for the intermittent and substantial supply of sediment to the estuary. In the absence of human interaction, an eruption of Mt. St. Helens, Mt. Hood, Mt. Adams, or other andesite volcano might be expected to provide airborne ash, an almost immediate influx of suspended sediment, and a longer term supply of coarser material. Although cataclysmic in human terms, over geologic time these major eruptions represent a relatively constant supply of sediment to the Columbia River system. The mineralogy of the estuarine sediments, and especially the volcanic rock fragments, pumice, and glass-mantled grains found in the estuary subsequent to the Mt. St. Helens eruption (Roy et al. 1982) point to the importance of the volcanic contribution to the estuarine sediments.

Marine sediments found adjacent to the Columbia River are similar in composition to the river sediments. Two reasons for this similarity exist: 1) most of the sediment found on the beaches of Washington and the continental shelves of northern Oregon and Washington is derived from the Columbia River drainage system, and 2) the sediment supplied to the Oregon continental shelf from numerous small rivers and coastal erosion is derived from comparable volcanic rocks and sediments (Hodge 1934, Runge 1966, White 1967, 1970; Scheidegger et al. 1979, Nittrouer 1978). Scheidegger et al. (1971) used subtle differences in the composition of the heavy mineral fraction to trace the sediments originating in the Klamath and Siskiyou Mountains, the Coast Range of Oregon, and the Pleistocene terrace deposits of Oregon on the continental shelf. They concluded that sediment generally moves northward along the Oregon shelf and that transport rates may have been higher in the past when sea level was lower. Several other lines of evidence also suggest that although seasonal changes occur, littoral drift and the net transport direction along the beaches and continental shelf of Oregon and Washington is northward (Hopkins 1971, Smith and Hopkins 1972, Sternberg and McManus 1972, Barnes et al. 1972).

Several lines of evidence suggest that some of the sediments in the estuary have been recently transported into the estuary from the adjacent nearshore and shelf regions. Current meter studies have documented a predominance of upstream flow in the deeper portions of the entrance channels (U.S. Army Corps of Engineers 1932, Lockett and Kidby 1961, Jay 1984), and various physical and numerical models indicate net upstream bottom flow and sediment transport through the entrance under low and moderate discharge conditions (O'Brien 1935, Herrmann 1968, Hamilton 1983, 1984; McAnally et al. 1983a,b). Morse et al. (1968) used seabed drifters to demonstrate that marine sediments could be transported into the estuary, and Walter (1980) and Walter et al. (1979) used a distinctive lamellar pyroxene as a mineral tracer of coastal sediment transported into the estuary. Lockett (1967) and Sherwood et al. (1984) used sediment size evidence to argue that positively skewed fine sand has been transported into the estuary. Sherwood et al. (1984) provided side-scan sonar data that indicate upstream bedform transport of sediments at some tide stages in the entrance and seasonal upstream transport in estuarine channels.

Additional sediment sources include local tributaries, erosion of older deposits within the estuary, and windblown transport. Cooper (1958) provides a discussion of the dune development on the prograding beach of Clatsop Spit following jetty construction. Hodge (1934) and O'Brien (1936) were concerned with eolian erosion and transport of beach sand into the estuary. O'Brien argued that wind transport to the NNE occurred at an average rate of $177-402 \text{ kg m}^{-1} \text{ day}^{-1}$ ($120-270 \text{ lbs ft}^{-1} \text{ day}^{-1}$) on the exposed and unvegetated portions of Clatsop Spit. Those rates, over a cross-section of 4 km, would provide more than a million cubic meters of sediment to the estuary each year, exceeding the average shoaling rate of Trestle Bay (see Chapter 5) by a factor of 8. Roy et al. (1982) examined sand grains from Clatsop Spit dunes with a scanning electron microscope and found that the grains were surprisingly fresh and displayed little of the characteristic pitting commonly associated with dune sands (Krinsky and Donahue 1968). The sand dunes were largely stabilized during re-vegetation efforts by the Soil Conservation District in 1935 (McLoughlin and Brown 1942) and eolian transport is probably less important now than in the period following jetty construction. Eolian supply of volcanic ash occurred following one of the Mt. St. Helens eruptions in 1980, but resulted in an insignificant deposit of sediment over the estuary. Although it is difficult to quantify the importance of eolian transport within the system, it is not believed to be a major process in the re-distribution of estuary sediments.

Erosion of the estuarine shoreline has been identified as a sediment source in other northwest estuaries, including Tillamook Bay (Glenn 1978) and Willapa Bay (Clifton 1983), but in both instances it was not considered a primary sediment source. Some of the rocky headlands in the Columbia River Estuary are eroding and contributing talus to the estuary, but the Tertiary bedrock does not appear to erode rapidly nor contribute significantly to the volume of estuarine sediments. Local erosion of younger (Pleistocene and Holocene) estuarine and fluvial deposits may represent a more important supply but is still thought to be minor relative to the fluvial source. Most of the other estuaries that have been studied along the Oregon and Washington coast have as their sediment sources some combination of either fluvial or marine sediments (Kulm and Byrne 1967, Boggs and Jones 1976, Scheidegger and Phipps 1976, Glenn 1980, Clifton and Phillips 1980, Peterson et al. 1982), and the Columbia River appears to exhibit similar characteristics.

Sediment from local tributaries may be a locally important source near the entrance to these rivers. Workers at Oregon State University have suggested that most of the sediment in the upper reaches of Youngs Bay are derived from erosion of Oligocene-Miocene sedimentary rocks in the drainages of the Youngs, Walluski, and Lewis and Clark Rivers (Oregon State University Ocean Engineering Programs 1975). It is likely that similar situations occur in the lower reaches of the Grays River, Elochoman River, and Skomokawa Creek, but the contribution of these tributaries to the overall sediment budget is expected to be minimal. In summary, sediment sources other than the Columbia River and the adjacent marine environment are believed to be quantitatively much less important to the sedimentology of the estuary.

2.4 ATMOSPHERIC AND COASTAL OCEANIC PROCESSES

This section concerns the atmospheric and coastal processes that determine flows, elevations, water types, and other inputs at the seaward boundary of the estuary, which is taken to be at the end of the jetties (RM-0).

2.4.1 Continental Shelf Circulation

The continental shelf circulation is important in that it determines the sea level and water types at the mouth of the estuary. The continental shelf circulation responds directly to the atmosphere and also to seasonal patterns in the northeast Pacific Ocean that are determined by seasonal atmospheric-oceanic interactions. The atmosphere accordingly affects the continental shelf circulation (and sea level at the entrance) on a variety of time scales, from a few days to inter-annual. Effects on two time scales (event, and seasonal to inter-annual) are of primary interest to this report.

Seasonal fluctuations in coastal sea level are associated with ocean-basin scale, seasonal changes in pressure, wind stress, and wind stress gradients (Chelton and Davis 1982; Hickey 1979; Hickey and Pola 1983). In summer the North Pacific High pressure system strengthens and moves north; winds directed to the south predominate off the Oregon and Washington coasts, atmospheric pressure is high, sea levels are low, and upwelling occurs. Shelf circulation in the winter is driven by north-directed winds, associated with the Aleutian Low. Downwelling occurs, atmospheric pressure is low, and sea level is elevated. The variability of all atmospheric parameters is much higher during the winter, and intense storms may be interspersed with periods of relatively good weather.

Atmospheric pressure also acts directly on coastal sea level through the inverse barometer effect (IBE). IBE is related to the fact that sea level (or a water barometer) will rise about 1 cm for every 1 millibar (mb) fall in sea level atmospheric pressure (Gill 1982). Removal of the inverse barometer effect from sea level data substantially reduces the variance (Jay 1984, Chelton and Davis 1982).

The Columbia River effluent has a substantial effect on the density of sea water in the adjacent coastal ocean by changing the salinity of surface layers (Barnes et al. 1972). The seasonal riverflow cycle may therefore have an effect on regional sea level, in addition to causing sea levels in the estuary to rise above the level of the adjacent coastal ocean so that more water may be discharged. Hickey and Pola (1983) found density-induced fluctuations of about eight dyn cm (dynamic centimeters) during a one-month period in March. This is about eight times the seasonal cycle due to temperature effects (Werner and Hickey 1983). Evaluation of the seasonal effects of the plume on sea level at the mouth of the estuary is, however, complicated by seasonal changes in the position of the plume.

Short-term fluctuations (lasting a few days to a week) in currents and sea level are often associated with storms. Storm surges may be as

large as 1 m, two to three times the amplitude of the seasonal cycle of sea level. Coastal sea level and currents may also be altered by energy transmitted along the coast by coastally trapped waves (Gill 1982). Despite the large magnitude of the storm surges associated with some storms, continental shelf events play only a small role in the circulation of the Columbia River Estuary (Jay 1984 and Section 3.1).

2.4.2 Winds, Storms, and Waves

The local effects of wind stress directly over the estuary must also be considered. Winter winds are directed to the north, and the average wind is directed offshore during some winter months (Table 2.2). Summer winds are directed to the south and onshore. The alongshore wind stress is to the north in all months, because the strongest (storm) winds are almost always directed to the north. The alongshore component of both winds and wind stress is considerably larger than the onshore component. The average winds are strong in both summer and winter and weaker in spring and fall. The winds appear to be nearly as strong in the summer as in the winter because summer winds are more persistent; the variability of the wind is much greater in the winter. Examination of the wind stresses (proportional to the square of the wind speed) and occurrence of extreme observations show that winter wind stresses are much stronger. Strong wind stresses (greater than $0.4 \text{ newtons/m}^{-2}$ in Table 2.2) are always directed onshore and almost always to the north.

The strongest winds are associated with major storms that occur a few times each year. According to Lilly (1983), the low pressure systems associated with these severe or "superstorms" have several important characteristics:

- They originate in the tropics or subtropics usually during fall, winter, or spring.
- The pressures at their centers are extremely low (935 to 970 mb).
- They grow, deepen, and move onshore very quickly.
- Interaction with the jet stream may cause significant strengthening of the system.
- They may bring winds in excess of 100 knots (50 m sec^{-1}) and wave height in excess of 35 feet (10 m) to the coast.
- Very strong winds and large changes in winds may be associated with passage of fronts during the storm.
- Weaker, secondary lows often follow behind the major low.

These storms, with strong winds and severe waves, are a very important factor in continental shelf circulation (Allen 1980, Hickey 1979) and in sediment transport at the mouth of the estuary (Sternberg et al. 1977, Kachel 1980). Sediment transport is strongly dependent upon extreme events because bottom shear stress, which controls sediment transport, varies non-linearly with velocity and is greatly increased by wave action.

The wave climate of the Pacific Northwest is severe. Wave

Table 2.2. Seasonal cycles of atmospheric parameters.

Geostrophic winds*, 1980-81
(46°N, 124°W)

	Pressure, mbar	wind		windstress, u				windstress, v			
		u, m sec ⁻¹	v, m sec ⁻¹	average newton (nt) m ⁻²	std. dev. nt m ⁻²	# of obs. >-0.4 nt m ⁻²	# of obs. <-0.4 nt m ⁻²	average nt m ⁻²	std. dev. nt m ⁻²	# of obs. >0.4 nt m ⁻²	# of obs. <-0.4 nt m ⁻²
Jan.	1015.9	-2.67	5.64	-0.049	0.094	2	0	0.132	0.198	17	0
Feb.	1015.2	-0.65	5.91	-0.003	0.091	1	0	0.108	0.129	9	6
Mar.	1017.4	2.17	0.20	0.028	0.069	1	0	0.007	0.079	1	0
Apr.	1018.1	2.52	0.19	0.033	0.053	0	0	0.003	0.063	0	0
May	1017.5	2.43	-3.31	0.024	0.027	0	0	-0.038	0.048	0	0
Jun.	1018.9	2.28	-2.69	0.021	0.028	0	0	-0.033	0.052	0	0
July	1018.8	1.38	-5.77	0.014	0.027	0	0	0.066	0.040	0	0
Aug.	1016.3	1.16	-4.61	0.011	0.022	0	0	-0.048	0.041	0	0
Sep.	1016.8	0.82	-0.75	0.008	0.038	0	0	-0.002	0.052	0	0
Oct.	1017.2	-0.24	2.14	-0.003	0.054	0	0	0.044	0.109	4	0
Nov.	1016.7	1.20	5.89	0.024	0.085	0	0	0.103	0.117	6	1
Dec.	1016.6	0.92	6.03	0.014	0.087	0	0	0.119	0.161	13	1
Mean	1017.14	0.96	0.68	0.0104	0.065	4	0	0.0263	0.123	49	8

*Calculated every 6 hours by NMFS from pressure distribution. High-frequency fluctuations removed with a lanczos low-passed filter with half-power point at (32 hours)⁻¹. The "u" indicates the onshore component

Table 2.3. Defining properties of surface ocean water (SOW) and sub-surface ocean water (SSOW), near mouth of Columbia River.

	<u>SOW</u>		<u>SSOW</u>	
	<u>Salinity ppt</u>	<u>Temp °C</u>	<u>Salinity ppt</u>	<u>Temp °C</u>
June				
11-20, 1965*	31.76 ±0.1	12.8 ±0.2	33.64 ±0.17	7.57 ±0.13
Sept.				
14-26, 1965*	31.92 ±0.45	13.6 ±0.3	33.36 ±0.21	7.80 ±0.11
June				
15-20, 1966*	31.65 ±0.55	12.5 ±0.7	33.76 ±0.09	7.25 ±0.16
Aug.				
13-23, 1966*	31.78 ±0.85	13.83 ±0.86	33.63 ±0.23	7.49 ±0.21
Jan. 13-				
Feb. 20, 1958**	32.0 - 32.5	10.2 - 10.9		not observed

*from Conomos et al. 1972

**from U.S. Navy Hydrographic Office 1960

climatology data are available for Newport, Oregon (Creech 1977), based on five years of data collected using a seismometer. The maximum observed significant wave height was 7.3 m with a period of 17 seconds. Compilations of wave statistics off the mouth of the Columbia River include O'Brien (1951), National Marine Consultants (1961a,b,c), and McAnally et al. (1983). The National Marine Consultants (1961a,b,c) and McAnally et al. (1983) statistics are based on meteorological hindcasting rather than actual observations. National Marine Consultants (1961a,b,c) emphasize the contribution of long-period waves originating in remote parts of the Pacific to the wave climate and hindcast a most severe wave at the South Jetty of 10 m amplitude and 13 sec period from 23°T.

The interaction of waves and currents plays a major role in causing severe bar conditions on ebb tides. The wave field can extract energy from the mean flow, just as turbulence does (Harris 1979; Vincent 1979). This occurs most effectively on a strong ebb tide, when the flow from the estuary assumes a jet-like form with strong horizontal gradients on either side of the jet. The ebb current steepens the waves and increases their energy. Most closures of the Columbia River entrance occur, accordingly, during the ebb, and prediction of rough bar conditions requires both knowledge of offshore wave conditions and tidal currents (Wang et al. 1979). Wave and storm effects upriver of RM-3 are, however, much smaller than at the entrance.

2.4.3 Water Types, Water Masses, and Mixing

In order to describe oceanographic mixing processes it is customary to define water types that have extreme water properties and that mix together to create the observed temperature and salinity properties in an area (the water masses). Water types in the Columbia River and adjacent ocean waters have been defined by Conomos et al. (1972). The three water types are River Water (RW), Surface Ocean Water (SOW), and Sub-Surface Ocean Water (SSOW).

River Water (RW) has a salinity of zero but has highly variable temperature characteristics. National Marine Fisheries Service (NMFS) records from Trojan (RM-72) show temperatures ranging from 0.2°C in January 1979 to 23.1°C in August 1977 (personal communication, R.J. McConnell, NMFS, Hammond, Oregon). CREDDP and National Ocean Service (NOS) records show temperatures above 20°C for periods of several weeks during the summers of both 1980 and 1981.

SOW is defined (Conomos et al. 1972 and Table 2.3) as the warmest water of near-oceanic salinity in the area. Pure SOW is found in the top 15 m more than 15 km offshore; it is a mixture of offshore water with the Columbia River plume. SSOW is the coldest and most saline water type. It is found at least 20 to 30 m below the surface offshore but is closer to the surface inshore, because of coastal and river plume-induced upwelling. The temperature-salinity (T-S) characteristics of SSOW are independent of riverine influence (Table 2.3). The seasonal variability of the SOW can be explained by seasonal differences in weather, riverflow, and mixing. SOW is warmest at the end of summer; it is colder and more saline in winter due to cold air temperatures and

strong winter mixing (Table 2.3). It is least saline during the spring freshet period. SSOW is not always observed in the nearshore area. Probably it is present only during periods when upwelling is occurring. While this may happen in any season, it is much less common in winter.

The magnitude of the riverflow and the strength of its influence on offshore water masses suggest that the river and estuary upriver of the jetties are only part of a larger river, estuary and plume system. While the offshore area has not been studied by CREDDP, the relationship between the river and estuary and the offshore processes is discussed in Chapter 9.

2.4.4 Ocean Tides of the Northeast Pacific

The tides are the dominant source of energy for circulatory processes in the Columbia River Estuary (Sections 3.2 and 3.5). The tidal energy that drives estuarine circulation is that which enters from the ocean; the effects of the sun and moon on the estuary itself are small in comparison. Ocean tides are generally inferred from coastal and island tidal height and offshore pressure records or from global tidal models. Model results (e.g., Parke 1980, Schwiderski 1980) show that both the diurnal and semidiurnal tides become larger and later to the north along the west coast of North America, but the model results are not detailed enough to determine coastal tidal characteristics at the mouth of the Columbia River Estuary. Since available offshore pressure records are too short to adequately define the tidal characteristics, recourse must be to the US Coast and Geodetic Survey (USCGS) and NOS coastal tidal gauge observations compiled by Callaway (1971) and Hopkins (1971) for stations between Crescent City, California, and Friday Harbor, Washington. These data generally confirm the model predictions concerning the phase and amplitude variation along the coast. Most stations show some modification of the tidal wave by local bay or river effects.

Hopkins (1971) has argued that the continental shelf off Oregon and Washington is too narrow to produce significant resonance or cross-shelf variation in the tides. He has also attempted to determine the alongshore variation of tides by an empirical method based on the observations at the various coastal stations. The amplitude suggested for the mouth of the Columbia River does not agree well with observations at Jetty A, North Jetty, and other stations near the mouth. The most reliable information concerning the offshore tide is that given by the Jetty A tide gauge at about RM-3. The tidal wave entering the estuary is of the mixed diurnal and semidiurnal type, with the semidiurnal tide predominating. The mean tidal range at the mouth is 1.81 m, the greater diurnal range is 2.4 m. Tidal processes are discussed more completely in Section 3.3.

2.5 PREVIOUS STUDIES OF GEOLOGIC AND CIRCULATORY PROCESSES

Scientific observations in the Columbia River Estuary began in the 1850's with the bathymetric and tidal surveys of USCGS, now NOS. The USCGS bathymetric studies from 1852 to 1958 are summarized in the maps prepared by Northwest Cartography, Inc. (Columbia River Estuary Data

Development Program, 1983); USCGS methodology is discussed by Shalowitz (1964). Major series of tidal observations occurred in 1867-75, 1935-39, and 1958 in connection with bathymetric surveys and from 1940-42 (the most extensive set of observations). The observations are summarized in an appendix in Jay (1984).

The need to satisfy navigational requirements has been the main impetus for circulatory and sedimentological research in the Columbia River. Navigational alterations to the estuary and river by the Corps of Engineers began in the 1870s (Hickson and Rodolf 1951; Lockett 1959, 1962). The Annual Reports of the Chief of Engineers contain sporadic observations and accounts of dredging, etc., beginning in the 1870s and continuing up to ca. 1920. The most useful of these is the 1903 Report of the Board of Engineers (U.S. Army Engineers Board of Engineers 1903), prepared because the newly completed South Jetty failed to stabilize the channel. Scattered current observations were made by the Portland District prior to 1920; these are summarized in Jay (1980). Early Corps of Engineers bathymetric surveys are summarized in Jay (1980) and Columbia River Estuary Data Development Program (1983). Valuable accounts of early dredging, jetty building, Corps of Engineers field observations, navigational problems, and morphological changes accompanying estuarine alterations include: Wilkes (1846), U.S. Army Engineers, Report of Chief Engineer (1884), Bagnall (1916), Hickson (1922, 1930, 1953, 1960, 1961), Moore and Hickson (1939), Kidby and Oliver (1965), and Gibbs (1973). Hickson's discussions (1959, 1960 and 1965) are important because they explain the strategy used by the Corps of Engineers in designing channel improvements up to about 1960. This simple strategy, which originated in the late Nineteenth Century civil engineering literature (U.S. Army Engineers Board of Engineers 1903), was to narrow the cross-section at points where dredging was required, until dredging was no longer required. Salinity intrusion effects were largely ignored.

Two major circulation studies of the estuary were conducted by the Corps of Engineers in 1932 and 1959 in conjunction with channel-deepening projects. The 1932 observations were analyzed from the point of view of conservation of mass in a valuable study by Hickson and his staff (Williams 1933). With the addition of a few salinity observations in 1936 and a study of sediment transport (U.S. Army Engineers 1933), the 1932 field work was the basis of all modeling work and analyses prior to 1960.

One useful analysis based on the 1932 data was that of O'Brien (1952), who attempted to determine the relative importance of density and boundary layer effects on the vertical structure of the flow. O'Brien was also responsible for extensive modeling work in the 1930's at the U.S. Tidal Model Laboratory in Berkeley California (summarized in O'Brien 1971). The foci of the modeling work were erosion problems on Clatsop Spit and the effects of various channel configurations on shoaling and erosion in the estuary below Harrington Point. O'Brien was hindered by the lack of salinity in the model (some parts of which had a movable sand bed), but he realized that salinity intrusion was pertinent to shoaling problems and that changes in channel configuration could have far-reaching effects. He was also the first to address the problem of shoaling in Baker Bay.

Field work by the Corps of Engineers in 1959 (U.S. Army Engineers, Portland District 1960) led to another generation of studies. These studies included the flushing time calculations of Neal (1965), the salt transport, estuarine classification, and circulation theory work of Rattray and co-workers (Hansen 1965a,b; Hansen and Rattray 1965, 1966; Hughes and Rattray 1980; Hughes 1968; Robe 1968), the hindcasting of waves (National Marine Consultants, 1961a,b,c), and engineering and modeling work (e.g. Lockett 1959, 1962; Herrman 1968, 1970). Potentially valuable offshore studies by the Navy in 1954 and 1958 (U.S. Navy Hydrographic Office 1960) remained classified until they were nearly obsolete.

In addition, there exist several works that summarize one or more aspects of circulation studies of the estuary. These include Callaway (1971), Neal (1972), Jay (1978a,b), Jay and Good (1978), Jay (1980), and Hamilton (1981). Anderson et al. (1961), Barwis (1975, 1976), Corps of Engineers (1954, 1955, 1957, 1959), Grier (1941), Love (1956), and Nittrouer (1977) are bibliographies that include relevant material.

The flood of 1948 (the largest since 1894) led to work on flood hydrology (Paulsen 1949, Nelson 1949, U.S. Army Engineers 1949, U.S. Geological Survey 1964).

Atomic Energy Commission studies (AEC) initiated to determine the fate of radionuclides from the Hanford Nuclear Reservation resulted in a wide range of studies; those relevant here include Forster (1972); Lutz et al. (1975), and Nelson et al. (1966) (hydrology and circulation); Conomos and co-workers (Conomos and Gross 1972; Conomos et al. 1972; water masses, suspended sediment and nutrients); and Duxbury (1972) and Barnes et al. (1972, Columbia River Plume). Studies by Hubbell et al. (1971), Hubbell and Glenn (1973), Glenn (1973), and Stevens et al. (1973) described the presence of a turbidity maximum in the estuary and delineated patterns of sediment-size distribution and bedform distribution.

Several studies unrelated to either navigation or radionuclide accumulation have provided sedimentological information, including the early studies of the dunes of Clatsop Spit (Cooper 1959), geochemical and physical studies in Youngs Bay (Johnson and Cutshall 1975, Oregon State University Engineering Programs 1975), and studies related to the resource potential of local concentrations of heavy-mineral enriched "black sands" (Norberg 1980, Dearborn Associates 1980). Studies of mineralogy and beach sands were made by Hodge (1933), Twenhofel (1946), Ballard (1964), and White (1967). More recent studies of the mineralogy of the Columbia River sediments have been performed by Whetten (1966), Knebel et al. (1968), Whetten et al. (1969), and Kelley and Whetten (1969).

The alteration of the freshwater flow cycle by dams and the planned construction of the Trojan Plant, plans for an aluminum plant near Warrenton, and the deepening of the entrance channel during a low flow year encouraged both observations (Snyder and McConnell 1973, McConnell et al. 1979, OSU Ocean Engineering Programs 1975) and modeling of transports and the heat budget (Callaway et al. 1969, Callaway and Byram 1970).

Plans for yet another round of deepening of the navigation channels led to field work by the Corps of Engineers in 1977-78 and analyses and modeling (McAnally et al. 1980, Hamilton 1983, McAnally et al. 1983a,b). Numerous studies have been performed by and for the U.S. Army Corps of Engineers (COE) on sediment transport in the vicinity of dredge disposal areas (Sternberg et al. 1977, Borgeld et al. 1978, Walter et al. 1979, Roy et al. 1979, Roy et al. 1982). Roberson et al. (1980) examined tidal circulation and sedimentation in Baker Bay.

2.6 PREVIOUS BIOLOGICAL STUDIES

Although Haertel and Osterberg (1967) have suggested how physical and biological attributes of the Columbia River Estuary were interrelated, there has been little information available on the underlying physical (e.g., sedimentation) and ecological (e.g., flow of trophic energy through the estuarine food web) processes influencing the dynamic structure of the estuary's biotic communities. Previous studies were typically confined to a few restricted locations and generally lacked time series data. However, they did provide enough descriptive information on the distribution and relative abundance of common taxa to provide focus and definition to the more process-oriented studies described in this report.

2.6.1 Primary Producers

The distribution and coverage of estuarine marshes had been described by Good (1977) and there was additional descriptive data on the succession of emergent plants on the dredged material disposal site at Miller Sands (Clairain et al. 1978, Heilman et al. 1978). These habitat development experiments provided some of the first areal biomass production estimates (averaging 6157 kg ha^{-1}) available for natural marsh habitat in the estuary. However, information was lacking on factors limiting production and on the fate of this macrophyte production in terms of its consumption by estuarine herbivores or decomposition and conversion to detritus.

Studies by Haertel et al. (1969), Haertel (1970), and Park et al. (1972) provided the most important distributional information on water column primary production. The Haertel publications described a 16-month time series of nutrient, phytoplankton, and zooplankton studies designed to determine seasonal and spatial distribution and the interrelationships among salinity, nutrients, and plankton. The results indicated that (1) freshwater phytoplankton taxa originating from upriver dominate the estuarine flora; (2) solar radiation was a potential limiting factor of phytoplankton production; (3) the bottom water mass in the central region of the estuary is generally nutrient-enriched. Park et al.'s (1972) monthly measurements of nine water chemistry parameters in the estuary during 1966 and 1967 also expanded the understanding of long-term variability in nutrient concentrations and their relationships to phytoplankton. Knowledge of phytoplankton taxa composition, however, was limited to data from a few isolated sites in the upper estuary (Williams 1964, 1972). Conomos et al. (1972) suggested that river discharge, tidal action, and coastal upwelling controlled nutrient concentrations in the estuary. Despite

their prominence on the estuary's tidal flats, the composition, distribution, and production rates of benthic microalgae were unknown.

2.6.2 Primary Consumers

Wildlife, in terms of the aquatic or wetland mammals which are primarily grazers of the estuary's emergent plant assemblages, had generally been assessed only qualitatively. Most documentation included descriptive inventories related to estuarine habitat usage (Ives and Saltzman 1970; Maser and Storm 1970; Claire et al. 1971; U.S. Army Corps Engineers 1972, 1975, 1976; Akins and Jefferson 1973; Thompson and Snow 1974; Washington Department of Game 1975; McKern 1976; Tabor 1976 a & b). There were, however, detailed quantitative data available for specific populations such as the Columbian white-tailed deer (Odocoileus virginianus leucurus) (U.S. Fish and Wildlife Service 1977; Davison 1979 a, b; Suring and Vohs 1979) and American beaver (Castor canadensis) (Scheffer 1925).

Haertel and Osterberg's (1967) comprehensive collections at five sites through the estuary stood as the only documentation of pelagic zooplankton and their occurrence and abundance as a function of prevailing physical parameters within the estuary proper. Their samples at five stations along 23 miles of the estuary indicated three distinguishable groups of zooplankton, including (1) freshwater; (2) marine; and (3) indigenous estuarine taxa. Probably one of the most important results was the evidence for a large population of the calanoid copepod, Eurytemora hirundoides (affinis), which dominates the indigenous zooplankton in the central region of the estuary.

Haertel and Osterberg (1967) also provided the only broad distributional information on benthic infauna and epifauna throughout the estuary; euryhaline polychaetes, gammarid amphipods, bivalve molluscs, and isopods were the predominant benthic macroinvertebrates at the five sampling stations. Considerably more data existed for specific dredging and dredge disposal sites (Durkin et al. 1979 a, b; Higley and Holton 1978; Higley et al. 1976; McConnell et al. 1978; Holton and Higley 1976) or other sites of environmental concern (Higley and Holton 1979). Durkin and Emmett (1980) also provided an inventory of benthic macroinvertebrates, water quality, and sediment structure in and adjacent to the two principal embayments (Baker and Youngs Bays) of the estuary. Specific studies had also focused on the distribution, abundance, and life history of several groups of benthic amphipods (i.e., Corophium spp., Anisogammarus sp., Eogammarus sp.) which were shown to be particularly important prey of out-migrating juvenile salmon (Higley and Holton 1975, Davis and Holton 1976, Holton and Higley 1976). Due to the coarse sieving of the benthos in most studies, no data existed for benthic or epibenthic meiofauna, although Haertel and Osterberg's (1976) information on the harpacticoid copepod, Canuella (Scottolana) canadensis, indicated the potential numerical importance of this epibenthic crustacean.

2.6.3 Predators

The occurrence, distribution, and relative abundance of

macroinvertebrate predators, principally Dungeness crab (Cancer magister) and crangonid shrimp (Crangon spp.), had also been surveyed in conjunction with demersal fish investigations (Durkin 1973, 1975, 1980; Durkin et al. 1981). Haertel and Osterberg (1967) also established that relatively large populations of Crangon utilized the estuary as a nursery ground for juveniles less than one year old. Although presumed to be prominent due to the presence of a small sport and commercial fishery, systematic data on crayfish (Pacifastacus leniusculus) was meager.

Larval and post-larval fishes had received some attention, principally in Misitano's (1977) excellent description of the composition, distribution, and abundance of ichthyoplankton at seven estuarine locations during winter 1973 and monthly at one station from March through December of that year. Misitano's results indicated that the peak occurrence of ichthyoplankton was in the lower region of the estuary during January through May, with mean abundances between 1.0 and 1.5 larvae m^{-3} ; the numerically dominant taxa during this period were longfin smelt, Sprinchus thaleichtys, eulachon, Thaleichtys pacificus, and prickly sculpin, Cottus asper.

With the exception of the extensive studies of juvenile salmonids migrating through the estuary (Greene 1911; Johnson and Sims 1973; Sims 1970, 1974; Durkin and Sims 1975; Dawley et al. 1978, 1979; Durkin 1982), most of the previous research on the estuary's fish assemblages involved site-specific studies of potential environmental impacts (Durkin 1973, 1974, 1975; Higley et al. 1976; McConnell et al. 1978; Durkin and Holton 1975). Westerheim's (1955) studies of the migrations of the principal estuarine flatfish (starry flounder, Platichthys stellatus) represents one of the few examples of basic research. Again, although biased by the singular use of bottom trawl sampling gear, the studies of Haertel and Osterberg (1967) stood out as the only comprehensive examination of the composition, abundance, and ecology of the fish fauna in relation to physiochemical conditions in the estuary. Significant findings included (1) the dominance of eurhaline species (e.g., starry flounder, prickly sculpin, longfin smelt, Pacific tomcod, snake prickleback) in the estuary's demersal fish assemblage; (2) the seasonal importance of copepods, amphipods, and mysids in the diets of the dominant fishes; and (3) utilization of the estuary as a nursery ground by juvenile starry flounder less than 2 to 2.5 years old.

Predatory wildlife had been surveyed in the case of Canadian river otter (Lutra canadensis) (Tabor 1974; Towell 1974) but little was known of other important carnivores such as raccoon (Procyon lotor). Similarly, historical documentation of the occurrence, distribution, abundance, or ecology of the upper level carnivores was limited to the purely descriptive accounts of avifauna by McMahon et al. (1974), Tabor (1976b), Seaman (1977), Werschkal et al. (1977), Crawford and Edwards (1978), Woodward-Clyde Consultants (1978), and Edwards (1979) and of marine mammals by Pearson and Verts (1970), Hirose (1977), and Johnson and Jeffries (1977). Quantitative data on food habits and other ecological relationships among these important mammalian and avian predators and their prey resources was almost completely lacking.

3. CIRCULATORY PROCESSES

The circulation described in this chapter and the sedimentary processes described in Chapter 4 provide the context in which the estuarine biological processes described in Chapters 7 and 8 occur. The most important time scales or frequencies of estuarine motion are those associated with the diurnal and semidiurnal tides, with the monthly changes in tidal range and density structure, and with seasonal hydrologic and atmospheric cycles. A variety of techniques ranging from theoretical analysis to numerical modeling have been used to understand the processes occurring at each of these frequencies. Not all of this information can be used in interpreting the available geological and biological data, but information on all three time scales is needed to plan future studies, to interpret historical changes, and to evaluate navigational, hydropower and shoreline developments. Finally, the definition of circulation patterns in a highly energetic estuary with both strong tides and riverflow is of scientific interest because such estuaries have not been extensively studied in the past; some of the results achieved here should be applicable in other energetic estuaries along the West Coast and elsewhere.

For the purposes of this chapter, the system is considered to extend from the mouth (RM-0 at the end of jetties) to the upstream limit of tidal influence. The position of this upstream boundary is variable, depending on the river flow, but is normally at least as far upriver as Vancouver, Washington (approximately RM-100). Salinity intrusion, in contrast, never extends much beyond RM-30. This choice of upstream boundary includes in the study area more of the river than is considered in some later chapters, but inclusion of the fluvial part of the system is dictated by the importance of tidal-fluvial interactions to circulatory and sedimentary processes.

Chapter 3 begins with a summary of the relevant physical oceanographic background. The material discussed includes the relationship between the tidal flow, the mean flow and the salinity distribution (Section 3.1.1 and 3.1.2), the factors influencing the residual (or mean) flow (Section 3.1.3), and the interaction between the density structure and vertical mixing. This material is essential to the understanding of circulatory processes and the relationship of sedimentary and biological processes to the circulation. It is not summarized in a concise and simple manner in any standard reference. The modes of circulation defined in Section 3.1.1 are used as a unifying framework for the discussion of the analytical and modeling results which follows.

The data base used for the analyses is discussed in Section 3.2, the tidal circulation in Section 3.3, tidal-fluvial interactions in Section 3.4 and the energy budget for the system in Section 3.5. Discussion of the spatial distribution of the dissipation of tidal and fluvial energy (Sections 3.4 and 3.5) sets the stage for the analysis of sedimentary processes (Chapters 4 and 5). The dependence of the vertical structure of both the tidal and the mean flows on the density

structure motivates an analysis of seasonal and tidal monthly changes in density structure and mean flow (Section 3.6) and a discussion of salt transport mechanisms (Section 3.7). Information on the peripheral bays is included in Section 3.8. Section 3.9 summarizes the results of Chapter 3.

The high energy level, short flushing time, and extreme variability of salinity intrusion strongly constrain biological processes in the Columbia River Estuary (Chapters 7 and 9). It is primarily on time scales longer than a few days that this influence of physical processes over biological processes is exercised (Lewis and Platt 1982). Thus, the discussions concerning the residual flow (Sections 3.1.3 and 3.3.5) and the density structure (Section 3.6) are particularly pertinent for readers of Chapters 7 and 8. The tidal monthly changes in mixing and density structure that determine the accumulation and cycling of detritus (Sections 4.4 and 5.4) also cause tidal monthly changes in biological processes. Although these tidal monthly biological changes cannot be completely defined with a biological data set designed primarily to determine seasonal patterns, their existence emphasizes the linkage of biological and physical processes (Chapters 7 and 9).

3.1 THE RELATIONSHIP BETWEEN TIDAL FLOW, MEAN FLOW, AND THE SALINITY DISTRIBUTION

The dominant factors in the circulation of the Columbia River Estuary are the high energy level, the strong horizontal salinity gradient, the high temporal variability provided by the strong tides and large riverflow, and the complex topography that consists of narrow (0.5 to 3 kilometer (km)), well-defined channels separated by broad sand banks (Figure 3.1). The resulting flow varies in all three spatial dimensions, is strongly influenced by friction and stratification, and is moderately influenced by the various non-linear tidal processes defined in Sections 3.1.1 and 3.1.3.

Despite the breadth of the lower estuary (5 to 12 km; Figure 3.1), most of the flow is confined to channels. Processes occurring on tidal flats are essential to biological and sedimentological processes, but circulatory studies and modeling have concentrated on the channels, where most of the flow is conveyed. Concentration of the flow in the channels allows the vital simplification that the flow at many locations is nearly two-dimensional in depth and along-channel distance. Use of this pragmatic assumption has permitted a detailed examination of the tidal-fluvial interactions and density effects that largely control circulation. A separate, vertically-averaged model with uniform density has been used to investigate flow outside the main channels and to demonstrate the adequacy of the assumption of two-dimensionality (Section 5.3 and Hamilton 1984).

3.1.1 Modes of Circulation

The ultimate aim of most physical oceanographic investigations is to explain the observed phenomena in terms of the governing hydrodynamic principles expressed in the equations of motion (conservation of momentum), continuity (conservation of mass), and salinity distribution or

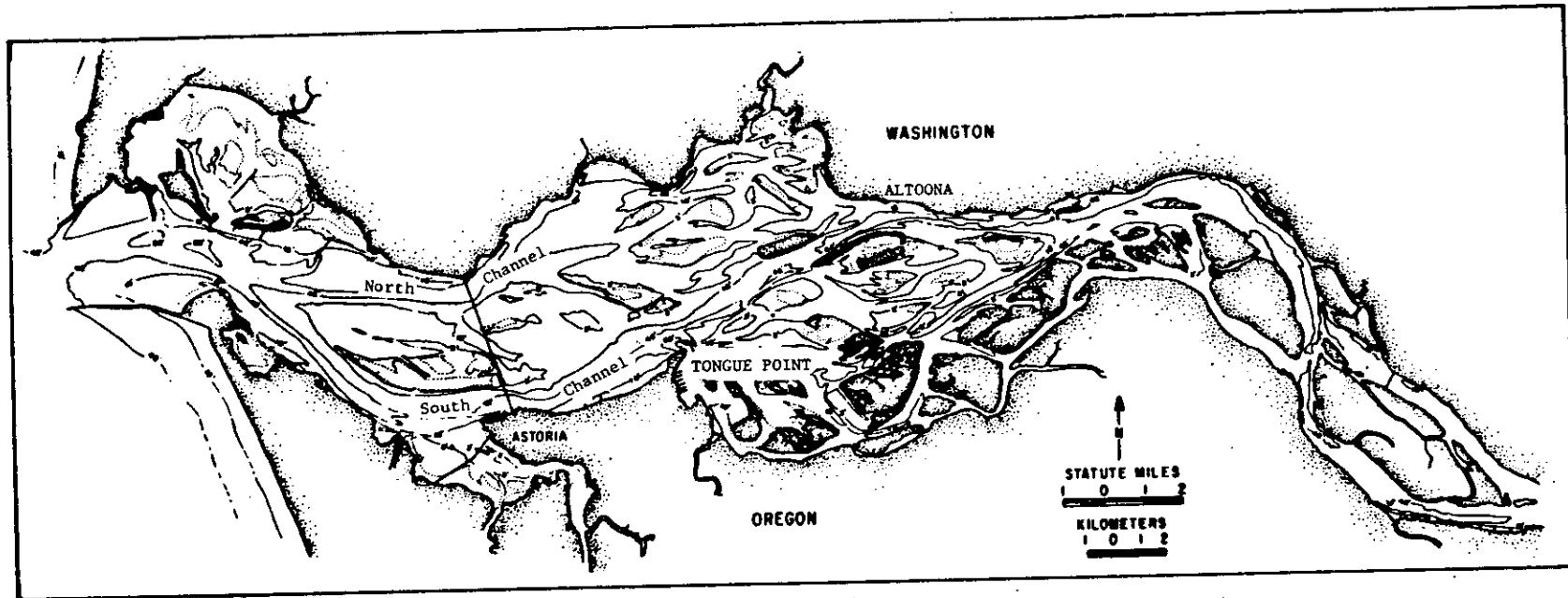


Figure 3.1. Columbia River Estuary bathymetry. Narrow channels are separated by broad sand bars. The principal channels seaward of Tongue Pt. are the north channel, along the north shore, and the south channel, off Astoria.-

salt continuity (conservation of salt). The most direct procedure is to solve these equations with the applicable boundary conditions and parameters. For a shallow, partially-mixed system with strong tidal forcing and complex topography, no analytical solutions are known, and numerical solution by a full three-dimensional model would be prohibitively expensive.

The domination of the circulation by processes occurring at tidal daily, tidal monthly, and seasonal frequencies (Section 3.3) and the importance of interactions between the processes occurring at these frequencies suggests another approach to analyzing the circulation. This theoretical method is called a scaling analysis and perturbation expansion. This approach is often used by oceanographers faced with complex non-linear phenomena for which no exact mathematical solutions are available. It uses the assumption of two-dimensionality and the frequency separation of different aspects the circulation to greatly simplify the governing equations. It also clearly shows the origins of the interactions between the processes occurring at the different frequencies. The method is used here, not to produce solutions, but to determine the importance of fluvial forcing, tidal forcing, etc., and to define modes of circulation. These circulation modes are used to interpret the observed flow and salinity distributions.

It is necessary here to explain the idea of the non-linearity of a process, because much of the complexity and richness of estuarine circulation, geology, and biology results from the non-linearity of important processes. A process is non-linear if any term in the differential equation(s) describing that process is non-linear in the unknown function, $f(x,z)$, where $f(x,z)$ is the velocity distribution, the population density of an organism, or some other quantity of interest. Terms such as $f(x,z)$, $\partial f/\partial x$, and $\partial^2 f/\partial x^2$ are all linear in the unknown function, but

$$f^2(x,z), f \frac{\partial f}{\partial x}, \frac{\partial f}{\partial x}, e^{-f(x,z)}, \text{ etc.,}$$

are all non-linear. Non-linear processes may exhibit complex interactions, transitions and non-proportional responses, not possible in linear systems. Of particular importance in this estuary is the non-linear transfer of tidal energy to both higher and lower frequencies.

The perturbation expansion is based on a parameter that has an important physical meaning. The perturbation parameter used in this work is that suggested by Ianniello (1977a,b); it is h/H , the ratio of tidal range (h) to mean depth (H). Large values of h/H (approaching one) occur in systems where non-linear processes associated with the tides are important and the tidal energy level is high. The value of h/H in the Columbia River Estuary is between about 0.05 and about 0.2. The estuary is therefore moderately non-linear in this respect. In contrast, Chesapeake Bay is weakly non-linear with respect to the tides because it is deeper, and the estuaries of the Atlantic Coast of France are strongly non-linear because they are shallower and have larger

tidal ranges (Allen et al. 1980).

The Tidal Circulation

The most important circulation mode in the estuary is the tidal flow, which occurs at diurnal and semidiurnal frequencies. The equation of motion is: acceleration of the tidal flow is balanced by bed friction (and the associated downward transfer of momentum in the flow), and the pressure gradient. The pressure gradient consists of two parts, which are called barotropic and baroclinic; they may be of equal magnitude. The barotropic part of the pressure gradient is that part caused by the surface slope; it is independent of depth. The baroclinic pressure gradient at any depth contains an integral from the surface to that depth of the horizontal salinity gradient $\partial S/\partial x$. This term in the equation of motion becomes more important near the bottom, in the part of the estuary where salinity is found. The sign of the total pressure gradient (barotropic plus baroclinic) may change with depth when the horizontal salinity gradient is large and opposes the surface slope. The tidal circulation is the most important circulation mode and dominates the energy balance for the estuary.

The interdependence of the circulation, stratification, and vertical mixing processes that is expressed in the vertical momentum transfer or friction term in the equation of motion is fundamental to the problem of estuarine circulation. Fluids have a very strong tendency to move, under the influence of gravity, along level surfaces. Vertical turbulent mixing and other processes such as breaking internal waves transfer both momentum and salt between layers. The loss of momentum to the sea bed (bottom friction) affects the flow higher in the water column as turbulence diffuses momentum toward the bed. Salinity stratification severely inhibits this vertical transfer (Section 3.1.4). Furthermore, tidal currents are the primary agent of up-estuary salt transport. That the circulation and salinity distribution are linked in this complex manner and that this interaction plays a major role in the primary tidal circulation means that no simple model can explain the behavior of the system.

The Secondary Circulation

The secondary circulation can be divided into three modes that occur at different frequencies, and that are (at least in part) driven by the primary tidal flow. These are: the secondary tidal circulation, which occurs at the same frequencies as the primary tidal circulation, the tidal higher harmonics or overtones (at frequencies which are multiples, sums, and differences of the basic tidal frequencies), and the nearly-steady residual circulation. The secondary tidal circulation modifies the primary tidal circulation and salinity distributions. The tidal higher harmonics are the result of friction and distortion in the tidal wave in shallow water (Section 3.1.3); this distortion transfers energy from tidal frequencies to higher frequencies.

The residual or mean circulation in the Columbia River Estuary is influenced primarily by the tides (with variations on tidal monthly time scales), the river flow (with variations on scales from a few days

to seasonal), and the density distribution (which varies with the tides, river inflow, and changes in salinity at the mouth). Atmospheric processes (which vary on time scales from a few days to seasons) are relatively unimportant in this estuary. They are much more important in larger, less energetic systems.

3.1.2 The Salinity Distribution

Perhaps the best place to begin in understanding the salinity distribution and salt transport is to consider how salt can be maintained in the estuary in the presence of a substantial outward transport of salt by the mean flow. The salt transport calculations presented in Section 3.7 show that salt is brought into the estuary primarily by the primary tidal circulation acting on the salinity gradient and secondarily by inward net flow near the bottom. Inward transport by the Stokes drift (associated with the tidal residual circulation; Section 3.1.3) is important near the entrance.

The salinity distribution and the circulation modes defined in Section 3.1.1 are linked to each other in a complex feedback system. To analyze this interaction, primary and secondary salinity distribution modes have been defined by application of the same perturbation expansion as used in Section 3.1.1. The resulting primary salinity distribution is: time change in salinity is balanced by advection of the salinity pattern by the primary tidal currents (including the baroclinic part of these currents), and vertical mixing and transfer of salt. Thus, the primary tidal circulation is, in the present analysis, the only circulation mode involved directly in determining the primary salinity distribution. Neither the residual circulation nor any form of vertical advection (entrainment) appear in the primary salt balance.

The secondary salinity distribution mode has also been defined, because the time-averaged horizontal salinity gradient and the vertical advection of salt are both secondary features; they are not accounted for by the primary circulation. The traditional picture of this problem is that the time-averaged salinity distribution maintains and is maintained by the density-driven part of the residual flow, as explained in Section 3.1.3. The perturbation expansion shows that the residual circulation does not control either the primary or secondary parts of the salinity distribution, because it is too small a feature to do so. This does not mean that the interaction between the flow and the density structure is unimportant, because the tidal flow, which controls the salinity distribution, is strongly influenced by the salinity distribution.

3.1.3 Residual Flow Processes

The term "residual flow" includes all of the processes that occur in the estuary at frequencies lower than the tidal daily oscillations. These processes include the classical, two-layer gravitational circulation of Hansen and Rattray (1965), in which a density-driven, inward flow of sea water along the bottom is coupled with a net outflow of river water at the surface, the tidal residual circulation (a non-linear tidal process important in shallow estuaries), and the

atmospherically driven residual (driven by winds over the estuary and wind and pressure-induced changes in coastal sea level). In addition to its physical oceanographic interest, the residual flow is important because the biological changes that take place in estuaries on time scales longer than a few days are often governed by the residual flow (Lewis and Platt 1982).

The classical, two-layer flow is probably the most familiar aspect of estuarine circulation to many readers. For many purposes it is a useful simplification to consider the response of this two-layer circulation or the tidal residual individually (as is done in the rest of this section), and to think of the time-averaged properties of the system as responding directly to low frequency forcing. However, the perturbation expansion shows that system response to low frequency external forcing (e.g., to a change in riverflow) does not occur directly through the residual flow or any part thereof. The response occurs through complex adjustments to the tidal circulation and salinity distribution, which then alter the residual flow as a whole. Thus, while it may be convenient to separate part or all of the residual flow from the tidal circulation, this simplification is not always applicable, because of the connections between the flow modes. This qualification also applies to ecological investigations.

Tidal Influence on the Residual Circulation

The tidally-driven part of the residual circulation is the result of the transfer of energy from the primary semidiurnal and diurnal tidal circulation to lower frequencies and of differences in the intensity of vertical mixing processes during the tidal month. The tidal residual resulting from the presence of a single tidal constituent (e.g., the lunar semidiurnal constituent (M2); Section 3.3) would be steady and would arise as follows. Consider a tidal wave entering one end of an idealized, narrow, shallow channel of simple form and infinite length, without riverflow or variations in water density. Even though the ebb and flood tidal currents at any level of the flow in this channel are equal, the upstream transport of water by the flood exceeds the downstream transport on ebb because the depth of the flood current is greater than that of the ebb current. This occurs because peak flood occurs near the time of high water and peak ebb near the time of low water. That is, the tidal height (h) and the current (U) are correlated and the product Uh has a positive time average over a tidal cycle ($[Uh]$ is greater than 1, where the brackets $[\]$ indicate time-average) that corresponds to a steady shoreward transport. This product is called the Stokes drift (Longuet-Higgins 1969). (In a wide channel, the expression for the Stokes drift is more complicated than this.)

The correlation of a tidal height and current has still another effect: distortion of the tidal wave, which produces the tidal harmonics. The peak of the tidal wave is in deeper water than the trough of the tidal wave. Since the propagation speed of the wave in shallow water is $(gd)^{1/2}$ where g is the gravitational acceleration and d is the water depth, the peak of the wave propagates more rapidly than the trough, distorting the wave. This distortion causes the tide (as

observed at any tide gauge) to rise rapidly and fall slowly, with strong, brief floods, and long, weak ebbs. Mathematically, this corresponds to reducing the M2 amplitude and adding overtones (e.g., M4 and M6), that occur at multiples of the basic M2 frequency.

There is a close connection between the net energy transported into an estuary by the tide and the Stokes drift (Section 3.5). In a shallow system like the Columbia River Estuary, much of the energy of the incoming tidal wave is lost to bottom friction. The outgoing (reflected) tidal wave is smaller and carries less energy out of the estuary. The tide is partially progressive, and the Stokes drift, which is proportional to the energy flux, is significant. In contrast, in a system with little friction, the incoming and reflected tidal waves will be of similar amplitude (a standing wave tide). In such a system high tide will occur at slack water, U and h will be weakly correlated, and there will be little Stokes drift and little net tidal energy flux into the estuary.

The Stokes drift is a property of the vertically integrated flow, in the sense that a current meter at any point in the flow in the above, idealized channel measures only the perfectly reversing tidal currents. Nonetheless, a particle in the fluid will be transported inward as it is moved back and forth by the tidal currents because of the greater channel cross-section on flood tide and frictional non-linearities of the flow. This is a case in which the Lagrangian motion (that following a particle) is different from the Eulerian motion (that observed at a fixed point in the flow field). Even though the Stokes drift itself is not directly measurable with a current meter, its consequences are. The shoreward transport of water by the Stokes drift in a real channel of finite length causes a surface slope sufficient to drive a steady return flow that carries an identical amount of water seaward. This Stokes drift compensation current (as measured by current meters) may, during low flow periods, be a substantial fraction of the total discharge (riverflow plus Stokes drift compensation flow; Section 3.4), and is distributed differently in the vertical than the Stokes drift itself. Thus, while the effect of the Stokes drift for the water column as a whole is compensated by the Stokes drift return flow, the net effect at any given level may be substantial (Ianniello 1977a,b, 1979, 1981).

A second major feature of the tidal residual circulation is its variation with tidal range during the tidal month. Jay (1984) has demonstrated that the changes in the barotropic part of the residual flow (those fluctuations associated with changes in surface slope) are dominated by changes in tidal range and riverflow. Changes in tidal range are the dominant factor downstream of Tongue Point (RM-19), changes in riverflow are the dominant factor upriver of Wauna (RM-43), and the two are about equally important between Wauna and Tongue Point. Atmospheric fluctuations do not play a major role in determining residual flows anywhere in the system, although these fluctuations may have a substantial effect on the water level.

With regard to tidal monthly variations, the strength of the tidal currents varies linearly with tidal range. The Stokes drift ($[U_h]$)

therefore varies with the square of the tidal range, and both the Stokes drift and the return flow it drives have the same 15 and 28 day (approximately) periodicities as the tidal range. Perhaps more important than the variation in Stokes drift during the tidal month is the variation in time-averaged surface slope. There are several reasons for this variation. One is the change in the Stokes drift compensation current; a larger Stokes drift on a spring tide requires a larger slope to drive a larger compensation current. Another is that the dissipation (frictional loss of tidal energy) varies as the cube of the tidal range and is greatly enhanced on spring tides. Vertical mixing is therefore also greatly increased on spring tides. The greater vertical mixing and resulting lesser stratification enhance vertical momentum transfer in the water column; a greater part of the total depth of the flow is affected by bottom friction. Because of the enhanced friction, a greater surface slope is needed to drive the same flow seaward. Thus, river slope increases on a spring tide, not only because Stokes drift compensation current increases, but also because of enhanced friction.

Riverflow and Density Effects on Residual Circulation

The riverflow enters the system from the upriver end of the estuary and increases the surface slope of the system so that flow may be transmitted through the estuary. Increased riverflow affects the stratification, mixing, friction, and the salinity distribution in a complex way. Fluvial effects greatly increase in the upriver direction, because the ratio of riverflow to tidal transport increases upriver. The tidal-fluvial interaction is examined in detail in Section 3.4. The seasonal cycle of riverflow is discussed in Section 2.2.

Most previous works on estuarine circulation have assumed that the density-driven part of the residual flow and the riverflow were the primary factors maintaining the salinity distribution. Theory (Section 3.1.2) and observations (Sections 3.7) show that tidal processes dominate in the Columbia River Estuary. Nonetheless, available theoretical studies of gravitational circulation yield important insights. The primary treatments of steady, density-driven estuarine flow are those of Hansen and Rattray (1965), Officer (1976) and Hamilton and Rattray (1978). The starting point for Hansen and Rattray (1965) theory is the division of the estuary into three regimes (Figure 3.2a). In the central regime of many estuaries the horizontal salinity gradient is nearly constant in time and space, as in Figure 3.2a. It is possible to use conservation of momentum, mass, and salt to obtain time-averaged salinity and horizontal velocity as a function of depth. Since the horizontal salinity gradient is assumed to be constant, the solutions have the same form throughout the central regime.

The Hansen and Rattray (1965) theory predicts a density-driven circulation that is increasingly inward toward the bottom. This is caused by the baroclinic pressure gradient (i.e., the salinity distribution). When this gravitational circulation is combined with a steady, outward riverflow of similar magnitude, the result is surface outflow and bottom inflow. This is the classical view of estuarine circulation. The time-averaged salinity gradient in the Columbia River Estuary (Figure 3.2b) is, however, spatially variable and sometimes

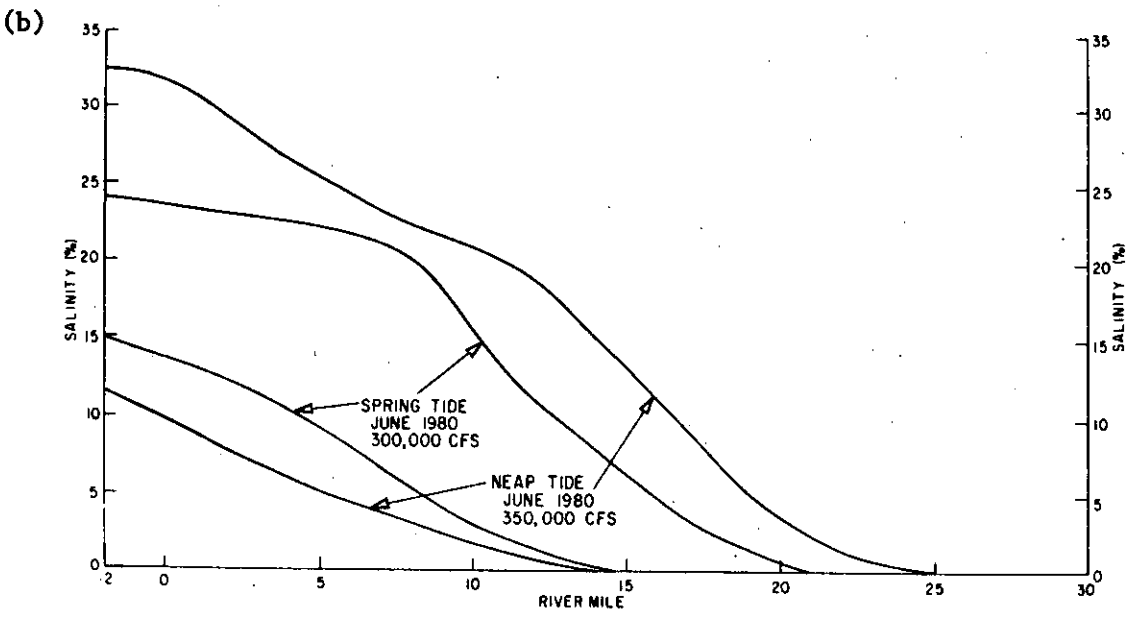
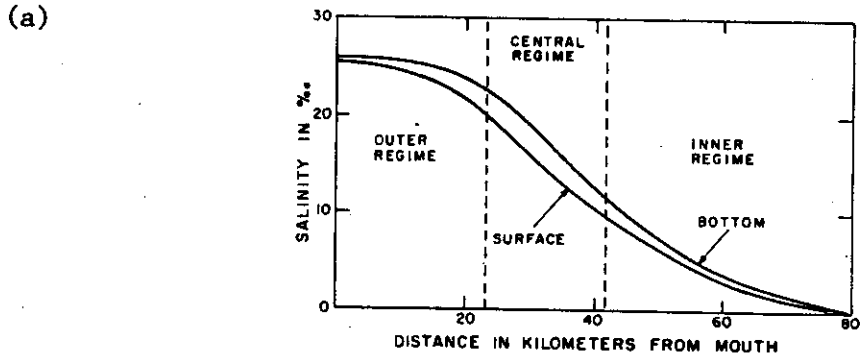


Figure 3.2. Tidal cycle average surface and bottom salinity in (a) a typical East Coast estuary (from Hamilton and Rattray, 1978), and (b) for spring and neap tide and moderate river flow in the Columbia River Estuary. The horizontal salinity gradient is much stronger and more variable in the Columbia River Estuary.

looks quite different from that in Figure 3.2a. Furthermore, the salinity gradient varies greatly during the daily tidal cycle and during the tidal month, and upstream bottom flow is totally absent in some reaches because of topographic effects (Section 3.3 and Hamilton 1984). It is in large part because of these complications that the perturbation expansion approach has been used in this section. This approach considers all major parts of the residual flow, and the connections between the residual flow and the tidal circulation are clarified.

Atmospheric Influence on Residual Circulation

It has been shown by means of a statistical analysis of sea level, surface slope, wind, and atmospheric pressure data that atmospheric fluctuations play a relatively minor role in governing the barotropic part of the residual circulation (Jay 1984). Preliminary statistical calculations based on velocity and salinity time series data suggest that the same conclusion also applies to the baroclinic (i.e. internal) circulation. These conclusions distinguish the Columbia River Estuary from larger, less energetic systems, where atmospheric effects on the estuary and over the continental shelf dominate the residual flow, e.g., Chesapeake Bay (Elliot and Wang 1978).

3.1.4 Vertical Mixing, Stratification, and Circulation

Vertical mixing plays an essential role in both the tidal circulation and the salinity distribution. It is important to know both the dependence of vertical turbulent mixing on stratification and under what circumstances other processes may be responsible for vertical momentum exchange. Dyer (1973) distinguishes between situations in which the vertical salt balance is satisfied primarily by vertical mixing and vertical tidal salt transport and those in which it is satisfied by entrainment. Entrainment occurs when a turbulent fluid flows over a relatively less turbulent layer; net vertical movements of momentum, water, and salt occur as the upper layer erodes the lower. In contrast, vertical mixing and vertical tidal salt transport transfer momentum and salt without a net movement of water.

There is a connection between the horizontal and vertical salt transport in an estuary. Conservation of mass requires that a strong, density-driven residual circulation be accompanied by significant entrainment. Water enters the estuary along the bottom (because of the baroclinic pressure gradient), is entrained into the surface layer, and is carried out of the estuary, diluted by river runoff. There will be substantial horizontal and vertical advective salt transports, both driven by the mean circulation.

The theoretical analysis of Section 3.1.2 suggests that both horizontal and vertical salt transport in the Columbia River Estuary should be dominated by tidal processes rather than the mean flow processes. Observations and model results (Sections 3.3 and 3.6) show that upstream net bottom flow is not continuous over the entire salinity intrusion length of the estuary and that tidal mechanisms dominate inward horizontal salt transport. This strongly suggests that vertical tidal salt transport and vertical mixing processes, rather than

entrainment, dominate the vertical salt transport in the Columbia River Estuary.

A further distinction can be made between the turbulent, bottom boundary layer dynamics that govern partially- to well-mixed locations in the flow and the more complex pycnocline processes that govern salt transfer in highly stratified situations (Gardner et al. 1980). In the first case, energy for turbulent mixing arises primarily from the frictional interaction of the flow with the bottom. The bottom layer of such a flow is turbulent and vertical mixing outweighs entrainment. This corresponds to maintenance of the horizontal salt balance by primarily tidal mechanisms. Vertical salt fluxes can occur both with and without net vertical movement of water at the pycnocline of a shallow, highly stratified flow. At this level of the flow, turbulence is suppressed to such a degree that it is not the principal agent of vertical salt transport. The processes bringing about vertical salt transport under these conditions are episodic, diverse, and poorly understood (Gardner et al. 1980).

The criterion for the suppression of vertical turbulent mixing by stratification (Phillips 1980) is that the energy lost by the turbulence to the mixing the stratified fluid (known as the buoyancy flux) must exceed the turbulent energy production. Where this occurs, the turbulence loses energy faster than it gains energy. In the absence of diffusion of turbulent energy from some other part of the flow, the flow ceases to be turbulent.

It is generally impossible in synoptic oceanographic studies to measure the properties of turbulence; they must be calculated from the the measurable, mean properties of the flow. The production of turbulent energy is represented in terms of the square of mean shear $((\partial u/\partial z)^2)$ times a proportionality constant. The buoyancy flux is represented in terms of the vertical salinity (density) gradient as $(g/\rho)(\partial\rho/\partial z)$. The condition for the cessation of turbulence can then be written in terms of the gradient Richardson number, which contains only measurable quantities (the mean velocity and density gradients):

$$Ri = \frac{\frac{g}{\rho} \frac{\partial\rho}{\partial z}}{\left(\frac{\partial u}{\partial z}\right)^2} > 0.25$$

The difficulty with a system such as the Columbia River Estuary is the variability of stratification and mixing processes; processes as diverse as vertical turbulent mixing and the breaking of internal waves are responsible for vertical momentum and salt transfer. It can be deduced from the profile data that the more complex interfacial processes associated with highly stratified systems occur under certain conditions in the Columbia River Estuary. The necessary data are not available to quantitatively describe such processes or to definitely state how important they are, on the average, to the dynamics of the system, because the profile data from the high flow season is very limited.

3.2 DATA COLLECTION

The 1980 CREDDP field program has been described in detail in an earlier report (Webster and Juhasz 1980). The field program consisted of a continuous monitoring program (March to November 1980) and two intensive cruises (during high riverflow in June 1980, and low riverflow in October 1980). The cruise periods and riverflow for the 1979-81 period are shown in Figure 2.9. The purpose of the continuous program was to assess seasonal and tidal monthly variability at important locations. The intensive cruises were designed to provide detailed information over half a tidal month under high and low flow conditions. Station locations are shown in Figures 3.3a,b and 3.4a,b.

The continuous monitoring program consisted of repeated deployments of five Aanderaa current meters on the Astoria-Megler Bridge (two in the north and three in the south channel). The Aanderaa current meters were equipped with conductivity, temperature, pressure (or in some cases, transmissivity), speed, and direction sensors. Tidal height data (Figure 3.3a) were available at Tongue Point (RM-18), Jetty A (RM-3), Wauna (RM-42), and Columbia City (RM-83). Each of the two intensive cruises consisted of two-week deployments of 17 Aanderaa current meters, 30-day deployments of seven Aanderaa pressure gauges, and a 15- to 30-day deployment of an Aanderaa anemometer. Extensive profiling was carried out during the October cruise with two velocity-conductivity-temperature-depth (VCTD) profilers. Because of the extensive current meter and profile data available, the CREDDP data for October 1980 constitute the best available data set for a low flow period.

The National Ocean Service (NOS) staged an extensive field program in the estuary in 1981 (Townsend and Hull 1981); their sampling stations are shown in Figures 3.5a,b and 3.6). These data provide, for some time periods, far more extensive time series data than were available through CREDDP. Moreover, the spring freshet in 1981 was the largest in the 1975-1982 period. Some CTD profile data are available, but no velocity profiles were collected. The NOS data provide the best realization of high flow conditions.

3.3 TIDAL PROCESSES

The tidal wave entering the mouth of the estuary and the potential energy of the riverflow are the major sources of energy for circulatory processes in the estuary and river; the tides are the major source of energy for the estuary below about RM-20. The strength of the tidal forcing and the well-defined frequencies involved can be seen in the power spectrum of tidal heights at Tongue Point (RM-18; Figure 3.4a). The largest peaks in Figure 3.4a are the semidiurnal (twice-daily) and diurnal (daily) tidal peaks which make up the primary tidal circulation. Numerous different effects, each represented in a harmonic analysis by a tidal constituent and each having a different frequency and magnitude, contribute to both of these peaks; the principal tidal constituents are identified in Section 3.3.1. The evenly spaced peaks to the right (at higher frequencies) are the tidal overtones that are generated by the interactions of the incoming diurnal and semidiurnal waves with the

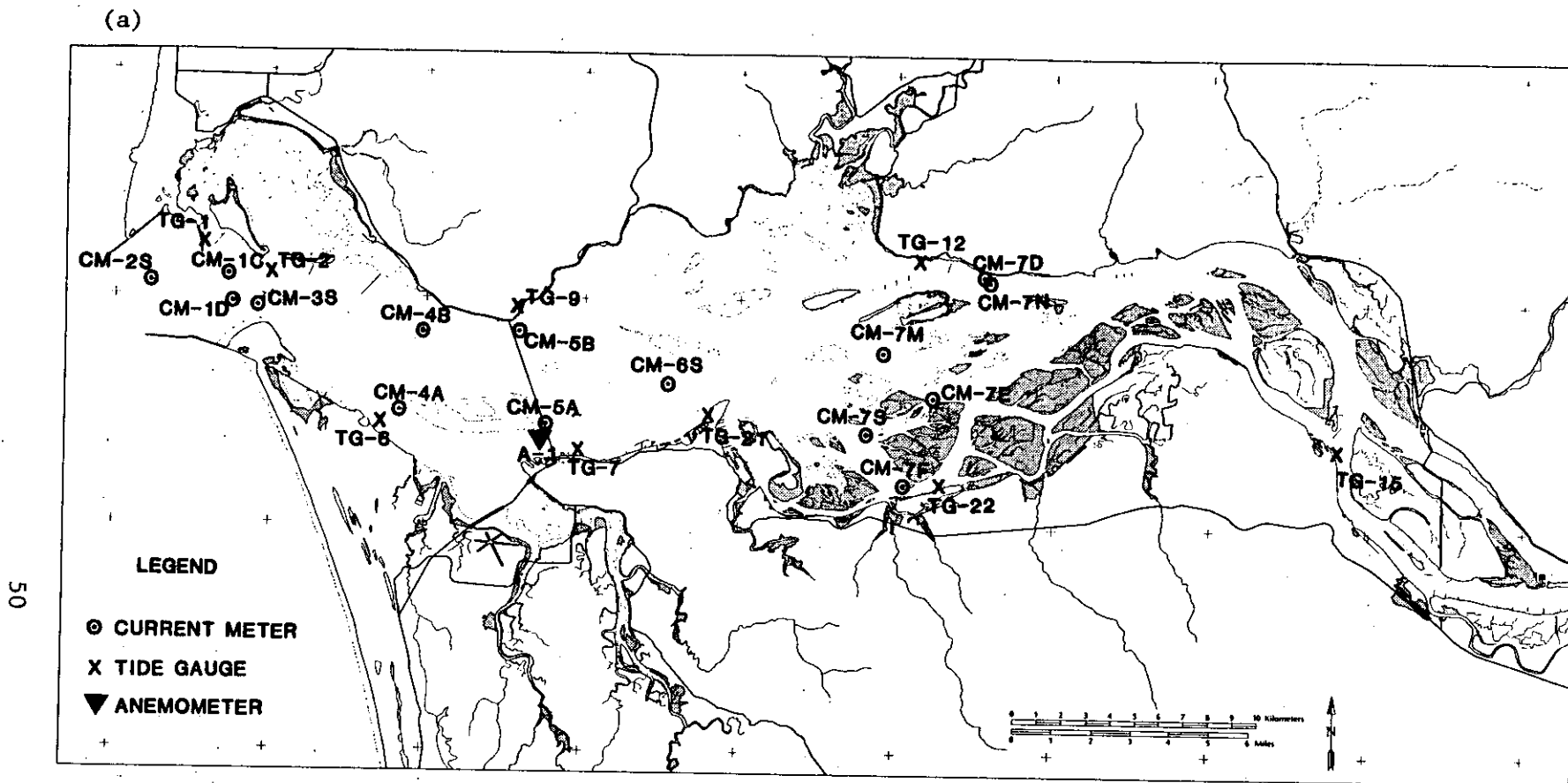
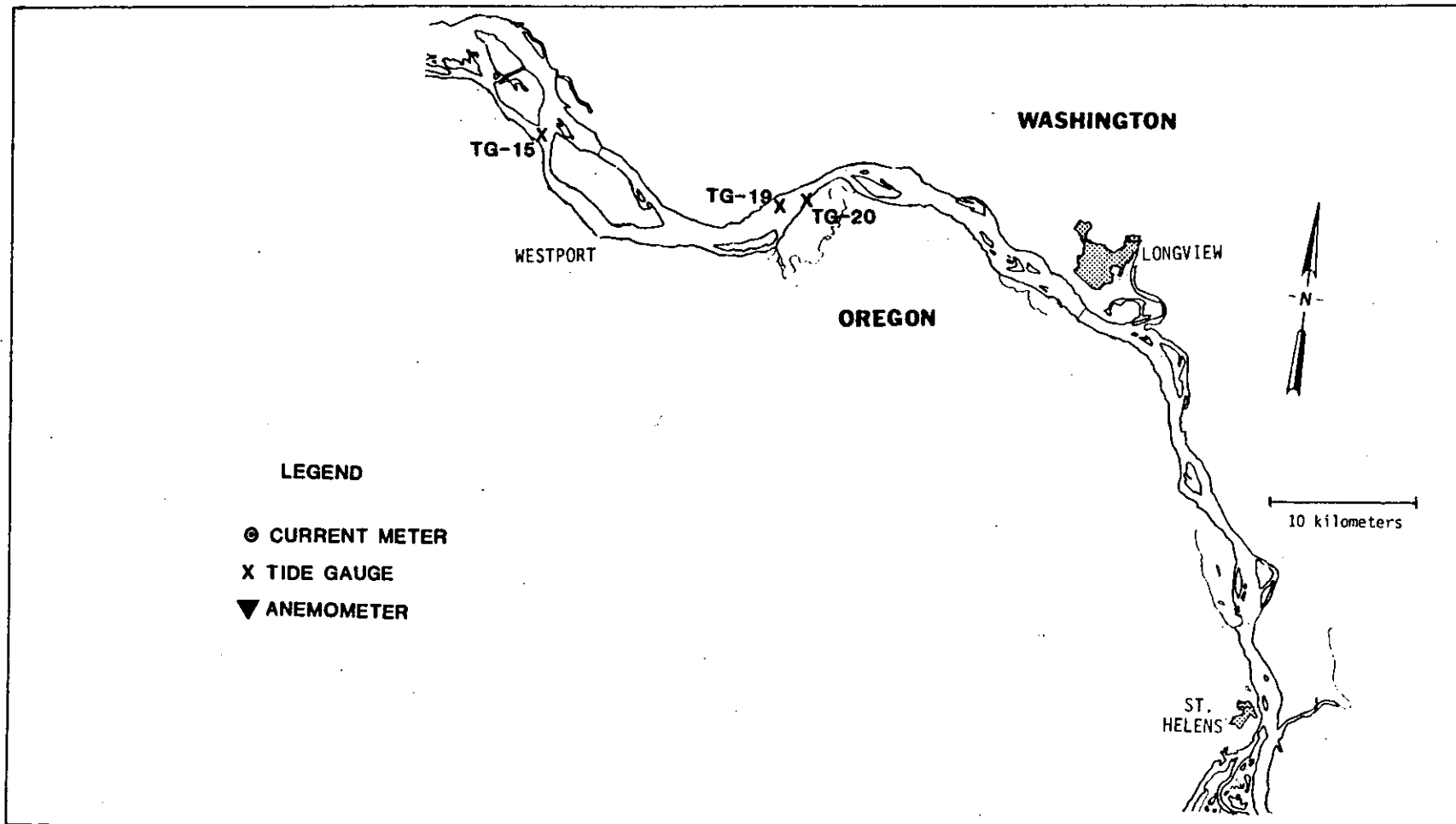


Figure 3.3. CREDDP 1980 sampling stations, (a) mouth to RM-47, and (b) above RM-47. Stations CM-5A, CM-5B, TG-1, TG-21, TG-19 and TG-20 were included in the continuous monitoring program. These and all other stations were used in one or both intensive cruises. Two additional tide gauge stations, TG-21 (NOS) and TG-1 (Geological Survey), are also shown.

(b)



51

Figure 3.3 (continued).

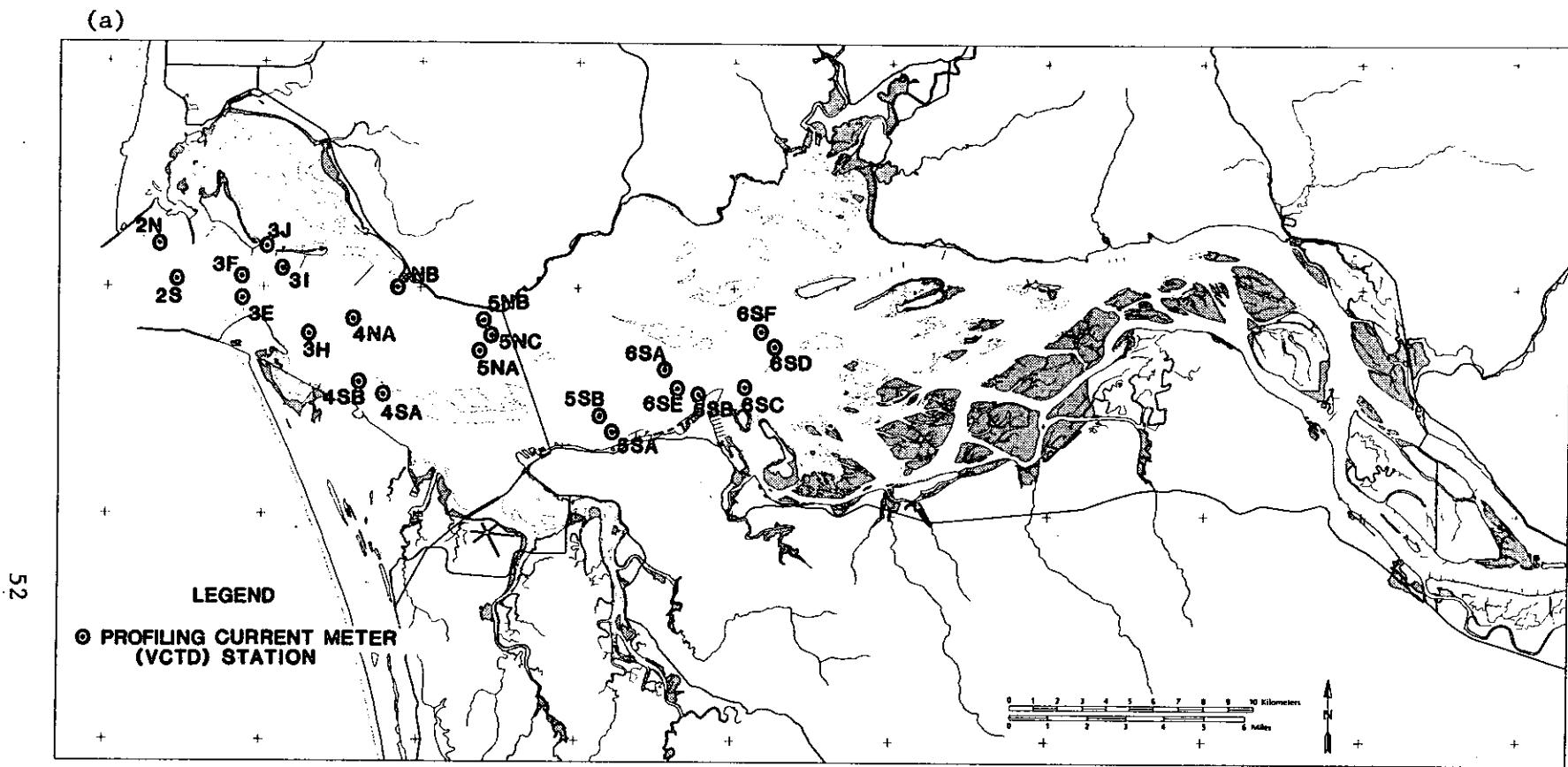
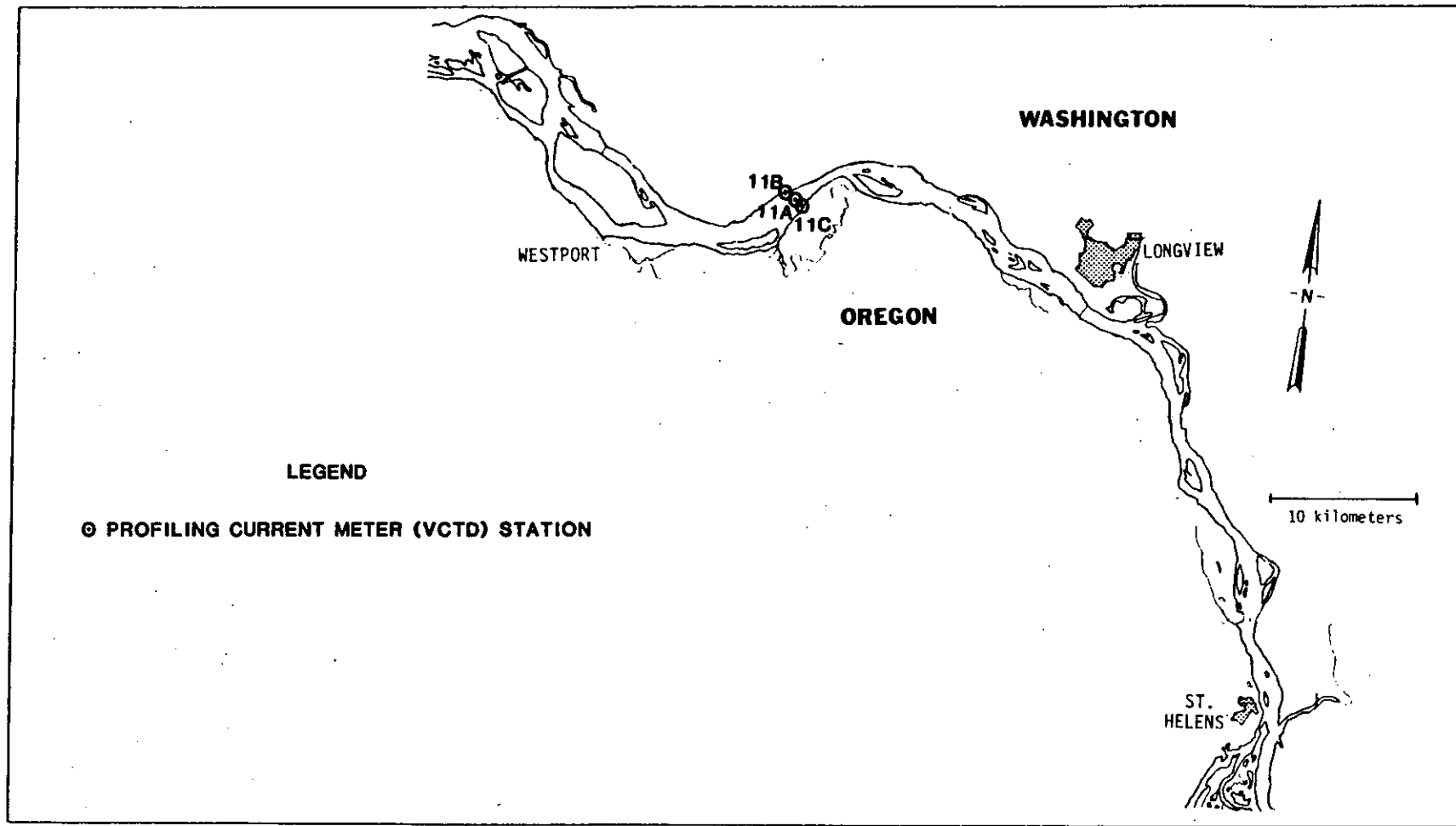


Figure 3.4. CREDDP October 1980 VCTD profile stations, (a) mouth to RM-47, and (b) above RM-47.

(b)



53

Figure 3.4 (continued).

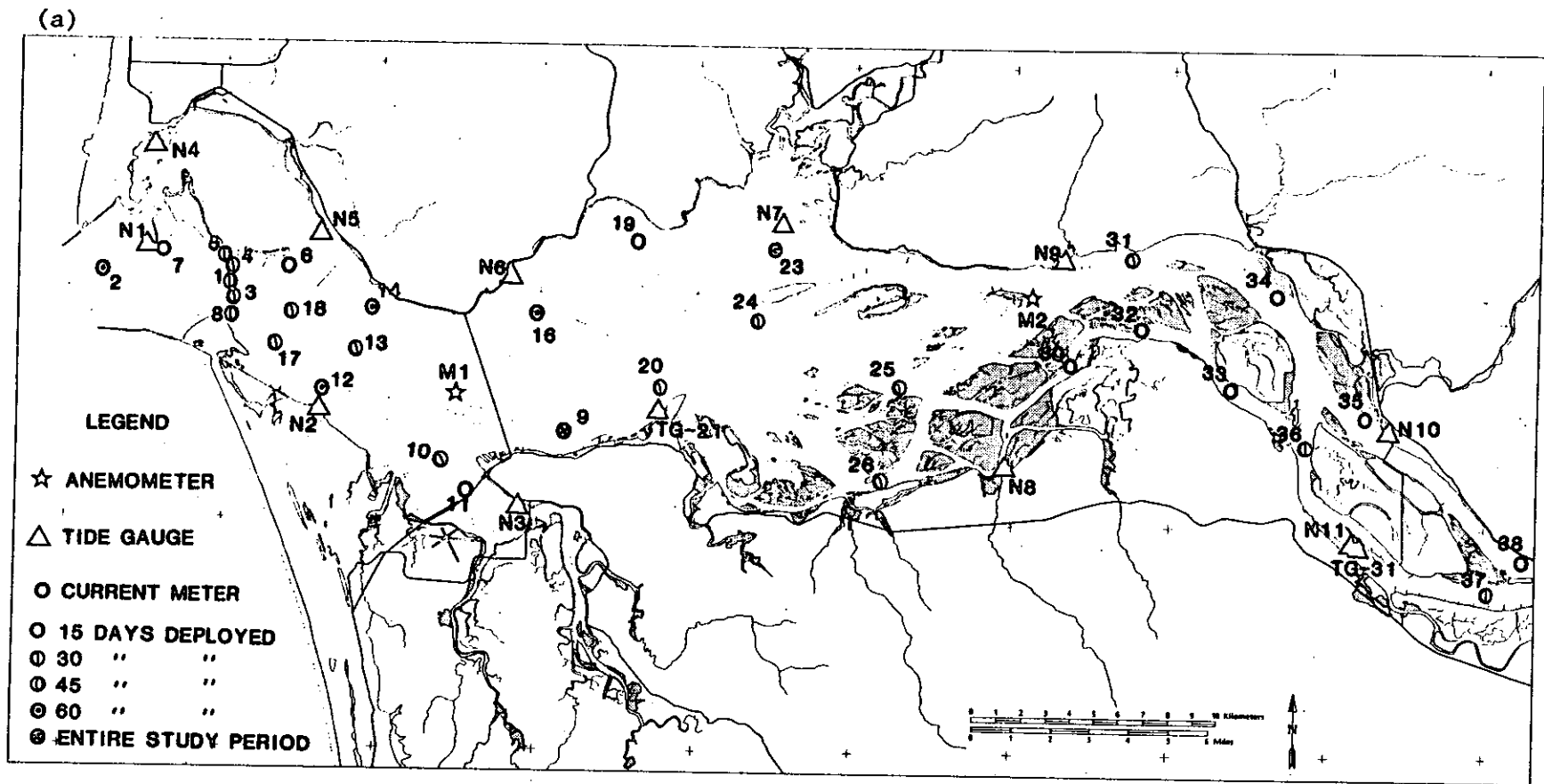


Figure 3.5. NOS 1981 current meter, tide and anemometer stations (a) mouth to RM-47, and (b) upriver of RM-47. Two additional Geological Survey tide gauge stations are shown, TG-31 and TG-41.

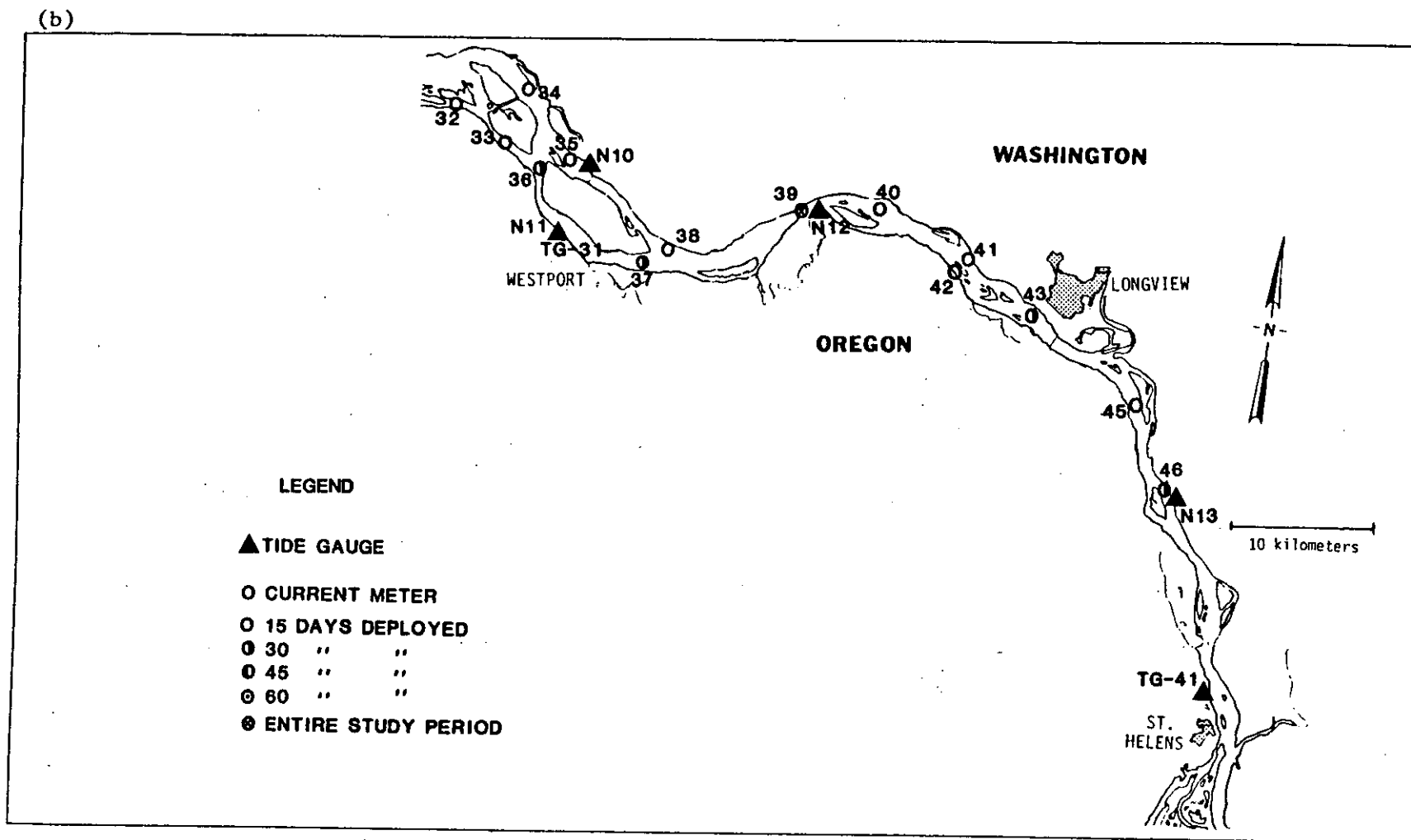


Figure 3.5 (continued).

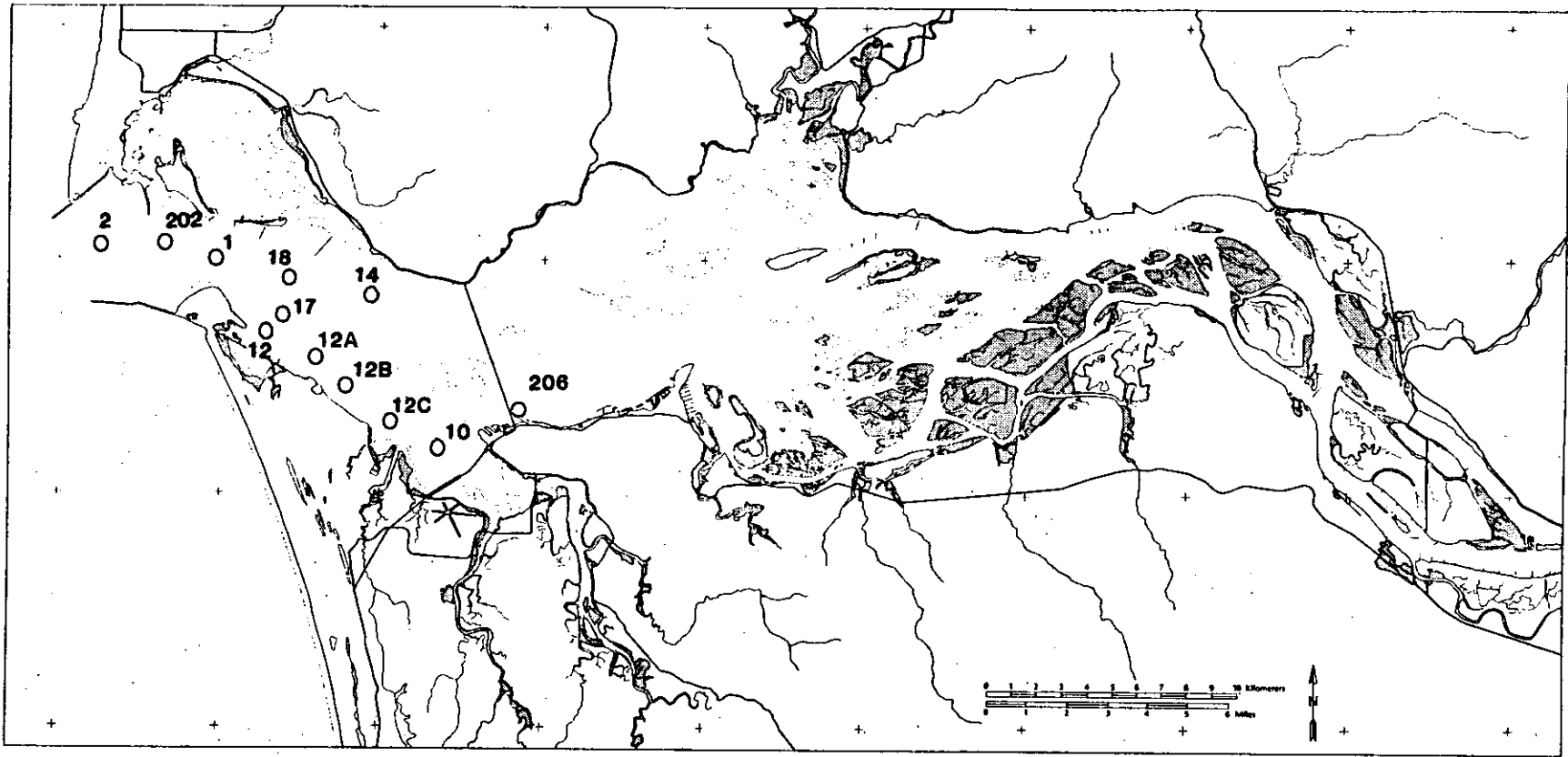
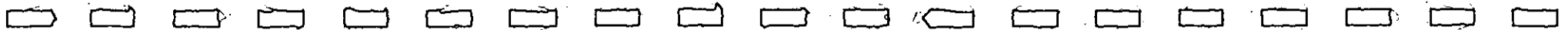


Figure 3.6. NOS 1981 CTD profile stations.



shallow water of the estuary. To the left of the diurnal and semidiurnal peaks are poorly resolved, low frequency peaks caused by tidal effects and riverflow fluctuations.

Tidal energy enters the estuary almost exclusively at diurnal and semidiurnal frequencies; it is effectively transferred by the non-linear processes described in Section 3.1 to higher and lower frequencies as the wave travels up the river. The power spectrum of the tidal heights at Wauna (RM-42; Figure 3.4b) shows that the main tidal peaks have diminished, the peaks corresponding to the higher harmonics and the residual flow have grown, relative to those of Figure 3.4a. Peaks at 15 and 28 days (approximately) are now resolved; these are caused by the tidal monthly variations in residual circulation.

3.3.1 Tidal Heights

Tidal height is perhaps the single most useful and most accurately known estuarine circulatory parameter. Harmonic analysis results for selected estuary stations are shown in Table 3.1. The energy contained in a tidal component is proportional to the tidal amplitude times the velocity. Virtually all of the tidal energy coming into the estuary is contained in the 3 largest semidiurnal constituents: M2 (the lunar semidiurnal component), S2 (the solar semidiurnal component), and N2 (the larger lunar elliptic component) and 2 largest diurnal constituents: K1 (the lunar-solar diurnal component) and O1 (the lunar diurnal component). The energy flux for M2 is nearly 8 times as large as the next most important constituent, K1. S2, N2, and O1 are still weaker. The effect of each of these constituents on the range of the tide is discussed in Section 3.3.2. The Tongue Point tidal height harmonic constants are similar to those of other nearby coastal systems; the tidal range and relative amplitudes of major constituents at Astoria differ from those of other stations between Waldport, Oregon and Aberdeen, Washington, by less than 20% (Callaway 1971; Hopkins 1971). Because the M2 tide accounts for such a large fraction of the total tidal energy in the system, it is useful to examine the propagation of the M2 tidal wave before considering the behavior of the other semidiurnal and diurnal constituents and higher harmonics.

Behavior of the M2 Tide - The Balance Between Topography and Friction

Figures 3.8 to 3.11a,b show model results for the amplitude and phase of the M2 tidal heights as a function of river mile for several different riverflows and tidal ranges. The model used is a one-dimensional, harmonic model of the M2 tide in the presence of variable channel cross-section and riverflow (Jay 1984). It is based on the method of Dronkers (1964). Figures 3.12a and b show the phase and amplitude of the M2 tidal heights, as determined from observations. Record lengths used in Figures 3.12a and b range from several months to a year; these results approximate a yearly average. The phase of the M2 tidal height increases nearly linearly with river mile (Figure 3.12a). The M2 tidal height amplitude (Figure 3.12b) first increases from the mouth to Astoria and then decreases almost linearly upriver. Figures 3.8 to 3.10 show that tidal heights upriver of Tongue Point

Table 3.1. Tidal constituent ratios for the Columbia River and Estuary.

<u>Length of Record</u>	<u>Station</u>	<u>RM</u>	M_2	$\frac{S_2}{M_2}$	$\frac{N_2}{M_2}$	$\frac{M_4}{M_2}$	$\frac{MK_3}{M_2}$	$\frac{K_1}{M_2}$	$\frac{O_1}{M_2}$	$\frac{O_1}{K_1}$	$\frac{M_2+S_2+N_2}{O_1+K_1+P_1}$
7 mos.	Jetty A	3	.833	.255	.207	.026	.015	.487	.328	.674	1.51
7 mos.	Ft. Stevens	8.3	.935	.256	.202	.027	.011	.441	.276	.625	1.72
1 yr.	Tongue Pt.	17.6	.947	.247	.189	.012	.025	.423	.252	.596	1.81
7 mos.	Altoona	24.4	.897	.238	.185	.042	.036	.400	.238	.595	1.91
1 yr.	Wauna	42.0	.736	.234	.188	.110	.089	.384	.205	.533	2.05
7 mos.	Beaver	53.3	.578	.236	.176	.155	.122	.385	.200	.519	2.10
1 yr.	Columbia City	83.0	.231	.236	.195	.208	.145	.478	.241	.504	1.78

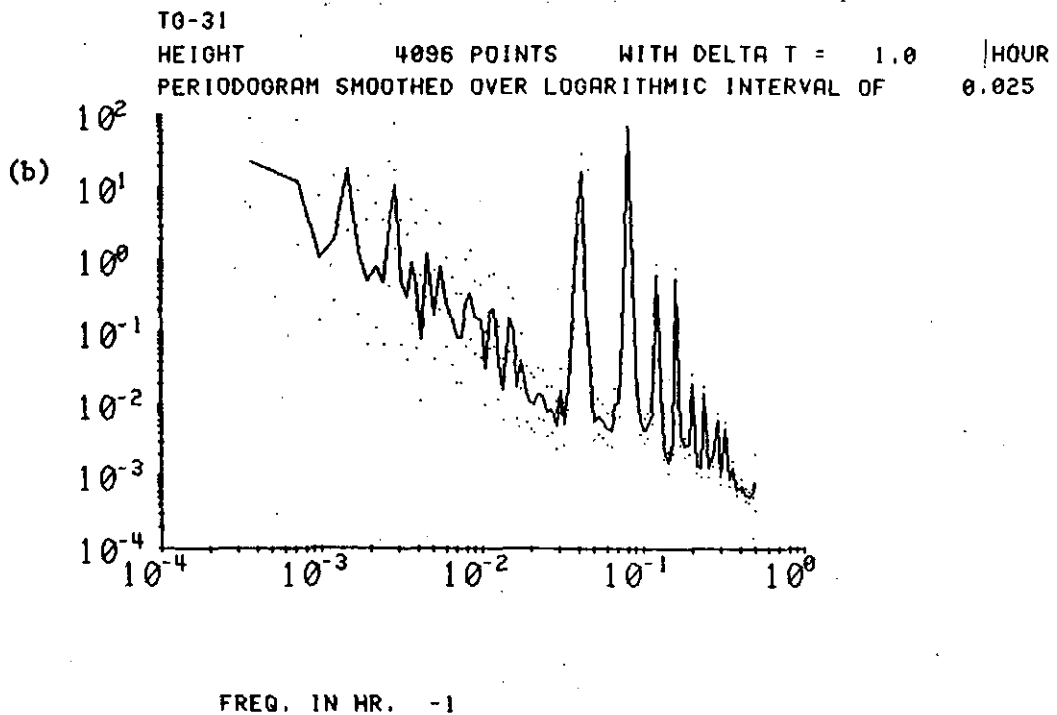
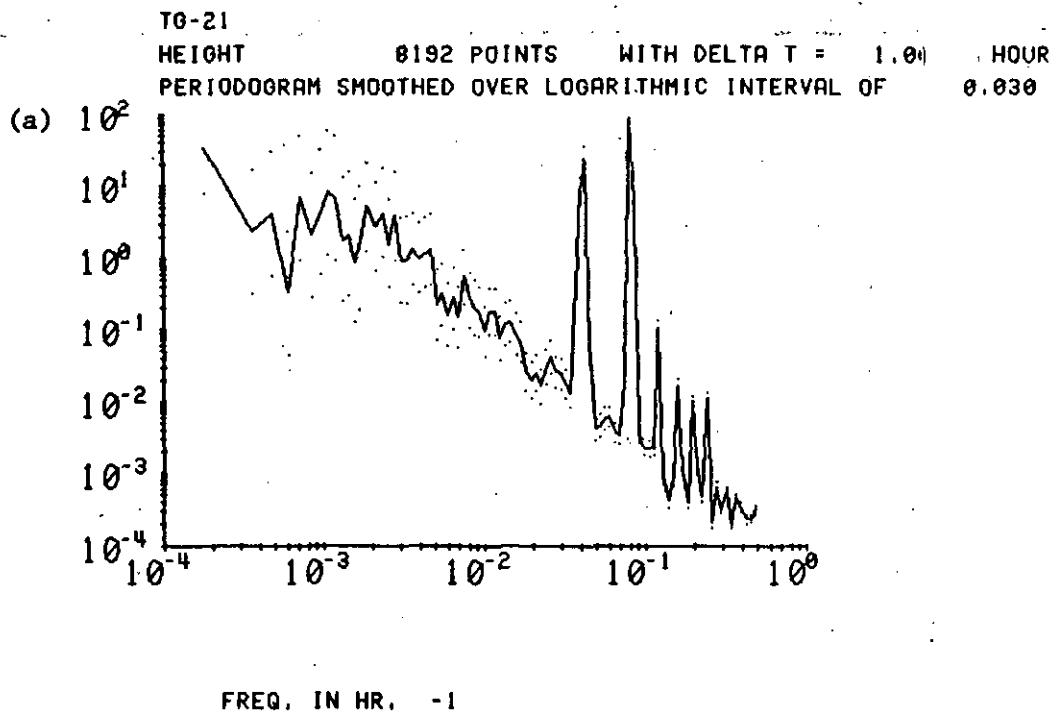
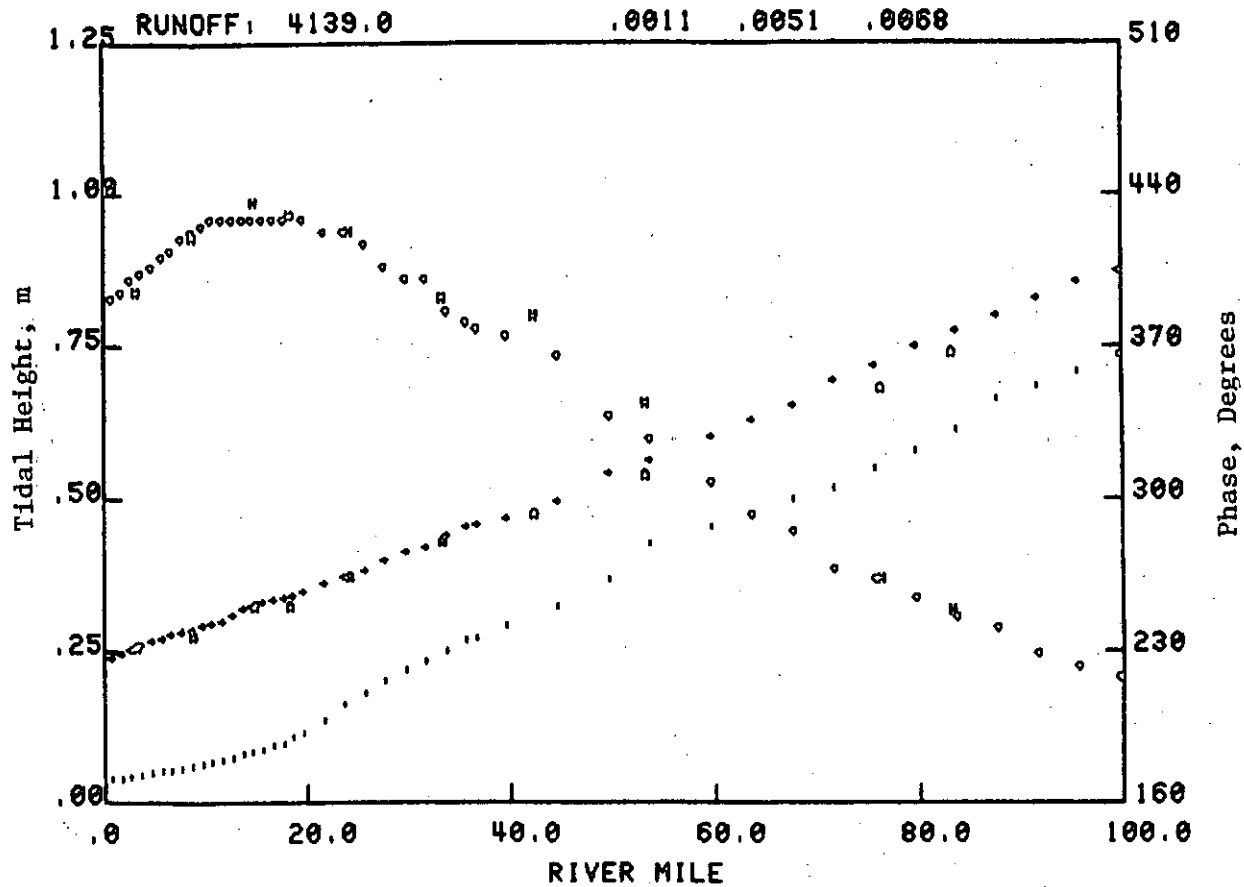
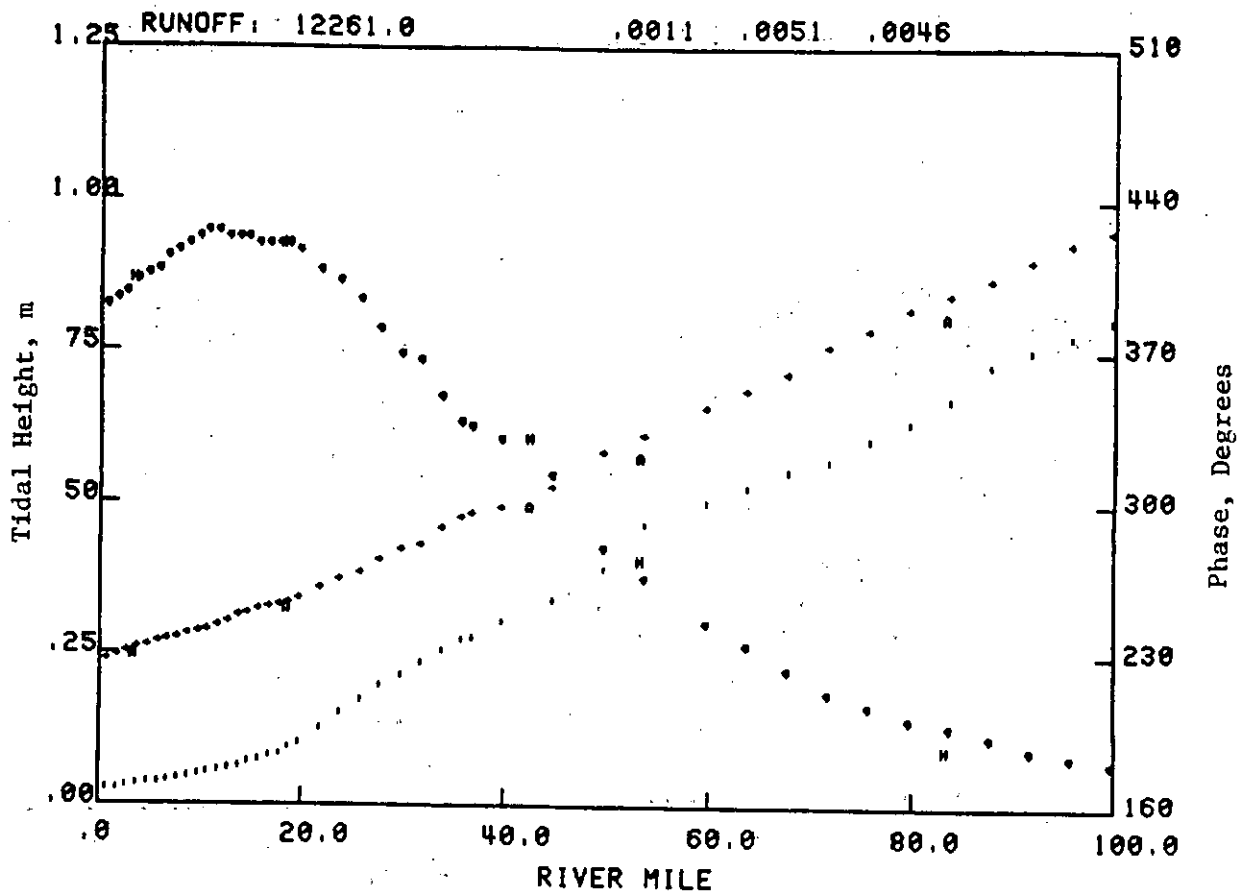


Figure 3.7. Power spectra of tidal height at (a) Tongue Point, and (b) Wauna. Dots indicate 95% confidence limits.



- * Model tidal height amplitude
- + Model tidal height phase
- | Model tidal current phase
- H Observed tidal height amplitude
- A Observed tidal height phase

Figure 3.8. Model results for river flow of 146 kcfs ($4,139 \text{ m}^3 \text{ sec}^{-1}$).



- * Model tidal height amplitude
- + Model tidal height phase
- | Model tidal current phase
- H Observed tidal height amplitude
- A Observed tidal height phase

Figure 3.9. Model results for river flow of 433 kcfs ($12,261 \text{ m}^3 \text{ sec}^{-1}$)

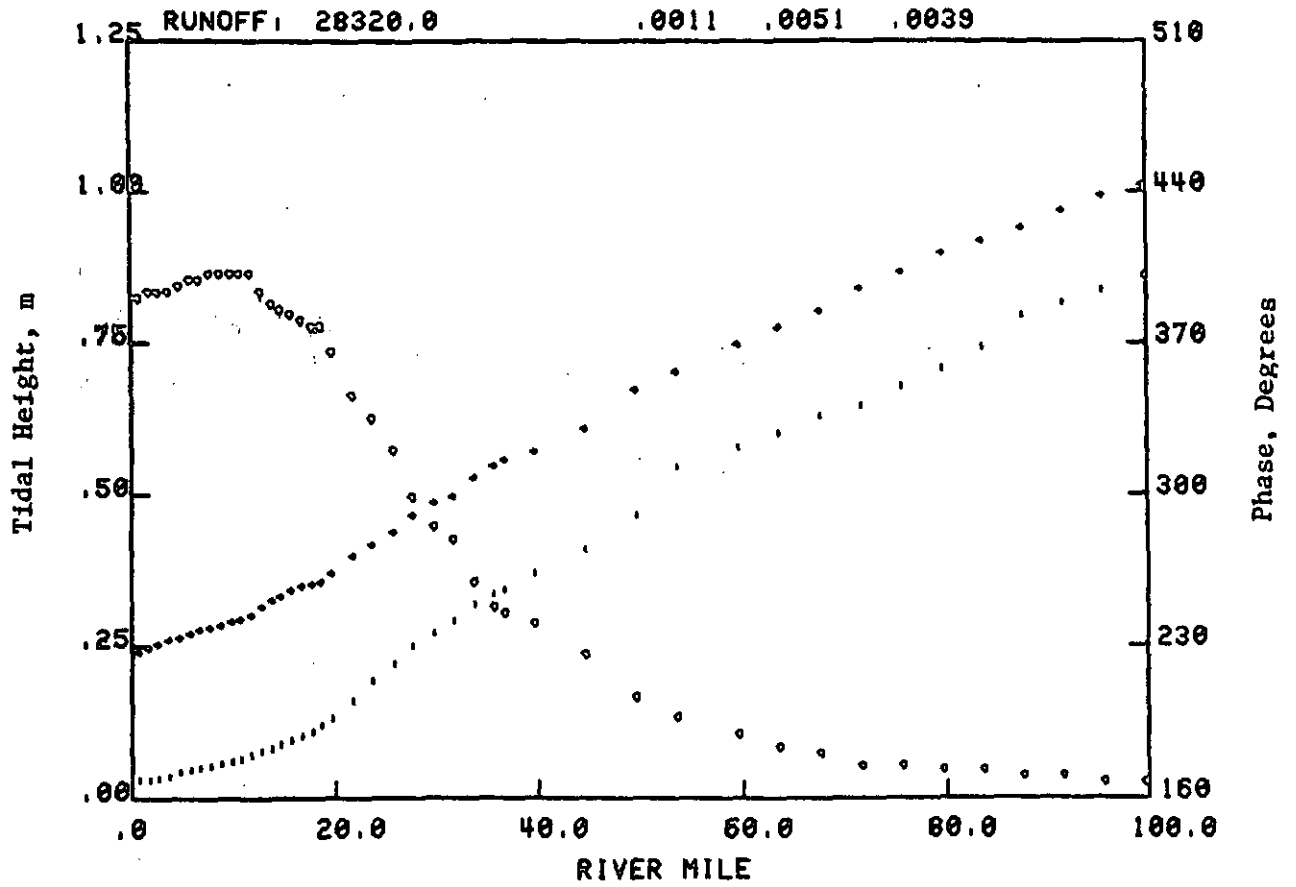


Figure 3.10. Model results for river flow of 1,000 kcfs ($28,320 \text{ m}^3 \text{ sec}^{-1}$).

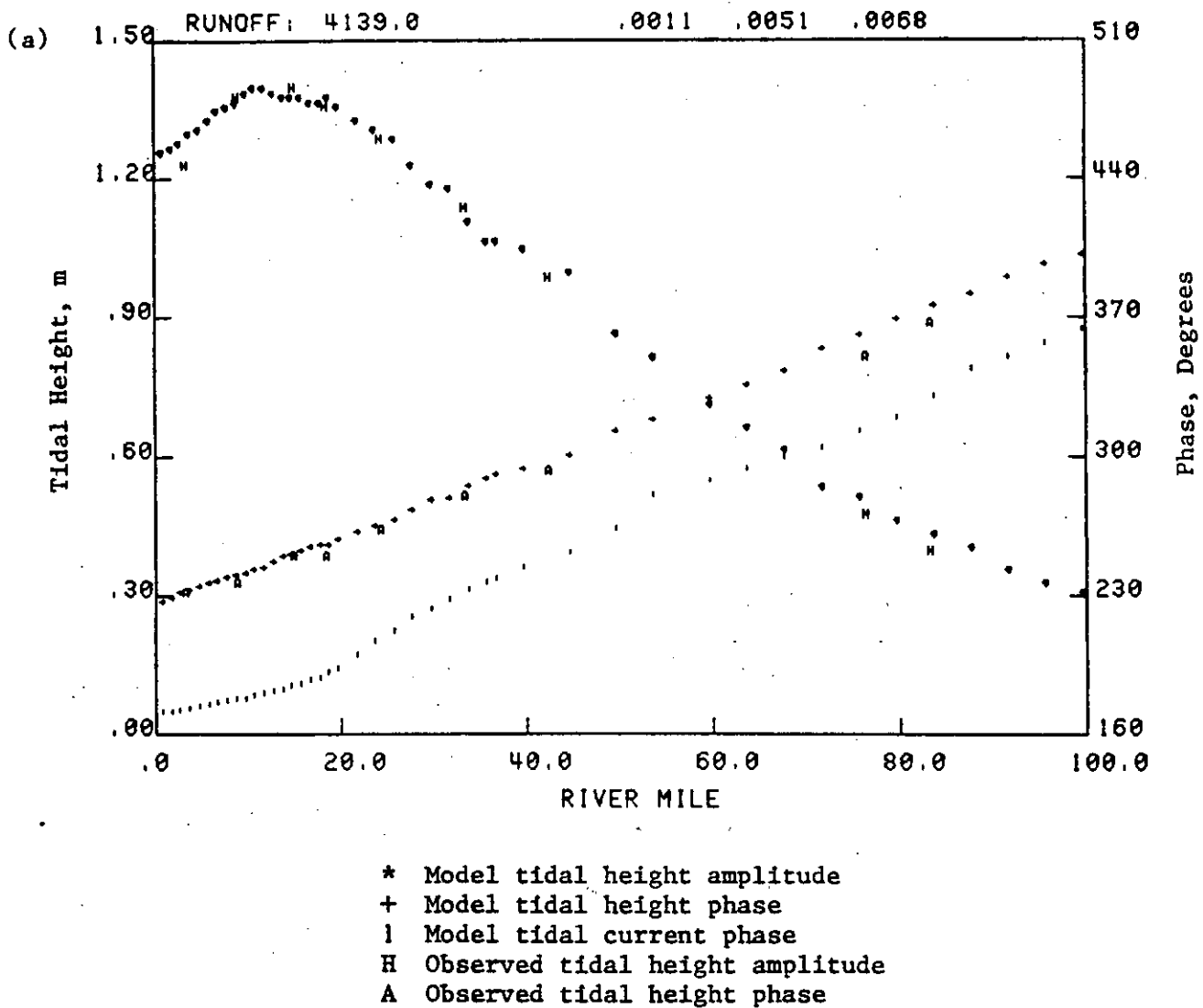


Figure 3.11. Model results for (a) $M2 + S2 + N2$, and (b) $M_s - S2 - N2$, with 146 kcfs ($4,139 \text{ m}^3 \text{ sec}^{-1}$). Note the difference in tidal height scale for (a).

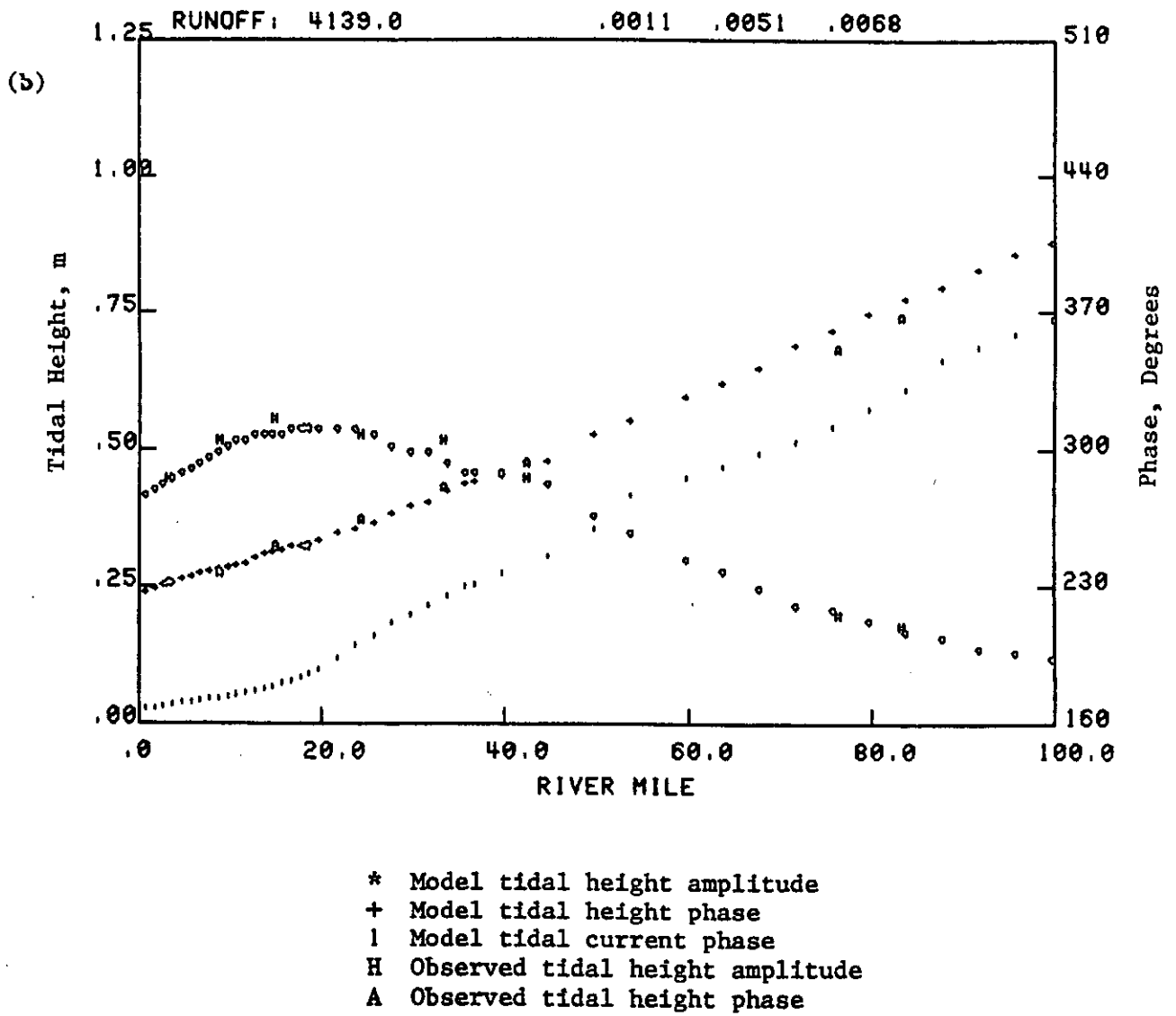
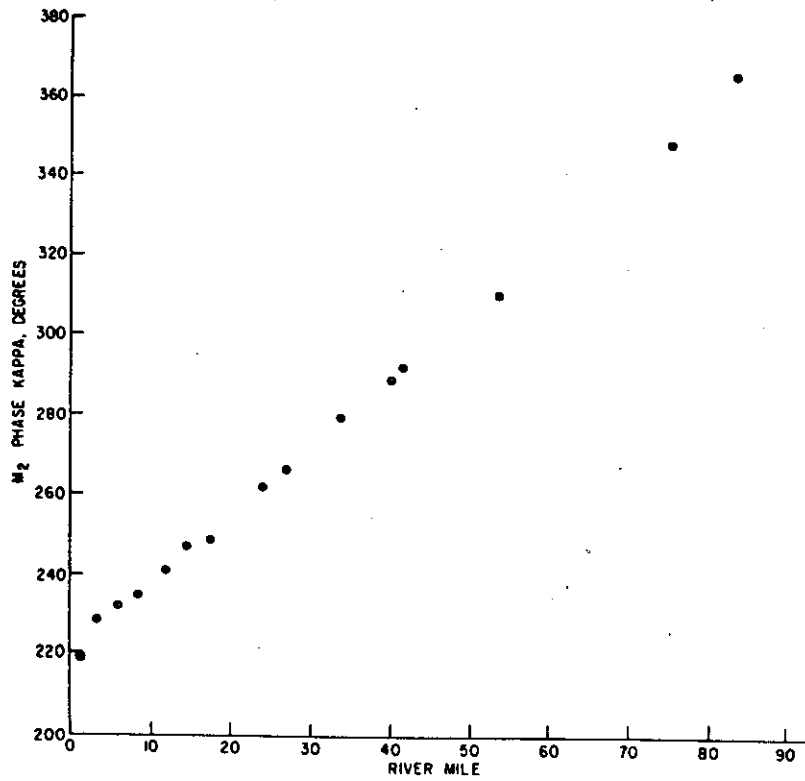


Figure 3.11 (continued).

(a)



(b)

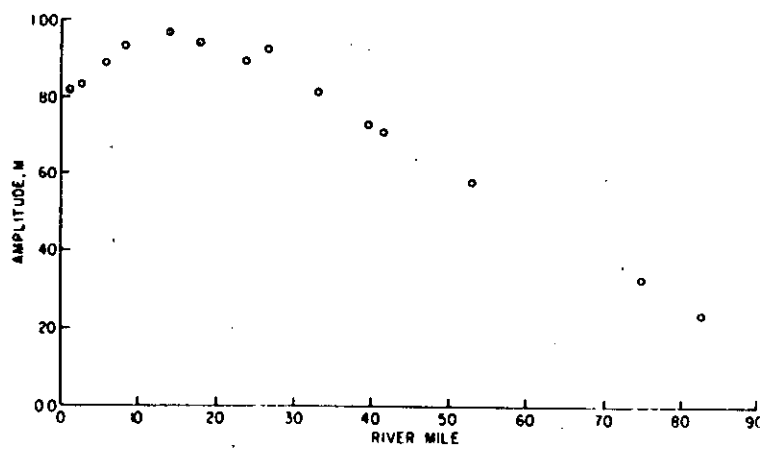


Figure 3.12. M_2 tidal height (a) phase and (b) amplitude vs. river mile in the Columbia River and Estuary.

(RM-19) are strongly affected by riverflow changes (Section 3.4).

Experimentation with the harmonic tidal model suggests that these patterns result from the balance between topography and friction. The M2 tide acts as a heavily damped wave in a channel with a constricted entrance, attached to a funnel that decreases in area almost linearly in the upstream direction. The tidal amplitude increases because of the partial standing wave character of the tide in the lower estuary and the funnel-like geometry; the highest amplitude occurs where the estuary narrows, between RM-13 and 20. This may be interpreted as partial reflection of the wave by the funnel-like topography above Astoria. The increasing friction in this reach, the shallowest part of the system, is also critical in determining the shape of the wave. As the tidal wave energy is more strongly dissipated upriver, friction eventually outweighs the funnel effect, and tidal range decreases and the tide becomes more progressive upriver (Figures 3.8 to 3.10).

The harmonic analysis results for Ilwaco, Chinook, Youngs Bay, Knappton, and Knappa show that the tides in the peripheral bays are similar to the tides in the rest of the estuary. There is a slight damping of the M2 wave in Baker Bay and slight amplification in Youngs Bay, Cathlamet Bay, and Grays Bay; the greatest M2 amplitudes in the entire estuary are found at Knappton and Youngs Bay (about 2 cm greater than at Tongue Point), and the M2 amplitude at Knappa is about 2 cm greater than that at Altoona.

Non-Linear Effects

The non-linearity of tides in shallow estuaries manifests itself in at least three other ways, in addition to the transfer of energy from the tidal circulation to the various secondary circulation modes (Section 3.1). First, the increase in riverflow during a freshet has a dramatic effect on the damping of the tidal wave in the tidal-fluvial portion of the system above Altoona (Figures 3.8 to 3.10). Second, the residual flow due to river inflow causes a marked flood-ebb asymmetry in the currents and the degree of mixing. So much more energy is dissipated by bottom friction during the ebb that much more mixing occurs on ebb than on flood; this difference is reflected in the velocity and salinity profiles and vertical mixing processes (Section 3.3.4). Third, it can be hypothesized that the above-noted tendency for the tides to be amplified slightly in most of the peripheral bays may be the result of the lower freshwater flow velocities there. This would reduce the bottom friction in the bays.

The Diurnal Constituents

The behavior of the diurnal constituents is different from that of M2. The ratio of semidiurnal constituents to diurnal constituents $((M2+S2+N2)/(O1+K1+P1))$ decreases sharply from the entrance to Ft. Stevens and more slowly from Ft. Stevens to Beaver (Table 3.1); it then increases again at Columbia City. The only diurnal constituent that increases in amplitude in the lower estuary is the largest, K1. The K1 and O1 phases do not vary linearly with river mile; the waves propagate much more quickly below Tongue Point than above, and K1 propagates more

quickly than O1. The much faster propagation of the diurnal wave in the estuary proper suggests a partial reflection of the diurnal wave, associated with the funnel shape of the channel upriver of Astoria.

The Tidal Overtones

The behavior of the tidal overtones also differs from that of the semidiurnal constituents. The amplitudes of M4 (the first overtide of M2) and MK3 (an overtide of M2 and K1) are both small and variable in the lower estuary below Tongue Point (Table 3.1). Both strongly increase relative to M2 upriver from Tongue Point. From Tongue Point upriver, the phase progression of both MK3 and M4 is quite uniform. These observations are consistent with the idea that the higher harmonics as measured below Tongue Point are in part those produced in the ocean. The higher harmonics observed in the tidal-fluvial part of the system are those of the non-linearly tidal circulation.

3.3.2 Factors Influencing the Tidal Range

The harmonic analysis results discussed are based on observations spaced evenly in time (i.e., hourly). The mariner and marine manager are commonly more interested in the traditional tidal parameters such as tidal range (distance between tidal extremes) and high and low water intervals (time of high or low water at a station) that appear in tide tables. Selected tidal parameters are therefore shown as a function of river mile in Table 3.2. The mean tidal range (Mean High Water-Mean Low Water (MHW-MLW)) at Tongue Point is about 2.03 m, the diurnal range (Mean Higher High Water-Mean Lower Low Water (MHHW-MLLW)) is about 2.62 m, and the spring range is about 2.44 m. There are three principal factors that influence the tidal range in a system with tides like those in the Columbia River Estuary (Marmer 1951). They are the phase of the moon (neap-spring effect), the declination of the moon above the equator as it passes over the longitude of the tide station (equatorial versus tropic tides, the diurnal inequality), and the distance of the moon from the earth (the apogee-perigee effect). A spring tide occurs when M2 and S2 are in phase, and a lunar apogean tide occurs when M2 and N2 are in phase. The spring-neap effect is about 1.3 times as important in the Columbia River Estuary as the apogee-perigee effect. The more extreme tides occur when several of these effects reinforce one another; for example, the higher of the two tides on the day of the spring tide each month will have a range larger than the spring range of 2.44 m, because of the effect of the diurnal tide or diurnal inequality. A really large higher high water occurs on those spring tides when the diurnal inequality is at its maximum, that is, when the moon is at its greatest distance from the equator. M2, S2, K1 and O1 are then in phase. The most extreme tide would occur when all the major constituents affecting the range of the tide were all in phase. The tidal range at Tongue Point would then be $2x(M2+S2+N2+K1+O1) =$ about 4.0 m. Such a tide is a rare occurrence. The ratio of spring and apogean to mean tide decreases with river mile (Table 3.2), since the ratio of N2 and S2 to M2 decrease with river mile (Table 3.1). This non-uniformity is a function of system energetics (Section 3.5). In the rest of this report, all tides of large range will be referred to as "spring tides" and those of small range as "neap tides", regardless of

the factors acting to produce the observed range.

The high and low water intervals in Table 3.2 give the number of hours after the passage of the moon over Greenwich that high and low waters occur at the station. The observed times of high and low water differ from those values that could be determined solely from the phase of the M2 tide, principally because of the distorting effect of the tidal overtones. A wave is considered to be in shallow water when the depth is less than half the wavelength (about 300 km for the tidal wave). The wave speed for shallow water waves is dependent on the depth of the water (Section 3.1.3). The average depth of the estuary is only about 6 to 12 m, and the change in depth of the estuary between high water and low water (~2 m) is a very large fraction of the average depth. Since the wave is in very shallow water, the peak of the wave travels somewhat faster than the trough of the wave. It can be seen in Figure 3.13 that considerable distortion of the wave occurs as it moves upstream. The time of low water approaches the time of high water, and the rise of the tide is much more rapid than the subsequent fall. In extreme situations the result is a tidal bore (e.g., on the Amazon River). This distortion appears in the harmonic analysis as the presence of the tidal overtones, shown in Figures 3.7a and b.

3.3.3 Tidal Inundation Time

The tidal inundation time curve for Tongue Point (based on 21 years of data) is shown in Figure 3.14. This curve may be compared to those for other west coast tide stations, given in National Oceanic and Atmospheric Administration (1980). The three basic factors governing inundation time curves are the tidal characteristics, the freshwater inflow, and atmospheric effects (both local and on the continental shelf). As discussed in Section 3.3.1, the tides are somewhat more diurnal near the mouth than elsewhere in the estuary, and the amplitude of the M2 tide drops almost linearly with river mile, above Tongue Point. The change in surface level associated with changes in riverflow are relatively minor in the estuary but increase rapidly upriver (Section 3.4).

3.3.4 Currents

The distribution of currents in the estuary is considerably more difficult to measure and explain than the distribution of the tidal heights, because of the importance of density and bottom boundary effects. Extensive analytical and modeling efforts have, therefore, been required to understand the currents.

Observed Spatial Distribution

Systematic variations in tidal currents occur both with river mile and depth. The M2 current phase and amplitude are shown as a function of river mile in Figures 3.15a through d. These results may be compared to the model results in Section 3.4 and Figures 3.8 to 3.10. The systematic vertical variations are a result of topography and stratified boundary layer effects. The strong effect of the sills between RM-6 and RM-10 in both channels is also evident in the salinity distribution

Table 3.2. Tidal properties as a function of River Mile.

Length of Record	Station	RM	Ranges, m								Greenwich		Inequalities, m	
			mean/ greater diurnal	spring/ neap	perigeon/ apogean	greater tropic/ lesser tropic	Intervals, Hours		Diurnal HW Inequality	Diurnal LW Inequality				
7 mos.	Jetty A	3.0	1.81	2.40	2.23	1.32	2.18	1.52	2.65	0.88	7.94	1.57	.21	.39
7 mos.	Ft. Stevens	8.3	2.01	2.62	2.47	1.49	2.42	1.71	2.85	1.07	8.22	1.81	.22	.39
1 yr.	Tongue Pt.	17.6	2.03	2.62	2.44	1.57	2.42	1.74	2.81	1.11	8.58	2.46	.21	.37
7 mos.	Altoona	24.4	1.93	2.46	2.28	1.52	2.28	1.66	.62	1.06	8.96	3.05	.20	.33
1 yr.	Wauna	42.0	1.59	2.01	1.86	1.27	1.89	1.38	2.07	0.86	9.72	4.38	.17	.24
7 mos.	Beaver	53.3	1.26	1.60	1.49	1.01	1.49	1.10	1.60	0.63	10.24	5.28	.15	.18
1 yr.	Columbia City	83.0	.51	.66	.59	.41	.61	.43	.74	.36	11.46	7.53	.11	.04

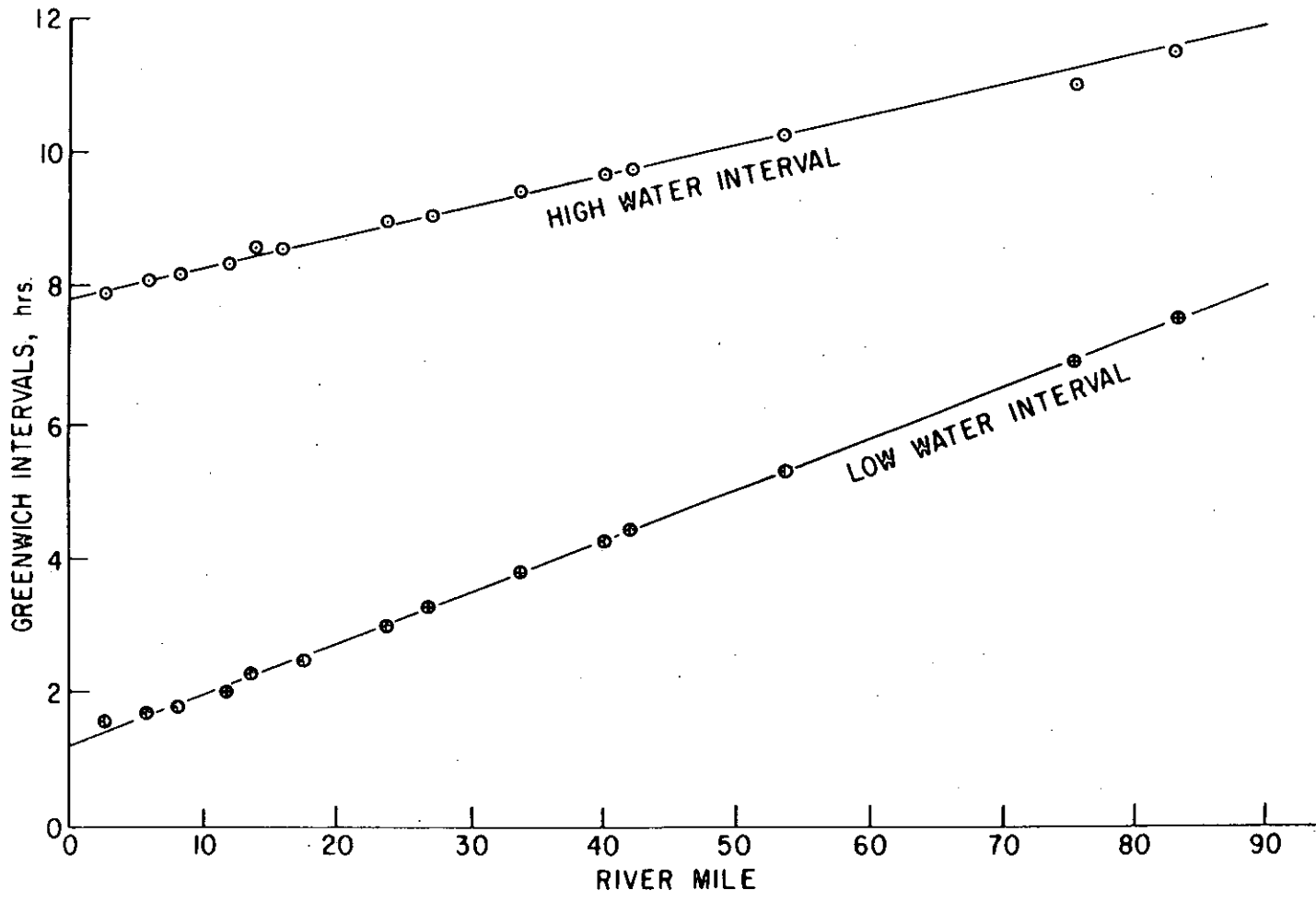
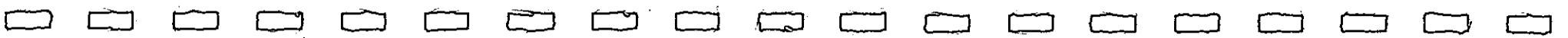


Figure 3.13. Greenwich intervals (times of high and low water) vs. river mile.



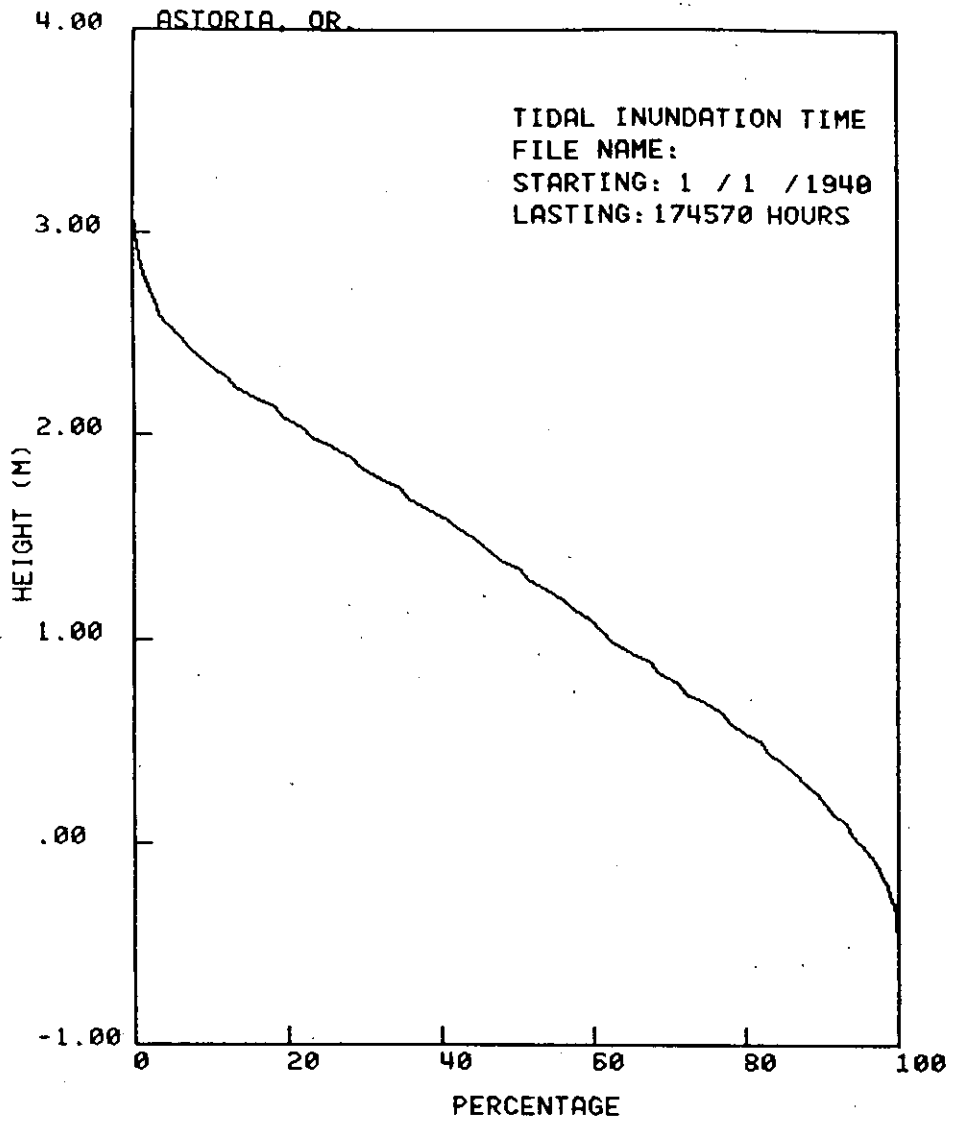


Figure 3.14. Tidal inundation time versus depth for NOS Tongue Point reference station, 1940-1961, referred to MLLW for the 1949-1959 epoch. An inundation time of 20% indicates that the intertidal land of the indicated level is inundated 20% of the time.

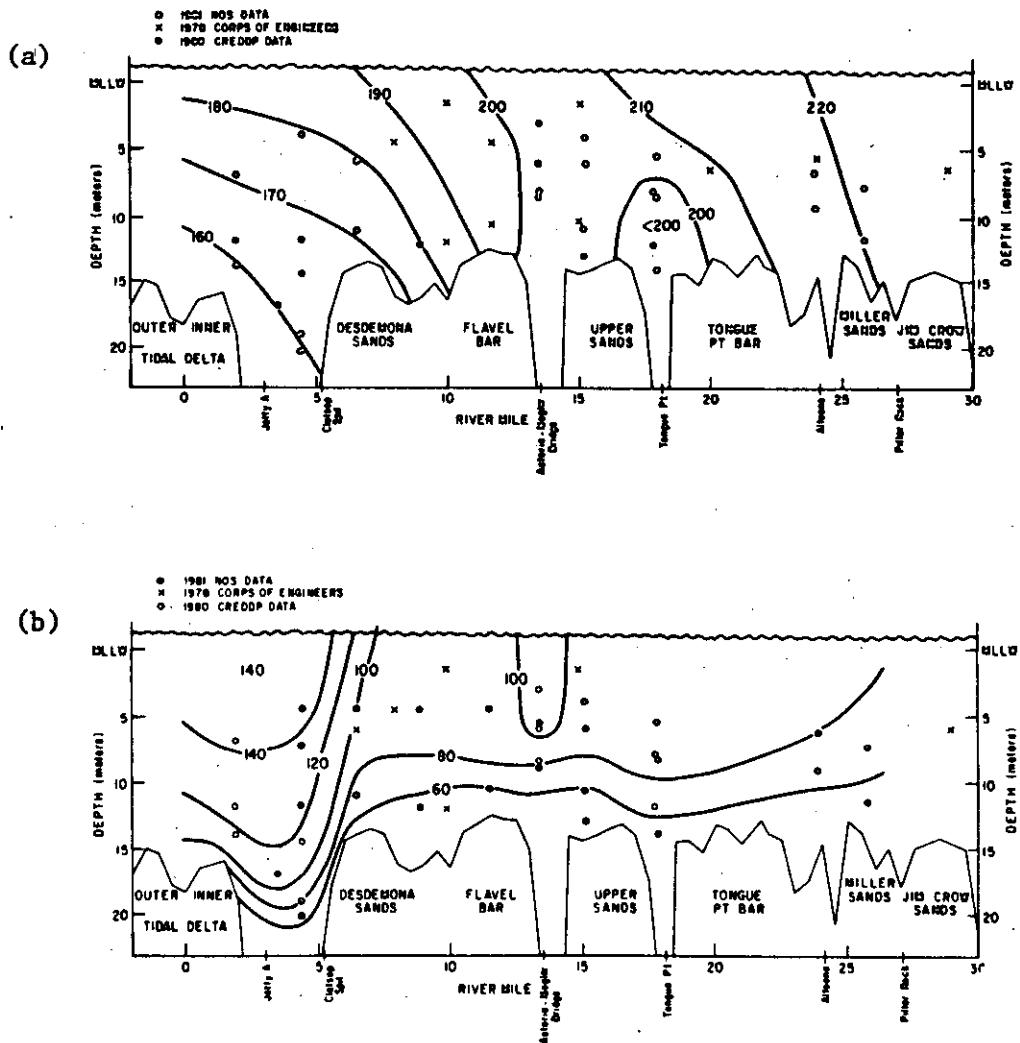


Figure 3.15. Phase in degrees (a) and amplitude in cm sec^{-1} (b) of M2 tidal currents in the south channel, and (c) and (d) in the north channel, based on all available current meter data. Vertical variations in phase and amplitude are greatest in deeper water near the entrance, where stratification effects are most important. The shallow bars in both channels at Desdemona Sands greatly reduce these vertical variations.

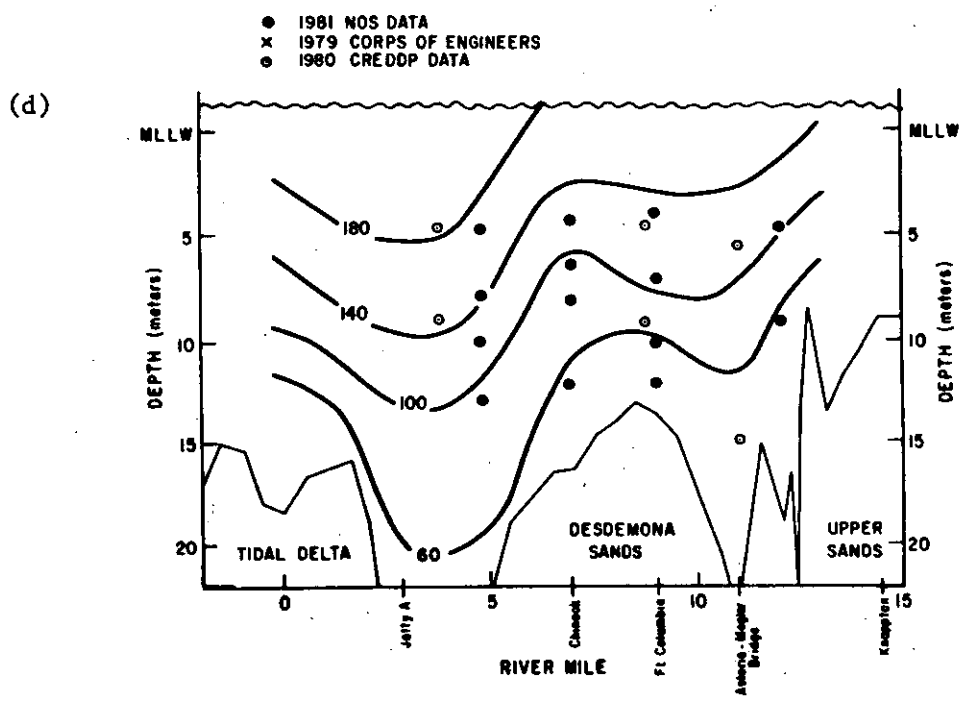
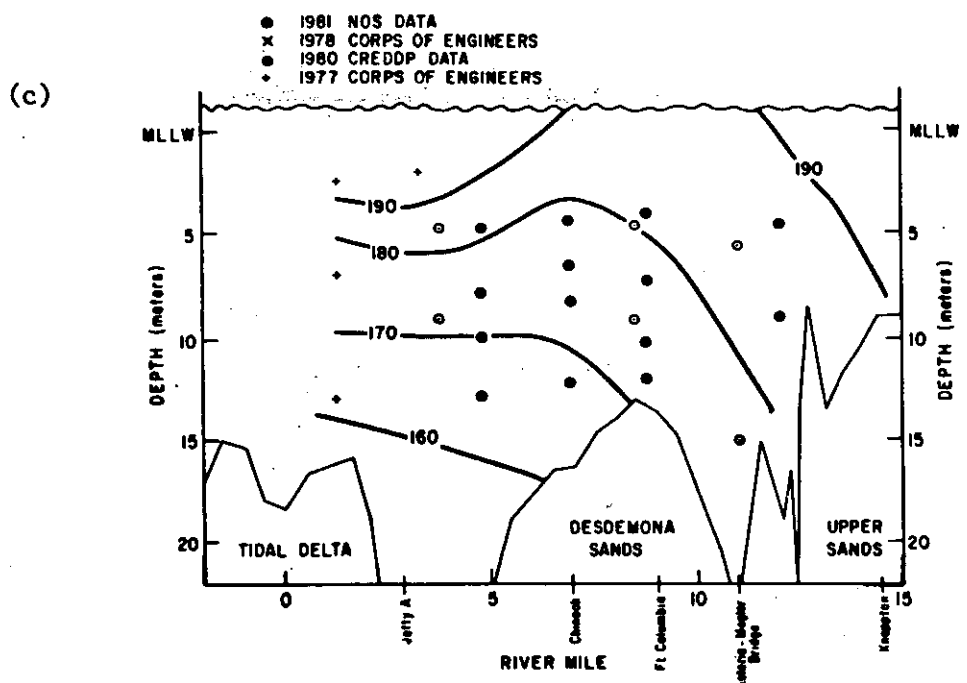


Figure 3.15. (continued)

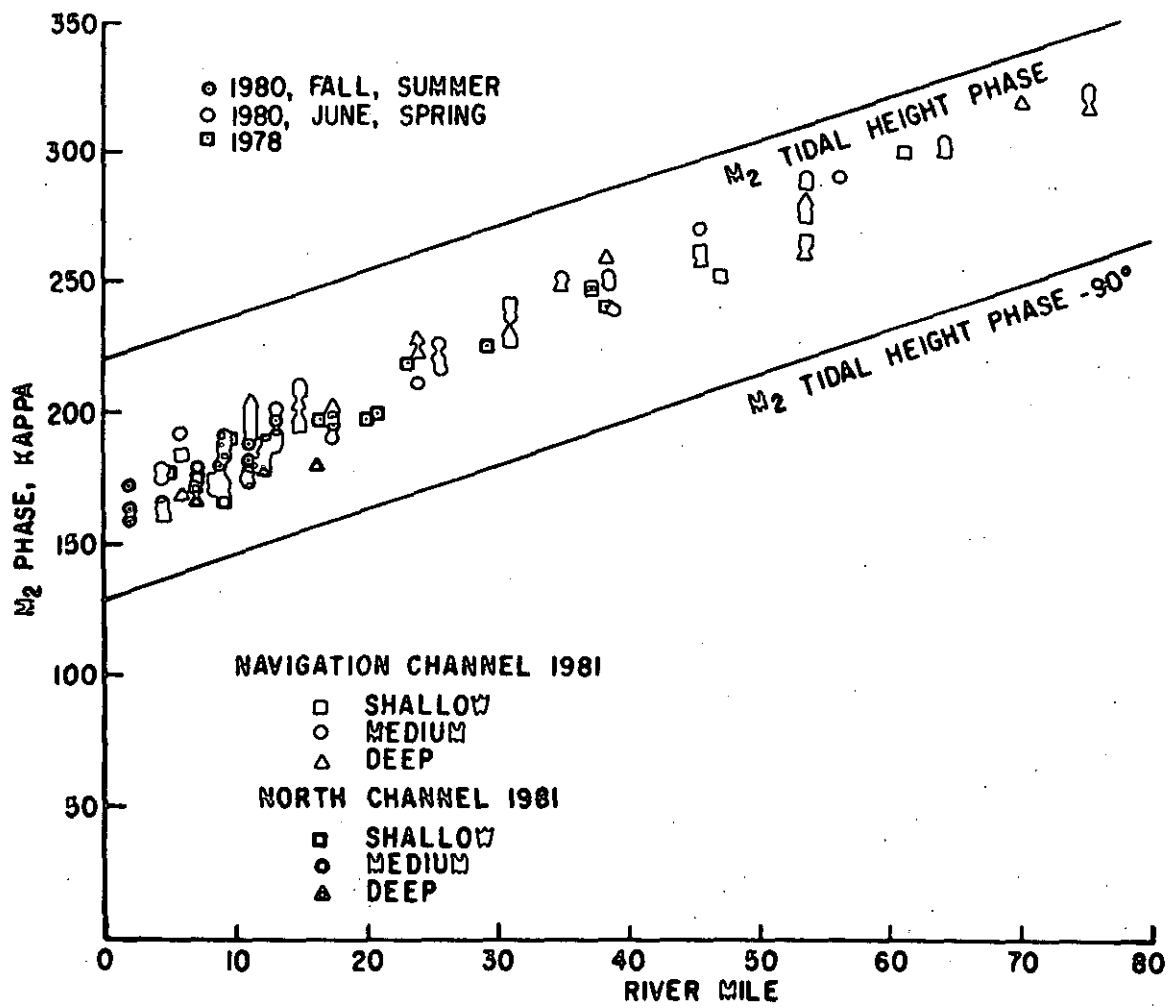


Figure 3.16. Phase of the M₂ tidal currents as a function of river mile in the north and south (navigation) channels, based on all available current meter data. Systematic variations of phase with depth occur, which are related to stratification and topographic effects.

(Section 3.6). The M2 current phase lags the tidal height phase by about 50 to 60° at the mouth and by about 45 to 50° upriver (Figure 3.16). These phase differences may be converted to time differences by use of a conversion factor of about 29° of phase hr^{-1} for the M2 tide. The current phase is intermediate between that for a progressive wave (tides and flow in phase) and a standing wave (tides and flow 90° out of phase). The currents become more closely in phase with the heights (more progressive) above Tongue Point; this is a result of the strong friction in the system. The strong decrease in currents (and tidal transport) upriver occurs because most of the tidal prism is near the mouth, where both the tidal range and width are large. Tidal currents are much stronger in the north channel than in the south channel (Figure 3.15); thus, most of the tidal flow below the Astoria-Megler Bridge is in the north channel, and most of the riverflow is in the south channel (section 3.7).

Figures 3.15 and 3.16 show that vertical variations in the phase and amplitude of the current are substantial and that this vertical structure varies in the along-channel direction. Examination of tidal currents at the Clatsop Spit-Sand Island cross-section show that cross-channel variations are also important (Figures 3.17a and b). The M2 amplitude is strongest and the phase latest at the surface in the north channel. The top to bottom phase difference is greater than 30° (about 1 hour) and the top to bottom shear in the tidal currents is more than 1.2 m sec^{-1} . The vertical shear and phase differences in the tidal circulation that are under consideration here should not be confused with the vertical variation in the mean flow.

Vertical Structure of the Tidal and Mean Flows - Boundary Layer and Density Effects

The factors that maintain the vertical structure of the tidal flow and that cause the variations of this vertical structure along and across the channel (Figures 3.15 to 3.17) are the subject of this subsection. It is useful to consider the entire flow as a stratified boundary layer; that is, that the bottom friction influences all parts of the flow. The vertical structure of a boundary layer flow is determined by stratification, the surface slope, the baroclinic pressure gradient, bottom roughness, and channel topography. These factors vary in time as well as space, so ebb-flood differences must be considered. Since the mean flow is essentially the difference between the ebb and flood tidal flows, the ebb-to-flood asymmetry determines the vertical structure of the mean flow.

Consider first the structure of a neutral boundary layer flow, one without stratification or a baroclinic pressure gradient. Most of the vertical shear and phase differences in neutral boundary layers occurs very close to the seabed (in the bottom 1 m). The shear is the result of deceleration of flow near the bed by bottom friction. The phase differences arise because of the shear (Lavelle and Mojfield 1983). For example, at the end of flood or ebb, the surface slope reverses some time before the flow changes direction, because the flow must first be decelerated before it can change direction. The parts of the flow with greater inertia (greater velocity) take longer to decelerate.

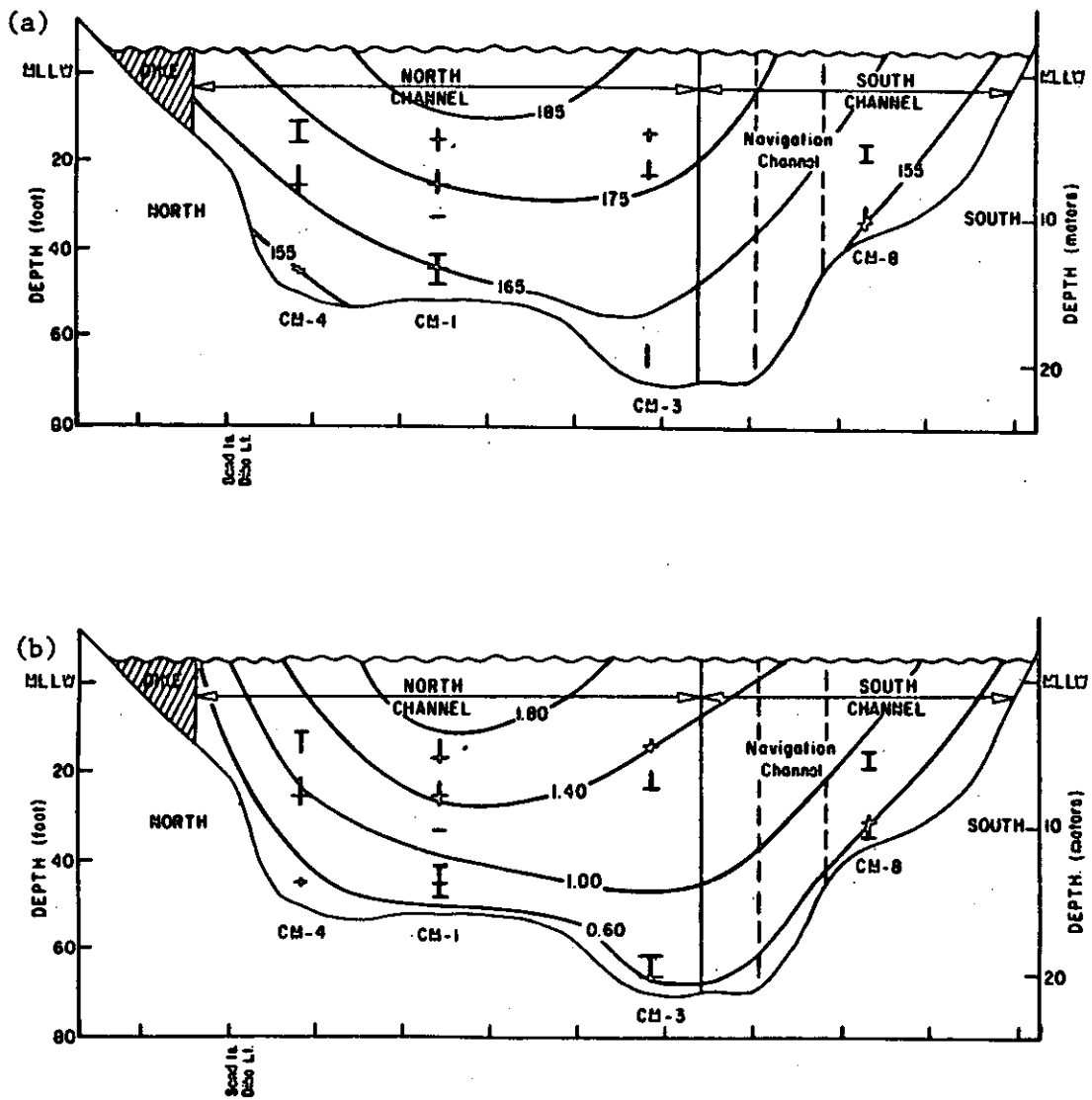


Figure 3.17. Phase in degrees (a) and amplitude in m sec^{-1} (b) of M2 tidal currents at Clatsop Spit at RM-5. Tidal currents are strongest in the north channel.

Reversal, therefore, occurs last in the parts of the flow with the greatest velocity (normally near the surface). The neutral boundary layer is an adequate model of the structure of the tidal flow in the tidal-fluvial areas, where salinity intrusion is not found, but this model cannot explain the the magnitude of the shear and phase differences seen at the Clatsop Spit-Sand Island section (Figures 3.17a and b) and elsewhere in the estuary.

To explain the magnitude of the shear and phase differences seen in the lower estuary, stratification, the baroclinic pressure gradient and the mean flow must also be considered. This can be done most easily in terms of figurative velocity and salinity profiles for the lower and upper estuary shown in Figure 3.18. These profiles are not observed data; they are, however, typical of profiles observed in the estuary during periods of low to moderate riverflow and tidal range. Consider first the profiles for the lower estuary. The ebb velocity profile shows more shear high in the water column than the flood profile, because the vertical structure of the total pressure gradient and the stratification effect on vertical mixing act together to allow large velocities to develop near the surface and, thus, to allow a large shear in the velocity structure. That is, on ebb (at least until after the time of peak ebb), the barotropic pressure gradient caused by the surface slope (independent of depth) accelerates the entire flow seaward, but is counteracted at depth by the baroclinic pressure gradient induced by the horizontal salinity gradient. The stratification allows layers of fluid to slide over each other easily, because it inhibits vertical momentum transfer, as was discussed in Section 3.1.4. Near-bottom velocities tend to remain small and, late in the ebb, the total pressure gradient may actually change sign with depth; this pushes the top and bottom of the water column in opposite directions. Thus, the stratification permits the development of large shears on the ebb.

On flood in the lower estuary (at least until after peak flood), the surface slope and horizontal salinity effect on the pressure gradient act in the same direction, and since the baroclinic pressure gradient increases with depth, the total inward pressure gradient is largest near the bottom. Although the stratification on flood is usually larger than on ebb and inhibits vertical momentum exchange, the pressure gradient favors large velocities near the bottom. The result is that stratification and pressure gradient effects act together on flood to minimize shear; the velocity is typically much more uniform with depth than on the ebb. At the end of flood, vertical differences in inertia are small and the reversal in flow occurs nearly simultaneously at all depths.

Thus, one aspect of the ebb-flood asymmetry is the differences in vertical structure that result from stratification, baroclinic, and inertia effects on boundary layer flow. To understand the vertical structure of the mean flow, one other factor must be considered; conservation of mass requires that ebb flow through any cross-section of the estuary be greater than the flood flow by an amount that is equal to the riverflow plus the Stokes drift compensation flow. The vertical distribution of this mean flow is simply the difference

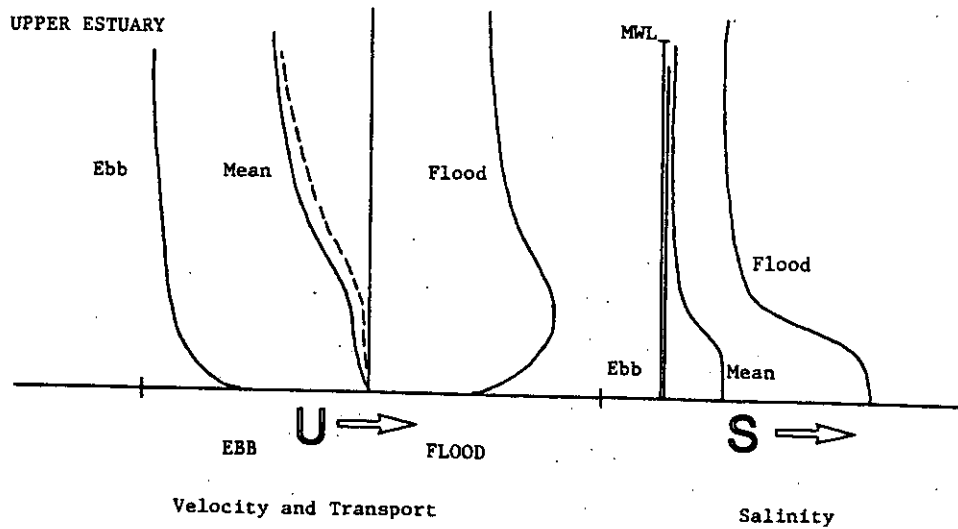
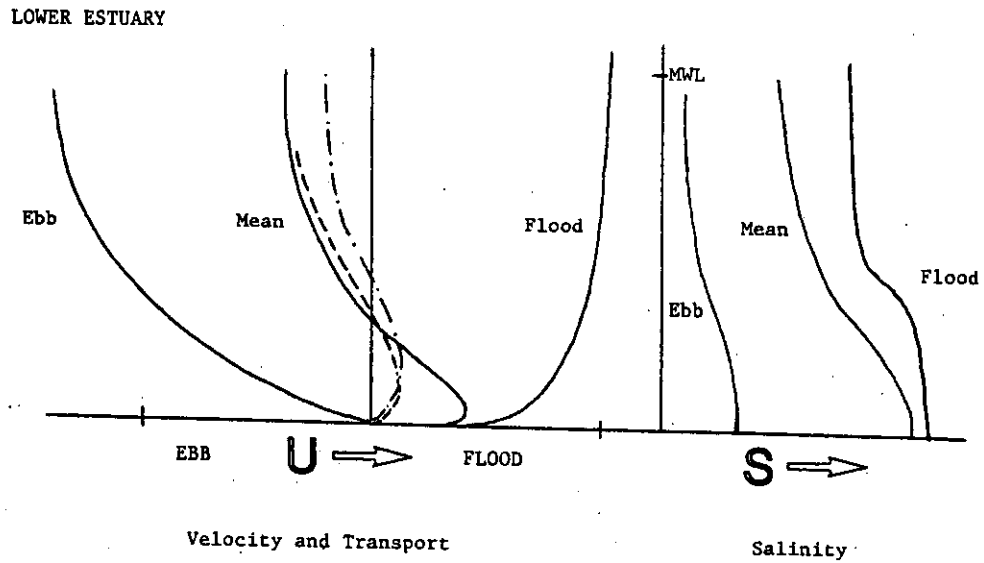


Figure 3.18. Typical profiles of flood, ebb and mean flows, and flood, ebb and mean salinities for (a) the lower estuary, and (b) the upper estuary. The dotted lines show the width-weighted flow and the effect of the Stokes drift. The Stokes drift is negligible in (b), and is not shown.

between the flood and ebb flows. Because of the strongly-sheared ebb and the more uniform flood, the net flow near the bottom is inward in many parts of the lower estuary. The dotted lines in Figure 3.18 show Eulerian transport per unit depth (i.e. velocity times channel width) and the sum of Eulerian and Lagrangian transport per unit depth. They show that very little inward transport is associated with the inward mean flow at the bottom, because the channel is narrow. The effect of the Stokes drift is felt mainly at the surface, where it is a substantial fraction of the total mean flow.

The situation in the upper estuary is somewhat different (Figure 3.18). Salt is absent during much of the ebb, so the ebb velocity profile is that of a neutral boundary layer and current reversal at the end of ebb is nearly simultaneous at all depths. The strongly-stratified flood flow frequently exhibits a velocity maximum in the pycnocline, as the adverse surface slope (after peak flood) decelerates the flow and the baroclinic pressure gradient continues to push the bottom flow upriver. The baroclinic pressure gradient and the sub-surface velocity maximum greatly delay current reversal at the end of flood near the bottom. The mean flow is outward at all depths despite the intrusion of salinity on flood, because the shear on the ebb is not large enough to allow net upstream bottom flow. The dotted line again shows the Eulerian net transport per unit depth; since the Stokes drift is small, the Lagrangian transport is not noticeably different from the Eulerian transport.

This discussion of boundary layer processes allows further interpretation of the spatial variations in the tidal flow in Figures 3.15 to 3.17. The shear and phase differences in Figures 3.15a through d are largest in the lower estuary. This is the area where salinity intrusion is present on both flood and ebb and where tidal flows are strongest; the potential for development of large shears is greatest there. The largest shears and phase differences on the Clatsop Spit-Sand Island section are found at the surface in the center of the section, where the inertia of the flow is greatest. It appears, however, that some of the spatial variations in structure of the tidal flow may be due to topographic effects. Bottom topography causes along-channel changes in the density structure (e.g. between RM-6 and RM-9 in both channels) that probably cause along-channel changes in velocity profiles in this reach. Modeling results are, therefore, used to further investigate the effects of bottom topography in Sections 3.5 and 3.6.

3.3.5 Tidal Effects on Residual Circulation

It has already been argued that the vertical distribution of the mean flow is determined by the tidal circulation. At low riverflow and larger tidal ranges, a significant fraction of the total mean flow is Stokes drift compensation flow (Section 3.4.2). However, the neap-to-spring changes in structure of the mean flow occur primarily because of the neap-to-spring changes in vertical mixing that change the vertical structure of the tidal flow.

The increase in vertical mixing that accompanies the increase in

tidal range on a spring tide decreases the stratification. Decreasing tidal range decreases vertical mixing and increases stratification. Whenever the ratio of stratification to shear (gradient Richardson number) becomes large enough, vertical turbulent mixing effectively ceases. Reduction of turbulent mixing during periods of weaker tides allows large shears and increased baroclinic circulation to develop, which tend to further increase the stratification. On neap tides, particularly during the low flow season, the system goes through a transition from a relatively well-mixed to a highly-stratified, two-layered state. The salinity intrusion length also increases greatly (Section 3.6). The increasing energy level in the estuary as the tidal range increases (after the neap) reverses this process: mixing increases and salinity intrusion length decreases.

The October 1980 period provides an excellent example of these tidal monthly changes. In a period of only 8 days, the tidal range increased from less than 2 m to more than 3.4 m. Results from the two-dimensional, time-dependent, laterally-averaged model (described in detail in Hamilton 1984) show that the density structure and vertical mixing processes were greatly altered as a result (Section 3.6). Figure 3.19 shows the geometry of the channel network used in the model; Figures 3.20 and 3.21 show model results (mean salinity and velocity) for the south channel (1 in Figure 3.19) and north channel (2 in Figure 3.19) for the same neap tide period in October 1980. There is substantial upstream bottom flow at sections 2 and 3 in the south channel, but upstream bottom flow is totally absent at section 4 (RM-6.2). The model then shows another zone of upstream bottom flow between sections 5 and 8 (RM-8 to 15.5). The maximum horizontal salinity gradient is somewhat farther downstream than observed in the prototype (Section 3.6), so the upstream bottom flow does not quite extend to Tongue Point. The north channel (Figure 3.21), which starts at section 4 of the south channel (RM-6.2), shows a similar pattern. Upstream bottom flow occurs between sections 3 and 7 (about McGowan to the upstream end of Taylor Sands), considerably further upstream than in the south channel. Spring tide results show much less stratification and a shorter intrusion length of the 5 ppt salinity contour, particularly in the south channel (Figures 3.22 and 3.23), but the neap-spring differences in salinity intrusion are weaker than in the prototype (Section 3.6). Net upstream bottom flow in both the north and south channels is discontinuous; it appears in three isolated cells in the south channel.

There are two probable causes of this pattern of isolated pockets of net upstream bottom flow: pockets of unusually saline, near bottom water (Figures 3.20 to 3.23) that are associated with the junction between the north and south channels, and longitudinal changes in the vertical distribution of the mean flow. These are caused by changes in mixing resulting from changes in channel cross-section (as suggested in Ianniello 1977a,b, 1979, 1981; and Simmons 1966). Ianniello (1981) has, on the basis of theoretical calculations for the constant density case, argued that topographic holes are accompanied by divergences in transport at the bottom that will tend to deepen the hole on its upstream side and shoal it on its downstream side (just as at sections 2 to 5 in the south channel, in Figures 3.20 and 3.22). The reversed

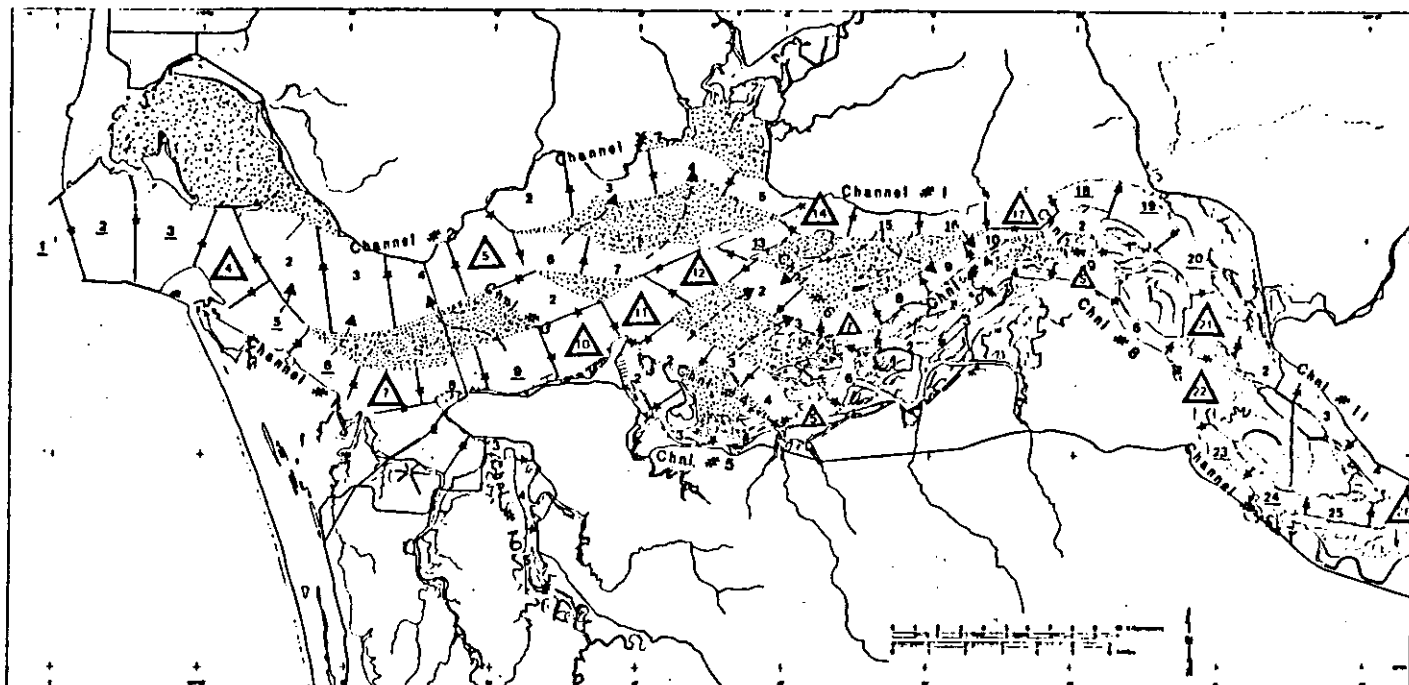


Figure 3.19 The channels and grid cells used for the schematization of the estuary. Grid cell number gives the position of elevation points, a star is the position of a transport point. Triangles denote channel junction grid points. Dashed arrows denote across barrier inter-channel connections.

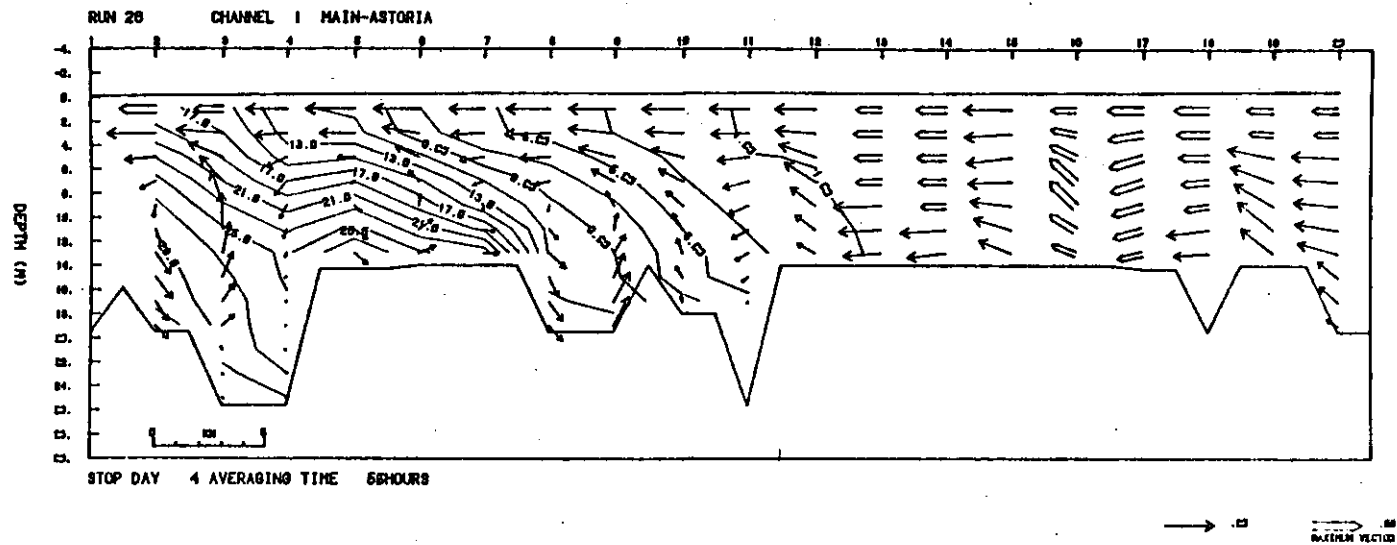


Figure 3.20. Channel 1, Neap tide period (Fall, 1980) mean currents and salinities (m sec^{-1} and ppt).

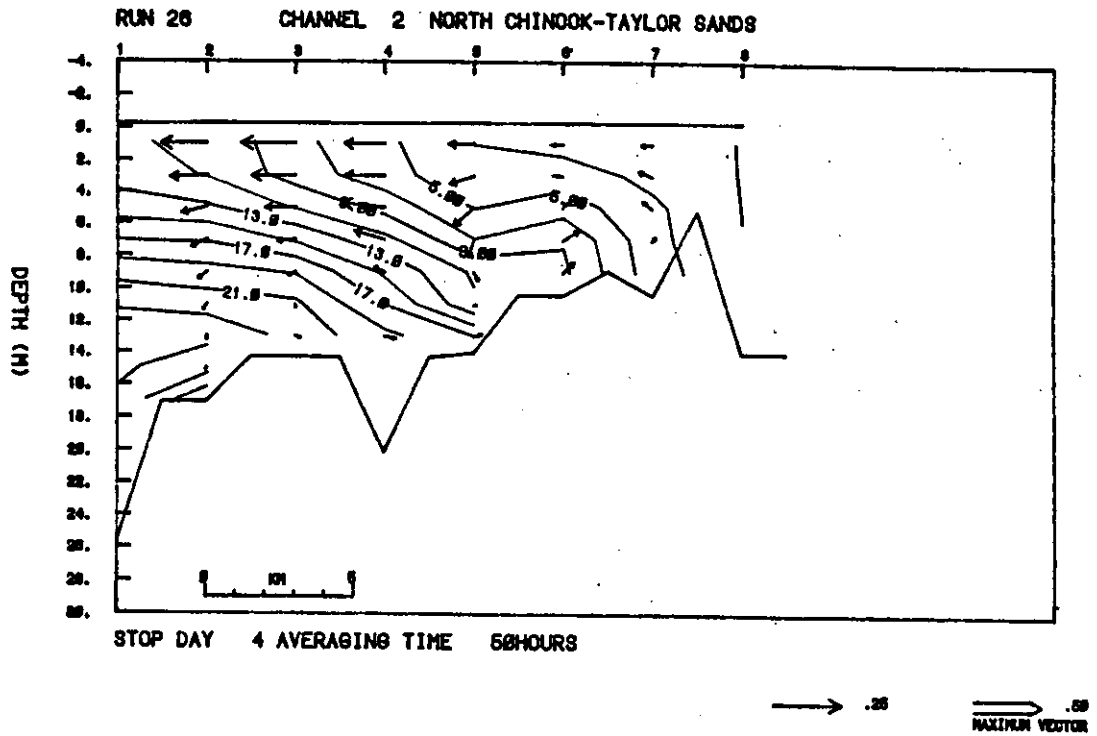


Figure 3.21. Channel 2, Neap tide period (Fall, 1980) mean currents and salinities (m sec^{-1} and ppt).

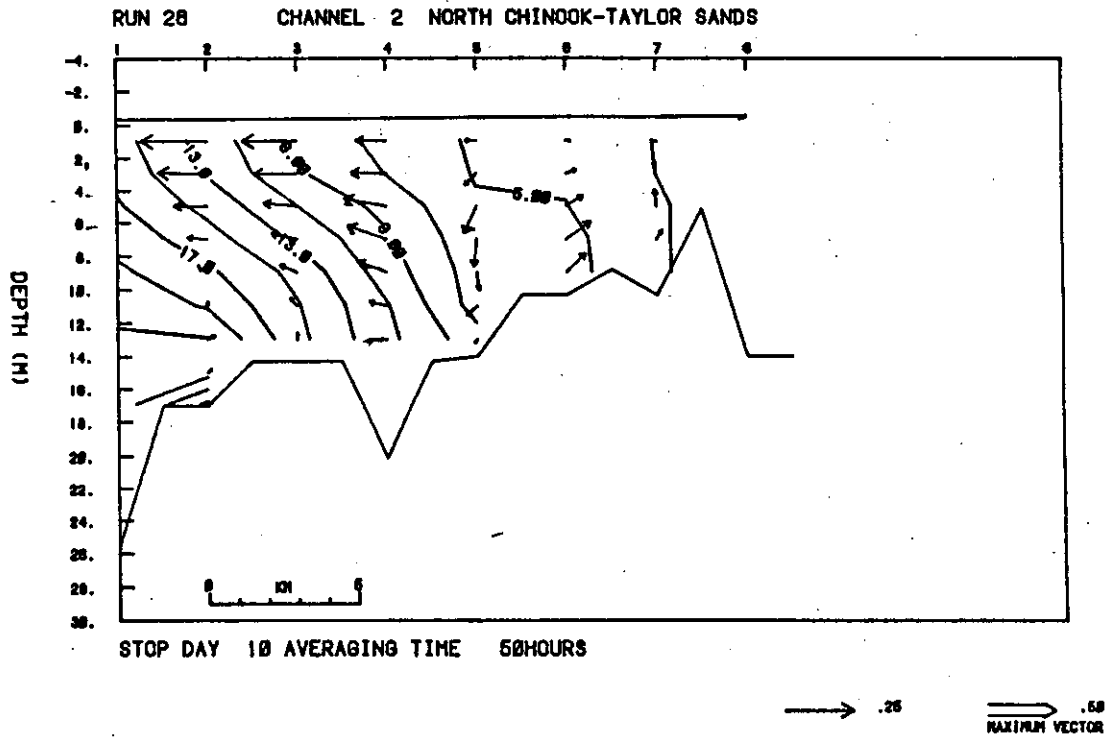


Figure 3.23. Channel 2, spring tide period (Fall, 1980) mean currents and salinities (m sec^{-1} and ppt).

salinity gradient tends to further increase the mean flow divergence. The theoretical calculations and the model predict a convergence in the bottom flow near a sill that would tend to maintain the sill (e.g., at the Upper Sands Shoal, RM-16, grid sections 9 and 10). Similar effects can also occur as a result of constrictions in breadth.

The divergences in the mean flow have important implications for sedimentary and biological processes. Suspended material tends to accumulate close to the bottom near the upstream limits of net upstream bottom flow. This accumulation is known as the turbidity maximum (Section 4.2). Multiple regions of upstream bottom flow may cause multiple turbidity maxima. The locations of these areas of upstream bottom flow change during the tidal month, as do the density structure (Section 3.6) and the concentrations of suspended materials (Section 4.2). The strength of these neap-spring changes is, in turn, dependent on the strength of the riverflow (Section 3.6.4). Finally, differences in topography and mean flow may bring about differences between the north and south channels in important sedimentary and biological processes. All of these factors may be expected to influence biological processes.

The profound effect of the sills between RM-6 and 9 in both channels on the mean flow raises the question of whether critical conditions for propagation of internal waves may occur at certain stages of the tide over the sills (or over the entrance bar). Such internal hydraulic controls have been found to exert a major influence on the density distribution (Gardner et al. 1980) in strongly stratified systems. They provide a mechanism for transfer of tidal energy into mixing that is often localized in time and space, but repeatable from tidal cycle to tidal cycle (Gardner et al. 1980). Neap-to-spring variations could be expected, because stratification and shear vary during the tidal month. The existence of such internal hydraulic controls might strongly affect the vertical structure of both the tidal and the mean flow. This is another possible explanation of the along-channel variations in the tidal (Section 3.3.4) and the mean flow.

Several qualifications are needed in interpreting the model results. First, although the vertical velocities in Figures 3.20 to 3.23 look very large, the vertical distortion in these figures is about 5500x; the velocity vectors are in fact very nearly horizontal. Second, the horizontal grid spacing is large (3 km) in the main channels in the model; thus the model provides a fairly simple approximation of the topography of the system. Determination of shoaling patterns and delineation of areas where turbidity maxima might be expected would probably require a closer grid spacing. However, the model prediction of strong outward transport at grid section 4 is supported by current meter data (Section 3.7). Third, it is possible that the reversals of salinity gradient near the bottom are artifacts caused by the channel schematization and/or numerical mixing effects in the model. Fourth, significant cross-channel variations occur in nature (Figure 3.17) that are averaged out by the model; these are strongest in the lower estuary. Fifth, conclusions concerning shoaling and sediment transport cannot be drawn from the mean flow alone. Flood-to-ebb differences in

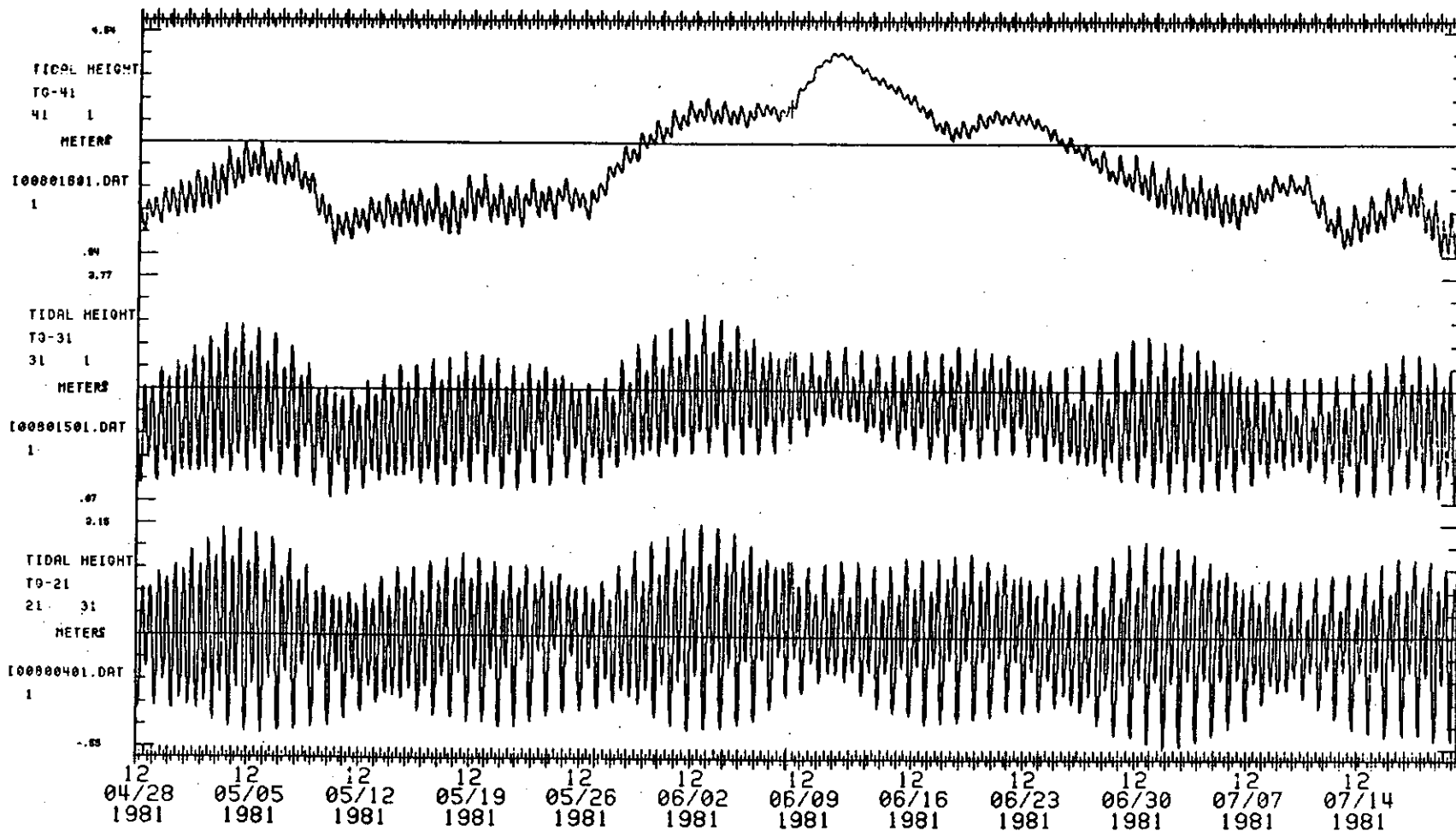


Figure 3.24. Tidal heights in m at (from bottom to top) Tongue Pt. (RM-18), Wauna (RM-42) and Columbia City (RM-83) during the June 1981 spring freshet. The highest flows occurred on June 10 and 11. Tides at upriver stations were suppressed by the high runoff for most of May and June.

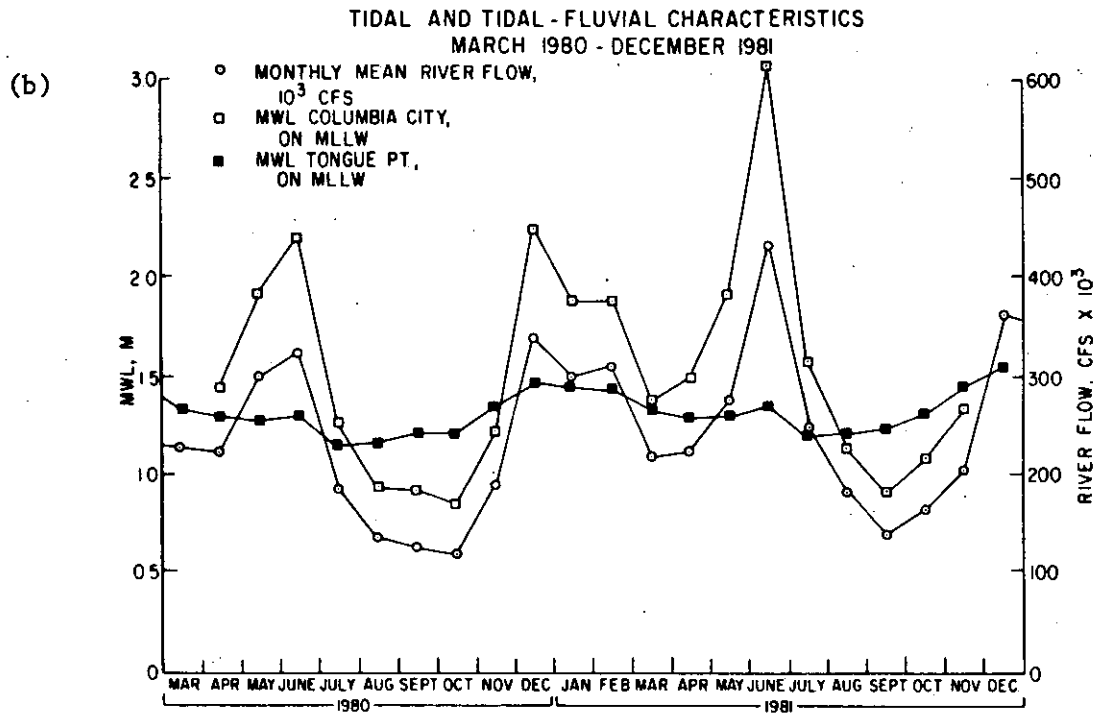
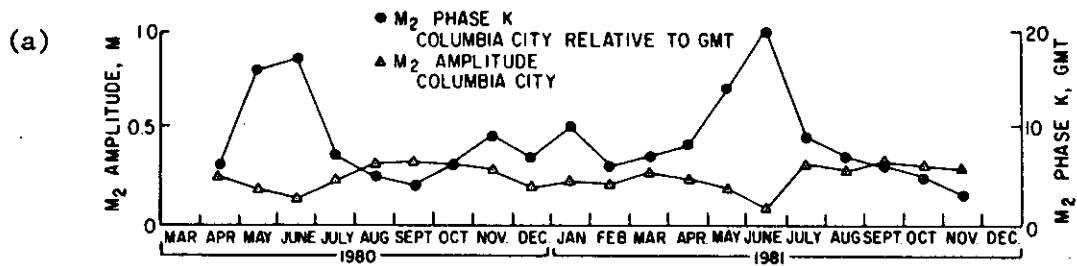


Figure 3.25. Tidal-fluvial effects. M₂ phase and amplitude at Columbia City (RM-83) (a), and monthly mean flow and MWL at Tongue Pt. (RM-18) and Columbia City (b) from March 1980 to December 1981.

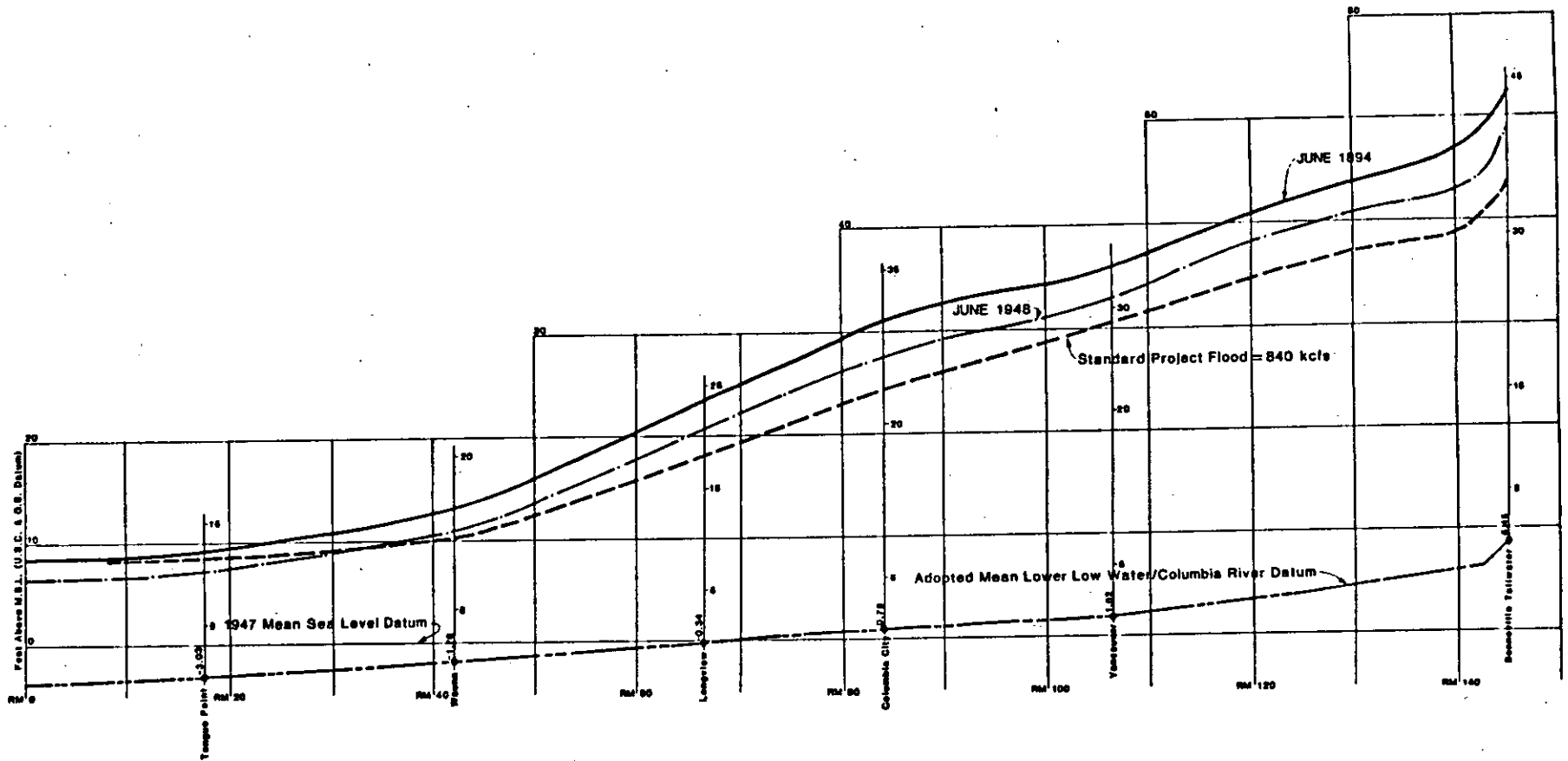


Figure 3.26. The effect of river flow on river stage. The lower line defines the slope of CRD. (Provided by the U. S. Army Corps of Engineers, Portland District.)

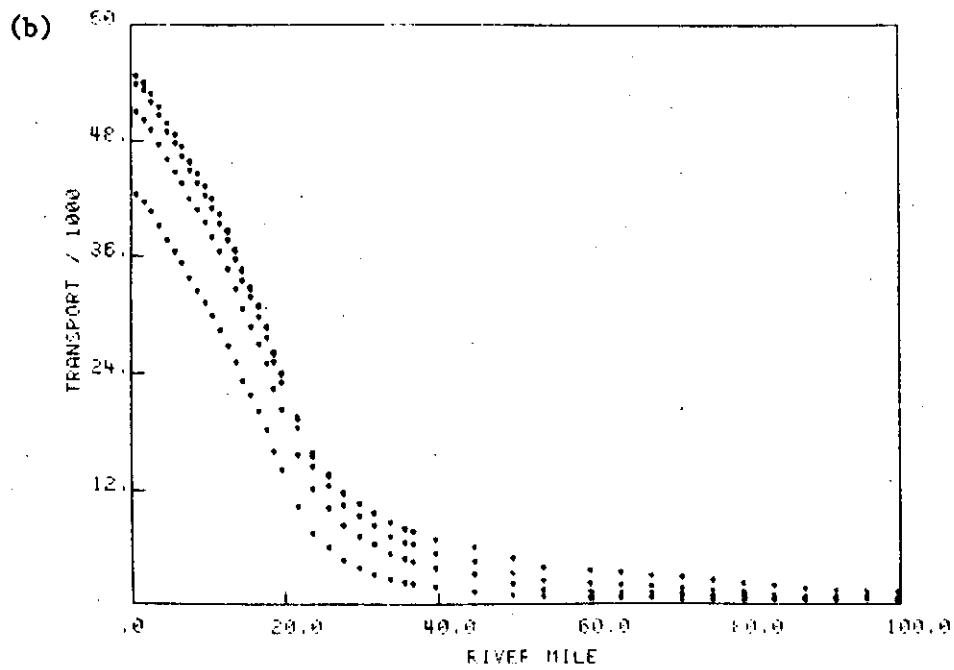
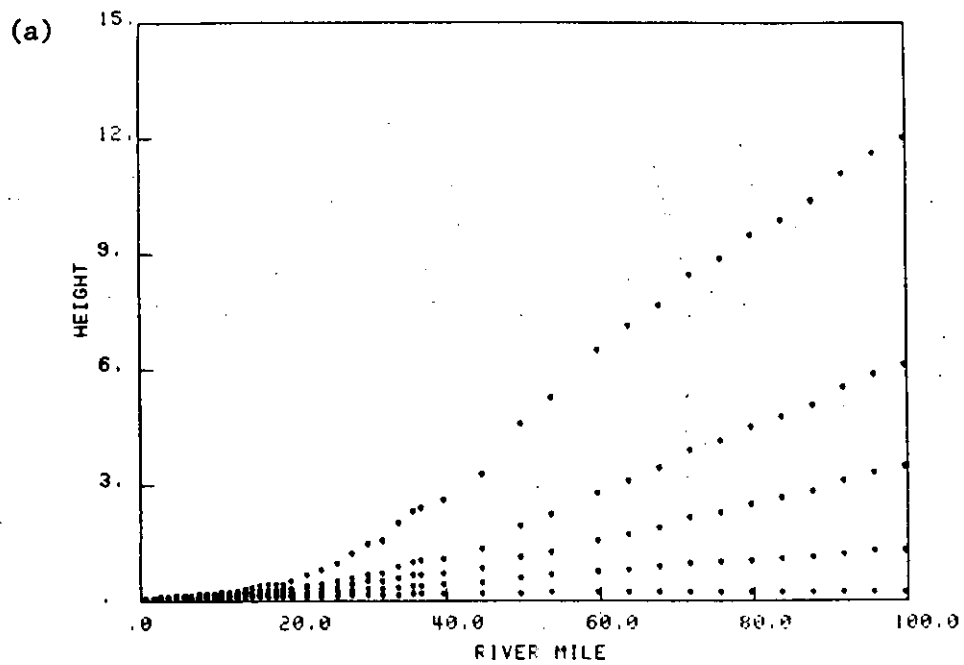


Figure 3.27. Predicted tide stage in meters (a), and tidal transport amplitude in $10^3 \text{ m}^3 \text{ sec}^{-1}$ (b) as a function of river mile for river flow rates (bottom to top) of 0, 100, 300, 500, and 1,000 kcfs (0, 2,831, 8,495, 14,159, and $28,317 \text{ m}^3 \text{ sec}^{-1}$) and a 2.0 m tidal range.

the tidal flow are clearly important, and sediment transport is a strongly non-linear phenomenon. Sediment transport should therefore be considered on the basis of the average of responses to the the full, time-dependent flow, not merely to the response to the mean flow.

Despite these qualifications, two important conclusions may be drawn: the change in energy available for mixing during the tidal month is large enough that neap-spring changes in mean flow are of substantial physical and biological importance; and the neap-spring differences are most important under low flow conditions, when a transition in density structure from well-mixed to stratified can take place during the tidal month.

3.4 TIDAL-FLUVIAL INTERACTIONS

Both model results and data have been used to examine the interaction between the riverflow and the primary tidal circulation.

3.4.1 Observations

There is a gradual change in the relative importance of riverine and tidal effects with river mile. The surface elevation changes at Tongue Point are dominated by the tides and atmospheric effects, and the riverflow has little effect on the tidal properties. The surface elevation at Columbia City (RM-83) is dominated by the riverflow, and tidal properties there are radically altered by changes in riverflow. June 1981 provides the best available example of the system response to a freshet. Flow was high for all of June 1981 and there was a sharp freshet between June 9 and 13, 1981, with peak flows of 560 kcfs (about $15,900 \text{ m}^3 \text{ s}^{-1}$; Figure 2.9). Figure 3.24 shows (from bottom to top) the response of the tidal heights at Tongue Point (RM-17.6), Wauna (RM-42), and Columbia City (RM-83) to this freshet. Larger freshets affect the tidal properties in the tidal-fluvial part of the system even more strongly; this is clear from Figures 3.8 to 3.10. The seasonal cycle of tidal-fluvial interactions is shown in Figure 3.25, which shows monthly-mean tidal and fluvial properties over a 20-month period. The mean water level at Columbia City closely follows the riverflow; it was 86 cm higher in June 1981 than in June 1980. The M2 amplitude at Columbia City in June 1980 was 14 cm, but only 9 cm in 1981. These are, respectively, 45 and 29% of the low flow amplitude of 31 cm. The tide is also delayed in reaching Columbia City by about 25 to 30 minutes under high flow conditions.

The tidal properties at Tongue Point show a different pattern. Mean water levels were highest in December of both years. While mean water level at Tongue Point is certainly influenced by the riverflow, continental shelf oceanography and atmospheric forcing predominate (Chelton and Davis 1982). The M2 phase and amplitude at Tongue Point are scarcely affected by the riverflow.

The increase in riverflow has at least three important effects on the dynamics of the system. First, the surface slope is increased, so that more water can be discharged. That is, surface elevations are much more strongly affected upriver than in the estuary (Figure 3.26).

The flood of 1894 (1,250 kcfs; $35,400 \text{ m}^3\text{sec}^{-1}$), for example, caused water levels of about 10 m above CRD (Columbia River Datum) at RM-100. Second, the increased adverse pressure gradient pushes the salinity intrusion downriver; this strengthens the horizontal and vertical salinity gradients and thus the baroclinic circulation. Third, the non-linear nature of bottom friction means that the friction on the tidal flow is greatly increased when the riverflow increases. It is this effect that explains the change in M2 amplitude at Columbia City, more than the increase in surface slope or effective depth.

3.4.2 Model Results

One of the primary purposes of the one-dimensional, harmonic model was to investigate, in a systematic manner, the interaction of the tides and the riverflow. Although the diurnal constituents cannot conveniently be included directly in the model, multiple tidal constituents and large range tides can be simulated by using the combined amplitude of two or more semidiurnal constituents. Thus, a spring tide (M2 and S2 in phase) can be approximated by using as a boundary condition at the mouth M2+S2.

To systematically investigate tidal-fluvial interactions, the one-dimensional model was run with riverflows of 0, 100, 300, 500, and 1000 kcfs (0, 2, 820, 8,500, 14,160, and $28,320 \text{ m}^3\text{sec}^{-1}$) and tidal amplitudes of 0.5, 1.0, 1.5, and 2.0 m (tidal ranges of 1.0, 2.0, 3.0, and 4.0 m); this encompasses all likely tidal ranges and riverflows. Calibration of the model and detailed results are discussed in Jay (1984). Stage and transport as a function of river mile are shown for all 5 riverflows in Figures 3.27a and b for a tidal range of 2.0 m. Tidal prism and Stokes drift transport at the mouth are given in Tables 3.3 and 3.4.

The variations of tidal height amplitude and tidal transport at the upriver stations with riverflow and tidal range (Figures 3.8 to 3.11 and 3.27b) show the effects of friction and the geometry. Increasing the tide at the entrance does not cause a proportional effect at Tongue Point and beyond (Figures 3.11a and b), because of greatly increased friction on larger range tides. Higher riverflow also considerably increases the frictional damping. The decrease in tidal height amplitude with increasing riverflow is much more severe upriver; the decrease in tidal amplitude is only about 20% at Tongue Point between 0 and 1000 kcfs (0 and $28,320 \text{ m}^3\text{sec}^{-1}$) but is more than 75% at Columbia City. These phenomena will be further discussed in Section 3.5.

The tidal transport drops off by 60 to 80% in the first 20 river miles (Figure 3.27b) because the width and tidal range both decrease upriver. Increasing the riverflow from 0 to 1000 kcfs (0 to $28,320 \text{ m}^3\text{sec}^{-1}$) decreases the transport at the mouth (the total tidal prism) by about 25%. The tidal transport at the mouth decreases with increasing riverflow, because high riverflow decreases the tidal range upriver. As the riverflow increases, flood transports (tidal transport - riverflow transport) and ebb transports (tidal transport + riverflow) diverge. More and more of the tidal prism is satisfied by the holdup of

riverflow. At the river mile where the flood transport is zero, the tidal transport (averaged over half a tidal cycle) is exactly balanced by riverflow. No net upriver transport occurs during the six lunar hours of flood, and the ebb transport is twice the tidal transport. The tidal prism upstream of this point is entirely filled by holdup of riverflow.

It is useful for many purposes to compare riverflow volume during a 12.42 hour tidal cycle to half-tidal cycle tidal transport volumes. The ratio of tidal transport volume over half a tidal cycle (tidal transport amplitude $\times 2/\pi \times 6.21$ solar hrs) to freshwater flow volume over a 12.42 hr tidal cycle is given in Table 3.3. The ebb/flood transport volume is the tidal transport volume \pm (the riverflow volume/2). A ratio of 0.5 in Table 3.3 corresponds to the condition where the riverflow volume over half a tidal cycle is equal to the tidal transport; the tidal prism is entirely satisfied by the holdup of riverflow. Except under high riverflow and low tidal range, the tidal exchange is considerably larger than the riverflow volume. Included in Table 3.4 is the Stokes drift volume ratio; this inward Stokes drift flow volume is very nearly compensated during each tidal cycle by the Stokes drift return flow. The Stokes drift is large relative to riverflow only at low riverflow levels and large tidal ranges, but under these conditions, the Stokes drift compensation flow is a significant fraction of the total outflow.

3.5 ENERGY CONSIDERATIONS

Energy for circulatory processes is provided by the tides and river flow and is ultimately lost to bottom friction and mixing of water masses. Determination of the spatial distribution of these processes by calculation of an energy budget provides further insight into tidal-fluvial interactions. The energy budget is also important to the interpretation of the modern and historical geologic processes in Chapters 4 and 5.

3.5.1 Formulation of the Energy Budget

The M2 tide accounts for most (more than 70%) of the total tidal energy that enters the system from the ocean, and the major semidiurnal constituents (M2+N2+S2) account for more than 80% of the total tidal energy input. Most of the energy available for circulation can, therefore, be accounted for by considering only the semidiurnal tide and the river inflow.

The riverflow in the system is sufficiently large that it dominates the energy budget in the tidal-fluvial part of the system. No estuarine energy budget that included riverflow was found in the oceanographic literature so it was necessary to develop such an energy budget. Consider a longitudinal section of estuary (e.g. from the mouth to some arbitrary river mile). The energy budget for this section of the system is found by multiplying the vertically and laterally integrated along-estuary equation of motion by the along-estuary velocity and the density. Integration with respect to longitudinal distance over some finite length of the estuary then yields an energy equation. This energy equation and the errors involved in calculation of the energy

Table 3.3. Tidal prism (km^3) and ratio of tidal prism to riverflow volume.

Tidal Range (m)	River Flow (kcfs)					
	0	100	300	500	1,000.	
	(kcfs)	0	2.83	8.50	14.2	28.30
	(km^3 / tidal [†] cycle)	0	.127	.38	.633	1.27
1.0	prism	0.44	0.44	0.41	0.37	0.29
	ratio	-	3.5	1.1	0.6	0.2
2.0	prism	0.79	0.79	0.78	0.74	0.62
	ratio	-	6.2	2.0	1.2	0.5
3.0	prism	1.12	1.12	1.11	1.08	0.96
	ratio	-	8.8	2.9	1.7	0.8
4.0	prism	1.44	1.44	1.43	1.41	1.29
	ratio	-	11.3	3.8	2.2	1.0

[†]One tidal cycle = 12.42 hours

Table 3.4. Stokes drift volume (km^3) and ratio of Stokes drift volume to riverflow volume.

		River Flow (kcfs)	0	100.	300.	500.	1,000.
		(kcms)	0	2.83	8.50	14.2	28.30
		($\text{km}^3/\text{tidal cycle}^\dagger$)	0	.127	.38	.633	1.27
Tidal Range (m)							
1.0	volume		.015	.015	.013	.012	.010
	ratio		-	.118	.035	.019	.008
2.0	volume		.053	.053	.050	.044	.037
	ratio		-	.417	.130	.070	.029
3.0	volume		.106	.108	.104	.097	.080
	ratio		-	.853	.275	.153	.062
4.0	volume		.174	.176	.174	.165	.137
	ratio		-	1.385	.459	.260	.108

[†]One tidal cycle = 12.42 hours

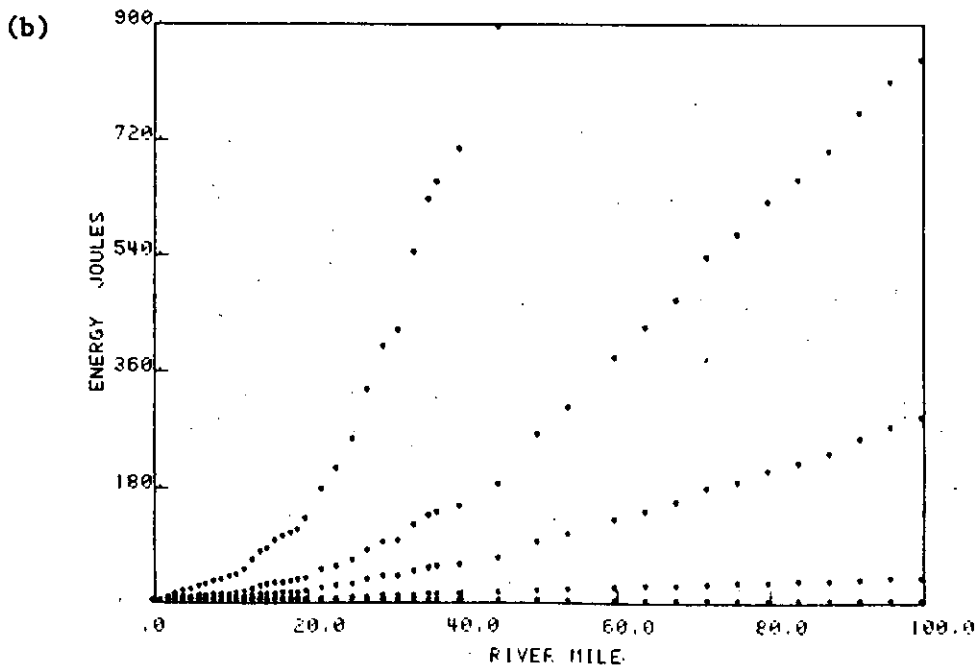
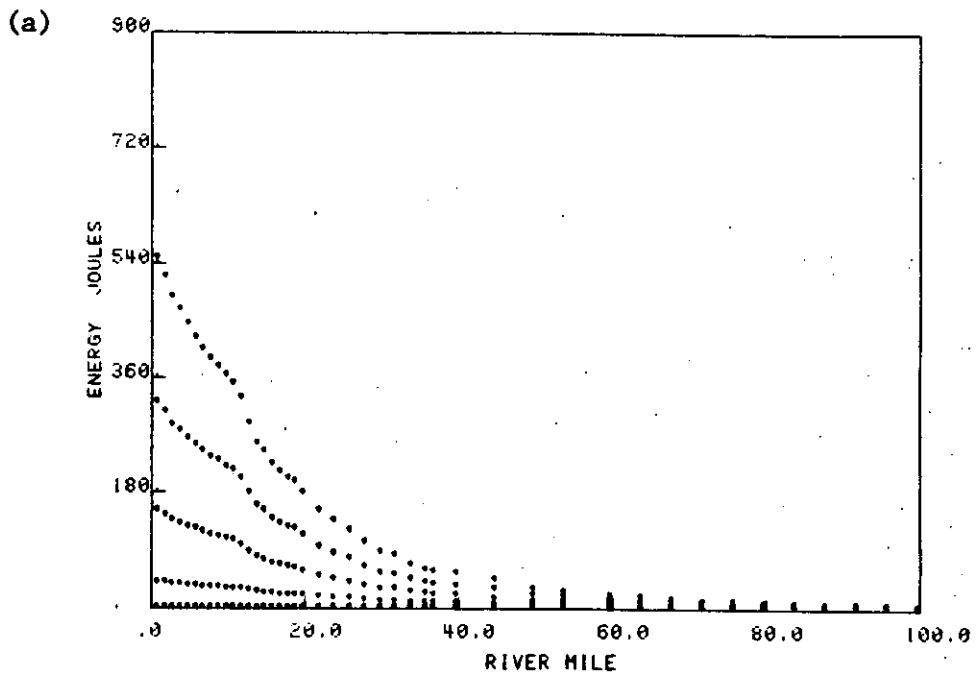


Figure 3.28. Model predictions of (a) tidal energy flux, and (b) mean flow potential energy flux, both in 10^6 joules, as functions of river mile for (a) (bottom to top) tidal ranges of 0, 1, 2, 3, and 4 m, and (b) river flow rates of 0, 100, 300, 500, and 1,000 kcfs (0, 2,832, 8,495, 14,160, and 28,320 $\text{m}^3 \text{sec}^{-1}$).

budget are discussed in Jay (1984). The detailed analysis shows that a simplified energy equation can be defined that includes all the terms that are important in the Columbia River Estuary:

$$\begin{aligned}
 & \Delta \text{ M2 energy flux} + \Delta \text{ potential energy flux of mean flow} \\
 & + \Delta \text{ mean flow kinetic energy flux} \\
 & + \Delta \text{ tidal/mean flow kinetic energy flux} \\
 & = \text{dissipation (tidal + mean flow + tidal/mean flow)},
 \end{aligned}
 \tag{1}$$

where the Δ indicates the difference between the flux into one end and out at the other end of a section of the estuary. All terms in eq (1) may be readily evaluated from the one-dimensional model described in Section 3.4.

There is a close connection (Section 3.1.3) between the M2 tidal energy flux (Figure 3.28a) entering any section of the estuary and the Stokes drift. The Stokes drift and the associated tidal energy input are large in systems with progressive or partially progressive tides. This occurs because the flow is deeper on flood than on ebb. This flood to ebb difference in elevation causes a net inflow (the Stokes drift) and an energy flux. The energy flux is simply the potential energy difference between the flood and ebb flows that is caused by the difference in surface elevation (and therefore potential energy) of the flood and ebb flows. The stronger the dissipation, the more progressive the wave is, and the greater the elevation difference and energy transport into the system.

The analogous potential energy term for the riverflow arises from the river slope; as the water flows downhill, gravitational potential energy is released. This term is largest in the upriver areas and increases sharply with increasing riverflow (Figure 3.28b). The mean flow kinetic energy flux term results from the decrease in flow velocity of the mean flow in the downstream direction as the cross-sectional area increases. The dissipation is the loss of energy caused by friction on the bottom and sides of the estuary channels. It is associated both with the form drag of bedforms, shoals, curves, etc., and skin friction of the sediment itself.

To summarize the balance of eq (1), both the tides and riverflow contribute potential energy and dissipation terms, but only the mean flow contributes a kinetic energy flux term. Interactions between the tidal and mean flow occur both in the dissipation and kinetic energy flux terms. The interaction terms in the dissipation occur because the dissipation is proportional to $[|U| U^2]$, where $U = \bar{u} + U'$, \bar{u} is the mean flow, U' the tidal velocity, $| \cdot |$ indicates the absolute value, and the brackets indicate a tidal cycle average. The tidal dissipation arises from $[|U'| U'^2]$, the mean flow dissipation from $[|\bar{u}| \bar{u}^2]$, and the interaction dissipation from mixed terms. The kinetic energy flux is also cubic in U , but without the absolute value. Odd powers of the tidal velocity average to zero over a tidal cycle; thus, there is no purely tidal kinetic energy flux term and only one interaction term.

The flood-ebb difference in energy dissipation can be seen as follows. On flood, the river and tidal flow are in opposite directions.

Thus, the flood dissipation is given by $||U'| - |\bar{u}|| (|U'| - |\bar{u}|)^2$. On ebb tide, the river and tidal flow are in the same direction, and the dissipation is given by $(|U'| + |\bar{u}|)^3$. The ebb dissipation will be substantially larger than the flood dissipation, if

$$\frac{|\bar{u}|}{|U'|}$$

is substantial.

3.5.2 Neap-spring Effects

The above formulation of the energy budget provides a useful framework to consider neap-spring variations. Consider the simplest possible case, in which the riverflow is negligibly small. The energy budget then contains only two terms, tidal input and dissipation. The tidal energy coming into the system is proportional to the Stokes drift at the entrance. Since the tidal transport is proportional to the tidal range, the tidal energy flux varies with the square of the tidal range at the entrance. The dissipation in the estuary varies with tidal range cubed. It is not immediately obvious how the tidal energy input and dissipation remain in balance as the tidal range varies during the tidal month, because they vary with different powers of the tidal range. The tidal model (Figures 3.11a and b) and the observed spatial distribution of the semidiurnal constituent amplitudes (Table 3.1) show that the balance between dissipation and the tidal energy flux is maintained by the changes in the spatial variation of tidal range in the estuary, as a function of the tidal range at the mouth. The tide is essentially composed of phase and amplitude modulated semidiurnal and diurnal tidal waves. The amplitude and phase modulation is accounted for in a harmonic analysis by introduction of various tidal constituents whose frequencies are determined from astronomical considerations. It was determined in Section 3.3 that the semidiurnal tidal wave is described primarily by three tidal constituents, M2, S2 and N2, that spring-neap tides were described by $M2 \pm S2$, that perigean-apogean tides were described by $M2 \pm N2$, and that S2 and N2 both decrease more rapidly in the upriver direction than does M2 (Table 3.1). The more rapid decrease of N2 and S2 can now be interpreted in a new light. The spring tide wave is described by $M2+S2$. The much greater dissipation on the spring tide in the interior of the estuary requires that the spring tide increase in tidal amplitude inside the estuary be less than proportional to that at the entrance. The more rapid decrease upriver of S2 than M2 provides exactly that response. The neap tide wave ($M2-S2$) is less rapidly damped than M2 alone or $M2+S2$. The situation is similar with $M2+N2$ and $M2+N2+S2$ and other constituent combinations.

Table 3.5. Total tidal and mean flow potential energy fluxes and total dissipation, 10^6 Joules

		<u>RIVER FLOWS</u>				
		0	100	300	500	1,000
Tidal Range (m)	(kcfs)	0	100	300	500	1,000
	(m^3sec^{-1})	0	2,832	8,395	14,160	28,320
1.0	Tidal Energy Flux	40				
	Potential Energy Flux	28				
	Total Dissipation	67				
2.0	Tidal Energy Flux	150	149	141	127	105
	Potential Energy Flux	0	35	284	824	3,318
	Total Dissipation	150	181	418	947	3,461
3.0	Tidal Energy Flux		319			
	Potential Energy Flux		42			
	Total Dissipation		354			
4.0	Tidal Energy Flux	549	546	540	505	422
	Potential Energy Flux	0	50	300	816	3,261
	Total Dissipation	549	585	811	1,283	3,659

3.5.3 Energy Budget Calculations

The energy budget was evaluated using the one-dimensional tidal model for selected cases in the same series of riverflows and tidal ranges used in Section 3.4; the riverflows were 0, 100, 300, 500 and 1000 kcfs (0, 2,832, 8,345, 14,160, 26,320 m^3sec^{-1}), and the tidal ranges were 1.0, 2.0, 3.0 and 4.0 m. These results are summarized in Table 3.5, which shows the total tidal energy flux, total mean flow potential energy flux, and total dissipation for the entire system for the various cases. It is evident from Table 3.5 that the largest energy fluxes are associated with the large tides and riverflows, and that major freshets provide by far the largest energy fluxes. The total dissipation for a 1,000 kcfs (28,320 m^3sec^{-1}) freshet is about 6 times that for the largest reasonable tide of 4 m. This very large mean flow potential energy flux is the result of the high river stage that accompanies floods; most of this potential energy does not reach the

estuary, however, because it is lost to dissipation upstream of RM-20.

Examination of the model results shows that not all of the terms included in eq. (1) are important, only the M2 tidal energy flux, the mean flow potential energy flux, and the tidal riverine dissipations need be considered here. We can, therefore, approximate the energy balance of eq (1) to about 10% as:

$$\begin{aligned} &\Delta \text{ M2 tidal energy flux} \\ &+ \Delta \text{ mean flow potential energy flux} \\ &= \text{mean flow dissipation} \\ &+ \text{tidal dissipation} \end{aligned} \quad (2)$$

Consideration of the spatial distribution of the various terms allows further simplification. It can be seen from Figures 3.28a and b, which show the tidal energy flux and the mean flow potential energy flux as a function of river mile for various riverflows and tidal ranges, that tidal energies are generally large only downriver of RM-20 and riverine terms large only upriver of RM-20. Thus, in the high-energy cases (i.e., riverflow and/or tidal range large) which are important for sediment transport, the energy balance at most locations in the system is either:

$$\begin{aligned} &\Delta \text{ tidal energy flux} \\ &= \text{tidal dissipation (in the estuary)} \end{aligned} \quad (3)$$

or

$$\begin{aligned} &\Delta \text{ mean flow potential energy flux} \\ &= \text{mean flow dissipation (in the fluvially-dominated section)} \end{aligned} \quad (4)$$

Eq (3) is the energy balance for a strongly-tidal estuary without major riverflow, and eq (4) is the expression for a non-tidal river. Eq (2) is necessary only in the tidal-fluvial reaches (RM-20 to RM-50, depending on the riverflow). Thus, the energy budget shows the same division of the system into estuarine, tidal-fluvial and fluvial reaches that is found in many other aspects of the physics, geology, and biology of the system.

Total dissipation (the sum of all terms on the right hand side of eq (1)) and energy inputs (the sum of all terms on the left hand side of eq (1)) are shown as a function of river mile for three typical cases in Figures 3.29a, b and c. Three points should be made in regard to these figures. First, the model does not conserve energy perfectly. Dissipation and energy inputs do not balance, although they balance within 2% at most sections and within 18% in the worst cases. Scaling analyses suggest that terms not evaluated are small, and that the errors result from approximations used to calculate the non-linear, convective acceleration term in the model (Jay 1984). Second, there is a broad area of minimum energy between about RM-18 and RM-30. As is also clear from Figures 3.28a and b, this reach of the estuary is never exposed to high energy fluxes, even in the largest floods. This relatively low energy level may account for the formation of the islands of Cathlamet Bay. The implications of this energy minimum are discussed further in Sections 4.5 and 5.4.

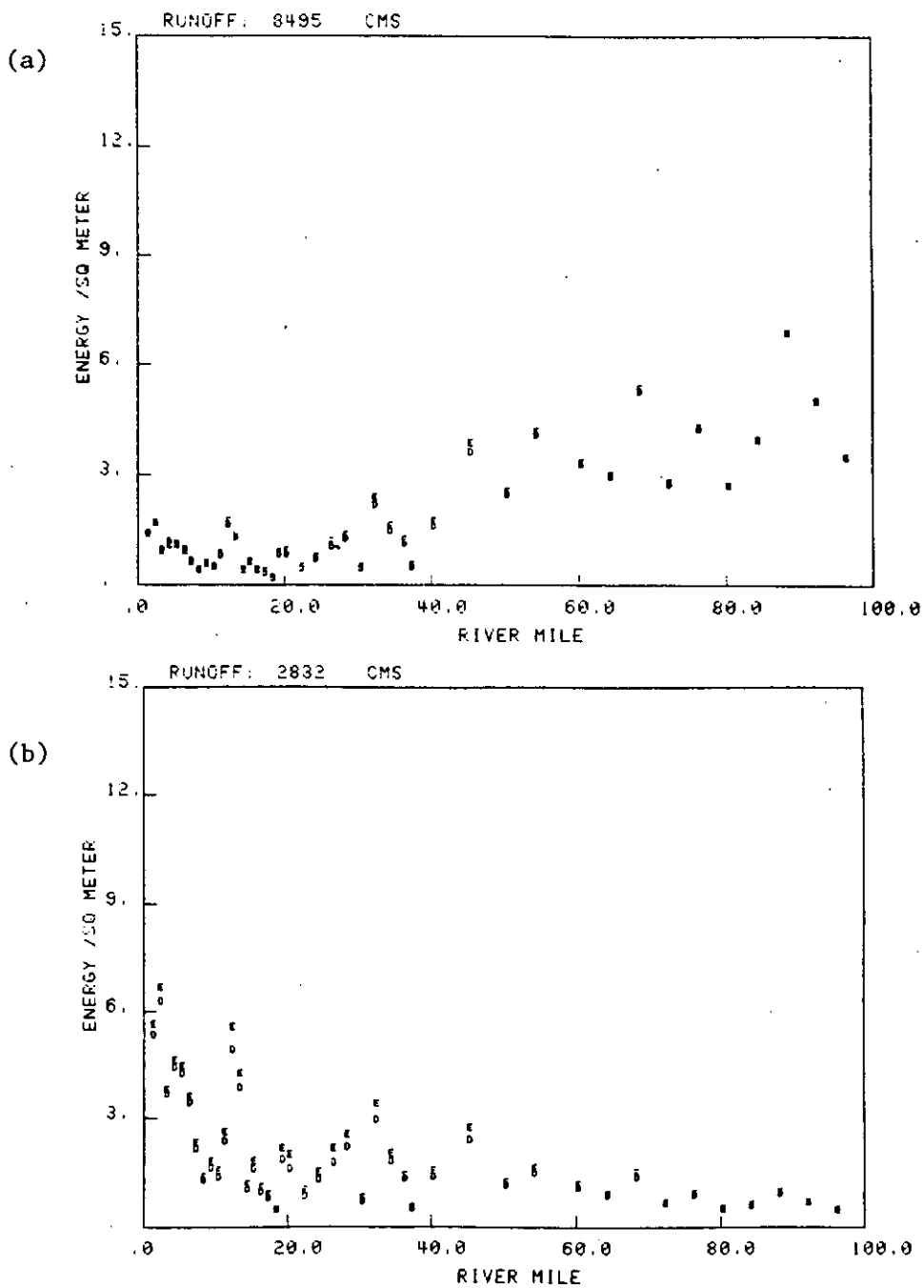


Figure 3.29. Model predictions of total energy flux unit area (E) and dissipation/unit area (D) both in joules m^2 , as a function of river mile for (a) tidal range of 2 m and river flow of 300 kcfs ($8,495 m^3 sec^{-1}$), (b) tidal range of 4 m and river flow of 100 kcfs ($2832 m^3 sec^{-1}$), and (c) tidal range of 4 m and river flow of 500 kcfs ($14,160 m^3 sec^{-1}$). Imbalances between D and E indicate errors in the model. The present annual maximum energy level corresponds roughly to (c); note energy minimum at RM-18 to RM-30.

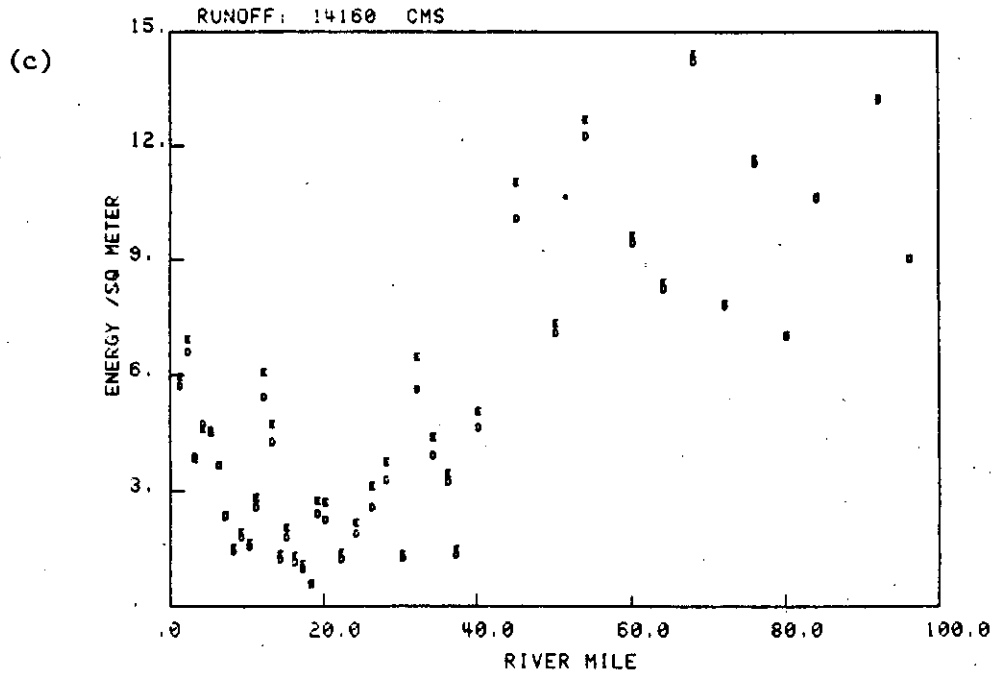


Figure 3.29 (continued).

Third, there are distinct maxima and minima in the dissipation vs. river mile curves (Figures 3.29a,b, and c). The dissipation maxima correspond to shallow sections of the estuary. In most cases, a distinct shoal in the channel can be observed that corresponds to each maximum, e.g., the inner tidal delta at RM-2, lower Desdemona Shoal between RM-6 and RM-9, Flavel Bar at RM-12 to RM-13, etc. It may initially seem paradoxical that a maximum of dissipation should correspond to a shoal. But considered from the point of view of a sediment particle moving downstream, a dissipation maximum is first (as the particle reaches the upstream side of the maximum) a reach of increasing energy, then one of decreasing energy. Thus, at least in the fluvial part of the system, where sediment is generally moving downriver, the downstream side of a dissipation maximum (topographic high) might correspond to an area of deposition, as would the upstream side of a dissipation minimum (topographic low). This corresponds to the convergences and divergences in the mean flow that are also associated with topographic highs and lows, discussed in Ianniello (1979, 1981) and Section 3.3. Salinity gradients in the estuary proper greatly complicate sedimentary processes, and this simple model is not alone adequate to explain processes there. The density structure is therefore considered in the next section.

3.6 THE DISTRIBUTIONS OF SALINITY AND MEAN FLOW

Previous sections have considered the tidal and mean flows from a dynamical point of view. In this section the distributions of salinity and the mean flow in the major channels are considered in more detail, because of their importance to both physical and biological processes. The salinity varies daily, tidal monthly, and seasonally; it is necessary to consider all three time scales. Seasonal average salinity distributions were compiled for the high and low flow seasons, using all available (1980 and 1981) time-series data. Salinity intrusion during spring-to-neap cycles was examined for low riverflow (October 1980), extreme low flow (model results only), and moderate flow (Hamilton 1984). High flow periods in June 1959 and June 1981 were also analyzed. Detailed results are given in Jay (1982, 1983, 1984) and Hamilton (1984). Salinity intrusion into peripheral bays is considered in Section 3.8.

The salinity distribution was determined from time-series of Aanderaa current meter salinity (with available profile data used as appropriate; Jay 1984) and from a two-dimensional (laterally-averaged), time-dependent, finite-difference model (Hamilton 1984). The use of current meter data to produce salinity sections provides synopticity not usually available with profile data and allows assessment of temporal variability. The wide spacing of current meter moorings, however, renders tentative interpretations based only on current meter results. The uncertainty is greatest at the surface, where the salinity is highly variable and no current meter data are available. Cross-channel variability, caused by channel curvature and the earth's rotation, also introduces errors that are probably greatest at and below RM-6, where the channel is wide. The two-dimensional model provides excellent temporal and superior spatial coverage and the ability to predict conditions not observed, but also fails to resolve

cross-channel variability. Since it has proven difficult to reproduce the observed neap-spring variations in density structure with the model, the model results are used here to augment, rather than replace, the field data.

The mean flow varies primarily with riverflow and tidal range (Section 3.1.3). It was not practical to contour current meter mean flow results, because of the complex dependence of the mean flow on bottom topography (e.g., Figures 3.20 to 3.23). The analysis of mean flow is therefore based entirely on model results. These plots are of the Eulerian mean (mean flow at a point); plots of Lagrangian mean flow (mean flow following a particle) have not been produced. The one-dimensional model shows that the Stokes drift is less than 10 cm sec⁻¹ under most conditions, and that it is small compared to the Eulerian flow at most locations. The Lagrangian flow (Eulerian flow plus Stokes drift) will therefore closely resemble the Eulerian flow plots presented here, except under low flow, large tidal range conditions, when the Stokes drift is a significant fraction of the total Lagrangian flow (Table 3.4).

3.6.1 Seasonal-average Salinity Distributions

All available data for March 25 to October 31, 1980, and April 30 to October 31, 1981, were used to construct high and low flow seasonal mean, minimum, and maximum salinity distributions for the north and south channels. The seasonal mean flow for the high flow season was about 310 kcfs (8,800 m³sec⁻¹); that for the low flow season was about 155 kcfs (4,400 m³sec⁻¹). The winter salinity distribution is not presented because insufficient winter data are available.

Many biological processes have time scales of weeks to months and may be expected to respond to the seasonal average salinity. The analysis of Section 3.1, however, emphasized the importance of non-linear processes in maintaining the circulation and salinity distributions. Many biological processes are undoubtedly also non-linear. The response of a non-linear process to average conditions is not likely to be the same as the average of the (non-linear) response to the series of individual states that form the average conditions. Great care should, therefore, be exercised in drawing conclusions concerning both physical and biological processes from the average salinity distributions.

The High Flow Season

Figures 3.30a and b and 3.31a and b show the high flow (about 310 kcfs or 8,800 m³sec⁻¹) season maximum and mean salinity distributions for the south and north channels, respectively. No minimum salinity plots are shown because the salinity is known (Section 3.6.3) to go to zero above RM-2 on the ebb under spring tide, freshet conditions, although this condition was not actually observed during the 1980-81 period.

The mean salinity plots for both channels for the high flow season show the influence of the sills between RM-6 and RM-9 and substantial

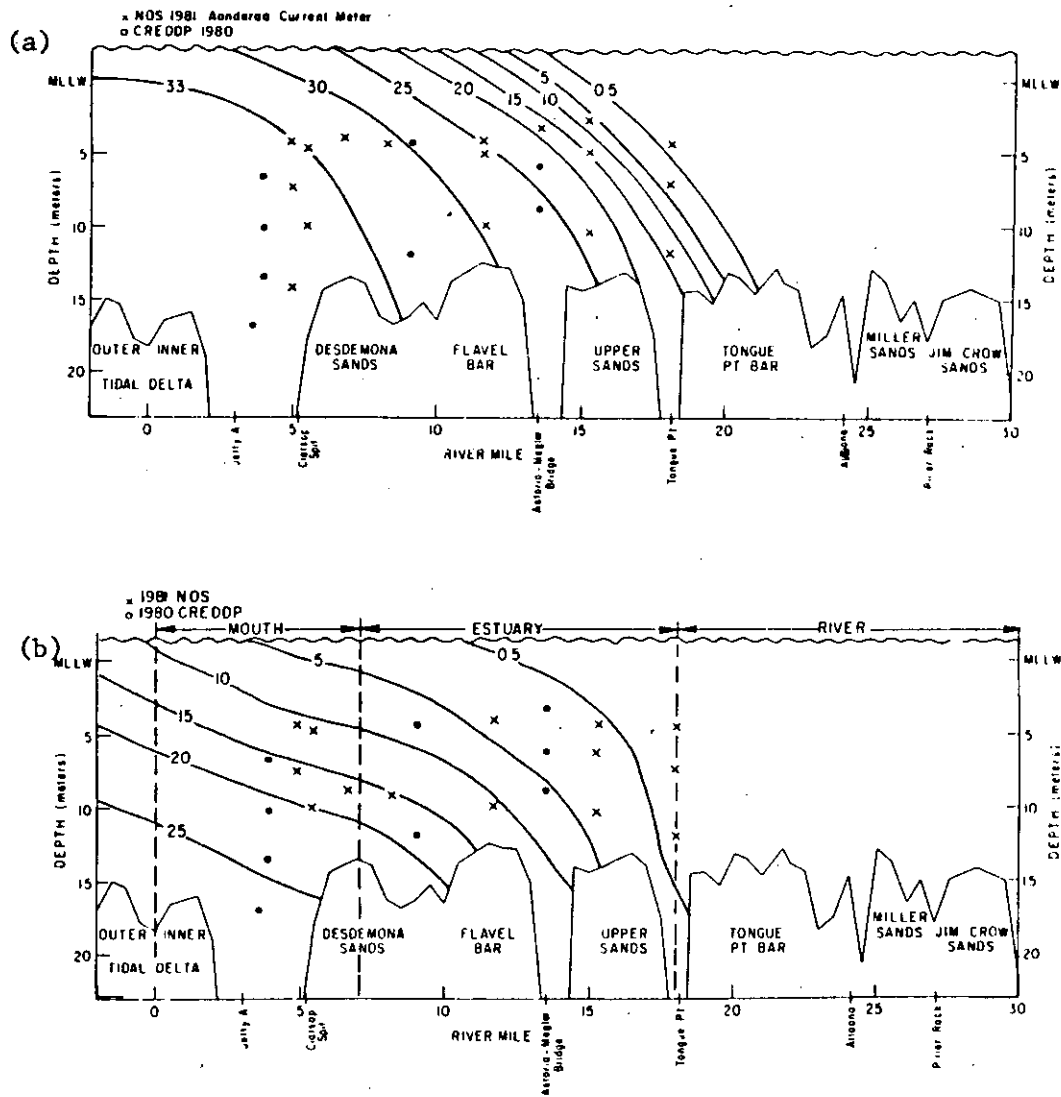


Figure 3.30. Maximum (a) and mean (b) salinity for the south channel for the high flow season (mean river flow 310 kcfs or $8,778 \text{ m}^3 \text{ sec}^{-1}$) based on all available 1980 and 1981 data.

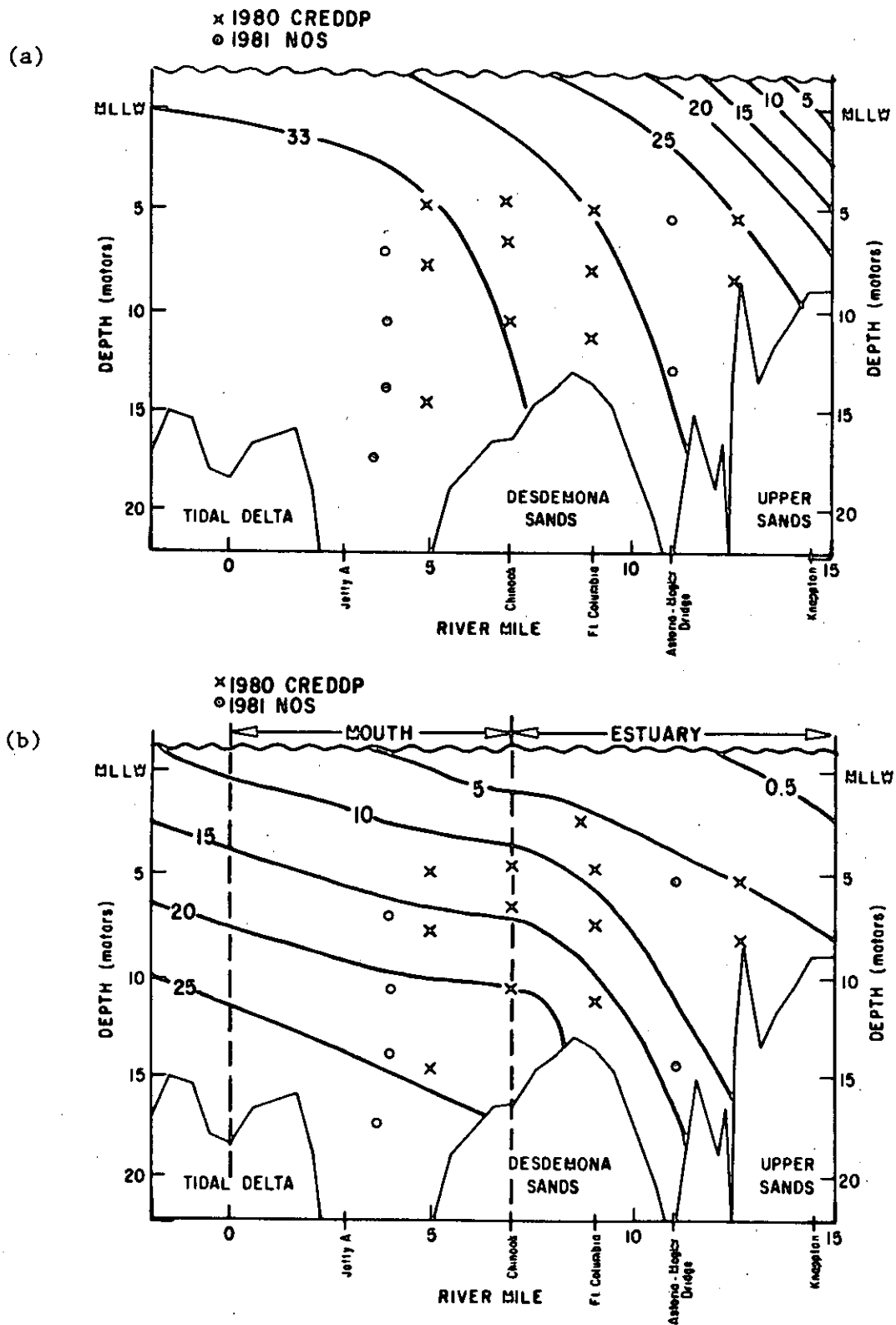


Figure 3.31. Maximum (a) and mean salinity (b) for the north channel for the high flow season (mean river flow 310 kcfs or $8,778 \text{ m}^3 \text{ sec}^{-1}$), based on all available data.

top to bottom salinity differences (10 to more than 20 ppt). The stratification and horizontal salinity gradient are, however, fairly uniform with depth (Figures 3.32 and 3.33). The apparent uniformity of the salinity distribution is largely a result of averaging. The density structure at most times during the high flow season shows sharp horizontal and vertical gradients. The stratification and horizontal salinity gradient are less uniform in the maximum salinity case than the mean salinity, because of the salt-wedge-like structure of the incoming flow. There is also greater maximum salinity intrusion in the north channel at mid-depth than in the south channel, despite the very shallow sill depths. This results from greater freshwater flow volume in the south channel. Note also that the salinity range exceeds 30 ppt between about RM-8 and RM-13 (Figure 3.33). Salinity ranges up to 33 ppt occasionally occur at individual current meters during a single tidal day.

The Low Flow Season

Figures 3.34a through f show the minimum, maximum, and mean salinity distributions for the low flow season (about 155 kcfs or $4,400 \text{ m}^3 \text{sec}^{-1}$) for the south and north channels, respectively. Top to bottom salinity differences are less (5 to 15 ppt), the slope of the isohalines is steeper, the horizontal density gradients are weaker, and the mean salinity intrusion length (about 25 miles) is much greater than in the high flow season. The maximum salinity (Figure 3.33) suggests salinity intrusion of about 5 ppt to Pillar Rock and beyond. Minimum salinity intrusion is substantial, and north channel-south channel differences are less prominent. The mean salinity gradient (Figure 3.32) is less variable than in the high-flow case, but far from constant.

3.6.2 The Variations of Salinity and Mean Flow During the Low Flow Season

Both profile and current meter data are available for the October 1980 low flow (120 to 150 kcfs or $3,400$ to $4,250 \text{ m}^3 \text{sec}^{-1}$) period. A detailed discussion of these data was presented in Jay (1982, 1984). This low flow period best exemplifies the neap-to-spring transition in mixing processes that occurs during most low flow periods. Model projections are used for the extreme low flow case (about 70 kcfs or $2,000 \text{ m}^3 \text{sec}^{-1}$).

The October 1980 Neap Tide Period

The data from this neap tide period exhibit one of the strongest neap-spring transitions so far observed in the Columbia River Estuary. The minimum tidal range occurred on the night of October 16 and 17, with a diurnal range of less than 2.0 m. The four-day period October 16 to 19 was a period of minimum vertical mixing, maximum stratification, and maximum salinity intrusion length. Comparison of maximum salinities at the Astoria-Megler Bridge for this and earlier neap tides suggests that this is one of perhaps 3 or 4 periods of maximum salinity intrusion for the year (Jay 1984). The salinity intrusion length was comparable or greater than that observed by McConnell et al. (1981).

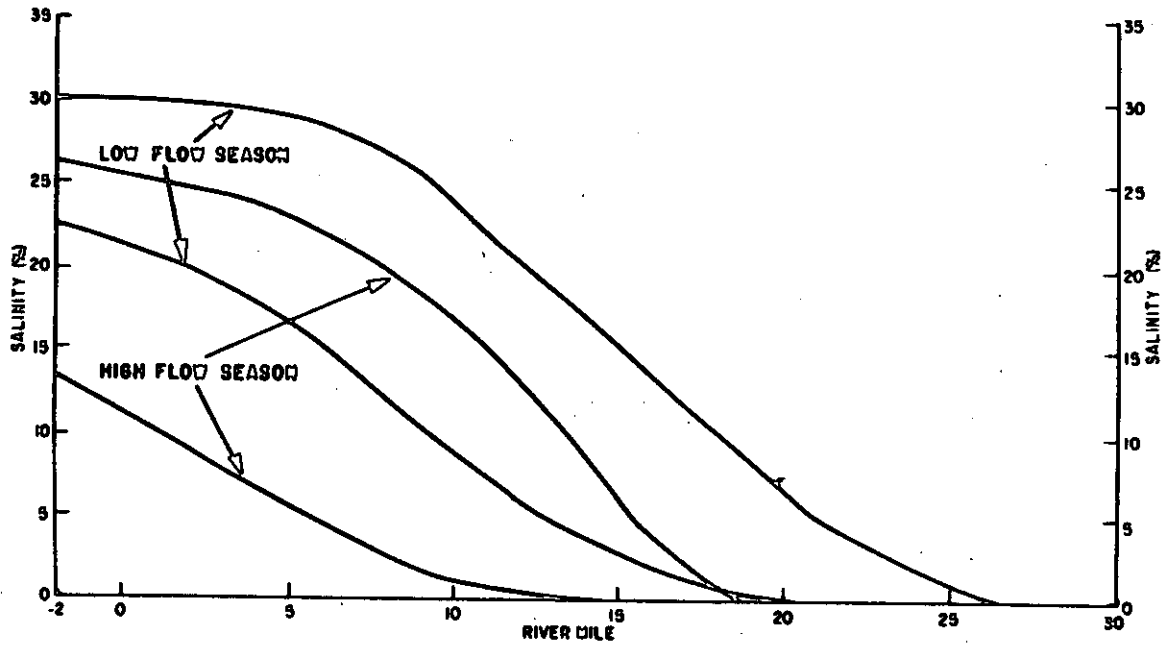


Figure 3.32. Seasonal mean salinity at MLLW and 12 m depth in the south channel for the high flow season (310 kcfs) and the low flow season (155 kcfs), based on all 1980-81 data.

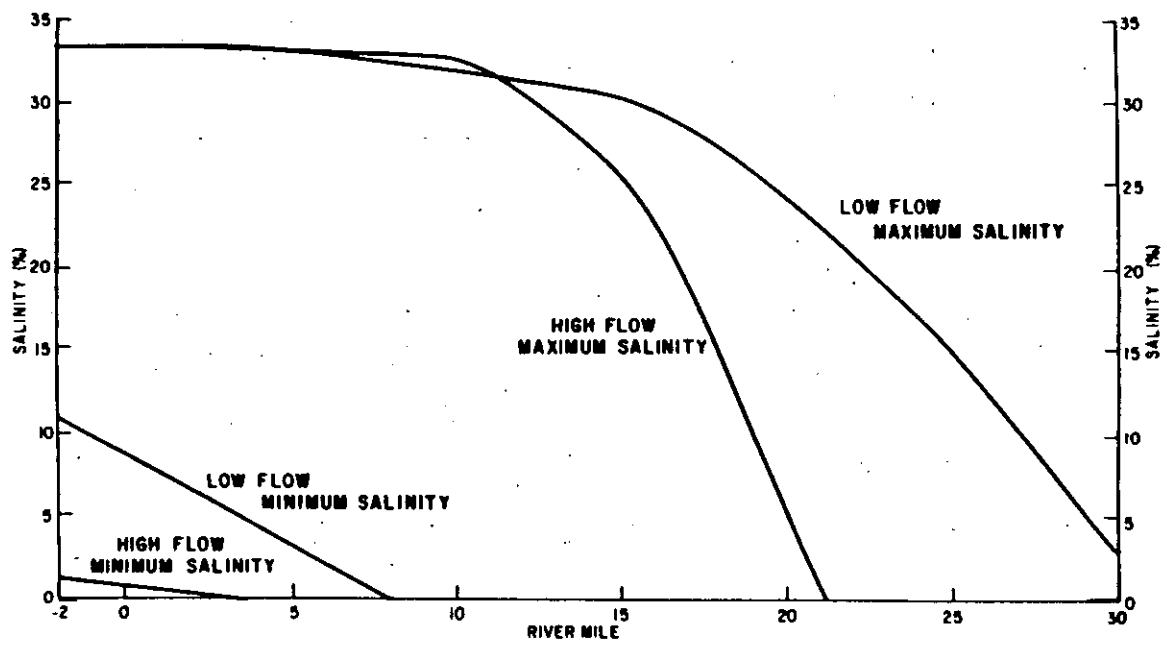


Figure 3.33. Seasonal minimum and maximum salinity in the south channel for the high flow seasonal (310 kcfs) and the low flow seasonal (155 kcfs).

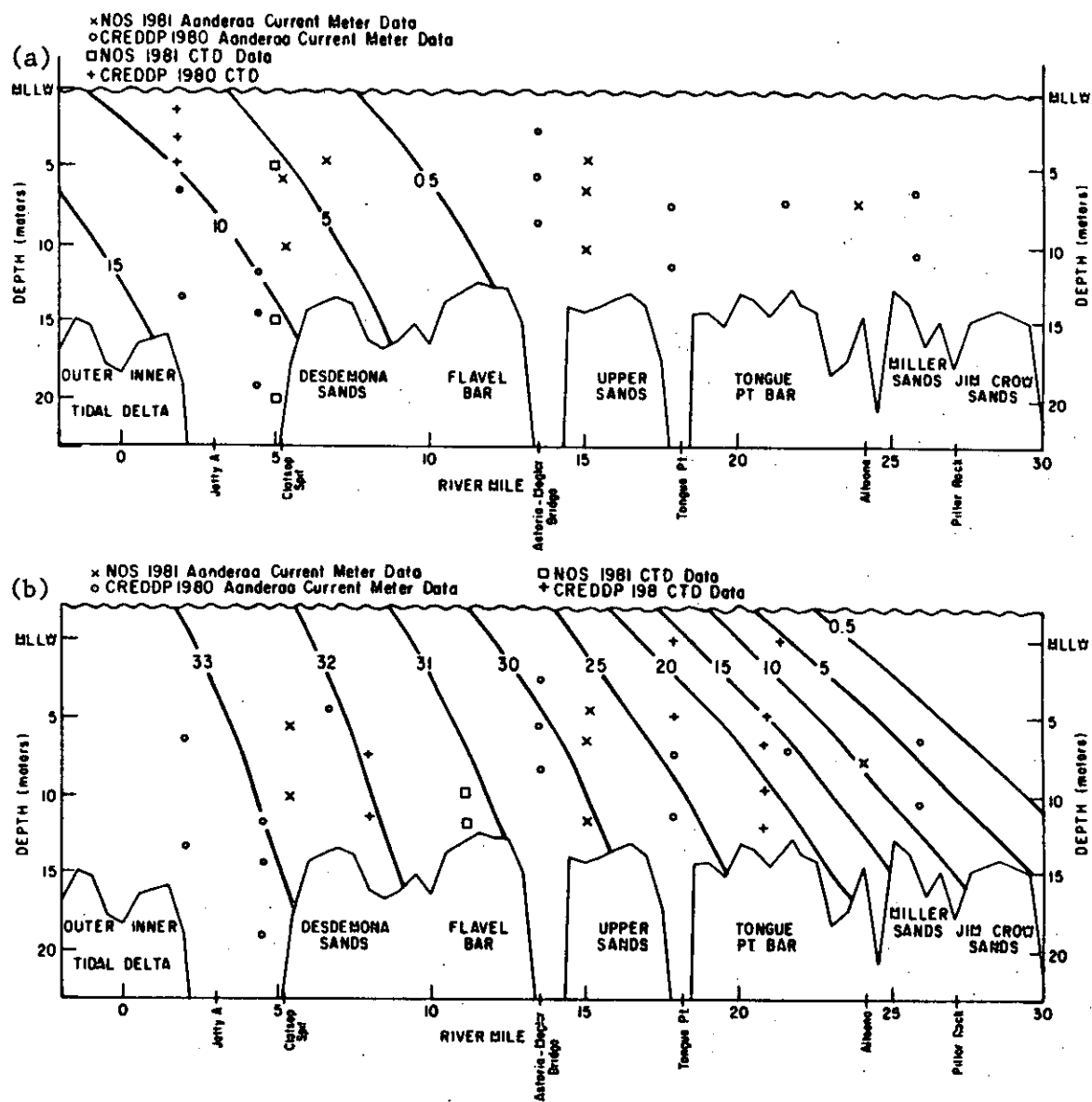


Figure 3.34. Seasonal minimum (a), maximum (b), and mean (c) salinity in the south channel and (d) to (f) in the north channel for the low flow season (155 kcfs).

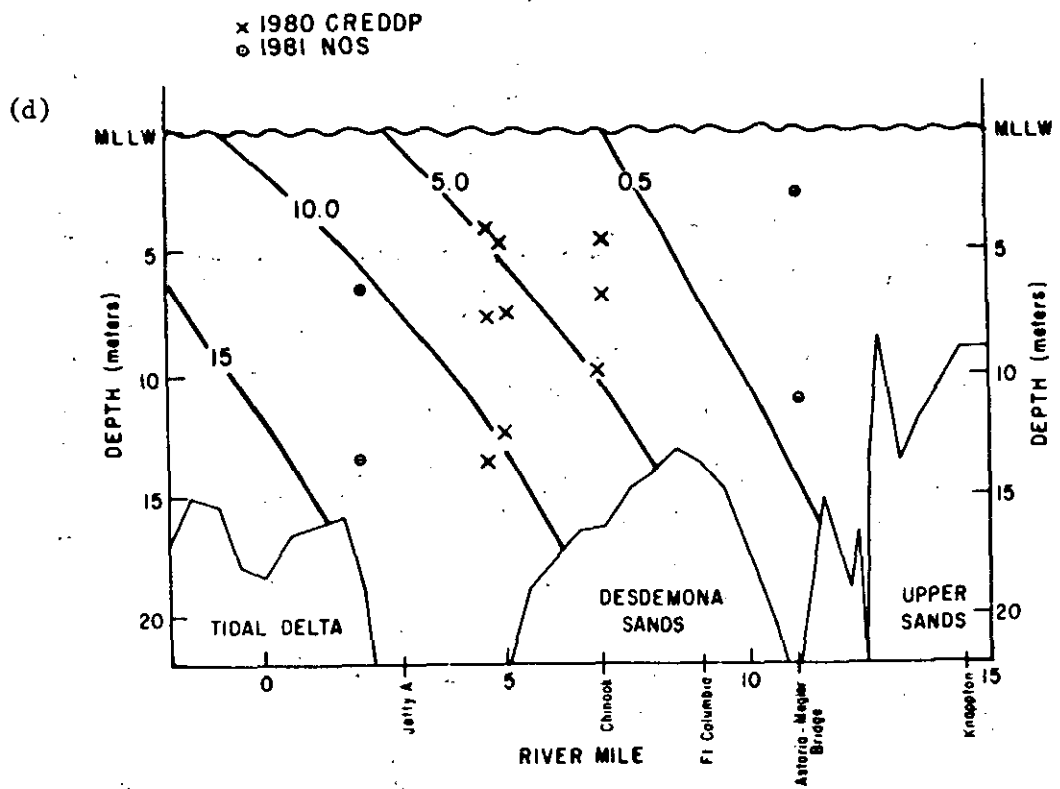
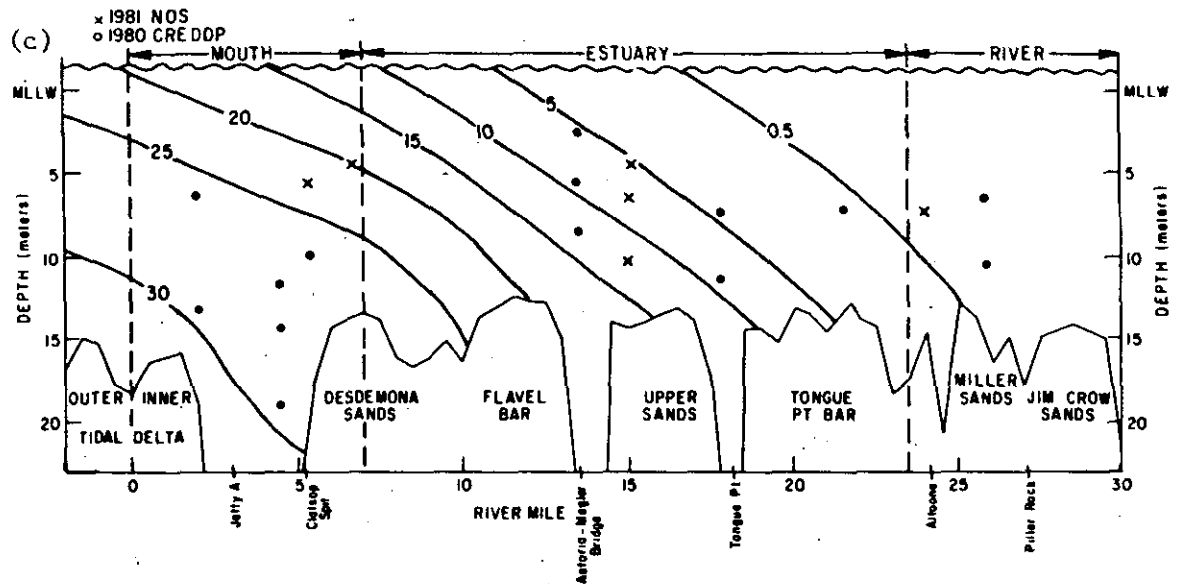


Figure 3.34 (continued).

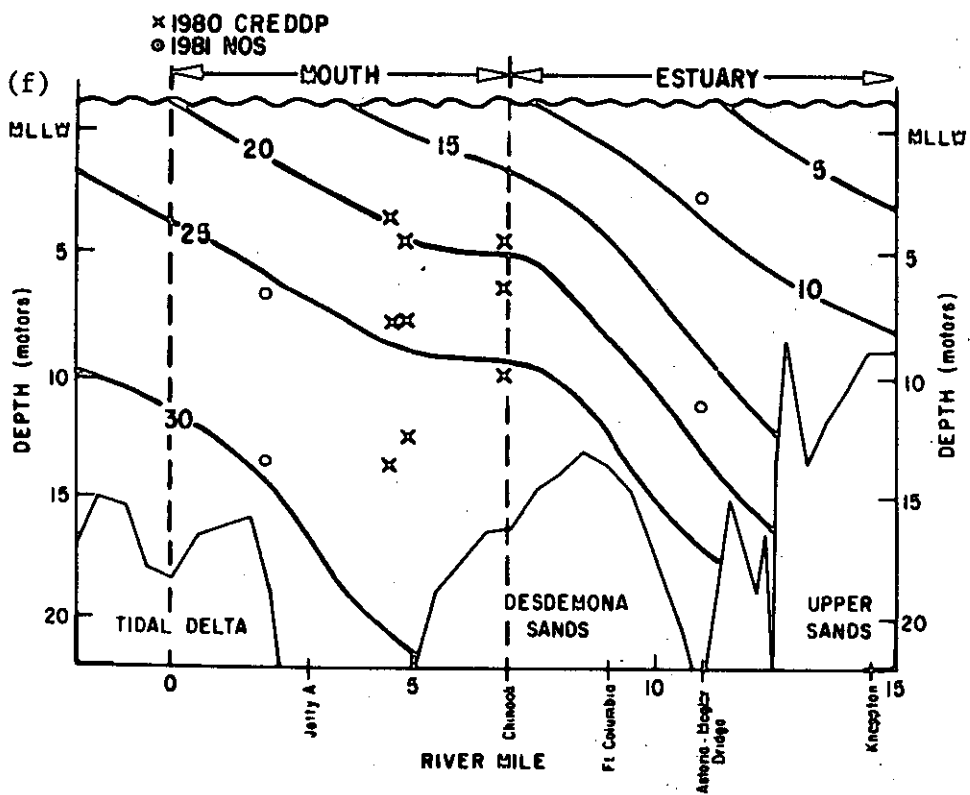
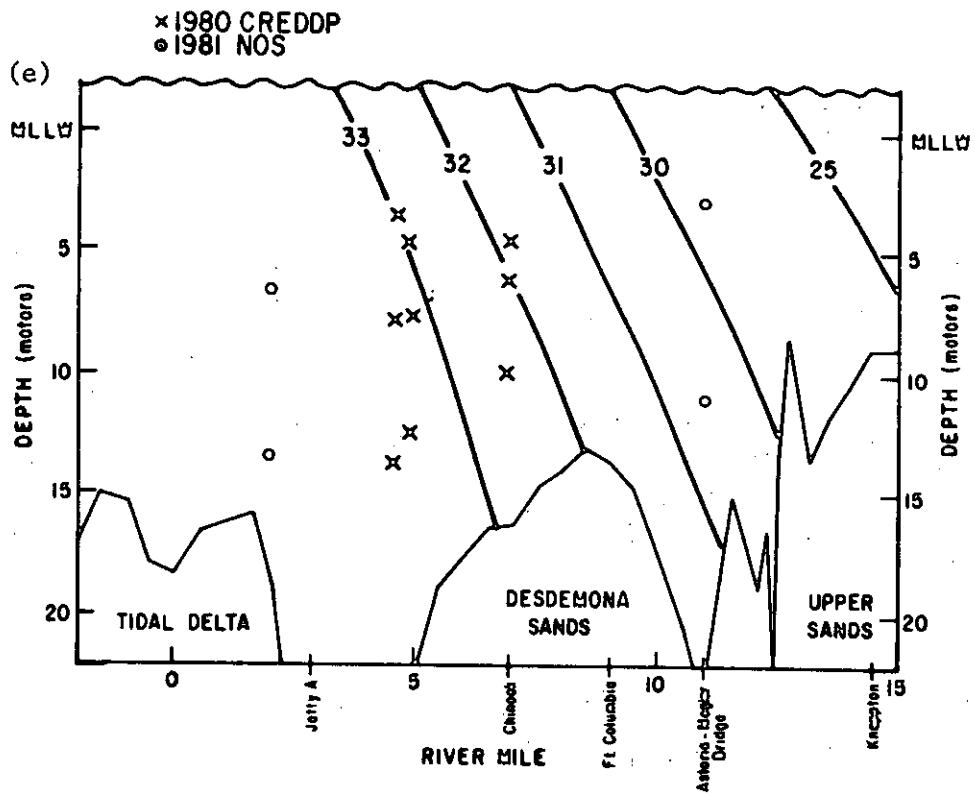


Figure 3.34 (continued).

Plots for the neap tide period of minimum, maximum, and mean salinity intrusion and salinity range are found in Figures 3.35a through d. The corresponding distribution of the mean flow is shown in Figure 3.20. Minimum and maximum salinity correspond roughly to end of ebb and end of flood pictures, but the data used are not truly synoptic, because maximum salinity occurred on a later tidal cycle above Tongue Point than nearer the entrance.

Typical late flood salinity and velocity profiles for the neap tide period for Tongue Point are shown in Figures 3.36a and b. The flow is divided into distinct upper and lower layers by the sharp interface at about 8 m. The lower, saline layer is still advancing slightly, and the upper layer has started to ebb. A smaller density interface occurs at about 6.4 m. On the ebb, stratification is reduced, as both vertical mixing and advection reduce bottom salinity. Early in the ebb, vertical mixing causes the salinity at mid-depth to increase despite outward advection.

One very prominent feature of Figures 3.35a through d is the temporal and spatial variability of the horizontal and vertical salinity gradients. Near the entrance, maximum stratification occurs at the end of the ebb, as the water of oceanic salinity (above 32 ppt) moves up-estuary beneath a surface layer that is still ebbing. Minimum stratification occurs later on the flood, when salinities of above 30 ppt occur at all depths below about MLLW. The greatest horizontal gradients are found at the end of flood at and above Tongue Point (Figure 3.35b) and at the end of ebb near the entrance (Figure 3.35a). Strong gradients are present at each location for only part of the tidal cycle. The horizontal gradient also varies by at least a factor of five between the surface and 5 m at Tongue Point at the end of a flood. The lack of synopticity and the wide spacing of the meters do not allow resolution of the form of the salinity intrusion (Figure 3.35a). Vertical and horizontal salinity gradients at the head of the salt wedge are actually much sharper than shown.

The observed (Figure 3.35d) distribution of the salinity range can be explained as the result of typical estuarine mixing processes. Nearly pure oceanic water is found at the bottom near the entrance during most stages of the tide. River water enters at the surface near the upstream end. Under conditions of weak mixing the result is an intermediate, high variance water mass that is beneath the river water at the upstream end of the estuary and over the oceanic water at the ocean end. The area downstream of the Astoria-Megler Bridge is one of very large (above 25 ppt) salinity range under most conditions; the shape and position of this maximum varies.

The October 1980 Spring Tide Period

The October 24 to 26, 1980, period of strong tides and low runoff probably represents the extreme well-mixed condition in the Columbia River Estuary; this period has the highest mean and maximum surface salinities and minimum mean vertical stratification at the Astoria-Megler Bridge for any 1980 spring tide for which data are available (Jay 1984). Figures 3.37a through d show the minimum,

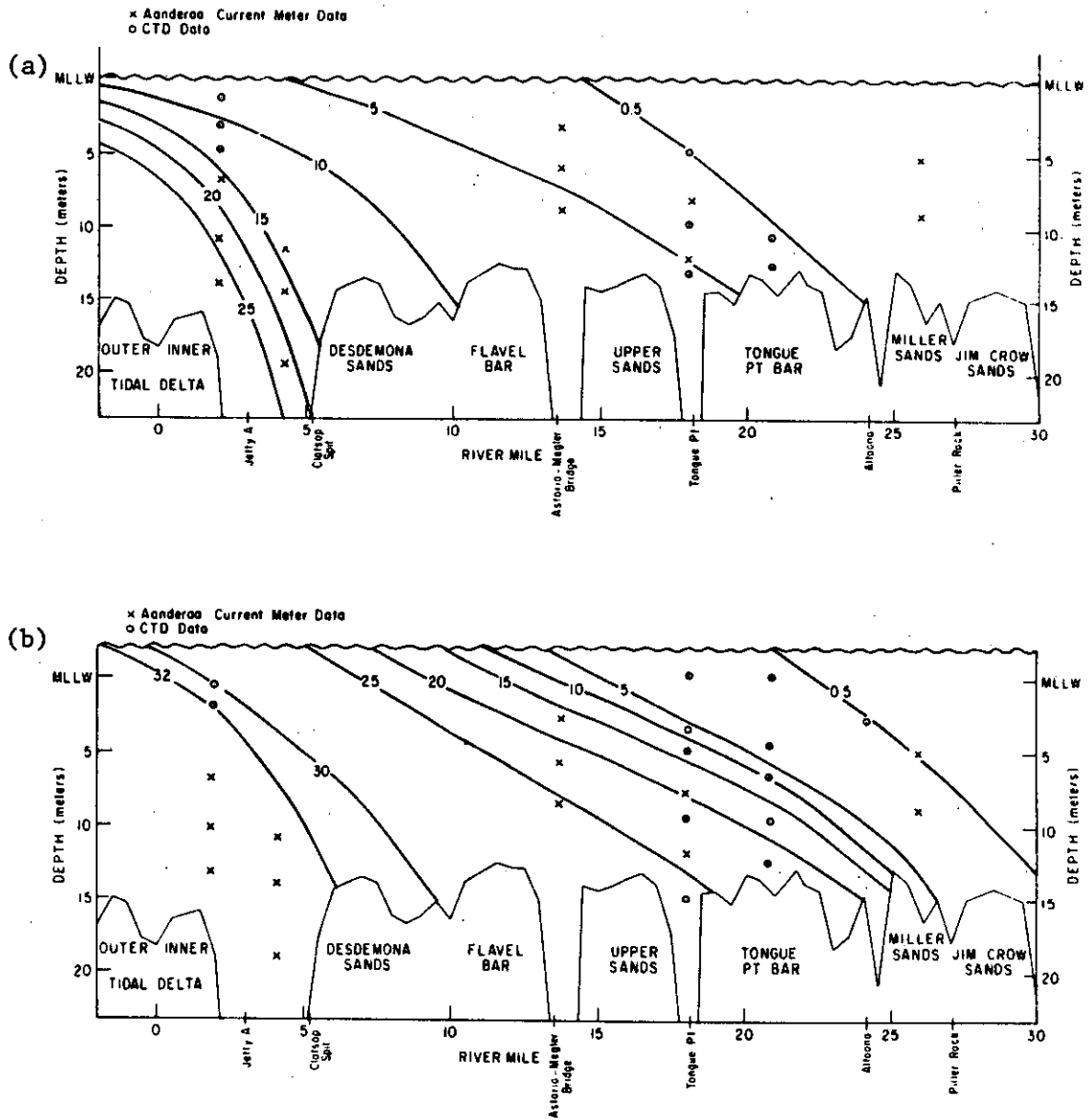


Figure 3.35. October 1980 neap tide minimum (a), maximum (b), and mean (c) salinity, and salinity range (d) for the south channel.

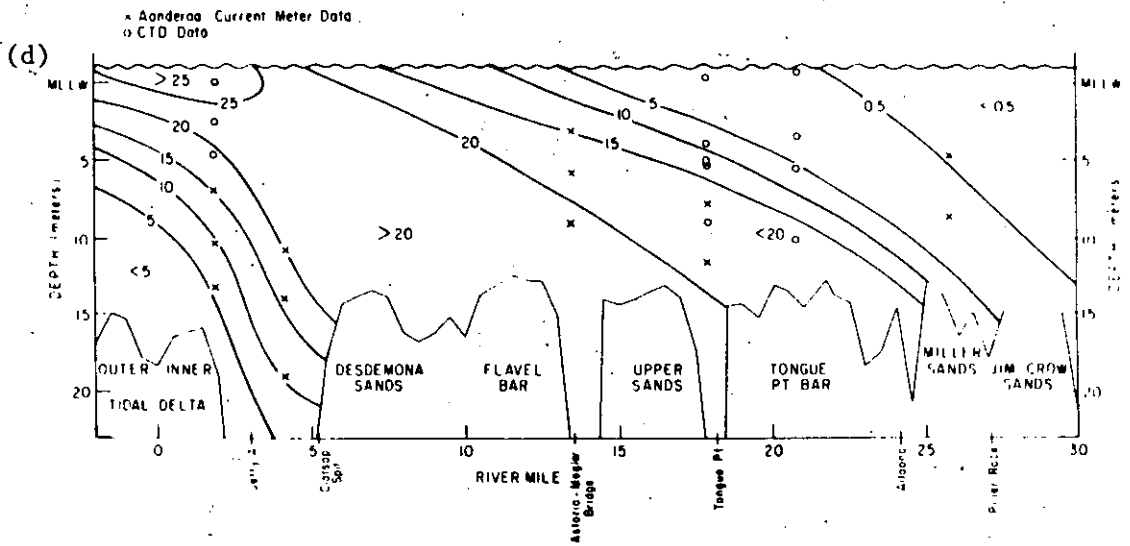
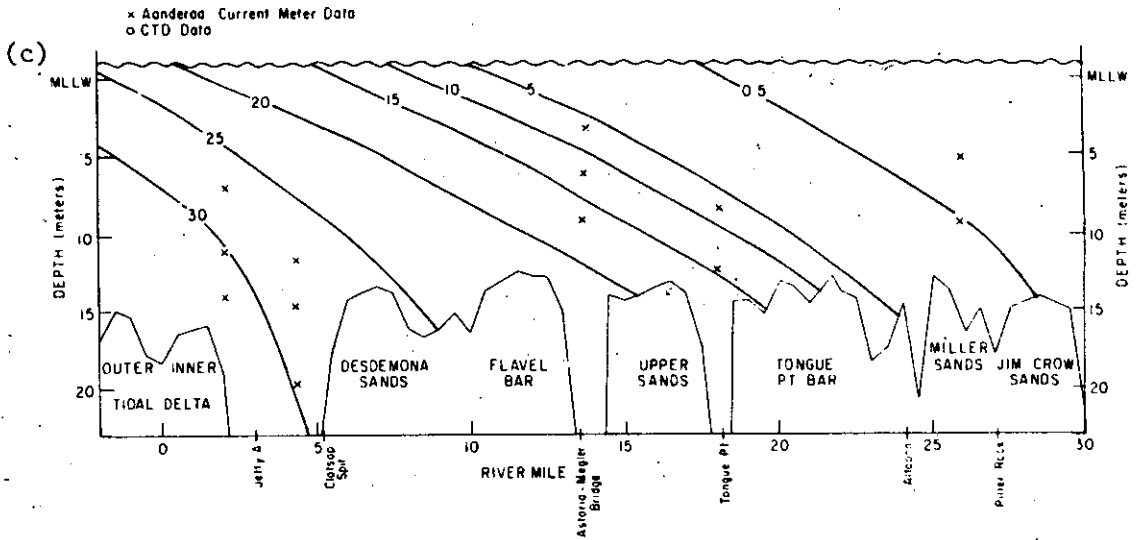


Figure 3.35 (continued).

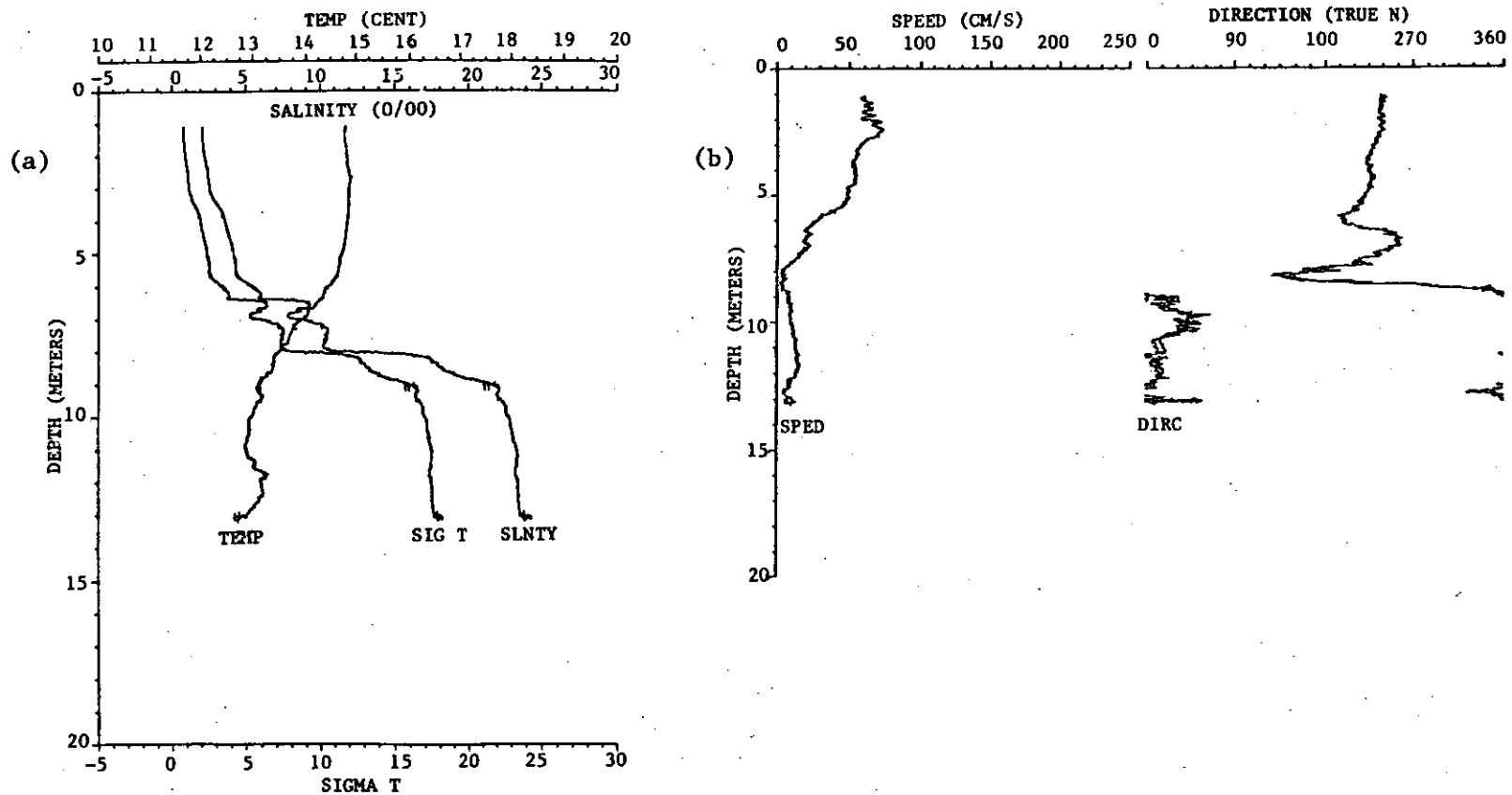


Figure 3.36. Salinity, temperature and sigma-t (a), and speed and direction (b) at station 6SA (Figure 3.4) on neap tide. Weak flood prevails at the bottom, but ebb has begun in the surface layer. Very strong stratification occurs at about 8 m, isolating the upper layer from the influence of the bottom boundary.

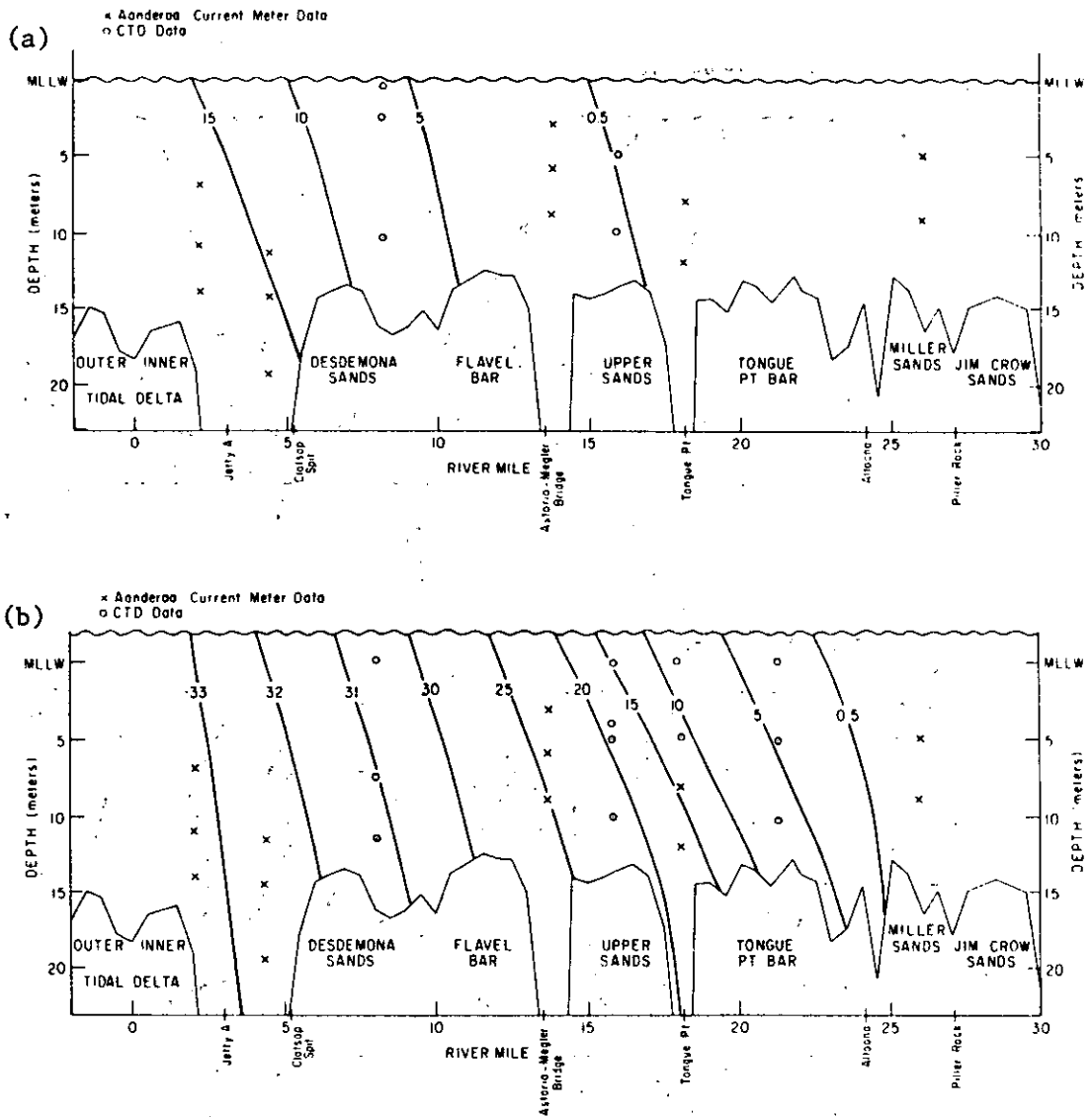


Figure 3.37. Minimum (a), maximum (b), and mean (c) salinity, and salinity range (d) in the south channel for the October 1980 spring tide period. Salinity intrusion length and stratification are both less than on neap tide.

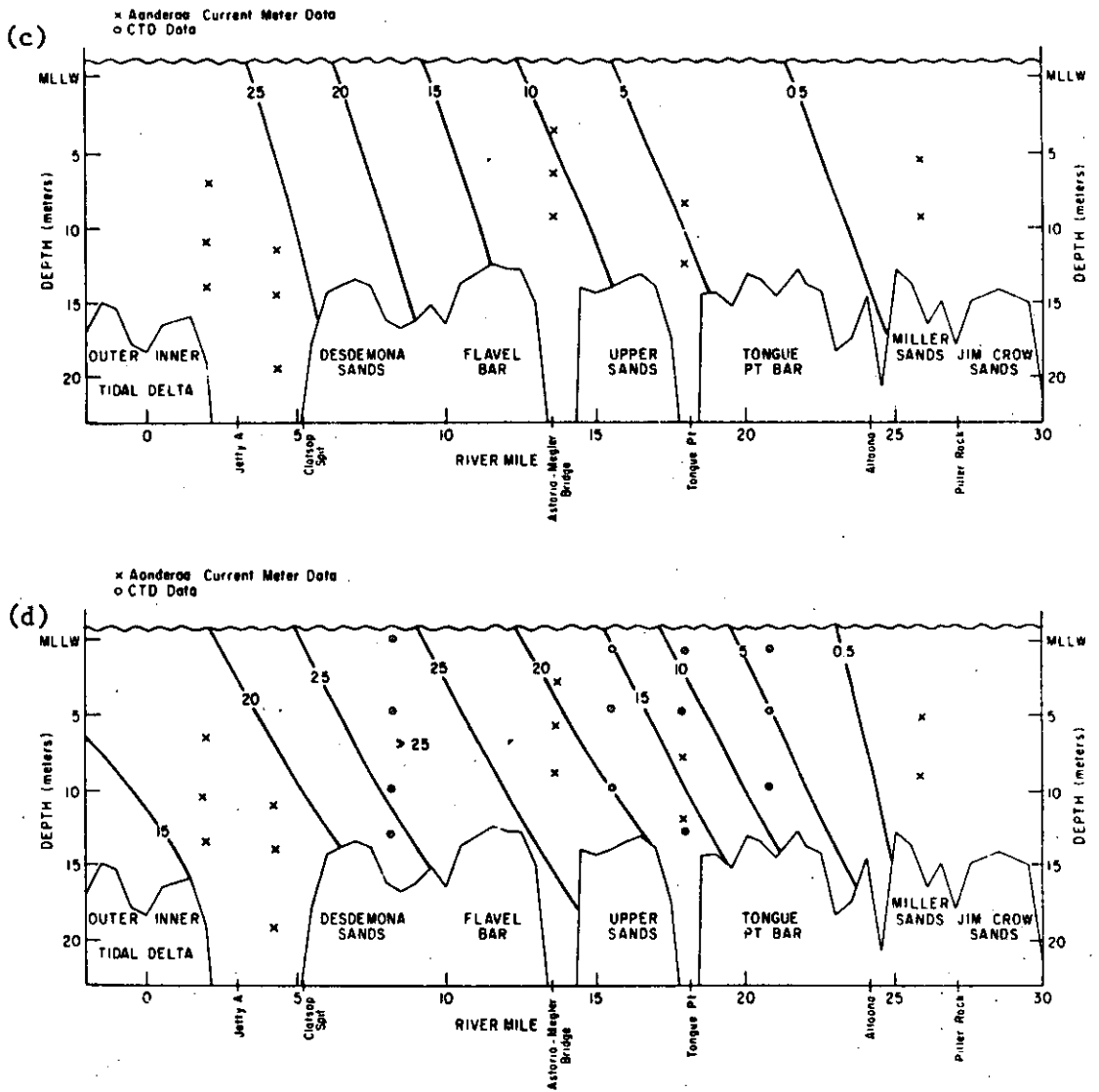


Figure 3.37 (continued).

maximum, and mean salinity intrusion and salinity range for this period. The mean flow predicted by the two-dimensional model is shown in Figure 3.22. The diurnal tidal range was above 3.4 m.

Spring tide salinity contours in Figures 3.37a through d are much more nearly vertical than those for the neap tide period (Figures 3.35a through d). The shorter salinity intrusion length and lesser stratification on spring tide are caused by the greater vertical mixing. The increased vertical mixing is clearly evident in profile data (Figures 3.38a,b). The velocity profile (Figure 3.38b) is that of a turbulent boundary layer modified by weak stratification. The decreased ebb bottom salinities at the entrance on the spring tide are related to both the increased vertical mixing and the greater tidal excursion.

The spring-to-neap differences in extreme (Figure 3.39) and time-averaged (Figure 3.40) salinities emphasize the difference in salinity intrusion length and in dynamics. Salinity intrusion on the neap tide was about 8 RM farther than on spring tide. Furthermore, the spring tide mean salinity distribution has a horizontal salinity gradient (Figure 3.40) that is much more regular than that for neap tide and that is nearly as regular as that of Figure 3.2a. Such uniformity in the salinity distribution is not typical of the Columbia River Estuary, and apparently only occurs on low flow spring tides. The neap tide mean salinity gradient is much more variable than the spring tide mean, because of the weaker mixing and stronger baroclinic circulation.

Model Predictions for Extreme Low Flow

The drought year of 1976-77 raised the question of the possible ecological effects of the increased salinity intrusion that would accompany a dramatic decrease in riverflow; further interest in this problem has been spurred by the proposed deepening of the navigation channel, which also would increase salinity intrusion. The results presented here (and in Hamilton 1984) for the decreased runoff case are, however, quite different from those for the increased channel depth case, discussed in Hamilton (1983).

The lowest monthly average "observed" flow at the mouth during the period of record was about 71 kcfs ($1,980 \text{ m}^3 \text{ sec}^{-1}$; Orem 1968 and Section 2.2). Daily flows significantly lower than this have been observed, but only in the coldest part of the winter. A model run was, therefore, made using a riverflow of $2,000 \text{ m}^3 \text{ sec}^{-1}$ (Hamilton 1984). The tides used were those for May 25 to June 3, 1981, for which other simulations had already been run. These tides provided a large change in tidal range in a short time period and were similar to the tides for the October 1980 low flow period already examined.

Model results for the $2,000 \text{ m}^3 \text{ sec}^{-1}$ case show much longer salinity intrusion lengths and somewhat less stratification (Figures 3.41 a through c) for the spring tide than the October 1980 model simulation (Figures 3.20 and 3.22). Neap tide results are similar and are not shown. There is much less stratification than the October 1980 observations (Figures 3.35a through d and 3.37a through d). The

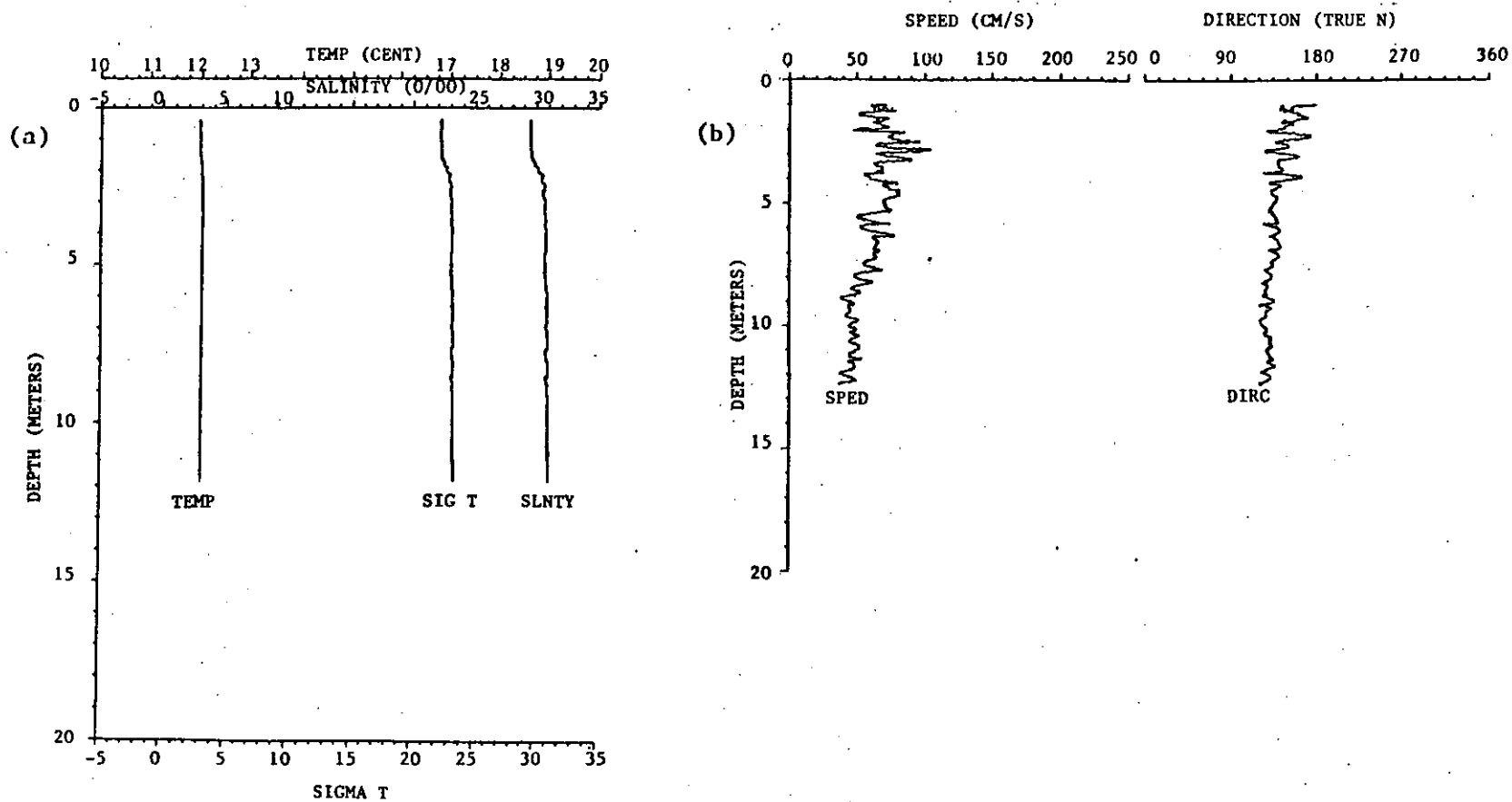


Figure 3.38. Salinity, temperature, and sigma-t (a), and speed and direction profiles (b) at station 4-SB (Figure 3.4) during flood tide in a period of very large tidal range. The stratification is small and much of the observed variation in the speed and direction profiles results from motion of the boat and water surface.

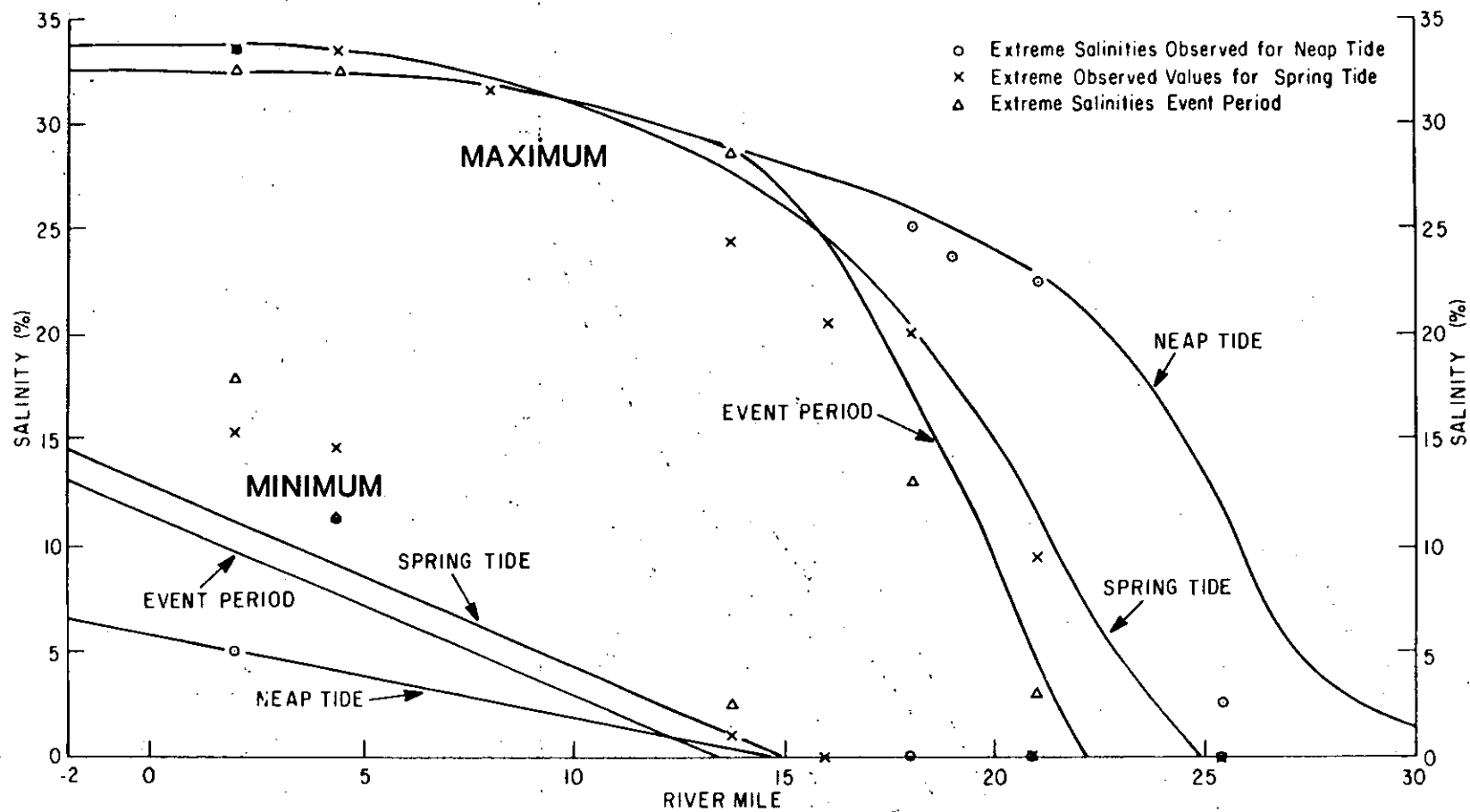


Figure 3.39. Maximum and minimum salinity intrusion for spring tide, neap tide, and "event period" in October 1980; riverflow 120 to 150 kcfs ($3,400$ to $4,250$ m^3 sec^{-1}). Reduced maximum salinity intrusion during the event period was caused by a wind-induced increase in surface slope.

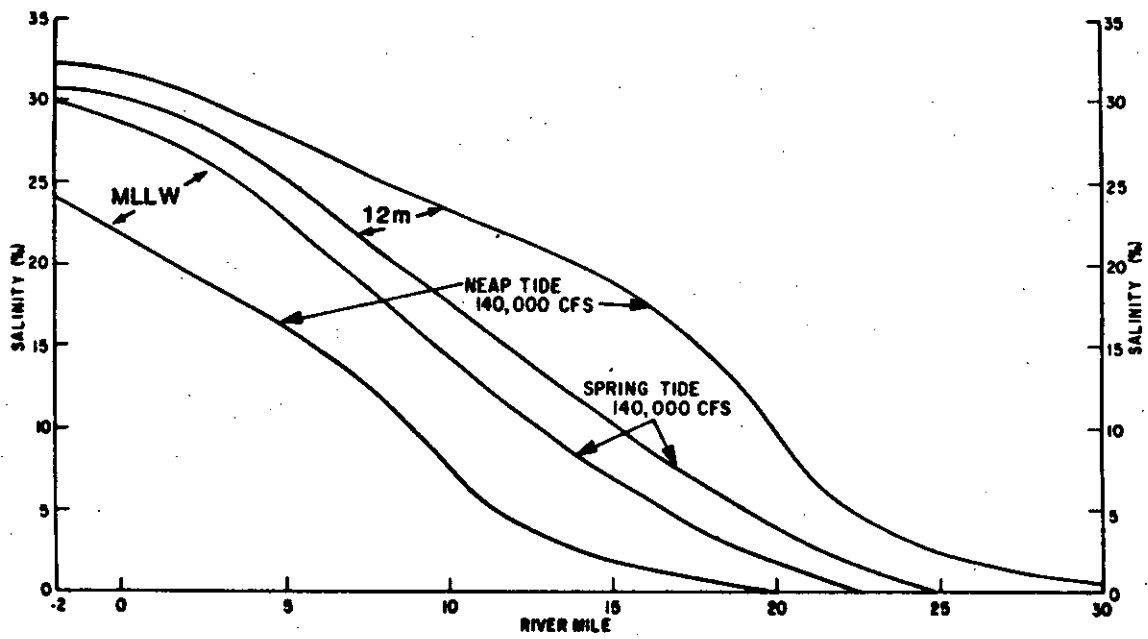


Figure 3.40. October 1980 mean salinity at MLLW and 12 m depth for neap and spring tide in the south channel.

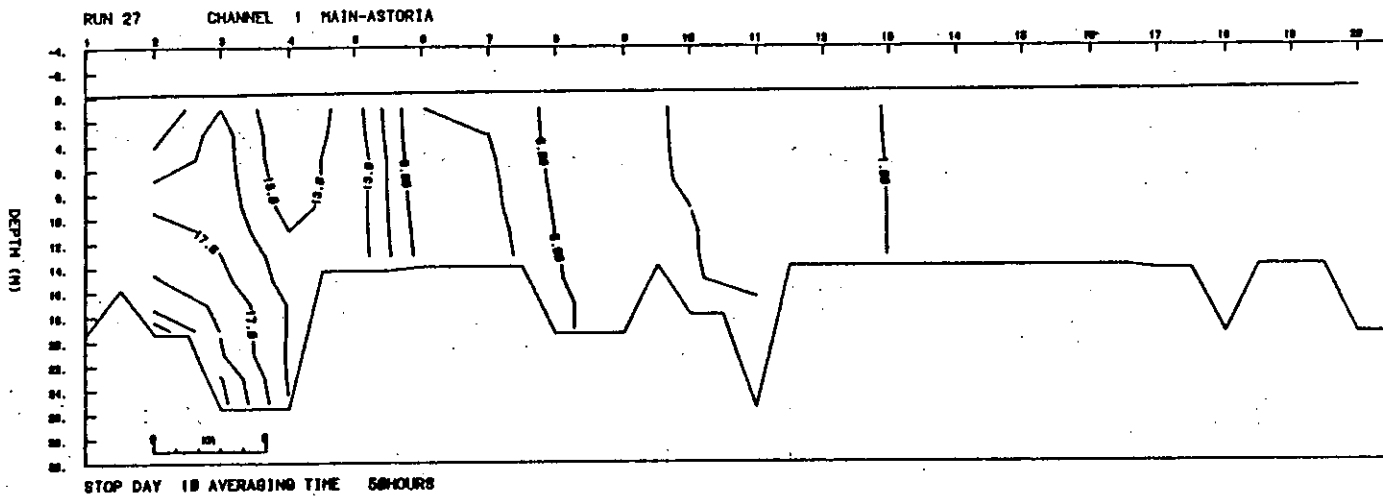


Figure 3.41a. Minimum salinity, 1980 estuary, $2000 \text{ m}^3 \text{ sec}^{-1}$, spring tide.

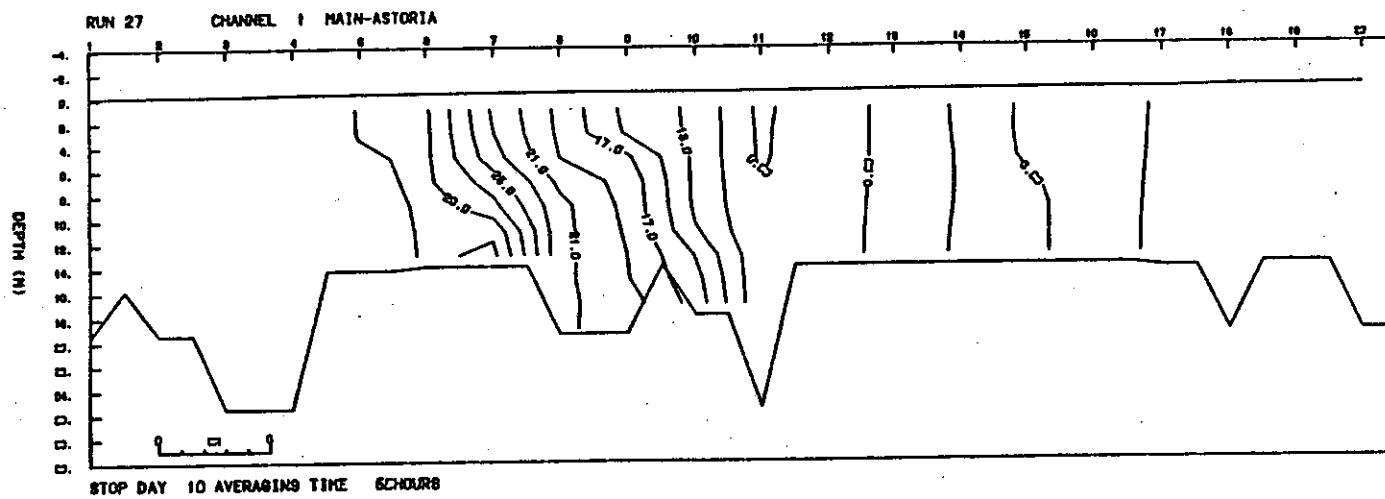


Figure 3.41b. Maximum salinities, 1980 estuary, $2000 \text{ m}^3 \text{ sec}^{-1}$, spring tide.

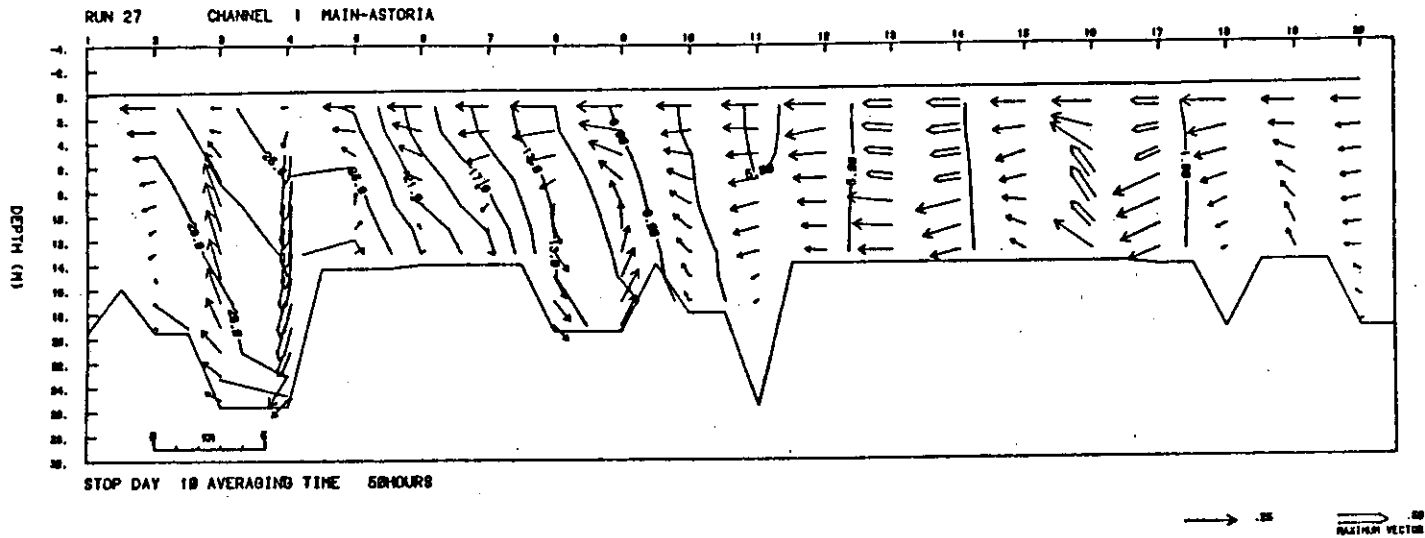


Figure 3.41c. Channel 1, spring tide period (constant riverflow = $2000 \text{ m}^3 \text{ sec}^{-1}$) mean currents and salinities (m sec^{-1} and ppt).

predicted extreme low flow salinity intrusion length is greatest on spring tide, rather than on neap tide. On spring tide, the 1 ppt contour is off the end of Figure 3.41b, and reaches to grid point 21, the downstream end of Puget Island. On neap tide, the 1 ppt contour reaches grid point 17.

If the model predictions for the extreme low flow case are correct, the most significant effect of the decreased riverflow would be the decrease in stratification and the increase in surface salinity. Surface salinities of 5 ppt would reach the interior of Cathlamet Bay in several channels, and 1 ppt would occur throughout the bay. The extreme, low flow scenario is, therefore, quite different than the deeper channel case investigated in Hamilton (1983). Deepening the channel was found to increase stratification by allowing increased salinity intrusion near the bottom; effects on shallow areas were insignificant.

3.6.3 The High Flow Distributions of Salinity and Mean Flow

High riverflows in excess of 500 kcfs ($14,130 \text{ m}^3 \text{ sec}^{-1}$) occur only a few days per year under the present flow regulation system. Salinity data are available for only two such periods, June 18-20, 1959, a spring tide, and June 8-11, 1981, a neap tide. The major difference between these two periods is not the difference in tidal range; it is that the flow was nearly steady in June 1959, but varied rapidly between June 8 and June 11, 1981.

Figures 3.42a and b show the maximum and mean salinity for a period of steady, high riverflow (535 to 570 kcfs or $15,150$ to $16,140 \text{ m}^3 \text{ sec}^{-1}$) during June 1959. Figures 3.42a and b are based on data collected from boats over a three-day period. The lack of synopticity is important because the tidal range increased from about 2.8 to about 3.1 m (spring tide) during the observation period and because a change in offshore water masses occurred. Salinities of more than 33 ppt were observed at the Clatsop Spit section (RM-5.5) on June 19, whereas the salinity at the entrance section (RM-2) did not exceed 32 ppt the previous day. For several hours during ebb the salinity observed did not exceed 0.5 ppt at any station. Thus, no minimum salinity plot is necessary, and the salinity range and maximum salinity are identical. The salinity data have been contoured using present day bathymetry, although controlling depths at the entrance and in the navigation channel at that time were 1 to 2 m shallower.

The June 1959 situation (Figures 3.42a and b) is notable for the very large salinity range (as much as 33 ppt), for strong stratification, and for a very large horizontal salinity gradient (up to 10 ppt km^{-1}). The strong gradients exist because the salinity intrusion occurs as a salt wedge. The total absence of freshwater at the end of ebb can be attributed to the large tidal range; the salt wedge is mixed and advected totally out of the estuary. The strong stratification is the result of the very large riverflow. There is undoubtedly a strong baroclinic circulation which allows strong flood intrusion of salt water despite the great riverflow.

A brief period of high riverflow was experienced in mid-June 1981 (Figure 2.9); the flow rose very quickly from about 400 kcfs ($11,330 \text{ m}^3\text{sec}^{-1}$), peaked at about 560 kcfs ($15,900 \text{ m}^3\text{sec}^{-1}$) on June 10 and 11, and then dropped back to about 400 kcfs ($11,330 \text{ m}^3\text{sec}^{-1}$). The total duration of flow greater than 500 kcfs ($14,130 \text{ m}^3\text{sec}^{-1}$) was only four days.

Comparison of the June 1981 data with the June 1959 data, collected during a period of steady flow of about 535 to 570 kcfs ($15,150$ to $16,140 \text{ m}^3\text{sec}^{-1}$), reveals that a transient flow increase produces a very different salinity regime from a steady flow of the same magnitude. Figures 3.43a through d show minimum, maximum, and mean salinity intrusion and salinity range for the transient flow event (June 1981). Model results for mean salinity and velocity are presented in Figure 3.44. The June 1981 situation is very different from June 1959 and is notable for the lack of stratification, because saline bottom water was absent. Apparently low salinities and minimal stratification during June 1981 were primarily caused by the transient response of the system to a change in riverflow. The initial decrease of salinity at all depths was caused by an adjustment of surface slope of the system at the onset of high flow. This adjustment was barotropic (occurred at all depths) and pushed a large part of the saline water mass out of the estuary in a short time (less than one day). Note that upstream bottom flow was absent upstream of grid section 3 (RM-4) and bottom salinities were depressed (Figure 3.44). After the salt water was nearly pushed out of the estuary, there then occurred a baroclinic adjustment (that was a function of depth) driven by the density structure that brought salinity back into the deeper parts of the estuary near the entrance. Salinities remained depressed near the surface and upriver because of the high riverflow. After the baroclinic adjustment occurred, stratification was greatly enhanced and the horizontal salinity gradient was greatly increased.

If Figures 3.43a through d (June 1981) capture the system in the midst of an adjustment to a change in external forcing, then Figures 3.42a and b (June 1959) represent the equilibrium state that would occur after this series of adjustments of flow to runoff. Such an equilibrium was never reached in June 1981, because the flow immediately dropped; the system remained out of adjustment with its external forcing. Figure 3.45 compares the mean salinity gradients for the June 1959 and 1981 periods. It can be seen that both the horizontal and vertical gradients are stronger in the 1959 equilibrium case. The gradient for the 1981 case resembles a gradient for much lower flows (e.g. Figure 3.40), but shifted in the down-river direction. This further supports the idea that the June 1981 data represent the transient response of the system, which was previously in equilibrium with a smaller flow, to a much higher flow.

In summary, the initial response of the system to a sharp increase in riverflow is very different from the final equilibrium with the high flow. Extreme, high flow events are now much less frequent than prior to regulation of the flow by dams. Nonetheless, the total absence of salt from the system for half a tidal cycle is still possible when strong riverflow coincides with strong tides.

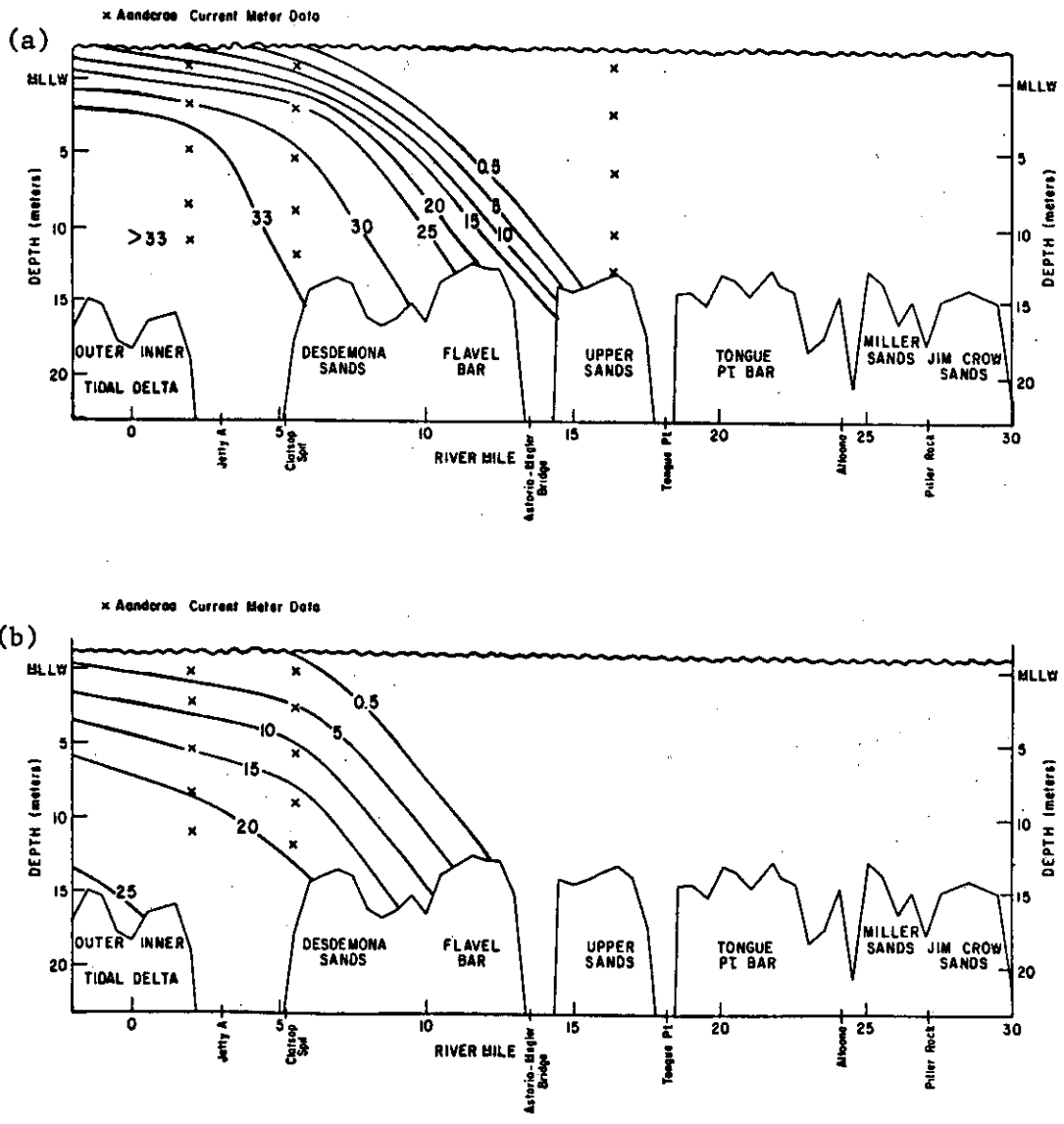


Figure 3.42. Maximum (a) and mean (b) salinity in the south channel during the 1959 spring freshet, as taken from U.S. Army Engineers (1960). Salinity was entirely absent from the system for several hours at the end of ebb.

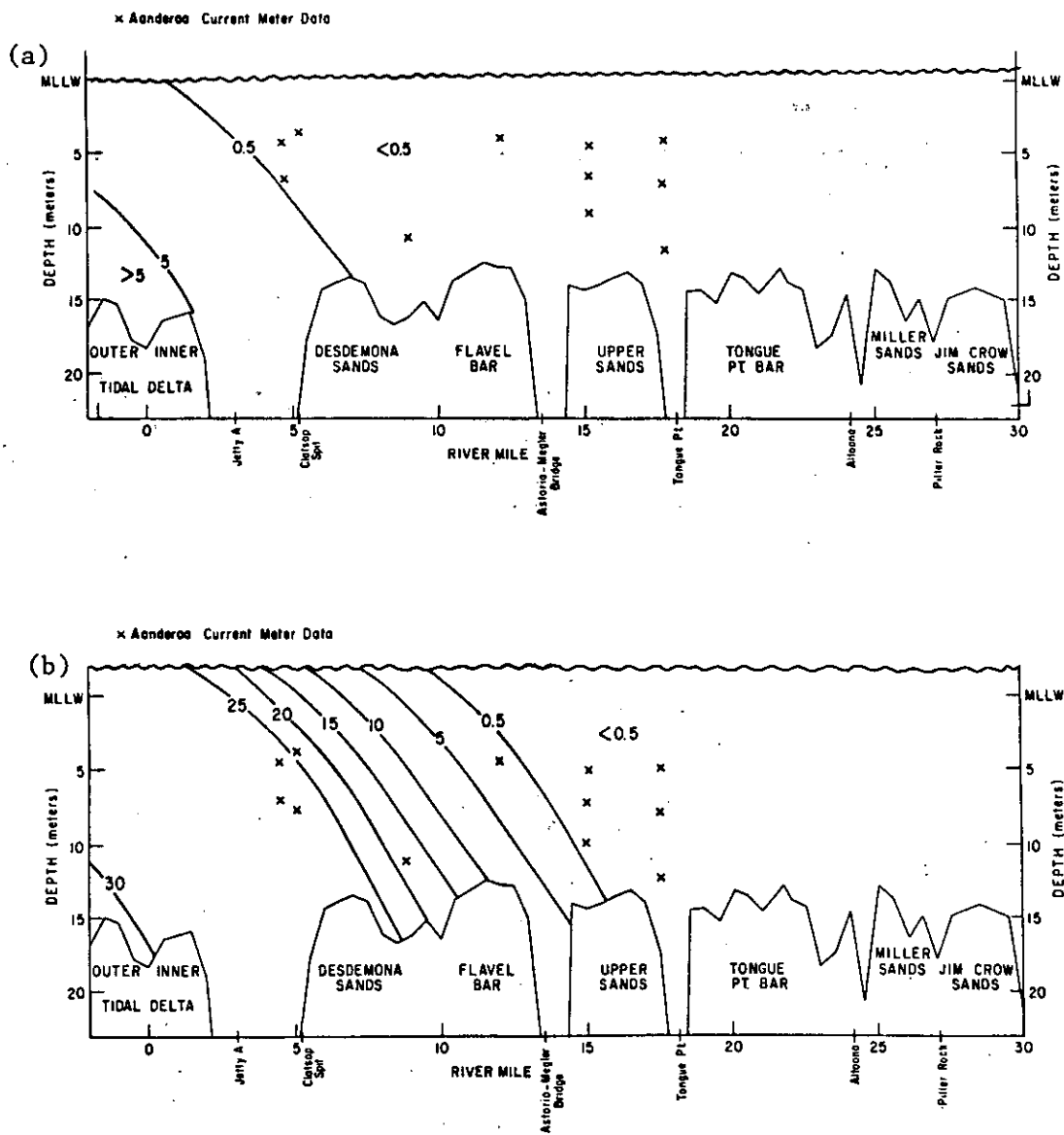


Figure 3.43. Minimum (a), maximum (b), and mean (c) salinity, and salinity range (d) for the south channel during the 1981 spring freshet.

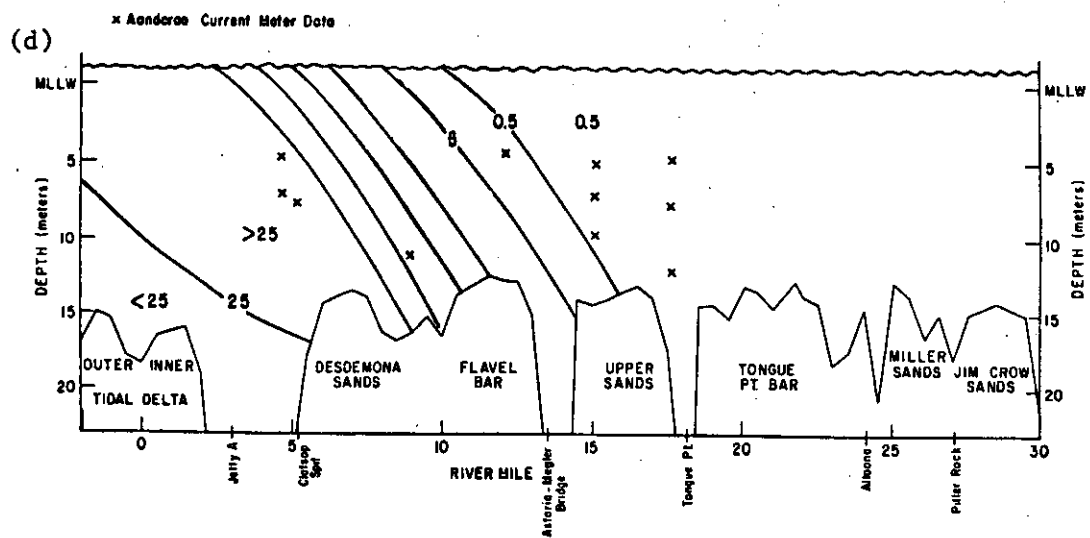
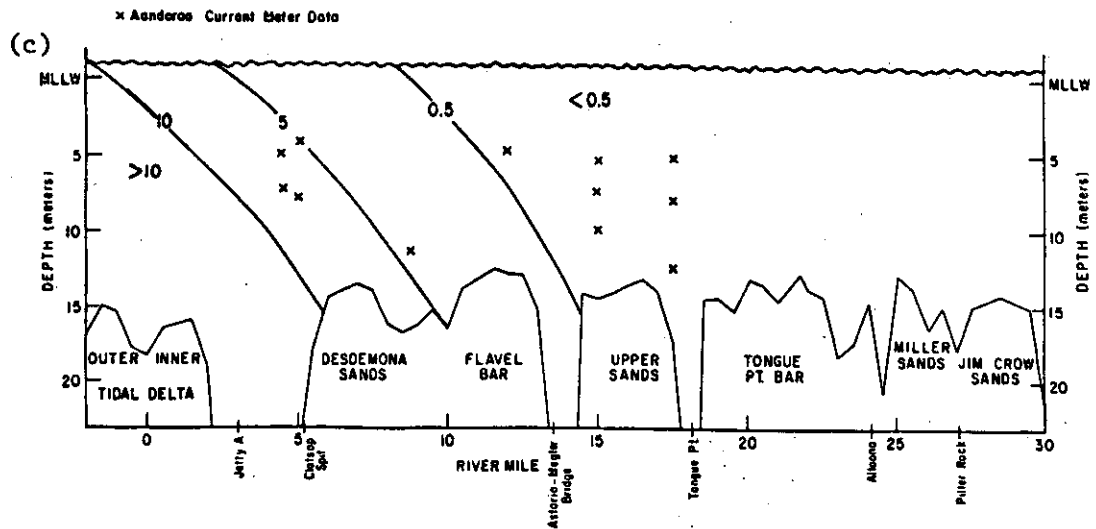


Figure 3.43 (continued).

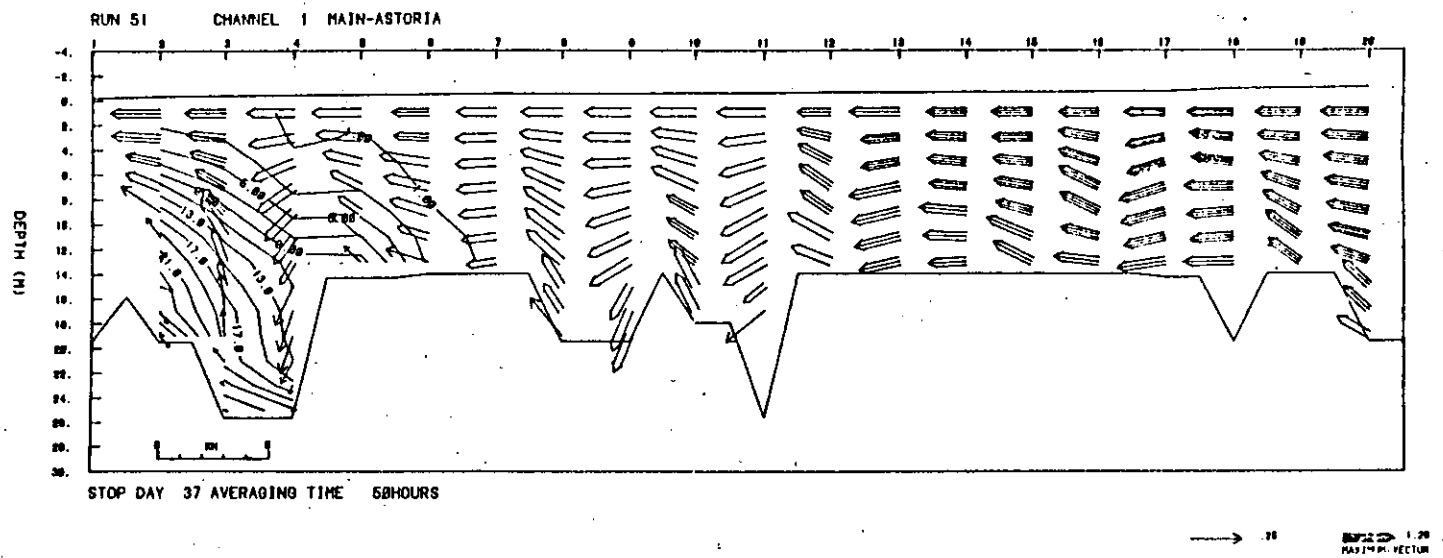


Figure 3.44. Channel 1 (Figure 3.19), Neap #2 (Spring, 1981). Mean currents and salinities (m sec^{-1} and ppt).

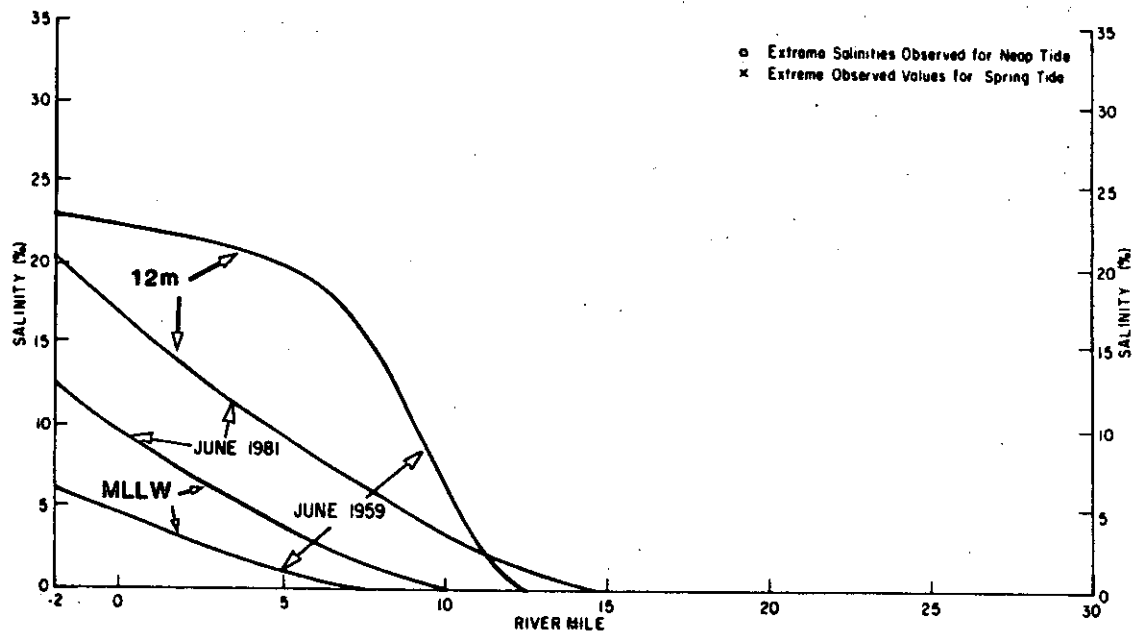


Figure 3.45. Salinity at MLLW and 12 m depth for high flow periods during June 1959 and June 1981.

3.6.4 Neap-to-spring Transitions, Riverflow, and Tidal Range

The results of Sections 3.6.2 and 3.6.3 suggest that neap-spring transitions in density structure are more important at times of low riverflow than at times of high riverflow. The dependence of this transition on the riverflow is the subject of this section. The salinity intrusion under moderate riverflow (300-350 kcfs or $8,500-9,900 \text{ m}^3\text{sec}^{-1}$) has been discussed in Hamilton (1984) and Jay (1983), and the mean salinity at MLLW and 12 m is shown in Figure 3.2b. Salinity intrusion length and tidal monthly changes in stratification are intermediate between those for low flow periods and freshet periods. Figure 3.46, which shows neap and spring values of maximum and minimum salinity intrusion length as functions of riverflow, has been prepared on the basis of the available data and reasonable assumptions about the asymptotic behavior of the system at very high and very low riverflows. It summarizes the present state of knowledge concerning neap-spring transitions.

With regard to the extreme low riverflow case, if the riverflow were decreased far enough, the neap-spring transition that is prominent in the present, low flow season data would disappear (e.g., in the $2,000 \text{ m}^3\text{sec}^{-1}$ riverflow case of Section 3.6.2), because riverflow is necessary for the occurrence of the stratification that makes the transition possible. Salinity intrusion in this hypothetical situation would be greatest on spring tide, because of the greater tidal excursion (Figure 3.41a through c). Increasing the riverflow would result in a situation where the system is highly-stratified on neap tide, and relatively well-mixed on spring tide. This is the existing low flow situation where salinity intrusion is greatest on neap tides (Figures 3.35a through d and 3.37a through d).

A further increase in riverflow would cause the estuary to be moderately- to highly-stratified under all tidal conditions, because the tidal mixing would be insufficient, for all real tidal ranges, to bring about a well-mixed system. This is the present moderate to high flow situation, which minimizes neap-spring differences in salinity intrusion length, because modest neap-spring changes in stratification more or less offset changes in tidal excursion (Figure 3.42a,b). At the highest riverflows, salinity intrusion would again be greatest on spring tide, because the system would be strongly stratified (probably a salt wedge) for all tidal ranges, and because the greater tidal excursion on spring tides would bring the salt water further into the system. Such flows rarely occur with the present, regulated flow cycle (Section 2.2).

In summary, the present neap-spring transition, with its enhanced neap-tide salinity intrusion, is something that can occur only within the range of riverflows defined approximately in Figure 3.46. Were the bathymetry or tidal range to be altered, then the range of flows leading to a neap-spring transition would also be changed (Chapter 5). Given the present regulated flow cycle, neap-spring transitions are prominent during the summer and fall (July to October), but may occur in any season (Jay 1984). Tidal monthly changes in turbidity maxima also occur during the same periods (Section 4.2). In this regard, the large seasonal differences in the amount and type of suspended material

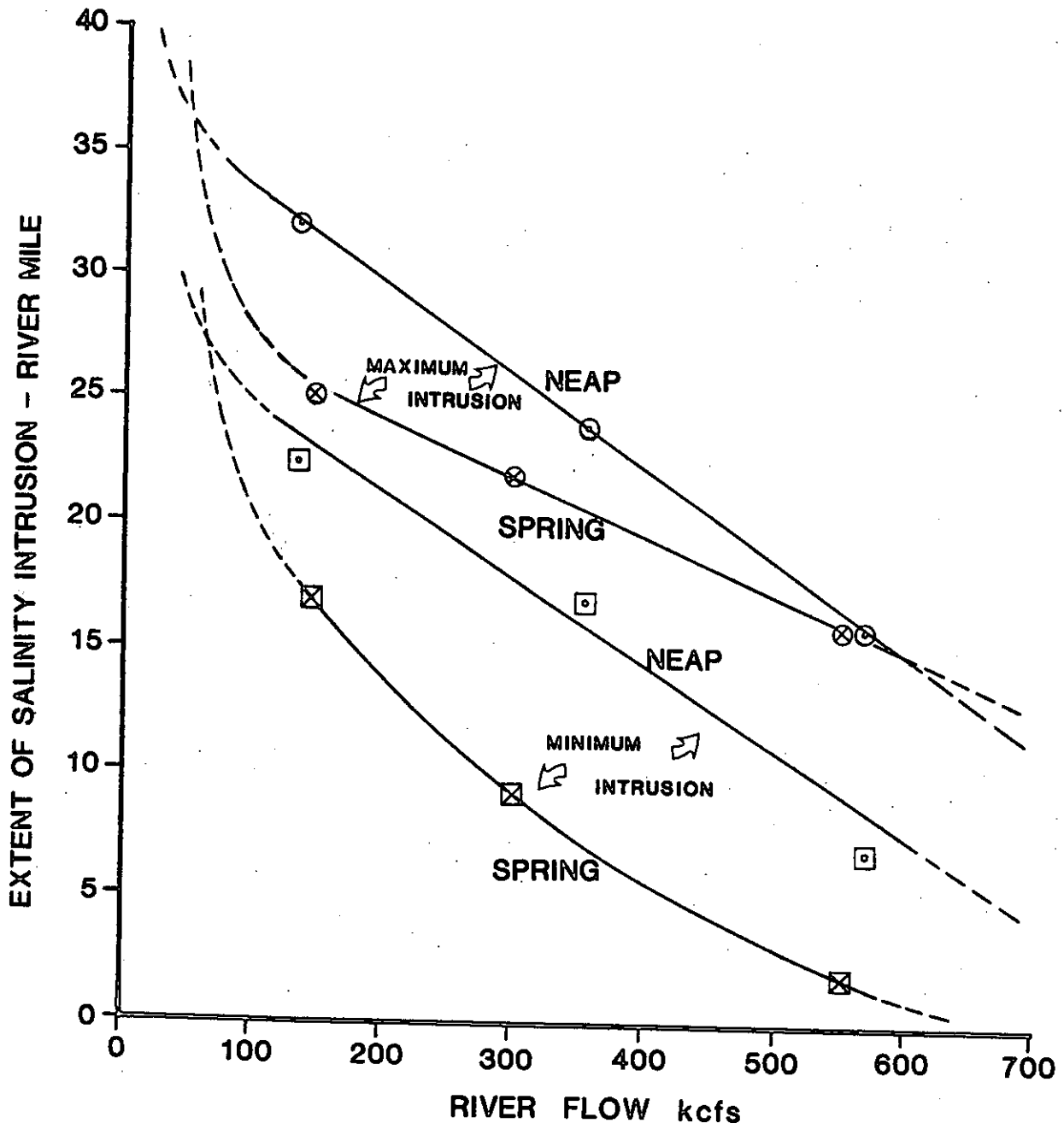


Figure 3.46. Maximum and minimum salinity intrusion length for spring and neap tides, as a function of river flow.

supplied to the estuary and river must also be considered (Section 4.2).

3.7 TRANSPORT PROCESSES

The transport of a conservative substance, such as salt, can be used as an indicator of the behavior of non-conservative substances, such as suspended sediment or organisms, for which insufficient data are available to calculate transports. Aanderaa current meter salinity and velocity records have therefore been used to calculate salt transport at selected cross-sections.

3.7.1 Salt Transport Calculation Method

The salt transport was calculated using the expansion of Robe (1968), adapted to a per unit area basis. The expansion is: transport per unit area in $\text{kg m}^{-2}\text{sec}^{-1}$ $\text{sup } -1 = us + [U'S']$

$$+ [U' \frac{h'}{H}]s + [S' \frac{h'}{H}]u + [S'U' \frac{h'}{H}] + \text{turbulent transport}$$

where the brackets indicate an average over a 24.84 hour tidal cycle and the primes indicate a tidal cycle deviation from the tidal cycle average, h' = tidal height, H is the mean depth, S' is the salinity deviation, U' is the velocity deviation, and s and u are the corresponding mean quantities.

The terms of the expansion represent (from left to right) advection by the mean flow (mean flow transport), tidal advective (or tidal oscillatory) transport, transport by the Stokes drift, the salinity-height correlation transport, the triple-product transport, and transport by turbulent processes. The first term is associated with the mean circulation and movement of riverflow through the system. The remaining terms are all associated with tidal processes. The second term is important when the salinity is, on the average, larger on flood than on ebb. The mean flow transport and the tidal transport are usually the dominant terms in the salt transport balance, but the Stokes drift transport is sometimes important. Previous studies in the Columbia River Estuary have found the last three terms on the right-hand side to be unimportant (Robe 1968; Hansen 1965a,b; Hughes and Rattray 1980).

3.7.2 Transports at Clatsop Spit

The Clatsop Spit-Sand Island cross-section provided the entrance boundary condition for the 1981 NOS study. As such, it was repeatedly and heavily instrumented. It is the only estuary cross-section at which more than a single current meter mooring was deployed for any length of time. The densest sampling occurred in August and September 1981, during which four stations were occupied. Results for the spring season are based on two stations. The number of hours of usable data for each meter for each season is shown in Figures 3.47a and b. The boxes in Figures 3.47a and b indicate the error bars on successive deployments of current meters. The average flows for the low and high flow season were

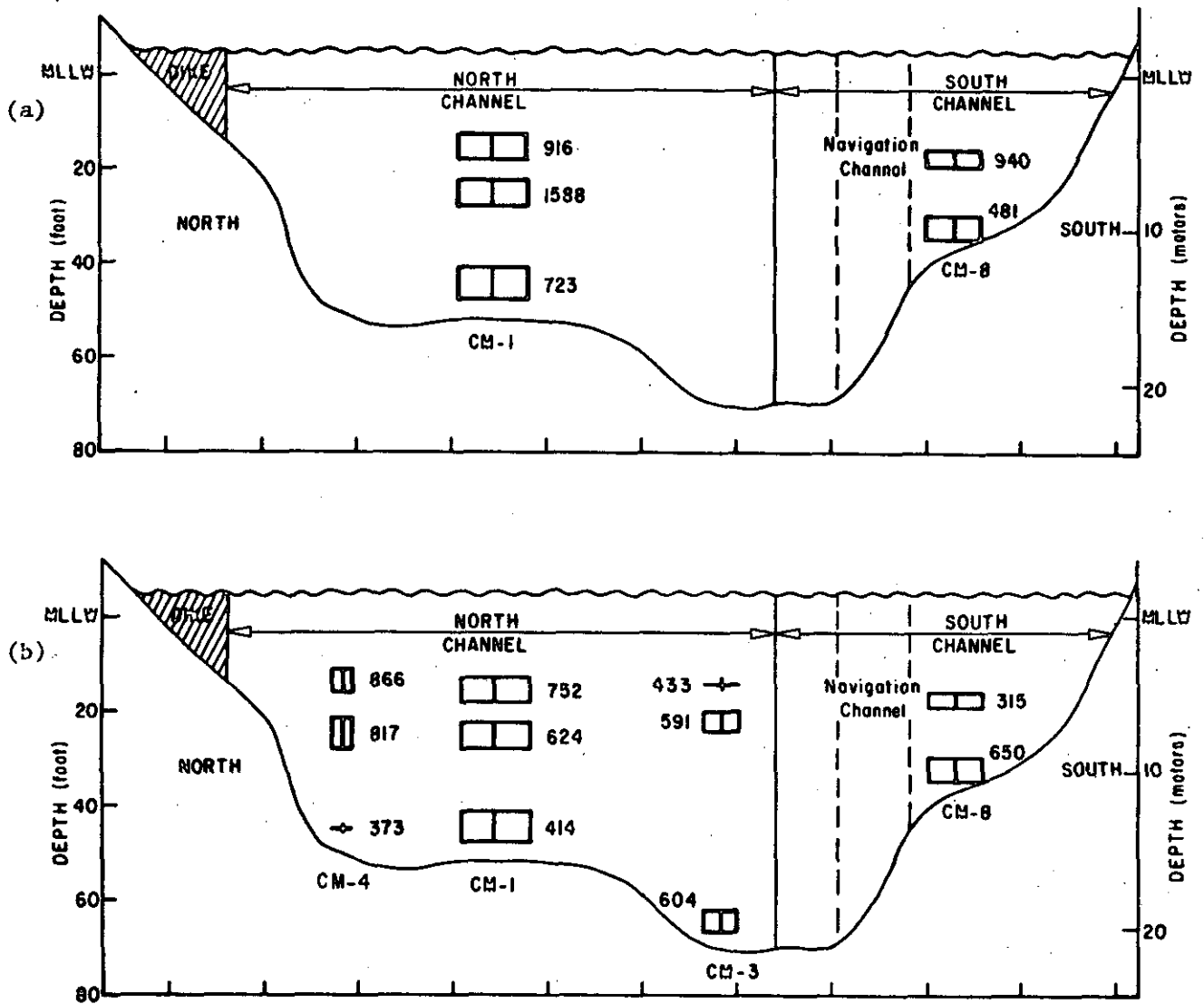


Figure 3.47. Length of record (in hours) and meter positions for current meters on the Clatsop Spit - Sand Island Section for 1981 high flow season (a) and 1981 low flow season (b). Boxes indicate range of depth and horizontal position for successive current meter deployments.

about 155 kcfs ($4,400 \text{ m}^3\text{sec}^{-1}$) and about 310 kcfs ($8,800 \text{ m}^3\text{sec}^{-1}$), respectively.

Mean Flow Properties

The tidal current characteristics at the Clatsop Spit-Sand Island cross-section were discussed in Section 3.3. The tidal flow varies spatially in strength and phase by a factor of at least three and by about one hr (Figure 3.17a and b), respectively, as a result of the influence of bottom friction and the density structure. The strongest tidal flow is at the surface in the middle of the north channel. The tidal prism of the lower estuary, particularly the mid-estuary sand flats, is filled from the north channel side; this interpretation is consistent with sedimentological results (Sherwood et al. 1984).

The mean flow is distributed differently in the cross-section than the tidal flow (Figures 3.48a and b). Outward flow is concentrated at the surface in the south channel, where mean flows reach 0.4 m sec^{-1} during the low flow season and 0.5 m sec^{-1} during the high flow season. During the high flow season there is also substantial (0.3 m sec^{-1}) outflow at the surface of the north channel. The outflow is strongest in the south channel, because the flow in the river channel upstream of Altoona is diverted into the south channel by a series of navigation structures and sand islands (Section 5.3). The outflow at the surface in the north channel probably reflects water transport from the south to the north channel across the sand flats between RM-10 and RM-20.

One striking feature of Figures 3.48a and b is the weakness of the upstream bottom flow during both seasons. The seasonal average net upstream flow does not exceed about 0.11 m sec^{-1} anywhere in the section for either season; it is strongest along the north side of the north channel, where it extends to the surface during the low flow season. Much of the shear in the mean flow is caused by frictional and stratification effects, just as is the case with the tidal flow (Section 3.3); these vary in the along- and cross-channel directions, according to the topography. The two-dimensional, laterally-averaged model also showed net downstream flow at the bottom in this reach (Figures 3.20, 3.22 and 3.44). It is probable that the curvature of the channel near Jetty A is responsible for the inward flow predominance on the north side. The inward flow is directed toward the north side of the channel at Jetty A. The outward flow is directed primarily by the relatively constricted channel topography of the north and south channels.

Salt Transport: Seasonal Averages

The forces maintaining the salt balance have been discussed in Section 3.1.2. Figures 3.49a and b through 3.52a and b show the salinity distribution, the tidal advective (or oscillatory) salt transport, the mean flow salt transport, and the total salt transport (which is the sum of tidal and mean flow transport, the Stokes drift transport, and two other small terms not shown individually) for the high and low flow seasons. The stratification and shear are somewhat greater in the south channel in both seasons, and the tidal currents are weaker. This does not result in upstream bottom flow or inward salt

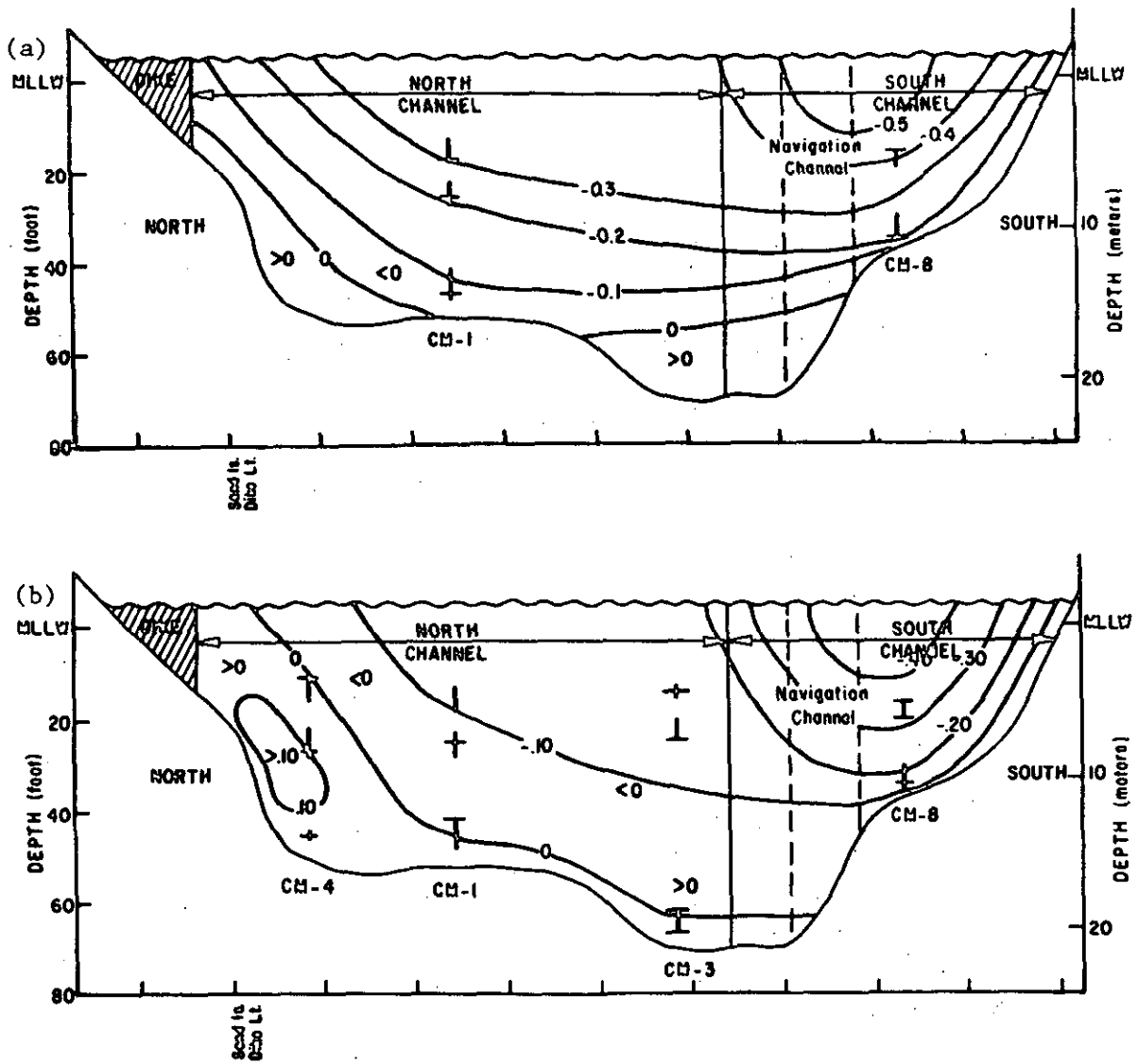


Figure 3.48. Mean flow of water through Clatsop Spit - Sand Island Section in m sec^{-1} during (a) high flow season and (b) low flow season.

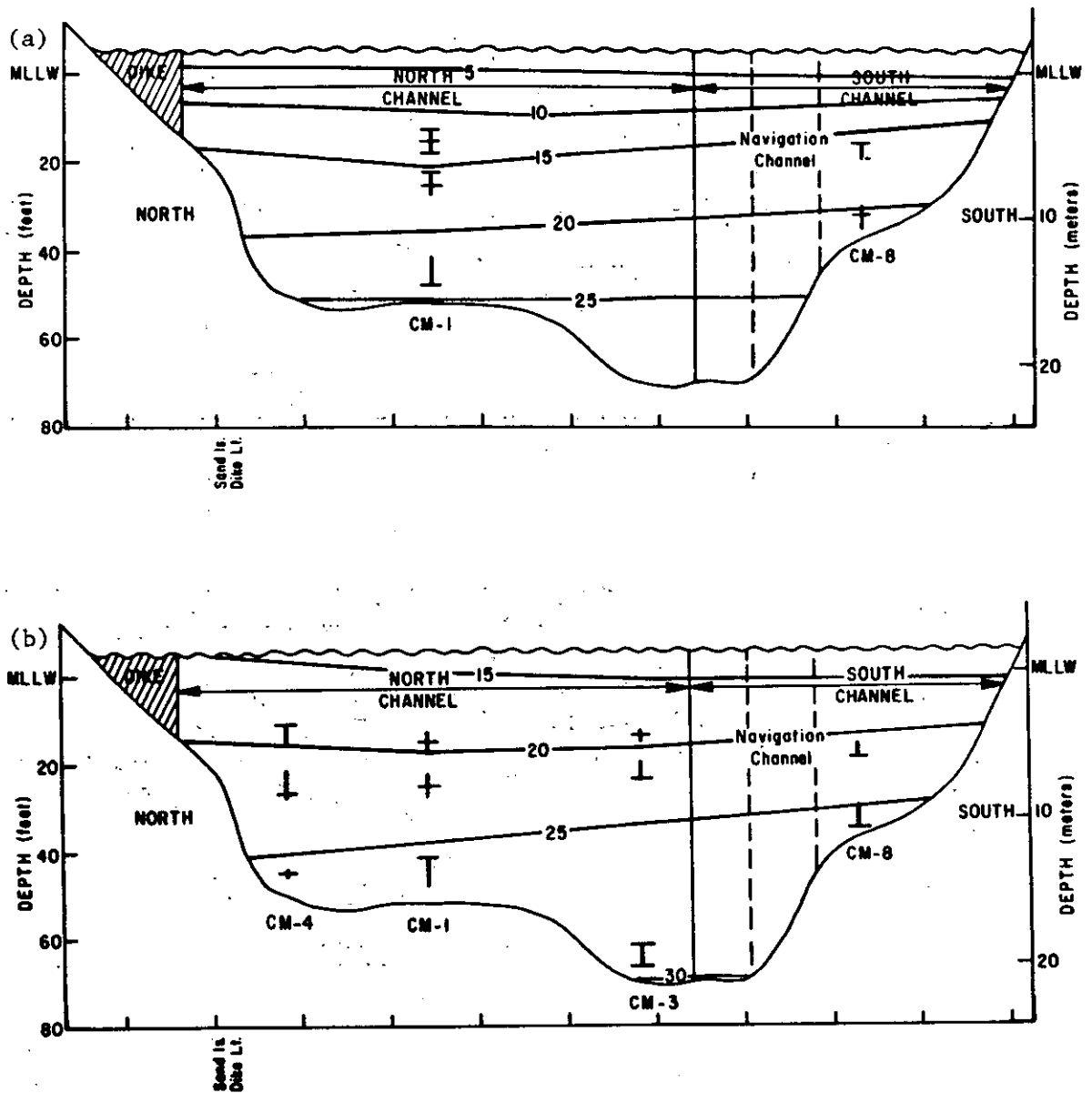


Figure 3.49. Salinity distribution at the Clatsop Spit - Sand Island Section, in ppt, during high flow season (a) and low flow season (b).

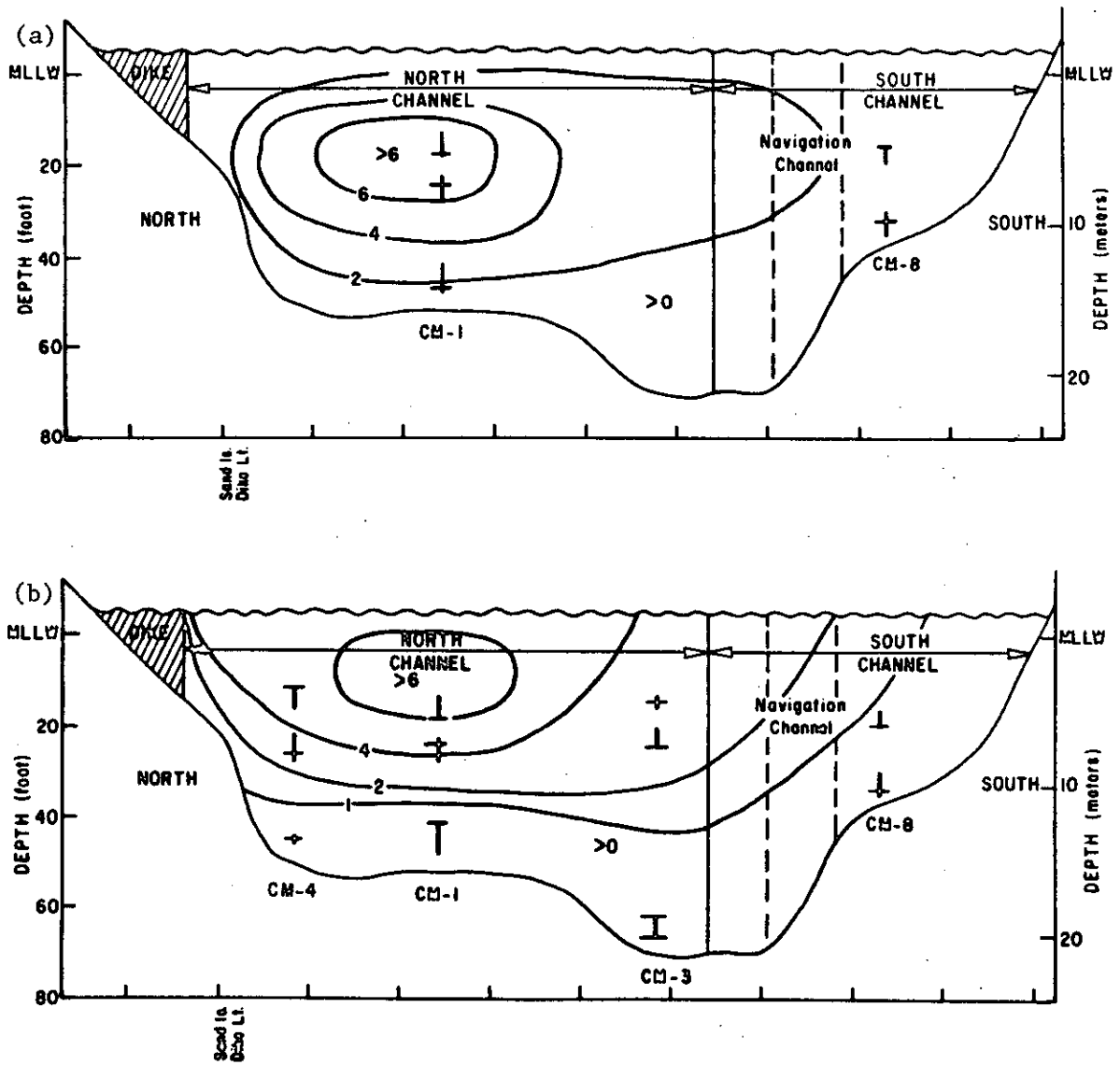


Figure 3.50. Tidal advective salt transport in $\text{kg (m}^2 \text{ sec)}^{-1}$ through the Clatsop Spit - Sand Island Section during (a) high flow season and (b) low flow season.

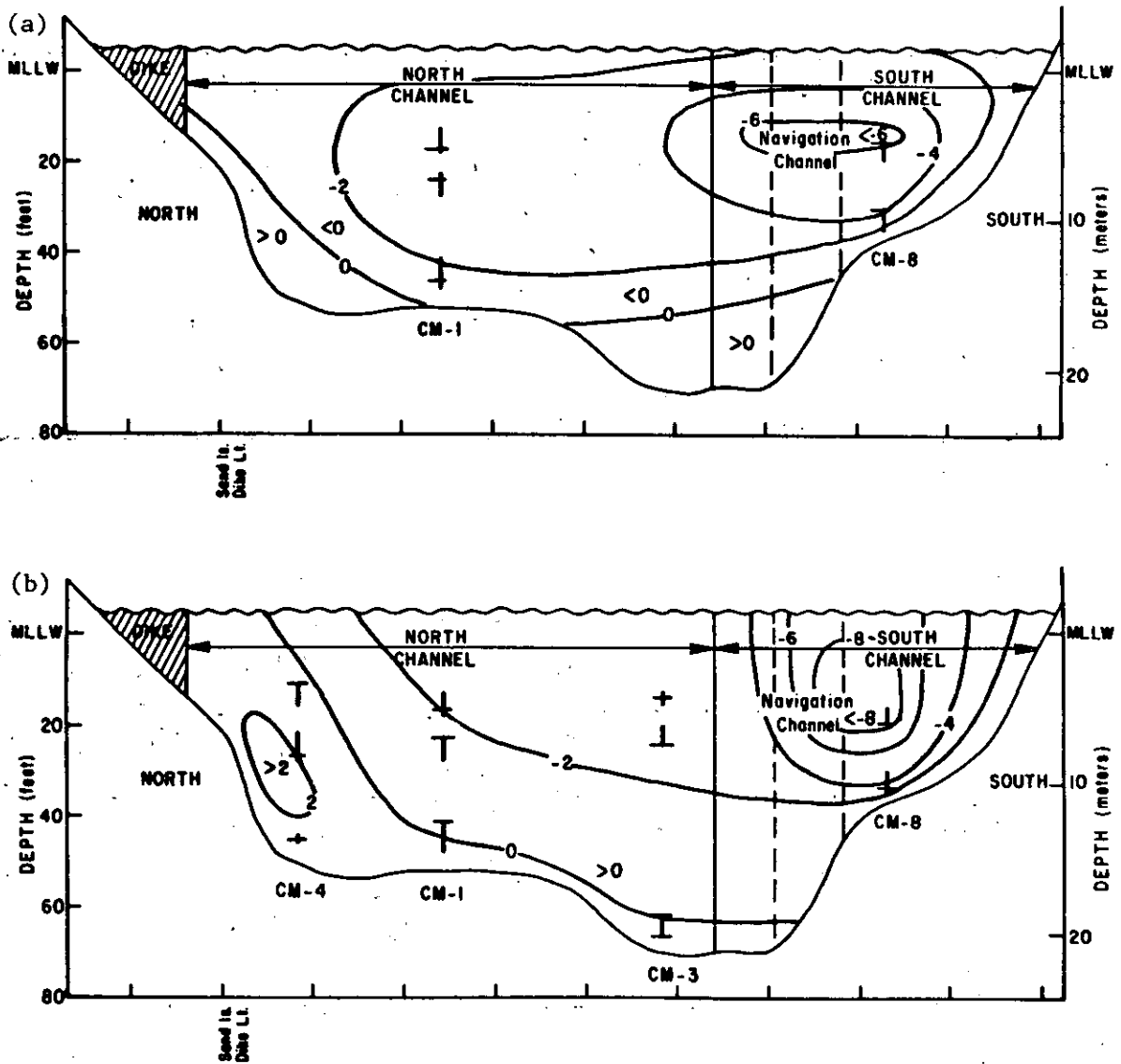


Figure 3.51. Mean flow salt transport in $\text{kg (m}^2 \text{ sec)}^{-1}$ through the Clatsop Spit - Sand Island Section during (a) high flow season and (b) low flow season.

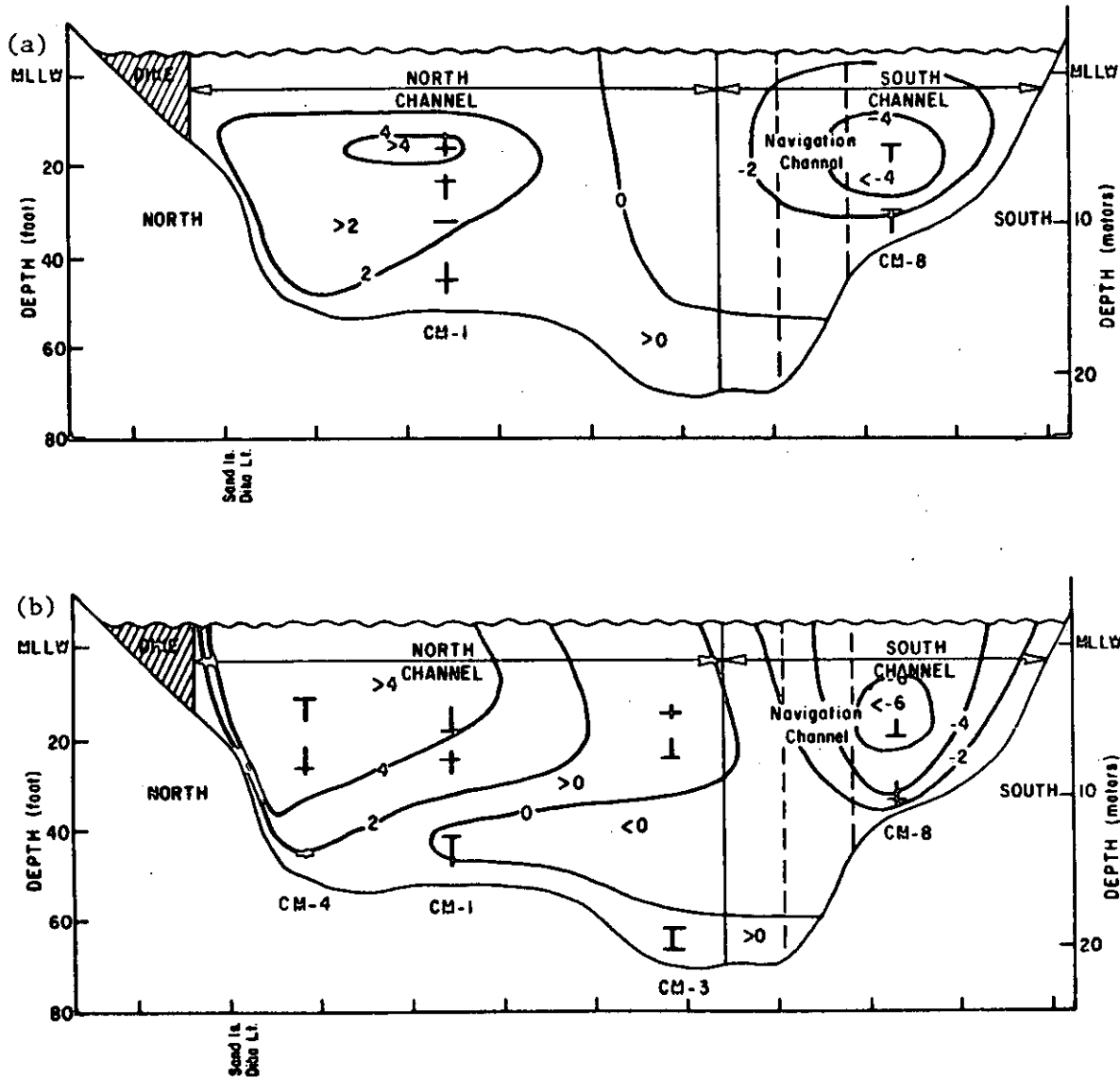


Figure 3.52. Total salt transport in $\text{kg (m}^2 \text{ sec)}^{-1}$ through the Clatsop Spit - Sand Island Section during (a) high-flow season and (b) low-flow season.

transport, because of the very large net outward flow of water in the south channel. The salinity is slightly higher (Figures 3.49a and b) on the north side, which is consistent with the larger net inflow there.

Inward salt transport is accomplished in a jet in the middle of the north channel (Figures 3.50a and b). The depth of the strongest transport is about 3 to 5 m below MLLW in the low flow season and about 5 to 6 m in the high flow season. The strongest tidal currents occur at the same lateral position, but at the surface. The salt transport drops off at the surface because the surface salinity is lower, particularly in the high flow season.

Outward salt transport by the mean flow is accomplished in a jet in the south channel at a depth of about 3 to 5 m in the high flow season and about 2 to 4 m in the low flow season (Figures 3.51a and b). As with the tidal transport in the north channel, the outward transport in the south channel occurs at slightly greater depth during the high flow season, because surface salinities are lower then. Inward transport by the mean flow is strongest along the north side during the low flow season. Salt transport near the bottom is weak in all seasons.

The total salt transport by all processes (Figures 3.52a and b) is inward in the north channel and outward in the south channel in both seasons. There are at least two important implications here. First, Figures 3.50a and b through 3.52a and b are striking confirmation of the analysis of Section 3.1, which argued that the salt balance was maintained (in the face of strong, outward surface transport of salt by the mean flow) by inward tidal transport of salt. The inward transport near the bottom by the mean flow is of secondary importance in maintaining this balance. The importance of tidal transport in the salt balance suggests that tidal mechanisms are also important in the transport of suspended material and phytoplankton. This conclusion is supported by the results of Chapter 7.

Second, inward and outward salt transports are laterally separated. The lateral separation is, in part, a function of the topography of this particular section, seaward of the junction of the north and south channels. A section closer to the entrance might show a very different lateral pattern, but Desdemona Sands (upstream of the Clatsop Spit-Sand Island section) provides a partial barrier to transport between channels. Net upstream transport should be found at stations in the north channel, and downstream transport at stations in the south channel for some distance upstream of Clatsop Spit. The water in the north channel has been in the system a shorter time, on the average, than water in the south channel. This suggests that substantial differences between the two channels in the concentration of suspended material (input primarily by the river) and organisms may occur. The observed separation of inward and outward transport does not fit the lateral gravitational circulation mechanism proposed by Fischer (1976), because Fischer's postulated mechanism did not include tidal processes.

Conservation of salt requires that the salt transported into the north channel somehow reach the south channel, so that it may return to the ocean. The most probable mechanism for this process is the same

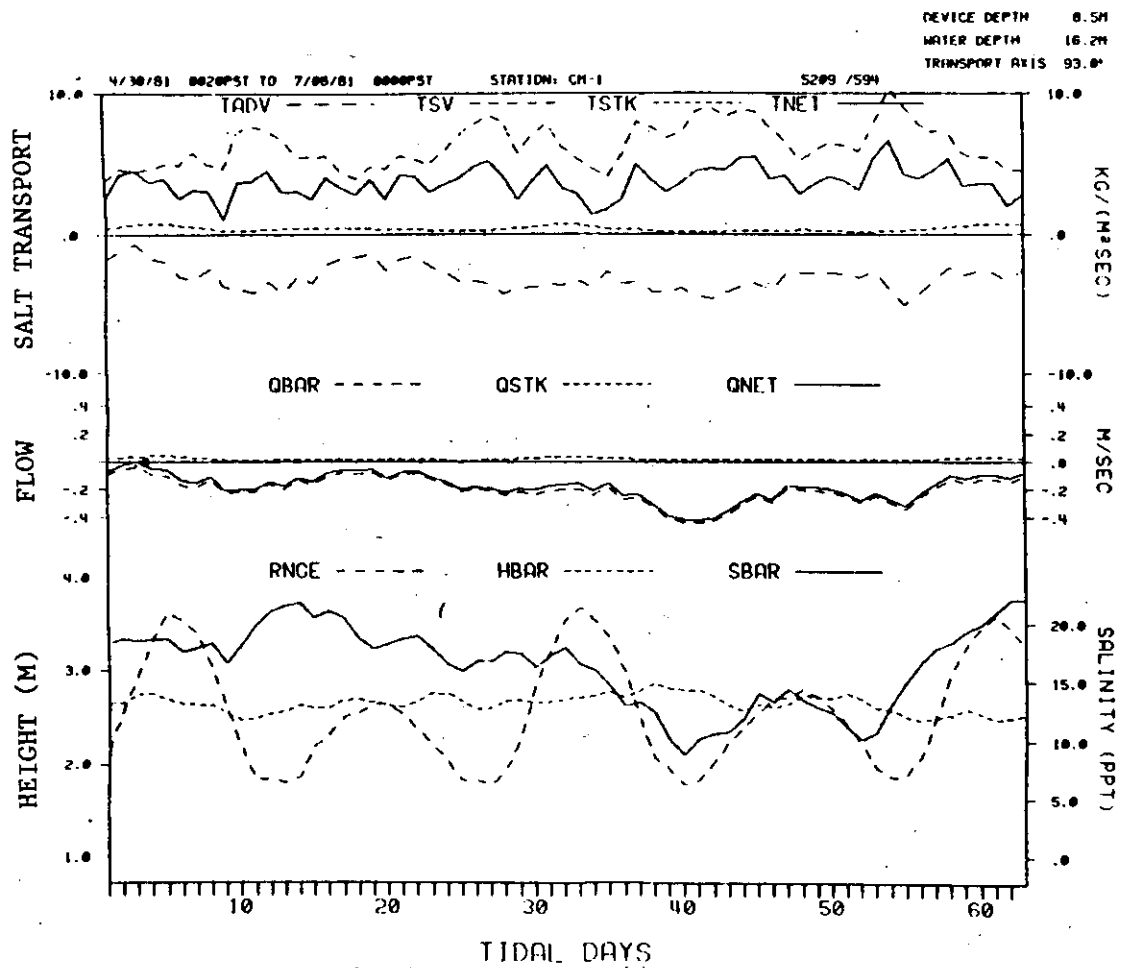
channels that transport water from south to north channel across the mid-estuary flats, between RM-10 and RM-20. Although they have a net water transport toward the north channel, they are ideally situated to have a salt transport in the opposite direction. These channels run diagonally from low river mile in the north channel to high river mile in south channel. They transport low-salinity water to the north channel on the ebb and high-salinity water to the south channel on flood. The strength of the transport in these channels may be augmented by the phase difference in tidal forcing at the two ends. Since these channels are very shallow, the Stokes drift may play an important role in the water and salt transport.

Salt Transport: Temporal Variations

The temporal variations in salt transport at Clatsop Spit have been examined by plotting time series of salt transport parameters for individual meters. The picture that emerges is one of complex, compensating changes in different parts of the cross-section. There is an increase of stratification on neap tides causing salinity increases at surface meters on spring tides. There is also some redistribution in the vertical of mean flow related to changes in stratification. In general, the tidal monthly changes at most Clatsop Spit meters were less dramatic than further up-estuary.

The longest continuous record for the Clatsop Spit-Sand Island section is for a mid-depth (about 6 to 8 m) meter at CM-1, for which 4 continuous deployments are available during the high flow season (Figure 3.53). The strongest tidal monthly changes at Clatsop Spit were also found in this record. Figure 3.53 covers slightly more than two tidal months and includes the 1981 spring freshet. The most striking features of Figure 3.53 are the increase in outward flow and decrease in average salinity during the freshet and the regular neap-to-spring changes in salt transport terms. The total salt transport is inward at all times despite the outward mean flow, because this meter is located just below the center of the jet of inward tidal transport. There is an increase in both tidal and mean flow salt transport during the freshet period. The outward mean flow salt transport increases slightly with increasing riverflow, but not in direct proportion to the flow. This occurs because an increase in outflow is associated with a decrease in salinity. The tidal transport at mid-depth increases as the riverflow increases and the flow becomes more stratified (as in Figures 3.54a and b). Under these conditions the salinity difference between flood and ebb can be very large at mid-depth as the interface moves up and down.

With regard to tidal-monthly changes, the inward tidal transport increases substantially with increased stratification on neap tides, without a large increase in average salinity. Small adjustments in both mean flow and salinity also cause substantial neap-to-spring adjustments in mean flow salt transport. These neap-to-spring changes in mean flow salt transport partially compensate for the neap tide increases in tidal transport, so that the total salt transport is less variable during the tidal month than either term individually. There is a slight tendency for a larger total inward salt transport at this station on a neap tide, which is in part compensated at other meters at this section and which



RNCE = tidal range	TADV = mean flow salt transport
HBAR = low-passed tidal height	TSV = tidal oscillatory salt transport
SBAR = low-passed salinity	TSTK = salt transport by stokes drift
QBAR = mean flow	TNET = net salt transport
QSTK = stokes drift	
QNET = net drift	

Figure 3.53. Time series of salt and water transport parameters at mid-depth at CM-1 (RM-5, middle of north channel) for spring 1981.

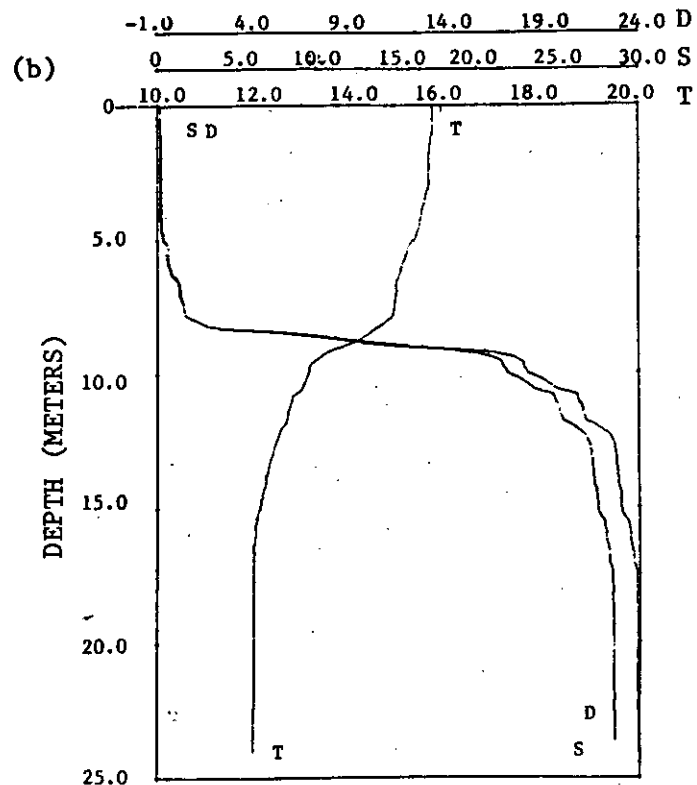
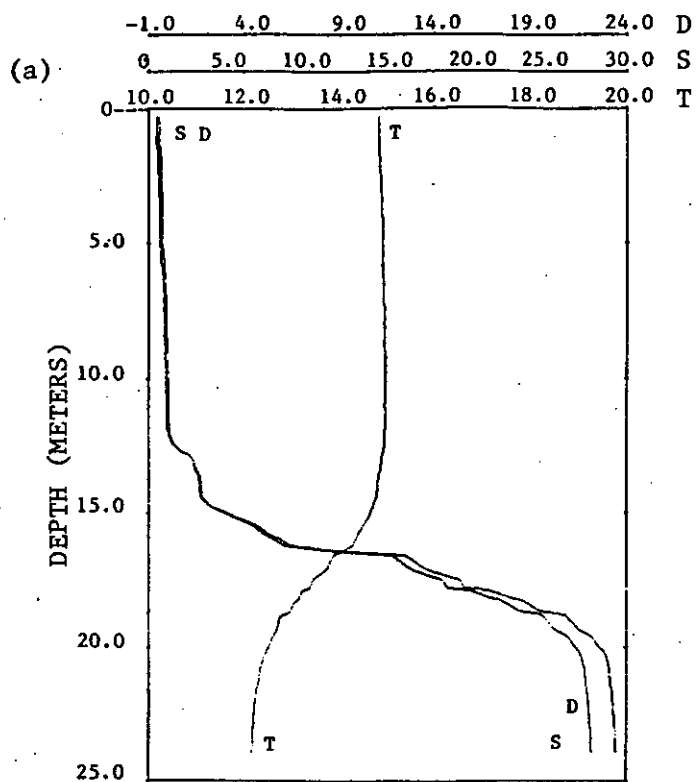


Figure 3.54. Temperature (T), salinity (S), and sigma-t (D) profiles at the end of weaker ebb (a), and the end of weaker flood (b).

in part contributes to the increase in average salinity during the neap at stations further up the estuary.

In summary, large changes in mean flow and tidal cycle average salinity during the spring season do not result in large changes in salt transport at the Clatsop Spit-Sand Island section, because the mean flow and the average salinity change in opposite directions. The mean flow salt transport and the tidal salt transport also tend to change in opposite directions during the neap to spring cycle so that the total salt transport is more stable than the individual terms contributing to it.

3.7.3 Salt Transport at Astoria (RM-15): Temporal Variations

Station CM-9 was one of the two highest priority stations during the 1981 NOS sampling. Extensive records are available for mid-depth meters, but results are spotty for near-surface and near-bottom meters. Figure 3.55 shows the salt transport parameters for a 110 tidal day period from May 5 to August 31, 1981, for successive deployments of meters at about 5 to 7 m below MLLW. Mean flow ranges from more than 0.4 m sec^{-1} in the downstream direction to near zero late in the record. Significant net upstream flow never occurs, and the net downstream flow is small only after two neap tides late in the record. Mean salinities range from near zero for 20 days during the freshet to about 13 ppt just after a neap tide in August.

Salt transports early in the record are small and variable. Salinity and salt transport terms vanish during the June 1981 freshet period. The post-freshet period is the most interesting. As at Clatsop Spit, there is a tendency (with important exceptions) for changes in the mean and the tidal salt transports to compensate one another, but the salt transports are greatest on spring rather than neap tides. The net salt transport is small and slightly inward, until the last 20 days of the record, during which two interesting events occur, following neap tides.

These two events are similar to the event observed in detail during the October 1980 cruise and events which are believed to have occurred on several other neap tides in 1980. At or after the period of minimum tidal range, the mean salinities increase dramatically (in one case in Figure 3.55, from about 4 to 13 ppt). This increase is accompanied by a sharp decrease in downstream mean flow salt transport and a resulting strong, upstream total salt transport. Meters located closer to the bottom show a maximum salinity in phase (in some cases) with that at mid-depth and somewhat earlier (closer to the neap tide) in other cases. The near-bottom salinity may increase by as much as 15 ppt. Near-surface meters show very little change in salinity; thus, the stratification is greatly increased.

These events have been interpreted in Section 3.6 as instances in which the system undergoes a transition from a moderately-stratified to a highly-stratified condition. The transition is a function of the decrease in tidal energy for mixing on the weaker tides. Note that each of the last four neap tides is accompanied by an increase in salinity,

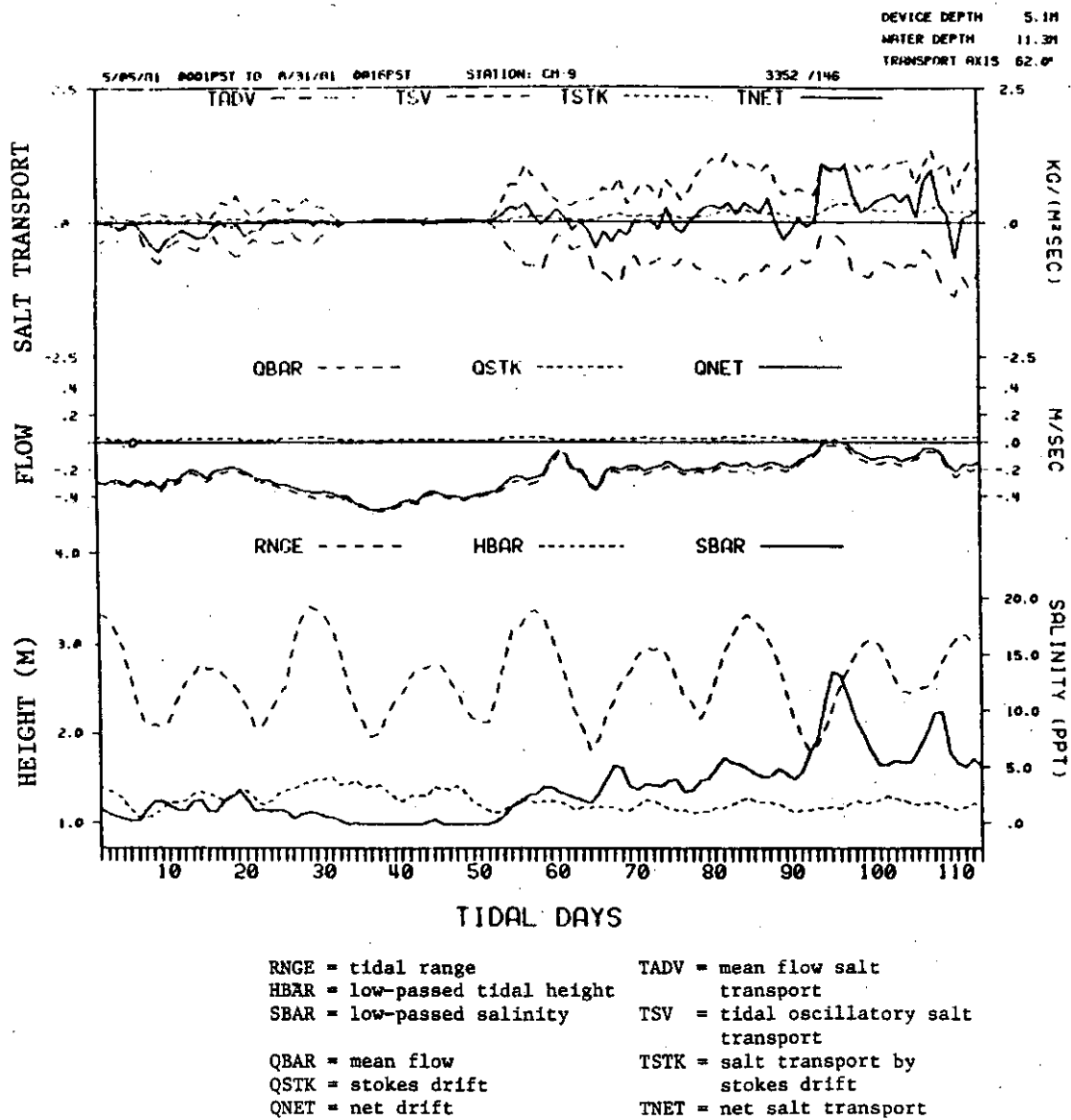


Figure 3.55. Time series of salt and water transport parameters at mid-depth at CM-9 (RM-15, off Astoria, in the south channel) for spring and summer 1981. The salinity is 0 ppt for about 20 days during the spring freshet (days 32 to 52). There is an increase in salinity after each neap tide. Apparently only the last two neap tides resulted in formation of a salt wedge and dramatically increased salinity intrusion and salt transport.

which increases as the riverflow and tidal range decrease. Only the last two neap tides have major effects on transport processes, presumably because the other events are too weak to cause the system to undergo a change in state from moderately to highly-stratified. It appears, therefore, that strong salinity intrusion events, during which the system becomes highly stratified above the Astoria-Megler Bridge and during which salinity intrusion above Tongue Point is greatly enhanced, are somewhat sporadic. Figures 3.46 and 3.55 show that the transition does not occur if the riverflow or the tidal energy is too high, but necessary and sufficient conditions have not yet been precisely defined.

In summary, the tidal monthly variation in tidal energy is the primary factor governing salt transport processes above the Astoria-Megler Bridge, during the low flow season. These processes are confined to the deeper part of the navigation channel and probably have little direct effect on the shallower parts of the estuary in that surface salinities are less strongly affected than salinities at depth. However, these tidal monthly changes are important with regard to the accumulation and cycling of detritus and other suspended material in the turbidity maximum (Section 4.4).

3.8 PERIPHERAL BAYS

As a result of the primitive state of knowledge concerning the circulation of the Columbia River Estuary prior to 1980, the NOS and CREDDP field programs both concentrated on circulatory processes in the main body of the estuary. The following section summarizes the small amount of information that is available for the peripheral bays.

3.8.1 Baker Bay

Baker Bay is tributary to the estuary between Jetty A (RM-3) and RM-9 of the north channel. It has three entrances and is predominantly shallow except for Sand Island Channel, in which depths of 30 ft (9 m) occur and through which most of the tidal exchange occurs. The outer side of the Sand Islands is affected by both strong currents and wind waves. Wind-driven currents and wind setup may be of some importance in the interior of the bay (Hamilton 1984). Local tributary inflow is insignificant.

No salinity data are available inside the bay. The 1980-81 data available for the three entrances suggest that stratification is probably minimal in the shallow interior of the bay and substantial in the deeper water of Sand Island Gap when the incoming flow from the north channel is stratified. Salinities at mid-depth in Sand Island Channel during the high flow season ranged from 0.1 to 30.3 ppt. During the summer-fall low flow season, they ranged from 6.4 to more than 32 ppt.

Tidal height data available for Jetty A, Ilwaco, Chinook, and Sand Island Gap (pressure gauge data) show that the semidiurnal tide is slightly damped inside the bay; M2 tidal height amplitudes are slightly lower (except for Sand Island Channel) than for stations at nearby locations outside the bay. There is no such effect on the diurnal

constituents, and the tide in Baker Bay, like the tide in the entrance, is more diurnal than that elsewhere in the rest of the estuary.

3.8.2 Youngs Bay

Youngs Bay is a tributary to the south channel between Tansy Point and the Port of Astoria. The channel into Youngs Bay has a controlling depth of about 10 ft (3 m) near its entrance to the Columbia River, limiting the intrusion of saline water. Deeper holes occur near the entrance to Youngs River. Construction of the two bridge causeways, diking, and extension of the Skipanon spits have greatly altered the form of Youngs Bay (Thomas 1983) and have isolated Alder Cove from the rest of the bay. The Youngs River (average flow about 560 cfs ($16 \text{ m}^3 \text{ sec}^{-1}$) and the Lewis and Clark River (average flow about 255 cfs or $7 \text{ m}^3 \text{ sec}^{-1}$; OSU Ocean Engineering Programs 1975) provide sufficient runoff that local tributary water may be distinguished as a water type from RW during winter highflow periods. The runoff pattern is similar to that of other coastal basins. About two-thirds of the annual average river inflow occurs during the months of December to March. Less than 5% of the flow occurs during the months of July to September. Salinities in the bay range from fresh under high flow conditions to more than 20 ppt under low flow conditions (OSU Ocean Engineering Programs 1975). Substantial stratification may occur in the deeper parts of the bay under low flow conditions.

The most important factors in the circulation of Youngs Bay are the very shallow depths (less than 15 ft or 5 m, except in isolated holes) and the standing wave tide in the bay. The tidal wave in Youngs Bay is less progressive than that in the main body of the estuary, because of the geometry, and because the small riverflow through Youngs Bay results in much less friction. The result is a slight amplification of the tide in Youngs Bay (mean tidal range 2.06 m as opposed to 2.03 m at the Port Docks). Because of the form of the tide in Youngs Bay, the tides and currents are nearly in phase, high water occurs nearly simultaneously throughout the bay above the bridge, and the current phase leads that in the adjacent Columbia River. Thus, early in the flood tide in Youngs Bay the Columbia River is still ebbing, and at the beginning of ebb in Youngs Bay the Columbia River is still flooding. Current meter harmonic analysis results show that the current in Youngs Bay is about 90 min earlier than in the adjacent south channel.

Another result of the phase difference between Youngs Bay and the main river is that the salinity in Youngs Bay often exhibits multiple maxima and minima. This occurs because the salinity on the flood (in Youngs Bay) first decreases (as the Columbia River ebbs) and then increases (as the Columbia River floods). The process is reversed on ebb.

Wind-driven circulation in Youngs Bay is probably not of great importance because the fetch is limited, except seaward of the causeway, where wind waves may be of some importance in disturbing the bottom in shallow water.

3.8.3 Grays Bay

Grays Bay is a topographically complex area of rocky, deep channels (along the north shore) and shallow flats separated by minor channels (the rest of the bay). The Grays River contributes an average of 14,130 cfs ($400 \text{ m}^3 \text{ sec}^{-1}$) of runoff; freshets may reach 20,000 cfs ($570 \text{ m}^3 \text{ sec}^{-1}$; Good and Jay 1978). This flow is too small to have an appreciable effect on circulation except in the bay. However, Grays Bay is relatively exposed to the wind and wind waves, and wind-driven set-up is expected to have a significant effect on the circulation in the bay.

The largest tidal range (M2 amplitude of 0.98 m) of any station in the estuary has been observed at Knappton on the west edge of the bay. This may be the result of limited freshwater flow and thus lower friction. It is not known whether the tide is further amplified in the interior of Grays Bay. Only one near-bottom current meter (off Knappton) has been installed in Grays Bay, in May 1981. This meter and the two-dimensional, vertically-integrated model suggest very minimal salinity intrusion into the deeper channels of Grays Bay under a freshwater flow of 250,000 cfs. More salinity intrusion must occur under lower flow conditions, but the channels of Grays Bay have very shallow sills which would prevent upstream penetration of a salt wedge.

3.8.4 Cathlamet Bay

Cathlamet Bay comprises the largest part of the surface of the estuary from RM-19 to RM-30, near and above the upper limits of salinity intrusion. It consists of a complex network of channels separating flats, marshes, and swamp islands. It is separated from the navigation channel to its north by numerous sand banks, both natural and artificial.

The proposed deepening of the navigation channel to Tongue Point raised questions concerning salinity intrusion into Cathlamet Bay. Data from several current meter moorings (Jay 1982) and the two-dimensional vertical model (Hamilton 1984) give some preliminary ideas concerning the salinity intrusion into the channels of the bay. The same ideas probably apply to Grays Bay. The complexity of the salinity distribution within Cathlamet Bay arises from the complexity of the circulatory processes outside the bay, the multiple entrances to the bay between Tongue Point and Miller Sands, the channel connections in the bay, and the topography of each channel. The entrances through which salt can enter the bay are Tongue Point Basin (sill depth 24 ft or 7m), Cathlamet Bay north channel (sill depth 30 ft or 9m), Woody Island Channel (sill depth 12 ft or 3.5m), and the channel near Miller Sands (sill depth 20 ft or 6m). Entrances upriver from Miller Sands are too shallow or too far upstream to allow salinity intrusion.

During periods of maximum salinity intrusion (low flow, neap tides) salt water moves up the navigation channel as a salt wedge (Section 3.6) that has very strong horizontal and vertical gradients. The distance up the navigation channel that this wedge penetrates is a complex function of tidal range, topography, riverflow and atmospheric forcing. The presence or absence of saline water at sill depth of each entrance of Cathlamet Bay is far more difficult to predict than for the other bays

that are closer to the ocean (Jay 1982). As in Grays Bay, the complex topography inside the bay also renders modeling of salinity intrusion difficult.

Salinity data collected during 1980-81 show that the water in the bay is fresh, except under low flow, neap tide conditions. The maximum salinity observed in the bay was 10.66 ppt, but higher salinities probably occur. Salinities are clearly greater in southern Cathlamet Bay because of the deeper sill depth and proximity to Tongue Point. Model results (Hamilton 1983, 1984) confirm that significant salinity intrusion occurs only on neap tides, and that surface salinities are probably always low. The model results also show that deepening the navigation channel would increase near-bottom salinities, without affecting surface salinities in the Bay.

3.9 SUMMARY

3.9.1 Summary of Present Knowledge

Circulatory studies were carried out in six areas: theory of estuarine circulation, tidal circulation, density distribution, salt transport, low-frequency flow processes, and estuarine modeling. Detailed results are reported in Jay (1984) and Hamilton (1984).

The primary theoretical results are the definition of modes of estuarine circulation and an analysis of the forces maintaining the salinity distribution. The circulation modes are defined by application of a scaling analysis and a perturbation expansion. This analysis separates the primary, tidal circulatory processes from the secondary, modifying features. The primary tidal circulation occurs at diurnal and semidiurnal frequencies and constitutes the first estuarine circulation mode. The secondary circulation modifies the primary circulation. It is divided into three modes that occur at different frequencies: the tidal higher harmonics or overtones (that occur at frequencies higher than semidiurnal and are produced by the distortion of the tidal wave as it moved upriver), the secondary tidal circulation (at diurnal and semidiurnal frequencies), and the residual (mean or time-averaged) circulation which varies over the tidal month and seasonally. The residual circulation is driven by the riverflow, the salinity distribution, energy transferred from the primary tidal circulation, and, to a lesser extent, atmospheric effects. The influence of the residual flow on biological processes is particularly important.

Use of the same perturbation expansion to define salinity distribution modes provides important insight into the forces that maintain salt in the estuary. The analysis indicates that the salinity distribution is maintained primarily by the tidal currents (including the density-driven part thereof) working on the salinity gradient (horizontal salinity variations), not by the mean flow.

With regard to the tidal circulation and its interaction with the mean flow and the density structure, the energy budget, data analysis and model results show that:

- 1) The three most important time scales of estuarine motion are tidal daily, tidal monthly and seasonal. Processes on these time scales are linked by various non-linear interactions. Important non-linear processes include bottom friction, distortion of the tidal wave in shallow water, the Stokes drift, and the interaction of vertical mixing and stratification. They influence the tidal flow, the mean flow, the salinity distribution, and sedimentary and biological processes.
- 2) Tidal range decreases more rapidly in the upriver direction on the tides of greater range; that is, an increase in tidal range at the mouth results in a less than proportional increase upriver. This occurs because the tidal energy flux into the estuary varies approximately with the square of the tidal range, but the frictional energy loss (dissipation) varies with the cube of tidal range.
- 3) Freshets reduce the tidal range and greatly increase the river stage (water surface level) above RM-20, because the riverflow increases the friction. Tides and river stage below Tongue Point are much less affected by such changes in riverflow.
- 4) Tidal exchange and tidal velocities are greater in the north channel than in the south channel. Most of the tidal prism of the lower estuary is filled by the flow in the north channel.
- 5) The tidal energy flux from the ocean is the dominant source of energy for circulatory processes in the estuary. The energy budget in the estuary is essentially: tidal energy flux is balanced by dissipation. The potential energy flux of the riverflow (i.e., energy released as the water flows downhill) is the dominant source of energy in the fluvial part of the system. The energy budget in the river is: potential energy is balanced by dissipation. The high riverflows during major freshets (e.g., 1894 and 1948) provide much more energy than any possible tide, but most of this energy is dissipated in the fluvial part of the system above RM-30.
- 6) There is a distinct energy minimum, between RM-18 and RM-30, where neither tidal nor fluvial energy inputs are large. This energy minimum may explain the location of the many deposition features of Cathlamet Bay.
- 7) There is more energy available for mixing on the ebb than on the flood, because of the strength of the riverflow. The greater mixing on the ebb and the effects of salinity intrusion combine to make the vertical structure of the ebb currents very different than that of flood currents; this is the ebb-flood asymmetry. The vertical distribution of the mean flow is determined by the differences between the ebb and flood flows. The large shear (vertical differences in velocity) on ebb, the relative vertical uniformity of the flood flow and the salinity intrusion combine to generate net upstream bottom currents in the lower estuary.
- 8) The vertical structure of the currents is, however, also strongly

influenced by along-channel changes in depth and width. Mean upstream bottom flow associated with strong horizontal salinity gradients is not continuous from the entrance to the upstream limits of salinity intrusion. Its continuity is often interrupted by pockets of mean downstream bottom flow caused by topographic features. This suggests that the accumulation and cycling of detritus and other suspended material in the turbidity maximum, which is dependent upon the upstream bottom flow, may occur preferentially in certain parts of the estuary or may be spatially discontinuous.

- 9) Neap-spring changes in tidal energy cause changes in vertical mixing that alter the density structure. Because of the relationship between stratification and vertical mixing, substantial neap-spring changes in mean and tidal flow occur. The changes in the spatial distribution of the mean flow cause neap-spring changes in suspended sediment concentrations and biological processes dependent on the cycling of detritus.
- 10) The neap-to-spring transition is most prominent during low flow periods and changes the salinity structure from partially-mixed or well-mixed (spring tide) to stratified (neap tide). The transition may occur abruptly, because of the interaction of vertical mixing and stratification. Increased stratification during the period of decreasing tidal range before the neap tide inhibits mixing which, in turn, allows a further increase in stratification. The process is reversed as the tidal range increases after the neap tide. Neap-to-spring changes in salinity structure become less important as the riverflow increases.
- 11) Salinity intrusion length is greatest under low flow, neap-tide conditions, when salinity intrusion may reach to about RM-30 in the navigation channel, because the stratification allows upstream movement of salt without significant mixing with the overlying river water. Under the highest flow conditions, salt may be absent upriver of RM-2 for several hours at the end of ebb.

The high flow (about 310 kcfs or $8,800 \text{ m}^3 \text{ sec}^{-1}$) and low flow (about 155 kcfs or $4,400 \text{ m}^3 \text{ s}^{-1}$) seasonal mean, minimum, and maximum salinity distributions have been defined for north and south channels. These seasonal distributions should be useful in understanding biological processes having seasonal time scales, but averaging obscures physical processes which are better understood in terms of the actual states of the system. The seasonal averages suggest that salinity intrusion into the north channel is somewhat greater than that into the south channel under high flow conditions, because of the stronger riverflow in the south channel. The difference is less pronounced under low flow conditions.

Salt and water transport calculations also show that most of the net outflow of water is near the surface in the south channel. Upstream bottom flow is strongest in the north channel. Salt enters the estuary primarily by tidal mechanisms in a near-surface jet in the north channel, at the same lateral position as the strongest tidal currents.

Unlike the currents the maximum salt transport is below the surface because the salinity is lower at the surface. The mean or residual circulation appears to be important in inward salt transport only on neap tides and in those parts of the estuary where horizontal salinity gradients are unusually strong. Salt transports near the bottom are otherwise small. The large, near-surface, net outflow in the south channel transports salt out of the estuary.

3.9.2 Areas for Future Work

The 1980 field program and the large NOS data set that arrived less than a year before the end of the program have provided one of the most intensive and extensive physical data bases available for any estuary of comparable size, but one which is still incompletely analyzed. There are, however, certain areas in which even this data base is inadequate and certain important processes that have not been examined at all. One area that has been found to be critical to the salt and mass balance of the estuary is the mid-estuary flats. Substantial exchanges of water and salt are believed to occur in the subsidiary channels that cross these flats, but no data are available to assess these transports.

The entrance has been a serious obstacle to navigators for over a century (Gibbs 1973), and severe working conditions have limited the acquisition of data seaward of Jetty A. Despite plans to deepen the entrance channel, knowledge of this area cannot be considered sufficient for prediction of tidal currents or severe waves, or for channel design and management of dredging. It is vital to know whether critical conditions are reached at any stage of the tide for propagation of internal waves; such hydraulic control at the entrance (or at the sills in both channels between RM-6 and RM-9) would affect circulatory processes throughout the estuary. Another geographic area where the data are inadequate is the peripheral bays. Data of all kinds are absent in Grays Bay and are incomplete in the other bays.

Moored-instrument studies have sampled near-surface processes in all parts of the estuary inadequately. The problems of floating debris, wave action, and vandalism often render near-surface moorings impractical, but profiling instruments show large shears and stratification near the surface under certain conditions. Prediction of severe wave conditions near the mouth particularly requires near-surface current and density observations.

Studies to date have focused on synoptic processes, not the details of turbulent mixing, internal waves, etc. To a certain extent it is productive to conduct small-scale, mechanistic studies in simpler systems; some results from these estuaries may then be used in the more complex Columbia River Estuary. However, the ability to do this is presently inhibited by the almost total absence of some measurements that are relatively easy to carry out. Profile data are lacking during the high flow season, and no acoustic echo sounding transects are available for any season. The acoustic echo sounding records are probably the simplest and most productive work that could be carried out. They provide a wealth of qualitative information concerning the form and extent of salinity intrusion, vertical mixing, transport

processes, and so on. These records, combined with conductivity-temperature-depth profiling, would be an inexpensive way to determine the extent of salinity intrusion into peripheral bays and the distribution of the fronts, which are known to be of high biological productivity in many bodies of water.

Further model studies would also be useful. The two-dimensional, laterally-averaged circulation model needs to be refined to calculate mean Lagrangian (particle motion) velocities. Further refinement of the vertical mixing and diffusion terms in the model and the use of a finer horizontal grid to better represent the actual topography would allow better model predictions of the salinity distribution and mean flow.

The one-dimensional model could be refined to include the diurnal tides and the tidal overtones. The north and south channels should also be treated individually. These changes would improve the tidal flows calculated by the model and allow a more accurate calculation of the energy budget.

4. SEDIMENTARY GEOLOGY

The study of estuarine sedimentary geology can be approached from several perspectives. Traditionally, geologists have studied estuaries from one of three reference frames, each of which suggests a different methodology and each of which has various advantages or disadvantages, depending on the eventual goal of the study. The three approaches are associated with distinct time scales.

The "modern processes/products" approach involves measuring the geologic events that are currently acting in an estuary. This approach is inevitably linked with the time scale of the research period and has the advantage of providing direct measurements of processes and results with some controllable precision. The drawbacks to studies of modern processes arise from the temporal and spatial variability of the ongoing processes and the difficulty in directly relating the ongoing processes to the resultant products (e.g. morphology or sediment distribution). It is seldom possible to measure rates over a sufficiently broad time spectrum to predict long-term changes; it is almost as difficult to ascertain whether the present state of an estuary is a result of present processes that have not and will not change over a suitable period (thus enabling predictions to be made) or whether the present state is a remnant of earlier processes that can no longer be measured.

As one solution to this dilemma, geologists have resorted to a second, "historical", approach to sedimentology. An historical approach allows integration of the processes over a much longer time span and may suggest the inclusion of infrequent but geologically important processes in future extrapolations. In Europe, this approach can provide as much as a thousand years of data; on the west coast of North America, good historical records barely exceed a hundred years. The historical approach allows long-term trends to be evaluated and incorporated into predictions and, when used in conjunction with modern process measurements, may provide the best overall perspective on the important human time scale. The drawback that arises most often is that the observed trends are largely confounded by human influences on the natural system. In the Columbia River Estuary, the changes wrought by humans dominate the historically observed changes. Predictions about future behavior of the natural system are inextricably tied to further development within and upriver of the estuary, and evaluation of the natural system over the historical time scale is extremely difficult.

The final recourse in developing an understanding of the relationship between geologic processes and the resulting morphology and sedimentary deposits in the estuary is the "stratigraphic" approach. Study of the deposits within an estuary leads to an emphasis on the geologically important depositional processes over either historical time scales, geologic time scales (thousands of years or much more), or both. The stratigraphic approach satisfactorily answers the question: What are the important natural processes that have resulted in sediments being deposited in the estuary? Because of its emphasis on the dominant processes, this approach might not shed much light on the prevailing

ambient conditions during that time period, nor on the important, but unpreserved, events.

Each approach has its own advantages and limitations and the relative merits of each must be evaluated in light of the time and space scales that are considered important and in light of the eventual application of the information. The research described here falls largely under the first of the three approaches: the process/product approach. However, in order to provide a longer-term perspective on the sedimentology of the estuary, the historical changes in bathymetry were analyzed. This chapter reports the results of three general research endeavors: 1) the study of modern processes within the estuary, including incorporation of the data gathered by the physical oceanographers and modellers (described in the previous chapter) with data on the sediment transport and erosion/deposition processes that were observed in the course of the project, 2) the distribution of sediments in the estuary, the variation in sediment with season and river location, and the relationship of sediments to the processes of erosion, transportation and deposition, and 3) an examination of the morphology of the estuarine deposits. Chapter 5 analyzes the historical changes in the estuarine morphology and the associated changes in circulation and sedimentation patterns.

4.1 SEDIMENT TRANSPORT

The erosion, transportation and deposition of sediments are major factors in controlling the configuration and morphology of the estuary. A discussion of the mechanics of sediment transport is introduced here to emphasize the importance of temporal and spatial variability to sediment transport.

Flows induced by river runoff, tides, density gradients, and wind-driven surface set-up are all sheared and decelerated by drag imposed on them by the estuary bottom. The total boundary shear stress $[(\tau_b)_t]$ exerted on the boundary by the fluid is composed of a form drag component $[(\tau_b)_p]$ and a skin friction component $[(\tau_b)_s]$, so $(\tau_b)_t = (\tau_b)_p + (\tau_b)_s$. The form drag component results from pressure differences as flow travels around large obstacles; in an estuary, form drag arises from bends in the channel, constrictions in the channel, and large topographic features such as bars and bedforms. The skin friction component results from the small-scale roughness of the bed itself and depends primarily on the grain size of the sediment and the flow strength.

The skin friction component of the total shear stress is the variable that controls the rate of sediment transport. The size of sediment that can be moved by a particular flow, and the rate at which sediment will move as bedload are directly dependent on skin friction $(\tau_b)_s$. Shields (1936) developed an empirical relationship that can be used to predict the critical value of skin friction that will erode a particular size of non-cohesive sediment. When simplifying assumptions are made, Shields' data can be plotted as a Hjulstrom diagram in terms of the flow velocity and the grain size, as in Figure 4.1.

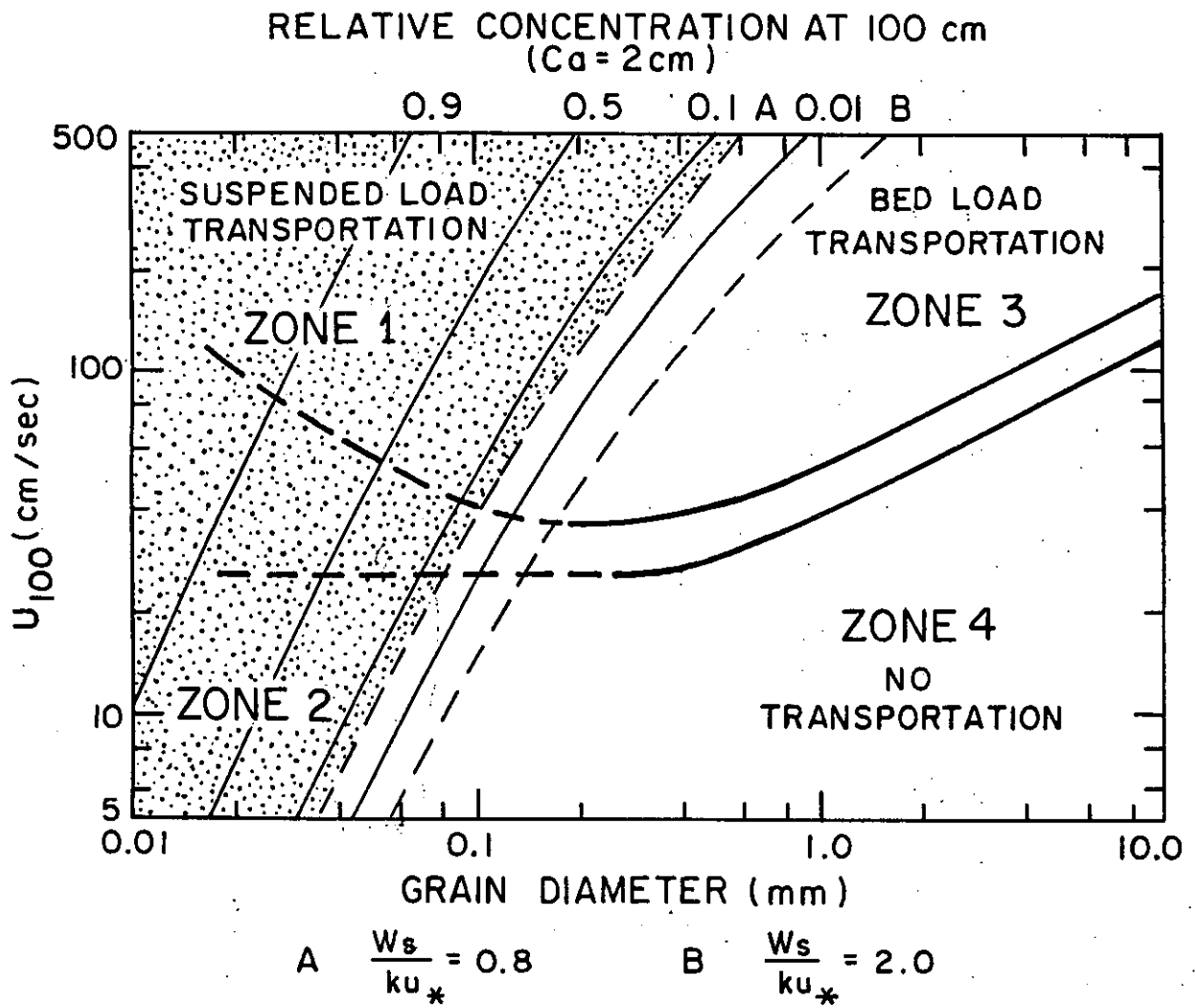


Figure 4.1 Hjulstrom diagram: relationship of critical erosion velocity to grain size (Sundborg, 1957).

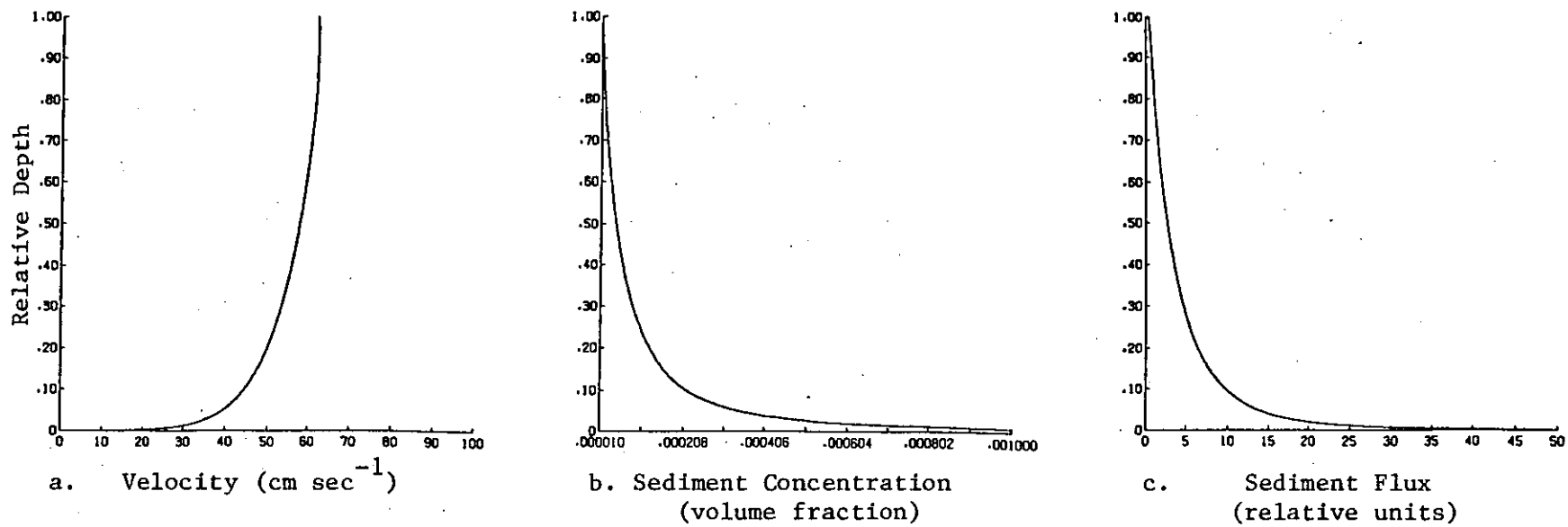


Figure 4.2. Results of suspended sediment transport model.

At sufficiently low values of $(\tau_{b,s})$, no sediment will move (Figure 4.1). As the skin friction increases, the threshold for sediment motion $[(\tau_{b,s})_{crit}]$ will be exceeded and bedload transport will occur. Initially, individual grains move along the bottom in traction transport and saltation. The grains are dragged, rolled and make short hops but are confined to within a few grain diameters of the bottom. The various modes of movement are collectively termed as "bedload transport." Most of the empirical and deterministic sediment-transport equations that have been developed can be written in terms that relate bedload transport rate to some high power of $(\tau_{b,s})$ (Smith 1977). As increasingly higher values of $(\tau_{b,s})$ are achieved, sediment grains leave the bed for longer periods of time and are accelerated to the speed of the flow some distance above the bed. This mode of intermittent suspended transport grades into entirely suspended load transport at higher skin-friction values. The rate of suspended sediment transport becomes a function of flow velocity, rather than shear stress; as a result intermittent and suspended sediment transport occur at much higher rates than bedload transport. Models that predict the flux rates of suspended sediment indicate that most of the transport occurs close to the bed. Figure 4.2 presents the results of a suspended sediment model developed by Smith and McClean (1977). The high rates of transport near the bed make flux measurements extremely difficult to perform in the natural environment, suggesting that alternate means of estimating sediment transport should be sought.

When sediment is moving under moderate skin friction $(\tau_{b,s})$ (relative to its grain size), minor instabilities in an otherwise steady, uniform flow cause ripples and larger bedforms to form and propagate along the bottom. These features exert a form drag on the flow, and because they extend to various heights into the shearing flow, skin friction varies along the surface of the bedform. The transport rates of sediment moving along the bedform vary accordingly, reaching a maximum near the crest (Smith and McLean 1977). At the crest, increased skin friction may be sufficient to cause sediment to go into suspension. If not, the sediment will fall down the steep lee face into a zone of low skin friction in the trough, to eventually be covered by later-deposited sediments. In this manner, the bedform advances along the bottom. When no sediment is being thrown into suspension at the crests, the rate of bedload transport will be determined by the geometry and rate at which the bedform is moving.

Erosion or deposition occurs when sediment transport diverges or converges in an area, or when sediment is suspended into or deposited from the water column. The "erosion equation" relates the rate of change of bed elevation (η) to the divergence of sediment transport ($\nabla \cdot Q_s$) and to changes in the amount of sediment suspended in the water column above the bed with time

$$\left(\frac{\partial v_s}{\partial t} \right) :$$

$$\frac{\partial \eta}{\partial t} = \frac{-1}{C_b} \left(\nabla \cdot Q_s + \frac{\partial v_s}{\partial t} \right)$$

where C_b is the fractional concentration of sediment (to water) in the bed, usually about 0.6. In the case of bedload transport, V_s and $\partial V_s / \partial t$ are relatively small; therefore, when the transport rate out of an area exceeds the transport rate into the area, erosion occurs. Conversely, when more sediment is carried into an area than is removed, accretion occurs. Rapid transport can occur without deposition or erosion, just as very steady accumulation can occur with continued, slow sediment input and no removal. The changes in bottom configuration that result from erosion or deposition affect the flow by changing the form drag (τ_b). Because sediment transport is a function of skin friction and skin friction is related to the form drag and the total boundary shear stress, a feedback loop exists that makes the interaction between the flow-field and sedimentation non-linear. As a result of this non-linearity, it is difficult to attain even a dynamic equilibrium among the sediments, the morphology of the bottom, and the flow fields.

As discussed in Chapter 3, tidal currents dominate the flow regime in the Columbia River Estuary and produce relatively strong currents. Much of the sediment supplied by the fluvial system is easily transported under normal spring tide current conditions, and as a result, the sediment transport field is dynamic and complex. Figure 4.3 provides an indication of the grain sizes found in the estuary and is included for comparison with the Hjulstrom curve of Figure 4.1. These data indicate that a large percentage of the estuary sediment is mobile under normally encountered higher currents (refer to Figure 3.17b for representative tidal velocities). Although several useful steps have been taken, only limited progress has been made to date in understanding the processes and budgets involved in sediment transport.

4.2 APPROACHES TO THE STUDY OF SEDIMENT TRANSPORT

Because of their different nature, bedload transport and suspended sediment transport were investigated using different techniques. This section discusses the underlying assumptions associated with each technique and presents the data and conclusions concerning bedload and suspended sediment transport in the Columbia River Estuary.

4.2.1 Bedload Transport

Very little data are available on the bedload budget in the estuary. As mentioned in Chapter 2, standard estimates of the fluvial supply of bedload sediment produce a figure of 1 million tons yr^{-1} (Whetten et al. 1969). This number is based on estimates of the total load of the river and has never been directly measured. No estimates have been made of the bedload transport rates into or out of the entrance, but the general consensus is that net transport is into the estuary, except possibly during extremely high runoff events (Lockett 1967, Sherwood et al. 1984). Both the river system and the adjacent continental shelf are potential sources of bedload sediment.

Research investigations were designed to delineate pathways and form qualitative estimates of bedload transport rates. In sand-bedded natural flows such as those occurring in the Columbia River Estuary, bedforms (ripples, dunes, and sandwaves) frequently are formed.

Previous studies indicated that bedforms were to be found in most areas of the estuary. Side-scan sonar studies (Roy et al. 1979, Sherwood et al. 1984) provided valuable information on the temporal and spatial distributions of bedforms in the estuary. In order to interpret these distributions in terms of rates and directions of bedload sediment transport, several assumptions must be made. The assumptions needed are based on research that has been performed on bedforms by sedimentologists over the last twenty years. Numerous flume studies are available which provide empirical relationships between some measure of flow strength, grain size, sediment transport rates and bedform morphology for shallow, steady flow (Simons et al. 1965, Allen 1968, Costello 1974, Costello and Southard 1981, Harms et al. 1975, 1982). The problem of relating transport rates to bedform morphology in unsteady, oscillatory flow of varying depth is much more complex and has motivated field investigations in intertidal and subtidal coastal environments. In these environments, it is more difficult to measure the parameters that effect bedform morphology and to know how important flow oscillations and depth variations are to the ultimate geometry of the bedforms. Nonetheless, several workers have extended the depth-velocity-flow concept from the flume to natural environments and discussed the relationships between sediment transport rates and bedform shape (e.g., Boothroyd and Hubbard 1975, Dalrymple et al. 1978, Rubin and McCulloch 1980). These studies permit the following assumptions to be made regarding the relationship of sediment transport rates to the morphology of bedforms in the estuary:

- 1) Bedform sediment transport occurs in a direction approximately normal to the strike of the crest axis and in the direction of the steeper side of the bedform.
- 2) Transport is more rapid and/or has occurred more recently when the steeper face is at the angle of repose (a "slip-face").
- 3) Conversely, the absence of a slip-face indicates that transport has occurred in both directions. In such instances, it is assumed that net transport has been in the direction of the steeper face, but it is recognized that both instantaneous and recent net transport directions may differ from the assumed longer-term net transport direction.
- 4) Because large bedforms contain more sediment, more sediment transport is necessary to significantly alter their characteristic geometry. Therefore, their morphology responds more slowly to changes in flow conditions than that of smaller features. Larger bedforms tend to integrate the effects of flow conditions over a longer period of time.
- 5) As a corollary to 4) it is assumed that smaller bedforms reflect instantaneous flow conditions more often than larger bedforms.
- 6) In areas where both large- and small-scale bedforms are present, and where the small bedforms change orientation in response to tidal flow oscillations, the rate and direction of net sediment transport is best estimated from the larger bedforms.

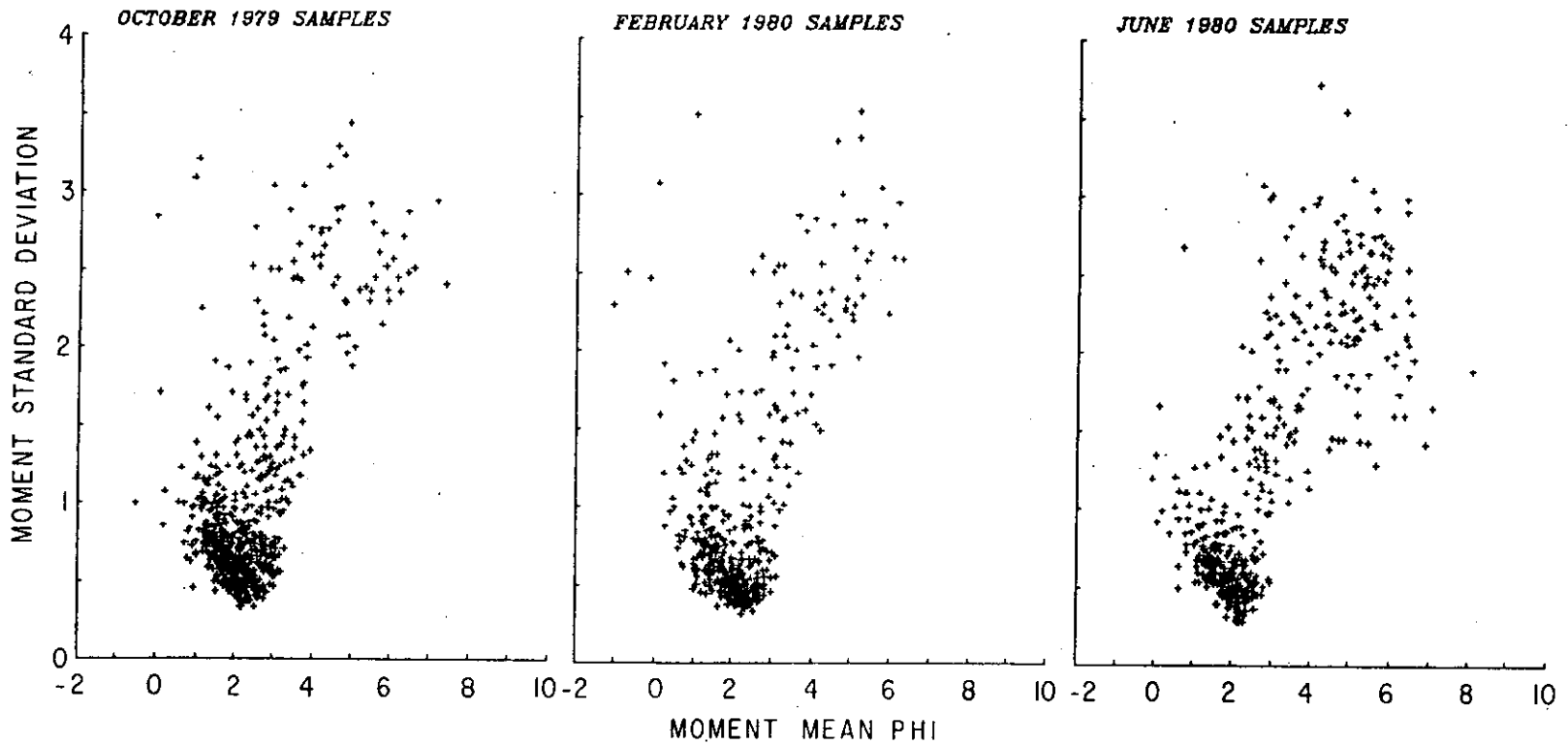


Figure 4.3 Grain size and standard deviation of CREDDP samples.

- 7) Among bedforms with slip-faces, the rate of bedform migration and therefore the rate of bedform sediment transport can be estimated by the crest geometry; when the crestlines become less linear and more sinuous or even cusped, they are reflecting stronger flow conditions and increased sediment transport rates.
- 8) Although interpretation of sediment transport rates is mostly based on the relation of bedform geometry and inferred rates and direction of bedform migration (i.e., bedform transport), bedform morphology may sometimes indicate that high flow conditions are placing bed material into suspension and high rates of suspended sediment transport is occurring. In particular, bedforms with irregular crest geometry or "planed-off" crests were used as indications that significant suspended sediment transport might be occurring.

Most of these assumptions appear to hold in the Columbia River Estuary. Sherwood et al. (1984) have utilized these assumptions and data acquired with side-scan sonar to map the distribution of bedforms in the Columbia River and infer bedform transport patterns from the distributions. They argue that areas of convergence indicate net accumulation of sediment and that areas of divergence indicate erosion. It is important to remember that in this situation, only the bedform transport is being considered; the total convergence of all transport (bedload and suspended load) must be included to correctly predict erosion or deposition. However, because convergence of bedload transport is apparently responsible for most of the shoaling in the estuary and because much of the deposition of finer sediments from suspension occurs on an ephemeral basis, the predictions of erosion and deposition based on the bedform transport field alone are of considerable value. The following sections discuss bedform distributions in the estuary and sediment transport at specific locations in the estuary, and then an overview of sediment transport patterns for the entire estuary is presented.

Figures 4.4, 4.5, and 4.6 are maps integrating the results of the side-scan sonar studies to date and depicting general bottom characteristics of the estuary. Various fields of bedforms are recognized and mapped on the basis of similar size and shape characteristics. The boundaries of some of these fields shift seasonally and will be discussed below. Many features of the bedform distribution pattern, however, were not observed to vary significantly over the study period, and may be discussed in a general manner.

Unidirectional downriver-oriented bedforms

Medium- and large-scale bedforms with downriver-oriented slip-faces are dominant in the portion of the estuary east of Tongue Point. In the deeper channels, these bedforms have heights of up to 10 ft (3 m) and wavelengths of more than 300 ft (100 m) (Figure 4.7). Smaller bedforms are commonly superimposed on the stoss sides of larger bedforms. Troughs of some of the larger bedforms appear as acoustically reflective on the side-scan sonar, suggesting that coarse lag sediments occupy these troughs. Sediment samples confirm that a substantial grain-size

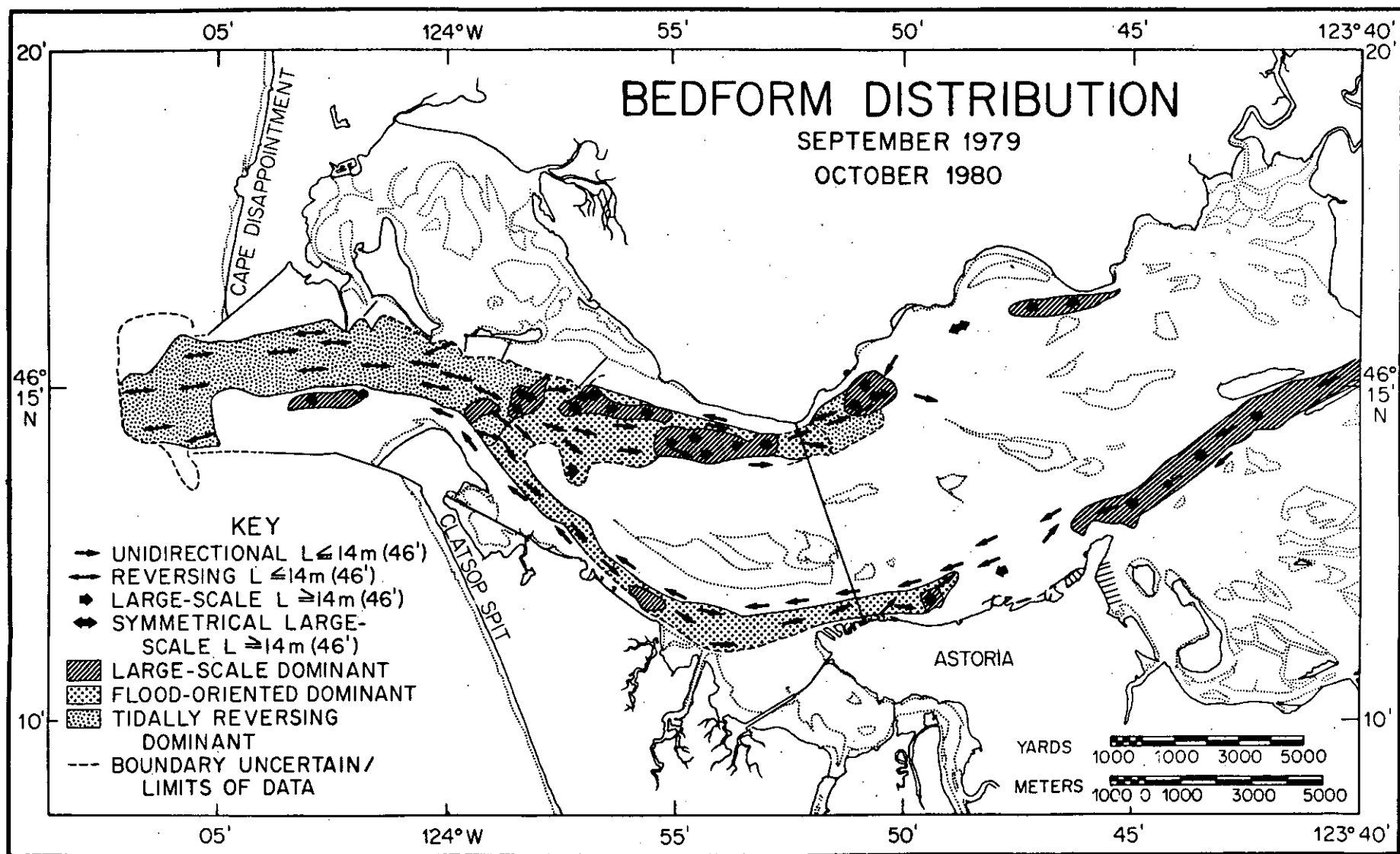


Figure 4.4 Bedform distribution - Fall.

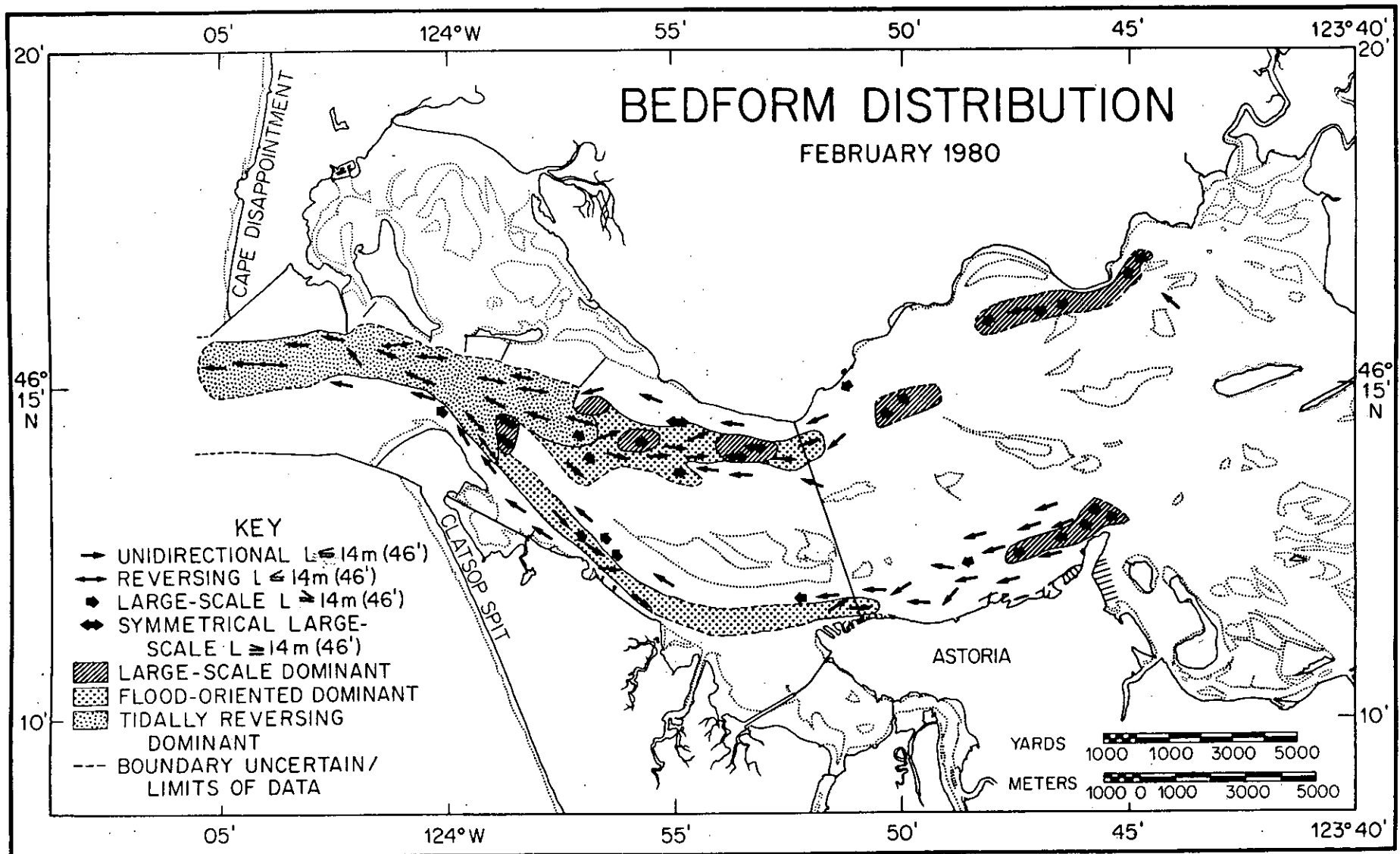


Figure 4.5 Bedform distribution - Winter.

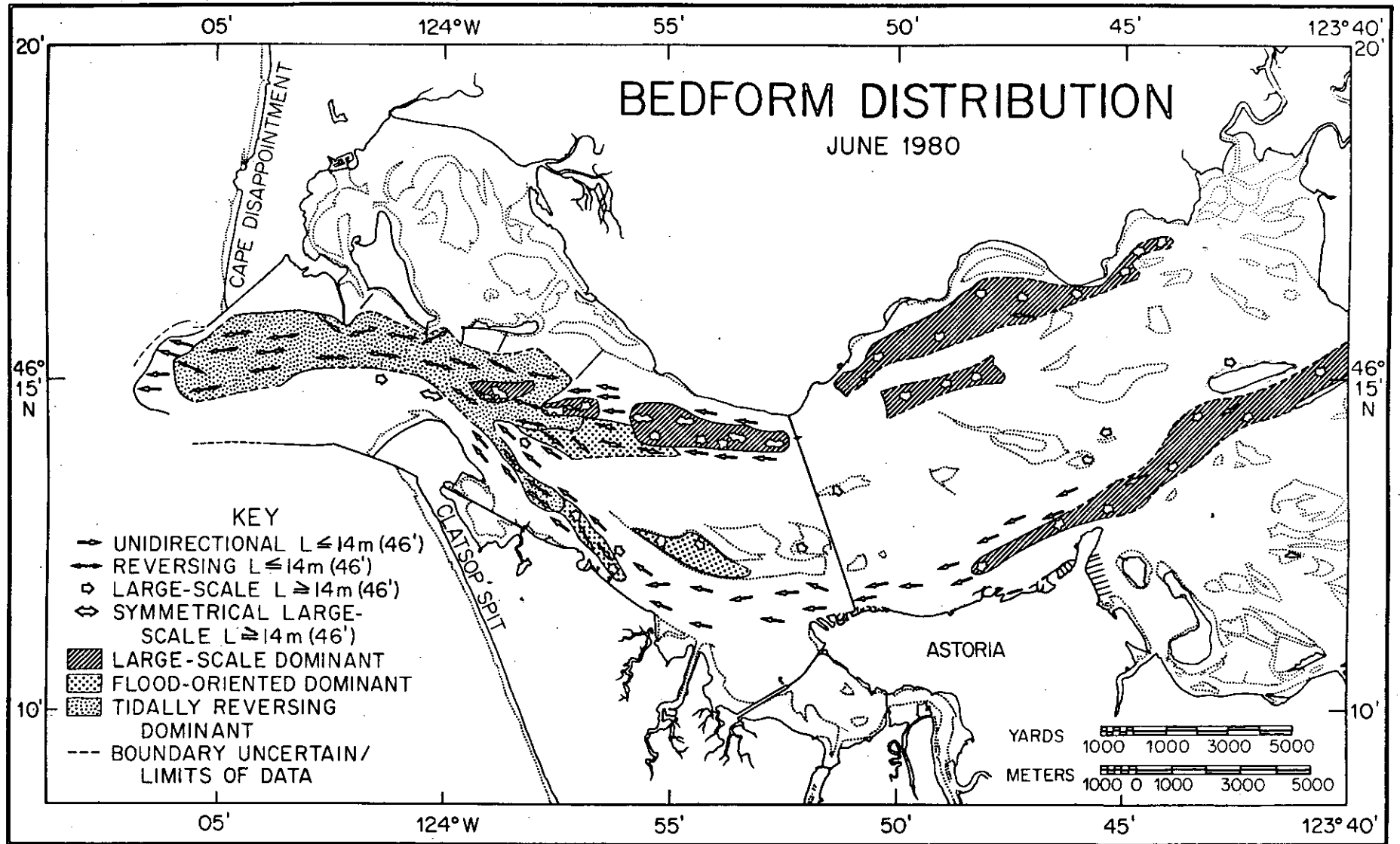


Figure 4.6 Bedform distribution - Spring.

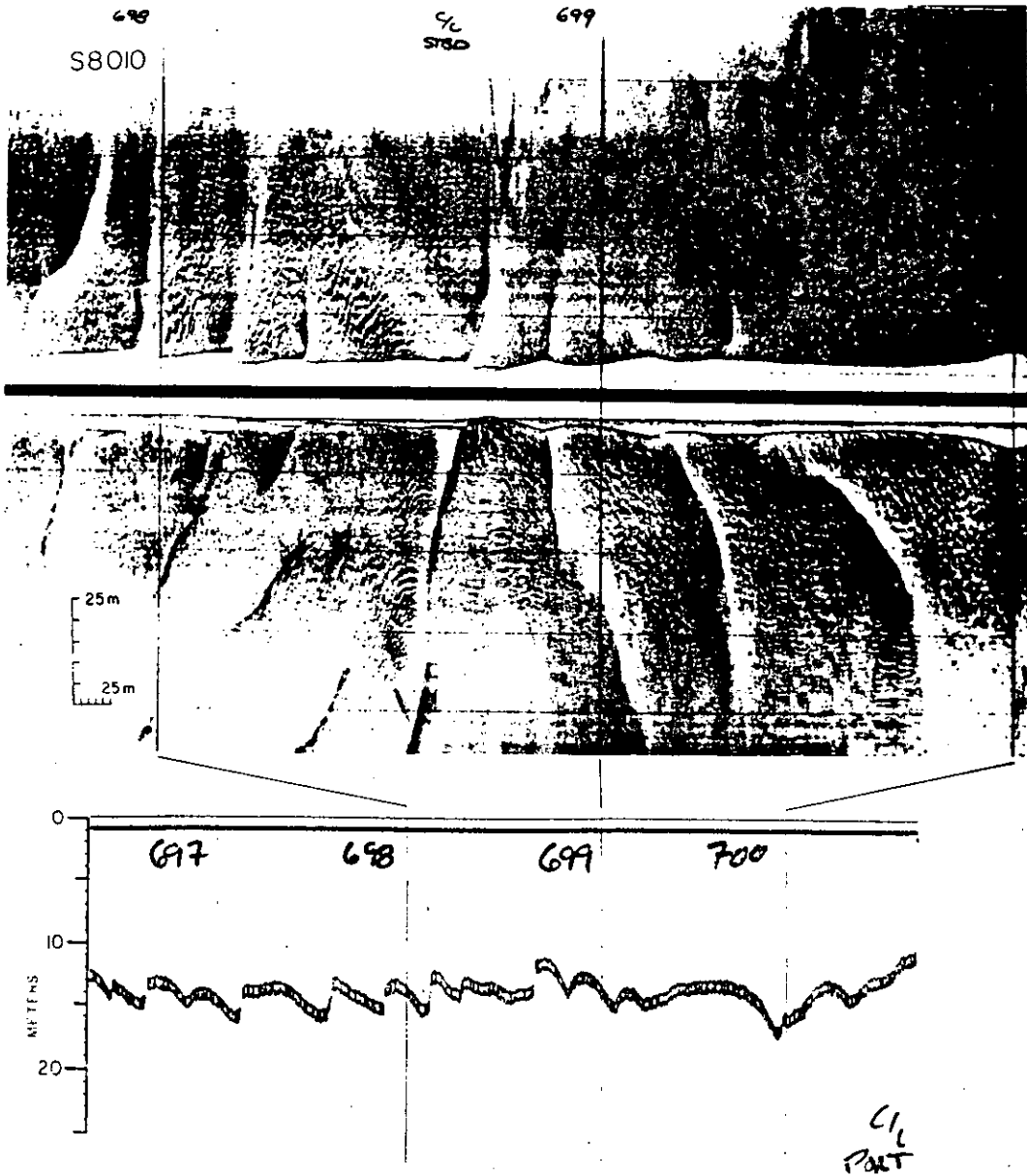


Figure 4.7. Side-scan sonar and echo sounder records of large-scale, downriver-oriented bedforms in the fluvially-dominated upper estuary (vicinity of Rice Island). Wavelengths - 100 meters; heights - 3 meters.

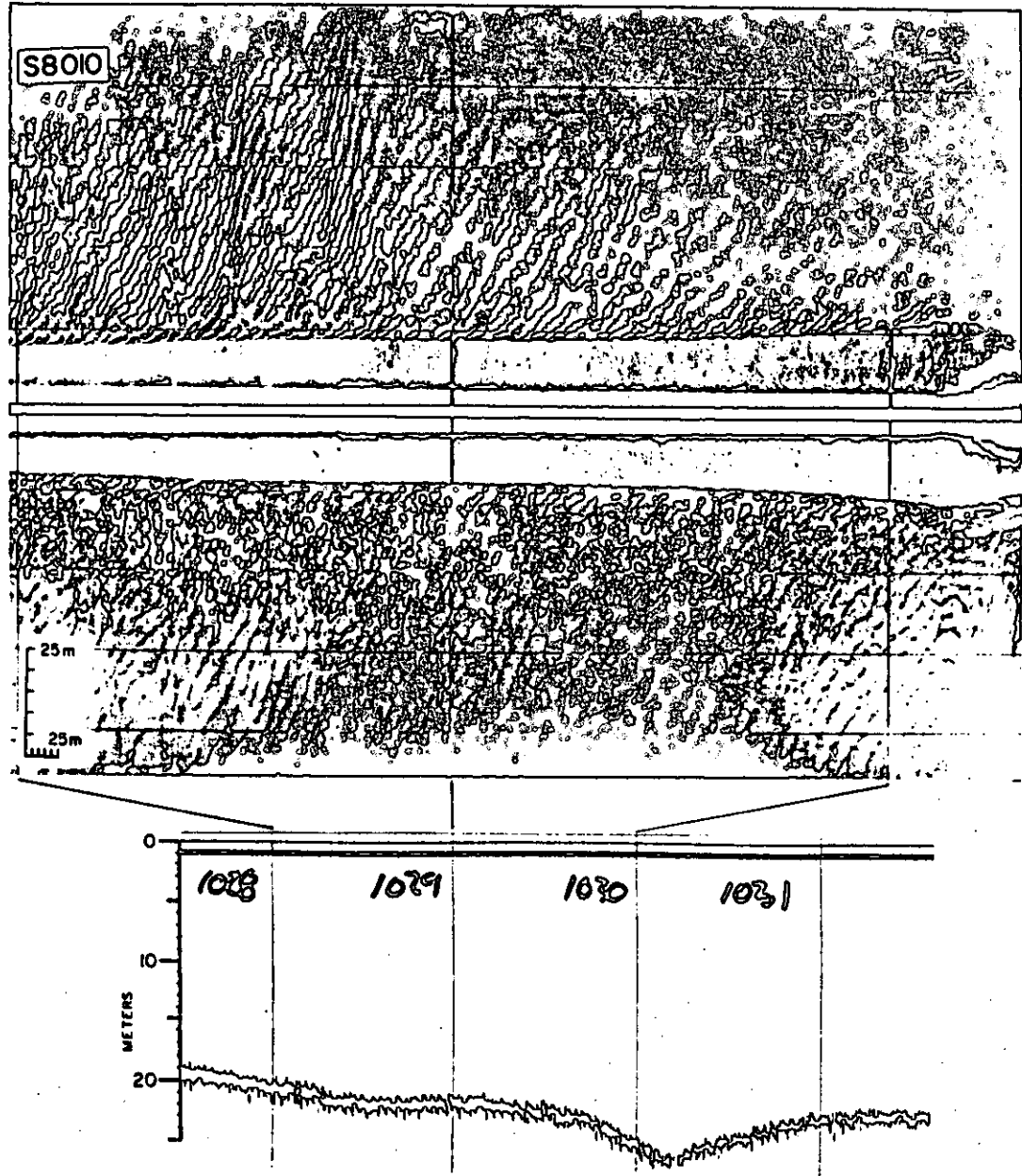


Figure 4.8 Side-scan sonar and echo-sounder records of small-scale reversing bedform in the tidally-dominated lower estuary (vicinity of Jetty A). Wavelengths - 4-7 meters; heights - 40 centimeters.

difference exists between crest and trough sediments: near Puget Island, the crests of bedforms are formed of well sorted coarse sand, whereas the troughs contain poorly-sorted gravel. Other troughs have a low reflectivity, probably indicating finer-grained sediments. Most of the bedforms in this upper portion of the estuary are unidirectional. The steeper faces (generally well-developed slip-faces) of even the small bedforms retain downriver orientations over the entire tidal cycle.

Bedforms with reversing orientations

Smaller bedforms are present from the outer tidal delta east to Hammond in the south channel and to the vicinity of the Chinook pile dike in the north channel. These areas are occupied by bedforms with wavelengths of approximately 10 to 30 ft (3 to 10 m), heights of up to 3 ft (1 m), and linear to slightly sinuous crests (Figure 4.8). At different tidal stages, these bedforms display various geometries ranging from asymmetric with slip-faces oriented in either an upriver or downriver direction to somewhat rounded and symmetric. Reversal of these bedforms over consecutive ebb and flood tides is documented in several instances, and orientation commensurate with the tidal current is the general rule for all of these bedforms. Bedforms with reversing orientations are commonly found in the channel portions of the estuary west of Chinook and Hammond and are found on some channel flanks and shoals in some seasons.

Upriver-oriented bedforms

In the channels upriver of the reversing bedforms described above, bedforms are found that do not reverse orientation; instead, they display upriver-oriented steeper faces over the tidal cycle. The appearance of the bedforms varies with season and location. Bedforms range in height from less than a foot (0.3 m) to six ft (2 m) and in wavelength from 10 to 120 ft (3 to 40 m). The degree of asymmetry also varies; some of the larger bedforms are nearly symmetric and rounded, while others are highly asymmetric and have slip faces. The large, nearly symmetric bedforms frequently have smaller bedforms superimposed on them that reverse orientation in response to tidal currents. They occur in small fields located on the northwestern extension of Desdemona Sands and on the shoal near Chinook.

The large asymmetric bedforms occur in deeper portions of the north and south channels, but their precise location varies seasonally. Figure 4.9 shows a particularly well-developed field of larger upriver-oriented bedforms. They have straight crests, upriver-oriented steeper faces, and smaller superimposed bedforms. Their wavelength is approximately 140 ft (43 m) and their maximum height is 6 ft (2 m).

Smaller bedforms with upriver-oriented steeper faces occupy large portions of both the North and south channels between Hammond and the Astoria-Megler Bridge. In much of this area, the channel flanks and shoals are occupied by bedforms with downriver-oriented steeper faces. As a result, cross-channel transects with the side-scan sonar show a reversal of bedform orientation with depth that remains constant over

the tidal cycle. Figure 4.10 illustrates this situation schematically, and Figure 4.11 is a portion of side-scan sonar record depicting a reversal with depth in the Flavel Bar region. In June, the depth of the depth-related reversals tends to increase with distance upriver. This trend is not well defined and is absent in the October data. The seasonal changes in the distribution of upriver-oriented bedforms and depth-related orientation reversals are discussed below.

Other bottom features

In addition to the features mapped in Figures 4.4, 4.5, and 4.6, other characteristics of the estuary bottom are evident in the side-scan sonar records. Some areas of the estuary are featureless at the resolution of the side-scan sonar. These areas are commonly found on channel flanks and rarely, and then only seasonally, found in channel bottoms. Occasionally these smooth areas grade into areas with indistinct bedforms having no clear orientation. The outer portion of the outer tidal delta is typified by these indistinct bedforms. The bay south and west of Cape Disappointment is an example of an area with no resolvable bedforms during any season. Seasonally, parts of the north channel and the north flank of the south channel are featureless.

The flanks of both channels occasionally display bedforms with non-linear crestline geometry ("three-dimensional" in Allen, 1968). They are generally found in water depths greater than 45 ft (14 m) and are not observed to reverse with daily tides, but change crest geometries on neap-spring and seasonal time scales.

The most common feature of the side-scan sonar records not associated with bedforms are areas of very high reflectivity and uneven, often precipitous, topography. These are attributed to areas of rock outcrops, boulder talus and gravel banks. These hard, erosion-resistant bottoms occur on the outside of river bends (notably the Port of Astoria region) and near rock headlands such as Grays Point, Chinook Point, and Tongue Point. Reflective areas are also frequently associated with deep bathymetric depressions, as at Tongue Point, Grays Point, the Chinook Jetty, and Jetty A, where they are probably a result of coarser sediments.

Pilings, pile dikes, rip-rap and sunken logs appear in the side-scan sonar images, as do fish (especially during salmon runs), salinity fronts, and turbulence. Longitudinal furrows located in the navigational channels (Figure 4.12) are the result of Corps of Engineers dredging activities. Correlation with Corps of Engineers dredging records suggests that these scour-marks remain identifiable for at least several days after the dredging activity, but are not present in later seasons.

Seasonal Changes

Of particular interest are the seasonal variations in bedform distribution. The upriver extent of upriver-oriented bedforms varies in response to discharge. During the low flow period of October 1980 (discharge: 140,000 cfs, $3,965 \text{ m}^3\text{sec}^{-1}$) upriver-oriented bedforms were

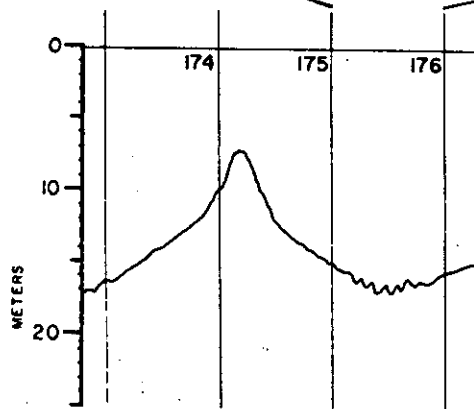
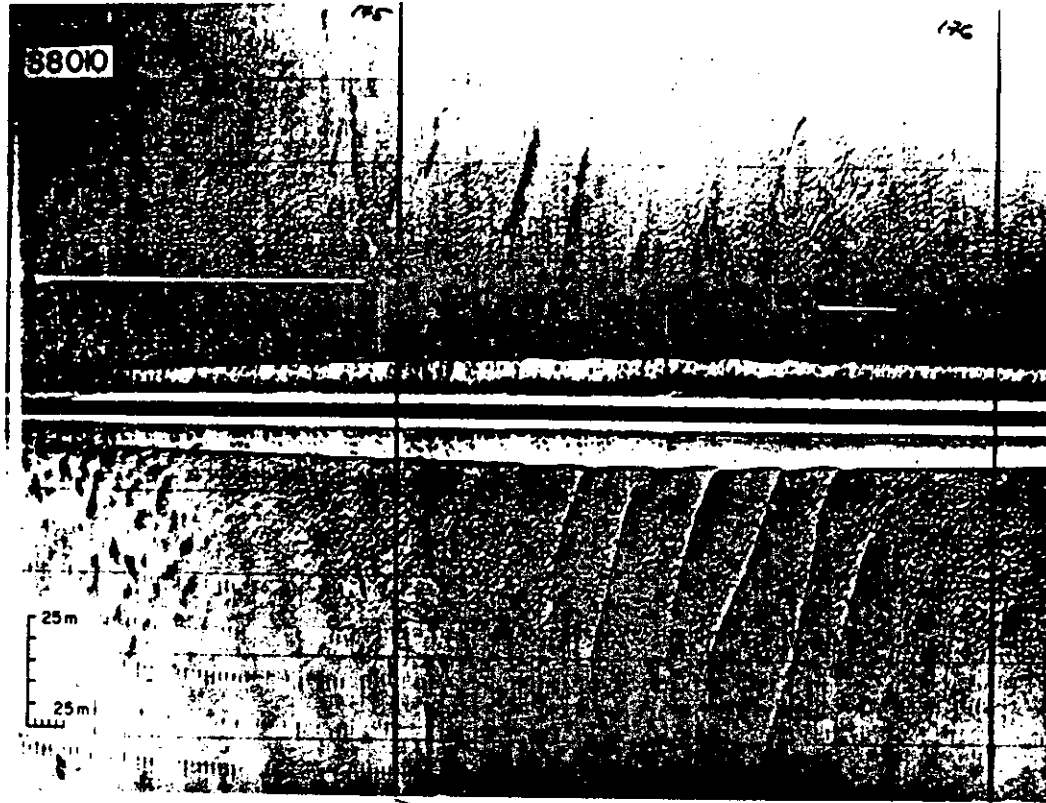


Figure 4.9. Side-scan sonar and echo-sounder records of upriver-oriented bedforms generated by estuarine circulation in the north channel (near Chinook). Wavelength - 43 meters; height - 2 meters.

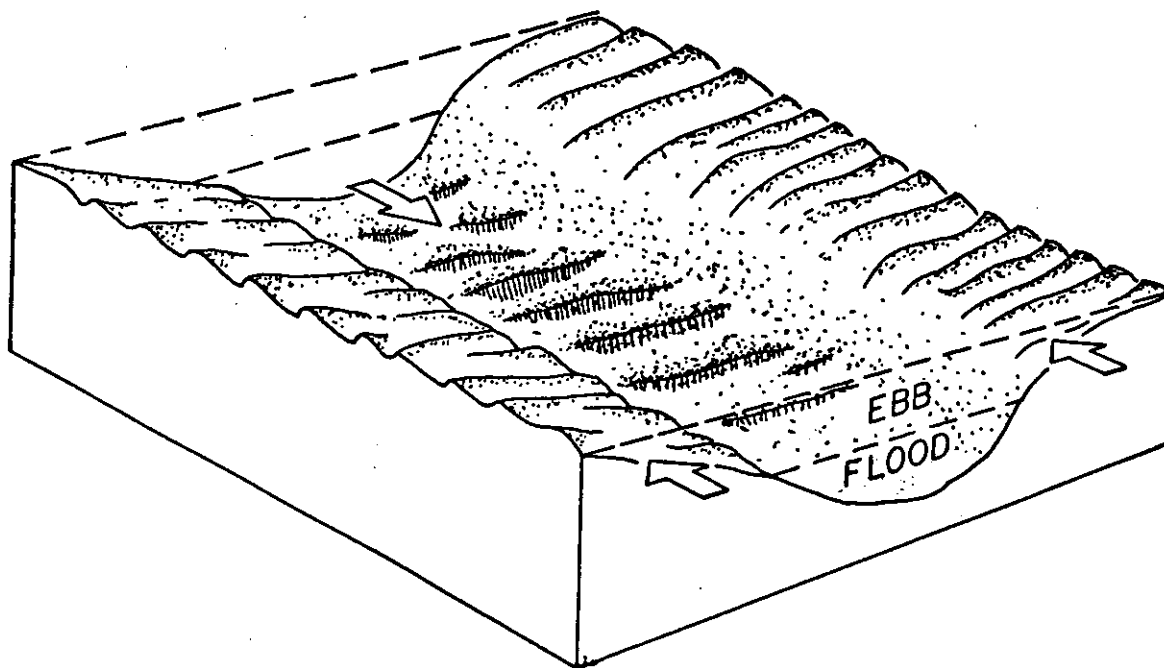


Figure 4.10. Schematic diagram of depth-related bedform orientation reversals. Bedforms on shallow flanks display downriver orientation while bedforms in channel display upriver orientation.

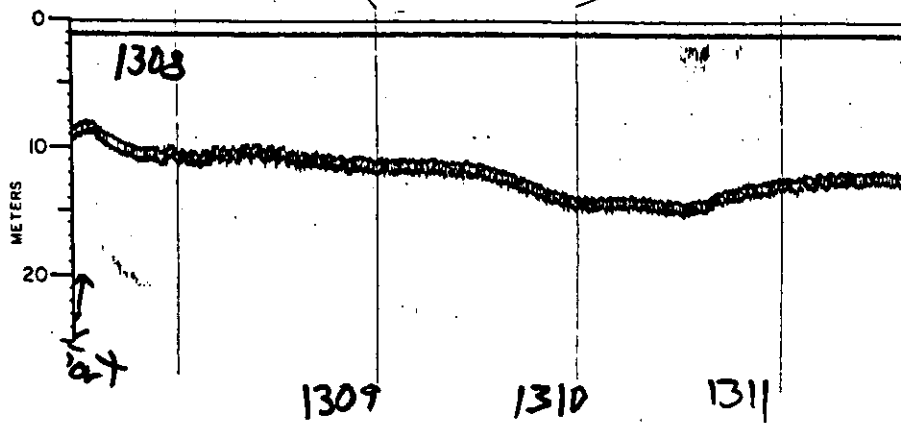
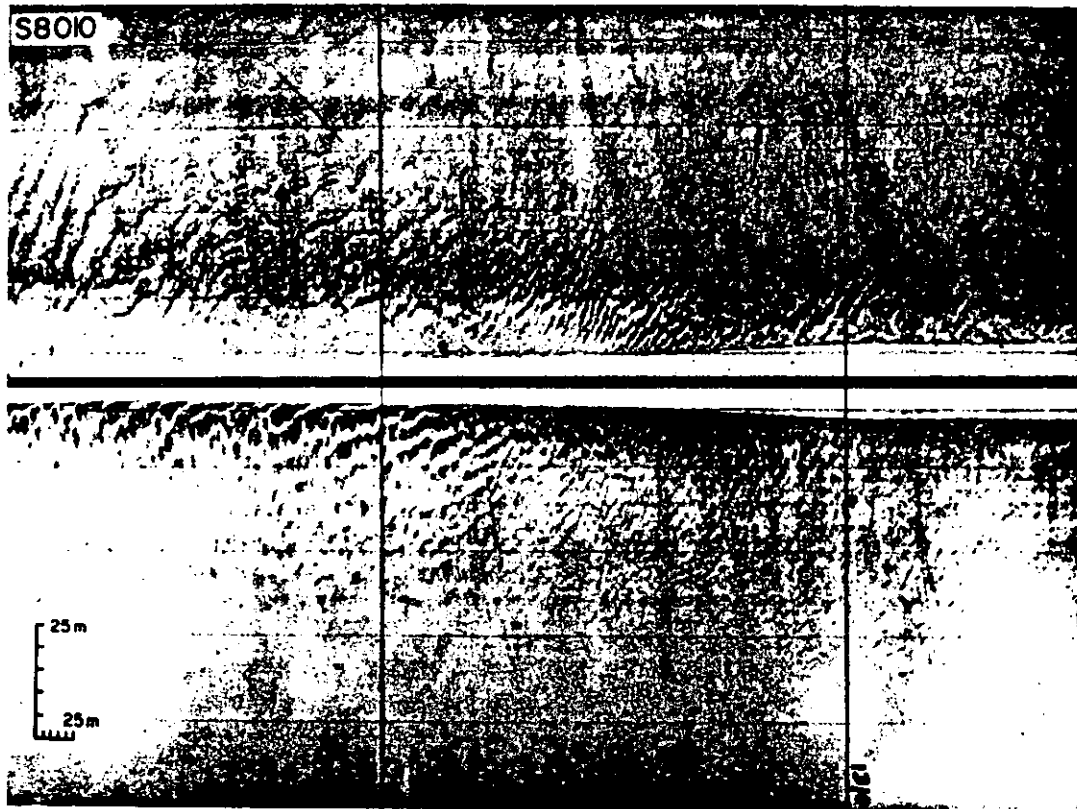


Figure 4.11. Side-scan sonar and echo-sounder records of bedforms whose orientation reverses with depth from the navigation channel (near Flavel Bar). Bedforms in the left-hand portion of the record display steeper faces oriented toward the bottom of the page (downriver) while the bedforms in the channel display steeper faces oriented upriver. Wavelength - 2.5 meters; height - 0.3 meters.

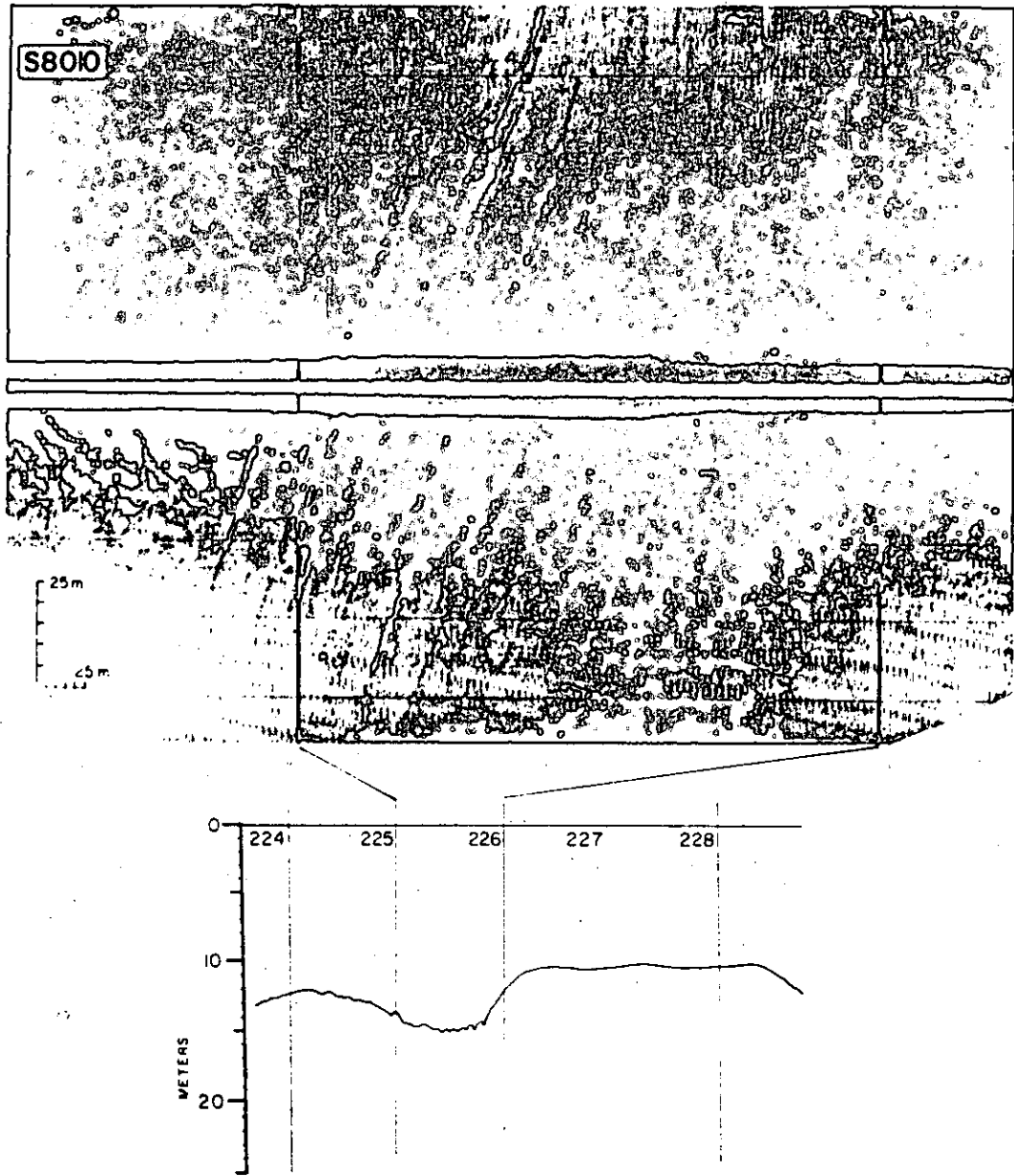


Figure 4.12 Side-scan sonar and echo-sounder records of dredge furrows in the navigation channel (Flavel Bar). Furrows are longitudinal, with depths of approximately 2 to 4 meters and widths of 1 to 2 meters.

observed nearly to Tongue Point in the south channel and extended into both forks of north channel south of Megler (Figure 4.13). Upriver-oriented bedforms and partially reversed bedforms were also found farther east near Grays Point, but these were probably isolated cases caused by unique topography, and not associated with estuarine circulation. In February, during higher discharge (191,200 cfs, $5415 \text{ m}^3\text{sec}^{-1}$), the limit of upriver-oriented bedforms in the south channel was pushed downriver to just east of the bridge. Similarly, in the north channel the limit of upriver-oriented bedforms was just east of the Astoria Megler Bridge. In June, with a high discharge (330,600 cfs, $9,363 \text{ m}^3\text{sec}^{-1}$), no upriver-oriented bedforms were found east of Tongue Point in the south channel (Figure 4.6). The eastern limit of upriver-oriented bedforms is pushed almost to Hammond in the south channel. In the north channel, while some symmetrical bedforms were observed east of the Astoria-Megler Bridge, the limit of upriver-oriented bedforms was pushed west of the bridge.

The bedform distribution on the channel flanks also varies seasonally. During the low flow period of October 1980, the south flank of the south (main) channel in the Flavel Bar region was dominated by upriver-oriented bedforms. Data in this region were sparse in February, but in June the region was occupied by downriver-oriented bedforms. Similarly, in October the south flank of the north channel was exclusively occupied by upriver-oriented bedforms, but in June and February the eastern half of this area was occupied by either tidally reversing or dominantly downriver-oriented bedforms. On the north flank of the main (south) channel, tidal reversals of the bedform orientations were seen in October but not in February or June.

Seasonal variations in the large upriver-oriented bedforms in both channels are noted in the records. In the north channel, during the low discharge season, large-scale bedforms with wavelengths of 120 to 210 ft (36 to 64 m) and heights of up to 8 ft (1.5 to 2 m) displayed steep, upriver-oriented slip-faces. In February, the bedforms in the eastern portion of the channel were rounded but still asymmetric and oriented upriver. In June, the asymmetric bedforms were replaced by symmetrical bedforms with superimposed downriver-oriented bedforms of a smaller scale. The eastern extent of upriver orientation of these large bedforms varied with discharge in a manner similar to that of smaller upriver-oriented bedforms in the south channel, which were observed as far east as Tansy Point in October, and were pushed downriver to west of Hammond in February and are not found at all in the south channel in June.

Patterns of bedform transport

The quality of the side-scan sonar data over the subaqueous extension of Clatsop Spit (opposite Cape Disappointment) was poor in all seasons. Much of the problem was attributable to strong wave activity, the presence of salinity fronts in the water column, and turbulence. The few satisfactory records showed a patchy distribution of small-scale bedforms and some large-scale vaguely undulatory topography. More often, the bottom was obscured by turbulence and, presumably, high concentrations of suspended sediments. Along the south shore of the

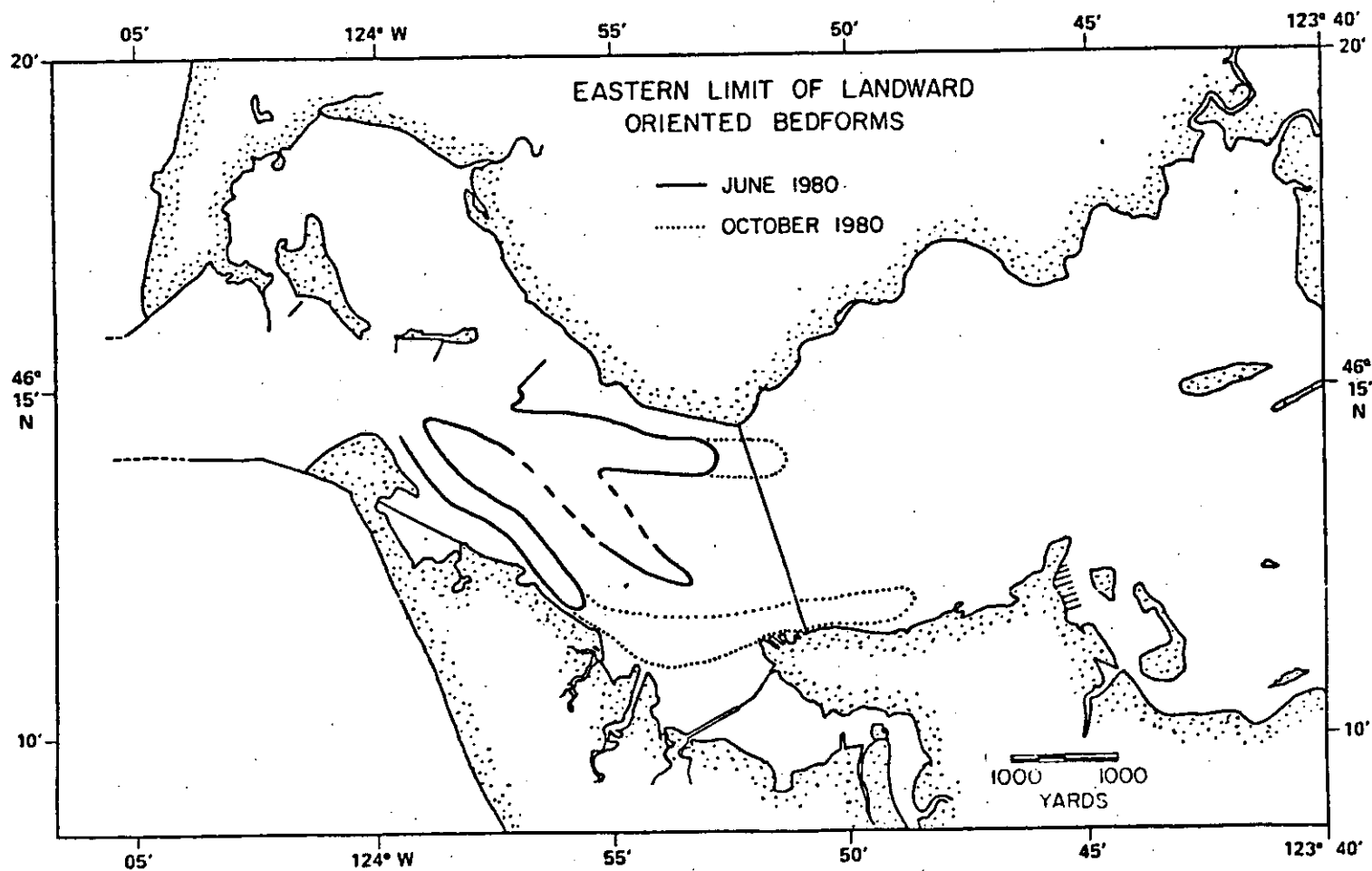


Figure 4.13. Schematic representation of the seasonal variation in the upriver limit of upriver-oriented bedforms for the high-riverflow season (June) and the low-riverflow season (October).

estuary east of Clatsop Spit, bedforms were oriented downriver, regardless of tidal stage, in all three seasons. West of Clatsop Spit, bedforms in the deeper waters of the entrance reversed tidally. The high energy nature of this area and the observed turbulence in side-scan sonar records suggested that the smooth topography of subaqueous Clatsop Spit was upper-flow regime plane bed (Simons et al. 1965) and was associated with a rapid flux of sediment. The predominately unidirectional downstream transport along the south flank of the south channel ended at Clatsop Spit. West of Clatsop Spit transport directions reversed tidally and the direction of the resultant net transport was ambiguous, but transport probably occurred at low rates.

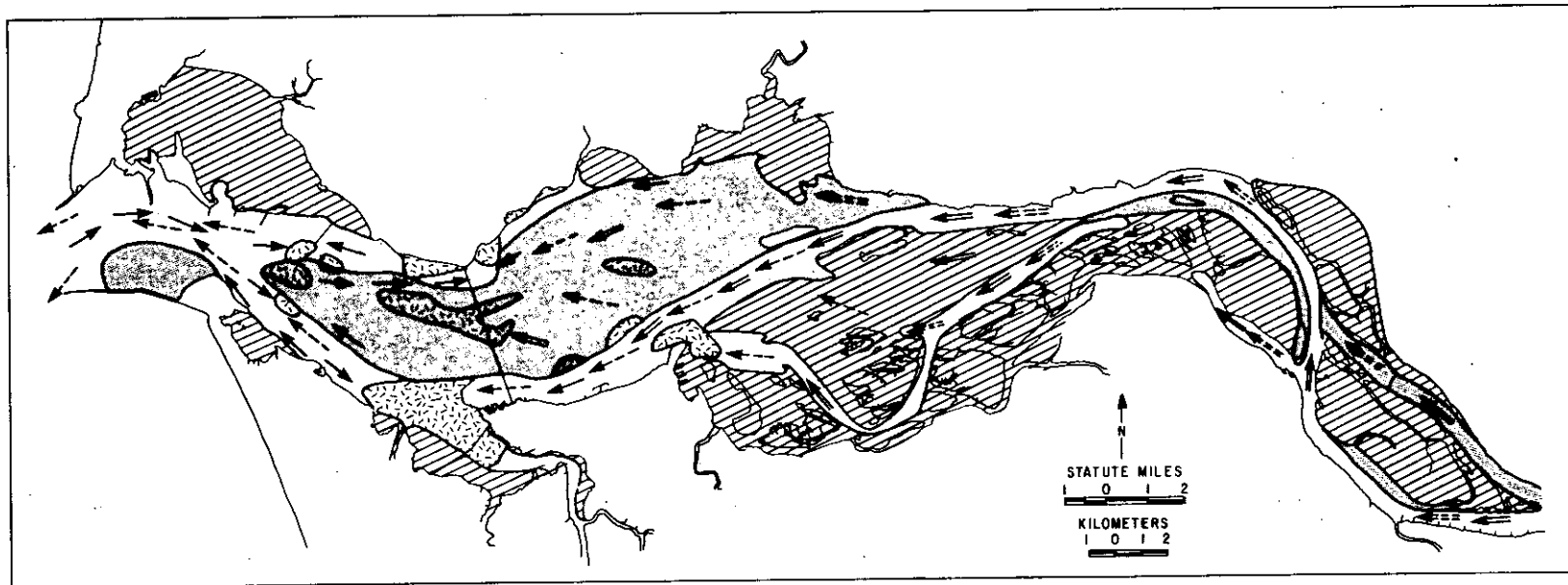
Tracer studies conducted in the Clatsop Spit region suggest that net transport was downstream at a low rate (Creager et al. 1980). High unidirectional flux rates into the Clatsop Spit area and low net transport away from this area resulted in a convergence of sediment transport, and suggest that the region has been depositional (Figure 4.14). Historically, the subaqueous extension of Clatsop Spit has grown northward and infringed on the navigation channel, requiring maintenance dredging.

The Flavel Bar region of the south channel has also required frequent dredging. Examination of the seasonal locations of the nodes of bedform transport reveals that Flavel Bar was midway between the seasonal extremes in upstream bedform transport (Figure 4.13). Downstream transport along the north side of the south channel converged with tidally reversing transport to the west at various locations dependent on season. In October, reversing bedforms on the channel flank extended past Tansy Point, but in June, transport was downstream nearly to the tip of Desdemona Sands. West of Tansy Point, strong downstream transport occurred on the south side of the south channel in all seasons, establishing a mechanism for removing sediment from this reach. However, east of Tansy Point on the south side, October data showed upstream transport. Hence, the south side of the south channel adjacent to Tansy Point was a zone of divergence and net erosion. A convergence of transport in the Flavel Bar region was suggested by both its location beneath the end of bedform transport in the channel (Figure 4.13 and 4.14), and by a confluence of transport, at least during low flow periods, along the bordering shoals (Figure 4.14).

In the north channel, upstream transport apparently occurred in the western portion of the channel during all seasons and extended upriver to the Astoria bridge and beyond during low flow periods (Figure 4.13). Downstream transport was rapid along the north flank in June, as evidenced by scour marks and cusped bedforms in this area. The shallow channel east of the Chinook pile dike exhibited downstream transport during most seasons, but the adjacent 35-ft shoal displayed various transport directions and occasionally large, rounded, somewhat symmetrical bedforms (Figures 4.4, 4.5 and 4.6). Historically, this shoal has grown since the completion of the Chinook pile dike in 1935. Transport along the downriver portion of the south side of the north channel and western tip of Desdemona Sands was dominantly upstream in all seasons. Downstream transport along the upriver portion of the south side of the north channel occurred only during February and June.

SCHEMATIC SUMMARY OF SEDIMENT TRANSPORT AND DEPOSITION PATTERNS

180



- | | | |
|--|--|---|
| <ul style="list-style-type: none"> Long-term deposition of coarser sediments in association with channel migration and/or split growth Ephemeral deposition of fine sediments in association with turbidity maximum processes Long-term deposition of fine sediments Non-deposition or erosion | <p>BEDLOAD TRANSPORT</p> <ul style="list-style-type: none"> Net of reversing transport Unidirectional transport | <p>SUSPENDED LOAD TRANSPORT</p> <ul style="list-style-type: none"> Net of reversing transport Unidirectional transport |
|--|--|---|

Figure 4.14 Sedimentation patterns in the Columbia River Estuary based on convergences and divergences of bedform sediment transport. Unidirectional transport arrows reflect dominant transport directions for all seasons. Net transport direction arrows reflect resultant direction of reversing transport indications, integrated over tidal and seasonal time frames.

These transport directions indicated convergence of sediment on the south flank of the north channel, which would suggest deposition. However, records from this area often displayed a highly reflective bottom, and step-like features along the south side of the channel resembled cut-bank features associated with differential erosion of sedimentary strata (Figure 4.15). Investigation of the historical bathymetry revealed that the north channel has recently migrated south, probably in response to the construction of the Chinook pile dike. Consequently, this area has been mapped as erosional in Figure 4.14.

The net upstream transport at depth in the north channel converged with downstream transport east of the Astoria-Megler Bridge. On the basis of this evidence and the presence of large, symmetrical bedforms in the north channel during June (Figure 4.6), the eastern end of the north channel has been mapped as depositional in Figure 4.14.

Relationship with model results

Many of the features of the bedload sediment transport are also suggested by the results of the two-dimensional (laterally averaged) model of Hamilton (1984) discussed in section 3.6. The model results for the low flow case (Figure 3.58) indicate that upstream mean bottom flow is found as far upriver as the Astoria Mooring Basin during spring tides; this position corresponds with the observed upriver limit of upriver-oriented bedforms as determined by the side-scan sonar. However, Figure 3.58 also indicates the presence of net downstream flow at the bottom in the bathymetric depression adjacent to Jetty A. In this region, the side-scan sonar data indicate that reversing bedforms are present. In section 3.6, this and other instances of mean bottom flow reversal are attributed to the effects of large scale bottom topography. Apparently, the reversing bedforms are dominated by the high diurnal tidal currents and do not reflect the mean flow in the entrance and lower estuary.

The model results agree well with the side-scan sonar data in several other instances. A dominance of upstream flow in the north channel that may extend well into Grays Bay is suggested in both investigations. The seasonal shift in the upriver limit of apparent upstream transport is consistent between the model and the side-scan sonar data. The tidal dominance of the entrance is apparent in the side-scan sonar data as well as the model results. As a result of the good agreement among the two approaches, the model results may be used to extrapolate to other flow conditions or topography, as well as to determine the net transport direction in areas with ambiguous bedform indications. In the latter case, model experiments at high discharges (Figure 3.63) indicate that net inward flow at the bottom exists even under the most adverse conditions, suggesting that the net transport direction of the reversing bedforms in the entrance is into the estuary under all modern conditions.

4.2.2 Suspended Sediment Transport

The suspended sediment budget of the estuary is also poorly understood. Fluvial supply of suspended material has been variously

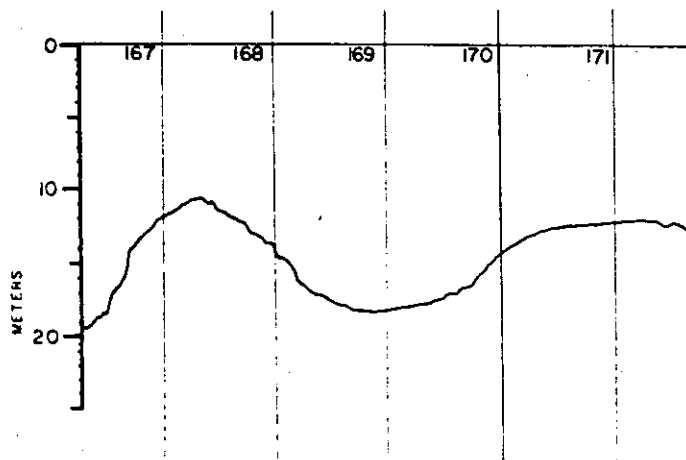
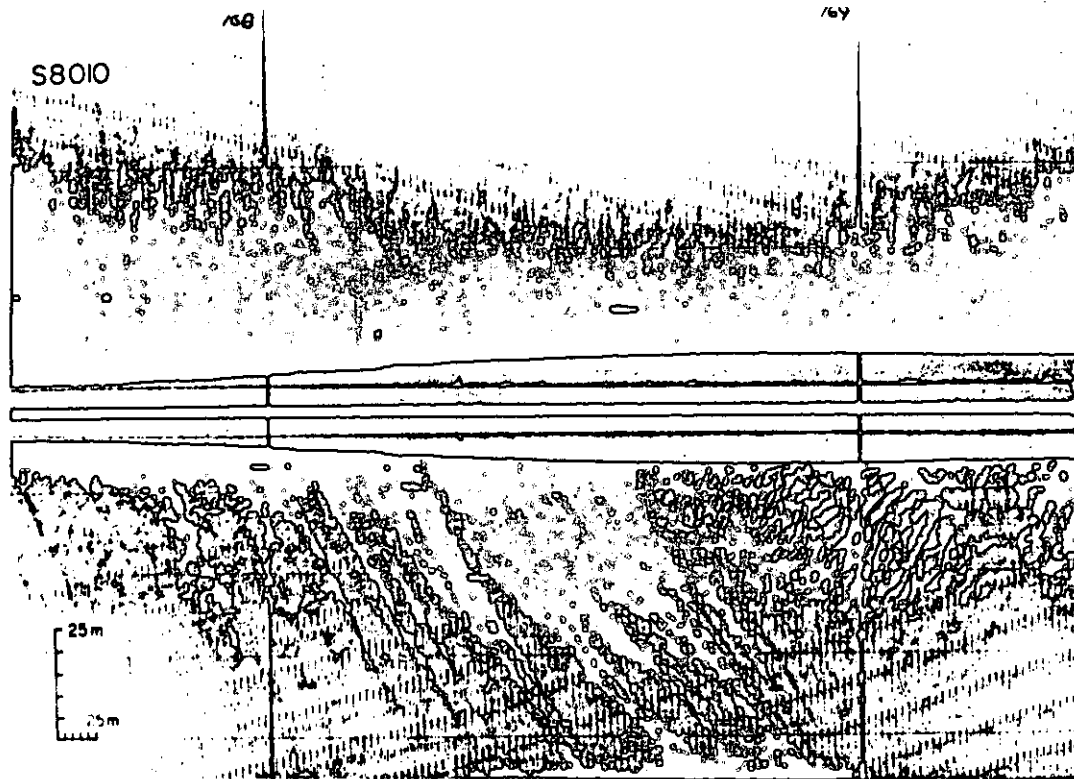


Figure 4.15 Side-scan and echo-sounder records of differential erosion of exposed strata along the south flank of the North Channel.

estimated at 7 to 30 million tons yr^{-1} (Van Winkle 1914 a,b, Judson and Ritter 1964, Haushild et al. 1966) and the generally accepted figure is 10 million tons yr^{-1} (Whetten et al. 1969). Most of the finer material is not retained in the estuary but is transported to the continental shelf either directly or following temporary deposition in the estuary. Nittrouer (1978) measured accumulation rates on the Washington continental shelf and estimated that two-thirds of the annual load of Columbia River sediments are deposited in the mid-shelf silt deposit.

Measurements of the suspended sediment field have been made in order to achieve a qualitative understanding of suspended sediment transport in the estuary. Turbidity profiles, continuous measurements with a nephelometer mounted on the Astoria-Megler Bridge and samples of suspended material have been obtained (Roy et al. 1979, Gelfenbaum 1983, Sherwood et al. 1984). The following discussion summarizes the results of those studies and is drawn almost exclusively from Gelfenbaum (1983).

Texture

Suspended sediment samples from station 11 (Figure 4.16) near Port Westward are representative of the river input of material to the estuarine system. Conomos (1968) found that the river-borne suspended material was predominately lithogenous, composed of discrete mineral grains and lithic fragments and, for low discharge conditions, had an average modal diameter of 6.5 phi (phi size is a measure of sediment grain size commonly used by sedimentologists, equal to $-\log_2$ (diameter of grain in mm). 6.5 phi is approximately 0.01 mm). Results from the present study show a similar predominance of organic lithogenous material. The organics, by weight, at this station were between 1 and 4 parts per thousand (ppt). Figure 4.17 shows the size frequency distribution for two samples from this station. A sample (Figure 4.17b) taken approximately 30 ft (9 m) above the bottom has a fine silt mode and is characteristic of most of the samples obtained from this station. The increase in volume percent at 10 phi (0.001 mm) is probably artificial, resulting from electronic noise in that channel during analysis. A second sample (Figure 4.17a) taken approximately 20 ft above the bottom at approximately the same location, has a medium to coarse silt mode, and characterizes those samples collected during the late ebb part of the tidal cycle. The mode at 7 1/3 phi (0.0072 mm) in Figure 4.17b and the shoulders in the phi distributions in both Figures 4.17a and b are evidence that the washload of the Columbia River is coarse clay-fine silt and that local resuspension at this station, occurring during late ebb, adds a medium- to coarse-silt component to the suspended load.

Suspended sediment samples from Station 2N (Figure 4.18) are representative of the oceanic input of material to the estuarine system. The oceanic source of suspended material to the estuary is predominately biogenous (Conomos et al. 1972). Samples obtained from stations near the mouth during this study had highly variable percentages of organic matter which tended to be fibrous and clogged the Coulter counter aperture, so that size distributions of the oceanic source are not available.

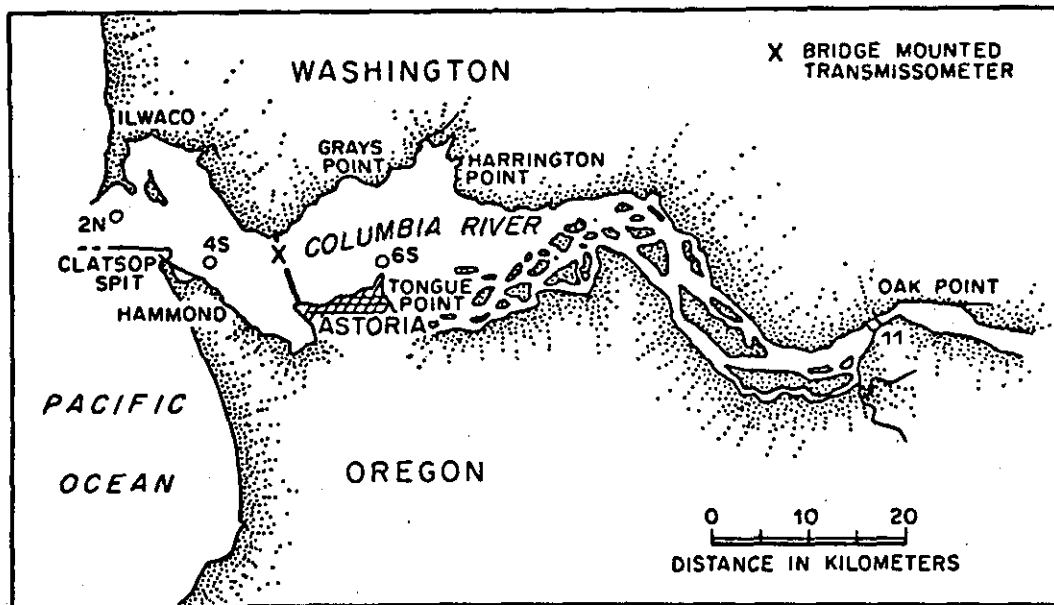


Figure 4.16 Locations of the suspended sediment sampling stations discussed in the text.

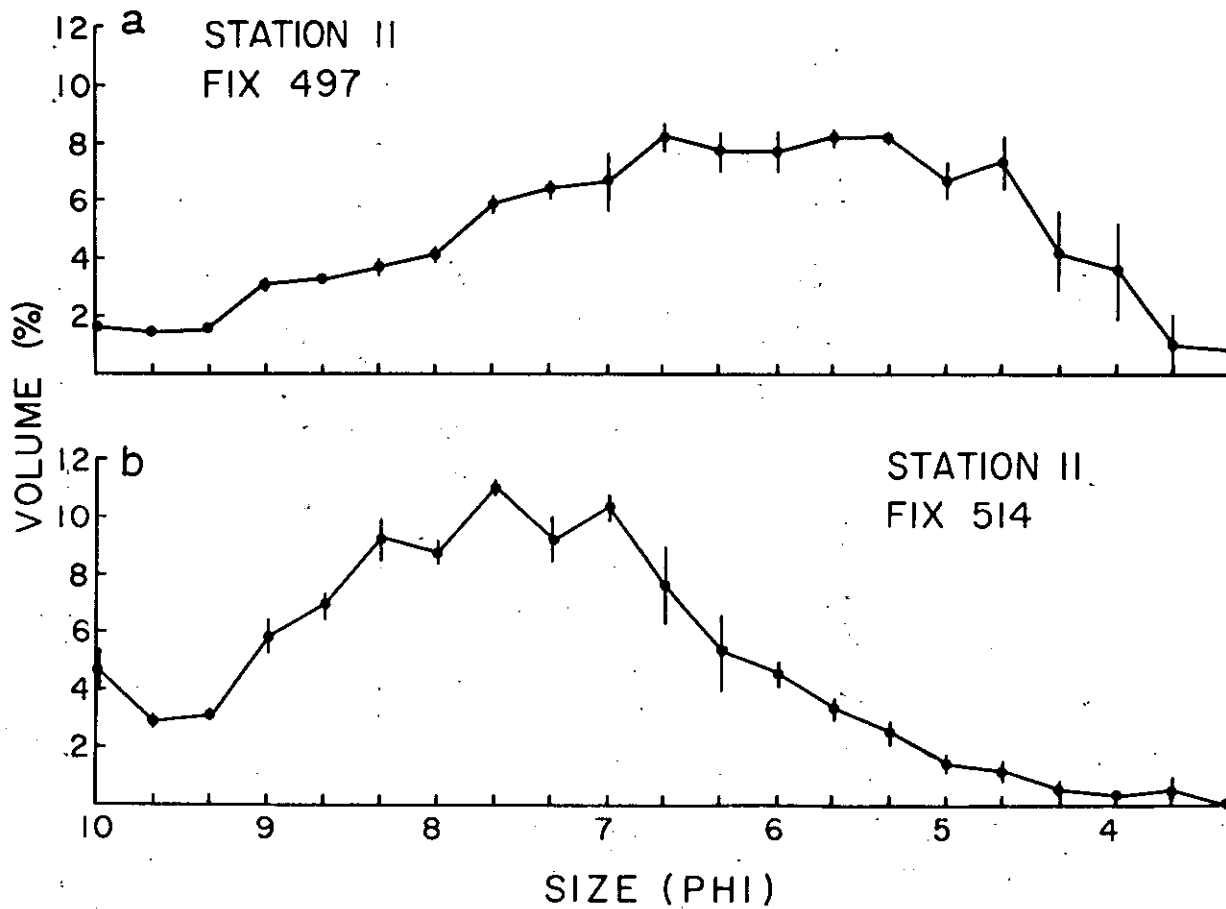


Figure 4.17 Size distributions of suspended sediment samples characteristic of the wash load (514) and locally resuspended material (497).

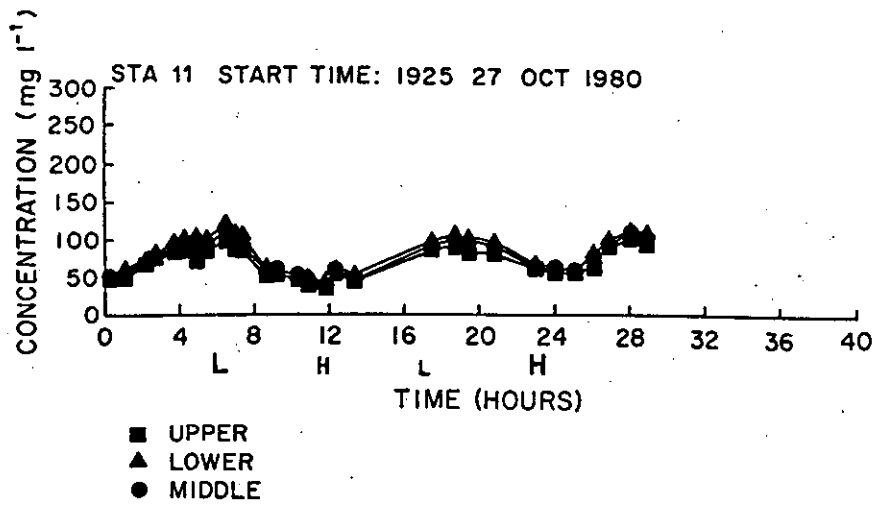
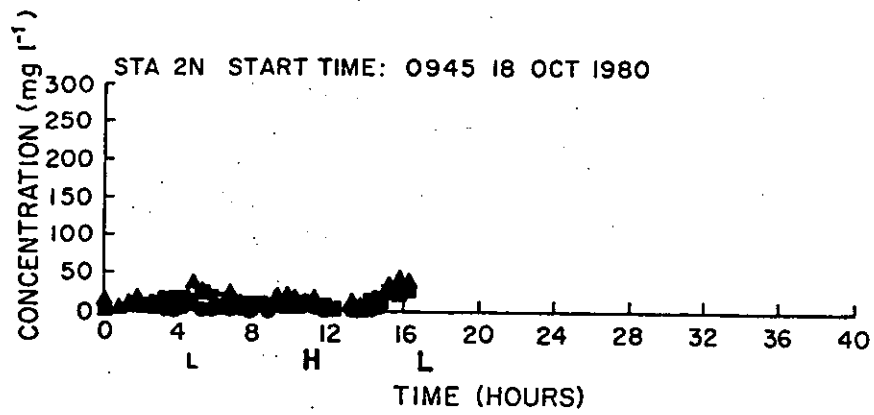


Figure 4.18 Time series of suspended sediment concentrations representative of the oceanic input (Station 2N) and the fluvial input (Station 11).

Transmissivity

Evidence for the importance of fortnightly tidal variations on the suspended sediment field can be seen in the time series in Figure 4.19. This time series displays results from a transmissometer instrument array mounted approximately 3 ft (1 m) above the bottom on the Astoria-Megler Bridge during the summer of 1980. The record clearly shows the correlation among current speed, salinity and transmissivity during both the spring and neap tides. During the spring tides there is a good correlation among higher flow speeds, lower average salinities, and lower percent transmission between approximately July 11 and 15 and again during July 27 to 31. Conversely, during the neap tides, from approximately July 18 to 22 and again from August 3 to 7, there is a strong correlation among lower flow speeds, higher average salinities, and higher percent transmission. The close association among these quantities is substantiated by observing that the second neap tide (August 3 to 7) has higher speeds than the first neap tide and that the percent transmission is correspondingly lower than during the first neap cycle.

Nephelometry

Data representing the upriver and downriver limits of the study area were obtained from station 2N near the entrance and from station 11 near Oak Point, respectively. A nephelometer time series of suspended sediment concentrations for station 2N, the farthest downriver station, is shown in Figure 4.18. At this station there is no vertical structure in the suspended sediment field (as shown by the superposition of the three curves), and concentrations are low, varying between 5 and 40 milligrams per liter (mg l^{-1}). These concentrations are some of the lowest found anywhere in the estuary. Figure 4.18 also presents results for station 11, the farthest upriver station, at approximately RM-50. These data show a similar lack of vertical stratification; however, the concentrations are higher than at the entrance, varying between approximately 40 and 100 mg l^{-1} .

A tidal periodicity exists in the suspended sediment concentrations at this station. The periodicity corresponds to the semidiurnal tide and, as discussed in the texture section above, is a result of local resuspension during the higher flow conditions of late ebb. The nephelometer records therefore indicate that at the boundaries of the estuary system, ocean waters contain low concentrations of suspended sediment and essentially no vertical stratification, while tidal-fluvial conditions are characterized by slightly higher concentrations, relatively little vertical stratification and a tidal periodicity in the suspended load.

The central part of the estuary, exemplified by stations 4S near Hammond and 6S near Tongue Point during spring tidal conditions, has high suspended sediment concentrations, implying the presence of a turbidity maximum (Figure 4.20). Suspended sediment concentrations in the turbidity maximum are almost an order of magnitude greater than incoming river concentrations and 10 to 20 times greater than the ocean concentrations. At both stations there is a strong semidiurnal dependence.

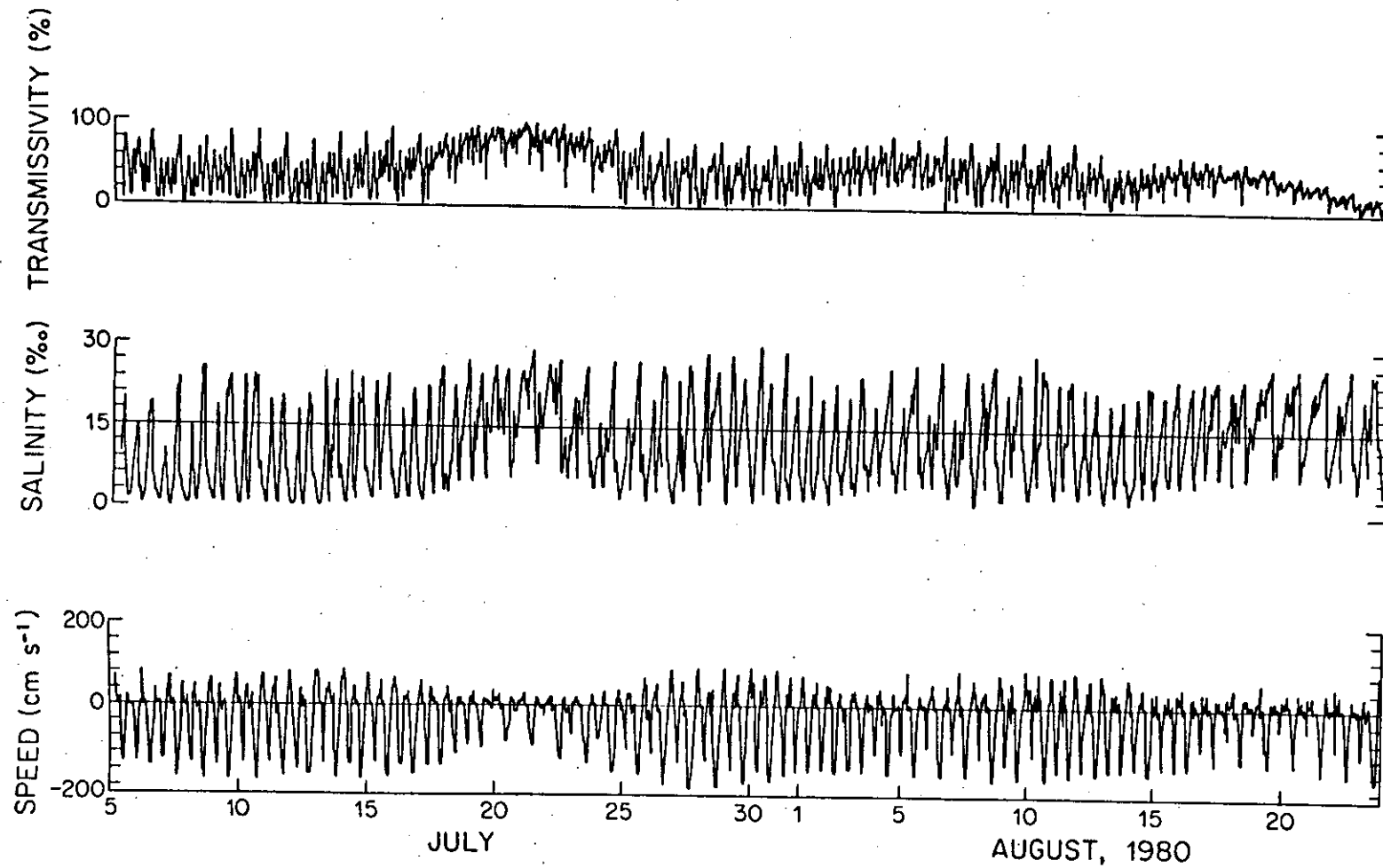


Figure 4.19 Time series of current speed, salinity, and transmissivity obtained from the bridge mounted instrument array.

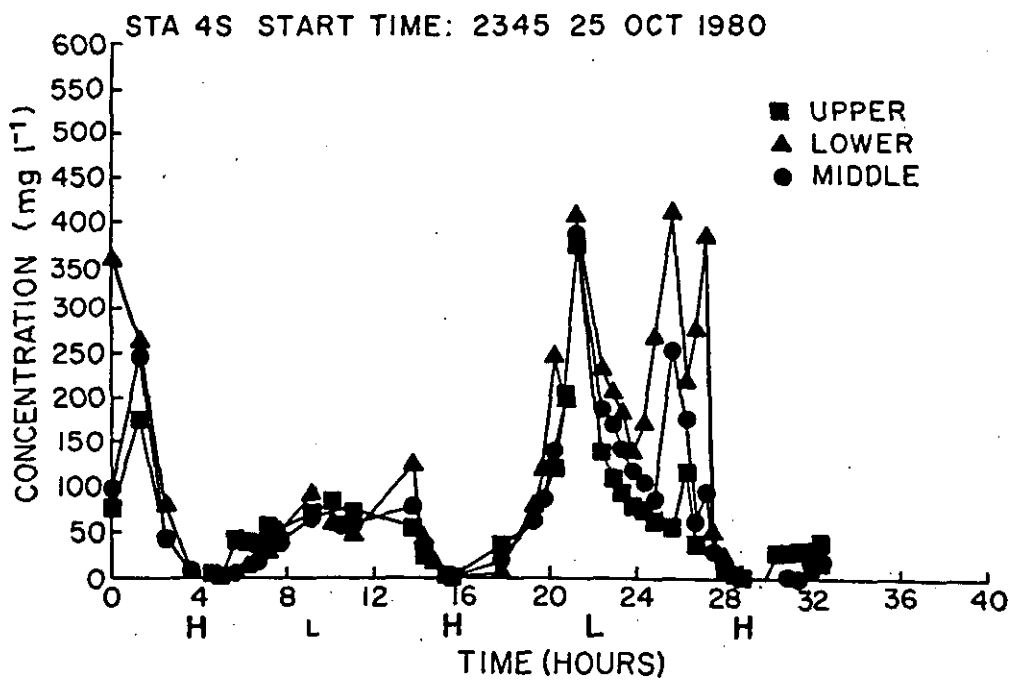
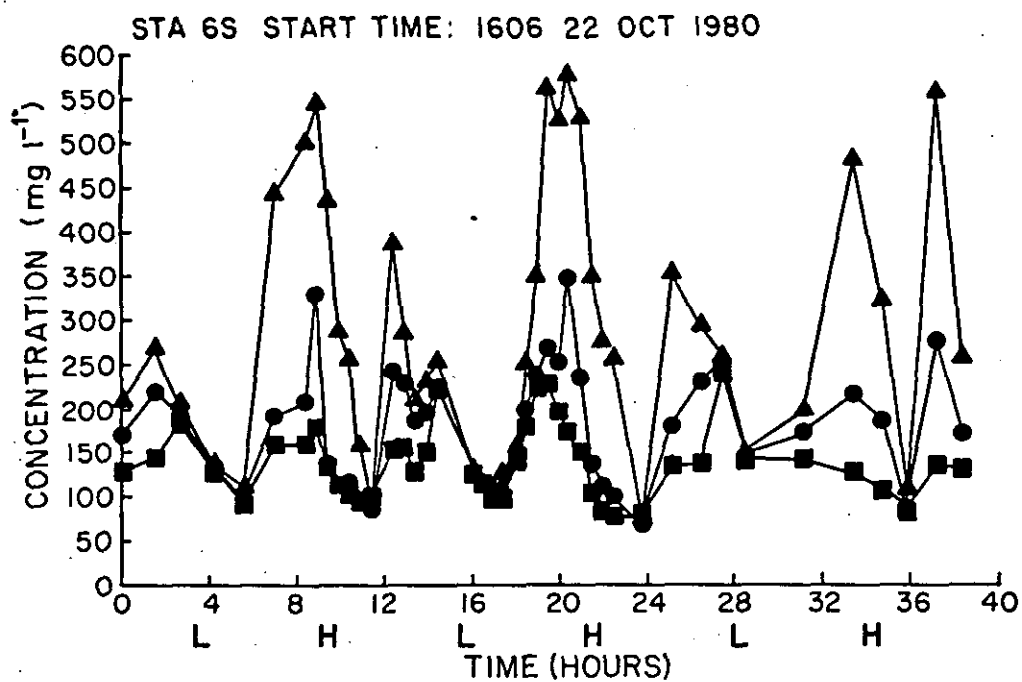


Figure 4.20 Time series of suspended sediment concentrations at the two mid-estuary stations.

Examination of the two time series in Figure 4.20 reveals the occurrence of pairs of high suspended sediment concentration peaks. At Station 4S the pairs of peaks are centered around a time which is approximately two hours after low water. Conversely, at Station 6S farther upriver, the pairs of peaks are centered approximately two hours after high water. The occurrence of these pairs of peaks suggests that the turbidity maximum is being advected alternately upstream with the flood tide and downstream with the ebb tide. Thus, the time period between peaks is related to the extent of upstream or downstream excursion beyond the sampling station. For example, from Station 6S the turbidity maximum is advected upstream, just beyond the sampling location during late flood, and then is advected downstream past the station again during early ebb. Therefore, the pairs of peaks centered around high water for Station 6S and around low water for Station 4S suggest that, for these discharge and tidal conditions, Station 6S is located just downriver of the maximum intrusion of the turbidity maximum and Station 4S is located just upriver of the maximum retreat of the turbidity maximum. As shown in the schematic representation of the excursion of the turbidity maximum (Figure 4.21), the approximate average longitudinal location of the turbidity maximum during this low river flow condition is RM-14 near Astoria. This location corresponds to the one reported by Hubbell et al. (1971) for similar discharge conditions.

A simple water-mass excursion calculation based on the assumption of a uniform channel supports these results. For an average maximum velocity of 150 cm sec^{-1} for the middle of the water column a tidal excursion for the turbidity maximum of 21 km is calculated. The distance between stations 4S and 6S is approximately 15 km. Although errors are inherent in this type of calculation, the relative agreement between the excursion calculation and the nephelometer results indicates the plausibility of the turbidity maximum advecting approximately 20 km tidally.

More sophisticated calculations performed using the one dimensional tidal model presented in Chapter 3 suggest that, in fact, there is not enough tidal excursion to allow the turbidity maximum to spend the observed amount of time below the downriver station and above the upriver station and still travel between the two. An alternate hypothesis to the simple advection scheme might be to attribute the changes to settling and resuspension, rather than advection. Calculations of the settling time (based on samples from the turbidity maximum), however, suggest that insufficient time exists for the relatively fine material to settle more than a few meters during the slack water interval (Guy Gelfenbaum, pers. communication 1984). Although settling and resuspension are clearly important in other estuaries (Schubel et al. 1978) and are equally if not more important in the Columbia River Estuary (see discussion below), the turbidity peaks centered around high and low water are believed to be related to advection processes. Since it seems that the diurnal excursion is insufficient to account for the observed data, it is suggested here that the mean location of the turbidity maximum is also advected on a neap-spring basis. This hypothesis accounts for the observed data (note that the data are not synoptic) and is in accordance with the change of the

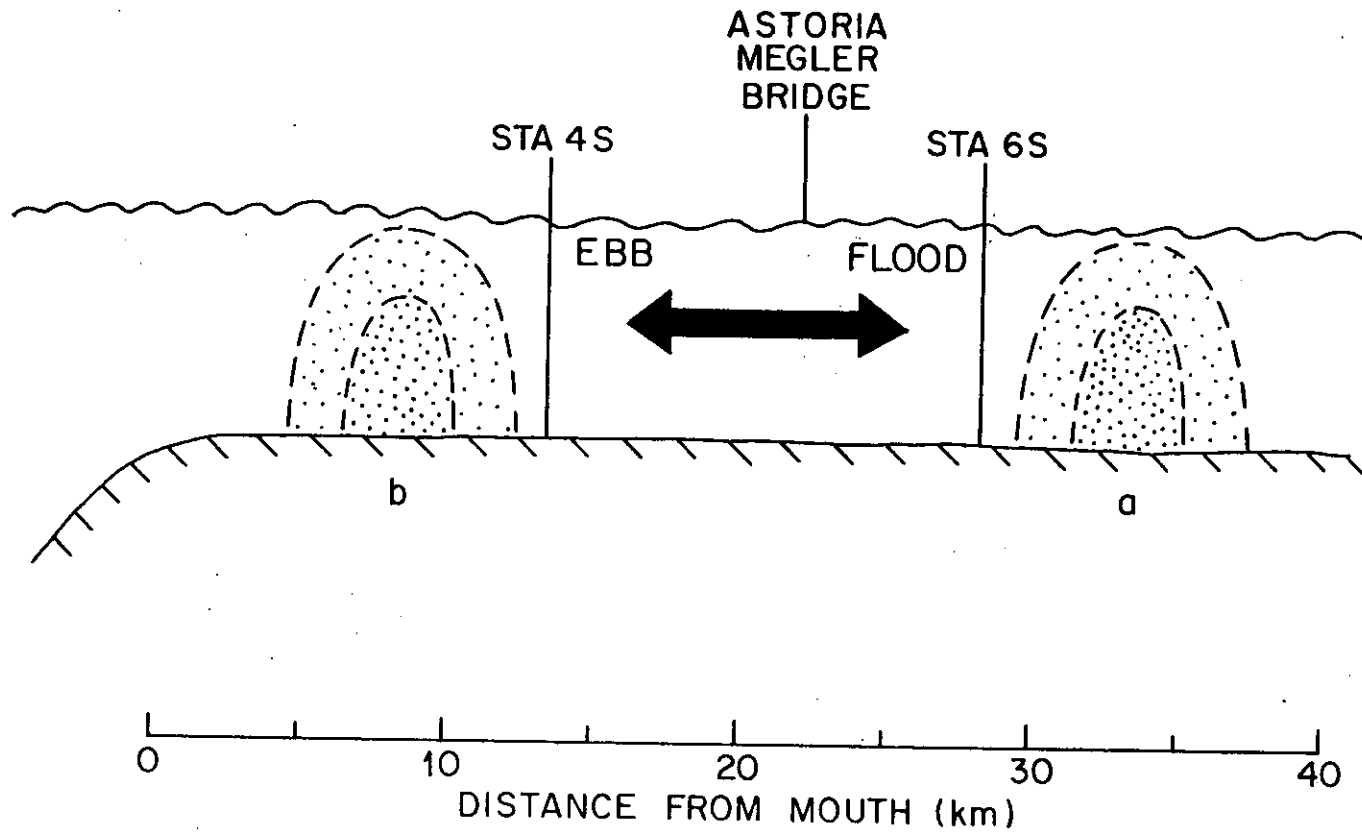


Figure 4.21 Schematic diagram illustrating the tidal excursion of the turbidity maximum.

mean position of the salinity distribution in the models presented by Hamilton (1984).

In addition to providing evidence for tidal advection of the turbidity maximum, the nephelometer profiles also demonstrate the importance of the fortnightly tidal variations on the suspended sediment concentration field. Nephelometer data comparing suspended-sediment concentrations during a spring and neap tide at a single location, Station 6S, are shown in Figures 4.22 and 4.23, respectively. Bottom salinity data, obtained concurrently with the nephelometer data during the spring tide, have a strong tidal dependence with variations between 0 and 15 ppt. Nephelometer data collected during the spring tide, as discussed above, show a vertical stratification of suspended sediments with maximum semidiurnal variations of 75 to 575 mg l⁻¹. Data collected during the previous neap tide at the same location show different results (Figure 4.23). Bottom salinities at this location during the neap tide are greater than during the spring tide, varying between 5 and 25 ppt. The nephelometer time series obtained during this neap tide shows a lack of vertical stratification and relatively low suspended sediment concentrations. These neap tide₁ suspended sediment concentrations, ranging between 25 and 75 mg l⁻¹, are comparable with the washload concentrations found at Station 11.

Both the nephelometer data and the transmissometer data suggest that the lower flow velocities during the neap tide cause a decrease in mixing such that the salt intrudes farther upriver. This lower flow condition also allows the turbidity maximum to degenerate, or decrease in concentration, as (1) resuspension of bottom sediment decreases due to lower boundary shear stresses, and (2) settling to the bottom of advected river material increases due to lower turbulent mixing. Conversely, during the spring tide the turbidity maximum will regenerate, or increase in concentration, as both boundary shear stresses and turbulent mixing are increased.

The behavior of suspended sediment in the estuary is clearly complex. Concentrations in the turbidity maximum vary in response to neap and spring variations in flow conditions, the turbidity maximum is advected on a diurnal and fortnightly basis, and seasonal variations in discharge and ocean water salinity are expected to cause it to shift location seasonally. In addition, settling and resuspension are important phenomena, and lateral mixing from the many side channels and bays is likely to further complicate the situation. The behavior of the turbidity maximum affects the ecosystem of the estuary, because high concentrations of detrital material are associated with the turbidity maximum. Despite the complexities included, suspended sediment behavior is an important aspect of the physical and biological estuarine system.

4.3 LARGE-SCALE MORPHOLOGY

As another approach to the study of the sedimentary geology of the estuary, examination of the large-scale morphology of the estuary was undertaken, using data from aerial photos and recent bathymetry. The gross morphology of the estuary (Figure 4.24) reflects the influence of tidal transport in the lower reaches, fluvial transport in the upper

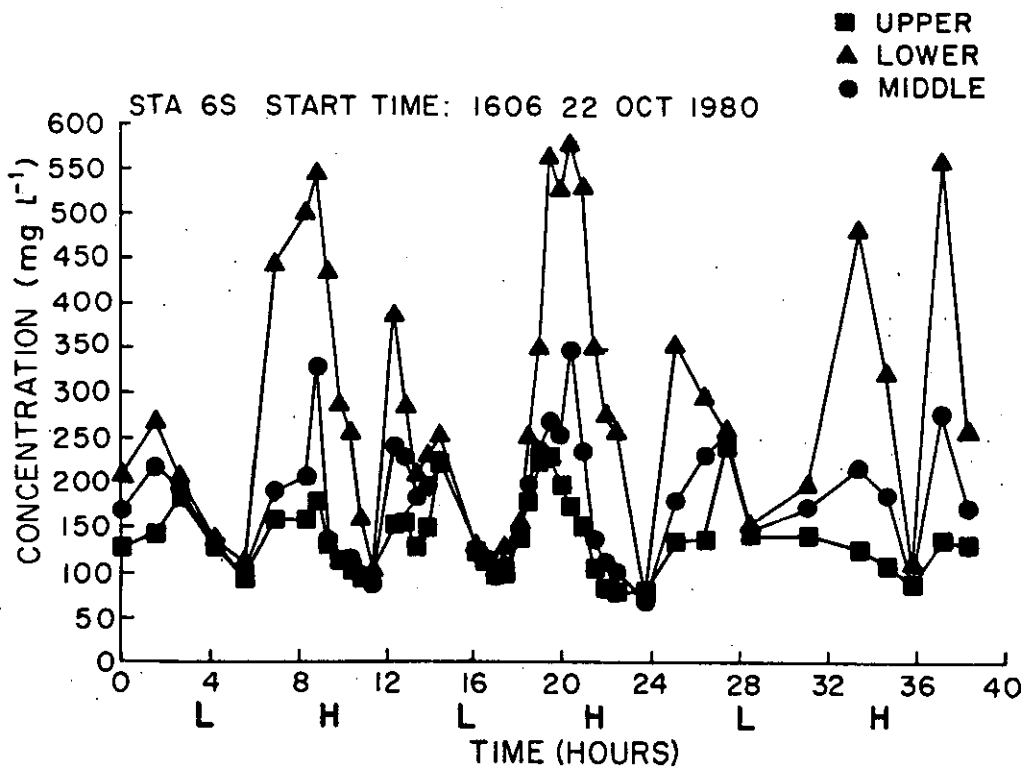
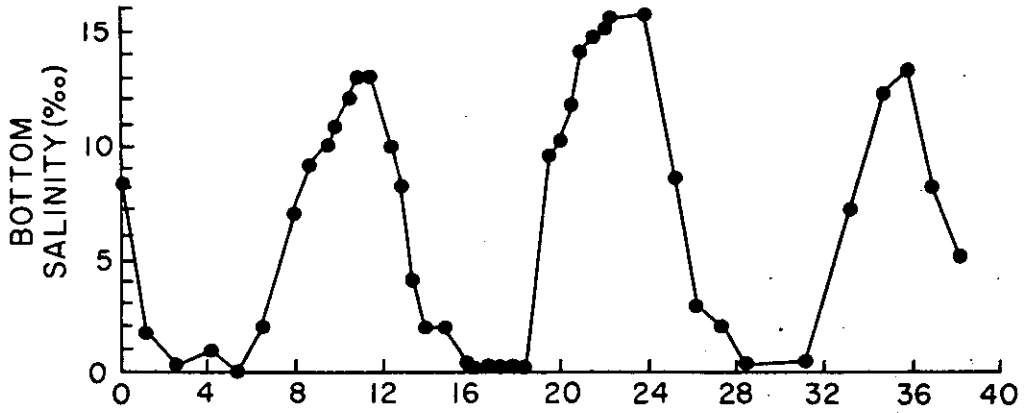


Figure 4.22 Time series of bottom salinity and suspended sediment concentrations (Station 6S) during a spring tide.

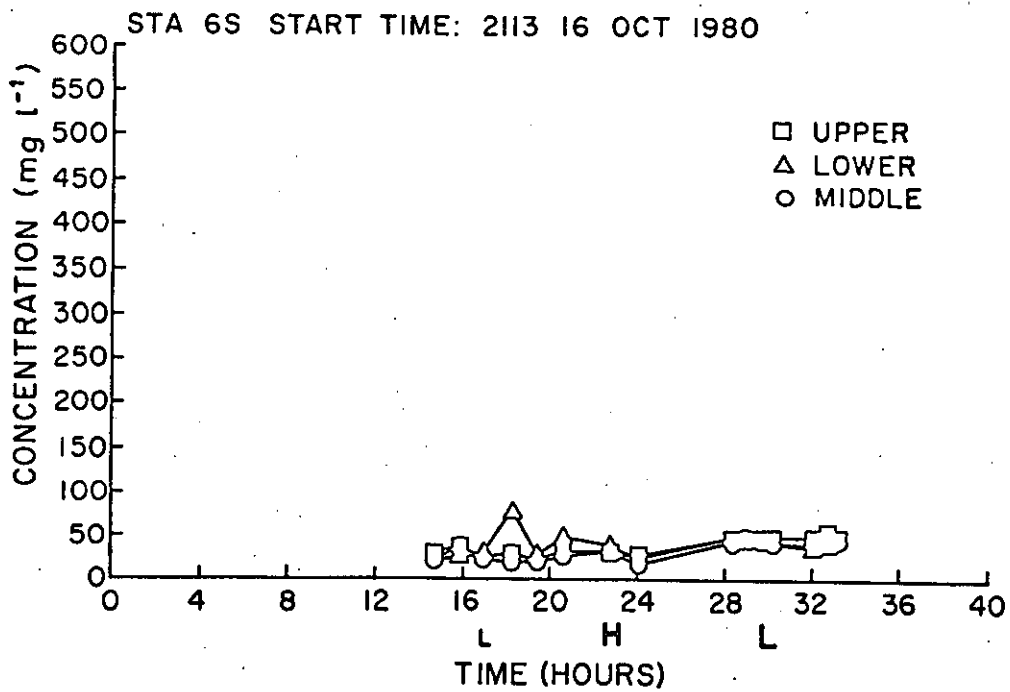
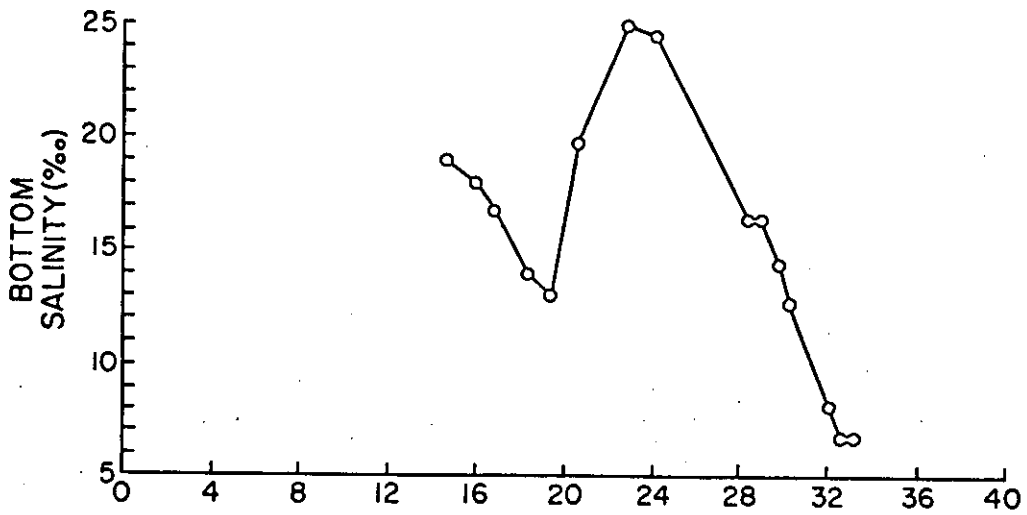


Figure 4.23 Time series of bottom salinity and suspended sediment concentrations (Station 6S) during a neap tide.

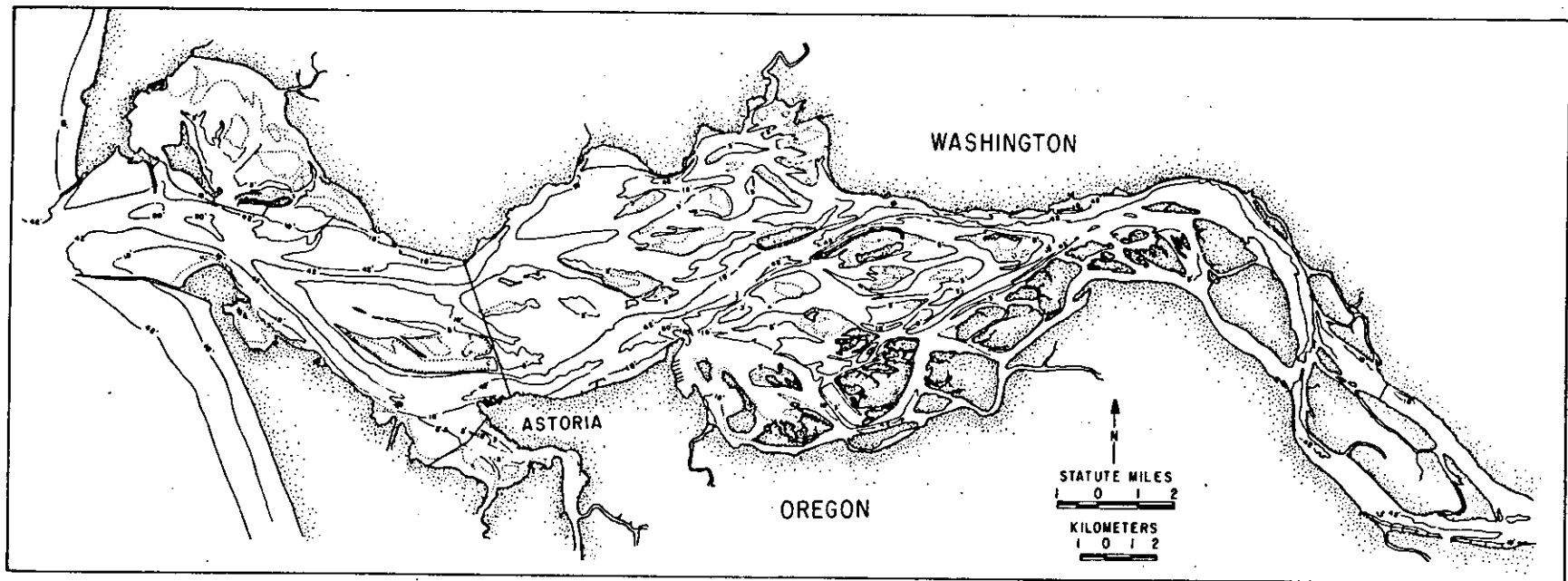


Figure 4.24 Bathymetry of the estuary.

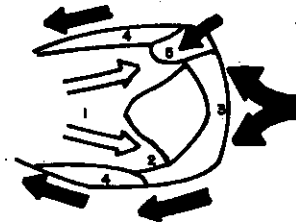
reaches, and a complex interaction between the two in the central portion of the estuary. The channel morphology in the reaches upriver of Tenasillahe Island are distinctly fluvial in nature. The channel has meandered across a narrow flood plain incised into Tertiary rock and, in most cases, the outside of river bends are confined by bedrock. The river channel exhibits bar-pool topography, with deep pools located on the outside of bends (especially adjacent to bedrock) and point-bar deposits on the inside of the bends. Much modification of the natural channel has occurred due to the construction of pile dikes. The channel modifications tend to confine the channel within a narrow cross-section, especially along the straight reaches, where the natural tendency would be to produce a relatively wide, flat-bottomed channel. Downriver of Tenasillahe Island, the bedrock channel broadens, and interaction of tidal flow and river discharge act to produce a complex series of anastomosing channels. These channels migrate and shift naturally where not confined by dikes or dredging. Examination of the historical bathymetry (Columbia River Estuary Data Development Program 1983) suggests that the locations of small channels shift more frequently with distance downriver, probably reflecting the stabilizing influence of vegetation on the more eastern islands. The channel morphology in the lower estuary is much simpler: a single entrance channel bifurcates to form two smaller channels. The location of the south (navigation) channel is controlled by regular channel maintenance activities. The north channel is a more natural system and has shifted its axis north and south during historical time.

Island and shoal morphology also reflect the dominant processes in the various parts of the estuary. The Sand Islands and Clatsop Spit (Figure 4.24) are located in the lower portion of the estuary and are exposed to Pacific Ocean waves. These areas display recurved spits that reflect the influence of wave-induced littoral drift. Desdemona Sands, located in the tidally-dominated lower estuary, displays many of the characteristics of the classic meso-tidal flood-tidal delta model of Hayes (1975) (Figure 4.25 a,b). The shoals in the upper portions of the estuary (for example, Taylor Sands, Figure 4.25c) reflect increasing shape modifications that appear to be related to increased influence of ebb flow and the action of wind-waves. The morphology of these shoals, located in the reaches between the Astoria-Megler Bridge and Harrington Point, is extremely complex, and no close analogues have been reported in other estuaries of the world. They appear to be a product of the time-variant influences of tidal currents during most of the year and nearly fluvial flow during high discharge periods.

In the southern parts of Cathlamet Bay and upriver of Harrington Point, the intertidal shoals grade into vegetated islands. The islands display a characteristic morphology that is related to the ebb-dominant flow of the upper estuary (Figure 4.25d). The upriver edge of the island is generally steep and erosional, while slopes on the downriver edge are gentle and probably reflect depositional processes. The centers of these islands are vegetated and dissected by tidal drainage channels.

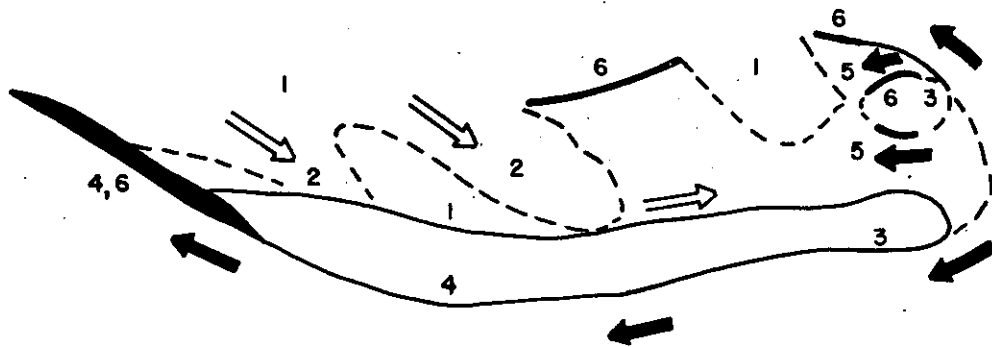
In the upper estuary, it appears that much of the deposition of sand-sized sediments occurs in conjunction with the lateral migration of

a. CLASSICAL FLOOD-TIDAL DELTA
(Hayes, 1975)



- ⇒ FLOOD
- ⇐ EBB
- 1 FLOOD RAMP
- 2 FLOOD CHANNEL
- 3 EBB SHEILD
- 4 EBB SPIT
- 5 SPILLOVER LOBE

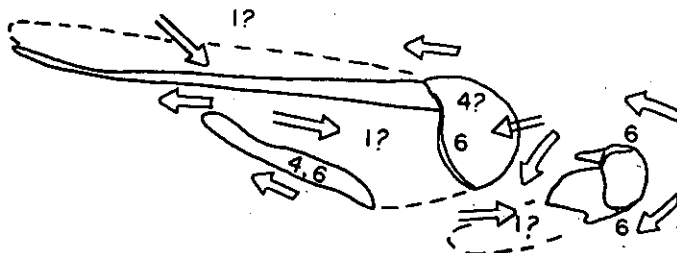
b. DESDEMONA SANDS



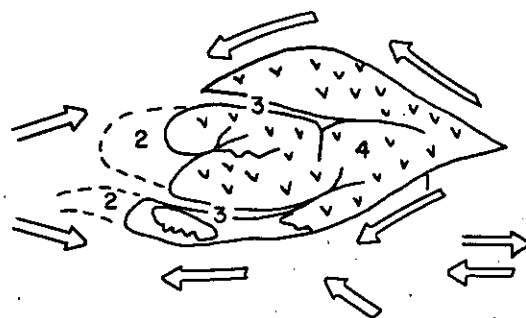
- ⇒ FLOOD
- ⇐ EBB
- 1-5 AS ABOVE
- 6 BEACH

Figure 4.25 Morphologies of intertidal shoals.
a. Classical flood-tidal delta
b. Desdemona Sands

c. TAYLOR SANDS



d. VEGETATED FLUVIAL ISLAND



- FLOOD
- EBB
- 1 EROSIONAL UPSTREAM EDGE
- 2 DEPOSITIONAL DOWNSTREAM EDGE
- 3 DRAINAGE CHANNELS
- 4 EMERGENT VEGETATED ISLAND

Figure 4.25 Morphologies of intertidal shoals.

- c. Taylor Sands
- d. Vegetated fluvial island

the small channels between islands and shoals. Channel migration in the upper reaches of the estuary results in a net downriver displacement of the channel. Evidence for downriver offset can be found by comparing the relative locations of cut-banks and point-bars among the small islands. In general, steep-sided channel margins are located on the upriver edge of the islands, while depositional bars tend to be found on the downriver side of the islands. Although relatively little data were obtained among the complex series of small channels and islands that occupy this region, it appears that horizontal aggradation of fluvially-associated point-bar deposits represents an important part of the natural depositional system of the Columbia River Estuary system. The point-bars represent deposition of bedload material and are genetically associated with the fluvial bedforms that have been observed in the channels of the upper estuary. The importance of lateral accretion is contrasted against the vertical accretion models that are invoked in many estuaries and which are also suggested for the peripheral bays in the Columbia River Estuary. Horizontal accretion explains many of the characteristics of the sediment distribution and morphology of the estuary, including the spatial variability of the sediment distribution, the discontinuous but linear trends in sediment distribution, the tendency for the sediments in the upper estuary to become finer in shallower water, and the shape of the islands and the general channel morphology of the estuary. Further, on the basis of a channel migration model, one would predict localized shoaling and erosion, rather than wide-spread deposition. This, in fact, is what is observed in the estuary.

The Corps of Engineers concentrates most of its dredging efforts in a few locations where shoaling of a fluvial nature occurs, including all of the bars upriver of Tongue Point. Only a few frequently dredged reaches in the lower estuary, notably Clatsop Spit and Flavel Bar, appear to reflect deposition that is dominated by reversing transport or effects of estuarine circulation. In short, the estuary resembles a fluvial system in many aspects of shoaling patterns and bottom morphology, and it is suggested here that the long-term accumulation of sediments occurring in the upper reaches of the estuary reflect mostly fluvial processes.

4.4 BOTTOM SEDIMENTS

An extensive bottom sediment sampling program was initiated in order to accomplish two objectives. The first of these was to provide a baseline data set in order to provide biologists and modelers with sediment size data for the purposes of habitat assessment and sediment transport modeling. The second was to characterize the grain size distributions in the hopes of gleaning additional information regarding the sediment transport and deposition regime in the estuary. Several problems are inherent in the latter approach, foremost of these is the difficulty in directly and unambiguously relating grain size data to sediment transport processes. Some of the best progress in sorting out the conceptual relationship between sediment sources and transported deposits via their grain size distributions has been made by McLaren (1981, 1982, McLaren and Bowles in prep. 1983). Nonetheless, the complications presented by limited sediment availability, complex

mineralogy (and thus complex size/settling velocity relationships), local grain size variability and limited sampling density remain formidable. The following discussion reviews the major conclusions that were drawn from the examination of the trends in bottom sediment size distributions.

4.4.1 Sediment Sampling and Analysis

In all, approximately 1850 samples were obtained in October 1979, 450 in February 1980, 400 in June 1980 and 400 in October 1980. The sampling efforts were designed to correspond with the river seasons discussed in Chapter 2, and will be referred to as fall, winter and spring samples. It should be noted at the outset that the spring samples are anomalous in that they were obtained between 3 and 5 weeks after the May 18, 1980, eruption of Mt. St. Helens, which caused mudflows from the Toutle-Cowlitz river system to enter the Columbia near Vancouver, Washington, approximately 110 statute river miles from the estuary. The effects of this eruption on the sedimentology of this estuary are discussed further below.

Grain-size analysis was originally performed on all seasonal samples from the June and February surveys and on more than 600 of the October 1979 samples. An additional 274 grain size analyses were performed on samples selected from the remaining October 1979 data pool to provide additional sample density in the central portions of the estuary. The locations of all samples chosen for analysis and all of the samples from October 1980 (none of which were analyzed) are provided in Sherwood et al (1984). The sample transects for October 1979 baseline samples are shown on Figure 4.26a. The seasonal samples were collected along the transects shown on Figure 26a. The seasonal samples from a series of earlier cruises, combined on Figure 4.26b, provide an indication of the sample density of the seasonal cruises. Most of the samples were collected utilizing microwave ranging techniques for navigational data and precision echo sounders for depth data. The positions are considered accurate to within +/- 30 m and depths (corrected to MLLW) are accurate to within ± 0.3 m. Standard sieve and pipette techniques were used in grain-size determination and most of the frequently used grain-size measurements were calculated (Krumbein and Pettijohn 1938, Inman 1952, Shepard 1954, Folk and Ward 1957, Folk 1974). The use of these standard techniques allowed comparison with several data sets obtained in and near the estuary during earlier studies for the Corps of Engineers (Sternberg et al. 1977, Borgeld et al. 1978, Walter et al. 1979, Roy et al. 1979, Roy et al. 1982); these data sets are included in the analysis presented here. More detailed descriptions of techniques are included in Sherwood et al. (1984).

In addition to producing maps of the standard grain-size statistics (mean, standard deviation, skewness, coarsest one-percentile, percent silt, sand and clay), several more sophisticated statistical techniques were used in an attempt to characterize the grain size data. These techniques included Q-mode factor analysis (variables were the normalized fraction weights in each size class), Q-mode cluster analysis (same variables), R-mode factor analysis (variables were depth, longitude, and moment measures of mean, standard deviation, skewness and

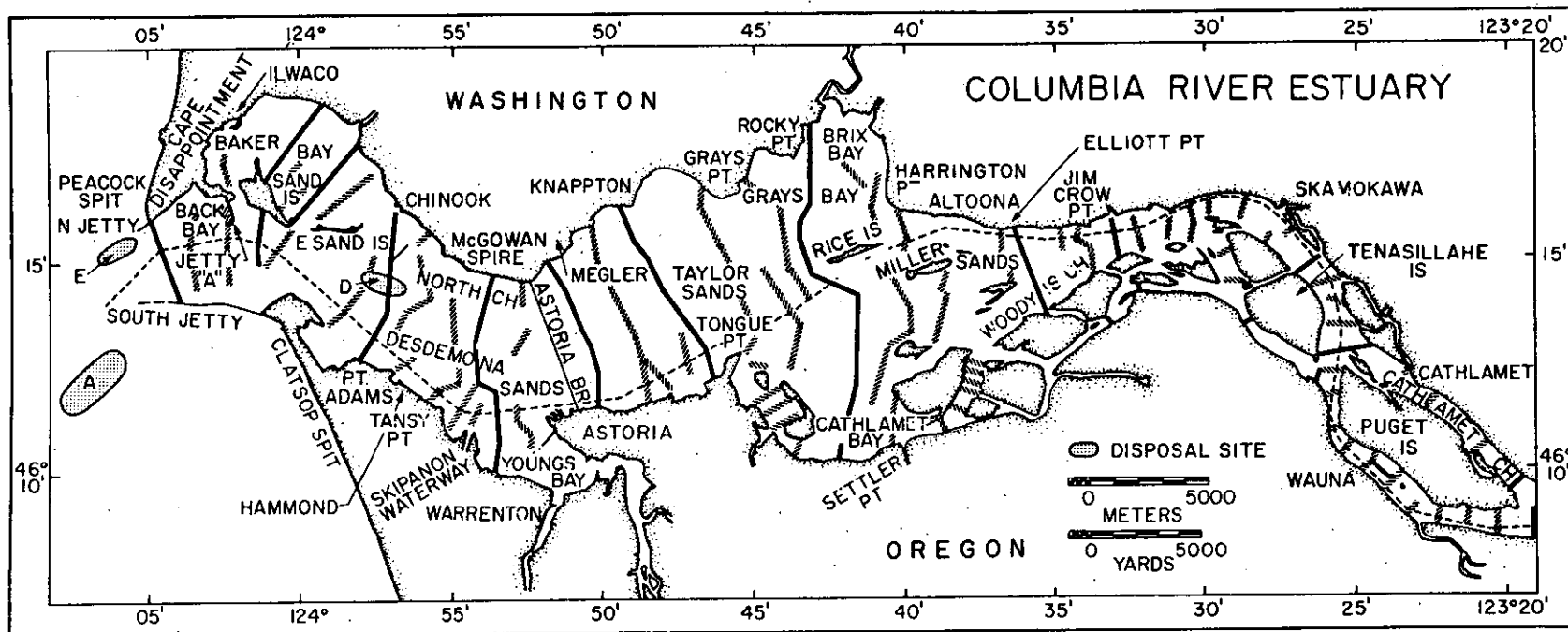


Figure 4.26a Sediment sample transects: dark line represents seasonal sample transects; hatched line represents fall baseline samples.

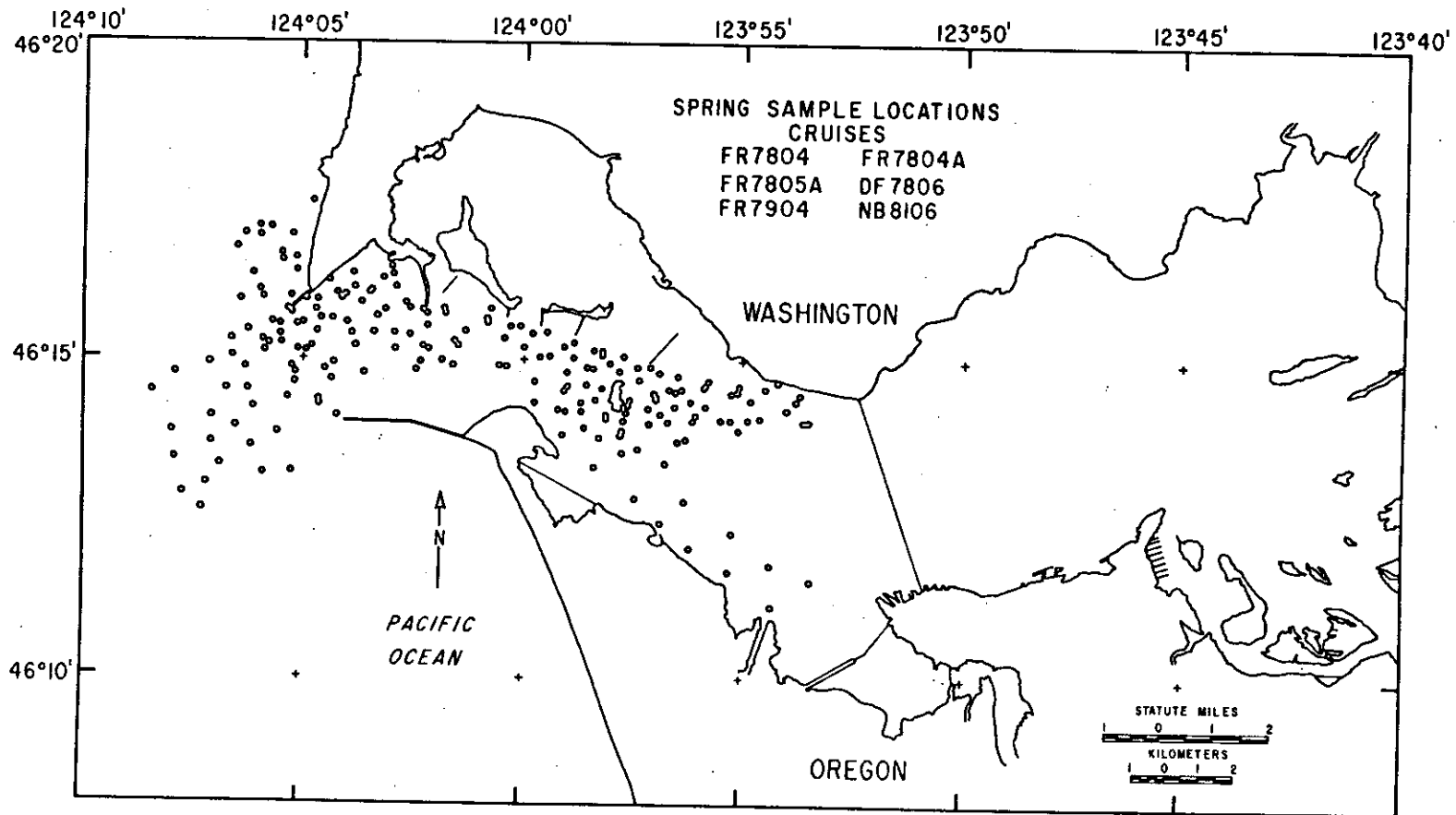


Figure 4.26b Sample locations during spring for several pre-CREDDP studies.

kurtosis), and R-mode cluster analysis (same variables). A number of graphic presentations and maps were generated using the various statistical results and employed in the interpretations. Details of the techniques and results are presented in Roy et al. (1982) and Sherwood et al. (1984) and the major conclusions of those reports are presented here.

4.4.2 Sediment Size Variation

The estuary bottom is predominantly fine sand: the overall average size of more than 2,000 samples is 2.48 phi (0.18 mm). Seasonal variations in the overall mean grain size are found. Overall, the coarsest samples are from winter, and the finest from spring (Table 4.1). The sorting (moment standard deviation) for the three seasons also varies, ranging from a value of 1.02-1.05 phi (1.10 mm) during the better-sorted fall and winter seasons to 1.22 phi (1.49 mm) in the spring (Table 4.1). A plot of mean grain size and sorting for all of the samples for each of the three seasons is shown in Figure 4.3. Despite a wide scatter in both the mean size and the sorting, several prominent features may be observed. The bulk of the samples have mean sizes between 1.00 and 3.50 phi (0.50 and 0.09 mm) and thus range from medium to very fine sand. Although some of the samples have means in the silt range (4.00 - 8.00 phi, 0.063 - 0.004 mm), no samples are found in either the clay range or the gravel range. Thus, despite significant variation in grain size within the estuary, the estuary is predominantly sandy, and the variability in sediment size occurs within a fairly narrow size range.

In Figure 4.27, which shows the relationship of grain size and sorting to distance downstream, the coarsest samples appear to become slightly finer downriver in the upriver sections (above RM-25). No trend with distance is noted in the upper or lower estuary until approximately RM-10. From RM-10 (approximately Hammond) downriver, the mean phi size of the coarsest samples increases steadily. The envelope surrounding the finest samples is more variable than that surrounding the coarsest samples. Several groups of fine samples are present on the graph over sections of the estuary; a large portion of these samples are from the peripheral bays. Many of the fine samples located between RM-3 and RM-9 are from Baker Bay; many of those in the fine group between RM-11 and RM-17 are from Youngs Bay; and many of the finer samples from RM-17 to RM-25 are from either Grays Bay or Cathlamet Bay.

When the estuary is subdivided by depth regime and by distance upriver from the entrance, changes in sediment size as a function of depth and distance from the entrance can be examined in more detail. In the upriver portion (above RM-25) a distinct trend of coarse sediments at depth (greater than 9 m, 30 ft) becoming finer upward to finer sediment in intertidal depths (less than 1 m, 3 ft) was observed in all three seasons (Figure 4.28). By contrast, in the entrance region (RM--5 to RM-2), intertidal sediments (less than 1 m) and shallow water sediments (1.5-5 m; 3-18 ft) are slightly coarser than moderately deep water sediments (5.5-9 m) and do not differ significantly from the deep water sediments except in spring (Figure 4.28). In the lower estuary (RM-5 to RM-14), the same relationship occurs between the intertidal

Table 4.1. Grand means of moment mean sediment size and moment standard deviation (sorting); phi values.

	<u>Fall</u>	<u>Winter</u>	<u>Spring</u>	<u>All</u>
Mean (S.D.) ¹	2.45 (0.99)	2.33 (1.15)	2.66 (1.37)	2.48 ³
Standard (S.D.) ² Deviation	1.05 (0.63)	1.02 (0.44)	1.22 (0.73)	1.10 ³
N	832	574	670	2076

1/ S.D. (Standard Deviation) around the mean of the means

2/ S.D. (Standard Deviation) around the mean of the standard deviations

3/ Weighted means, no standard deviations

MEAN GRAIN SIZE and SORTING
of
ALL SAMPLES

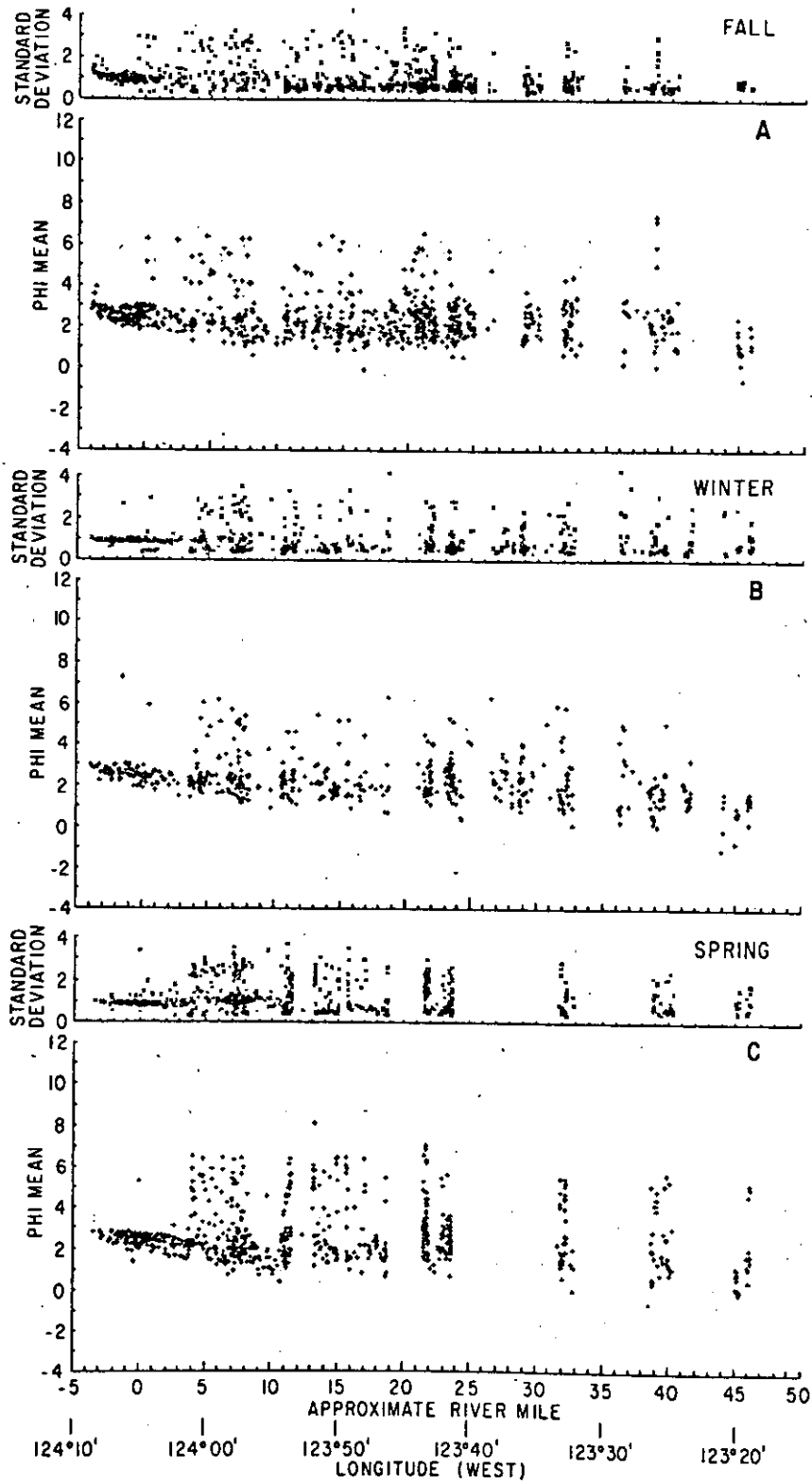


Figure 4.27 Mean size and sorting versus river mile.

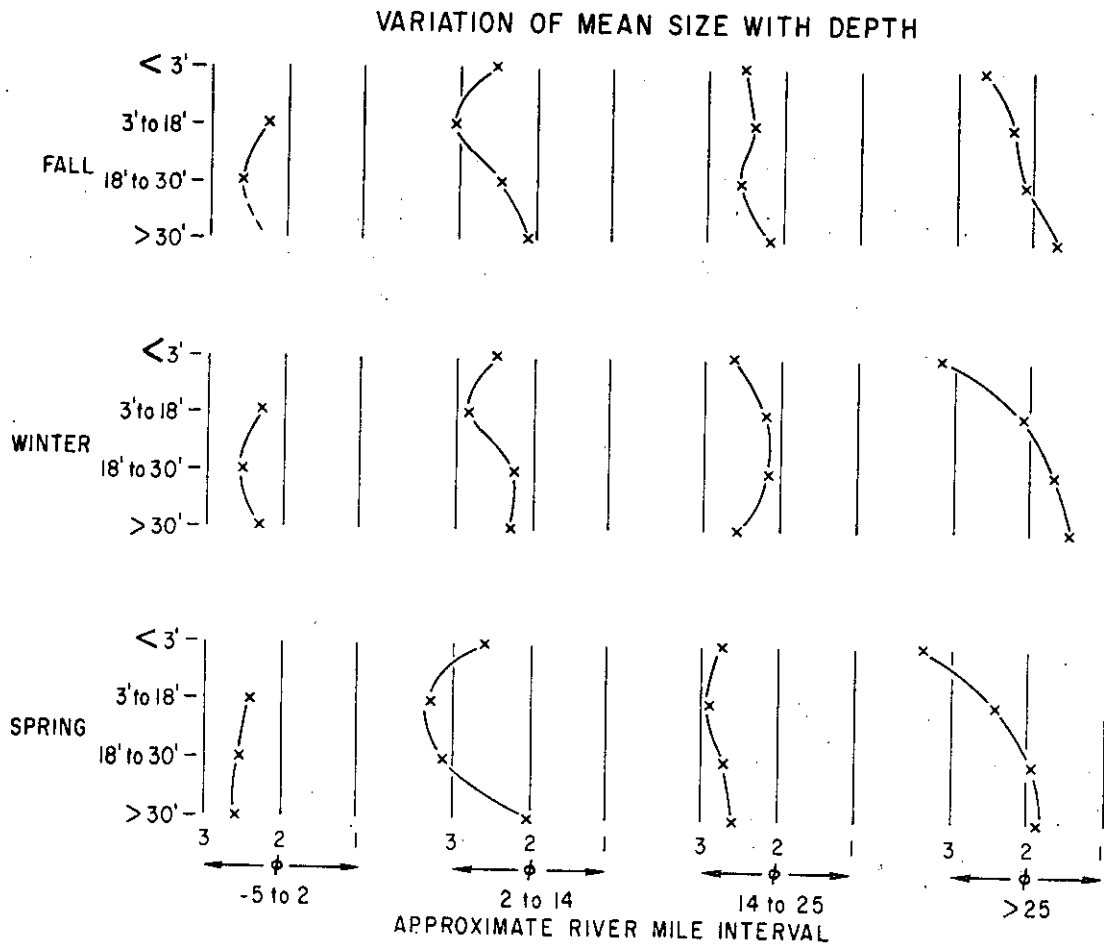


Figure 4.28 Variation of mean size with depth.

sediments and the shallow water sediments: the intertidal sediments are distinctly coarser and slightly better sorted (Figure 4.28). In most seasons, the shallow water sediments of the lower estuary are among the finest in the system. The sediments in deep water in the lower estuary have mean sizes between 2.10 and 2.53 phi (0.23 and 0.17 mm) during the three seasons, with the finest sediments again occurring in spring (Figure 4.28). In the upper estuary (RM-14 to RM-25), no consistent trends related to depth are evident. Sediments in this reach are slightly finer in spring.

Grain-size trends in the along-estuary direction are shown in Figure 4.29. In the intertidal sediments, grain size becomes finer with distance upriver from the entrance. The coarsest sediments are found in the upriver section (above RM-25) in deep water. The finest sediments are found in the upriver section at intertidal depths and in the lower estuary (RM-2 to RM-14) in shallow water (Figure 4.29). In the spring, anomalously fine sediments occur at moderate depths in the lower estuary. Although not evident in Figure 4.29, a distinct trend occurs in the deepest samples (depths greater than 9 m) and can be seen in Figure 4.30). Figure 4.30a depicts the relationship between mean size and distance from the entrance, while Figure 4.30b shows the relationship of the size of the coarsest one-percentile with distance from the entrance. Both plots indicate that the deepest sediments become finer downriver. The plotted standard deviations (the standard deviation about the mean of the mean sizes; this is a measure of variability among samples, rather than a measure of the sorting of one sample) suggest that there is a very narrow range of sediment types in the entrance region, and a greater diversity in the upper and lower estuary regions. The upriver sediments show less variation than the estuary sediments, but more than the entrance sediments.

High local variation in sediment texture occasionally occurs, and has implications on the interpretation of textural distributions. Figures 4.31 and 4.32 (from Roy et al. 1982) show the bathymetry and a measure of grain size (based on the factor extremals) of two north-south transects, one across the boundary between the entrance and the lower estuary, and one across Grays Bay in the upper estuary. Despite the greater depth variation in the downriver transect (Figure 4.31), there is less variation in the sediment size, especially in comparison with the upper estuary transect (Figure 4.32), which includes troughs of bedforms. As can be seen in the side-scan sonar image of Figure 4.7, the troughs of larger bedforms (in this case, heights of 3 m and wavelengths of approximately 100 m) appear more acoustically reflective than the crests. When similar bedforms are selectively sampled, crest-trough differences in sediment size were striking (Table 4.2). In most cases, the troughs are substantially coarser and more poorly sorted. They may be either scoured lag deposits or an old pavement of earlier deposits across which the bedforms are migrating. In other areas, troughs are found that appear less reflective, suggesting that finer sediments have accumulated in the troughs, but these were not specifically sampled. The relatively high local variability of sediment size tends to obscure large scale and seasonal trends in the estuary and render interpretations of the trends more subjective.

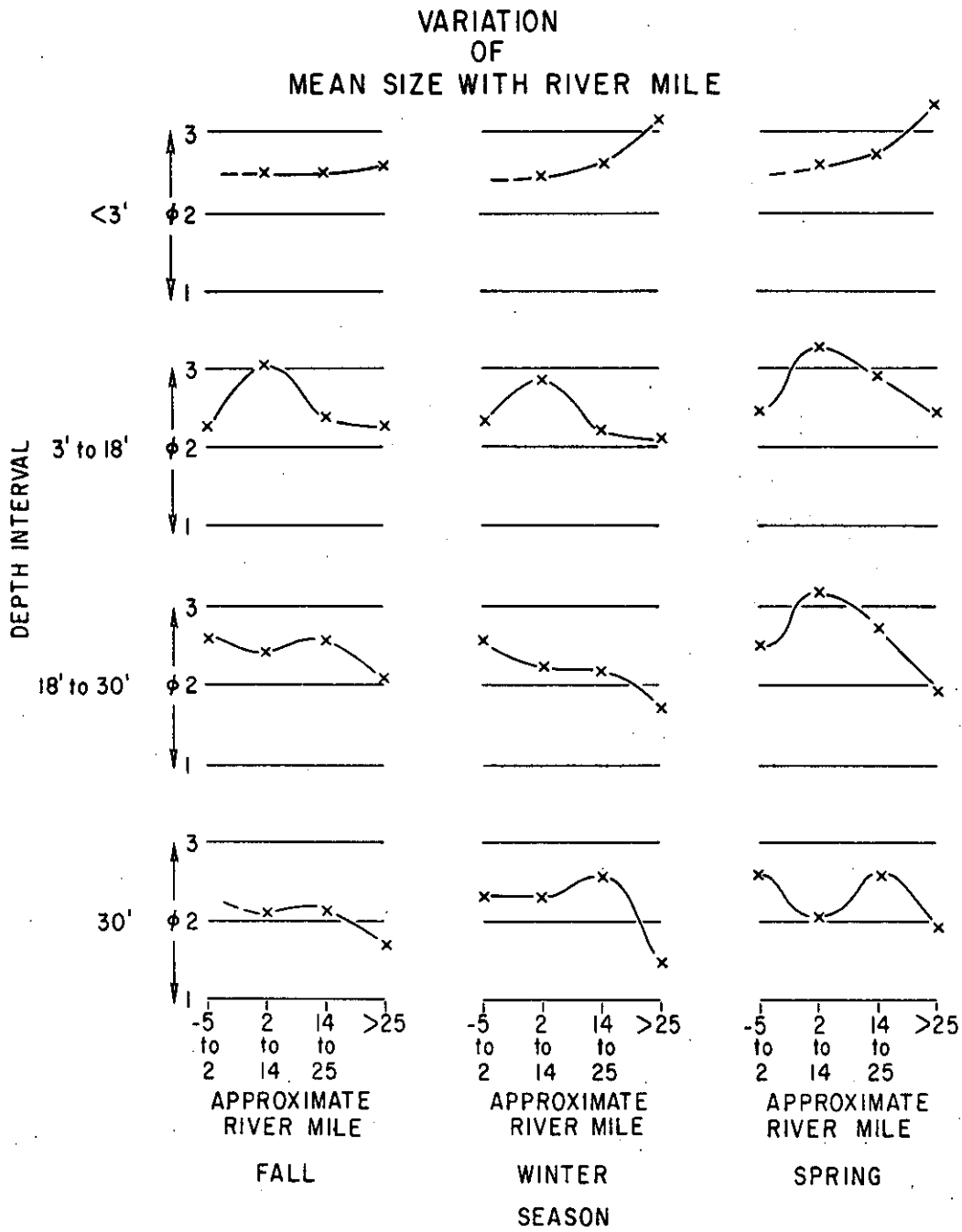


Figure 4.29 Variation of mean size with river mile.

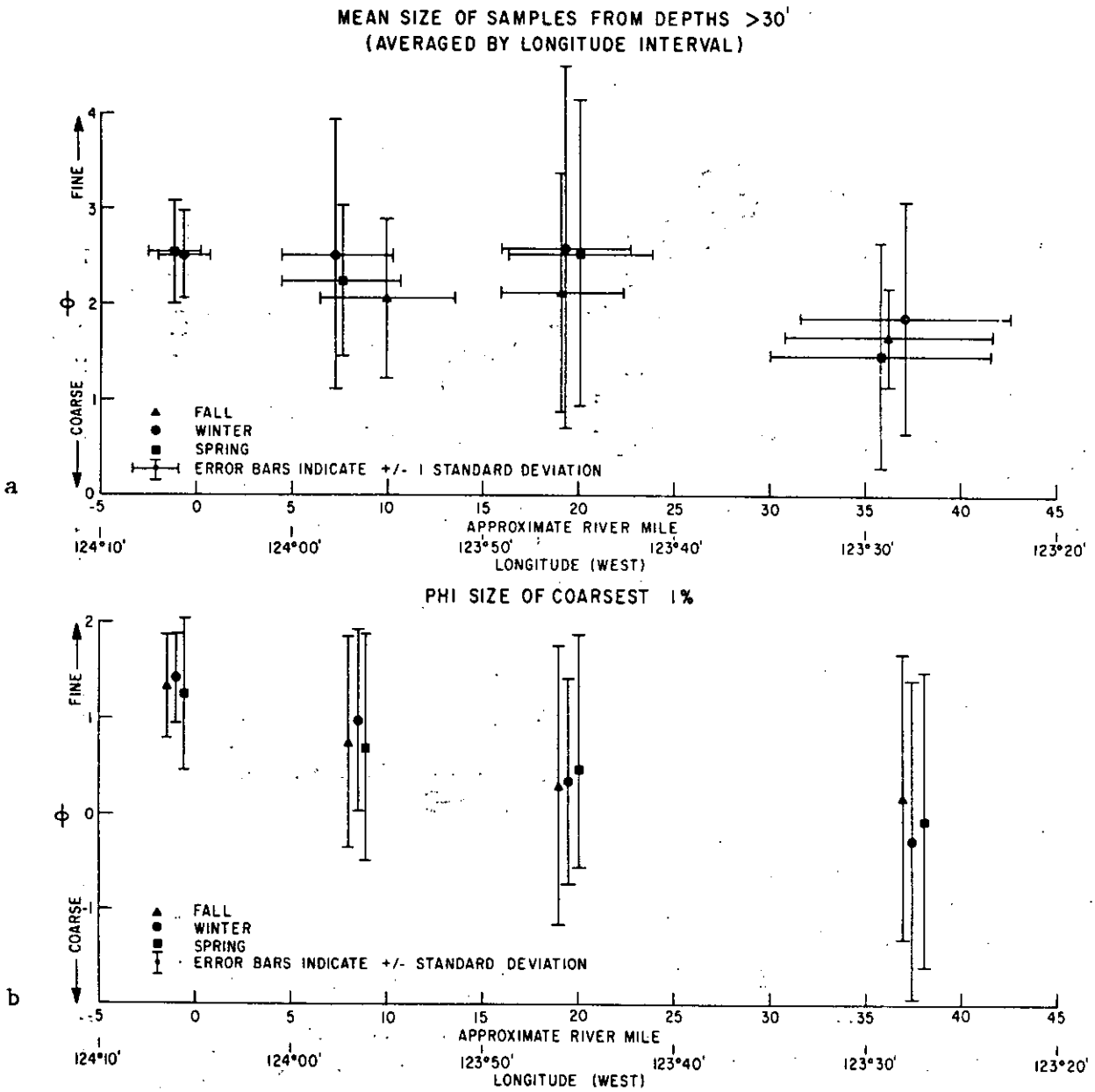


Figure 4.30 Mean size and phi size of the coarsest one percentile of samples from depths greater than 9.1 meters.

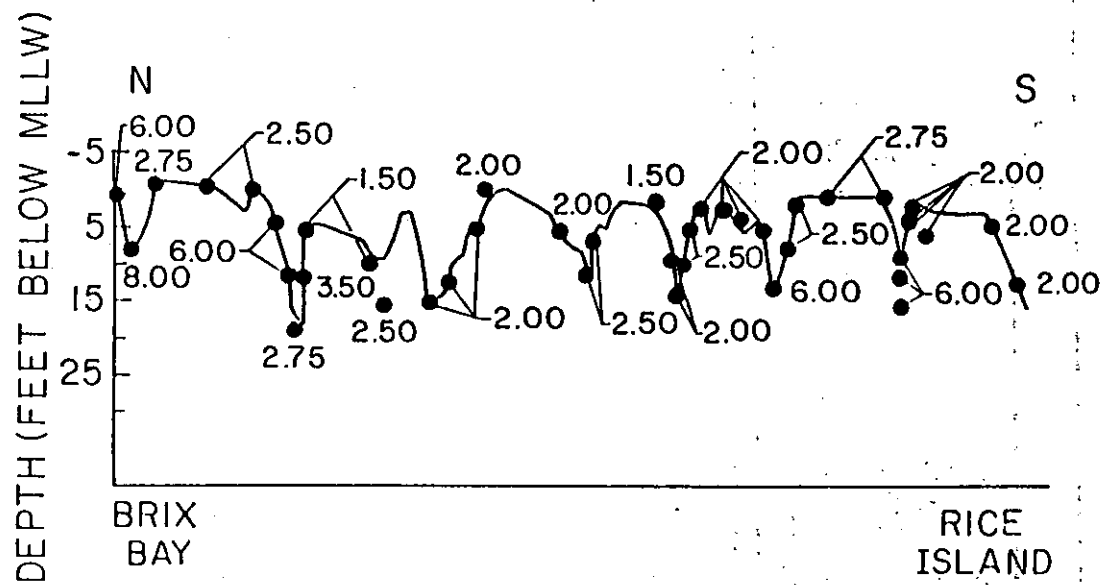


Figure 4.32 Sediment size and bathymetry across transect in Grays Bay.

Table 4.2. Summary of results of sediment grain-size differences between crests and troughs of large-scale bedforms.

PARAMETER	CRESTS	TROUGHS
Average modal phi size	1.50	-0.13
Average percent gravel	0.0	49.66
Average percent mud	0.29	0.47
Average sorting	1.19	5.00
Average mean phi size	1.37	-0.58

From Roy et al. (1982)

4.4.3 Areal and Seasonal Variation in Sediments

In order to most simply present the areal distribution of sediments, the parameters that provided the most information were compiled on two kinds of maps: 1) the generalized sediment distribution maps, one for each of the three seasons (Figures 4.33, 4.34, and 4.35), and 2) a generalized silt plus clay map which combines the data from all three seasons and summarizes the results of more than 2000 grain size analyses (Figure 4.36). The density of data and the variability of the sediments in some areas precludes adequate resolution of the distributions at the map scale required for this report, and the reader is encouraged to refer to Fox et al. (1984) for a more detailed representation of the sediment distribution in the estuary. On the other hand, sample density in some areas was insufficient to allow extrapolations to be made with confidence. In the absence of other data, most extrapolations were made along bathymetric contours.

The following parameters are mapped on the generalized sediment distribution maps (Figures 4.33, 4.34, and 4.35): 1) mean grain size, in three broad intervals: less than 2.25 phi, 2.25 phi to 3.00 phi, and greater than 3.00 phi, 2) skewness, less than 0.0 or greater than or equal to 0.0, 3) location of obviously stratified (two-layered) samples, shown as coarse sediments overlying fine or fine over coarse, 4) location of sandy-silt clasts ("mudballs" in Roy et al. 1982), and 5) location of acoustically reflective bottoms (as with the side-scan sonar) that are interpreted as bedrock, talus, or coarse gravel.

Overall Trends

The gross pattern of sediment distribution is similar in all three seasons. Most of the estuary is floored in either fine or medium sand. The offshore regions, including the outer tidal delta and most of the lower portions of the estuary but excluding the channel proper, are characterized by fine sand. Fine sand is also found on most of the large sandy shoals in the lower and upper estuary, especially the Sand Islands, Desdemona Sands, and Taylor Sands, and the unvegetated shoals of Cathlamet Bay. Medium sand predominates in most of the remaining channel areas. The sands with the coarsest mean grain size are generally found along the main (navigation) channel in the fluvial reaches and the upper estuary. These sands are usually negatively-skewed and have coarsest one-percentiles that are coarser than 0.0 phi. The coarsest sands are obtained from the deep bathymetric depressions found near some of the Tertiary bedrock headlands and man-made dikes and jetties, or when the troughs of large bedforms in the fluvial reaches are intentionally sampled. Only a few samples containing any gravel-sized material were recovered, and these were located in the immediate vicinity of rock headlands or talus slopes. The sampling equipment was not ideal for recovering gravel-sized material; the talus and gravel distributions indicated on the maps are inferred from highly reflective bottoms recorded with the side-scan sonar. Some of these reflections may also be bedrock outcrops.

The finest sediments are found in the peripheral bays, notably Baker Bay, Youngs Bay, Cathlamet Bay, and Mott Basin. Very fine

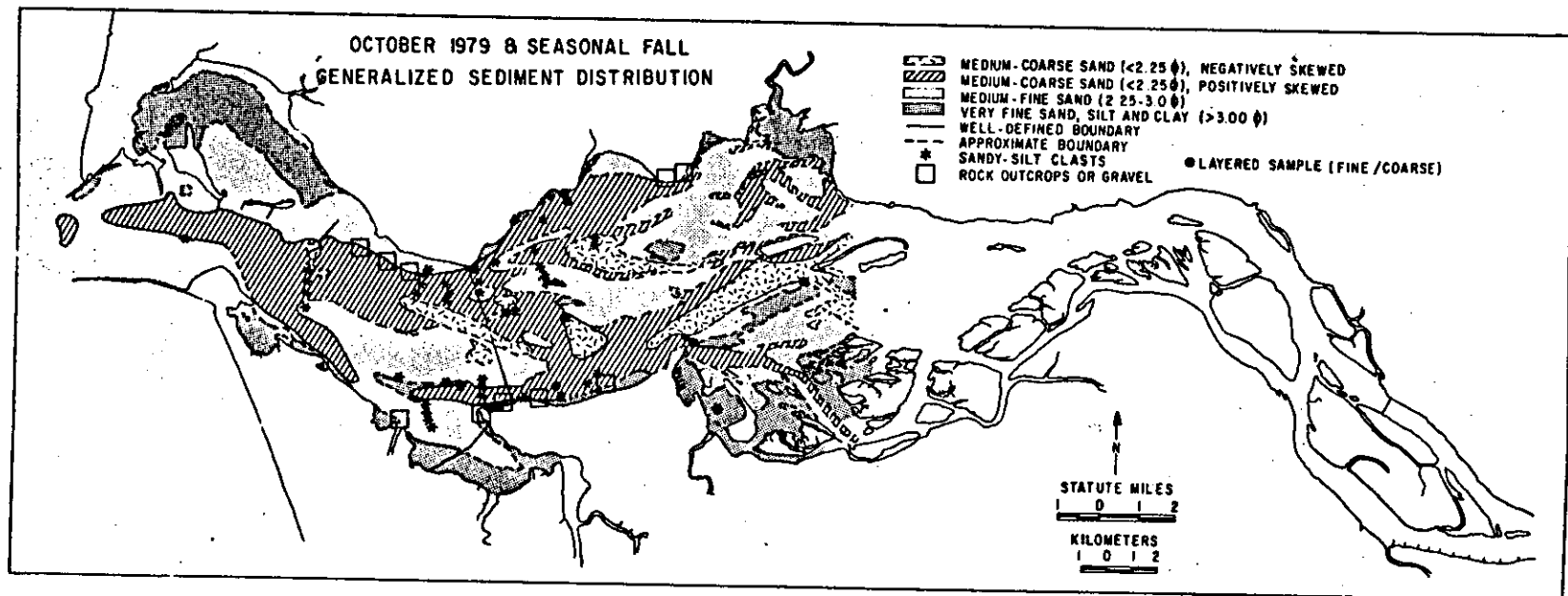


Figure 4.33 Generalized sediment distribution in fall.

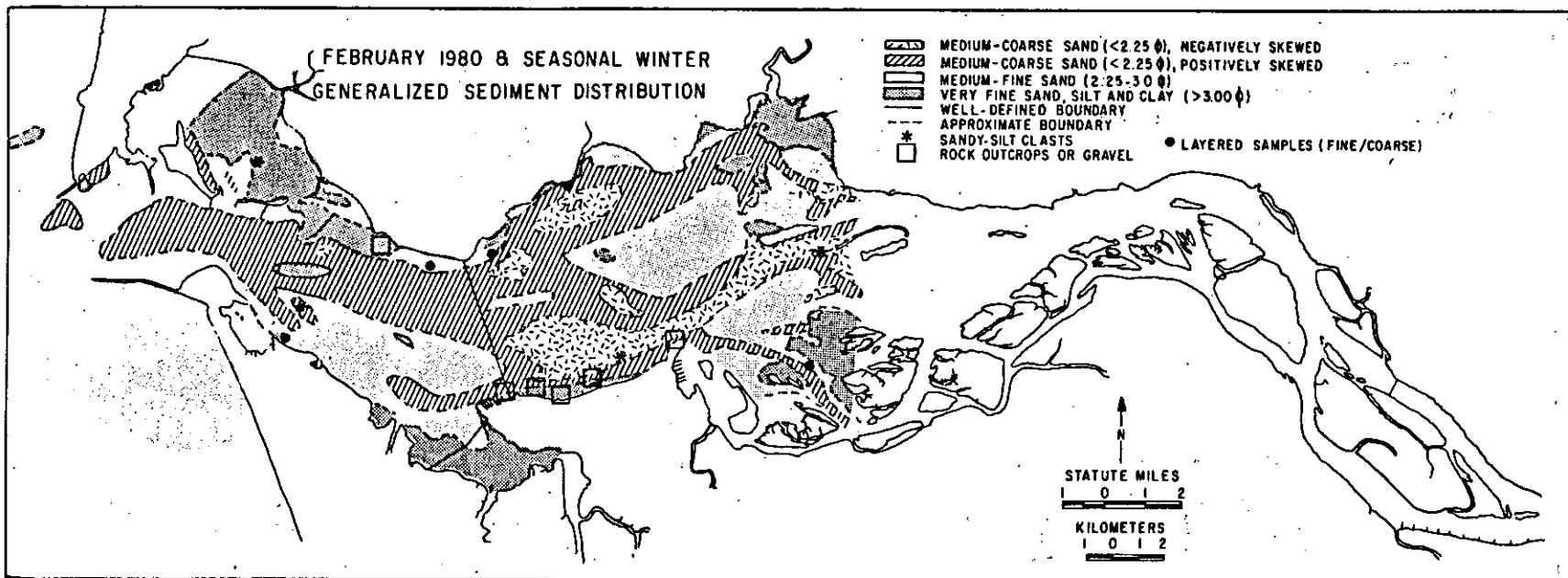


Figure 4.34 Generalized sediment distribution in winter.

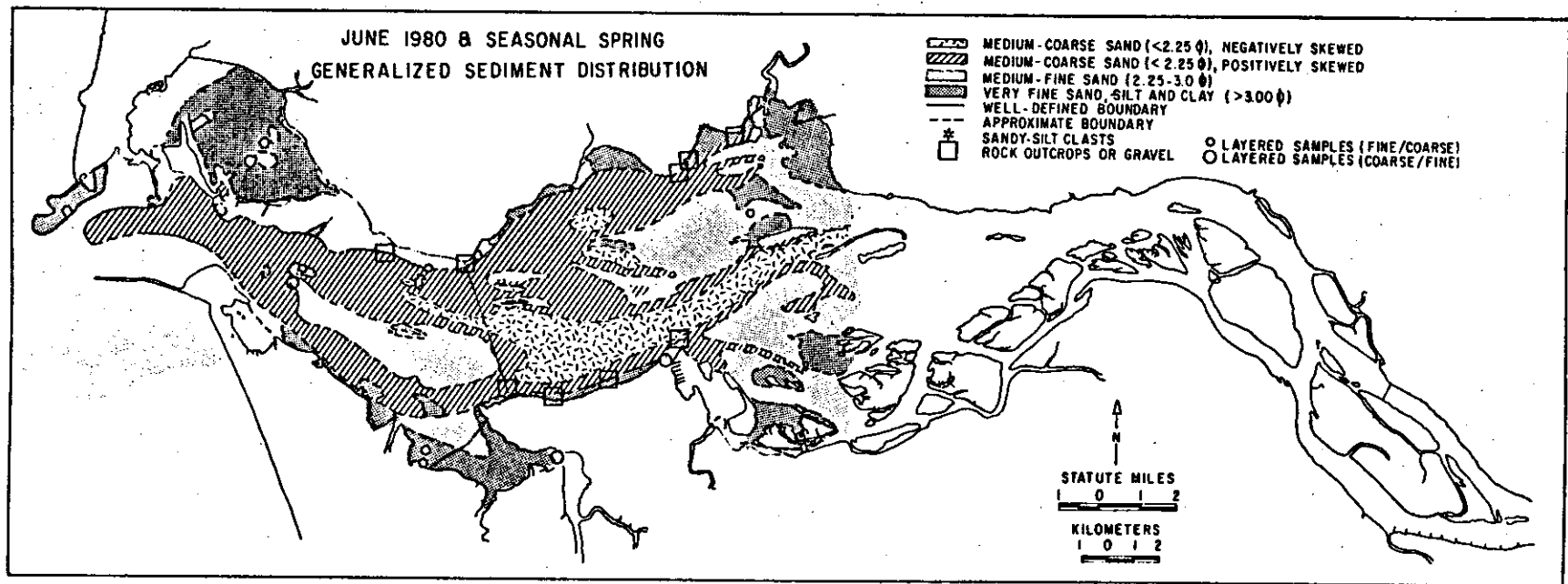


Figure 4.35 Generalized sediment distribution in spring.

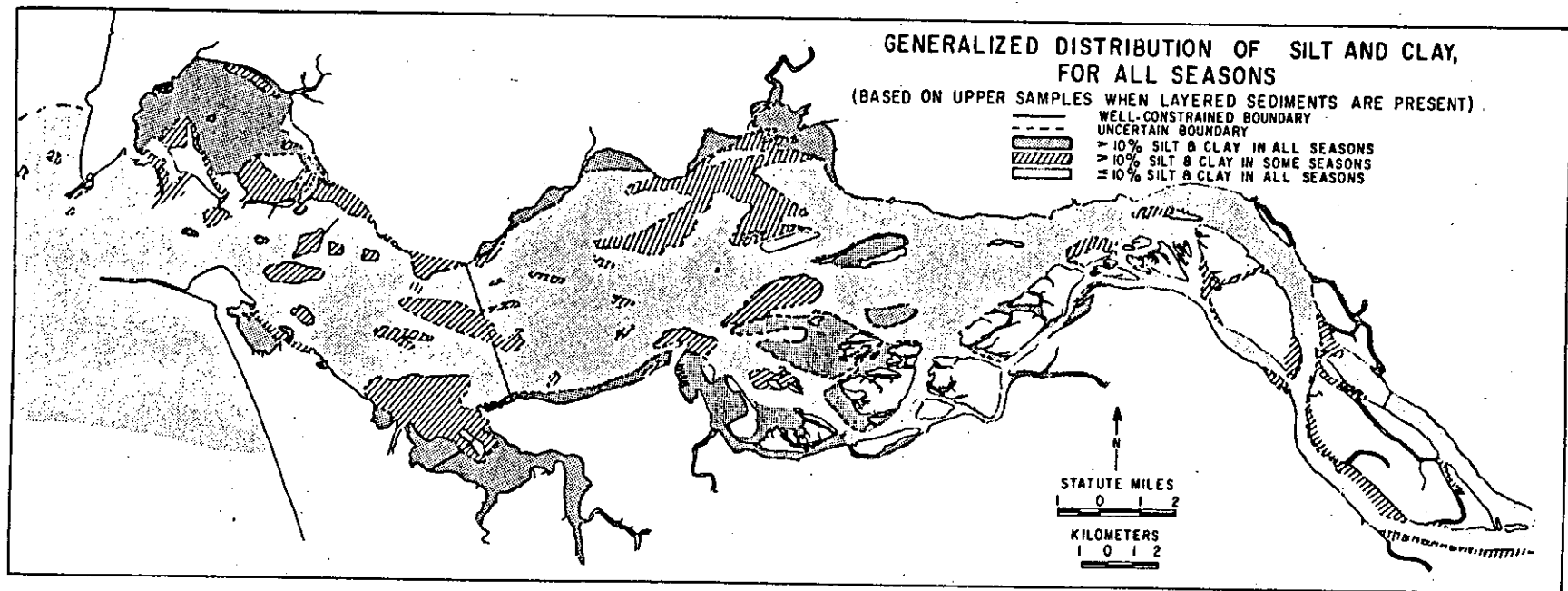


Figure 4.36 Generalized distribution of silt and clay in all seasons.

sediments (sandy-silt and silt-clay) were also found in both small and large channels in samples from some seasons. These channel silts were often found in thin (2- to 5-cm) layers that were deposited over fine to medium, well-sorted sands. The locations of samples that contained any obvious stratigraphy are indicated on the three seasonal sediment distribution maps. Only a few of these layered samples displayed the inverse relationship of coarse material overlying finer sediments.

Seasonal Variation

The overall sediment distribution is remarkably similar to that described by Hubbell and Glenn (1973) even though they had many fewer samples from only one season. They describe the variation of grain size with location as follows:

"For samples from the channels, [mean grain-size] increases (samples become finer), [sorting] remains relatively unchanged, and [skewness] becomes positive or less negative (distributions become less skewed toward the coarse particles) from the head to mouth of the estuary" (Hubbell and Glenn 1973, p. L-18).

The present study, however, has been able to detect seasonal changes in the grain-size distribution patterns. Comparison of Figures 4.33, 4.34, and 4.35 reveals that the distribution of negatively-skewed, coarse- to medium-sand varies considerably with season. In spring, a tongue of this coarse material extends downriver along the main channel to approximately Astoria. It crosses to the north channel along the trend of the broad diagonal channel separating Taylor Sands and Desdemona Sands. In fall, this coarse material is observed in the main river channel to Tongue Point, but downriver of Tongue Point, the distribution becomes patchy along the diagonal channel. In winter, the upriver pattern is similar and continuous to almost Astoria, where it terminates without crossing the diagonal channel. In all three seasons, areas with the coarse (less than 2.25 phi) negatively-skewed sand are found in the channels of Grays Bay. There is only one small patch of negatively-skewed material in the lower estuary, present only in fall and winter and located in the bathymetric depression near the Chinook pile dike.

The distribution of the coarse to medium-grained, negatively-skewed sand varies in response to the shifts in the positively-skewed material, and displays further seasonal changes in the south (main navigation) channel between Hammond and Astoria (RM-5 to RM-15). In spring, this portion of the south channel, which crosses Flavel Bar, contains coarse material along the entire reach. In fall, however, coarse sand extends downriver from Astoria only part of the way across Flavel Bar and extends upriver from the entrance only as far as Hammond (Figure 4.33). An even longer "gap" in the distribution of coarse material in the south channel is found in winter (Figure 4.34). The distribution of this grain size does not appear to vary significantly near the entrance among seasons.

Various distributions of fine-grained sediments (greater than 3.00

phi) occur in in the three seasons. Fine sediments appear most commonly in spring, when they dominate the grain size distributions in Baker Bay, Youngs Bay and Cathlamet Bay. These areas are also predominantly fine-grained in winter, but in the fall the number of samples with fine to medium sand (2.50 to 3.00 phi) increases in these areas. In addition to the shallow bays, very fine sand-, silt- and clay-sized material is found in both the large and small channels of the estuary. Small channels in Grays Bay and Cathlamet Bay and the sloughs in the upriver portions of the study area occasionally have finer sediments than their respective flanks (Roy et al. 1982). Fine-grained deposits in the large channels are localized, mostly in the lower estuary. In spring, patches of fine-grained material occur in the vicinity of Flavel Bar in the south channel and near Chinook in the north channel. In the fall and winter, the only sizable deposits of material finer than 3.00 phi occur in the north channel at and slightly downriver of Chinook.

Sandy-Silt Clasts and Layered Samples

The distribution of sandy-silt clasts recovered in numerous samples and the distribution of layered samples are also included in Figures 4.33 to 4.35. As noted by Roy et al. (1982) the sandy-silt clasts are usually slightly consolidated, rounded, disc-shaped clasts with a mean size in the coarse silt range. They are found predominantly in the lower estuary, often associated with otherwise fine to medium sands. Most of the few that are found upriver of Tongue Point are more highly compacted clays, some of which have root traces, and appear to have been eroded from older deposits now forming banks or channel beds. More mudballs were found in the fall cruises, even when the increased number of samples is taken into account.

Two-layered samples were obtained over a range of depths and in various parts of the estuary and, except for three samples found in spring, finer material was always found overlying the coarser material. Typical two-layer samples exhibit a sandy-silt layer (mean size from 3.00 to 6.00 phi) over fine to medium sand (mean size between 2.00 and 2.75 phi). The composition of the sandy-silt layers is very similar to the composition of the sandy-silt clasts described above, suggesting that the clasts are in fact rip-up clasts resulting from the erosion of ephemeral fine deposits. The distribution of both the clasts and the thin, fine deposits coincide with the region beneath and to the side of the turbidity maximum. This suggests that silt and very fine sand settling out of the turbidity maximum may be deposited as a thin layer over coarser material only to be eroded by higher currents under later conditions of higher tidal range or river discharge. Whether this scenario allows sufficient time for consolidation of this material into somewhat durable clasts remains open to question; an alternative hypothesis for their origin is the erosion of much older silt deposits from subaqueously exposed strata.

Ephemeral Deposition of Silt and Clay

Figure 4.36 is a map of the distribution of percent silt and clay as either greater than 10% or less than 10%. An overlap exists where samples obtained from the same area in different seasons fall into

different categories; in these areas, deposition of silt and clay is ephemeral. Silt and clay occur throughout the discharge year only along the margins of the estuary, in the peripheral bays, and among the vegetated islands of the upriver portions of the study area. However, from time to time, fine-grained sediments appear on some parts of the mid-estuary shoals (Desdemona Sands, Taylor Sands, and the shoals in Cathlamet and Grays Bays). Silt and clay also appear on an intermittent basis in both the large channels (including the main navigation channel and the north channel) and in the smaller channels dissecting the shoals. When present in the large channels, fine-grained deposits are confined to the lower estuary; in fact, they appear mostly in the vicinity of Flavel Bar in the south channel and in the north channel between the sized material is found over this entire area, ranging from coarse sand (usually finer than 0.0 phi) to very fine sand (3.00 phi). Much of this material actually falls into the highly-mobile sand range between 1.75 phi and 3.00 phi.

4.4.4 Factor and Cluster Analyses

The factor and cluster analysis techniques were used as an exploratory statistical technique. They were intended to produce groupings of sediment types whose distributions would suggest a testable geologic hypothesis. In earlier studies in the estuary, Q-mode factor analysis was found effective in delineating sediment distribution patterns near the entrance and in the lower estuary (Borgeld et al. 1978, Roy et al. 1979), but results of factor analysis over the entire estuary (Roy et al. 1982) proved more difficult to interpret. After extensive investigation and experimentation with both factor and cluster analysis, a reasonable explanation for the difficulties in interpreting data using these methods is proposed. A brief discussion of the results is included here because it contributes to a general understanding of the estuarine sedimentology.

Both factor analysis and cluster analysis, when used in the Q-mode, utilize the sediment size information to group similar samples. In factor analysis, between 7 and 11 groups (factors) are mathematically chosen to characterize the suite of samples, and each factor is characterized by an archetypical sample: the factor extremel. All other samples can then be described in terms of how similar they appear to each of the 7 to 11 extremels; this is the factor loading. Table 4.3 (from Roy et al. 1982) lists the factor extremels chosen in each of the three seasons and, for reference, their modal phi sizes. The final column in each season indicates the percent of samples that are highly similar to the extremels. Note that the modal phi size and the number of factors required to describe the data set vary for each season. Figure 4.37 provides a graphic view of similar information from Sherwood et al. (1984) which shows the effect of choosing 6, 8, or 10 factors from the same data set. These and other results from the factor analysis data suggest that there are no stable, discrete groups of sediment that exist in the estuary during all three seasons.

Similar conclusions can be drawn from the cluster analyses. Cluster analysis is a more simple grouping system: a measure of the similarity of each pair of sediment samples is computed on the basis of the

Table 4.3. Summary of seasonal factor analysis results. Secondary modal phi sizes are in parentheses.

October 1979		February 1980		June 1980	
Modal Phi Size	% of Loadings >.5	Modal Phi Size	% of Loadings >.5	Modal Phi Size	% of Loadings >.5
		-2.0 (-3.0, 1.75, -4.0)	1	.25	1
.25	1	.75	4	1.00	2
1.00	5				
1.75	22	1.50	28	1.50	18
				2.00	28
2.25	33	2.25	35	2.50	20
2.75	23	2.75	20	2.75	11
3.25	8	3.50	6	3.5 (4.5)	5
4.50 (12.50)	8	4.50	4	4.50	5
				4.50 (12.0, -2.75)	2
				6.0 (2.0)	6
		12.50	2	9.0 (12.0)	2

From Roy et al., 1982.

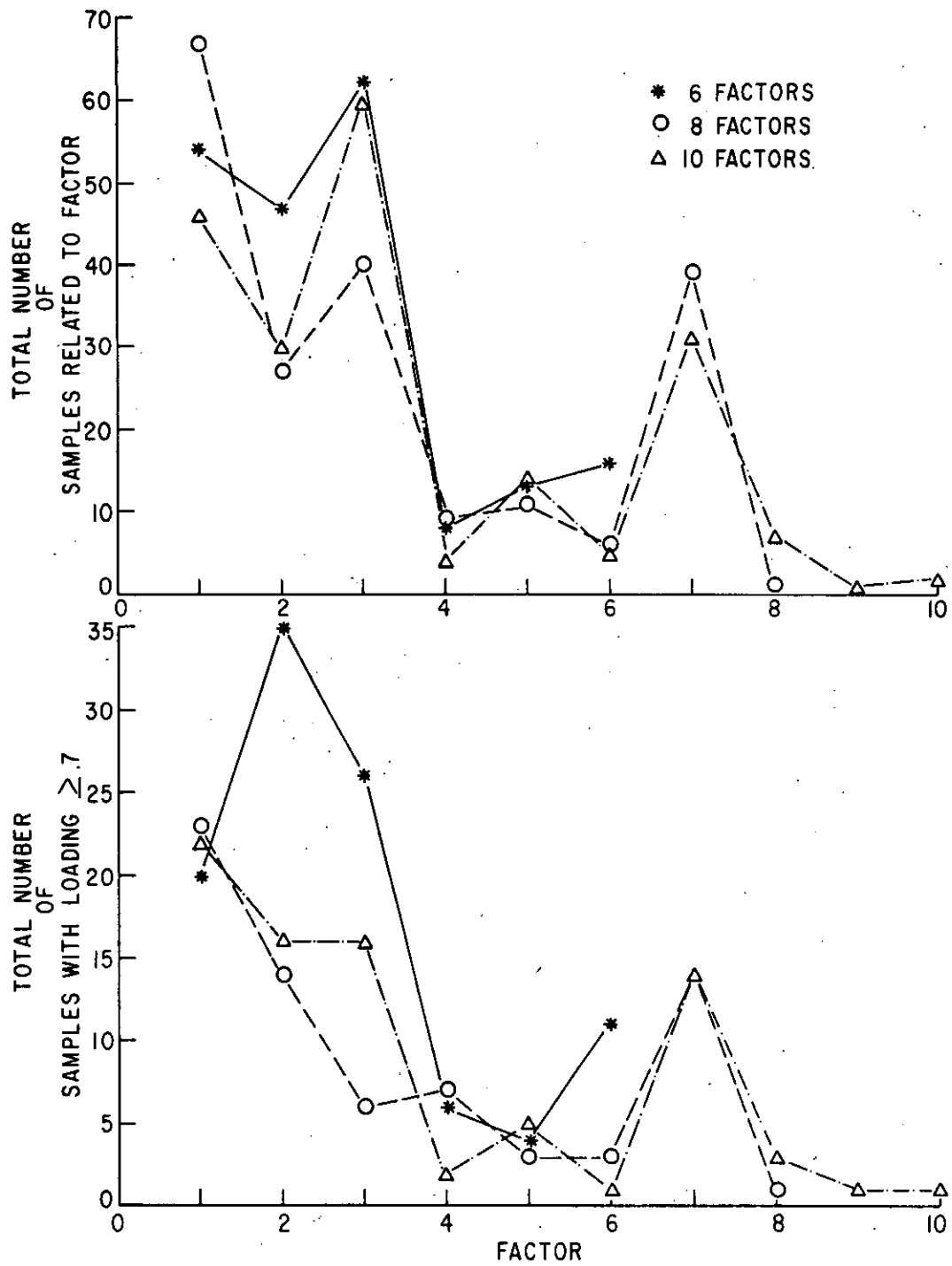


Figure 4.37 Relative importance of factors. Mean grain size generally decreases with increasing factor number.

samples' size distributions and the most similar pairs are grouped. The groups (clusters) of pairs are then compared and grouped, those groups compared and grouped and so on until all of the samples have been interrelated. A popular way of describing the results of this operation is in the form of a dendrogram, such as the one shown in Figure 4.38. Although this technique efficiently groups samples, it makes no attempt to characterize the properties of the clusters. To accomplish this, the grain size distributions of the clusters differentiated at the 0.65 correlation level were averaged. The averaged grain-size distributions are shown as Figure 4.39 together with their related statistics and the number of samples included in the cluster. As with the factor analysis, similar but not identical groupings emerged for each season. The clusters were assigned standard numbers, and the importance of the six standard clusters and their modes is shown on Figure 4.40. The cumulative curves of the standard clusters from each season are shown in Figure 4.41. Within each season, although more than one curve representing the standard cluster might appear (each from a different sample set), the standard clusters are well differentiated and apparently represent somewhat discrete assemblages of samples. When all of the standard curves are plotted on the same axes (also on Figure 4.41), it becomes apparent that the cluster technique has not identified six or even 11 discrete groups of sediment sizes.

The inability of either factor or cluster analysis to consistently group the sediment size data and the subsequent difficulty in interpreting the results lies in the premise that several unique and distinct populations exist and are obscured by mixing processes. Although this premise is useful in many geologic applications, it does not apply to the Columbia River Estuary. In fact, the major conclusion to be drawn from the factor and the cluster analyses is that the sediments in the estuary represent a continuous size distribution. No fundamental sub-groups are being admixed to produce the observed sediment distributions; rather, sediment from a single source is being continuously sorted, winnowed, transported, and remixed to produce the observed sediment distributions.

4.4.5 Implications of Sediment Size Data

There are several implications that can be drawn from the wealth of sediment data collected during these studies. The first of these concerns the continuous nature of the grain-size distribution within a fairly narrow overall range of sediment sizes in the estuary. Apparently, there are not multiple sediment sources contributing different size materials to the estuary. In fact, consideration of the overall energy levels in the estuary and the potential sources of sediment to the estuary suggests that the only likely sources are the river and the adjacent marine environment. Because it is likely that the marine source consists almost entirely of older (or even very recent) Columbia River sediment, essentially one ultimate source supplies sediment for the estuary. The sediment distribution in the estuary is a result of the ongoing sediment transport processes acting on the range of sediment sizes provided by the river. This size distribution includes two broad size ranges; those normally transported as suspended sediment and those normally transported as either bedload

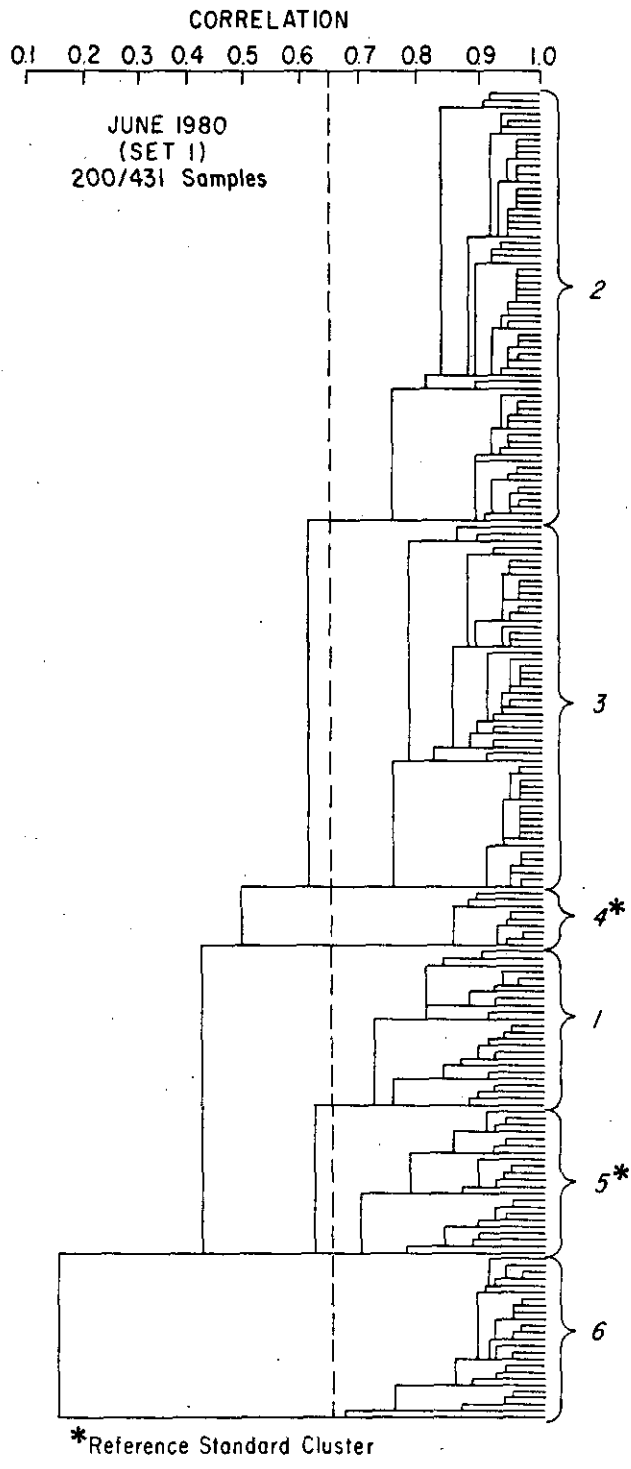


Figure 4.38 Dendrogram of the clusters chosen from one set of samples. Standard clusters are numbered to the right.

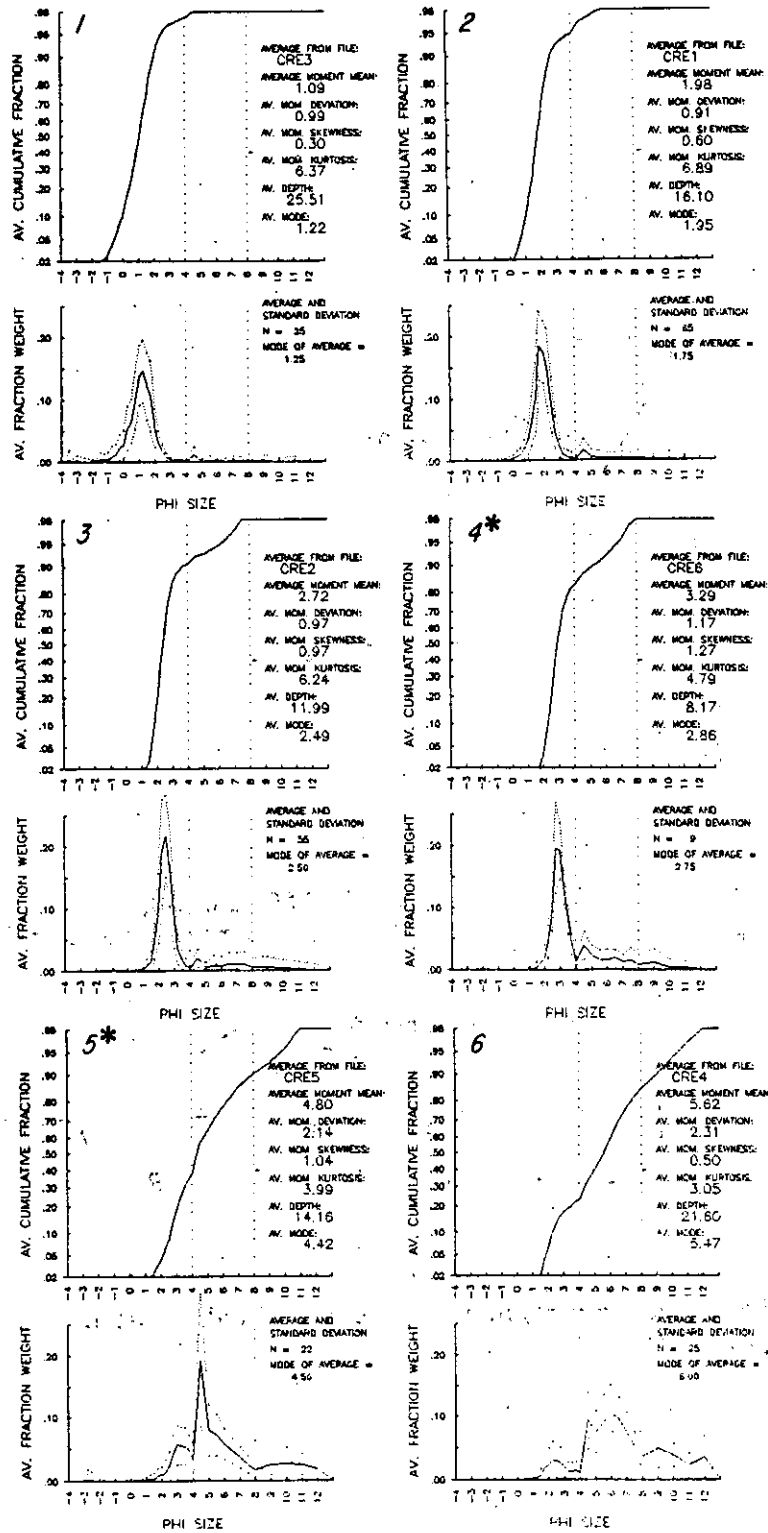


Figure 4.39 Sediment distributions of the standard clusters.

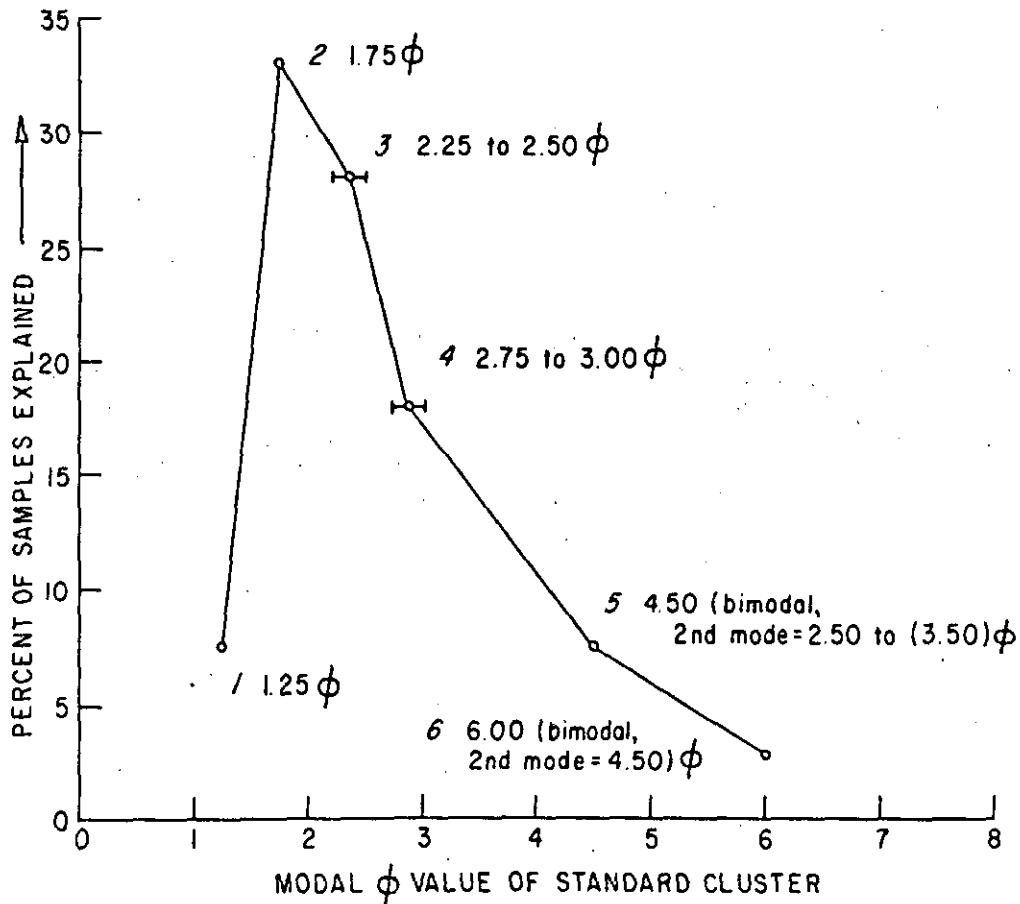


Figure 4.40 Relative importance of the standard clusters. Modal ϕ size as indicated.

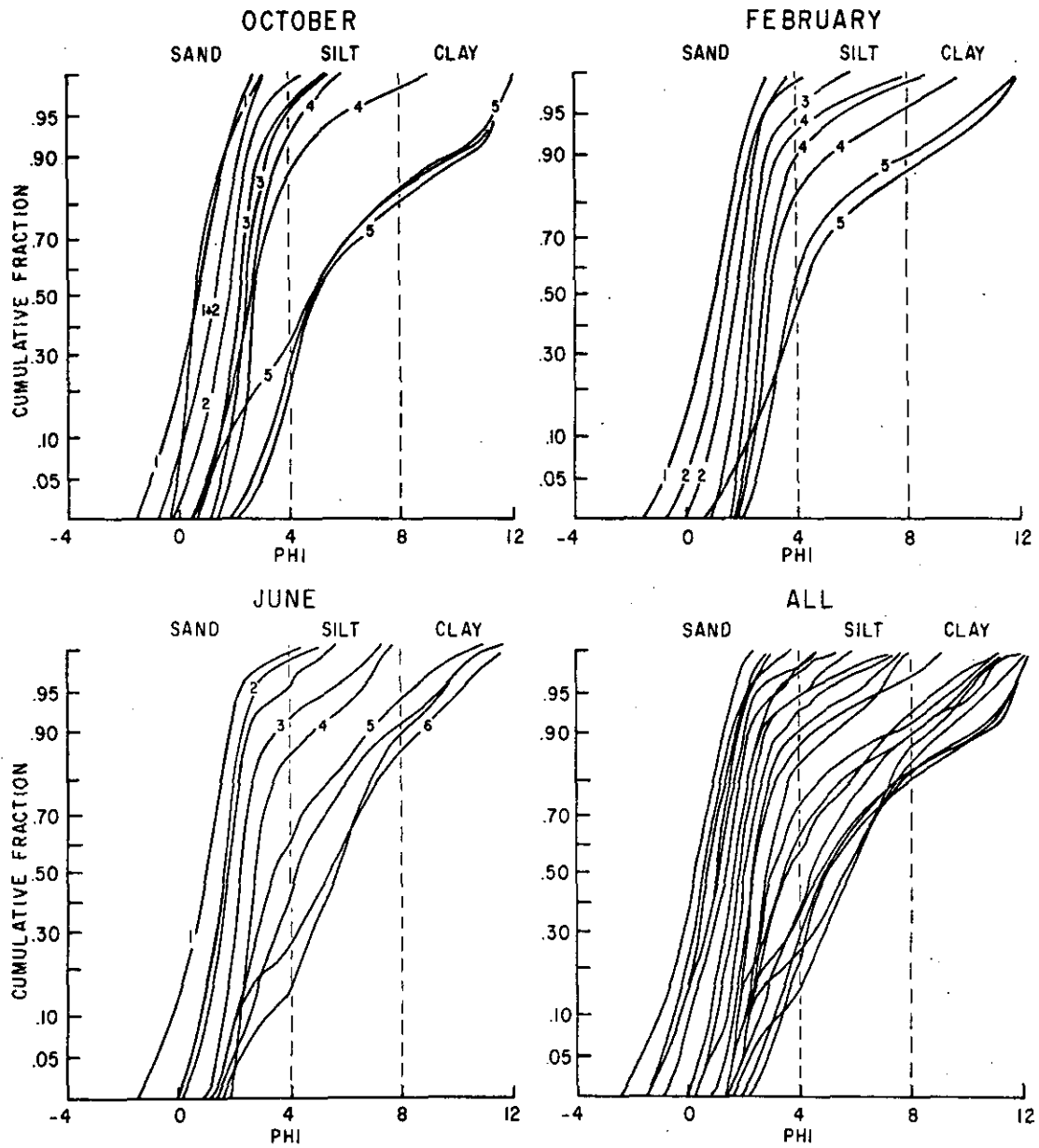


Figure 4.41 Cumulative curves of standard clusters from three seasons.

or intermittently suspended material. These appear on the plots of Figure 4.42. These broad groups are best delineated by their mean size, as is also done on Figure 4.42. They may be further differentiated on the basis of skewness within each group. As is apparent in Figure 4.42, more positively-skewed samples are generally finer than more negatively-skewed samples and are more likely to be transported as intermittently suspended material. Thus the distinction between the products of various sedimentary processes can be made largely on the basis of the two parameters: mean size and skewness.

The second implication of the grain size data concerns trends in mean size and skewness, which are related to processes acting within the estuary. Several examples will be discussed here. A general tendency for mean sediment size to decrease downriver in the fluvial and upper estuary channels is noted. This is interpreted as an indication of decreasing sediment transporting energy in the channels deeper than 9.1 m. This is caused by a broadening of the estuary and diversion of flow from a single channel to more numerous small channels and across shoals. A tongue of negatively-skewed sediment is observed crossing from the main navigation (south) channel to the north channel in some seasons (Figures 4.34 and 4.35). This is an extension of the coarser, negatively-skewed sediments that are apparently characteristic of the fluvial source in the upper estuary. In addition to emphasizing the importance of cross-channel sediment transport trends, the seasonal nature of this trend reflects the importance of fluvial processes relative to tidal energy during the high discharge seasons. The fact that the distribution of the coarser negatively-skewed sediment does not extend downriver of Chinook during any season is evidence that fluvial transport of bedload material out of the estuary is not occurring under present conditions.

The decrease in grain size associated with positively-skewed and relatively well-sorted sediments from the entrance downriver is a second indication that very little bedload material is transported out of the estuary, at least not at discharges encountered during the sample period. The downriver limit of the positively-skewed coarse to medium sand never extends beyond the entrance jetties (Figure 4.34 and 4.35). This size range is associated with bedload and the lower range of intermittent suspended-load transport. This and the coarser negatively-skewed material are commonly associated with downriver-oriented bedforms, and the distributions largely coincide (Figures 4.33, 4.34 and 4.35). The more mobile medium to fine sands are found on shoals, in the channels of the peripheral bays and downriver of the entrance. This sand is easily moved from the channels during higher current periods and is generally deposited in regions of lower energy. As most of the marine material on the adjacent continental shelf falls into this size range, it is difficult to use grain size evidence to determine whether the fine sand which moves as intermittently suspended material is being transported into or out of the estuary. This question is addressed using other evidence drawn from Section 4.5.

Another example of the association of grain size with process is found in the accumulation of the finest material. The broad, protected bays (Baker Bay, Youngs Bay, Cathlamet Bay and Grays Bay) are isolated

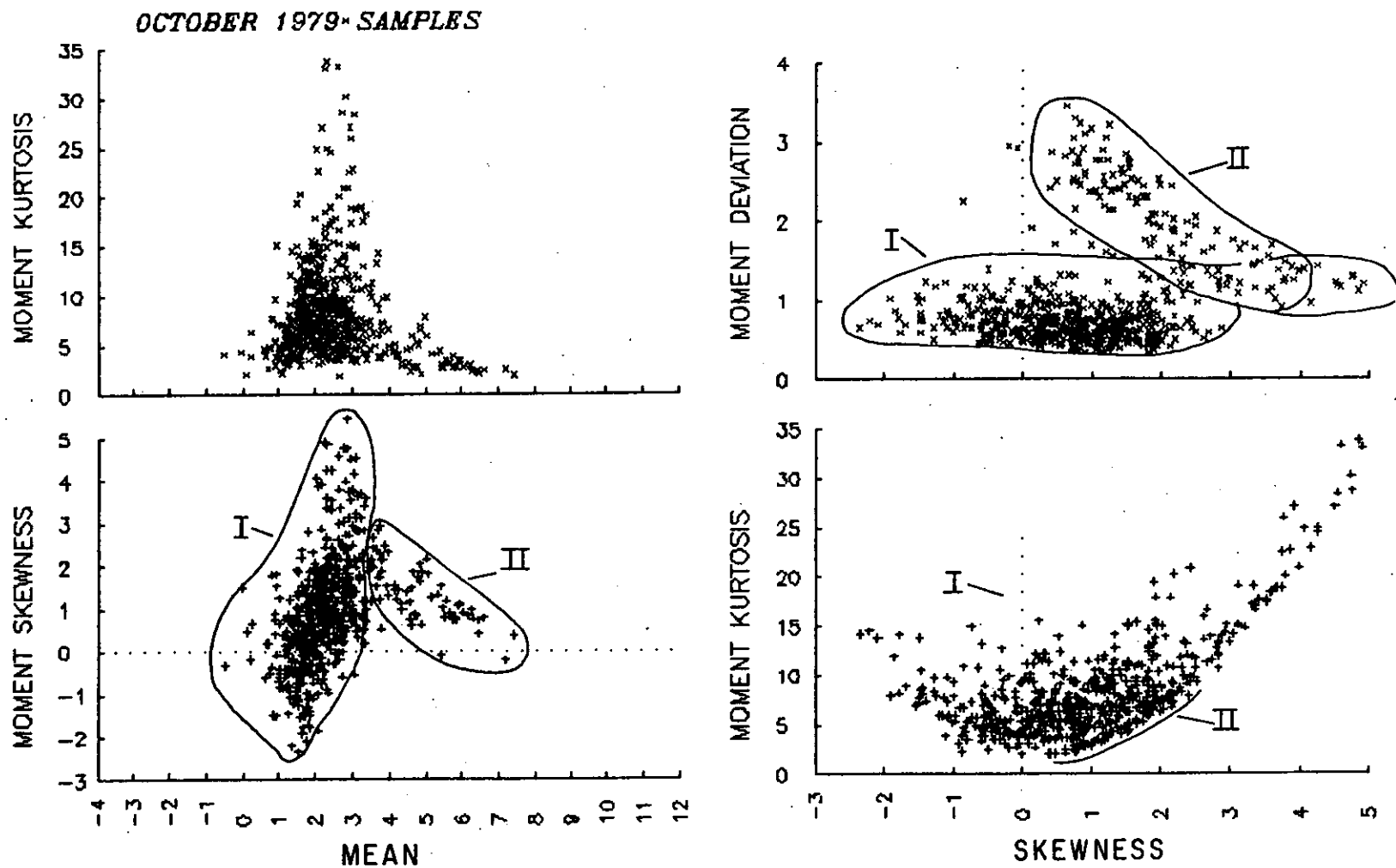


Figure 4.42 Relationships between mean and skewness, mean and kurtosis, skewness and kurtosis, and skewness and standard deviation for fall samples.

from most of the main tidal and fluvial flow of the estuary. Sediment initially suspended by high currents in the main estuary will be deposited in these bays with less likelihood of subsequent resuspension. In contrast, the fine materials deposited in the channels of the central estuary on waning tidal currents or during low amplitude neap tides are likely to be resuspended during subsequent spring tides. On resuspension, this fine material will represent the coarser fraction of the turbidity maximum (the finer fraction is derived from the wash-load). Some of this very fine sand and silt is likely to be mixed up into overlying surface waters. Once in the surface waters, suspended sediment is readily transported either out of the estuary in the river plume, or into an adjoining peripheral bay, where it may settle out. Some settles back into deeper water and is advected back into the turbidity maximum. Several lines of evidence have already been introduced suggesting that this is a reasonable mechanism for explaining not only the accumulation of fine material in the bays, but also the ephemeral appearance of fine sediment, layered samples, and rip-up clast in the channels of the lower estuary.

4.5 ENERGY CONSIDERATIONS AND SEDIMENTARY ENVIRONMENTS

The energy available in the form of wave and current motion ultimately controls sediment transport and deposition. This section discusses the relative importance of fluvial and tidal energy, as well as the important modifications caused by the interaction of these energy sources with stratification, topography and biological activity.

4.5.1 Influences on Sedimentation and Erosion

As discussed in Chapter 3, there are several sources of energy available in the estuary that can generate currents and transport sediment. Overall, the tidal energy dominates the flow regime in the estuary, but it is not always the most important in determining where sediment will erode or eventually accumulate. To evaluate the relative importance of various influences on sedimentation in the estuary, a wide variety of information was considered. Morphologic information in the form of bedform distributions, shoal morphology, island shape, and channel pattern was considered. Grain size data and the processes implied by sediment size were considered. The data relating to measured processes, especially those occurring in the turbidity maximum were included. A tabulation of many of the characteristics associated with each of the major energy inputs and with the biological influence on sedimentation or erosion is presented in Table 4.4, and the results are presented qualitatively in Figure 4.43. Figure 4.43 depicts the relative importance of each of the energy inputs with distance along the estuary. Although highly subjective, Figure 4.43 is useful in relating the sedimentary environments and processes within the estuary and may be used as a basis for comparison with other estuaries.

Several features of Figure 4.43 are important to note. Wave energy plays an important role in the transport and deposition of shallow-water sediments near and seaward of the entrance. Wave energy is less important in the lower estuary, due to relatively short fetches and generally deep water. In the upper estuary, longer fetches and the

Table 4.4. Characteristics used to delineate the importance of sedimentary processes.

Wave activity:	Morphology	- spits, beaches, shallow depths
	Sediments	- fine to medium sand, relatively well sorted
	Processes	- wave transport, current transport
Fluvial currents:	Morphology	- ebb-oriented bedforms, bar/pool topography, island shape, ebb-oriented spits
	Sediments	- coarse to medium, negatively-skewed, more poorly sorted
	Processes	- current transport, channel migration
Tidal currents:	Morphology	- ebb and flood oriented bedforms, transverse bars, flood ramps, flood oriented spits, reversing bedforms.
	Sediments	- fine to medium, varied but often moderate sorting, positive skewness, fine in bays
	Processes	- tidal current transport, settling lag
Residual currents:	Morphology	- flood oriented bedforms, channel shoals
	Sediments	- fine to medium, occasionally very fine, poorly sorted, ephemeral, layered, rip-up clasts
	Processes	- currents, turbidity maximum processes

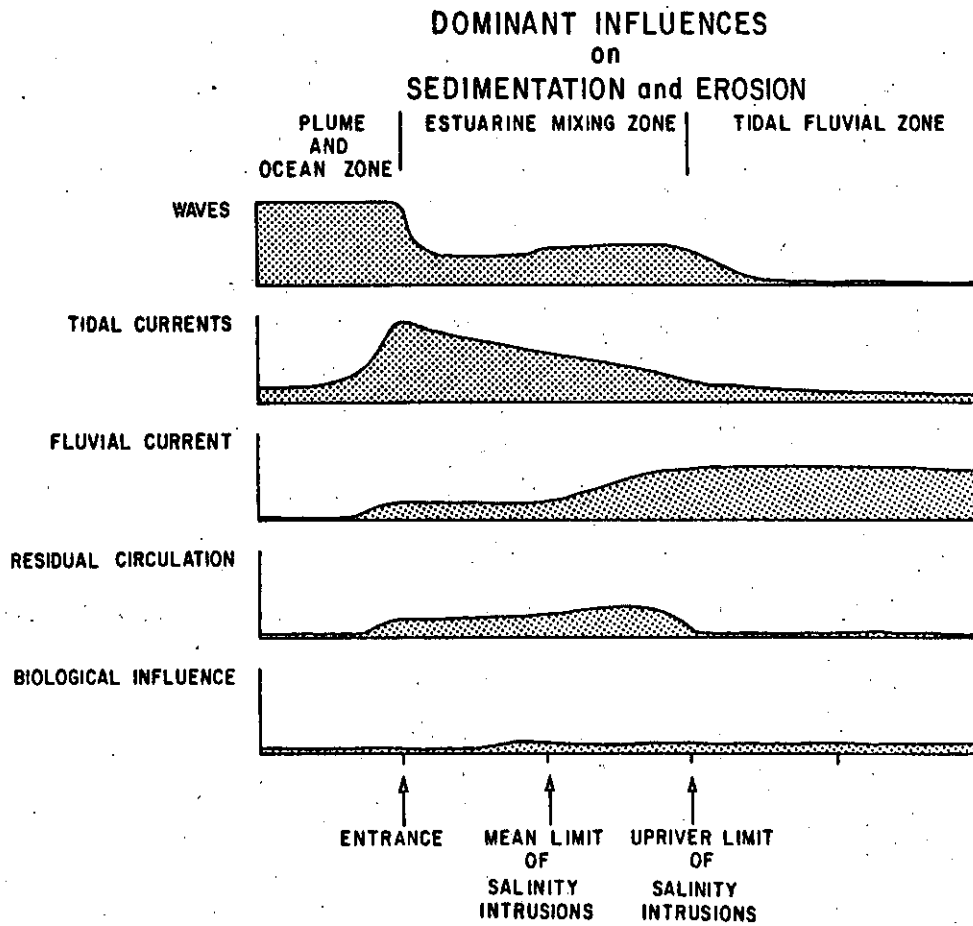


Figure 4.43. Dominant influences on sedimentation and erosion.

presence of intertidal shoals result in several intertidal beaches and it is likely that wave action is relatively important in winnowing the finest material off the intertidal shoals in Grays Bay. Wave energy becomes negligible in protected and relatively deep fluvial reaches of the upper estuary.

Tidal energy influence on sediment transport is the highest in the entrance and declines upriver. The influence of tidal energy declines seaward of the entrance as water depths increase and flows are not confined. Although the tidal amplitude peaks in the mid-estuary (Jay 1984 and Chapter 3), the current velocities associated with the major tidal components are at a maximum in the confined entrance region. This corresponds with the zone of reversing bedforms noted earlier. In the lower and upper estuary, tidal energy manifests itself in the advection of the turbidity maximum and the formation of distinctive intertidal morphology including flood-oriented bedforms, flood ramps, and flood-oriented spits.

Fluvial currents clearly dominate the sedimentology in the upriver reaches of the estuary, but are gradually overshadowed by tidal currents in the lower estuary. The fluvial effects on the bottom morphology and sediment distribution are greatly reduced when saline bottom water present in the estuary, because the salinity stratification prevents strong shears from impinging on the bottom and because net upstream bottom flow is established by the baroclinic pressure gradients. In most of the upper estuary, the fluvial processes of sedimentation seem to dominate: channel migration, point bar sedimentation and bar/pool topography are all present. Large and small bedforms east of Tongue Point are always ebb-oriented and sediment textures are closely related to those in the fluvial reaches. In the lower estuary and seaward, the influence of the fluvial currents is confined to surface water and shallow depths except during high discharge and low tidal range periods.

The circulation of the estuary is inherently more complex than that of the river because of the effects of salinity intrusion. Although tidal energy dominates the system (Section 3.1), the effects of salinity stratification and the secondary circulation caused by tidally-induced transport produce circulation patterns that differ dramatically from those that would be obtained from purely tidal or purely fluvial processes. Two effects are clearly identified in the distribution of sediments and bedforms. First, in the channels of the lower estuary the baroclinic pressure gradient and the difference in the vertical structure of the ebb and flood flows combine to create a tendency for net upstream sediment transport. The effects of this upstream transport are distinguishable in the sediment distributions and in the bedform morphology. Second, the interaction of the tidal currents with the salinity gradients cause the development of the turbidity maximum. The tidal effects on the turbidity maximum are demonstrated by the changes in suspended sediment concentrations measured between neap and spring tides (Section 4.2).

Because the rate of sediment transport is highly dependent on the local, instantaneous shear stress exerted on the bottom, and because the value of the local shear stress varies in response to tidal forcing,

bottom topography, and stratification (which in turn depend on many other factors such as river discharge and human influences), it is extremely difficult to predict sediment transport rates in the estuary. The evidence presented in preceding sections suggests that despite the relative importance of the tidal energy in the estuary, these secondary effects of topography, stratification, and density-driven circulation ultimately control the sedimentation patterns. In Figure 4.43, these effects are attributed to the residual circulation, although this does not emphasize the importance of the differences in the ebb and flood vertical velocity profiles and evokes an image of the classical estuarine circulation which is probably oversimplified for the Columbia River Estuary. Secondary effects are most important near the mean limit of salinity intrusion (which varies seasonally; Section 3.6). In the lower estuary and near the entrance, tidal energy tends to control sediment transport. Evidence for this is found in the distribution of reversing bedforms (Figures 4.33, 4.34 and 4.35), which ends near the bifurcation of north and south channels, giving way to upriver-oriented bedforms that extend upriver to limits controlled by the seasonal variation in fluvial energy. The importance of the residual circulation diminishes upriver of this seasonal boundary, and the system becomes fluvially dominated.

The biological influence on sedimentation and erosion in the estuary is low relative to many other estuaries. In fact, current and wave energies are substantial factors in determining habitat. Bioturbation by infauna and epifauna is low relative to natural sediment mixing depths. Sufficient energy exists in most of the estuary to erode the algal mats that can occur in the intertidal region. Marine grasses such as Zostera and Potamogeton are at best patchily distributed and exhibit very little effect in the estuary. The processes that control the turbidity maximum are also important in the distribution of detritus. The major biological influence on the sedimentology of the estuary is the stabilization of the islands of the upper estuary and fluvial reaches by marsh grasses and woody vegetation. Even these effects may be overestimated on Figure 4.43.

4.5.2 Interpretation of the Energy Budget

The energy budget calculated in Chapter 3 has distinct implications for the long-term sedimentation patterns in the estuary. The continuous decrease in fluvial energy downstream, considered by itself, would suggest continually increasing sediment deposition. The tidal energy, considered separately, would transport sediment at the highest rates near the entrance of the estuary and at decreasing rates upriver. The summation of these two energy inputs provides a gross measure of the total sediment transporting capability of the system. One result of the combined energy inputs is addition to the decreasing fluvial energy by the tidal energy with distance downstream. The effect of the added tidal energy is to provide sufficient currents to transport sediment in the lower reaches of the estuary despite the decreased fluvial energy. When the net downstream component of the fluvial current is superimposed on the oscillatory tides, sediment can be carried out of the estuary. The trapping of sediment in the turbidity maximum occurs despite the net downstream flux, because sediment tends to settle into the underlying,

flood-dominated layers.

An important result of the energy budget study is the appearance of an energy minimum in the upper estuary/lower fluvial region, at the physiographic "head" of the estuary (near Harrington Point). It is in this region that the least amount of energy is available to transport sediment and it is in this region that long term deposition of sediment would be expected. In fact, this region is where the estuary begins to broaden and branch into a series of complex channels and islands. The transition from this region to the more open waters and intertidal shoals of the upper estuary does not appear to be controlled by bedrock because the width of the floodplain remains relatively constant in the transition zone (Figure 4.44). The newly vegetated islands and the small, migrating channels in this region appear to represent the present area of long-term net deposition in the estuary, in accordance with the discussions of morphology above. The association of the zone of energy minimum with the site of long term deposition is not unreasonable in light of this discussion.

If, in fact, the energy minimum as described in Section 3.5 is associated with the site of long-term deposition in the estuary, there are some implications which may be drawn regarding the evolution of drowned river valley estuaries. As deposition continues, it will gradually reduce the tidal prism of the estuary by reduction of the intertidal volume from the head. The reduction in tidal prism will lower the tidal energy curve, with the result that the position of the energy minimum will be shifted downriver, down the river energy slope. The site of deposition will shift downriver as well, and in this manner the estuary will progressively fill downriver from the head.

When the river energy slope is so moderate that little displacement of the location of the energy minimum occurs with changes in the tidal prism, sediment will not be able to prograde downriver, and the estuary will be in equilibrium with the sediment supply, discharge and tidal range. Transitory displacements of the energy minimum downriver by large floods will not permanently affect the tidal prism, but will effectively remove sediment from the lower estuary by briefly increasing the minimum energy levels. For this reason, large floods are apt to play an important role on the morphology of estuary.

One final implication of the energy budget to the conceptual classification of estuary morphology should be mentioned. When a large discharge and moderate or low tides combine to force the energy minimum completely out of the estuary for most of the discharge year, a fluviially-dominated system will result. A supply of sediment can force a rapid evolution to this stage and promote the development of a delta, but a steep stream gradient may be sufficient to classify the estuary as fluviially-dominated. The alternative in the conceptual classification scheme is the tidally-dominated system, in which no discharge is present. In intermediate cases, the energy minimum should be located at the head of the estuary under equilibrium conditions; a position elsewhere is an indication that the system is not in equilibrium.

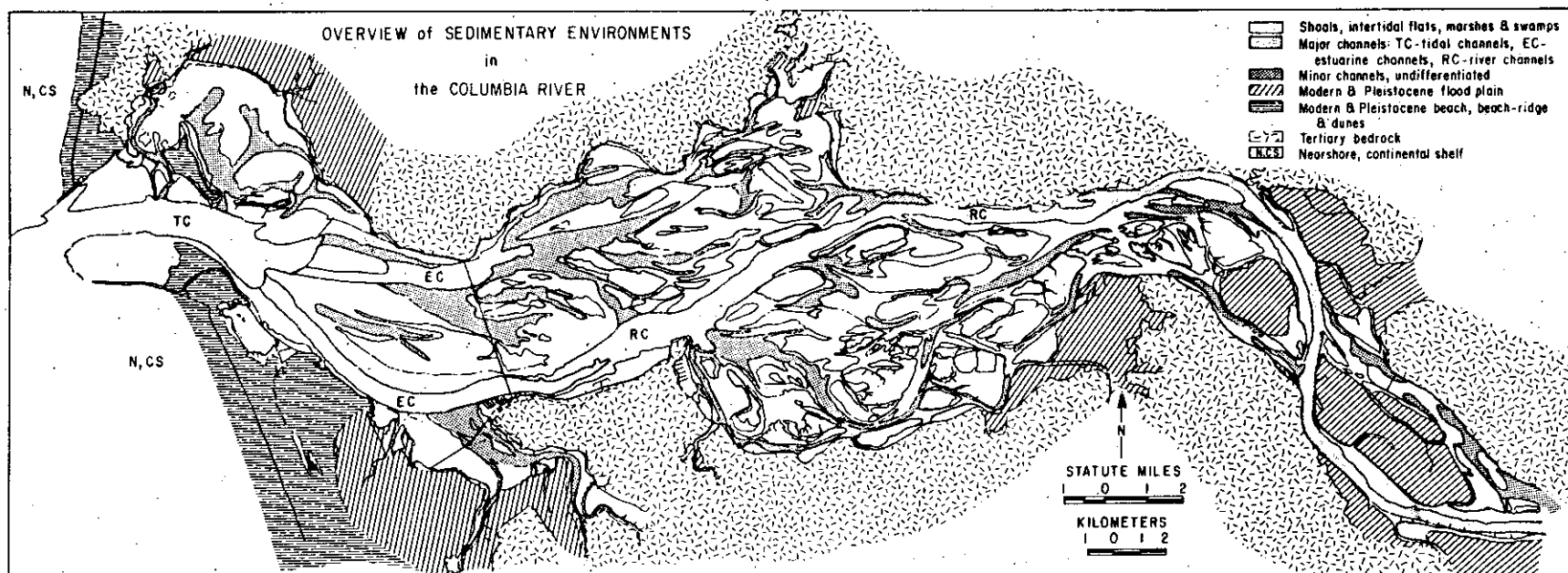


Figure 4.44 Sedimentary environments of the Columbia River.

4.5.3 Sedimentary Environments

Considerations of the energy levels, sediment textures, processes and morphology of the estuary can be incorporated into a sedimentary environments map. A detailed sedimentary environments map is included in Fox et al. (1984) and a simplified version is presented in Figure 4.44. The classification scheme used in delineating the sedimentary environments is primarily based on the dominant processes and subdivided by morphological characteristics. The most striking feature of the sedimentary environment map is the complexity and wide variety of environments to be found. In addition to longitudinal trends noted in the discussion above, lateral changes across the estuary and variation in depth combine to produce a suite of environments that can only be completely described in four dimensions: along-estuary, cross-estuary, depth and time. This complex variability in processes makes measurement and prediction of physical changes and their ecological consequences difficult. However, an understanding of the process relationships at all levels is crucial to an understanding of the resultant distributions and ecological systems. These can be more easily observed and measured, and provide data that has been naturally intergrated over time and influenced by the dominant underlying factors.

4.6 SUMMARY

Several conclusions have been drawn regarding the sedimentology of the Columbia River Estuary in the course of both this discussion and the earlier works summarized in Chapter 2. They are enumerated here:

- 1) The energy levels available for transporting sediment in the Columbia River Estuary are high relative to many of the estuaries of the world. The combined effects of large tidal range, large fluvial discharge, high ocean wave regime, and the various residual circulations produced by the interaction of these three energy inputs with the density distribution and the morphology of the estuary results in currents that are frequently more than sufficient to move most of the sediment found in the estuary.
- 2) The energy sources are highly time-dependent, resulting in a continuously changing current regime in the estuary. Although the circulation in the estuary is dominated by the semidiurnal tides, large diurnal and fortnightly effects are apparent in tide heights and circulation. Seasonal variations in the discharge and oceanic regimes are less energetic but still important in modifying the circulatory processes that effect sediment transport. Long-term changes in sea-level and river discharge introduce an even longer time scale that must be considered in evaluating the sedimentology of the estuary.
- 3) The relative importance of each of the energy inputs varies not only in time, but with position in the estuary. Fluvial influence decreases downriver, tidal energy decreases upriver, wave energy is related to ocean exposure and local fetch, and residual circulation, especially the net upstream bottom flow, is dependent on local topography.

- 4) The ultimate source of sediment for the estuary is the Columbia River which contributes a somewhat restricted range of sizes generally finer than 1.00 phi. Local sources and allochthonous marine sources contribute only minor amounts of sediment to the estuary. Evidence suggests that some marine sediment consisting of older and/or relatively recent Columbia River sediment and minor amounts of sediment from headland erosion along the Oregon coast is being transported into the estuary.
- 5) The patterns of sediment distribution within the estuary are complex and reflect the variety of processes acting over various time scales. Most of the estuary reflects an even more restricted range of sediment size than is supplied by the river; the mean size of the estuary sediment is 2.50 phi. Sediment is moved as bedload, intermittently suspended local, and suspended load. The intermittently suspended sediment is highly mobile and is an especially important fraction in determining the grain-size distributions. Finer sediment, because it is more easily transported, is quantitatively less important in the Columbia River Estuary. Sediment in the adjacent fluvial reaches is generally coarser than that of the estuary, while sediment in the adjacent marine environment is generally finer.
- 6) Details of the sediment distribution suggest that bedload sediment is not being transported out of the estuary. Finer sediment that may be intermittently suspended may be both entering and leaving the estuary through the tidally-dominated entrance, but the net transport direction appears to be inward at depth.
- 7) Fine sediment that is normally transported in suspension comprises only a small percentage of the sediment found in the estuary. Fine sediment is found in the peripheral bays, and minor, inactive channels, especially in Cathlamet Bay. Fine sediments also occur in the channels of the central estuary, but they are ephemeral deposits and do not contribute to long-term deposition in the estuary.
- 8) Studies of bedform transport with side-scan sonar indicate that bedload transport is tidally-dominated near the entrance, where bedform reversals occur, and fluvially-dominated in the upper estuary. In the central estuary, bedforms indicate the upriver sediment transport occurs in response to the net upstream bottom flow, causing a bedload transport node in the main channels. The location of this node moves seasonally in response to discharge changes.
- 9) Studies of suspended sediment indicate the presence of a turbidity maximum that is related to both a trapping effect of the net circulation and a resuspension effect by the tidal currents. The turbidity maximum advects with the semidiurnal tide over much of the lower estuary. Concentrations in the turbidity maximum change in response to tidal energy on both a diurnal and neap-spring time scale. The location of the turbidity maximum is expected to generally shift with discharge changes.

- 10) Inspection of the distribution of rip-up clasts, fine sediment deposition, and the excursion of the turbidity maximum suggest that suspended sediments concentrated in the turbidity maximum may be mixed into upper layers of the water column and advected either out of the estuary or into one of the peripheral bays. In the latter instance, currents will be insufficient to resuspend the sediment if it settles to the bottom, and a mechanism for an advection and settling lag deposition in the fine bays is established. Deposition of fine sediments in the main channels occurs on an ephemeral basis beneath the turbidity maximum, but does not result in a significant long term accumulation of fine material in the estuary.
- 11) The net effect of the behavior of the turbidity maximum is to increase the residence time of fine material in the estuary and to provide some fine material to the peripheral bays. However, in the long run, most (80%) of the fine material that enters the estuary is eventually discharged into the marine environment in the river plume.
- 12) The morphology of the estuary reflects the processes that dominate the eventual deposition of sediment. Most of the upper estuary and above is characterized by a distinctly fluvial morphology, indicating the importance of fluvial processes such as point bar deposition and channel migration. In conjunction with other data, this suggests that the long-term accumulation in the estuary is associated with gradual horizontal accretion of bedload sediment via channel migration, rather than vertical accretion of fine material being deposited from suspension. This style of horizontal accretion of sandy sediments is in contrast to the vertical accretion that is often associated with estuarine sedimentation.
- 13) A complex set of depositional environments is created by the processes acting in an estuary with varied topography. These processes are highly time-dependent, producing a suite of sedimentary environments that also change in time.

These conclusions, together with those developed in Chapter 3, set the physical background in which the even more complex web of biological interactions must be analyzed. Chapter 5 will utilize the results of a model simulation and bathymetric comparisons to set an historical perspective on these processes.

5. HISTORICAL CHANGES IN COLUMBIA RIVER ESTUARINE PHYSICAL PROCESSES

The Columbia River Estuary is a more natural system than many of the more-studied estuaries of the Atlantic seaboard, where human influence has been overwhelming. Nonetheless, substantial areas have been diked, filled, or otherwise removed from the estuary. The shoreline has been urbanized, farmed, or logged. Dredging, dredged material disposal and pile dikes have altered the hypsometric curve and distribution of flow in the system. The jetties at the entrance have moved the mouth of the estuary and the tidal delta seaward, the hydrologic regime has been greatly altered by storage and diversion of water in the river basin (Section 2.2), the enormous salmon runs that once passed through the estuary have been decimated, and non-native fish species have been introduced. Changes in the quality of incoming water have also occurred, but water quality has not become the major problem that it is in many, less dynamic estuaries.

This report documents the present state of the system and analyzes the functioning of the ecosystem in relation to the physical environment. An understanding of the present functioning of the system inevitably implies a temporal dimension extending through historical time and beyond. The larger questions to be addressed by looking at historical trends include the effects of flow regulation and diversion, jetties, pile dikes, dredging, and dredged material disposal on the sediment budget, sediment distribution and circulation; the effects of habitat loss on the estuarine biota; and the effects of estuarine alterations on migratory salmonids.

The analysis of historical changes is limited by the data base. Aside from accounts of historical alterations (summarized in Section 5.2), the only data available from the time prior to navigational alterations and large-scale commercial fishing (which both became significant in the 1870's; Oregon Historical Society 1980) are the tidal observations and the bathymetric surveys and charts of the U.S. Coast Survey (discussed in Section 2.5 and Columbia River Estuary Data Development Program 1983). The bathymetric data were exploited systematically by mapping bathymetric changes between surveys conducted at 20- to 50-year intervals between 1867 and 1981. These bathymetric changes are analyzed in Section 5.2 to determine shoaling and erosion rates. The same surveys and charts were used to determine changes in shoreline and vegetative cover (Thomas 1983). Both bathymetric and tidal data were used in the two-dimensional, laterally-averaged circulation model (Hamilton 1984) to determine circulation and salinity patterns prior to human alteration (Section 5.3). The results of Sections 5.2 and 5.3 and available sediment transport information (Chapter 4) are used in Sections 5.4 and 5.5 to discuss changes in suspended sediment accumulation in the turbidity maximum and to define an approximate sediment budget. Historical issues related to the physical environment of the estuary are further addressed in Section 5.5, and the ecological implications are discussed in Chapter 9.

5.1 HISTORICAL CHANGES IN THE COLUMBIA RIVER ESTUARY

Human influence on the physical environment of the Columbia River Estuary began about fifty years after the arrival of the first white settlers. Although native populations had lived and fished in the area for centuries, it was not until the construction of the salmon canneries and the beginning of lumber exports in the 1840's and 1850's that men and women began to shape the estuary to their own needs (Oregon Historical Society 1980). Until 1885, human influence on the morphology of the estuary was probably negligible; it was confined to the construction of pilings, weirs, and some sporadic scrape-dredging of the bars. In 1885, however, construction of the South Jetty began, and a new era in the evolution of the estuary was inaugurated.

Several surveys made prior to 1885 demonstrated the dynamic nature of the entrance to the estuary before the construction of the entrance jetties. Shifting shoals and channels occupied the entrance regions. Early charts (collected by the Oregon Historical Society 1980) and descriptions of the entrance region (U.S. Army Engineers 1903; Moore and Hickson 1939; Lockett 1962, 1963; Borgeld et al. 1978) indicate that the number of channels crossing the tidal delta (the "bar") varied. The earliest survey by Vancouver in 1792 shows a single channel, but by the time of the 1839 survey by Belcher, two channels existed, separated by an intertidal sand body seaward of Clatsop Spit (Middle Sands) which was connected to Sand Island immediately east of the entrance. The entrance morphology changed continuously through 1880, but two channels existed across the tidal delta for the entire period. During this time, Clatsop Spit prograded north and west, forcing the south channels and Sand Island north. In 1868, the south channel was well suited for navigation, but by 1881, the continued northward migration of the south channel had caused the two channels to merge, creating a single broad, shallow channel across the delta. Clatsop Spit was eroded and lost elevation during the same time. The result of these changes was that the best channel across the delta provided only 5.8 m (19 ft) of depth at the time of the 1881 survey.

The Board of Engineers prepared the plans for an improvement project in 1882, and construction of the original South Jetty began in 1885 (U.S. Army Engineers 1903; Hickson 1922). There was little effect on the entrance region in the first four years, but beginning in 1889, the channel across the tidal delta began to swing north and deepen until, in 1895, a depth of 10.6 m (35 ft) was obtained. However, the channel continued to swing north and began to shoal, and by 1902, the channel had broadened and bifurcated, again creating two channels across the outer tidal delta. At this point, the best channel into the estuary was only 6.7 m (22 ft) and plans for the extension of the South Jetty and construction of the North Jetty were initiated (U.S. Army Engineers 1903).

Construction of the South Jetty extension began in 1903 and was completed in 1914. The North Jetty was begun in 1913 and completed in 1917, and dredging of the entrance channels began in 1903. Rapid changes in the channel occurred as a result of the jetty construction

and the dredging (Hickson 1922). Subsequent rehabilitation of the jetties, construction of Jetty A and the Sand Island dikes in 1939, and dredging associated with increases in the project depth of the entrance channel have resulted in further modifications to the morphology of the entrance region (Lockett 1962, 1963; Borgeld et al. 1978).

While these changes were occurring near the entrance as a result of jetty construction, the upriver channels were being modified by the construction of pile dikes and by dredging. In the upper estuary, the complex channel system was gradually replaced by a single deep channel. Previously important channels like Cordell Channel and Cathlamet Channel were isolated from the main flow by pile dikes, and bars in the main channel were removed by dredging. The greatest changes occurred during the initial development of the river for navigation; by 1935 the 10.7 m (35 ft) river channel had been obtained. Concurrent with the channel modifications and continuing into the 1940's, extensive diking of marsh and swampland occurred in the estuary and lower reaches of the river. Thomas (1983) indicates that a total of $1.2 \times 10^8 \text{ m}^2$ (30,000 acres) of estuarine wetland (tidal swamps and tidal marshes) has been lost by diking and filling activities.

Meanwhile, development was continuing in the drainage basin and upper reaches of the Columbia River, affecting the river discharge and possibly the sediment load. Beginning in the 1840's, water was diverted for irrigation, and beginning with the construction of the first major dam on the Columbia River (the Rock Island Dam, in 1933) changes in the hydrology of the river were effected. Chapter 2 discusses the historical changes in river discharge that have occurred as a result of climatic variations, diversion, and flow regulation by the dams.

A chronology of many of the important developments in the river and estuary system is listed in Table 5.1. This table has been compiled from a variety of sources and is presented here as a brief history of the physical changes that have altered the form of the estuary.

The following sections will summarize historical changes in estuarine volume and surface area and discuss the historical changes in the processes that act in the estuary, beginning with changes in the circulation and continuing with the effects on sedimentation.

5.2 CHANGES IN THE MORPHOLOGY OF THE ESTUARY

5.2.1 Causes

The substantial changes that have taken place in the structure of the estuary in historical time are the result of natural processes, human activity, and sedimentological responses to human activity. The dredging of material from channels and the transfer of dredged material into shallow water or onto land may be the least important cause of structural change in the estuary. The natural response to the construction of permeable pile dikes and jetties, especially the jetties at the entrance, has probably caused the largest changes in the location of sediment in the estuarine system. The accumulation of sediment behind these dikes, and the associated scour of the adjacent river

channel, has resulted in deeper channels and broader, shallower expanses of shallow intertidal and supratidal areas. Many previously important channels, such as Cordell Channel, Prairie Channel, Cathlamet Channel, and the channels of eastern Grays Bay have been isolated from the main flow by pile dikes and have subsequently shoaled. The processes that have caused these changes were anticipated by the Corps of Engineers (COE) in designing their "training" structures. They have taken advantage of the fact that in order for the river to maintain a relatively constant discharge in the face of an artificially reduced channel width, velocities must increase. In the absence of salinity intrusion effects, the resulting increased shear stresses will erode sediment from the channel bottom until the increased depth compensates for the reduced channel width. The displaced sediment will move down-current to a regime of lower shear stress, where it will be deposited. The system of permeable pile dikes is highly effective in the riverine part of the system, for it narrows the channel cross section and provides a protected region of lower current velocities that receives the material displaced from the channels. Dredging efforts have been concentrated on obtaining new project depths, channel realignments, and maintenance dredging on a finite number of troublesome bars.

The natural movement of sediment down the river channel has probably been greatly affected by 1) changes in sediment supply from the drainage basin of the Columbia River and its tributaries, 2) changes in the hydrographic regime of the river, 3) removal of material from the river bed by dredging and by storage behind pile dikes, and 4) transitory increases in the transport rates immediately following the construction of new pile dikes. The net result of these effects is unknown; to date insufficient progress has been made in developing a sediment budget for the lower reaches of the river, and the individual contribution of each of these changes is not well understood. While increased agricultural and logging activity has probably accelerated erosion rates in the drainage basin of the Columbia River, sediment supply to the lower Columbia River may not have increased because of storage behind dams, removal from the system by dredging, and reduction in transport rates due to the damping of the hydrographic curve. On the other hand, Fullam (1969) argues that during high flow periods the dams of the Columbia River permit sediment to pass freely and the analysis of flow regulation in Chapter 2 of this report indicates that substantial damping of the discharge curve did not occur until about 1969. In fact, the effect of pile dike construction along the lower reaches of the river may have been to hasten transport of bed sediment down the river, producing an artificial and transient increase in sediment supply to the estuary. Regardless of whether the rate of sediment supply to the estuary from the river has been altered substantially in historic times, the river has undoubtedly been the primary source of sediments in the estuary, and the sediment budget of the lower reaches of the river will need to be examined in the future to completely interpret the results of sediment budget estimates in the estuary.

5.2.2 Measurements of Structural Changes

In order to approach the changes in the estuary quantitatively, the digitized bathymetric information compiled in the preparation of the

Table 5.1. Chronology of important events affecting the physical evolution of the Columbia River Estuary

1792	Captain George Vancouver, commanding, sent Lt. Broughton to chart river and mouth: single entrance channel, controlling depth 8 m (27 ft); Robert Gray prepared harbor sketch.
1805	Lewis and Clark expedition arrived.
1811	Fort Astoria constructed by Pacific Fur Company.
1839	Sir Edward Belcher survey: two entrance channels, controlling depth 8 m (27 ft).
1840's	Irrigation began in Columbia River basin. 1841 Wilkes survey.
1844 to present	Log and lumber exports.
1849	Large June freshet.
1849-50	First USCGS bathymetric survey (Lt. Commander McArthur).
1850's	First salmon canneries.
1863	June freshet more than $26,900 \text{ m}^3 \text{ sec}^{-1}$ (950,000 cfs).
1867-77	USCGS survey of estuary and river.
1867	Dredging begun in Willamette River.
1868	First dikes in place in Youngs Bay.
1873-74	Dredging of the Hogsback bar, Cordell Channel.
1876	June freshet more than $27,180 \text{ m}^3 \text{ sec}^{-1}$ (960,000 cfs).
1877	Navigation channel from mouth to Vancouver/Portland approved by Congress.
1878	First current observations.
1880	June freshet more than $26,050 \text{ m}^3 \text{ sec}^{-1}$ (920,000 cfs); first scrape-dredging on bar.
1882	9 m (30 ft) entrance channel approved.
1883	Peak of cannery operations.
pre-1885	Only occasional dredging and a few training structures were employed to date.
mid-1880's	Minor dredging in Cordell Channel.
1885	South Jetty construction began. 1890 Cordell Channel no longer in use.
1890's	First pile dikes constructed in river channel.
1893	Snag Island dike (and Green Island and Marsh Island dikes?) built: Cordell Channel closed and flow diverted to north channel.
1894	June freshet more than $33,980 \text{ m}^3 \text{ sec}^{-1}$ (1.2 kcfs); first extensive dredging ($305,820 \text{ m}^3$, $400,000 \text{ yd}^3$) after freshet.
1895	6.8 km (4.25 mi) South Jetty completed with four groins; 9.5 m (31 ft) controlling depth in entrance channel; rock ledge near upper Astoria blasted.

Table 5.1. (continued)

1899	7.6 m (25 ft) river channel from mouth to Portland authorized.
1899-1903	Dredging across Upper Sands Shoal: navigation channel re-aligned.
1902	Three entrance channels, controlling depth 6.7 m (22 ft).
1903	Dredge Grant arrived.
1904	Dredge Chinook arrived.
1905	River and Harbor Act of 3 March.
1905	Approved 12.2 m (40 ft) Entrance Project, including extension of South Jetty.
1909	Grays River channel obstructions cleared.
1912	River and Harbor Act, 9.1 m (30 ft) channel authorized from Brookfield to Portland.
1913	North Jetty construction began; Cowlitz River channel dredged to 1.2 m (4 ft); Oregon slough dredged to 7.6 m (25 ft); Baker Bay (east) channel dredged to 3.4 m (11 ft).
1914	South Jetty extension completed; 7.3 m (24 ft) entrance channel obtained; extensive dredging and pile dike construction in Columbia River channel to Portland begins.
1917	North Jetty extension completed; 9.1 m (30 ft) channel authorized from mouth to Brookfield.
1918	Entrance channel controlling depth 12.2 m (40 ft).
1920	Skamokawa Creek channel cleared to 2 m (6.5 ft).
1924	Clatskanie River channel dredged to 1.8 m (6 ft).
1927	Entrance channel controlling depth 14.3 m (47 ft).
1928	Deep River channel cleared to 2.4 m (8 ft); 10.7 m (35 ft) river channel recommended.
1931	South Jetty rehabilitation begun; Lake River channel dredged to 1.8 m (6 ft).
1932	Chinook pile dike constructed; COE current survey at mouth.
1933	Rock Island Dam.
1934	Ilwaco (east) Channel completed (3.1 m, 10 ft).
1935	10.7 m (35 ft) Columbia River Channel completed; dikes along Columbia River completed, channel revision at Harrington Point completed; Multnomah channel completed (7.6m, 25ft); Cathlamet side channel (3.1 m, 10 ft) completed.
1935-1939	USCGS bathymetric survey of estuary and river.
1936	Flood Control Act of 22 June.
1936	Extensive COE diking begun.
1938	Bonneville Dam constructed; Youngs Bay channel cleared (3.1 m, 10 ft); North Jetty rehabilitation begun (concrete terminal and asphalt added).
1939	Jetty A completed; four Sand Island pile dikes completed; North Jetty rehabilitation completed; Skipanon channel dredged (9.1 m, 30 ft); Skipanon peninsula created with dredged material; Westport slough dredged (8.5 m, 28 ft); Elochoman slough dredged (3.1 m, 10 ft).

Table 5.1. (continued)

1939-1955 Dredging at entrance confined to Clatsop Spit.	
1940	Chinook Channel (3.1 m, 10 ft), mooring basin, and breakwaters completed.
1941	Grand Coulee Dam constructed; concrete terminal added to South Jetty.
1942	South Jetty rehabilitated (asphalt added); COE salinity measurements.
1942-1945 Mott Basin dredged, Lois Island created/enlarged?	
1944	Ilwaco (west) Channel mostly completed (3.1 m, 10 ft).
1945	Regular annual dredging (of outer bar?) initiated.
1947-1958 USCGS bathymetric survey of estuary and river.	
1948	June freshet more than $28,320 \text{ m}^3 \text{ sec}^{-1}$ (1 kcfs); Ilwaco (west) Channel (2.4 m, 8 ft) and three pile dikes (on larger Sand Island) completed.
1950	Flood Control Act of 17 May
1950	Astoria east boat basin completed.
1951	Channel alignment on Desdemona shoal.
1953	McNary Dam constructed; fourth pile dike on larger Sand Island completed.
1954	River and Harbor Act of 3 September.
1954	14.6 m (48 ft) entrance channel project approved.
1955	Chief Joseph Dam constructed.
1956	Dredging of 14.6 m (48 ft) entrance channel begun.
1957	The Dalles Dam constructed; Warrenton mooring basin (3.7 m, 12 ft) completed; Ilwaco (west) Channel (3.1 m, 10 ft) completed; 14.6 m (48 ft) entrance channel obtained.
1958	Westport slough cleared (8.5 m, 28 ft); Chinook harbor breakwaters extended; dredge material disposal Sites A and C abandoned, Site B used extensively.
1959	Priest Rapids Dam constructed; COE current meter study.
1960	Cowlitz River channel dredged to 2.7 m (9 ft).
1961	Rocky Reach Dam constructed; South Jetty and Jetty A rehabilitated.
1962	12.2 m (40 ft) Columbia River channel to RM-105 and 18.5 km (11.5 mi) up Willamette River authorized; completion of WES physical model of Columbia River.
1965	Radionuclide studies of estuarine sediments (AEC, USGS).
1963	Wanapum Dam constructed; prototype physical measurements initiated by WES. 1966 Astoria-Megler Bridge completed.
1967	Wells Dam constructed.
1968	Mica Lake, Arrow Lake Dams constructed.
1975	COE current meter studies.
1976	12.2 m (40 ft) river channel completed from mouth to Portland/Vancouver; Oregon slough deepened to 12.2 m (40 ft).

Table 5.1. (continued)

1977	15.9 m (52 ft) entrance project initiated; COE current meter studies.
1978	COE current meter studies.
1979	Initiation of CREDDP fieldwork.
1980	Mt. St. Helens eruption and associated mudflows into the Columbia River at Kelso/Longview.
1980-1983	5-11 million m ³ of material dredged from the Cowlitz/Columbia confluence.
1981	NOS current meter survey.
1982	Coal port channel (16.7-18.3 m, 55-60 ft) to Tongue Point (RM-18) proposed.

Sources: U.S. Army Engineers (1875, 1903), various Congressional documents (House of Representatives Document 1899, 1900, 1917, 1919, 1921, 1928, 1946; House of Representatives Report 1906; Senate Documents 1881, 1917), U.S. Army Engineers (1960), Lockett (1963, 1967), Oregon Historical Society (1980), Roy et al. (1982), George Blomberg (pers. communication), David Jay (pers. communication).

Columbia River Estuary Data Development Program (1983) bathymetric atlas was used. These data represent the most comprehensive collection of bathymetric data available for the Columbia River Estuary in a format suitable for comparison. Surveys from four composite periods were chosen for analysis:

- 1868: includes U.S. Coast and Geodetic Survey (USCGS) charts made between 1867 and 1877, before any major influences of jetty construction;
- 1935: includes USCGS surveys made between 1926 and 1937, post-dating jetty construction and coincident with construction of numerous pile dikes and channel alignments;
- 1938: includes USCGS surveys made between 1949 and 1958, post-dating the completion of the 14.6 m (48 ft) entrance channel but pre-dating the initiation of the 12.2 m (40 ft) river channel and much of the flow regulation;
- 1982: includes COE surveys made between 1979-1982 and represents the most recent available bathymetry.

The various surveys were compiled at identical scale relative to the same datum. The resulting suite of charts and differencing maps and the bathymetric atlas (Columbia River Estuary Data Development Program 1983) form the basis for the discussions in this chapter. Shalowitz (1964) was used in interpreting the surveys.

Calculations of surface area in each of several depth regimes were made utilizing the digitized bathymetric data. The estuary was subdivided into thirteen subareas on the basis of physical, geological, and biological criteria (Figure 5.1). The areas within each of fourteen depth intervals were calculated for each of the subareas (Table 5.2) using two methods. The first of these methods provided an approximation of the surface area over the actual topography of the bottom, while the second calculated the surface area projected onto a level plane (the "normal" surface area). The actual surface area is most appropriate in biological analyses requiring surface area estimates, but the normal area is more convenient in that it conserves area within the surveyed region from year to year regardless of any bathymetric changes. The two areas differ by less than 1% in all cases. The bathymetric data used in the analysis were interpolated onto a latitude-longitude grid which contained one bathymetric data point every 29 m along the north-south axis and every 21 m along the east-west axis. Areas calculated from this grid should not be considered accurate to more than 1000 m² (generally much less than 0.1% of the total area of the depth interval). Greater inaccuracies may be present in the original data as a result of the difficulties encountered during compilation of the historical bathymetric series. The contours and shoreline are considered to be accurate to within 51 m. Although errors of up to 30% in the measurement of a 100,000 m² area could occur with uncompensated boundary displacements of 50 m, this is considered the maximum error involved in the calculations, and the much larger area of many of the polygons and internally consistent comparisons are likely to produce fairly precise

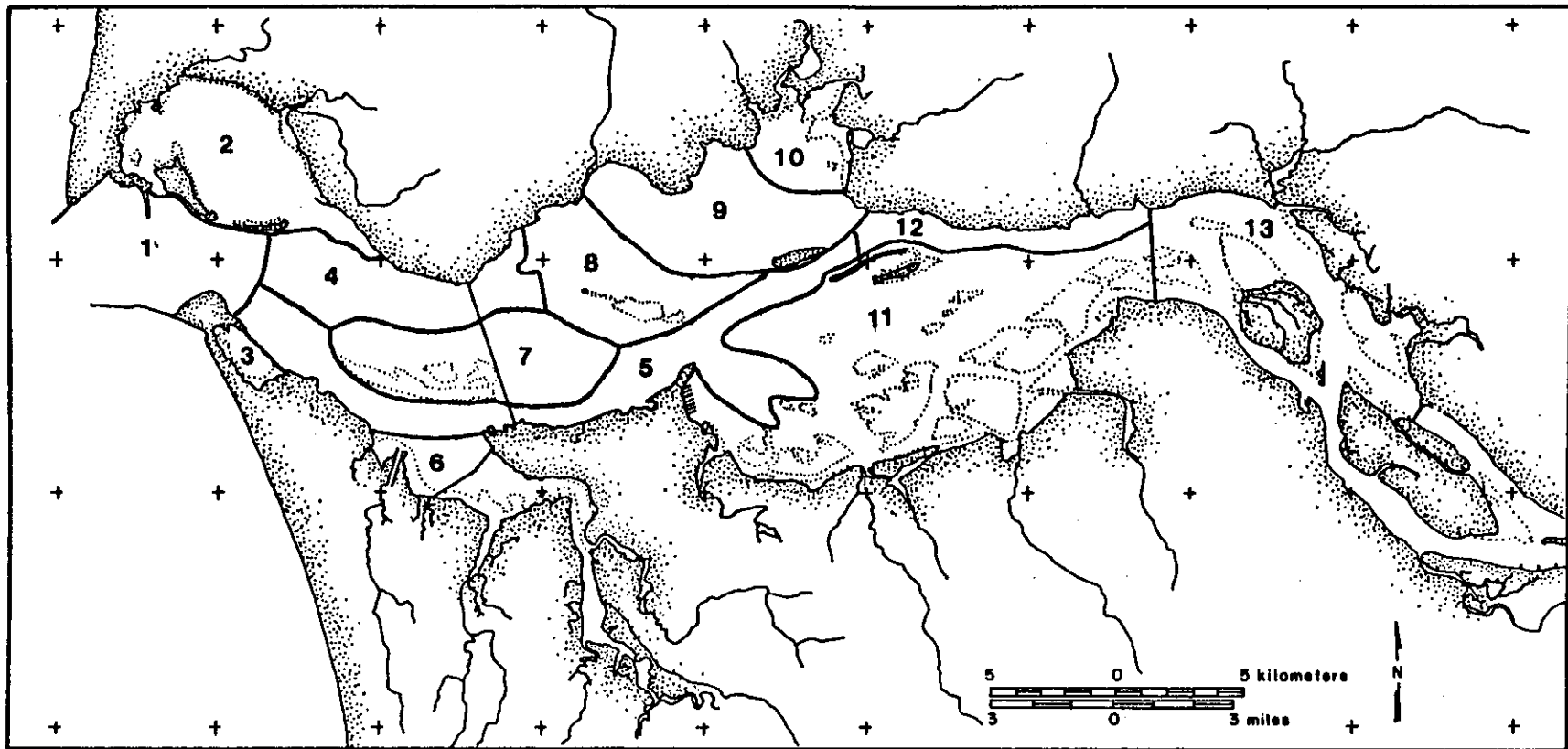


Figure 5.1 Map of the Columbia River Estuary showing 13 subareas used in volume and area calculations: 1) Entrance; 2) Baker Bay; 3) Trestle Bay; 4) North Channel; 5) South Channel; 6) Youngs Bay; 7) Desdemona Sands; 8) Mid-Estuary Shoals; 9) Grays Bay; 10) Brix Bay; 11) Cathlamet Bay; 12) Lower River Channel; 13) Upper River Channel.

numbers. The vertical control on the bathymetric data is considered reliable to within several centimeters in the estuary proper but degrades to 0.5 m in the upriver sections due to datum inconsistencies and runoff effects on river height. A bias toward the shallowest soundings is probably included, as all of the data were collected for navigational purposes and more modern data were collected with acoustic echo-sounders. Small scale topographic features such as bedforms, which are known to exist over much of the estuary, are not resolved, but as the areas are computed for relatively broad depth intervals, the error is negligible. In the upper intertidal regions more serious errors occur for two reasons: 1) bank to bank surveys were not performed in all four time periods, and shoreline locations are often uncertain, especially in marshes and swamps; 2) the digital scheme, designed for bathymetry, assigned all "land" the value of -2.1 m (-7 ft); therefore the depth interval -2.1 to -0.9 m (-7 to -3 ft) includes not only intertidal areas, but in some cases upland areas with greater elevations. (Note that the depth intervals are discussed using the shallower of the bracketing depths; Table 5.2.) In these areas, the estimates provided by Thomas (1983) may prove more accurate and are used in portions of the discussion. In the subtidal depths, the digitized data allow fairly precise calculations for a number of depth intervals.

In addition to area calculations, the digital bathymetric data were used to calculate volume changes in the estuary between the four survey periods. For the overlapping regions of each survey, the change in volume of each triangular prism defined by three bathymetry data points was summed over the estuary subarea, providing an estimate of the change in sediment volume of that subarea between the survey periods. Many of the same sources of error discussed above are inherent in these calculations. In addition, the volume estimates are highly sensitive to area changes and more sensitive than the area calculations to errors in depth measurements. It is difficult to assign error estimates to the volume calculations: although a systematic error in depth could cause large errors if multiplied over a large area, errors in depth are thought to be random. These errors should not bias the volume calculations. It is believed that the important errors are those of omission, rather than calculation errors. Several dredged material disposal sites and broad expanses of beach near the entrance jetties grew rapidly from intertidal or subtidal depths to elevations in excess of 2.1 m (7 ft) between survey periods. In the subsequent survey these are considered land and are assigned maximum elevations of 2.1 m or omitted from the survey. In the first instance, the volume differences presented underestimate the amount of shoaling occurring in the estuary. In the second case, no comparison between the two areas is made (only the intersecting regions of consecutive surveys are compared). Although in this case the error can fall in either direction, the accumulation of sediment is again usually underestimated. Therefore, the volume difference numbers presented in the following section are conservative in the sense that they provide a minimum estimate of the amount of material that has accumulated in the estuary since the 1868 survey period.

As another approach to the volume changes in the estuary, estimates of water volume were calculated from the area estimates. These volume figures are based on the midpoint of the depth interval over which the

Table 5.2. Depth intervals used in area calculations (relative to MLLW).

Interval		Applicable depth range (ft)
(m)	(ft)	
-2.1	-7.0	$-7.0 \leq z < -3.0$
-.9	-3.0	$-3.0 \leq z < 0.0$
0.0	0.0	$0.0 \leq z < 3.0$
.9	3.0	$3.0 \leq z < 6.0$
1.8	6.0	$6.0 \leq z < 12.0$
3.7	12.0	$12.0 \leq z < 18.0$
5.5	18.0	$18.0 \leq z < 24.0$
7.3	24.0	$24.0 \leq z < 30.0$
9.1	30.0	$30.0 \leq z < 36.0$
11.0	36.0	$36.0 \leq z < 42.0$
12.8	42.0	$42.0 \leq z < 60.0$
18.3	60.0	$60.0 \leq z < 80.0$
24.4	80.0	$80.0 \leq z < 100.0$
36.5	100.0	$100.0 \leq z$

areas were obtained, and they tend to overestimate the water volume in the estuary because there is generally more shallow water area than deep water area in a given depth interval. In the absence of errors, changes in the water volume between survey periods should equal the changes in sediment volume and be opposite in sign. This was generally true, and discrepancies were helpful in resolving problems in areas where particular biases of one technique or the other were encountered.

5.2.3 Area Changes

The results of the area calculations are presented, in part, as Tables 5.3 and 5.4. The entrance region areas, which have shown dramatic changes, have been omitted from the areas shown in Table 5.4 to emphasize the changes within the estuary proper. The normal surface area of the surveyed area (in 1958) of each of the thirteen subareas labeled on Figure 5.1 is shown on Figure 5.2. The area included in the digital bathymetry is identical for each of the first three survey periods (1868, 1935, and 1958) in all of the areas except those showing a minus sign (-). The coverage of these three areas decreased over the 90-year period due mostly to extensive shoreline changes and, as a result, the areas are not strictly comparable. The effects of these omissions on the interpretation of the data are discussed before the final conclusions are presented. The results of the 1982 survey have been entirely omitted because the survey did not produce comparable coverage and excludes large areas, especially near shore, that were surveyed in the previous periods.

Although not tabulated in this report, the area changes in each depth regime of the thirteen subareas were calculated (Sherwood et al. 1984). The following discussion relies on the changes observed in the individual depth intervals of the subareas, which may be found in Sherwood et al. (1984).

The largest area changes occurred in the entrance region as a result of jetty construction and shoaling. Area losses of 35 million m^2 in the 0.0 m interval between 1868 and 1935 represent 70% of the total area lost in the estuary for the entire 90-year period. Most of this area, which had been low intertidal shoal area in 1868, was transferred to supratidal environments on Clatsop Spit and Peacock Spit during beach accretion around the newly constructed jetties. Nearly 38 million m^2 were omitted from the 1935 surveys as a result of the land growth, creating discrepancies in the surveyed areas. The 1868 survey included 212.33 million m^2 , the 1935 survey included 173.95 million m^2 , and the 1958 survey covered 172.45 million m^2 . In addition to these changes, large gains in the area above MLLW were noted between the 1868 and 1935 surveys, also reflecting the spit growth. Area was lost during the same period in the 0.9, 1.8, 3.7, 5.5, and 7.3 m intervals (36 million m^2) but a nearly equal area was gained in the deeper 9.1, 11.0, and 12.8 m intervals (32 million m^2). Areas of the deepest water were somewhat reduced as the outer tidal delta was forced seaward. Changes in the entrance region were much less dramatic in the period between 1935 and 1958, suggesting that an equilibrium had been reached. Area was lost in the 9.1 and 11.0 m intervals and gained in the 12.8 and 24.4 m intervals, probably reflecting dredging of the 14.6 m (48 ft) entrance

Table 5.3. Areas, volumes, volume changes, and area changes by depth regime for 1868, 1935, and 1958.

Depth regimes		Area (10^6 m^2)			Water volume [†] (10^6 m^3)			Volume changes (10^6 m^3)			Area changes (10^6 m^2)				
(m)	(ft)	1868	1935	1958	1868	1935	1958	1868-1935	1935-1958	1868-1958	1868-1935	1935-1958	1868-1958		
-2.1	-7.00	294.22	339.33	326.31	-448.39	-517.14	-497.15	-68.75	19.99	-48.76	45.11	-13.12	31.99		
-0.9	-3.00	38.05	54.46	50.91	-17.40	-24.90	-23.27	-7.50	1.62	-5.88	16.41	-3.55	12.86		
0.0	0.00	113.85	69.48	65.11	52.05	31.77	29.77	-20.28	-2.00	-22.28	-44.36	-4.37	-48.74		
0.9	3.00	47.65	50.23	48.66	65.36	68.90	676.75	3.54	-2.15	1.38	2.58	-1.57	1.01		
-1.8	6.00	104.43	74.19	75.72	286.47	203.52	207.72	-82.95	4.20	-78.74	-30.24	1.53	-28.71		
3.7	12.00	70.71	53.33	55.39	323.31	342.85	253.25	-79.46	9.40	-70.06	-17.38	2.06	-15.32		
5.5	18.00	61.63	43.36	38.65	394.50	277.51	247.37	-116.98	-30.14	-147.13	-18.28	-4.71	-22.99		
7.3	24.00	45.41	35.62	31.48	373.72	293.13	259.91	-80.59	-33.22	-113.81	-9.79	-4.04	-13.83		
9.1	30.00	28.82	33.56	33.30	289.85	337.59	334.96	47.74	-2.63	45.11	4.75	-0.26	4.49		
11.0	36.00	21.42	32.33	30.87	254.58	384.31	366.98	129.73	-17.33	112.41	10.91	-1.46	9.46		
12.8	42.00	44.93	62.38	66.19	698.36	969.68	1028.94	271.32	59.26	330.59	17.45	3.81	21.27		
18.3	60.00	24.63	22.16	25.86	525.51	472.88	551.83	-52.63	78.95	26.32	-2.47	3.70	1.23		
24.4	80.00	17.98	13.79	11.51	493.16	378.33	315.79	-114.83	-62.54	-177.37	-4.19	-2.28	-6.47		
36.5	100.00	8.52	9.19	7.81	285.71	308.27	261.90	22.56	-46.37	-23.81	0.67	-1.38	-0.71		
Total		922.24	893.43	867.78	4042.57	3969.74	3925.17	-72.83	-44.57	-117.40	-28.82	-25.64	-54.46		
Summed depth regimes*															
-0.9<	0.9	-3<	3	151.89	123.94	116.01	69.45	56.66	53.04	-12.78	-3.62	-16.40	-27.96	-7.92	-35.88
0.9<	5.5	3<	18	222.80	177.76	179.78	675.13	516.26	527.71	-158.87	11.45	-147.42	-45.04	2.02	-43.02
5.5<	12.8	18<	42	157.28	144.87	134.40	1312.64	1292.54	1209.22	-20.10	-83.32	-103.42	-12.41	-10.46	-22.87
12.8-		42-		96.06	107.53	111.38	2002.75	2129.16	2158.47	126.42	29.30	155.72	11.47	3.85	15.32
Total below -3		628.02	554.09	541.57	4059.96	3994.63	3948.44	-65.33	-46.19	-111.52	-73.93	-12.52	-86.45		

[†]Volumes above MLLW are expressed as negative.

*Volume sums do not include volume above 0.9 m (3 ft) above MLLW.

Table 5.4. Areas, volumes, volume changes, and area changes by depth regime for 1868, 1935, and 1958 (excluding entrance).

Depth regimes		Area (10^6 m^2)			Water volume [†] (10^6 m^3)			Volume changes (10^6 m^3)			Area changes (10^6 m^2)		
(m)	(ft)	1868	1935	1958	1868	1935	1958	1868-1935	1935-1958	1868-1958	1868-1935	1935-1958	1868-1958
-2.1	-7.00	285.44	323.82	310.67	-435.01	0493.50	-473.45	-58.50	20.05	-38.45	38.39	-13.16	25.23
-0.9	-3.00	36.40	50.76	48.66	-16.64	-23.21	-22.25	-6.56	0.96	-5.60	14.35	-2.09	12.26
0.0	0.00	74.12	67.50	63.28	33.89	30.86	28.93	-3.02	-1.93	-4.96	-6.62	-4.22	-10.84
0.9	3.00	45.34	48.29	46.68	62.18	66.23	64.03	4.05	-2.20	1.85	2.95	-1.61	1.35
-1.8	6.00	88.21	69.56	70.56	241.97	190.81	193.57	-51.16	2.77	-48.39	-18.65	1.01	-17.64
3.7	12.00	58.19	48.18	49.22	266.06	220.27	225.05	-45.80	4.78	-41.01	-10.02	1.05	-8.97
5.5	18.00	45.04	35.88	31.43	288.28	229.66	201.20	-58.61	-28.47	-87.08	-9.16	-4.45	-13.60
7.3	24.00	29.30	26.61	22.09	241.15	219.00	181.78	-22.15	-37.22	-59.36	-2.69	-4.52	-7.21
9.1	30.00	17.12	21.42	21.79	172.18	215.41	219.17	43.23	3.76	46.99	4.30	0.37	4.67
11.0	36.00	10.35	14.17	16.18	123.07	168.39	192.38	45.32	23.99	69.31	3.81	2.02	5.83
12.8	42.00	17.79	11.25	12.89	276.55	174.88	200.44	-101.67	25.56	-76.11	-6.54	1.64	-4.90
18.3	60.00	2.17	1.83	1.68	46.25	39.07	35.88	-7.18	-3.19	-10.37	-0.34	-0.15	-0.49
24.4	80.00	0.41	0.11	0.19	11.28	3.08	5.13	-8.20	2.05	-6.15	-0.30	0.07	-0.22
36.5	100.00	0.04	0.11	0.00	1.25	3.76	0.00	2.51	-3.76	-1.25	0.07	-0.11	-0.04
Total		709.91	719.48	695.33	1764.11	1561.42	1547.56	-202.69	-13.85	-216.54	9.57	-24.14	-14.58
Summed depth regimes*													
-0.9 <	0.9 -3-3	110.52	118.26	111.94	50.53	54.07	51.18	3.54	-2.89	0.65	7.74	-6.32	1.42
0.9 <	5.5 3-18	191.74	166.02	166.47	570.21	477.30	482.65	-92.91	5.35	-87.56	-25.71	0.45	-25.27
5.5 <	12.8 18-42	101.81	98.07	91.50	824.67	832.46	794.53	7.79	-37.93	-30.14	-3.74	-6.58	-10.32
12.8 -	42-	20.41	13.31	14.76	335.34	220.79	241.45	-114.55	20.67	-93.88	-7.10	1.46	-5.64
Total below -3		424.47	395.66	384.67	1780.75	1584.62	1569.81	-196.13	-14.81	-210.94	-28.82	-10.99	-39.80

[†]Volumes above MLLW are expressed as negative.

*Volume sums do not include volume above 0.9 m (3 ft) above MLLW.

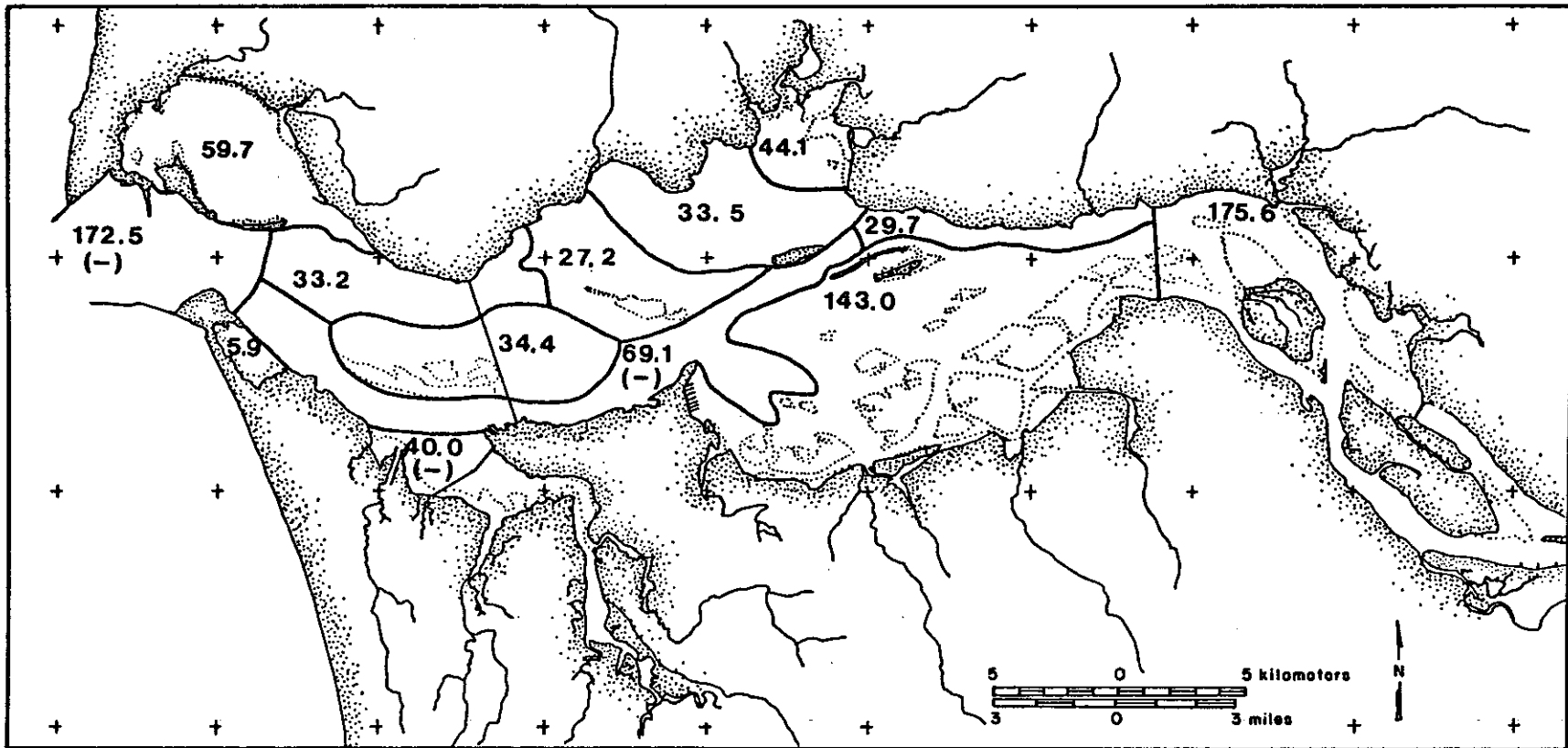


Figure 5.2 Map of the Columbia River Estuary showing the normal surveyed area in each of the 13 sub-areas. ($m^2 \cdot 10^6$) in 1958. The (-) indicate reduction in surveyed area since earlier surveys.

channel which was begun in 1956.

The relative changes among the depth regimes in the entrance are apparent in the hypsometric curve of the entrance region, presented as Figure 5.3. The hypsometric curve plots the cumulative area beneath a particular depth in the estuary. Integration of the area to the left of the curve provides a water volume estimate. The shape of the hypsometric curve and the amount of water stored in various water depths has changed dramatically since 1868. Large water volumes have been removed from the shallow intertidal and subtidal areas. Smaller volume losses have occurred in the deepest areas, and large increases of water volumes in the mid-depth ranges has nearly offset the volume losses in shallower and deeper water. Figure 5.3 also indicates that most of the changes occurred in the 1868-1935 period, following jetty construction.

Changes have also occurred in two other subareas that have affected the area calculations to some extent. The Youngs Bay subarea has been modified greatly in historic time by the dredging of the Skipanon waterway and the filling of the surrounding marsh. Thomas (1983) estimates that 40% of the original estuarine area has been converted to developed floodplain by diking and filling which began prior to even the 1868 survey. Survey coverage of the Youngs Bay area is inconsistent as a result of the changes, and more area was included in the 1935 survey than either the earlier or later survey. As a result, a large gain in the -2.1 m interval of 20 million m^2 was noted between 1868 and 1935. A loss of 12 million m^2 occurred in the same period from the 0.0 m interval. The latter number probably more accurately reflects the loss of intertidal area to diking and filling. In the subsequent period (from 1935 to 1958), an additional loss of 18 million m^2 from the -2.1 m interval was calculated: at least some of this loss is the result of reduced coverage in the 1958 survey. These calculations underestimate the change in intertidal area measured by Thomas (1983) in the same regions of the estuary.

There are also minor differences in the area covered by the 1935 and 1958 surveys in the south channel. The total area covered in 1868 and 1935 is 70.75 million m^2 , but it decreases to 69.07 million m^2 in 1958. Most of this probably appears in the difference calculations as a loss of 1.38 million m^2 in the -2.1 m interval over the period 1935 to 1958. It is likely that the decrease in the survey coverage was related to the dredging of Mott Basin for use as a seaplane base during World War II and the construction of Mott and Lois Islands with the dredged materials.

The hypsometric curve for the south channel subarea is included as Figure 5.4. The changes are similar in trend to those of the entrance but involve smaller areas and volumes. Area and water volume in the shallow intervals has decreased since 1968, while large increases in area and water volume have occurred in the mid-depths. Examination of the specific area numbers reveals that the areas in the 5.5 to 11.0 m intervals increased between 1868 and 1935 (Sherwood et al. 1984). In the subsequent period (1935 to 1958) area was lost in the 5.5 and 7.3 m intervals and gained in the 12.8 m interval. This trend probably reflects the increased navigation channel depths maintained in the more

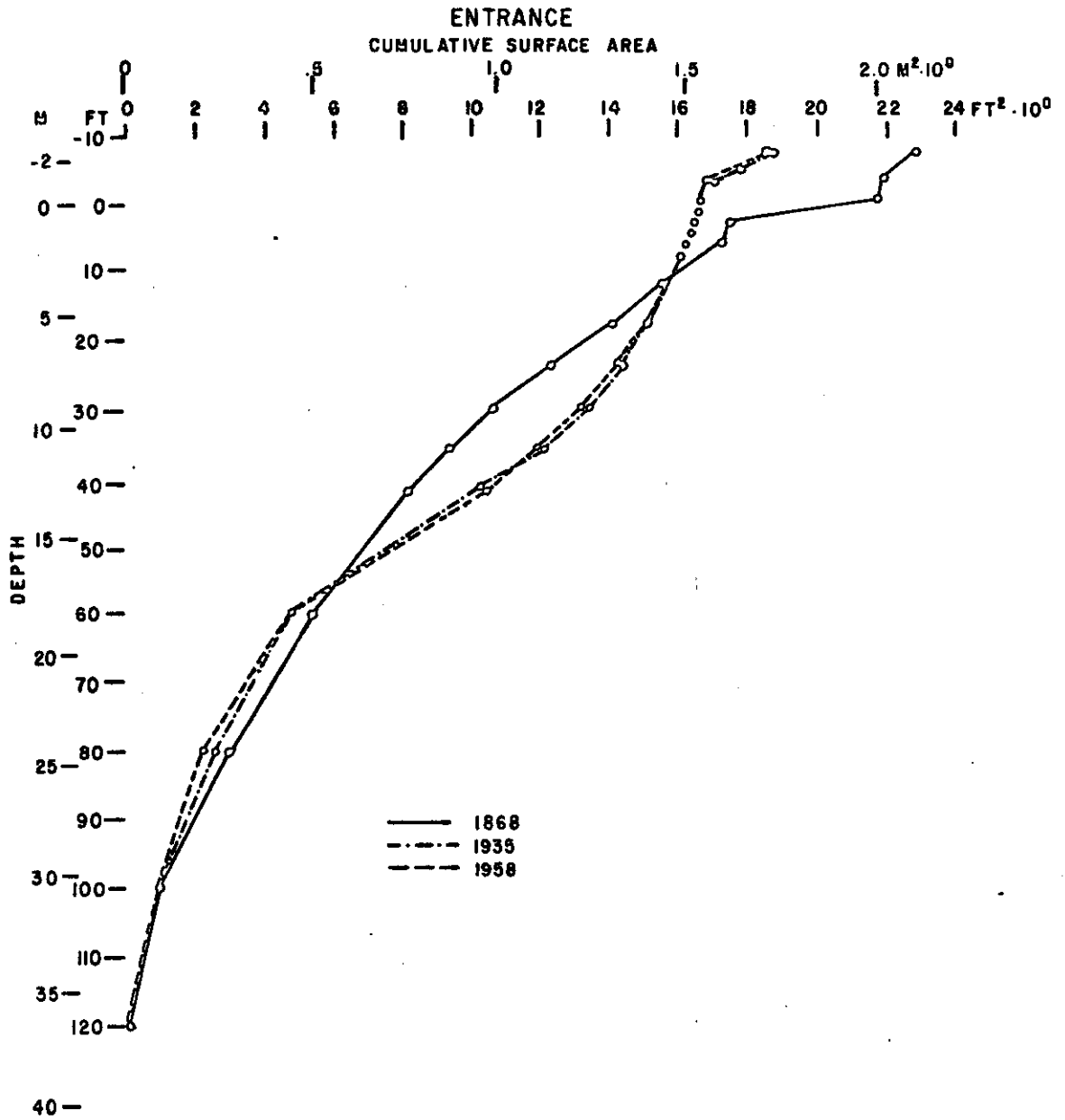


Figure 5.3 Hypsometric curve relating cumulative surface area with depth in the entrance region for 1868, 1935, and 1958.

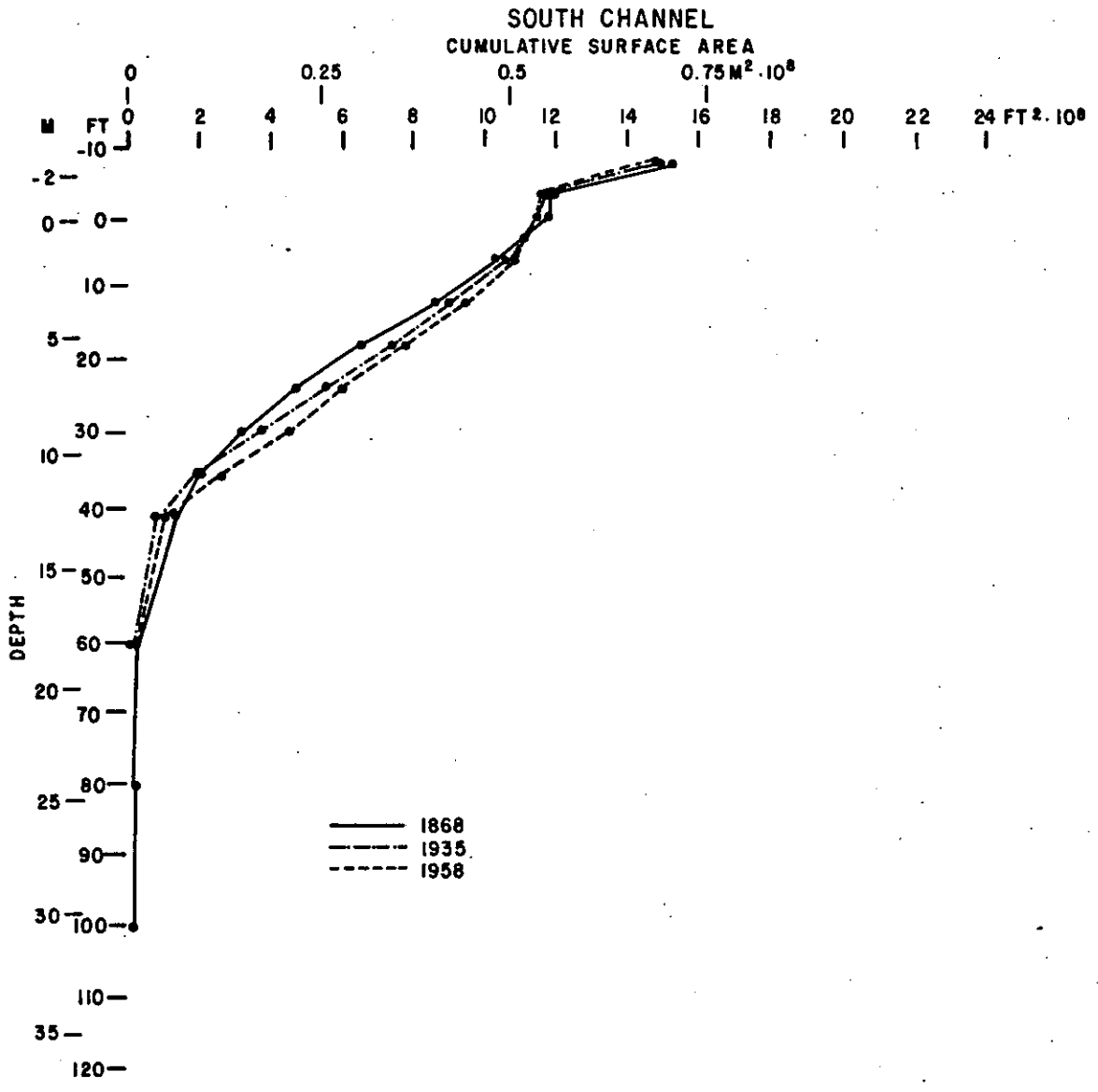


Figure 5.4 Hypsometric curve relating cumulative surface area with depth in the South Channel in 1868, 1935, and 1958.

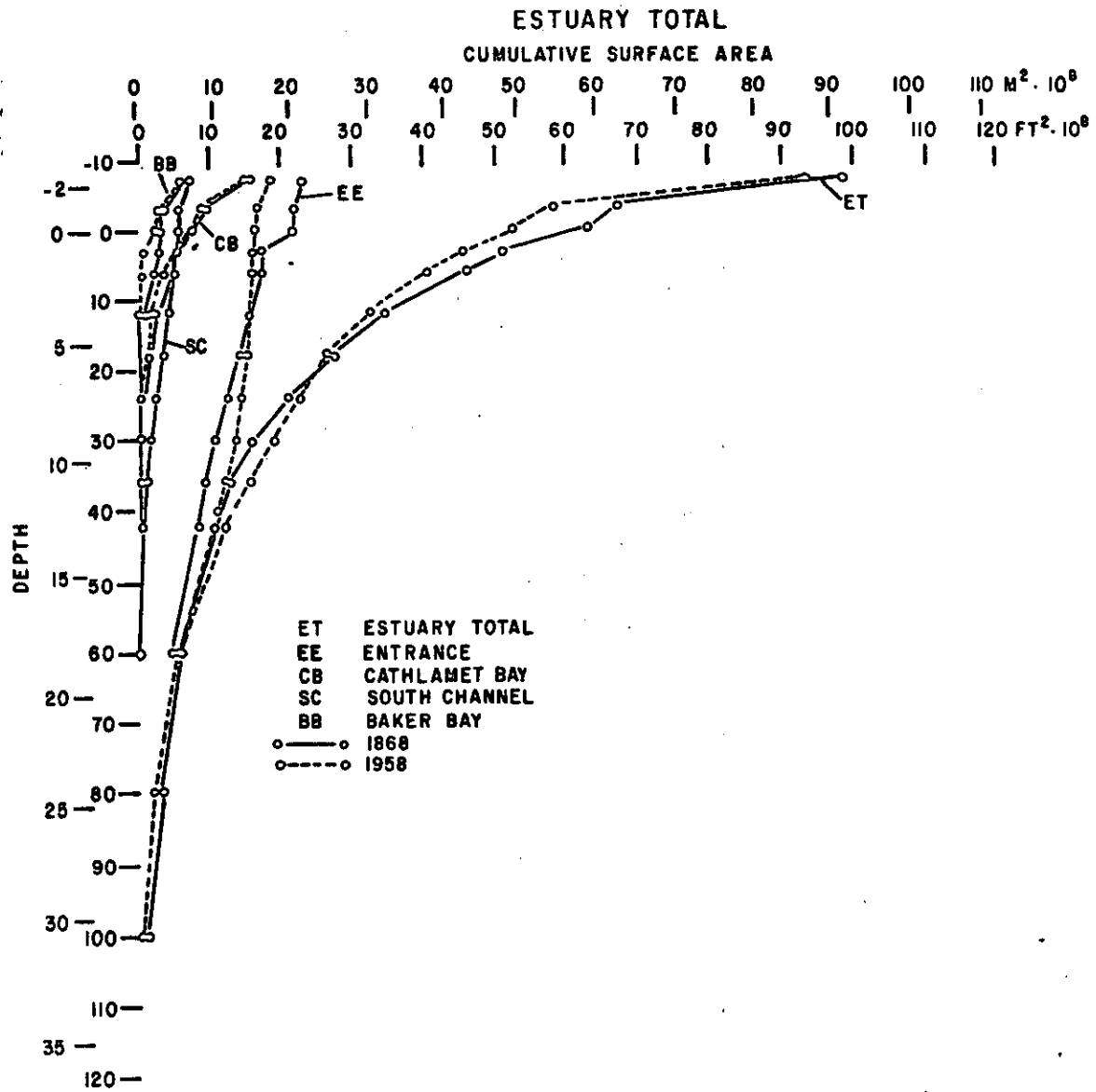


Figure 5.5 Hypsometric curve relating cumulative surface area to depth for the estuary as a whole and several subareas in 1868 and 1958.

recent period. It is interesting to note that there has been a loss of deeper water since 1868 in the south channel subarea (Figure 5.4).

With the exception of the survey discrepancies that have been discussed, the numbers from each of the time periods provide accurate estimates of the area changes in the estuary. Some exchange between upper intertidal elevations and "dry" land may occur in the -2.1 m interval, and for many calculations, the area below in the -0.9 m interval and below should be used as the most accurate estimate of estuary areas. Area totals below MLLW are very reliable.

Tables 5.3 and 5.4 summarize the area changes that have occurred in the estuary since 1868. Water volumes approximated by multiplying the area of each depth regime by the mid-point of the depth interval are also shown on the tables. The changes in both areas and volumes have been computed and summations of the volume below MLLW and the area (total; i.e., complete survey area) appear at the bottom of each column. A breakdown of the totals into depth regimes compatible with Thomas (1983) is appended at the bottom of each column, as well as totals of the areas and volumes below -0.9 m. The volumes above MLLW are flagged as negative volumes, but in calculating the volume sums, the volume of the -0.9 interval has been subtracted, effectively adding to the volume total.

Several trends in the long-term changes are apparent from Table 5.4 (which does not include the large changes that have occurred in the entrance region). An overall loss in the area of the estuary has occurred since 1868. Nearly 40 million m² of area below -0.9 m (3 feet above MLLW) have been lost, representing a decrease of 9% relative to the 1868 area of 424.47 million m². Most of the loss has been from the shallow subtidal depths in the intervals from 0.9 to 3.7 m (64% of the total loss), but significant losses from the deeper intervals (5.5 to 11.0 m, 26%; and 12.8 and deeper, 14%) have also occurred. Most of the change occurred during the longer early period (1868 to 1935); it was during this period that most of the relatively shallow area was lost (loss of 26 million m² from the 0.9 to 3.7 m intervals). In the more recent period (1935 to 1958) there has been a slight increase in the area of this shallow interval; the losses in the intervals between 5.5 and 11.0 m are twice the losses in the same intervals for the preceding period. A slight gain in the area deeper than 12.8 m occurred during the more recent period, probably reflecting increased depths in the navigation channel.

It is difficult to estimate the changes in the upper intertidal area from the figures shown in Tables 5.3 and 5.4 because of the survey inconsistencies. Thomas (1983) estimates that 121.6 million m² of area (30,050 acres) has been lost in the tidal marshes and swamps. This amounts to a loss of approximately 20% of the original estuary area. The loss of some of this area has been important in decreasing the tidal prism of the estuary; however, the diked and filled areas were originally high and many were upriver, where the tidal prism was small.

The effects of these area changes on the water volumes of the estuary are depicted graphically in Figure 5.5, which shows a

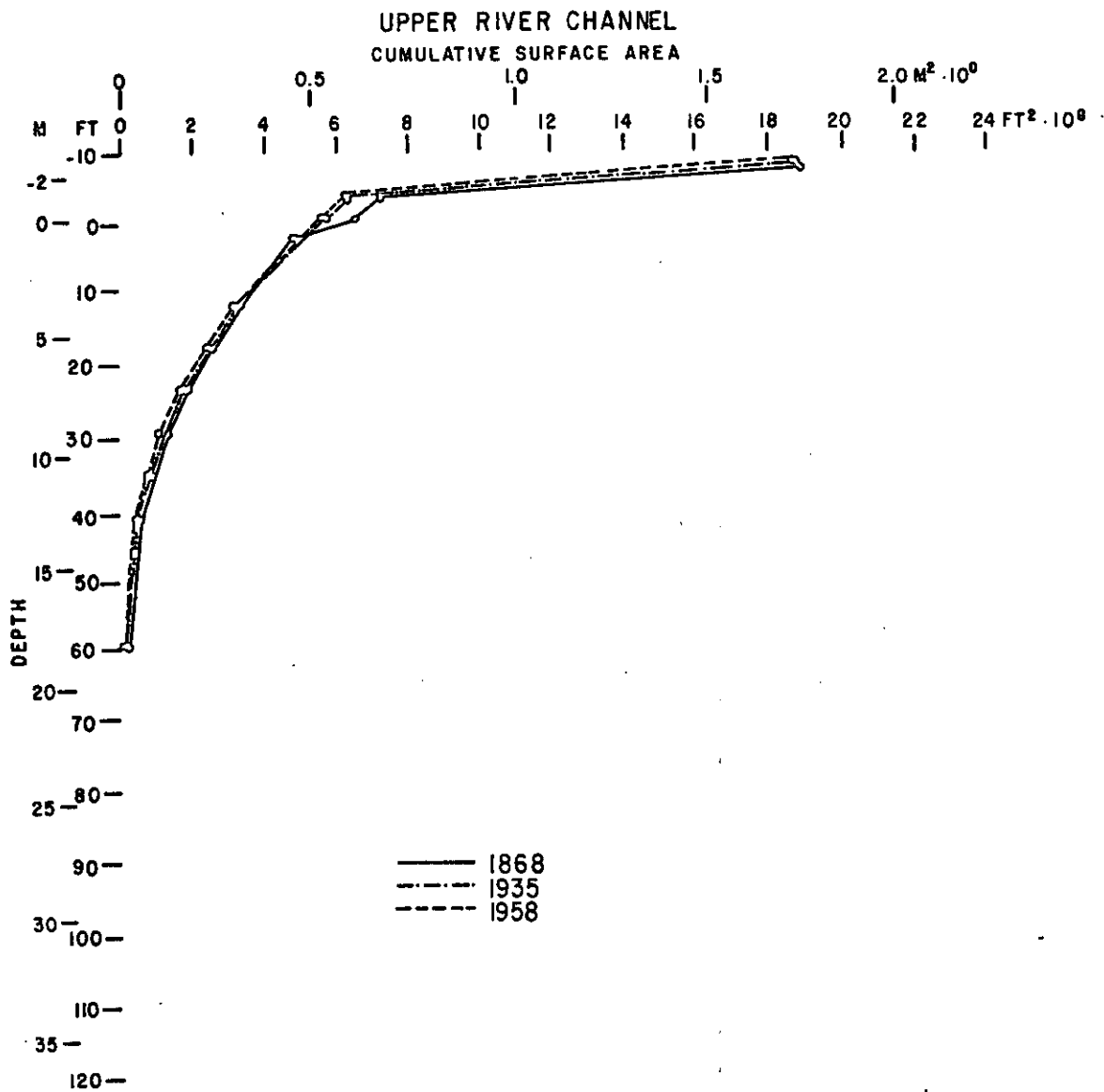


Figure 5.6 Hypsometric curve relating cumulative surface area to depth in the upper river channel in 1868, 1935, and 1958.

hypso-metric curve for the estuary as a whole and for four of the subareas. Curves for both 1868 area and 1958 areas are shown. The shift in area from the shallow subtidal depths to deeper depths between 1868 and 1958 is readily apparent. Much of the shift can be attributed to changes in the entrance, but separate examination of the south channel (also shown in Figure 5.4) and the upper river channel (Figure 5.6) show similar trends. The subareas of Baker Bay and Cathlamet Bay are filling in more uniformly, with no marked shift to relatively deeper water (Figures 5.5 and 5.7).

The same trends observed on the hypso-metric curves may also be seen in the volume figures of Tables 5.3, 5.4, and 5.5. It should be noted that the choice of the depth interval midpoint results in an overestimate of the water volume associated with each area, so these numbers should be used mostly for comparison. They indicate that there has been little change in the intertidal intervals (between -0.9 and 0.0 m) and large volume losses in all of the deeper intervals. The greatest volume losses have apparently occurred in the deepest intervals (deeper than 12.8 m) and nearly equivalent losses have occurred in the intervals deeper than 12.8 m. Somewhat less water volume has been lost from the intervals between 0.9 and 11.0 m. The intertidal water volume loss again can not be estimated from these numbers, but based on Thomas' (1983) figures it is apparent that a substantial loss in water volume has occurred in the shallow regions of the estuary.

The net effect of the area changes in the estuary has been to reduce the total area of the estuary, while shifting a larger percentage of the estuary area and water volume into deeper water. Both the total volume of the estuary and the intertidal volume of the estuary have been substantially decreased by the changes in the distribution of area among the depth regimes. One effect of the area loss has been to reduce the tidal prism significantly in historical time. A 12% loss of deep water area, coupled with additional changes in the intertidal areas (Thomas 1983), has resulted in a 10-15% reduction of the tidal prism of the estuary.

5.2.4 Volume Changes and Sedimentation Estimates

The digitized bathymetric data were used to directly calculate the volume changes in each of the subareas between the surveys. These calculations are not subject to the same errors as the area calculations because only overlapping areas from consecutive surveys were used in the calculations. Thus, although volume differences were not computed for all of the area of the estuary among all of the surveys, those numbers that were calculated contain no particular biases. The subareas which do not overlap exactly between surveys are marked with a (-) on Figure 5.2: the entrance, the south channel, and Youngs Bay. As discussed in the first part of the preceding section, the areas omitted from subsequent surveys were often newly developed land, so it is reasonable to assume that the figures generally underestimate shoaling in the estuary. The lumping of all elevations greater than 2.1 m (7 ft) above MLLW probably also serves to produce underestimates of the amount of shoaling. Furthermore, shoaling rates are calculated on the basis of the entire surveyed area in the

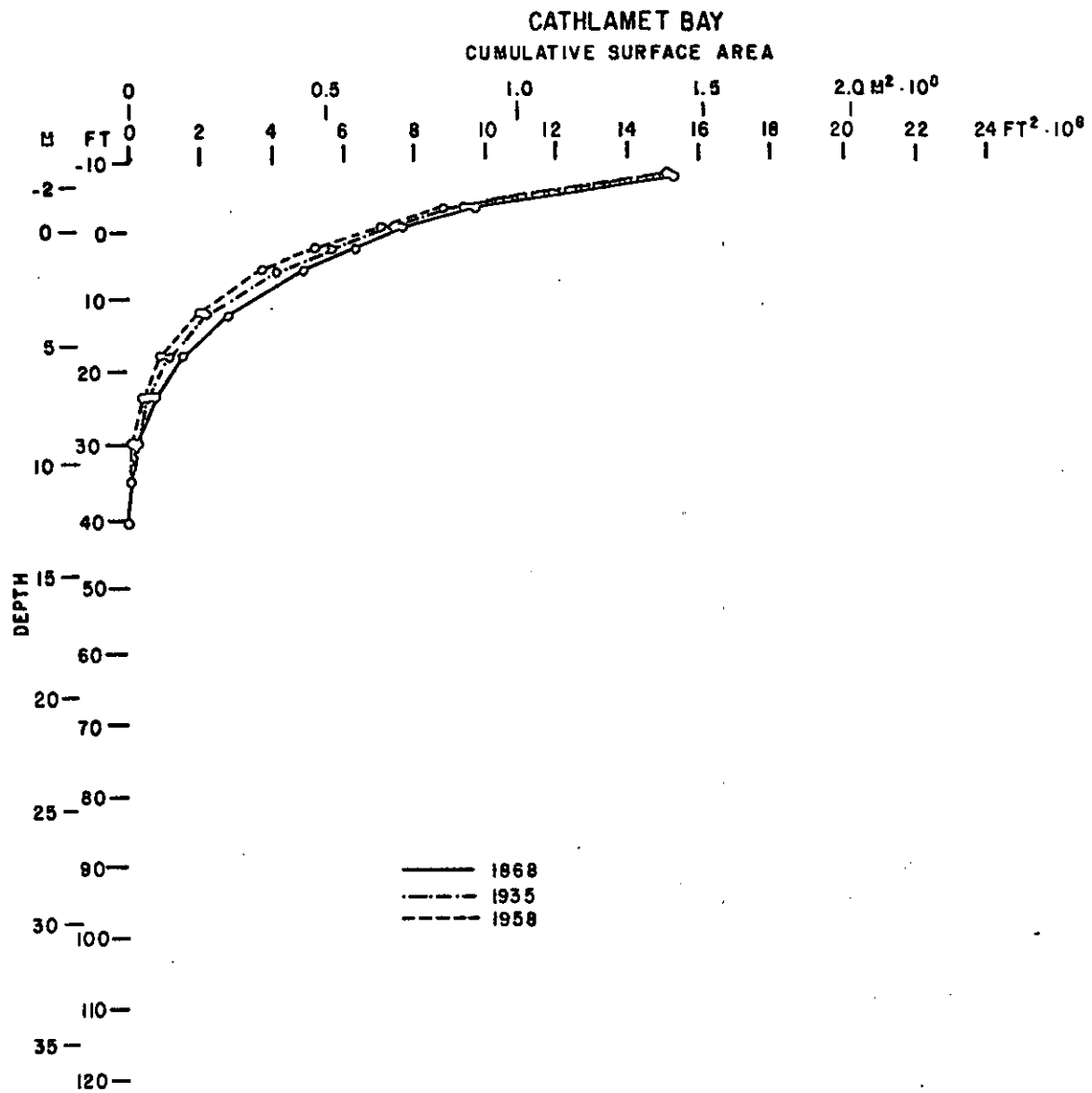


Figure 5.7 Hypsometric curve relating cumulative surface area to depth in Cathlamet Bay in 1868, 1935, and 1958.

Table 5.5. Volumes, volume changes, and sedimentation by subarea.

Estuary subarea	Volumes ⁽¹⁾ (10^6 m^3)			Volume changes (10^6 m^3)					
	1868	1935	1958	1868-1935		1935-1958		1868-1958	
				(1)	(2)	(1)	(2)	(1)	(2)
1 Entrance	2279.23	2410.03	2378.64	130.80*	-212.86	-31.39*	-33.87	99.41*	-246.73
2 Baker Bay	103.14	23.34	27.05	-79.80	90.89	3.71	-4.76	-76.09	86.13
3 Trestle Bay	9.76	3.23	1.61	-6.53	9.03	-1.62	3.96	-8.15	12.99
4 North Channel	226.25	228.56	238.40	2.31	-3.42	9.84	-5.63	12.15	-9.05
5 South Channel	379.44	391.28	413.50	11.84*	-9.96	22.22	17.64	34.06*	7.68
6 Youngs Bay	35.44	25.15	16.22	-10.29*	31.43	-8.93*	3.88	-19.22*	35.31
7 Desdemona Sands	159.57	115.31	100.82	-44.26	45.93	-14.49	12.92	-58.75	58.85
8 Mid-estuary Shoals	87.68	86.84	86.88	-0.84	1.26	0.04	-0.29	-0.80	0.97
9 Grays Bay	92.50	71.70	74.33	-20.80	23.13	2.63	-4.00	-18.17	19.13
10 Brix Bay	8.40	6.40	6.67	-2.00	6.18	0.27	-0.58	-1.73	5.60
11 Cathlamet Bay	249.33	207.87	191.31	-41.46	49.34	-16.56	26.86	-58.02	76.20
12 Lower River Channel	101.34	108.40	107.24	7.06	-7.11	-1.16	0.88	5.90	-6.23
13 Upper River Channel	311.73	303.18	291.41	-8.55	19.32	-11.77	8.24	-20.32	27.56
Estuary w/o entrance	1764.58	1571.26	1555.44	-193.32	256.02	-15.82	59.12	-209.14	315.14
Estuary total	4043.81	3981.29	3934.08	-62.52	43.16	-47.21	25.25	-109.73	68.41

(1) Based on water volume estimates.

(2) Based on bathymetric differencing; negative numbers indicate erosion, positive indicate shoaling.

*Numbers biased by unequal survey coverage (see text).

individual subareas, rather than just the intertidal area, again underestimating the rate of shoaling. Therefore, these calculations are conservative estimates of the amount of sedimentation that has occurred in the estuary during historical time.

Table 5.5 presents the water volumes of the individual subareas for each of the three survey periods. These are the water volumes calculated as the product of the depth interval midpoint and the area, and they include the inherent limitations discussed in the last section. The volume changes based on these numbers are tabulated in the successive columns, alternating with the estimates of shoaling calculated from the bathymetric differencing. Ideally, the changes in water volume and the volume of sediment accumulation or loss should be of equal magnitude and opposite sign. Except for the areas marked with an asterisk (*), which have survey coverage inconsistencies that have been discussed, there is reasonable agreement between the two methods of estimating the amount of shoaling in the estuary. The shoaling estimates based on the water volume changes are less reliable due to the overestimate of volume, especially in deep water, and the remainder of this discussion will focus on the sedimentation estimates derived from the differencing technique.

The largest volume change in sediments occurred in the entrance between 1868 and 1935, following jetty construction. Nearly 312 million m^3 of sediment was lost during this period, and another 34 million m^3 was lost in the subsequent period. However, the adjacent subareas of Trestle Bay and Baker Bay showed large gains during the early period; Trestle Bay showed an increase of 9 million m^3 and Baker Bay an increase of 91 million m^3 . In the rest of the lower estuary, Desdemona Sands showed an increase of 46 million m^3 of sediment, while the north and south channels exhibited a sediment loss of 3 and 10 million m^3 , respectively. Youngs Bay gained approximately 31 million m^3 , but overall, the losses in the entrance and the lower estuary exceeded the gains by nearly 50 million m^3 . However, gains in the upper estuary, notably Grays Bay (23 million m^3) and Cathlamet Bay (49 million m^3), were more than sufficient to offset the loss in the lower estuary, and the system as a whole gained 43 million m^3 . If the losses in the entrance region are ignored, over 256 million m^3 of sediment accumulated in the estuary.

In the subsequent period (1935 to 1958) the changes are less dramatic but nonetheless quite significant. Again, large losses of sediment occurred in the entrance region (34 million m^3). Slight losses occurred in the previously depositional subarea of Baker Bay and continued in the north channel. Trestle Bay remained depositional, and substantial accumulation occurred on Desdemona Sands (13 million m^3). The south channel became depositional, gaining nearly 18 million m^3 . Cathlamet Bay remained depositional and accumulated 27 million m^3 of sediment. The system as a whole gained 25 million m^3 . If the large losses from the entrance are not considered, the estuary gained 59 million m^3 .

Over the 90-year period, net deposition in the entire system amounted to 68 million m^3 ; losses in the entrance region amounted to

247 million m^3 ; therefore, the accumulation in the estuary (not including the entrance) totaled 315 million m^3 .

The normalized area of the various subareas has been used to calculate the rate of sediment deposition or erosion. The values appear in Tables 5.6 and Figures 5.8a, 5.8b, and 5.8c as shoaling rates in $cm\ yr^{-1}$ and are presented for the periods between each of the two surveys and for the entire 90-year period. Shoaling rates vary from a maximum of $3.33\ cm\ yr^{-1}$ (Trestle Bay between 1935 and 1958) to -1.84 (erosion in the entrance between 1868 and 1935). The highest rate of accumulation over the 90-year period also occurred in Trestle Bay ($2.43\ cm\ yr^{-1}$) and the highest erosion rate occurred in the entrance ($-1.59\ cm\ yr^{-1}$). The averages do not depend greatly on whether the 1868 area for each of the subareas or the 1958 values are used (compare in Table 5.7). The grand average for the entire system is a shoaling rate of $0.08\ cm\ yr^{-1}$; when the erosion at the entrance is ignored, the average shoaling rate for the remainder of the estuary becomes $0.49\ cm\ yr^{-1}$.

5.3 ANALYSIS OF HISTORICAL CIRCULATION PATTERNS

5.3.1 Modeling Procedure

The laterally-averaged, time-dependent circulation model described in Hamilton (1984) was used to simulate the circulation of the estuary prior to human modification. The data used to define the channels were the 1867-77 U.S. Coast Survey bathymetric surveys described in Section 5.1. The channels defined are shown in Figure 5.9; these may be compared to Figure 3.19 for the modern estuary. The grid spacing in the vertical was the same as in the modern case, and the horizontal spacing was similar.

All the available historical tidal height data (summarized in Appendix C of Jay (1984)) were used to define historical tidal conditions. In most instances, harmonic analyses were not available, and the data were tabulated as mean and diurnal range and Greenwich intervals (times of high and low water). There was considerable variability within the historical observations, because of the short and variable record lengths and because reference stations as distant as San Francisco Bay were used in reducing the raw observations, but minimal differences between present and historical tidal data were found. The same Jetty A tidal data were, therefore, used to drive the model for the historical runs as were used for the $2,000\ m^3\ sec^{-1}$ (71 kcfs) case for the modern bathymetry. These were the tides actually observed during a 10-day period in the spring of 1981 (Section 3.6.2). The model predicted tides in the upriver area for the historical runs that were nearly identical to those predicted for the comparable modern runs. River flows used were 2,000, 4,000, and $12,000\ m^3\ sec^{-1}$ (71, 141, and 424 kcfs), comparable to flows used with the modern bathymetry.

5.3.2 Changes in Transport Patterns

Perhaps the largest difference between the present and historical flows is one that is not directly portrayed by the model; the present-day estuary is less variable and has a smaller mean flow, because of the

Table 5.6. Shoaling rates.

Estuary subarea	1958 area (10 ⁶ m ²)	Shoaling (cm/yr)			1868 area (10 ⁶ m ²)	Shoaling (cm/yr)		
		1868-1935	1935-1958	1868-1958		1868-1935	1935-1958	1868-1958
1 Entrance	-172.45	-1.84	-0.98	-1.59	212.33	-1.50	-0.80	-1.29
2 Baker Bay	-59.69	2.27	-0.40	1.60	59.69	2.27	-0.40	1.60
3 Trestle Bay	5.94	2.27	3.33	2.43	5.94	2.27	3.33	2.43
4 North Channel	33.19	-0.15	-0.85	-0.30	33.19	-0.15	-0.85	-0.30
5 South Channel	69.07	-0.22	1.28	0.12	70.75	-0.21	1.25	0.12
6 Youngs Bay	40.07	1.17	0.48	0.98	52.96	0.89	0.37	0.74
7 Desdemona Sands	34.35	2.00	1.88	1.90	34.35	2.00	1.88	1.90
8 Mid-estuary Shoals	27.17	0.07	-0.05	0.04	27.17	0.07	-0.05	0.04
9 Grays Bay	33.49	1.03	-0.60	0.63	33.49	1.03	-0.60	0.63
10 Brix Bay	44.07	0.21	-0.07	0.14	44.07	0.21	-0.07	0.14
11 Cathlamet Bay	143.00	0.51	0.94	0.59	143.00	0.51	0.94	0.59
12 Lower River Channel	29.71	-0.36	0.15	-0.23	29.71	-0.36	0.15	-0.23
13 Upper River Channel	175.59	0.16	0.23	0.17	175.59	0.16	0.23	0.17
	Area Totals	Average shoaling rates (unweighted)			Area Totals	Average shoaling rates (unweighted)		
Estuary w/o entrance	695.34	0.75	0.53	0.67	709.91	0.72	0.52	0.65
Estuary total	867.79	0.55	0.41	0.50	922.24	0.55	0.41	0.50

Table 5.7. Average shoaling rates based on 1868 estuary area (cm yr^{-1}).

	1868-1935	1935-1958	1868-1958
Excluding entrance	.54	.36	.49
Total	.07	.12	.08

Average shoaling rates based on 1958 estuary area (cm/yr)

	1868-1935	1935-1958	1868-1958
Excluding entrance	.55	.37	.50
Total	.21	.13	.09

Estimated time (years) to fill the estuary, based on volume below MLLW in 1958 and above rates (1868/1958)

Excluding entrance	800	(average depth: ~4 m)
Total	7,778	(average depth: ~7 m)

Note: would be higher if based on estuary area deeper than -0.9 m.

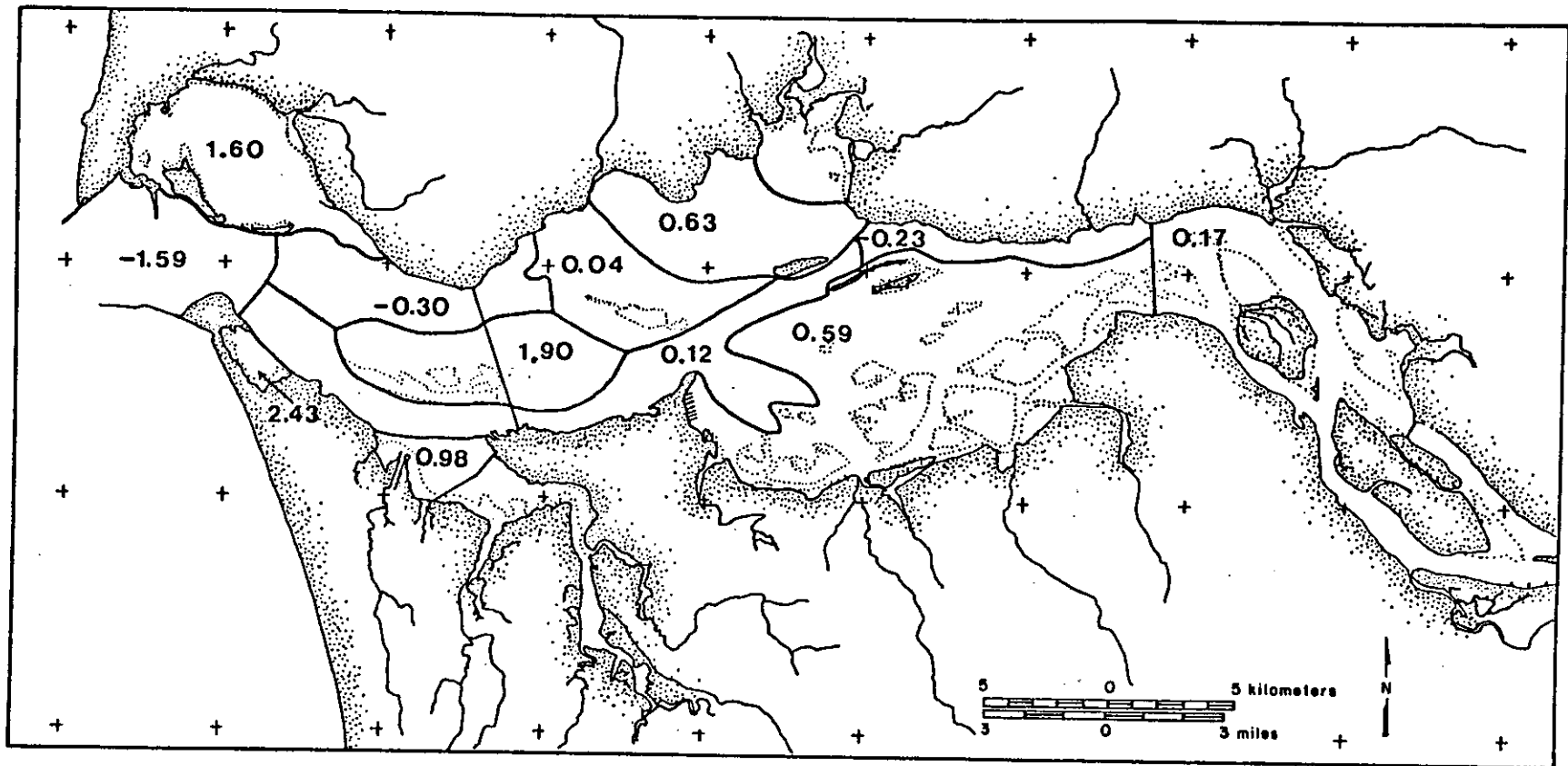


Figure 5.8a. Shoaling rates (cm yr^{-1}) between 1868 and 1935.

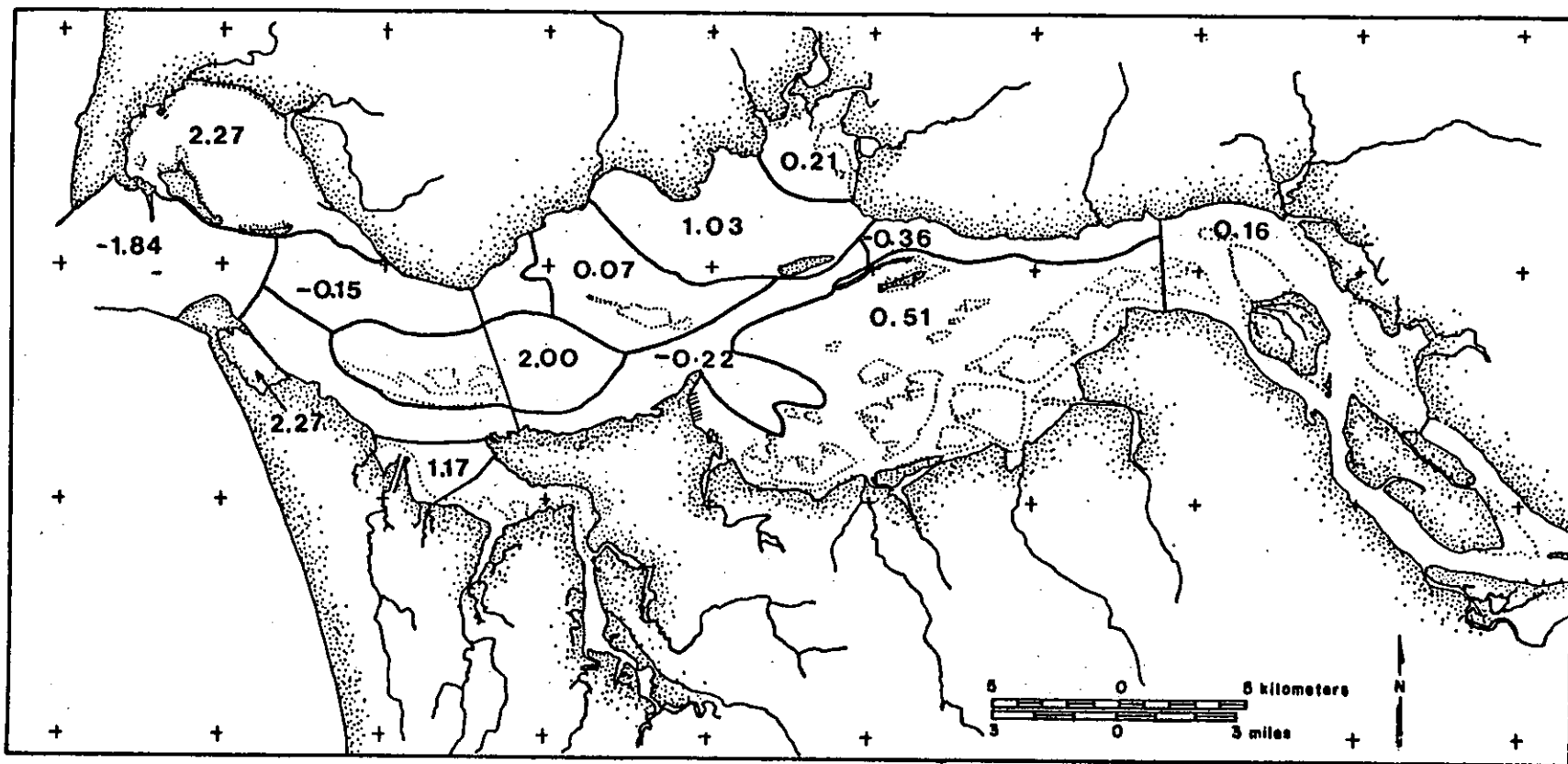


Figure 5.8b. Shoaling rates (cm yr⁻¹) between 1935 and 1958.

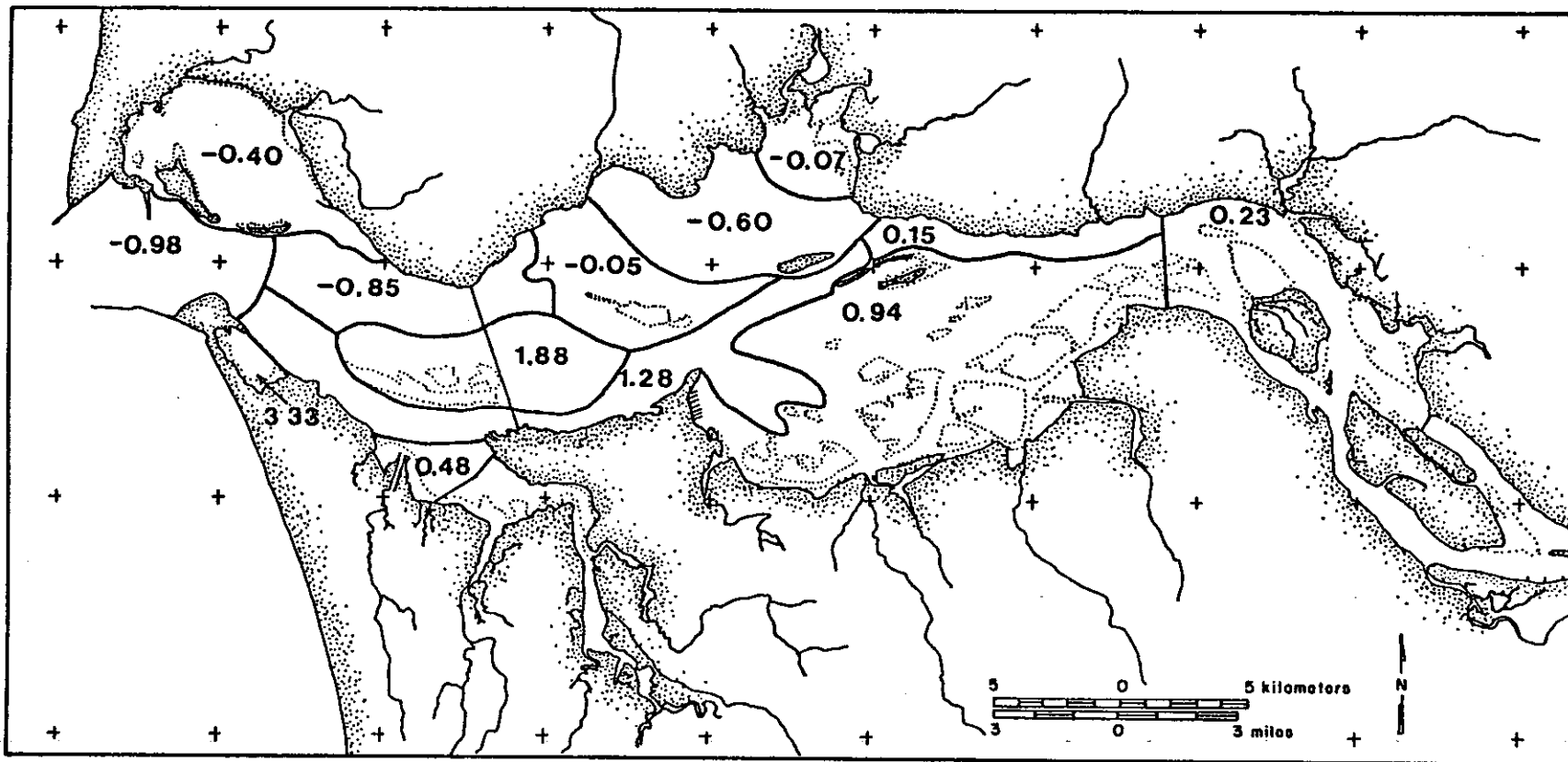


Figure 5.8c. Shoaling rates (cm yr^{-1}) for the entire 90 year interval (1868-1958).

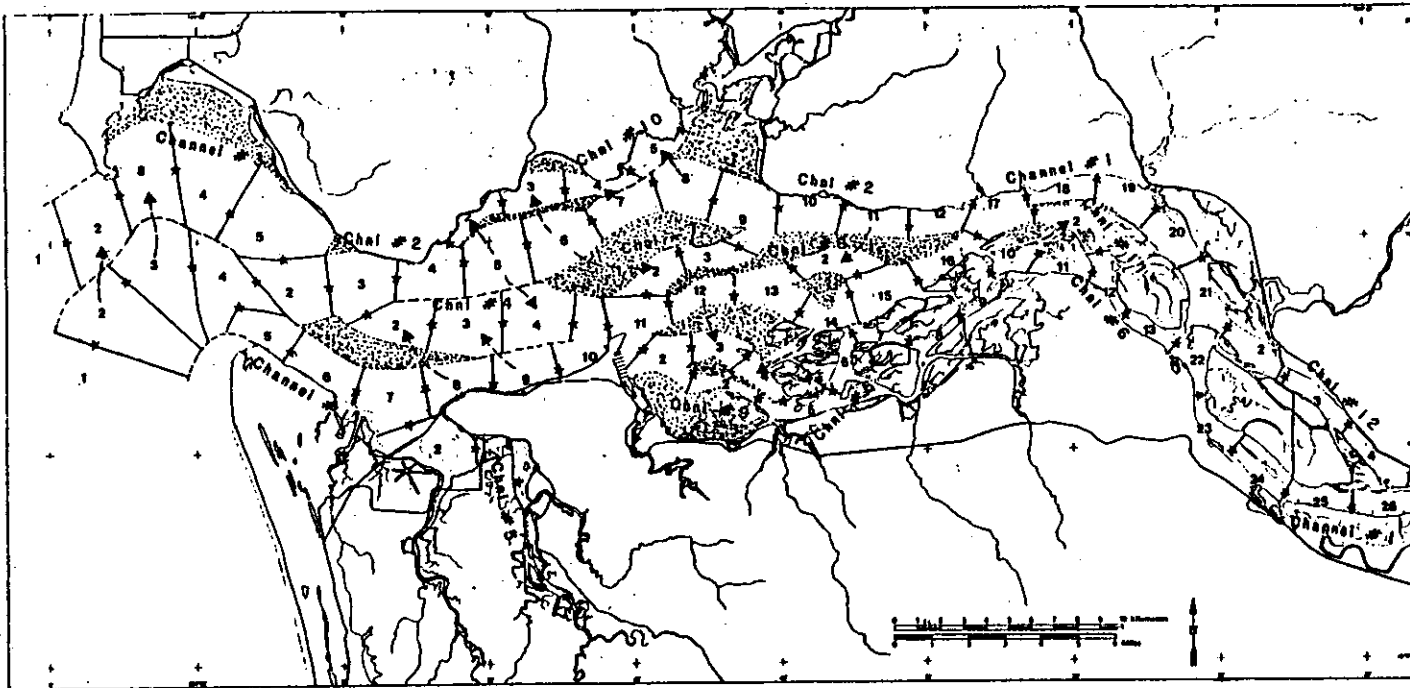


Figure 5.9. Model schematization of the 1868 estuary.

diversion and regulation of freshwater flow (described in Section 2.2). Modern river flows rarely exceed 600 kcfs ($17,000 \text{ m}^3 \text{ sec}^{-1}$) or fall below 100 kcfs ($2,830 \text{ m}^3 \text{ sec}^{-1}$), whereas such conditions probably occurred in most years before flow regulation by the dams. Despite the elimination of extreme low-flows, the residence time of water in the river has been increased because of storage of water in reservoirs. This has increased river water temperatures during the summer. The major freshets (e.g. 1894 and 1948) that have really large impacts, as judged by the energy budget (Section 3.5), have been totally eliminated. Flow processes internal to the 1868 estuary also enhanced the variability over that of the modern estuary.

One of the most striking historical changes that is portrayed by the model is the difference in the distribution of transport; dredging/dredged material disposal and pile dikes have concentrated flow in the navigation channel, depriving other parts of the estuary of flow and changing the balance between flood and ebb flows in the north and south channels. This is demonstrated in Figures 5.10 to 5.15 which show flood, ebb, and mean transports as predicted by the model for the historical and modern bathymetry. While the tides used to generate Figures 5.10 and 5.11 are somewhat different than those for Figures 5.13 and 5.14, they are similar enough that direct comparisons may be made between the historical and modern cases. Comparing Figures 5.11 and 5.14, it is evident that ebb flows are generally stronger in the south channel at present (Figure 5.11) than in 1868 (Figure 5.14). This has been accomplished by diversion of the ebb flow away from the north channel and peripheral channels. The distribution of flood tide flows (Figures 5.10 and 5.13) has been much less affected. The result is that flow in the south channel is now far more ebb-oriented (Section 3.8) than in 1868 and flow in the north channel is less so.

The mean flow plots (Figures 5.12 and 5.15) summarize these changes. In 1868 (Figure 5.15), strong ebb flows occurred in Cathlamet Channel, Clifton Channel, and Cordell Channel in the northern part of Cathlamet Bay. Flow has been diverted from all of these areas, the most obvious cases being the total blocking of the Cordell Channel by the Snag Island Jetty in 1893 and the diversion of riverflow away from Grays Bay by construction of Rice Island and the pile dikes at Harrington Point. Much more flow also crossed the shoals off Astoria in 1868, because these shoals were generally deeper at that time.

It was demonstrated in Section 5.2 that the tidal prism of the estuary decreased by about 10-15% between 1868 and 1958. The tidal transports in Figures 5.10 and 5.11 are, accordingly, smaller than for the historical case (Figures 5.13 and 5.14), but this is difficult to discern, because of the change in distribution of the transports. The change in the distribution of depths (the hypsometric curve) discussed in Section 5.2 has also influenced the circulation; it can be seen in Figure 5.16 that the channels of the lower estuary are now deeper and greater in cross-section than were the corresponding channels in 1868. Previously submerged flats are now shallower and, in some cases, have been filled. The model assumes that the flow is conveyed in the channels and that the flats are only storage areas. Because more flow was conveyed in channels of lesser cross-section, the model predicts

that current velocities for comparable tidal ranges were greater in 1868.

The validity of the assumption that most of the flow was (and is) conveyed in the channels is clearly critical. Two arguments can be advanced to show that this assumption is a good approximation for the present bathymetry. First, the distribution of mean transport calculated by the laterally-averaged model (Figures 5.10 to 5.12) is very similar to that calculated for the same flow conditions by the vertically-integrated model (Hamilton 1984), even though the latter does not confine flow to the channels (Figures 5.17a, b, and c). (Note that, in some cases, the channels of Figure 5.12 are two grid points wide in Figures 5.17a,b,c.) Second, the laterally-averaged model underestimates, rather than overestimates, current speeds in the wider channels. This occurs because the current meters generally measure the flow near the center of the channel, but the model calculates the average flow over the entire width of the channel. If, however, the model overestimated the fraction of the the total transport conveyed in the channel, speeds predicted by the model would tend to be too large, rather than too small. We cannot directly test the hypothesis that most of the flow was conveyed in the channels in the 1868 estuary. The 1868 estuary was less channelized than the present system, and it is possible that more of the flow was conveyed by areas considered in the model to be storage areas. This remains one of the uncertainties in attempting to model circulation in the 1868 estuary.

5.3.3 Changes in Tidal Currents, Mean Flow, and Salinity Distribution

Differences in circulation between the modern and 1868 cases may be further evaluated by comparing model predictions for minimum, maximum, and mean salinity and mean flow for the $4,000 \text{ m}^3 \text{ sec}^{-1}$ case (141 kcfs) for spring and neap tides for the two time periods. Figures 5.15 to 5.23 for the south channel and Figures 5.30 to 5.35 for the north channel for the 1868 bathymetry may be compared to the analogous plots for fall 1980 (Figures 5.24 to 5.29 and 5.36 to 5.41).

One major difference between the modern and 1868 estuary is the greater salinity intrusion into the 1868 estuary for all flow conditions. The model predicts that mean salinity intrusion in 1868 was considerably larger, despite the decrease in mean flow in the modern estuary. Maximum salinity intrusion was certainly greater in 1868, because minimum flows were lower then (Section 2.2). The greater salinity intrusion is particularly prominent in the south channel, because the ebb flows are smaller there with the 1868 bathymetry. The excursion of salinity contours in both channels is also substantially larger in the 1868 case than at present. These differences occur despite the shallower channel depths and are believed to be a result of the greater tidal currents in the 1868 case. This further confirms the conclusion of Sections 3.1 and 3.8, that the major factor maintaining salinity in the estuary is the tidal currents working on the gradient. Were density currents the primary factor maintaining salinity intrusion, the shallower controlling depths of the channels in 1868 would have severely limited salinity intrusion, because the strength of the density current varies with the cube of the depth (Hamilton and Rattray 1978).

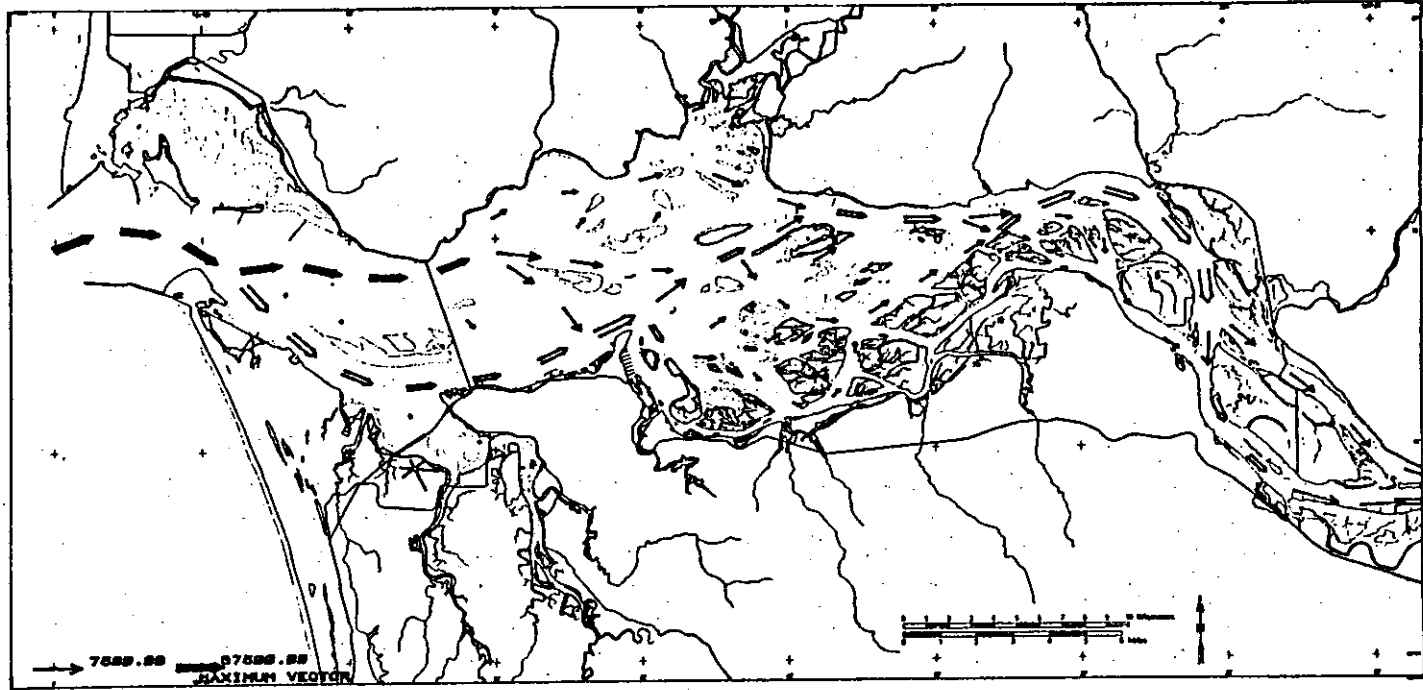


Figure 5.10. Flood tide transport, 1980 estuary, $4000 \text{ m}^3 \text{ sec}^{-1}$, neap tide.

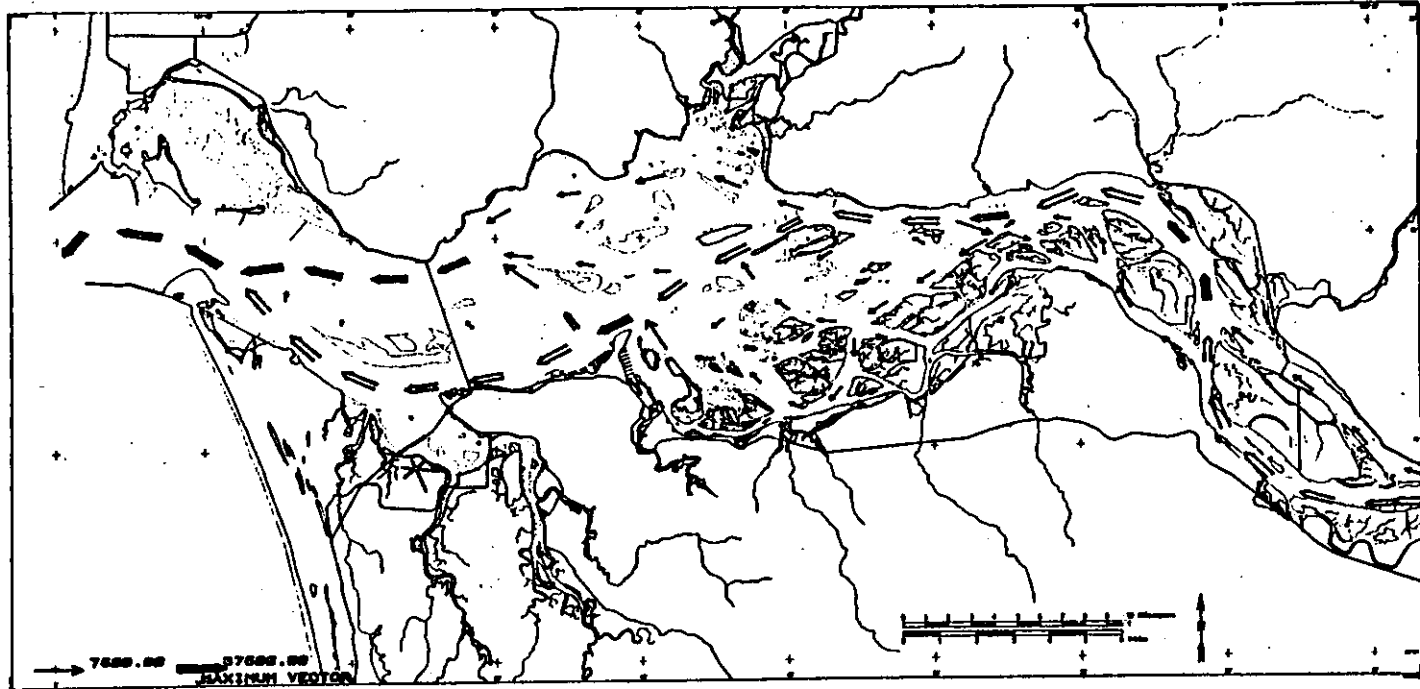


Figure 5.11. Ebb tide transport 1980 estuary, $4000 \text{ m}^3 \text{ sec}^{-1}$, neap tide.

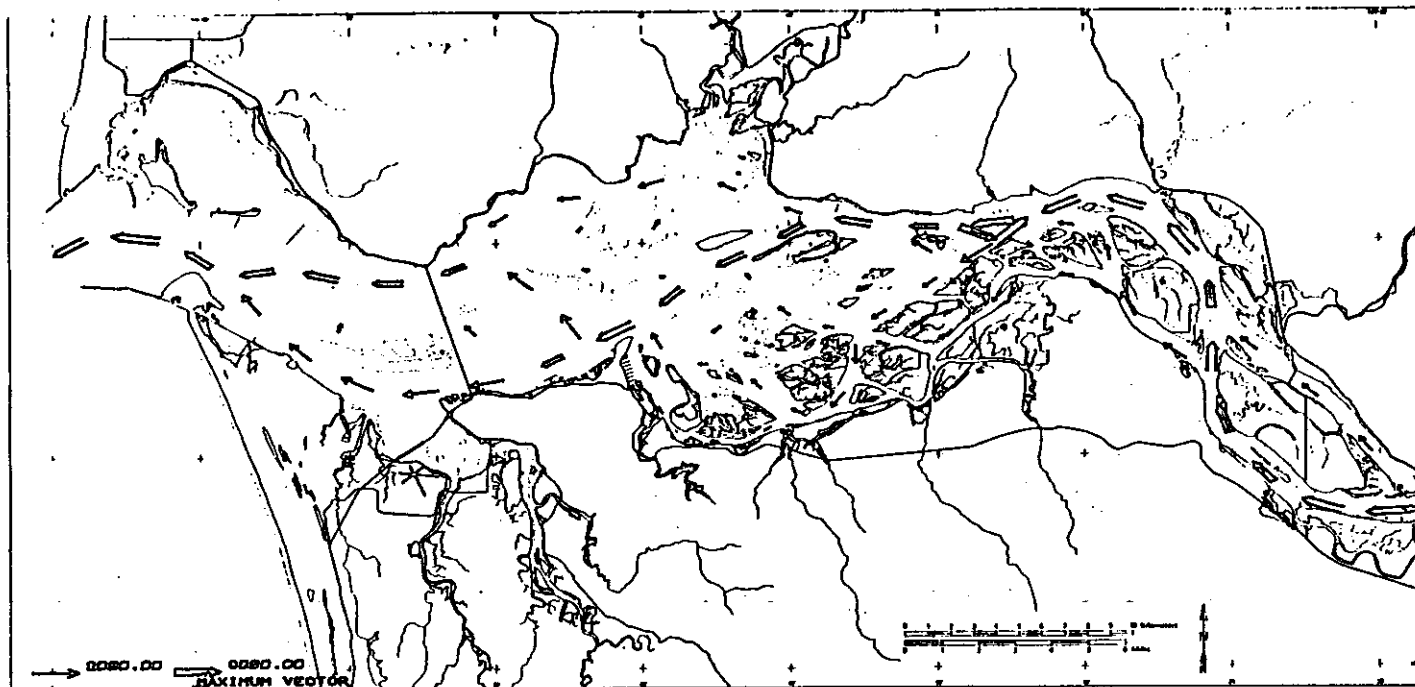


Figure 5.12. Mean transport in the 1980 estuary, $4000 \text{ m}^3 \text{ sec}^{-1}$, neap tide.

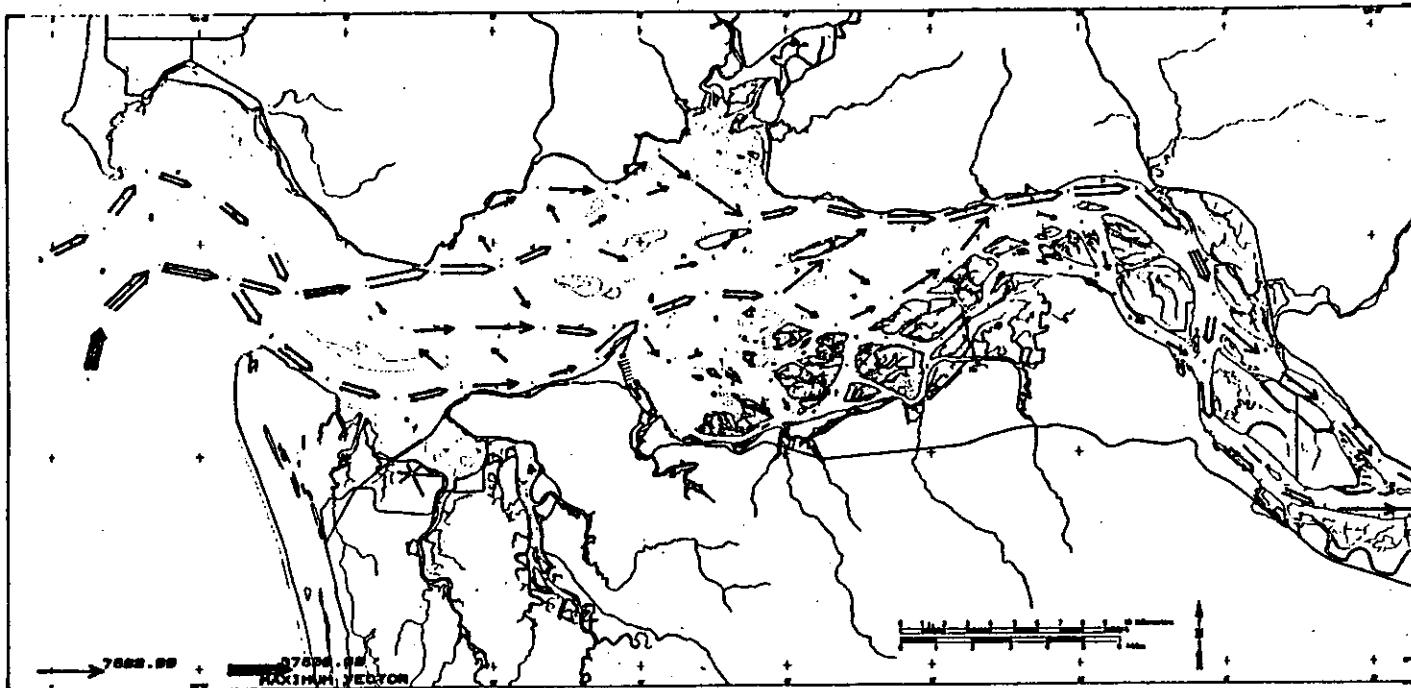


Figure 5.13. Flood tide transport, 1868 estuary, $4000 \text{ m}^3 \text{ sec}^{-1}$, neap tide.

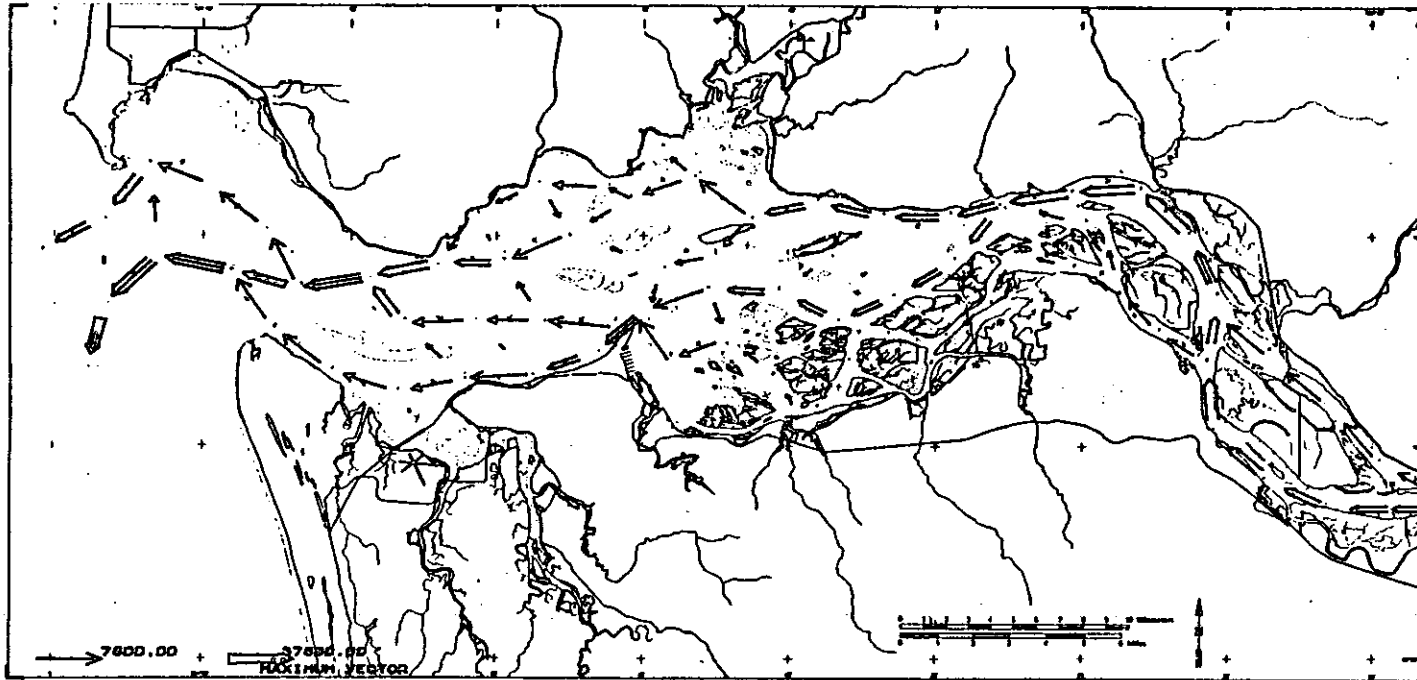


Figure 5.14. Ebb tide transport, 1868 estuary, $4000 \text{ m}^3 \text{ sec}^{-1}$, neap tide. Note ebb tide predominance in the north channel and substantial flows across the mid-estuary flats.

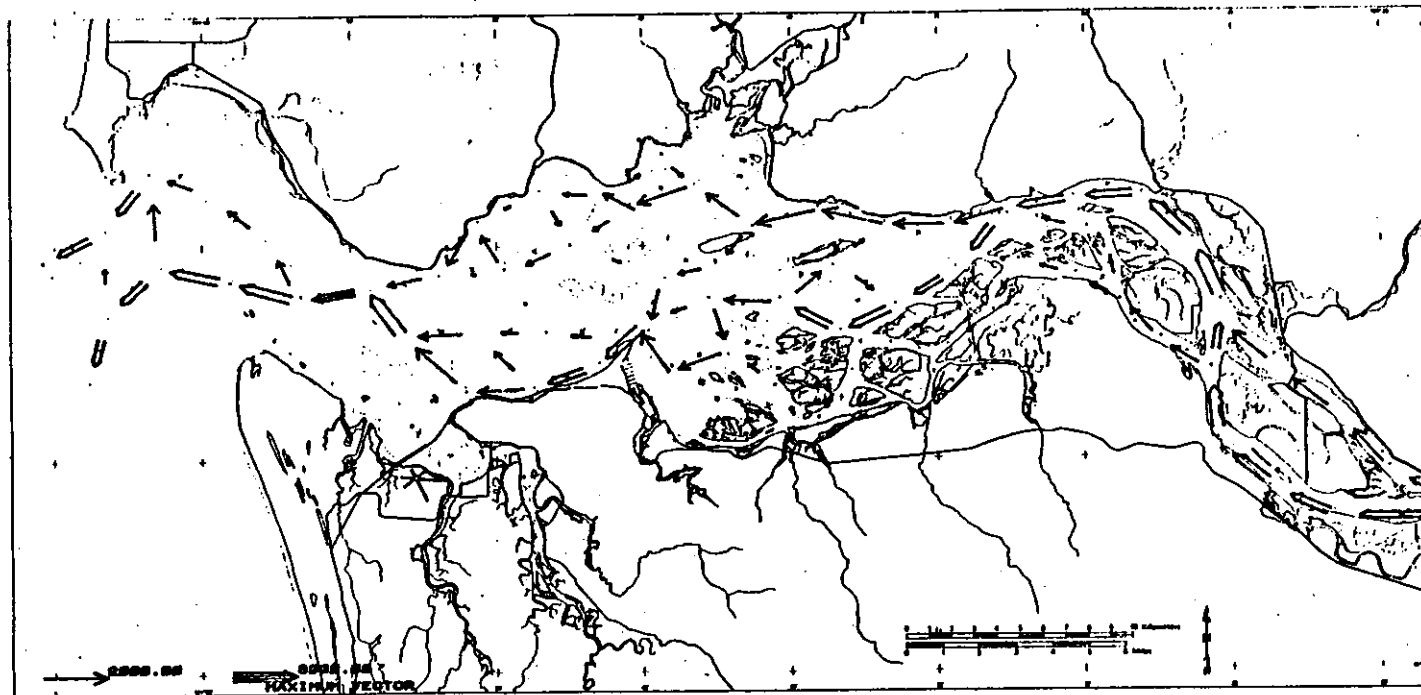


Figure 5.15. Mean transport in the 1868 estuary, neap tide $4000 \text{ m}^3 \text{ sec}^{-1}$. Note large mean flow in the north channel, through Grays Bay.

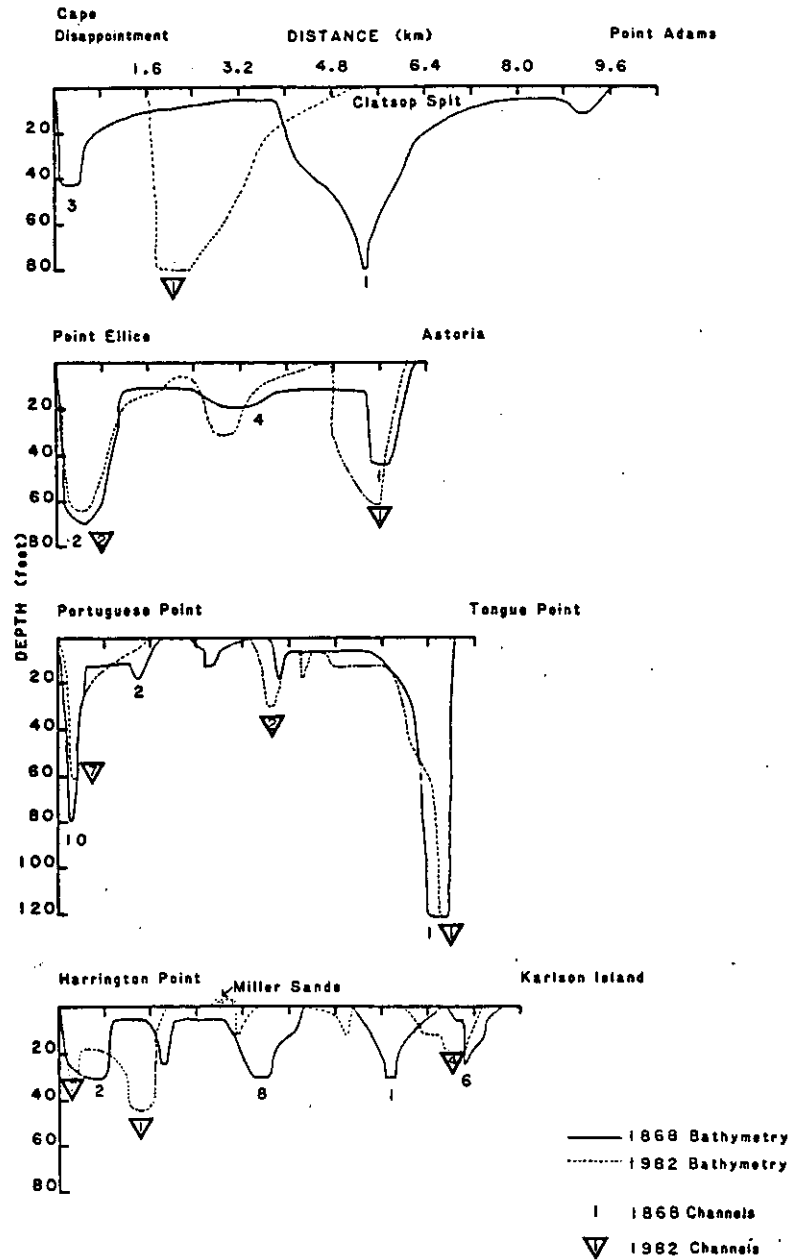


Figure 5.16. Channel cross-sections; 1860 and 1980 channels in the lower estuary (upper two sections) had smaller cross-sections in 1868 than in 1980.

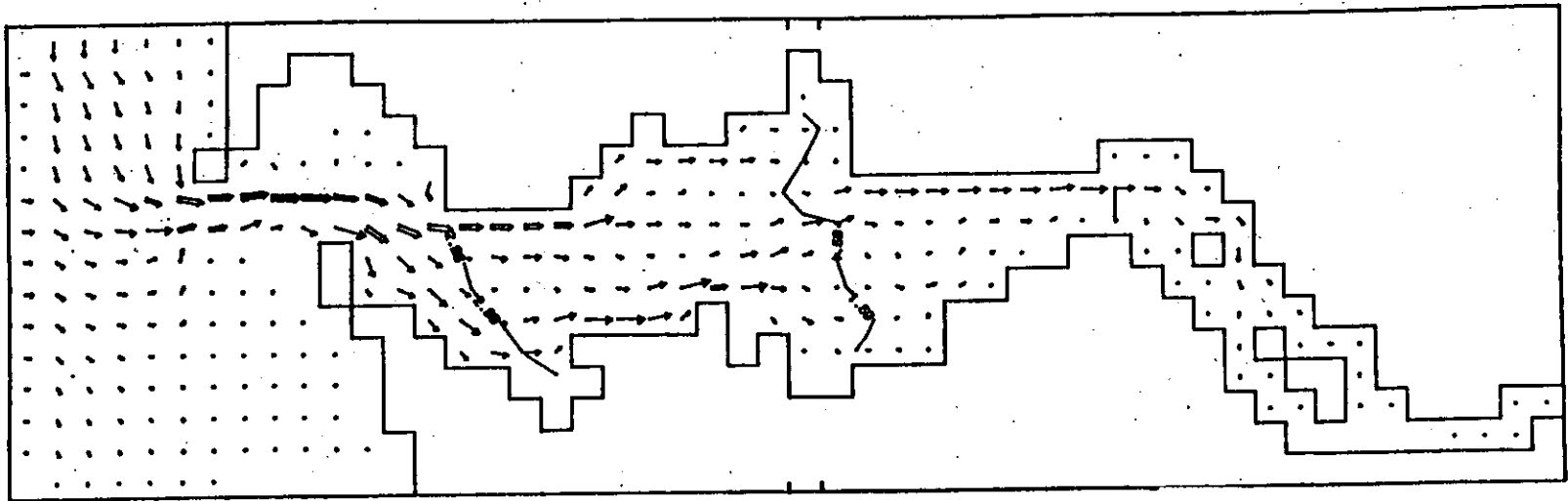


Figure 5.17a. Flood-tide volume transport in the two-dimensional, vertically-integrated model of Hamilton (1984). The distribution of transport is similar to that in Figure 5.10.

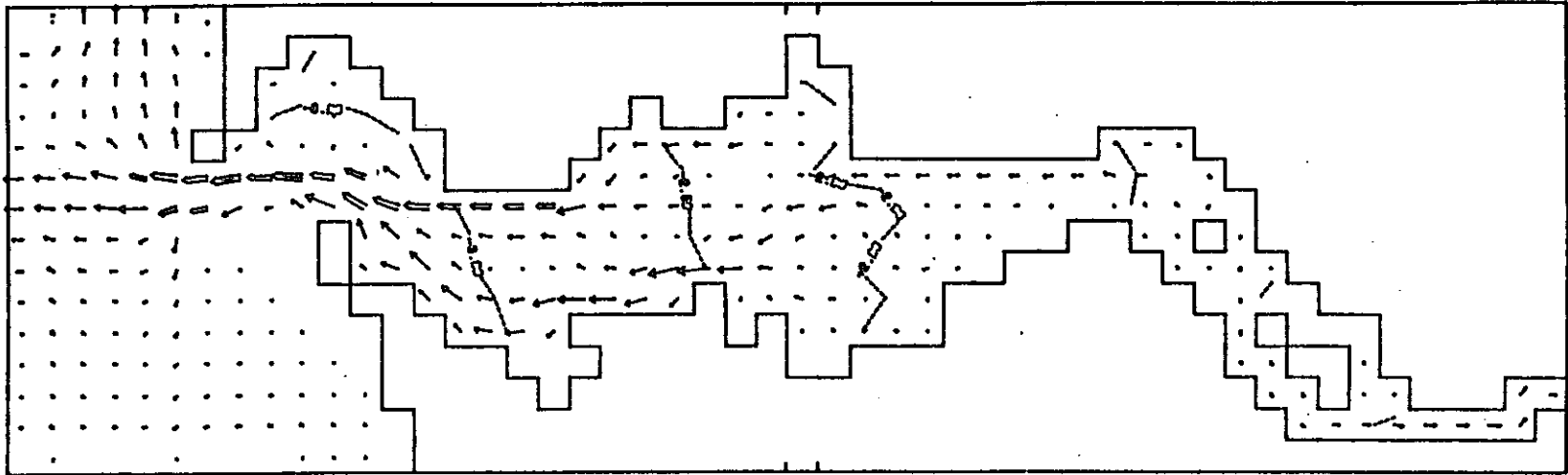
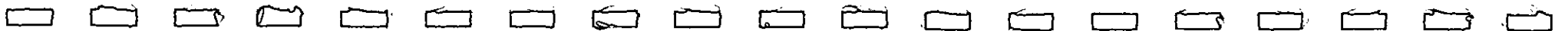


Figure 5.17b. Ebb-tide volume transport in the two-dimensional, vertically-integrated model of Hamilton (1984). The distribution of transport is similar to that in Figure 5.11.



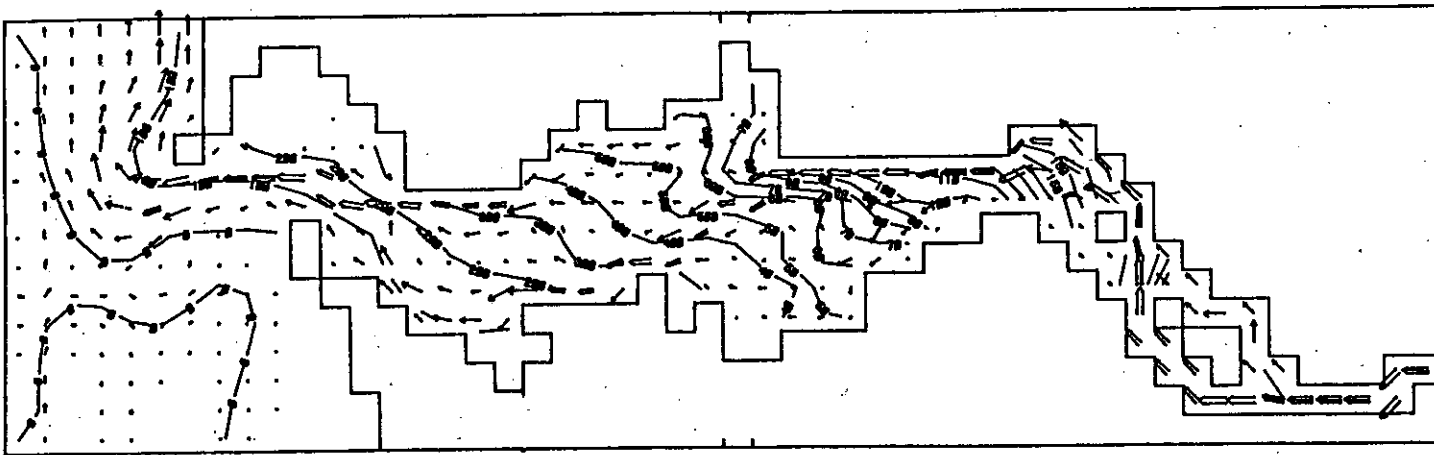


Figure 5.17c. Mean volume transport in the two-dimensional, vertically-integrated model of Hamilton (1984). The distribution of transport is similar to that in Figure 5.12.

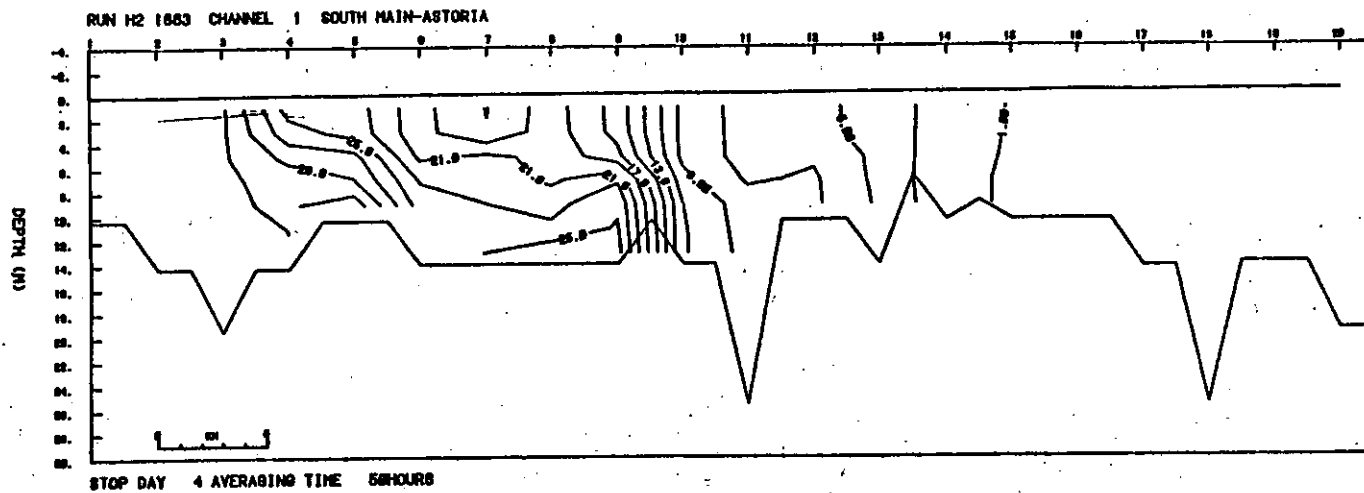


Figure 5.19. 1868 estuary, south channel, $4000 \text{ m}^3 \text{ sec}^{-1}$, neap tide, maximum salinity.

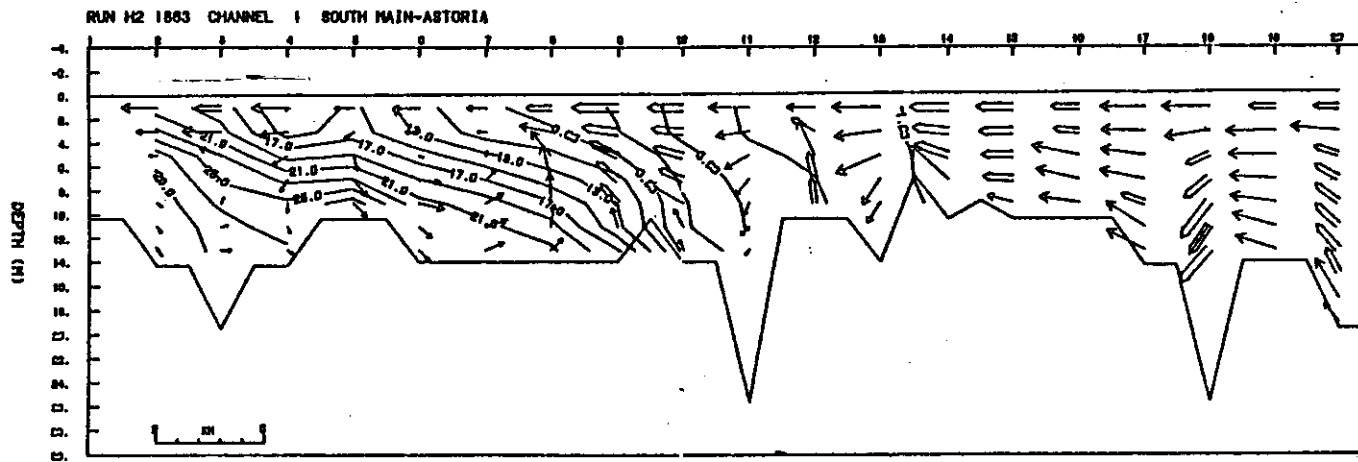


Figure 5.20. 1868 estuary, south channel, $4000 \text{ m}^3 \text{ sec}^{-1}$, neap tide, mean salinity and currents.

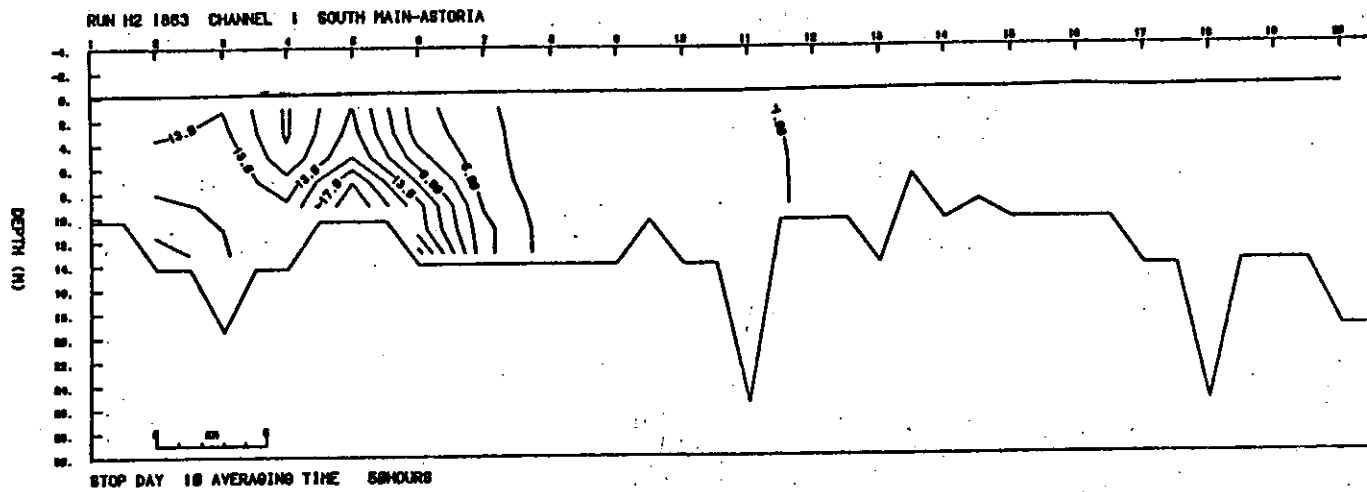


Figure 5.21. 1868 estuary, south channel, $4000 \text{ m}^3 \text{ sec}^{-1}$, spring tide, minimum salinity.

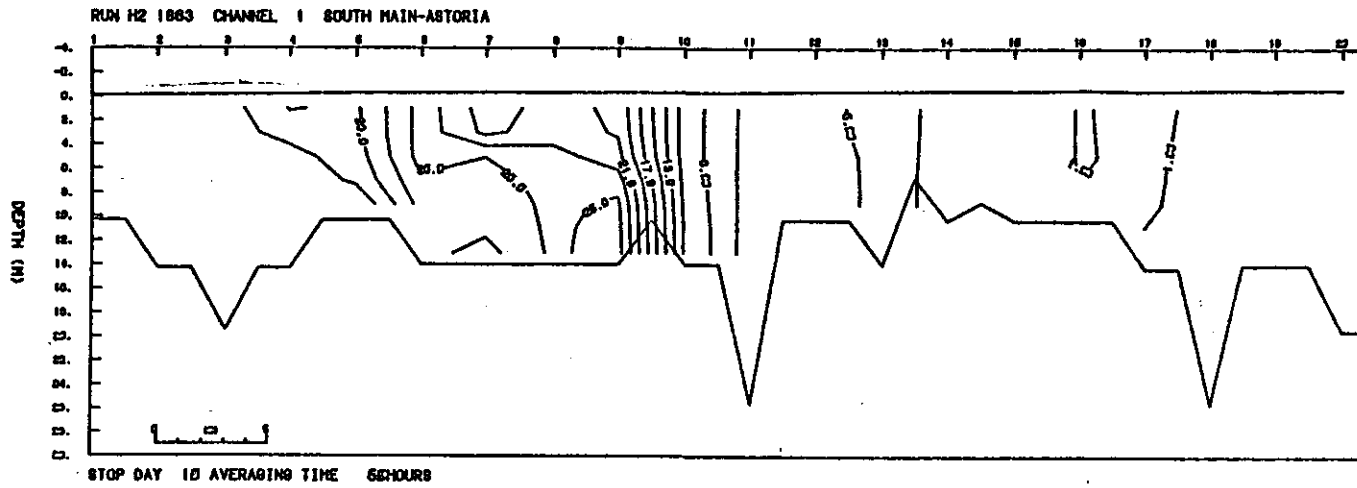


Figure 5.22. 1868 estuary, south channel, $4000 \text{ m}^3 \text{ sec}^{-1}$, spring tide, maximum salinity.

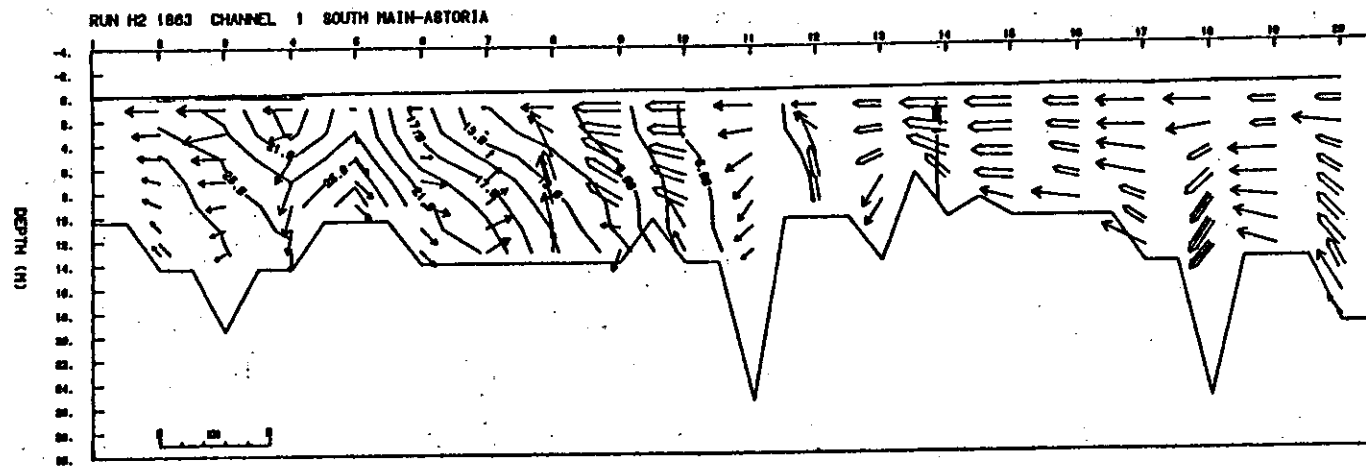


Figure 5.23. 1868 estuary, south channel, $4000 \text{ m}^3 \text{ sec}^{-1}$, spring tide, mean salinity and currents.

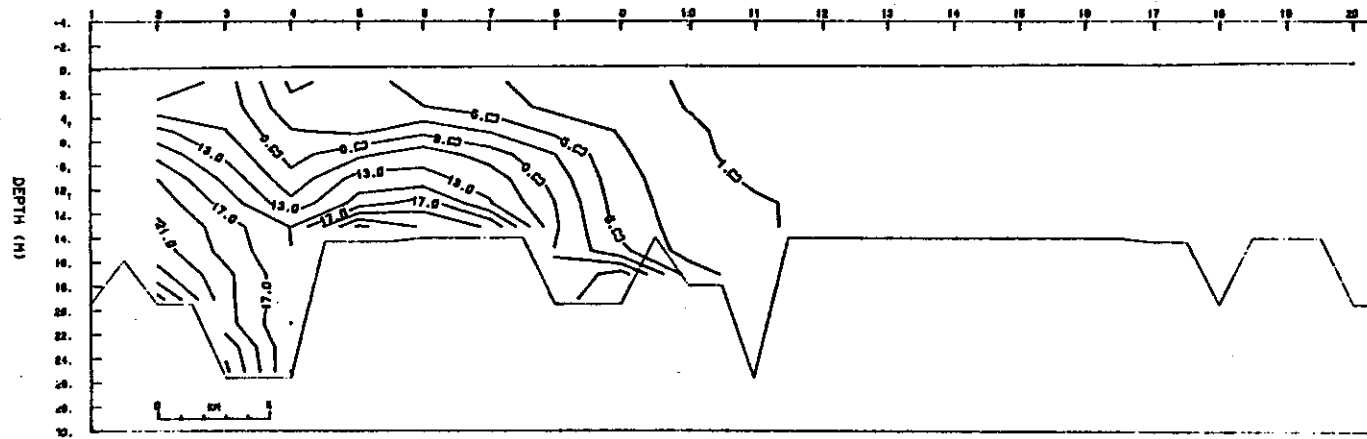


Figure 5.24. 1980 estuary, south channel, $4000 \text{ m}^3 \text{ sec}^{-1}$, neap tide, minimum salinity.

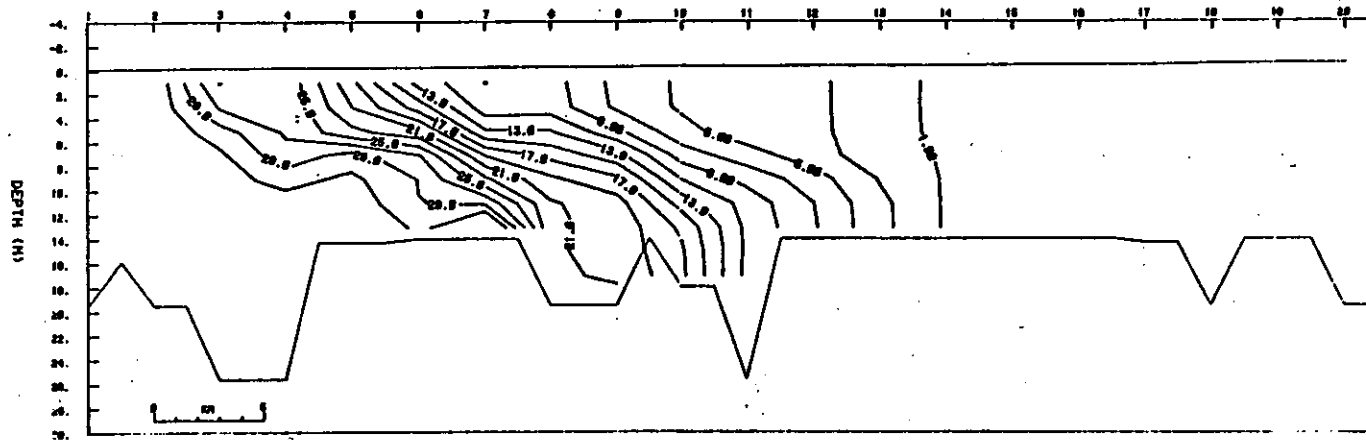


Figure 5.25. 1980 estuary, south channel, $4000 \text{ m}^3 \text{ sec}^{-1}$, neap tide, maximum salinity.

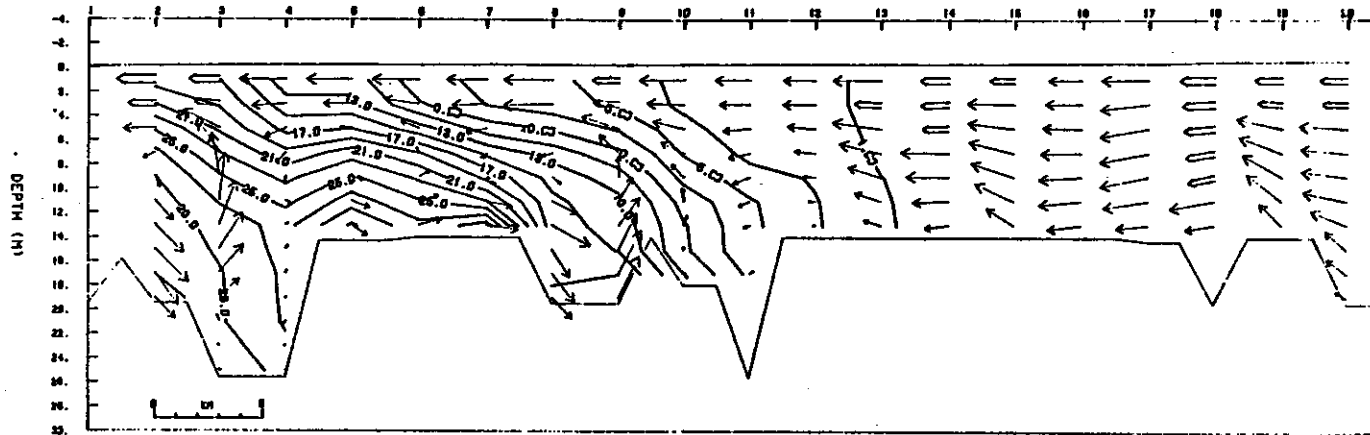


Figure 5.26. 1980 estuary, south channel, $4000 \text{ m}^3 \text{ sec}^{-1}$, neap tide, mean salinity and currents.

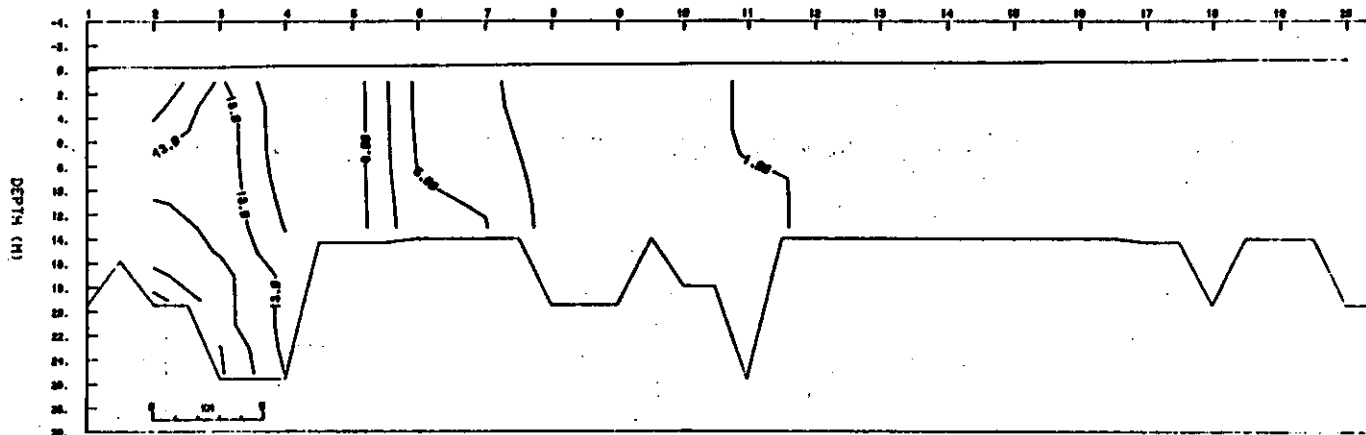


Figure 5.27. 1980 estuary, south channel, $4000 \text{ m}^3 \text{ sec}^{-1}$, spring tide, minimum salinity.

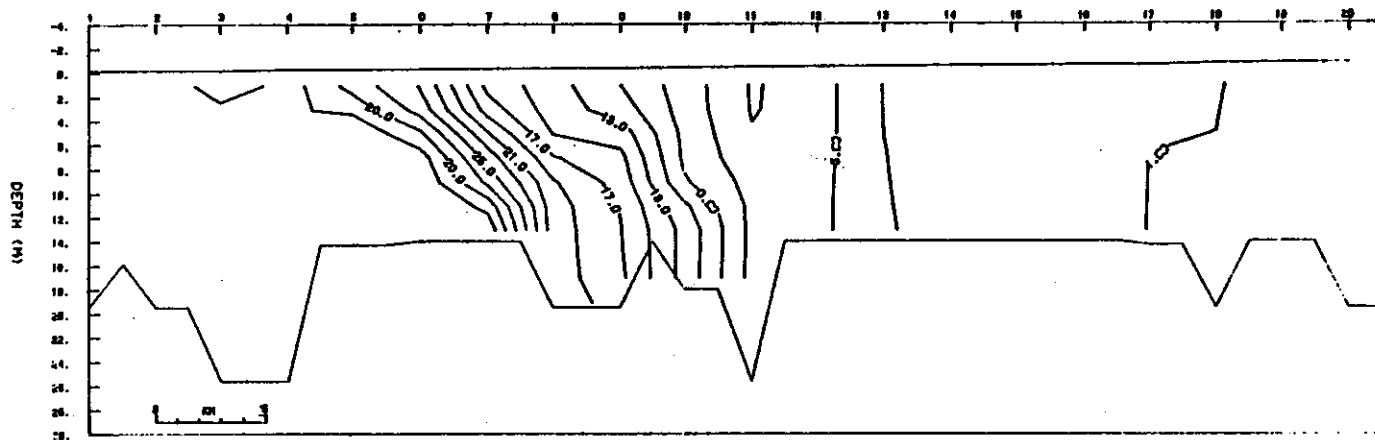


Figure 5.28. 1980 estuary, south channel, $4000 \text{ m}^3 \text{ sec}^{-1}$, spring tide, maximum salinity.

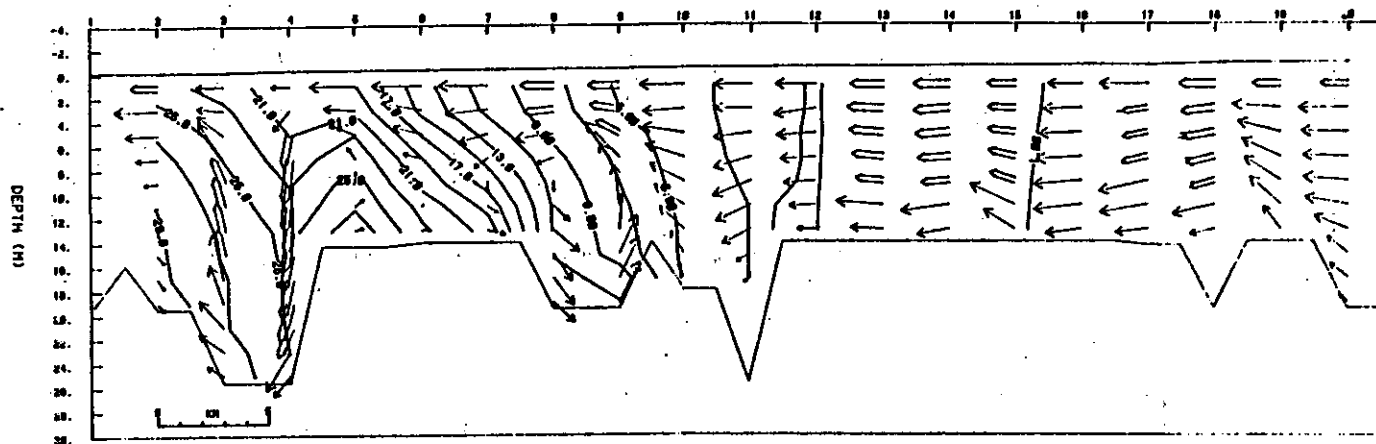


Figure 5.29. 1980 estuary, south channel, $4000 \text{ m}^3 \text{ sec}^{-1}$, spring tide, mean salinity and currents.

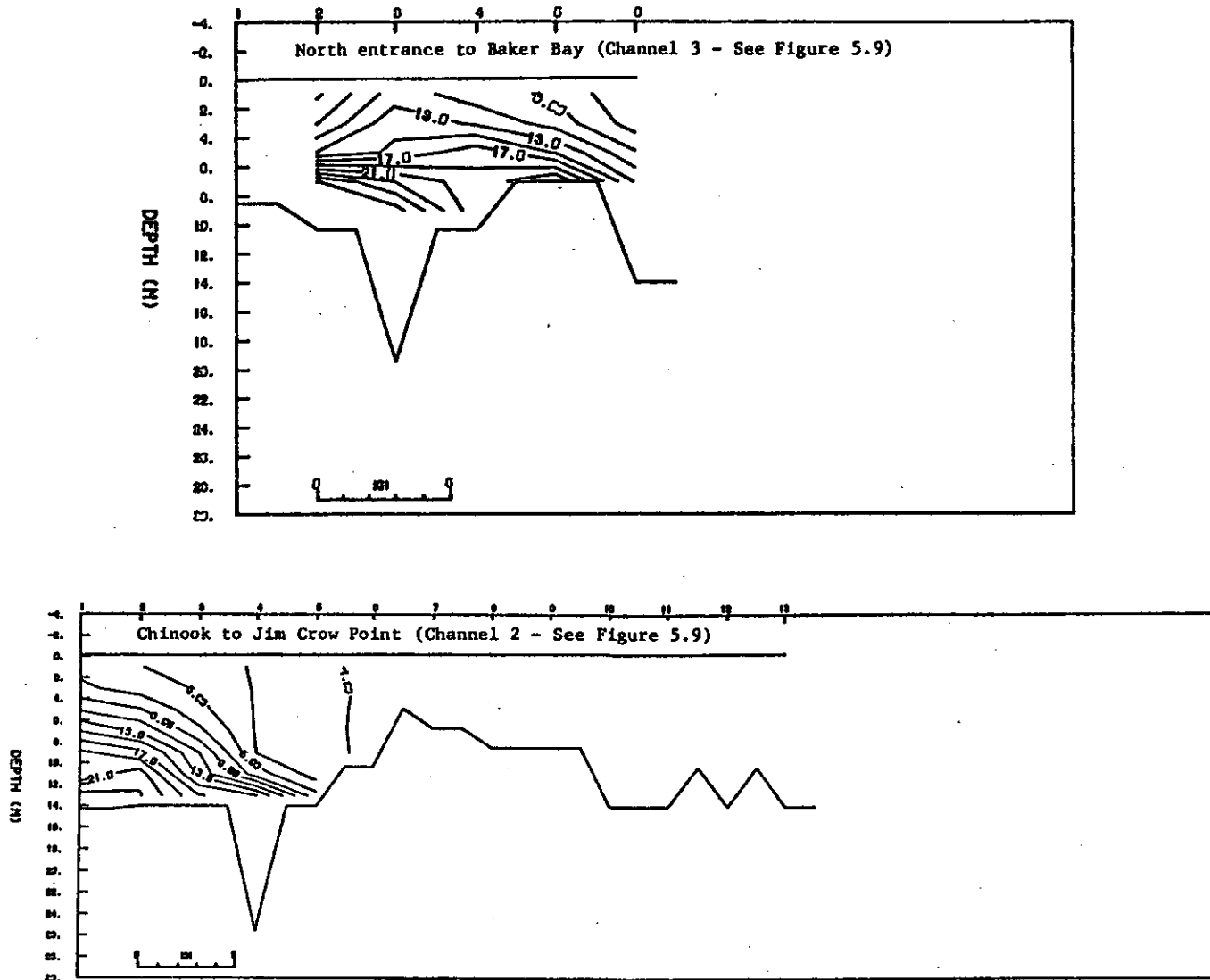


Figure 5.30. 1868 estuary, north channel, $4000 \text{ m}^3 \text{ sec}^{-1}$, neap tide, minimum salinity.

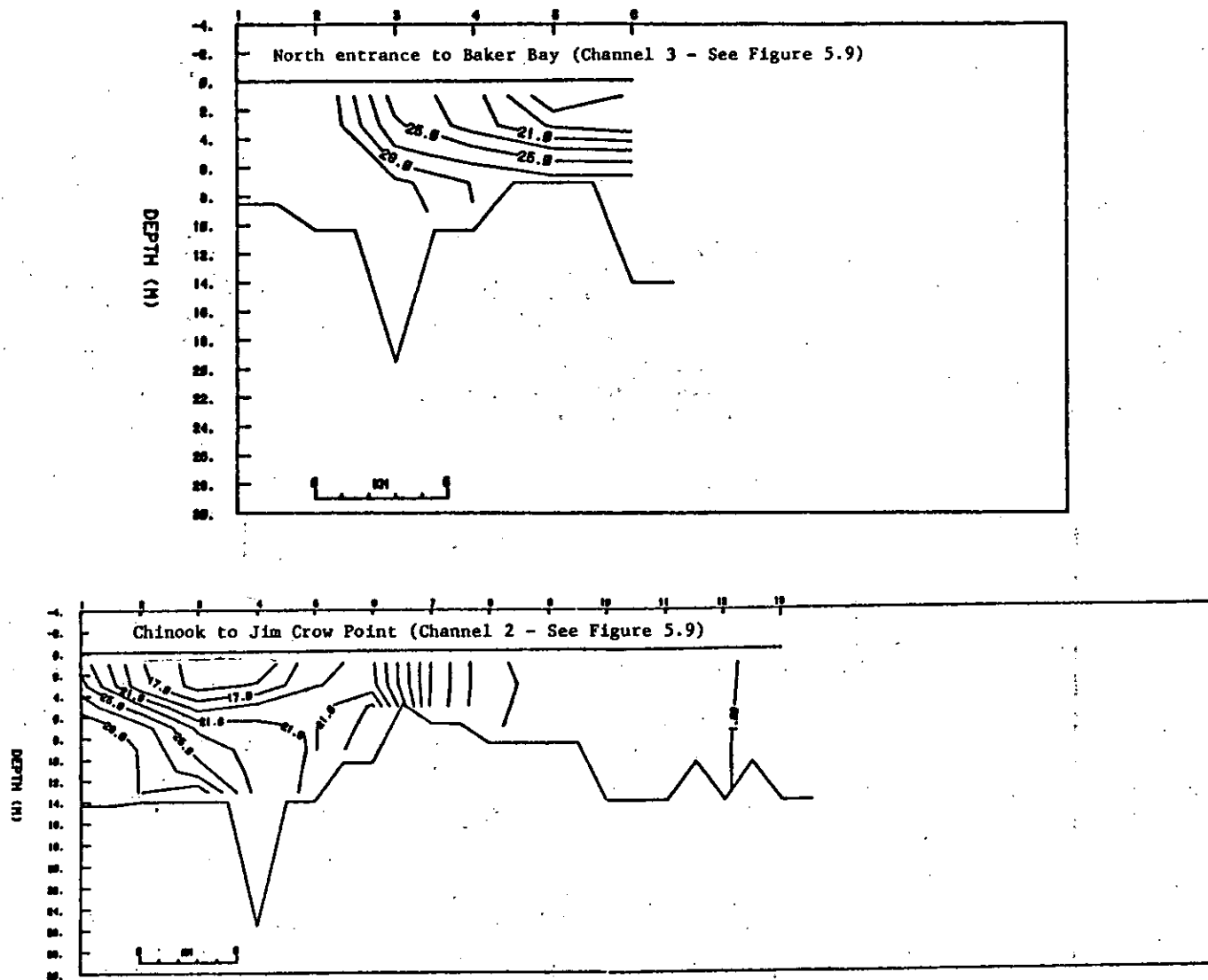


Figure 5.31. 1868 estuary, north channel, $4000 \text{ m}^3 \text{ sec}^{-1}$, neap tide, maximum salinity.

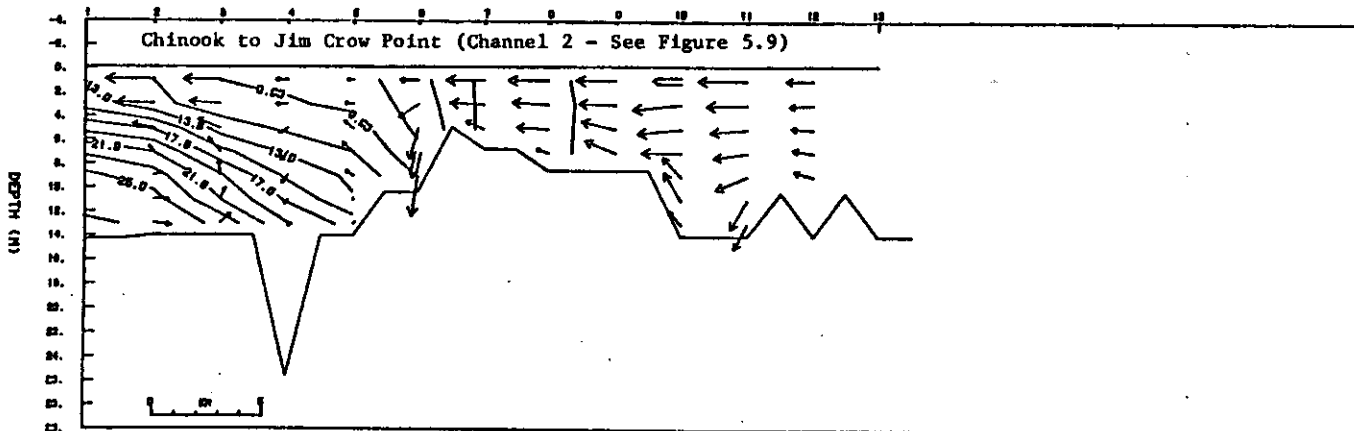
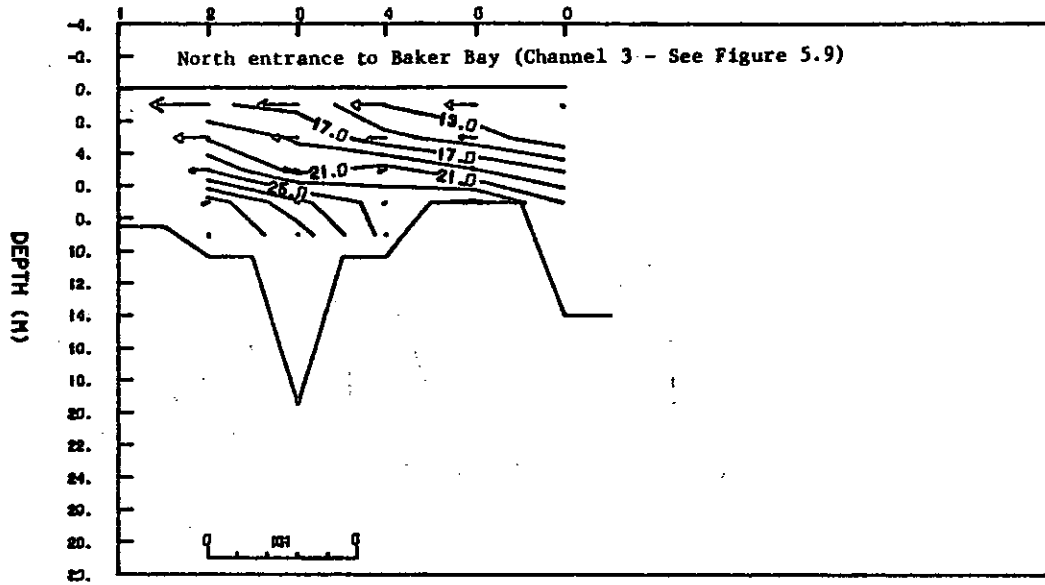


Figure 5.32. 1868 estuary, north channel, $4000 \text{ m}^3 \text{ sec}^{-1}$, neap tide, mean salinity and currents.

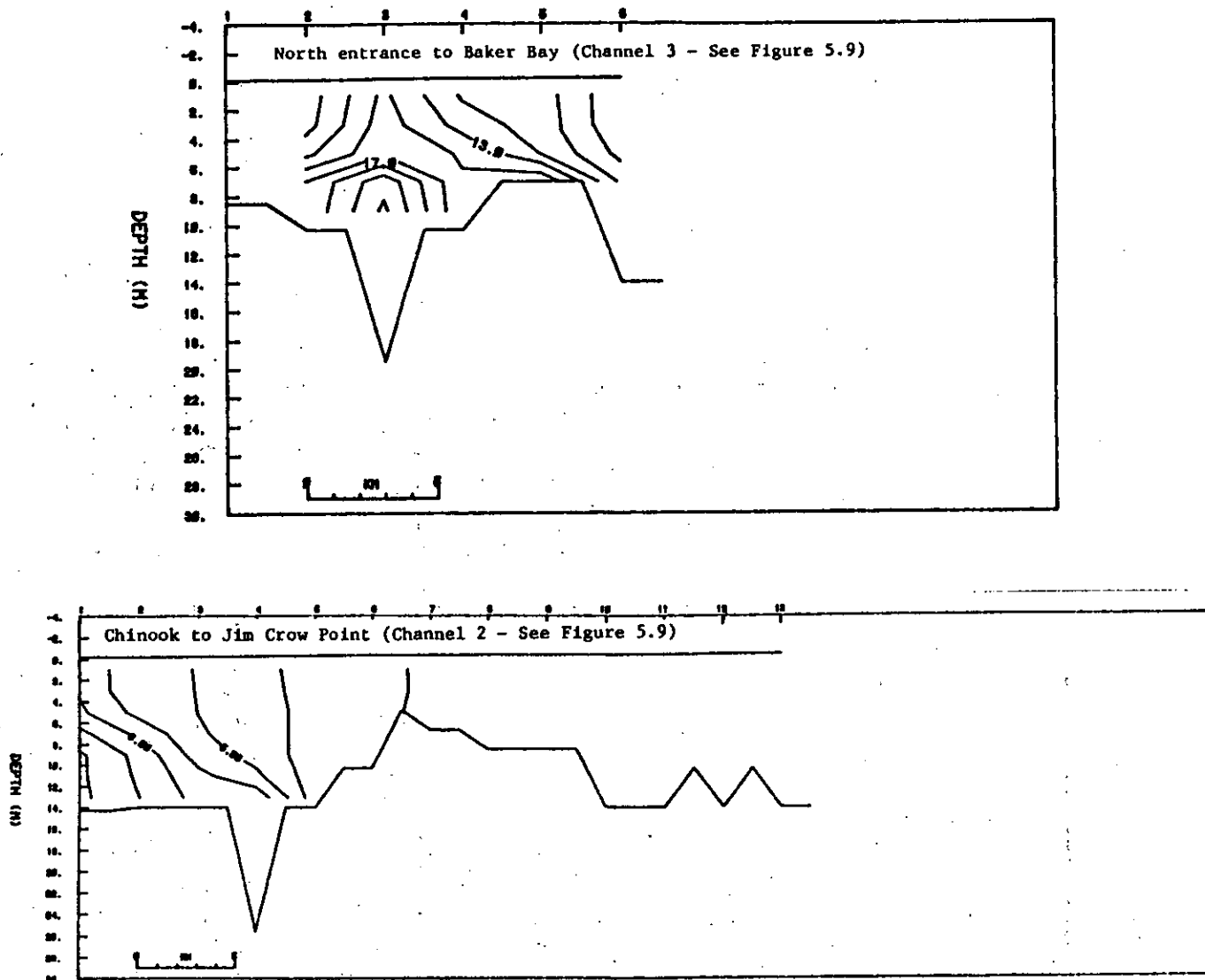


Figure 5.33. 1868 estuary, north channel, $4000 \text{ m}^3 \text{ sec}^{-1}$, spring tide, minimum salinity.

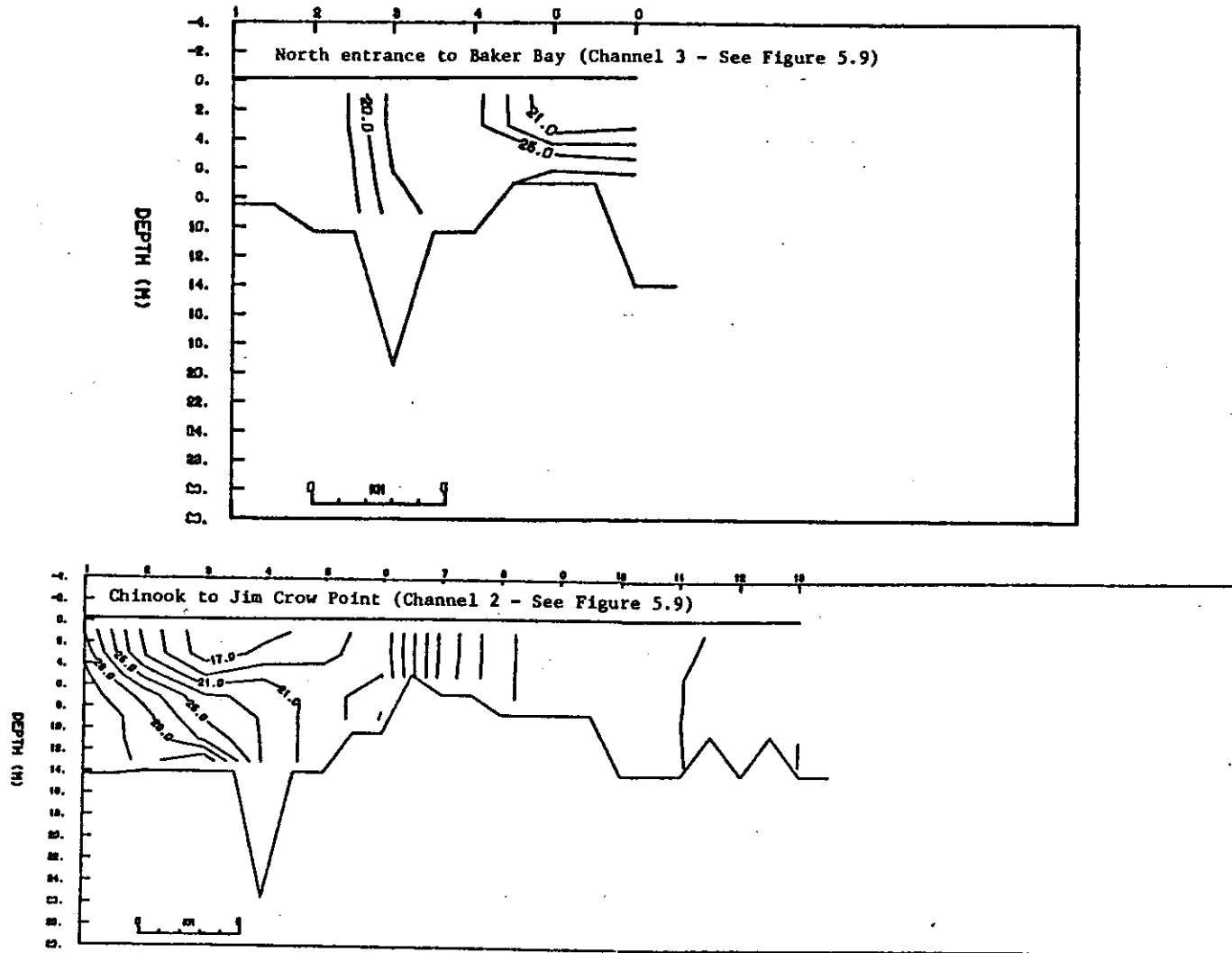


Figure 5.34. 1868 estuary, north channel, $4000 \text{ m}^3 \text{ sec}^{-1}$, spring tide, maximum salinity.

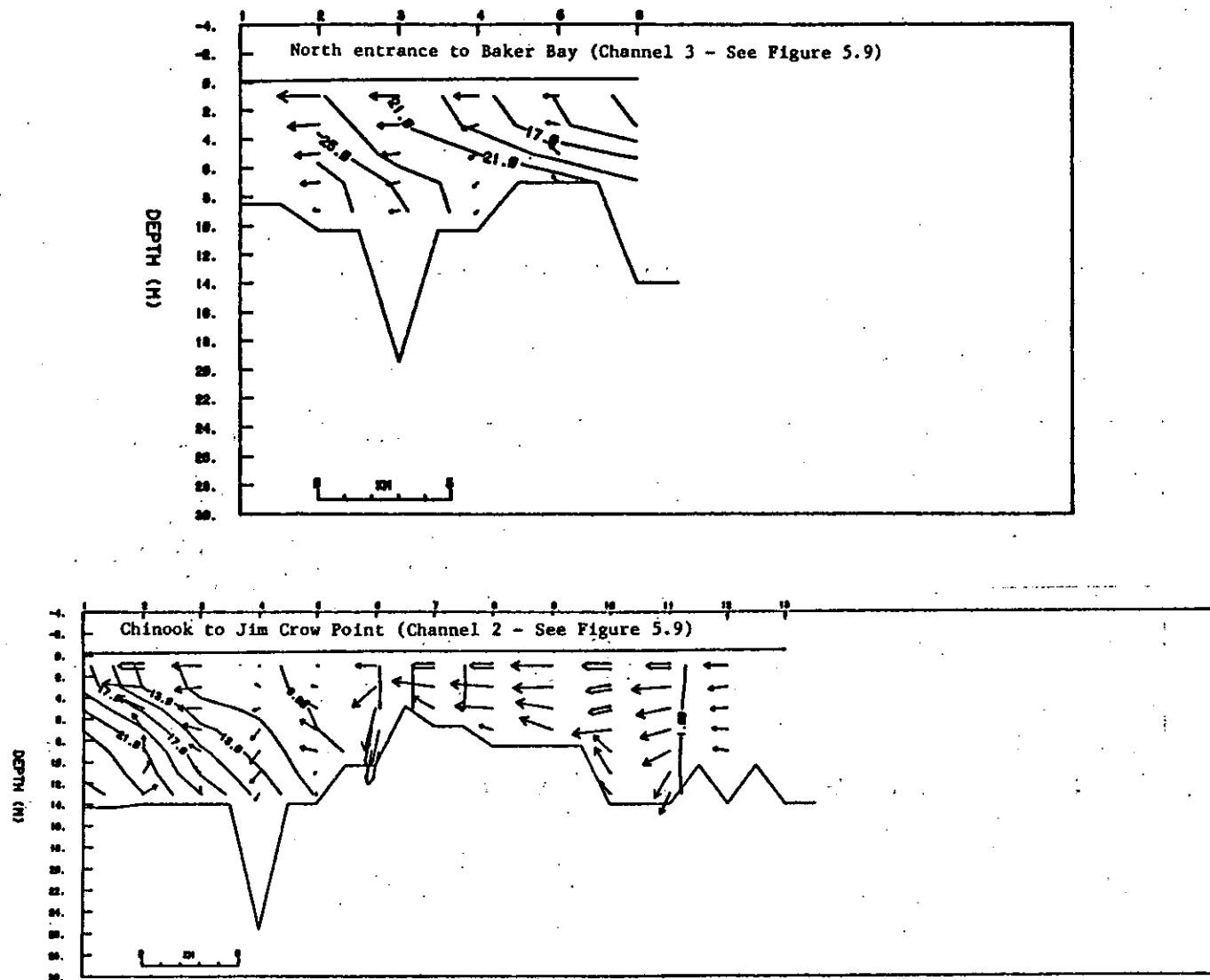


Figure 5.35. 1868 estuary, north channel, $4000 \text{ m}^3 \text{ sec}^{-1}$, spring tide, mean salinity and currents.

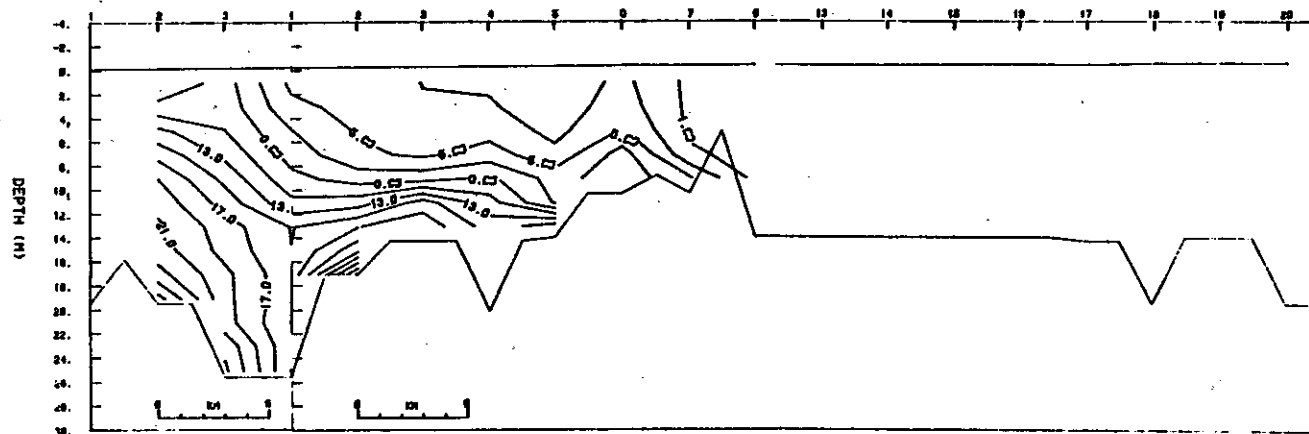


Figure 5.36. 1980 estuary, north channel, $4000 \text{ m}^3 \text{ sec}^{-1}$, neap tide, minimum salinity.

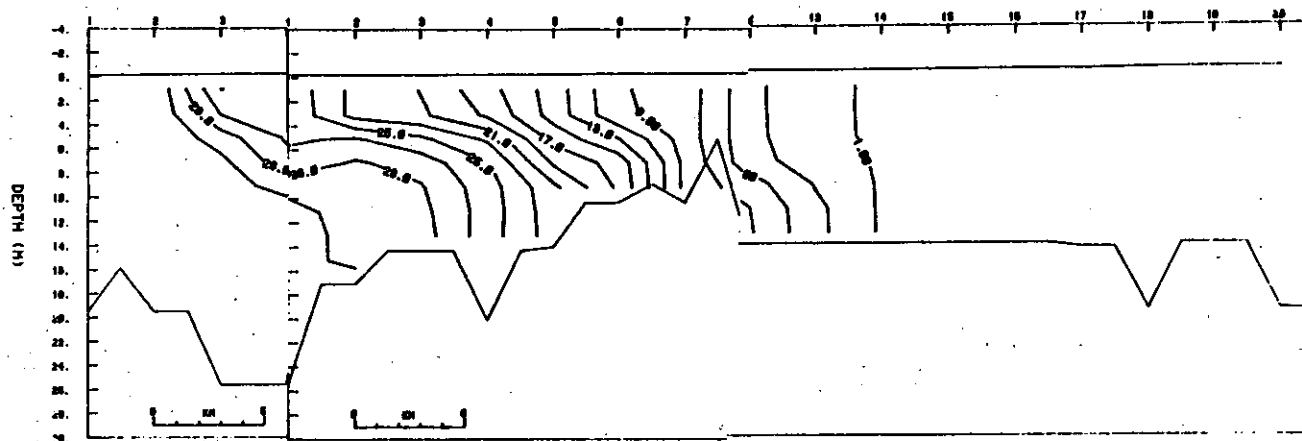


Figure 5.37. 1980 estuary, north channel, $4000 \text{ m}^3 \text{ sec}^{-1}$, neap tide, maximum salinity.

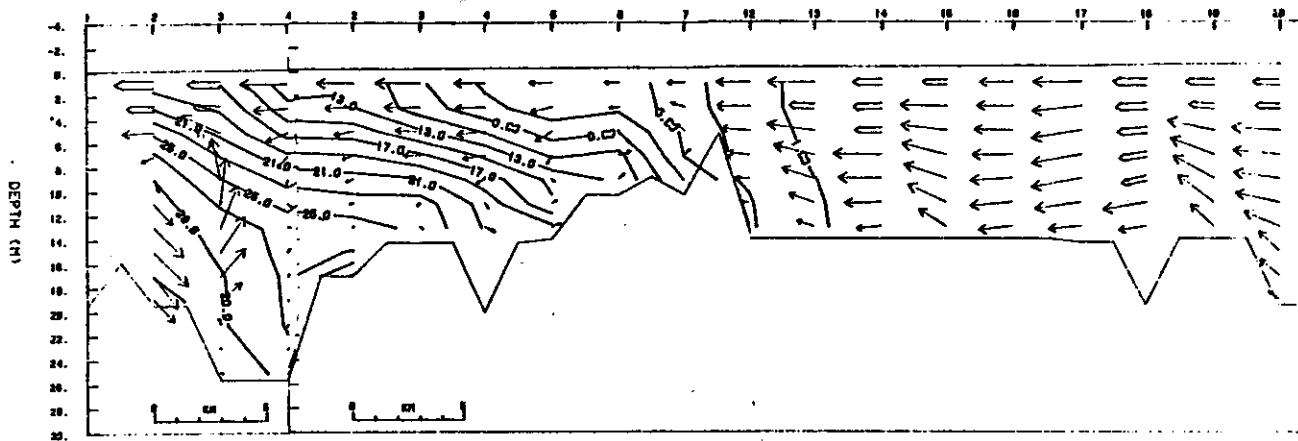


Figure 5.38. 1980 estuary, north channel, $4000 \text{ m}^3 \text{ sec}^{-1}$, neap tide, mean salinity and currents.

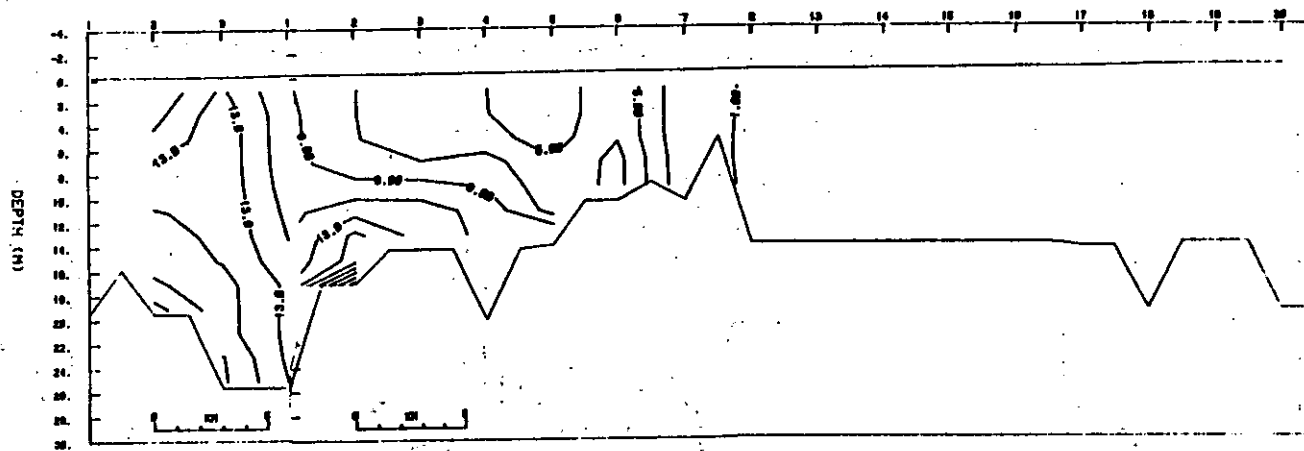


Figure 5.39. 1980 estuary, north channel, $4000 \text{ m}^3 \text{ sec}^{-1}$, spring tide, minimum salinity.

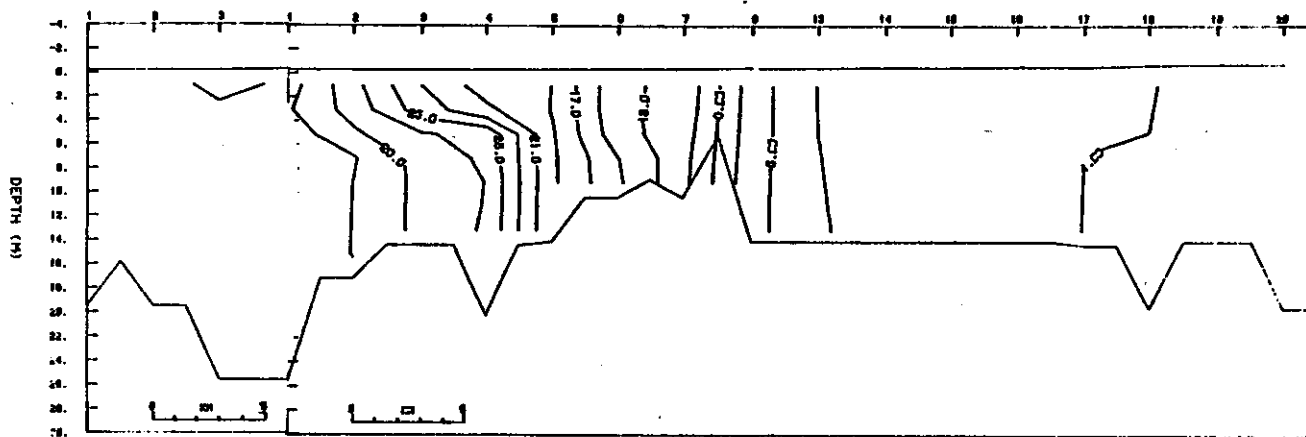


Figure 5.40. 1980 estuary, north channel, $4000 \text{ m}^3 \text{ sec}^{-1}$, spring tide, maximum salinity.

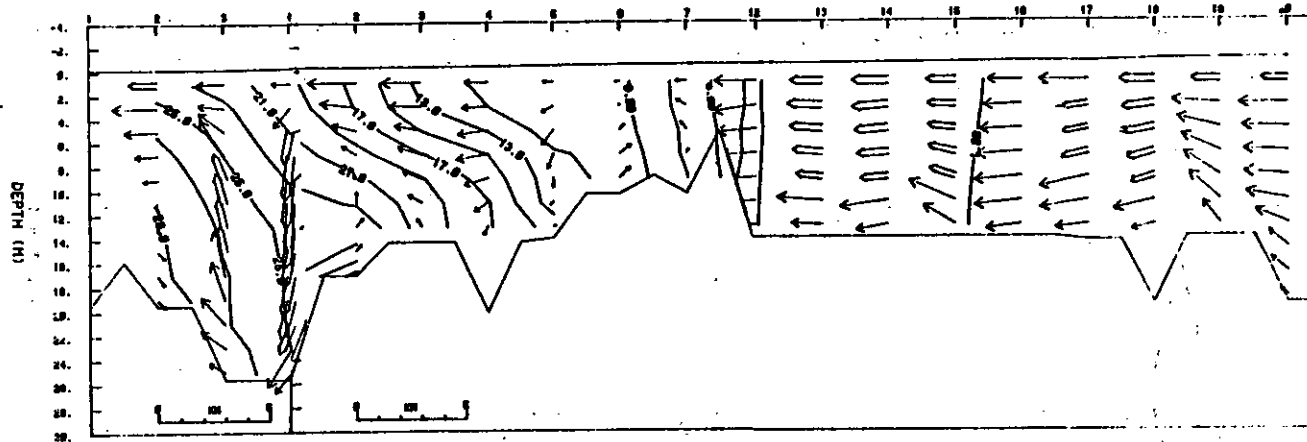


Figure 5.41. 1980 estuary, north channel, $4000 \text{ m}^3 \text{ sec}^{-1}$, spring tide, mean currents and salinity.

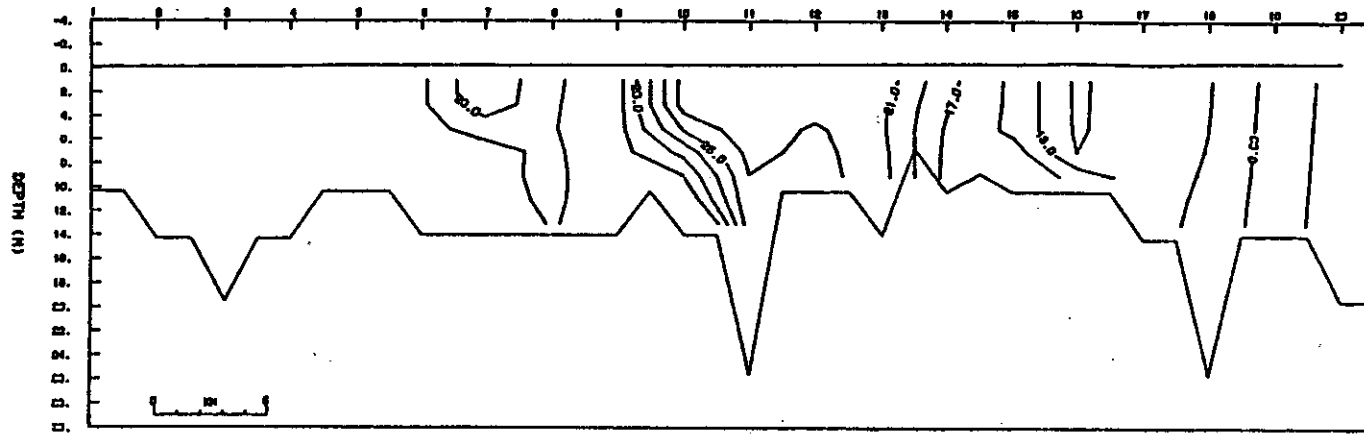


Figure 5.42. 1868 estuary, south channel, $2000 \text{ m}^3 \text{ sec}^{-1}$, spring tide, maximum salinity.

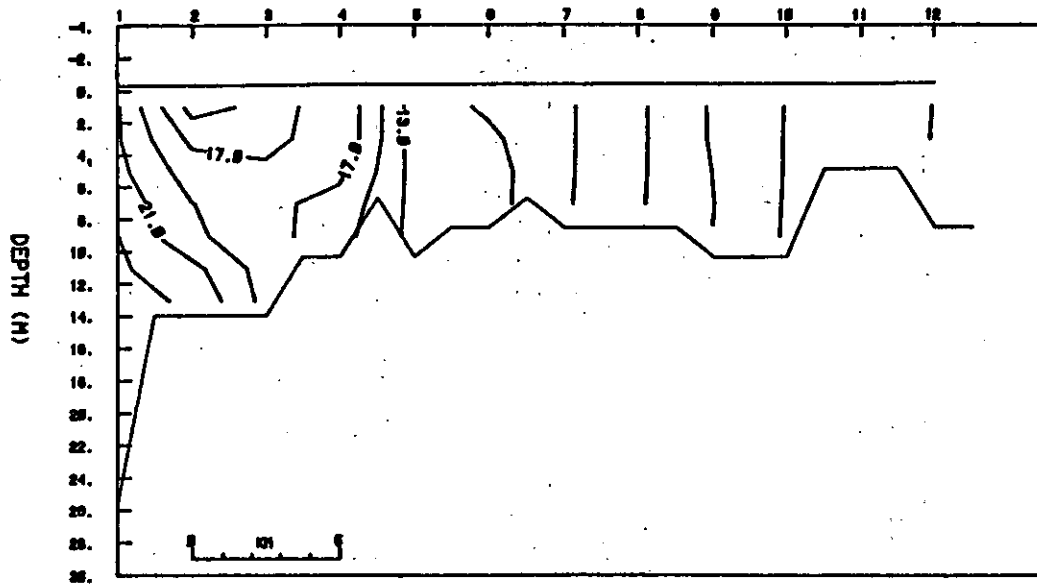


Figure 5.43. 1868 estuary, $2000 \text{ m}^3 \text{ sec}^{-1}$, maximum salinities in Cathlamet Bay.

Figure 5.22 shows salinity intrusion of 1 ppt to about Skamokawa (grid point 18), about 5 river miles further than in 1980 for the spring tide, low flow case. Thus, given present-day, autumn river flows and 1868 bathymetry, salinity intrusion of about 1 to 5 ppt could be expected throughout Cathlamet Bay. Autumn river flows in 1868 were substantially lower than at present, so even larger salinity intrusion probably occurred on a sporadic basis. Figures 5.42 and 5.43 show maximum spring tide salinity intrusion for the extreme low flow ($2,000 \text{ m}^3\text{sec}^{-1}$ or 71 kcfs) in the navigation channel and into Cathlamet Bay. Salinities of 10 to 15 ppt occur in the interior of Cathlamet Bay and the 5 ppt contour reaches the downstream end of Puget Island in Figure 5.42. The difference in the salinity distribution between the present and historical bathymetry appears to increase as the flow is decreased.

The model predicts that sharp fronts should occur on flood tide at sills in both channels for the $2,000$ and $4,000 \text{ m}^3\text{sec}^{-1}$ (71 and 141 kcfs) cases, with the 1868 bathymetry (e.g. in Figures 5.22 and 5.34). The flow upriver of the sills on flood tide is much less stratified than that seaward of them. The most prominent such sill is just downstream of Tongue Point, and the strong mixing here brings saline water to the surface, so that it can enter Cathlamet Bay. Since light, rather than nutrients, is generally limiting for primary productivity, it is not likely that the fronts would have the significance for primary productivity that they might in other systems. The model also shows trapping of pockets of high salinity water behind topographic features and/or near channel junctions (e.g. in Figures 5.21 and 5.22); these features are more prominent than with the modern bathymetry, because of the greater complexity of the channel network and the shallow depths. The fronts and reversals of salinity gradient can be expected to exert a substantial influence on the mean flow.

With regard to neap-spring changes in stratification and salinity intrusion, the 1868 bathymetry produces different results than the present bathymetry. Salinity intrusion is greater on spring tide rather than neap tide and no clear neap-spring change in stratification occurs, except in the $12,000 \text{ m}^3\text{sec}^{-1}$ (424 kcfs) case (not shown), where the neap-spring difference in stratification is somewhat greater than at present. As discussed in Section 3.6.5, it is to be expected that decreasing the riverflow would eliminate the neap-spring transition, as the riverflow became insufficient to create stratification, even with the smallest tides. The model suggests that the flow below which no neap-spring transition can occur is much higher with the 1868 bathymetry, probably because of the shallow depths and stronger tidal currents in 1868. It is reasonable to infer that the neap-spring transition occurred at higher flows with the 1868 bathymetry; however, the model has difficulty reproducing the present-day neap-spring changes described in Section 3.6.5, and it not clear that the model can, in present form, be used to establish the range of flows over which a neap-spring would occur with either modern or 1868 bathymetry.

All of the factors which influence the mean flow (the strength and distribution of the tidal currents, the stratification and horizontal salinity gradient, and the topography) are different in the 1868 model. It is no surprise that the distribution of the mean flow is somewhat

different in the 1868 cases. The most obvious difference in the mean flows between Figures 5.12 and 5.15, 5.20, and 5.26, and 5.32 and 5.38 is the shift in ebb predominance from north channel (1868) to south channel (1980). The increased salinity intrusion lengths in the 1868 case do not generally increase the lateral extent of upstream bottom flow, because the increased salinity intrusion length decreases the horizontal salinity gradient and stratification, which are required for net upstream bottom flow to occur. Furthermore, the influence of topography is very strong. Upstream bottom flow in the north channel never extends beyond the shallow sill near Taylor Sands, regardless of the riverflow, in either the modern or historic case. Upstream bottom flow in the south channel never extends much beyond Tongue Point, and the model does not show significant, upstream bottom flow anywhere in Cathlamet Bay in any case.

5.4 EFFECTS OF THE CHANGES IN MORPHOLOGY AND CIRCULATION

The remainder of this chapter is a discussion of the implications of the historical changes that have occurred in the estuary. The first subsection attempts to relate the changes that have occurred in the circulation and salinity distribution to the changes that might be expected in the behavior of the turbidity maximum and the deposition of fine sediment. The second subsection provides an analysis of the bathymetric differencing data in terms of a long term sediment budget for the estuary. The final subsection and the summary (Section 5.5) approach the question of long term trends and "equilibrium" in the Columbia River Estuary and conclude the physical discussion in this volume.

5.4.1 Implications for Turbidity Maximum Processes

The existence of a mid-estuary accumulation of suspended material, the turbidity maximum (Section 3.4), is of considerable importance as a sink for primary productivity and as a detrital food source, and its presence demonstrates that a mechanism must exist by which organisms may remain in the estuary in the face of the outward mean flow. It is, therefore, of interest to consider the effects of the alteration of estuarine flow patterns on the turbidity maximum. This is by no means a simple question, and only a few conclusions can be drawn.

Consider first the flushing time of the estuary, how it has changed, and how this has affected the turbidity maximum. The flushing time of an estuary (or any part thereof) is a simple concept: how long will a conservative substance injected into the system remain there before being removed to the ocean by the the action of tides and riverflow, assuming that it is mixed uniformly throughout the system? The flushing time cannot be measured directly but can be calculated in a variety of ways. Flushing times in the modern Columbia River Estuary are very short (on the order of a few days; Neal 1972), relative to those of most other major estuaries. Flushing time varies both seasonally and during the tidal month, because of the variations in tidal and river flows, and density structure. The residence time of a particle or organism in the estuary may be longer than the flushing time of the system as a whole, if the particle spends part of its time on the

bottom, in areas of weak currents (e.g. the peripheral bays) or in parts of the system where the residual flow is inward (e.g. in the bottom of the channel in certain reaches). Particles tend preferentially to accumulate in such locations and particularly in the bottom of the deeper channels; this is the trapping mechanism that leads to the turbidity maximum (or maxima) of the estuary (Chapter 4).

The flushing time of the 1868 estuary was, on the average, less than that of the modern estuary, primarily because tidal exchange was greater, but secondarily because the average riverflow was greater before diversion and regulation. Flushing time was also seasonally more variable, because the freshwater inflow was more variable. A decrease in temporal variability in flushing has been accompanied by an increase in the spatial variability of flushing rates. The concentration of tidal and mean flow in the subsidiary channels and the diversion of flow away from subsidiary channels (compare Figures 5.12 and 5.15) has undoubtedly increased the flushing time of the main channels. Not only will a parcel of water remain longer in such a channel, but a particle may spend more time on the bottom, because of reduced shear stress. In this sense, the modern estuary is more favorable for the deposition of fine material in peripheral areas, exclusive of any changes that may have occurred in the supply of this material.

It was concluded in Section 4.3.2 that lateral movement of suspended material into these peripheral areas from the turbidity maximum in the channel was probably an important mechanism for deposition of fine material. It was further concluded that more suspended sediment is presently found in the south channel than in the north channel, because the south channel is more directly connected to the source of the material (the river), because the seawater in the south channel has been in the estuary longer, and because the greater tidal exchange in the north channel leads to a lower residence time there. It is probable that the difference between channels in suspended sediment concentrations was less in 1868, because of the more direct connection of the north channel to the river at that time. It is a reasonable question whether this difference in the distribution of the turbidity maximum has shifted the pattern of deposition from north to south.

The flushing time of the estuary, even under low flow conditions, is, and was in 1868, short relative to the tidal monthly periodicities (15 and 28 days, approximately) over which the tidal range and density structure vary. The residence time of inorganic suspended material in the modern estuary appears to be regulated by neap-spring changes in tides and stratification, at least during low flow periods. Material is deposited during neap tides and eroded and transported seaward during spring tides, because of the stronger tides and weaker stratification. Data are not available to assess the importance of neap-spring changes in the modern turbidity maximum except under low flow conditions; probably such changes are less important when the flow is higher. Although no data are available to assess the possibility, it is not unlikely that zooplankton populations may exhibit tidal monthly variability, during periods of strong, tidal-monthly variations in density structure.

It was suggested in Section 5.3.2 that the season during which strong neap-spring changes in density structure occur has shifted from the high flow season in 1868 to the low flow season in 1980. If the boundary shear stress was greater in 1868 on low flow neap tides, because neap-spring changes in density structure were smaller and tidal currents stronger, then outward transport of suspended material might have been a more continuous process and the spring tide turbidity maximum may have been less prominent. It is also possible that the neap-spring changes in turbidity maximum were more prominent during the spring high flow period, when both sediment supply and primary productivity are now at a maximum. This may indicate that neap-spring transitions in biological processes were more important in 1868 than they are presently.

5.4.2 Long-Term Shoaling Patterns and the Sediment Budget

Some evidence regarding the historical shoaling patterns in the estuary can be derived from further examination of Table 5.5. The net accumulation in the system has totaled approximately 68 million m^3 since 1868. When adjusted for the loss of 247 million m^3 that occurred in the entrance region, it becomes clear that 315 million m^3 of sediment accumulated in the estuary proper in the 90-year period, an annual rate of 3.5 million m^3 . However, several lines of evidence suggest that not all of this 315 million m^3 was derived from the river. The history of change at the entrance, as related by Hickson (1922, 1930), Lockett (1963, 1967), the Columbia River Estuary Data Development Program (1983) bathymetric differencing maps, and sedimentological evidence (Borgeld et al. 1978; Walter et al. 1979; Roy et al. 1979, 1982; Sherwood et al. 1984) all suggest that much of the accumulation on Desdemona Sands, Baker Bay, and Trestle Bay is related to the displacement of sediment from the natural tidal delta as a result of the construction of the entrance jetties. Scouring of the entrance channel by the constrained tidal currents has transported sediment both offshore and into the estuary. Whereas the inner and outer tidal deltas were relatively close to each other in 1868, they are now separated by several miles of deep channel and by the spits formed around the jetties. The inner tidal delta in 1868 was a distinct, if dynamic, feature consisting of intertidal islands (the old Sand Islands) or shoals. The modern inner tidal delta has been forced further into the estuary and is no longer a distinct feature. The sandy sediment that made up the 1868 inner tidal delta is now found in Baker Bay and Desdemona Sands.

In this scenario, sandy sediments deposited in the lower estuary, including Trestle Bay, Baker Bay, Desdemona Sands, and the north and south channels, account for more than half of the sediment lost from the entrance region (157 million m^3). The remainder of the 247 million m^3 lost from the entrance region (90 million m^3) has been either deposited on Clatsop or Peacock spits or has been lost entirely from the system. The portion that was lost from the system has been either pushed farther offshore or carried along the coast with the littoral drift. The patterns of erosion and deposition in the entrance region, discussed in Lockett (1963) and evident in the bathymetric atlas (Columbia River Estuary Data Development Program 1983) suggest that much of the displaced sediment has in fact moved seaward and north. This direction

is consistent with studies of shelf sediment transport on the Oregon and Washington shelves and with the flux of winter wave energy. One possible implication is that the erosion of the outer tidal delta (since jetty construction was initiated in 1885) has provided sediment for the littoral drift system north of the Columbia River in unusually large quantities. In effect, a large pulse of sediment may have been introduced to the Washington beaches by jetty construction. The effects of the pulse, which may have been seen as jetty and beach accretion along Long Beach and sedimentation in Willapa Bay, may now be wearing off, and future littoral supply from the Columbia River will be dependent on the amount of bedload escaping from the mouth.

The 157 million m^3 that was deposited in the lower estuary accounts for half of the 315 million m^3 that accumulated in the estuary in the 90-year period. The remaining 158 million m^3 must represent the contribution from fluvial sources at an apparent rate of 1.76 million m^3 yr^{-1} . Using the accepted estimate of a total load amounting to 10 million metric tons per year for the Columbia River (Whetten et al. 1969) and assuming that sediment deposits in the estuary have a porosity of 40% and a density of 2.65 g cm^{-3} , there is an annual sediment supply of 6.3 million m^3 yr^{-1} . If all of the bedload material is trapped in the estuary (10% of the total load, or 0.63 million m^3 yr^{-1}), 20% of the remaining suspended load (1.13 million m^3 yr^{-1}) must also be deposited in the estuary to balance the sedimentation rate with the supply. The correctness of this estimate is subject to the correctness of the bedload supply estimate; it could be either high or low. However, even if no bedload were trapped in the estuary, an upper limit of 30% of the fine sediment could be retained. Clearly, most of the fine sediment escapes to the ocean. The estimate of 20% retention of the fine sediment in the estuary is slightly lower than the value of approximately 30% retention calculated by Hubbell and Glenn (1973).

These budget estimates may be used to emphasize the potential importance of infrequent catastrophic effects such as volcanic eruptions. Estimates of the volume of sediment in the mudflows from the May 18, 1980, eruption of Mt. St. Helens that reached the confluence of the Cowlitz and Toutle rivers approach 100 million m^3 (Fairchild and Wigmosta 1983). As much as 34 million m^3 of this sediment accumulated in the Columbia River adjacent to the mouth of the Cowlitz River (Schuster 1981). The Corps of Engineers has since removed more than 11.5 million m^3 of sediment from this reach, but the Cowlitz River continues to contribute 5 million tons of sediment to the Columbia River each year (Schuster 1981; Dunne and Leopold 1981). The amount of this sediment that has reached or will reach the estuary is unknown; much less will arrive, because of the land disposal of dredged material, than would have reached the estuary from an eruption 100 years ago. However, the magnitude of sediment involved clearly suggests that a few comparable eruptions over long periods of time would have a profound effect on the sediment budget of the estuary.

The major spring freshets that have been eliminated by flow regulation carried large total loads and may also have been of considerable importance to the sediment budget. U.S. Geological Survey data for 1963 to 1970 (summarized in Jay and Good 1978) show average

annual suspended loads at Vancouver ranging from 4 to 28 million metric tons yr^{-1} , with the spring freshet of 1965 carrying 12 million metric tons and a winter freshet the same year carrying about 8 million tons. None of these freshets were major in comparison with the much larger freshets which occurred before 1963 (e.g., in 1894 and 1948).

While the historical calculations show that most of the suspended sediment carried by such freshets was lost to the ocean, the former effects of major floods on the bedload are harder to analyze. It is reasonable to suppose that large pulses of bedload were brought into the estuary by the major freshets (Hickson 1930). Given the energy budget discussion of Sections 3.5 and 4.6, it is improbable that even the largest freshets would have resulted in more transport of bedload out of the mouth of the estuary than entered from the river. Thus the larger freshets of the 1868-1958 period may have had a substantial impact on the total accumulation. Significant regulation of flow (post-1969) is too recent to be evaluated by the historical methodology, and it cannot be determined whether the estuarine shoaling rate has been altered by elimination of large freshets.

5.4.3 Equilibrium

The concept of an equilibrium morphology was approached in Section 4.5 using energy considerations. The results presented in Section 5.2 may be used to suggest that the estuary has not reached an equilibrium. Average shoaling rates and the hypothetical time required to fill the estuary at those rates are presented in Table 5.7. These estimates suggest that only 800 years would be required to fill the estuary entirely at the present rate. Because sea level reached its present height between 3,000 and 5,000 years ago, and the estuary is clearly still filling, it appears that the recent rate of 0.5 cm yr^{-1} is abnormally high for the Columbia River Estuary. This may be used as circumstantial evidence to suggest that the changes that have occurred in historical time have caused relatively rapid shoaling, compared to longer-term, natural shoaling rates.

5.5 SUMMARY OF HISTORICAL TRENDS IN THE ESTUARY AND IMPLICATIONS FOR THE FUTURE

Preliminary analysis of historical bathymetric data indicates a historical shoaling rate in the estuary of 0.5 cm yr^{-1} , substantially larger than that rate sustainable over geologic time. This is believed to be the result of navigational development of the estuary. The effects of flow regulation cannot be evaluated by the historical methodology employed, because significant flow regulation is too recent a phenomenon. Changes in the shoaling rate of the estuary are almost certainly a result of movements of sand (i.e., bedload), because the permanent retention of fine material was, and is, small.

The temporary retention of fine material is, nonetheless, extremely important to biological processes in the estuary. Numerical modeling of the circulation and salinity distribution suggests that the decrease in tidal prism and diversion of flow away from subsidiary channels has

decreased salinities throughout the estuary, increased the stratification and residence time of suspended material in the estuary, and perhaps caused increased shoaling in peripheral areas. Neap-to-spring changes in density structure and mean flow are now more prominent during low flow periods; in 1868 they were more prominent during high flow periods. Diversion of river flow from the north channel to the south channel may also have reduced the supply of resuspended material to the north side of the estuary.

Although the Columbia River Estuary is dominated by tidal currents and is a highly energetic system, the trends that have emerged from this analysis of the historical changes in the estuary are alarming. Unfavorable results of estuarine development have included: a major loss of wetlands, decreased estuary surface area and tidal prism, reduced tidal mixing and increased flushing time, and increased sedimentation. The river discharge curve has also been damped and the mean flow reduced, with the result that major floods no longer occur, and the residence time and temperature of water in the river have been increased by storage reservoirs. Residence times in the estuary for detritus and nutrients have increased and vertical mixing has decreased. These hydrodynamic changes have probably enhanced the primary productivity within the estuary, not, however, to the extreme of producing the eutrophication that is occurring, for example, in Chesapeake Bay. In short, the Columbia River Estuary is responding to human influence in much the same manner as less energetic systems studied elsewhere. Although it remains a dynamic system, it is important to recognize these trends and address them in planning future navigation projects and flow diversion or regulation.

LITERATURE CITED
(Volume I)

- Akins, G.J.; Jefferson, C.A. 1973. Coastal wetlands of Oregon. Natural Res. Invent. rep. to Ore. Coastal Conserv. Dev. Comm. 159 pp.
- Allen, G.P.; Solomon, J.C.; DuPenhoat, Y.; De Grandpre, C. 1980. Effects of tides on mixing and suspended sediment transport in macrotidal estuaries. *Sed. Geol.* 26:69-80.
- Allen, J.R.L. 1968. Current ripples: their relation to patterns of water and sediment motion. Amsterdam: North Holland.
- Allen, J.S. 1980. Models of wind-driven currents on the continental shelf. *Ann. Rev. Fluid Mech.* 12:389-433.
- Anderson, G.C.; Barnes, C.A.; Buddinger, T.F.; Love, C.M.; McManus, D.A. 1961. The Columbia River discharge area of the northeast Pacific Ocean, a literature survey. Seattle: University of Washington, Department of Oceanography. 83 pp.
- Ando, M.; Balazas, E.I. 1979. Geodetic evidence for a seismic subduction of the Juan de Fuca plate. *J. Geophys. Res.* 84:3023-3028.
- Atwater, T. 1970. Implications of plate tectonics for the Cenozoic tectonic evolution of western North America. *Geol. Soc. Am. Bull.* 81:3513-3536.
- Bagnall, M.G. 1916. Improvement of the mouth of the Columbia River. U.S. Corps of Engineers, Professional Memoirs 8:687-720.
- Bakun, A. 1975. Daily and weekly upwelling indices, west coast of North America, 1967-73. NOAA Tech. Rep. 16, NMFS SSRF-693. 114 pp.
- Ballard, R. L. 1964. Distribution of beach sediment near the Columbia River. Technical Report No. 98. Seattle: University of Washington, Department of Oceanography.
- Barnes, C.A.; Duxbury, A.C.; Morse, B.-A. 1972. Circulation and selected properties of the Columbia River effluent at sea. Pruter, A.T.; Alverson, D.L. eds. The Columbia River Estuary and adjacent ocean waters, pp. 41-80 Seattle: University of Washington Press.
- Barwis, J.H. 1975. Catalog of tidal inlet aerial photography. U.S. Army Engineers, WES GITI Report 75-2. Vicksburg, MI.
- Barwis, J.H. 1976. Annotated bibliography of the geologic, hydraulic, and engineering aspects of tidal inlets. U.S. Army Engineers WES, GITI Report #4. Vicksburg, MI.

- Blatt, H.; Middleton G.; Murray, R. 1972. Origin of sedimentary rocks. New York: Prentice-Hall, Inc.
- Boggs, S. Jr.; Jones, C.A. 1976. Seasonal reversal of flood-tide dominant sediment transport in a small Oregon estuary. G.S.A. Bull. 87:419-426.
- Boothroyd, J.C.; Hubbard, D.K. 1975. Genesis of bedforms in mesotidal estuaries, Cronin, L.E. ed. Estuarine research, II. New York: Academic Press.
- Borgeld, J.C.; Creager, J.S.; Walter, S.R.; Roy, E.H. 1978. A geological investigation of the sedimentary environment at sites E, G, and H near the mouth of the Columbia River. Portland: Department of the Army, Corps of Engineers, Portland District.
- Callaway, R.J. 1971. Applications of some numerical models to Pacific Northwest estuaries. Proceedings of the 1971 technical conference on estuaries of the Pacific Northwest. Circ. #42, Engineering Experiment Station, Oregon State University, Corvallis, OR.
- Callaway, R.J.; Byram, K.V. 1970. Mathematical model of Columbia River from the Pacific Ocean to Bonneville Dam, part II: Input-output and verification procedures. Corvallis, OR: EPA. 49 pp.
- Callaway, R.J.; Byram, K.V.; Ditsworth, G.R. 1969. Mathematical model of the Columbia River from the Pacific Ocean to Bonneville Dam, part I: Theory, program notes and program. Corvallis, OR: EPA. 155 pp.
- Chelton, D.B.; Davis, R.E. 1982. Monthly mean sea-level variability along the west coast of North America. J. Phys. Oceanogr. 12:757-784.
- Clairain, E.J.; Cole, R.A.; Diaz, R.J.; Ford, A.W.; Huffman, R.T.; Hunt, L.J.; Wells, B.R. 1978. Habitat development field investigations, Miller Sands marsh and upland habitat development site, Columbia River, Oregon. Tech. Rep. D-77-38, U.S. Army Corps Engineers Waterways Exp. Sta., Dredged Material Res. Prog., Vicksburg, MI. 78 pp. + append.
- Claire, E.W., et al. 1971. The potential impact of severe water fluctuations on wildlife resources of the lower Columbia River. Spec. Rep. Ore. State Game Comm., Portland, OR.
- Clark, S.M., Snyder, G.R. Timing and extent of a flow reversal in the lower Columbia River. Limnol. Oceanogr. 24:960-965.
- Clifton, H.E. 1983. Discrimination between subtidal and intertidal facies in Pleistocene deposits, Willapa Bay, Washington. J. Sed. Petrol. 53:353-370.

- Clifton, H.E.; Phillips, R.L. 1980. Lateral trends and vertical sequences in estuarine sediments, Willapa Bay, Washington. Pacific Coast Paleography Symposium 4: Quaternary depositional environments of the Pacific Coast. Los Angeles, CA: Pacific Section, S.E.P.M.
- Columbia River Estuary Data Development Program (CREDDP). 1983. Bathymetric atlas of the Columbia River Estuary. Astoria, OR.
- Conomos, T.J. 1968. Processes affecting suspended particulate matter in the Columbia River effluent system, summer, 1965, 1966. Ph.D. thesis. Seattle: University of Washington.
- Conomos, T.J.; Gross, M.G. 1972. River-ocean suspended particulate matter relations in summer. Pruter, A.T.; Alverson, D.L. eds. The Columbia River Estuary and adjacent ocean waters, pp. 176-202. Seattle, WA. University of Washington Press.
- Conomos, T.J.; Gross, M.G.; Barnes, C.A.; Richards, F.A. 1972. River-ocean nutrient relations in summer. Pruter, A.T.; Alverson, D.L. eds. The Columbia River Estuary and adjacent ocean waters Seattle, WA: University of Washington Press.
- Cooper, W.S. 1959. Sand-dune development and sea-level changes on the coast of North Oregon (abstract). Geol. Soc. Am. Bull. 65:1373.
- Costello, W.R. 1974. Development of bed configurations in coarse sands. Report No. 74-1. M.I.T. Dept. of Earth and Planet. Sci.
- Costello, W.R.; Southard, J.B. 1981. Flume experiments on lower-flow-regime bedforms in coarse sand. J. Sed. Pet. 51:849-864.
- Crawford, J.A.; Edwards, D.K. 1978. Postpropagation assessment of wildlife resources on dredged material. Clairain, E.J. ed. Habitat development field investigations, Miller Sands marsh and upland habitat development site, Columbia River, Oregon, Appendix F. Tech. Rep. D-77-38, Dredged Material Res. Prog., U.S. Army Corps Engineers Waterways Exp. Sta., Vicksburg, MI. 67 pp.
- Creager, J.S.; Sims, L.; Sherwood, C.; Roy, E.; Stewart, R.; Barnett J.; Gelfenbaum, G. 1980. A sedimentological study of the Columbia River Estuary. Annual Report. Vancouver, WA: Pacific Northwest River Basins Commission.
- Creech, C. 1977. Five-year climatology (1972-1976) off Yaquina Bay, Oregon. Oregon State U. Sea Grant Pub. #ORES-U-77-011, Corvallis, OR. 16 pp.
- Dalrymple, R.W.; Knight, R.J.; Lambiase, J.J. 1978. Bedforms and their hydraulic stability relationships in a tidal environment, Bay of Fundy, Canada. Nature 275:100-104.
- Davis, J.S.; Holton, R.L. 1976. Diel activity of benthic crustaceans in the Columbia River Estuary. M.S. thesis. Corvallis: Ore. State Univ. 170 pp. + append.

- Davison, M.A. 1979a. Completion report: Columbian white-tailed deer literature review and study plan (unpubl.). Project E-2. Olympia Washington Department of Game.
- Davison, M.A. 1979b. Columbian white-tailed deer status and potential on off refuge habitat. Columbian White-tailed Deer Study Completion Rep., Proj. E-1. Olympia: Wash. Dept. Game.
- Dawley, E.M.; Sims, C.W.; Ledgerwood, R.D. 1978. A study to define the migrational characteristics of chinook and coho salmon and steelhead trout in the Columbia River Estuary. Ann. Rep. 1977. Proj. 712, NOAA, Natl. Mar. Fish. Serv., NW Alaska Fish. Cntr., Seattle, WA. 23 pp. + append.
- Dawley, E.M.; Sims, C.W. Ledgerwood, R.D.; Miller, D.R.; Thrower, F.P. 1979. A study to define the migrational characteristics of chinook and coho salmon and steelhead trout in the Columbia River Estuary. Ann. Rep. 1978, Proj. 712, NOAA, Natl. Mar. Fish. Serv., NW Alaska Fish. Cntr., Seattle, WA. 35 pp + append.
- Dearborn Associates. 1980. Black sand mining project: draft environmental impact statement. Prepared for the State of Washington and Pacific County Department of Natural Resources. Olympia, WA.
- Depletions Task Force. 1983. 1980 level modified streamflow 1928-1978 Columbia River and coastal basins. Columbia River Water Management Group. Portland, OR. 340 pp.
- Dronkers, J.J. 1964. Tidal computations in rivers and coastal waters. Amsterdam: North-Holland Publishing Company. 518 pp.
- Dunne, T.; Leopold, L.B. 1981. Flood and sedimentation hazard in the Toutle and Cowlitz River system as a result of the Mt. St. Helens eruptions. Report to the Federal Emergency Management Agency, Region X, January 1981.
- Durkin, J.T. 1973. A list of crustacean shellfish of the lower Columbia River between the mouth and river mile 108, July to October 1973. Unpubl. rep., NOAA, Natl. Mar. Fish. Serv., NW Alaska Fish. Cntr., Seattle, WA. 4 pp.
- Durkin, J.T. 1974. A survey report of fish species found in a proposed fill area west of the Port of Astoria docks. Unpubl. rep., NOAA, Natl. Mar. Fish. Serv., NW Alaska Fish. Cntr., Seattle, WA. 5 pp.
- Durkin, J.T. 1975. An investigation of fish and decapod shellfish found at four dredge material disposal sites and two dredge sites adjacent to the mouth of the Columbia River. Compl. Rep. to U.S. Army Corps Engineers Portland Dist., NOAA, Natl. Mar. Fish. Serv., NW Alaska Fish. Cntr., Seattle, WA. 29 pp.

- Durkin, J.T. 1980. Columbia River Estuary finfish and shellfish utilization. Proc. 60th Ann. Conf. Western Assoc. Fish Wildl. Agen., July 13-17, 1980, Kalispell, Montana, pp. 334-342.
- Durkin, J.T. 1982. Migration characteristics of coho salmon (Oncorhynchus kisutch) smolts in the Columbia River and its estuary. Kennedy, V.S. ed. Estuarine comparison, pp. 365-376. New York: Academic Press, Inc.
- Durkin, J.T.; Emmett, R.L. 1980. Benthic invertebrates, water quality, and substrate texture in Baker Bay, Youngs Bay, and adjacent areas of the Columbia River Estuary. Fin. Rep. to U.S. Fish Wildl. Serv., Ecol. Serv. Div., Coastal Zone Est. Studies, NOAA, Natl. Mar. Fish. Serv., NW Alaska Fish. Cntr., Seattle, WA. 44 pp. + append.
- Durkin, J.T. Sims, C.W. 1975. Migrations of juvenile coho salmon, Oncorhynchus kisutch, into the Columbia River Estuary, 1966-71. Unpubl. rep., NOAA, Natl. Mar. Fish. Serv., NW Alaska Fish. Cntr., Seattle, WA.
- Durkin, J.T.; Lipovsky, S.J.; Snyder, G.R.; Tuttle, M.E. 1977. Environmental studies of three Columbia River estuarine beaches. NOAA, Natl. Mar. Fish. Serv., NW Alaska Fish. Cntr., Seattle, WA. 68 pp.
- Durkin, J.T.; Lipovsky, S.J.; McConnell, R.J. 1979a. Biological impact of a flowlane disposal project near Pillar Rock in the Columbia River Estuary. Final Rep. to U.S. Army Corps Engineers Portland Dist. NOAA, Natl. Mar. Fish. Serv., NW Alaska Fish. Cntr., Coastal Zone Est. Studies Seattle, WA. 92 pp.
- Durkin, J.T.; Lipovsky, S.J.; Snyder, G.R.; Shelton, J.M. 1979b. Changes in epibenthic estuarine fish and invertebrates from propeller agitation dredging. U.S. Army Corps Engineers, N. Pac. Div. Impact of propeller agitation dredging on fish and invertebrates at Chinook Channel in the Columbia River Estuary, Part II, Section I. Portland, OR. 57 pp.
- Durkin, J.T.; Coley, T.C.; Verner, K.; Emmett, R.L. 1981. An aquatic species evaluation at four self-scouring sites in the Columbia River estuary. Final Rep. to U.S. Army Corps Engineers. NOAA, Natl. Mar. Fish. Serv., NW Alaska Fish. Cntr., Seattle, WA. 46 pp.
- Duxbury, A.C. 1972. Variability of salinity and nutrients off the Columbia River mouth. Pruter, A.T.; Alverson, D.L. eds. The Columbia River Estuary and adjacent ocean waters, pp. 135-150. Seattle, WA: University of Washington Press.
- Dyer, K.R. 1973. Estuaries: a physical introduction. London: John Wiley & Sons. 140 pp.
- Edwards, D.K. 1979. An analysis of avian communities on a dredged material island. M.S. thesis. Corvallis: Ore. State Univ. 48 pp.

- Elliot, A.J.; Wang, D.-P. 1978. The effect of meteorological forcing on the Chesapeake Bay: The coupling between an estuarine system and its adjacent coastal waters. Nihoul, J.C.J. ed. Hydrodynamics of estuaries and fjords, pp. 127-146 New York: Elsevier Scientific Publishing Co. 546 pp.
- Fairchild, L.H.; Wigmosta, M. 1983. Dynamic and volumetric characteristics at the 18 May 1980 lahars on the Toutle River, Washington. Proc. Symp. on Erosion Control in Volcanic Areas, July 6-9, 1982, Seattle and Vancouver, WA. Tech. Memo of P.W.R.I. No. 1908. February 1983. Sabo (Erosion Control) Division, Erosion Control Dept., Public Works Res. Ins., Ministry of Construction, Govt. of Japan.
- Festa, J.F.; Hansen, D.V. 1978. Turbidity maxima in partially mixed estuaries: a two-dimensional numerical model. Estuarine and Coastal Mar. Sci. 7:347-359.
- Fischer, H.P. 1976. Mixing and dispersion in estuaries. van Dyke, M.G.; Wehausen, J.V. eds. Annual review of fluid mechanics pp. 107-133 Palo Alto, California.
- Folk, R.L. 1974. Petrology of sedimentary rocks. Austin, TX: Hemphill.
- Folk, R.L.; Ward, W.C. 1957. Brazos River bar: a study in the significance of grain-size parameters. J. Sed. Pet. 27:3-26.
- Forster, W.O. 1972. Radioactive and stable nuclides in the Columbia River and adjacent ocean waters. Pruter, A.T.; Alverson, D.L. eds. The Columbia River Estuary and adjacent ocean waters, pp. 663-700. Seattle: University of Washington Press.
- Fox, D.S.; Bell, S.; Nehlsen, W.; Damron, J. 1984. The Columbia River Estuary: atlas of physical and biological characteristics. Astoria, OR: Columbia River Estuary Data Development Program.
- Fullam, T.J. 1969. Measurement of bedload from sand wave migration in Bonneville Reservoir on the Columbia River. Ph.D. thesis. Seattle: University of Washington.
- Gardner, G.B.; Nowell, A.R.M.; Smith, J.D. 1980. Turbulent processes in estuaries. Hamilton, P.; MacDonald, K.B. eds. Estuarine and wetland processes. New York: Plenum Publishing Corp.
- Gelfenbaum, G. 1983. Suspended-sediment response to semidiurnal and fortnightly tidal variations in a mesotidal estuary: Columbia River, U.S.A. Mar. Geology 52:39-57.
- Gibbs, J.A. 1973. Pacific graveyard. Portland, OR: Binford and Mort. 296 pp.
- Gill, A.E. 1982. Atmosphere-ocean dynamics. New York: Academic Press. 662 pp.

- Glenn, J.L. 1973. Relations among radionuclide content and physical, chemical, and mineral characteristics of Columbia River sediments. Professional Paper 433M. Denver: U.S. Geological Survey.
- Glenn, J.L. 1978. Sediment sources and Holocene sedimentation history in Tillamook Bay, Oregon: data and preliminary interpretations. Open-file report 78-680. Denver: U.S. Geological Survey.
- Good, J.W. 1977. Columbia River Estuary tidal marshes. Seaman, M.H. ed. Columbia River Estuary: inventory of physical, biological and cultural characteristics, pp. 1019. Astoria, OR: Columbia River Estuary Study Taskforce.
- Good, J.W.; Jay, D.A. 1978. Columbia River Estuary freshwater resources, Seaman, M.H. ed. Columbia River Estuary inventory of physical, biological and cultural characteristics. Astoria, OR: Columbia River Estuary Study Taskforce.
- Greene, C.W. 1911. The migration of salmon in the Columbia River. Bull. U.S. Bur. Fish. 19:129-148.
- Grier, M.C. 1941. Oceanography of the North Pacific Ocean, Bering Sea and Bering Strait: a contribution toward a bibliography. Seattle: University of Washington, Dept. of Oceanogr. 290 pp.
- Haertel, L.S. 1970. Plankton and nutrient ecology of the Columbia River Estuary. Ph.D. thesis. Corvallis: Oregon State University.
- Halpern, D.; Pillsbury, R.D.; Smith, R.L. 1974. An intercomparison of three current meters operated in shallow water. Deep-Sea Research 21:489-497.
- Hamilton, P. 1983. Numerical modeling of the depth dependent salinity intrusion for the Coal Point Deepening Project in the Columbia River Estuary. Final report. Portland: U.S. Army Engineer District.
- Hamilton, P. 1984. Hydrodynamic Modeling of the Columbia River Estuary. Astoria: Columbia River Data Development Program.
- Hamilton, P.; Rattray, M. Jr. 1978. Theoretical aspects of estuarine circulation. Kjerfve, B. ed. Estuarine transport processes. Columbia: University of South Carolina Press.
- Hansen, D.V. 1965a. Currents and mixing in the Columbia River Estuary. Ocean Sci. Ocean Engin. 1965, Vol 2, Mar. Technol. Soc. and Am. Soc. Limnol. and Oceanogr.:943-955.
- Hansen, D.V. 1965b. Salt balance and circulation in partially mixed estuaries. Estuaries, pp. 45-51 Publication No. 83. Washington, D.C.: American Association for the Advancement of Science.
- Hansen, D.V.; Rattray, M. Jr. 1965. Gravitational circulation in straits and estuaries. J. Mar. Res. 23:104-122.

- Hansen, D.V.; Rattray, M. Jr. 1966. New dimensions in estuary classification. *Limnol. Oceanogr.* 11:319-326.
- Harms, J.C.; Southard, J.B.; Spearing D.R.; Walker, R.G. 1975. Depositional environments as interpreted from primary sedimentary structures and stratification sequences. Short Course No. 2. Tulsa: Society of Economic Paleontologists and Mineralogists.
- Harms, J.C.; Southard, J.B.; Walker, R.G. 1982. Structures and sequences in clastic rocks. Short Course No. 9. Tulsa: Society of Economic Paleontologists and Mineralogists.
- Harris, D.L. 1979. A note on the interaction between waves and tides with reference to the Columbia River entrance. Overland, J. E. ed. *Waves at the Columbia River entrance*, pp. 29-35. Seattle, WA: Pacific Marine Environmental Laboratory, NOAA.
- Haushild, W.L.; Perkins, R.W.; Stevens, H.H.; Dempster G.R.; Glenn, J.L. 1966. Radionuclide transport in the Pasco to Vancouver, Washington reach of the Columbia River July 1962 to September 1963. Open File Report. Portland: U.S. Geological Survey.
- Hayes, M.O. 1975. Morphology of sand accumulations in estuaries: an introduction to the symposium. Cronin, L.E. ed. *Estuarine research*, Vol. 2. New York: Academic Press, Inc.
- Heath, R.A. 1981. Tidal energy loss in coastal embayments. *Est. Coast. Shelf Sci.* 12: 279-290.
- Heilman, P.E.; Greer, D.M.; Braun, S.E.; Baker, A.S. 1978. Postpropagation assessment of botanical and soil resources on dredged material. Habitat development field investigations, Miller Sands marsh and upland habitat development site, Columbia River, Oregon, Appendix E. Tech. Rep. D-77-38, Dredged Material Res. Prog., U.S. Army Corps Engineers Waterways Exp. Sta., Vicksburg, MI. 78 pp.
- Henshaw, F.F.; Dean, H.J. 1915. Surface water supply of Oregon 1878-1910. Water Supply Paper 370. Washington, D.C.: U.S. Geological Survey.
- Herrmann, F.A. 1968. Model studies of navigation improvements, Columbia River Estuary Report I: hydraulic and salinity verification. U.S. Army Engineers WES Tech Report 2-735, Vicksburg, MI. 24 pp., 15 photos, 218 plates.
- Herrmann, F.A. 1970. Tidal prism measurements at the mouth of the Columbia River. U.S. Army Engineers WES Misc paper H-70-3, Vicksburg, MI. 4 pp., 36 plates.
- Hickey, B.M. 1979. The California current system - hypotheses and facts. *Prog. Oceanog.* 8:191-279.

- Hickey, B.M.; Pola, N.E. 1983. The seasonal alongshore pressure gradient on the west coast of the United States. *J. Geophys. Res.* 88:7623-7633.
- Hicks, S.D. 1972. On the classification and trends of long period sea-level series. *Shore Beach*: 20-23.
- Hicks, S.D. 1978. An average geopotential sea-level series for the United States. *J. Geophys. Res.* 83:1377-1379.
- Hickson, R.E. 1922. Changes at the mouth of the Columbia River 1903 to 1921. *Milit. Engin.* 14(76):2111-214,257-58.
- Hickson, R.E. 1930. Shoaling on the lower Columbia River. *Milit. Engin.* 22(123):217-219.
- Hickson, R.E. 1953. Salinity observations Columbia River in 1936. Unpublished Memorandum. U.S. Army Engineer District, Portland. 4pp., 6 charts.
- Hickson, R.E. 1959. Discussion of paper 'Interim Considerations of the Columbia River Entrance'. *Proc. Am. Soc. Civ. Eng., J. Hydr. Div.* 85(hy8):95-108.
- Hickson, R.E. 1960. Open river channel improvement. Portland District, U.S. Army Engineers. 15 pp, App.
- Hickson, R.E. 1961. Columbia River ship channel improvement and maintenance. *Proc. Am. Soc. Civ. Eng., J. Waterways Harbors Div.* 87(13):71-93, paper #2883.
- Hickson, R.E. 1965. Columbia River stabilization and improvement for navigation. Symposium on channel stabilization problems, Chapter IV. Tech Rep #1, Vol. 3, U.S. Army Engineers WES, Vicksburg, MI.
- Hickson, R.E.; Rodolf, F.W. 1951. History of the Columbia River Jetties. *Proc. 1st Conf. Coast. Eng.*, pp. 283-298.
- Higley, D.L.; Holton, R.L. 1975. Biological baseline data: Youngs Bay, Oregon 1974. Fin. Rep. to Alumax Pac. Alumin. Corp., Ocean. ref. 75-6, School Ocean., Ore. State Univ., Corvallis, OR. 91 pp.
- Higley, D.L.; Holton, R.L. 1978. A grab-sample study of the benthic invertebrates of the Columbia River Estuary. Suppl. Data Rep. to Ocean. Ref. 76-3, School Ocean., Ore. State Univ., Corvallis, OR. 27 pp.
- Higley, D.L.; Holton, R.L. 1979. Biological baseline and fluoride effects data for Youngs Bay, Oregon, 1974-1975. Corvallis: School Ocean., Ore. State Univ. 91 pp.
- Higley, D.L.; Holton, R.L.; Komar, P.D. 1976. Analysis of benthic infauna communities and sedimentation patterns of a proposed fill site and nearby regions in the Columbia River Estuary. Corvallis: School Ocean., Ore. State Univ. 78 pp.

- Hirose, P. 1977. Incidence of seal-damaged salmonids sampled from the lower Columbia River gill-net fishery, 1972-1976. Info. Rep. 77-4. Portland: Ore. Dept. Fish Wildl. 6 pp.
- Hjulstrom, F. 1939. Transportation of detritus by moving water. Trask, P. D. ed. Recent marine sediments. Tulsa: Symposium American Association of Petroleum Geologists.
- Hodge, E.T. 1934. Geology of beaches adjacent to mouth of Columbia River and petrography of their sands. Final report to Corps of Engineers, Pacific Division, Beach Erosion Investigation.
- Holton, R.L.; Higley, D.L. 1976. Gammaridean amphipods in the Columbia River Estuary. Proc. 5th Tech. Conf. Est. in the Pac. Northwest. pp. 9-12. Circ. 51. Engineering Exp. Sta. Corvallis: Ore. State Univ.
- Hopkins, T.S. 1971. On the barotropic tide over the continental shelf off the Washington-Oregon coast. Special Report #46. Seattle: University of Washington, Dept. of Oceanogr. 22 pp.
- House of Representatives Document 94. 1899. 56th Congress, 1st Session. 10 pp.
- House of Representatives Document 673. 1900. 56th Congress, 1st Session. 16 pp.
- House of Representatives Document 2096. 1917. 64th Congress, 2nd Session. 11 pp.
- House of Representatives Document 1222. 1919. 65th Congress, 2nd Session. 15 pp.
- House of Representatives Document 1009. 1921. 66th Congress, 3rd Session. 35 pp.
- House of Representatives Document 195. 1928. 70th Congress, 1st Session. 50 pp.
- House of Representatives Document 692. 1946. 79th Congress, 2nd Session. 23 pp.
- House of Representatives, Report 3213. 1906. 59th Congress, 1st Session. 12 pp.
- Hubbell, D.W.; Glenn, J.L. Distribution of radionuclides in bottom sediments of the Columbia River Estuary. Geol. Soc. Am. Professional Paper 433-L. Washington, D.C.: U.S. Government Printing Office.
- Hubbell, D.W.; Glenn J.L.; Stevens, H.H. Jr. 1971. Studies of sediment transport in the Columbia River Estuary. Proceedings 1971 Technical Conference on Estuaries of the Pacific Northwest. Proc. Circ. 42, Eng. Experiment Station. Corvallis: Oregon State University.

- Hughes, F.W. 1968. Salt flux and mixing processes in the Columbia River Estuary during high discharge. M.S. thesis. Seattle: University of Washington.
- Hughes, F.W., Rattray, M. Jr. 1980. Salt flux and mixing in the Columbia River Estuary. *Est. Coast. Mar. Sci.* 10:479-493.
- Hutton, C.O. 1950. Studies of heavy detrital minerals. *Geol. Soc. Am. Bull.* 61:655-716.
- Ianniello, J.P. 1977a. Non-linearly induced residual currents in tidally dominated estuaries. Ph.D. thesis. University of Connecticut. 250 pp.
- Ianniello, J.P. 1977b. Tidally induced residual currents in estuaries of constant breadth and width. *J. Mar. Res.* 35(4):755-786.
- Ianniello, J.P. 1979. Tidally induced residual currents in estuaries of variable breadth and depth. *J. Phys. Oceanogr.* 9:962-974.
- Ianniello, J.P. 1981. Comments on tidally induced residual currents in estuaries: dynamics and near-bottom flow characteristics. *J. Phys. Oceanogr.* 11:126-134.
- Inman, D.L. 1952. Measures for describing the size distribution of sediments. *J. Sed. Pet.* 22:125-145.
- Ives, F.; Saltzman, W. 1970. A special report to the State Department of Transportation. Portland: Ore. State Game Comm. 17 pp.
- Jay, D.A. 1978a. Columbia River estuarine circulation. Seaman, M.H. ed. Columbia River Estuary inventory of physical, biological and cultural characteristics. Astoria, OR: Columbia River Estuary Study Taskforce.
- Jay, D.A. 1978b. Columbia River Estuary tides and tidal currents. Seaman, M.H. ed. Columbia River Estuary inventory of physical, biological and cultural characteristics. Astoria, OR: Columbia River Estuary Study Taskforce.
- Jay, D.A.; Good, J.W. 1978. Columbia River Estuary sediment and sediment transport, Seaman, M.H. ed. Columbia River Estuary inventory of physical and biological Characteristics. Astoria, OR: Columbia River Estuary Study Taskforce.
- Jay, D.A. 1980. Columbia River Estuary Data Development Program literature review: circulation studies. Bellevue, WA: Mathematical Sciences NW.
- Jay, D.A. 1982. Columbia River Estuary salinity distribution. Submitted to the U. S. Army Corps of Engineers, Portland District. 113 pp.

- Jay, D.A. 1983. Interim report: circulatory processes in the Columbia River Estuary. Seattle: University of Washington. 111 pp., 7 appendices.
- Jay, D.A. 1984. Circulatory Processes in the Columbia River Estuary. Astoria, OR: Columbia River Estuary Data Development Program.
- Johnson, R.C.; Sims, C.W. 1973. Purse seining for juvenile salmon and trout in the Columbia River Estuary. Trans. Am. Fish. Soc. 102:341-345.
- Johnson, M.L.; Jefferies, S.J. 1977. Population evaluation of the harbor seal (Phoca vitulina richardsi) in the waters of the State of Washington. Rep. to U.S. Marine Mammal Comm., Contract MM5AC019. Tacoma, WA: Univ. Puget Sound. 27 pp.
- Judson, S.; Ritter, D.F. 1964. Rates of regional denudation in the United States. J. Geophys. Res. 69:3395-3401.
- Kachel, N.B. 1980. A time-dependent model of sediment transport and strata formation on a continental shelf. Ph.D. thesis. Seattle: University of Washington. 122 pp.
- Kelley, J.C.; Whetten, J.T. 1969. Quantitative statistical analysis of Columbia River sediment samples. J. Sed. Pet. 39:1167-1173.
- Kidby, H.A.; Oliver, J.G. 1965. Erosion and accretion along Clatsop Spit. Chapter 26 in Coastal Engineering Santa Barbara Specialty Conference, October 1965. A.S.C.E.
- Knebel, H.J.; Kelley, J.C.; Whetten, J.T. 1968. Clay minerals of the Columbia River: a qualitative, quantitative, and statistical evaluation. J. Sed. Pet. 38:600-611.
- Kraft, J.C. 1971. Sedimentary environment facies patterns and geologic history of a Holocene marine transgression. Geol. Soc. Am. Bull. 82:2131-2158.
- Krumbein, W.C.; Pettijohn, F.J. 1938. Manual of sedimentary petrography. New York: Appleton-Century-Crafts Inc.
- Lavelle, J.W.; Mojfield, H. 1983. Effects of time varying viscosity on oscillatory turbulent channel flow. J. Geophys. Res. 88:7607-7616.
- Lewis, M.R.; Platt, T. 1982. Scales of variability in estuarine ecosystems. Kennedy, V.S. ed. Estuarine Comparisons, pp. 3-20 New York: Academic Press.
- Lilly, K.E. 1983. Marine weather of western Washington. Seattle: Starpath. 150 pp.
- Lipman, P.W.; Mullineaux, D.R. eds. 1981. The 1980 eruption of Mt. St. Helens, Washington. U.S.G.S. Prof. Paper 1250.

- Lockett, J.B. 1959. Interim considerations of the Columbia River entrance. Paper 1902, Proc. A.S.C.E. Journal of the Hydraulics Division 85 HY-1:17-40.
- Lockett, J.B. 1962. Phenomena affecting improvement of the lower Columbia Estuary and entrance. Presented at 8th Conference on Coastal Engineering, Mexico City, Mexico. Portland: U.S. Army Engr. Division.
- Lockett, J.B. 1963. Phenomena affecting improvement of the lower Columbia River Estuary and entrance. Prepared for Federal Interagency Sedimentation. Jackson: I.C.W.R.
- Lockett, J.R. 1967. Sediment transport and diffusion: Columbia Estuary and entrance. WW-4, Proc. A.S.C.E., J. Waterways and Harbors Div. 93:167-175.
- Lombard, R.E.; Miles, M.B.; Nelson, L.M.; Kresh D.L.; Carpenter, P.J. 1980. The impact of mudflows of May 18 on the lower Toutle and Cowlitz Rivers. Lipman, P.W.; Mullineaux, D.R. eds. The 1980 eruption of Mt. St. Helens, Washington. U.S.G.S. Prof. Paper 1250.
- Longuet-Higgins, M.S. 1969. On the transport of mass by time-varying ocean currents. Deep-Sea Research 16:431-447.
- Love, C.M. 1956. Sources of oceanographic data for a portion of the North Pacific Ocean. Dept. of Oceanogr. Spec. Rep. #25. Seattle: University of Washington.
- Lutz, G.A.; Hubbell, D.W.; Stevens, H.H. Jr. 1975. Discharge and flow distribution, Columbia River Estuary. Geological Survey Professional Paper 433-P. Washington, D. C.: U. S. Government Printing Office.
- Marmer, H.A. 1951. Tidal datum planes. Special Publication No. 135. Revised (1951) Edition. Washington, D. C.: U. S. Government Printing Office.
- Maser, C.; Storm, R.M. 1970. A key to the Microtinae of the Pacific Northwest. Corvallis: Ore. State Univ. Bookstores.
- McAnally, W.H. Jr.; Brogdon, N.J.; Letter, J.V.; Stewart, J.P. Thomas, W.A. 1983a. Columbia River Estuary hybrid model studies, report 1: verification of hybrid modeling of the Columbia River mouth. U.S. Army Engineers WES, Vicksburg, MI: 83 pp., appendices.
- McAnally, W.H. Jr.; Brogden N.J.; Stewart, J.P. 1983b. Columbia River Estuary Hybrid Models, report 4: entrance channel tests. U.S. Army Engineers.
- McAnally, W.H.; Thomas, W.A.; Letter, J.V. Jr. 1980. Physical and numerical modelling of estuarine sedimentation. Paper presented at the International Symposium on River Sedimentation, Beijing, China.

- McConnell, R.J.; Lipovsky, S.J.; Misitano, D.A.; Craddock, D.R.; Hughes, J.R. 1978. Inventory and assessment of predisposal and postdisposal aquatic habitats. Clairain, E.J. ed. Habitat development field investigations, Miller Sands marsh and upland habitat development site, Columbia River, Oregon, Appendix B. Tech. Rep. D-77-38, U.S. Army Corps Engineers Waterway Exp. Sta., Dredged Material Res. Prog., Vicksburg, MI.
- McConnell, R.J.; Snyder, G.R.; Durkin, J.T.; Blahm, T.H. 1981. Concentration, extent and duration of salinity intrusion into the Columbia River Estuary September-October 1977-78. Proceedings of the National Symposium on Freshwater Inflow to Estuaries, Vol. 2, pp. 41-54.
- McKee, B. 1972. Cascadia. New York: McGraw Hill.
- McKern, J.L. 1976. Inventory of riparian habitats and associated wildlife along the Columbia and Snake Rivers, vol. I. Rep. to U.S. Army Corps of Engineers, North Pacific Division, Portland, OR.
- McLaren, P. 1981. An interpretation of trends in grain size measures. *J. Sed. Pet.* 51:611-624.
- McLaren, P. 1982. Discussion: hydraulic control of grain-size distributions in a macrotidal estuary. *Sedimentology* 29:437-439.
- McLaren, P.; Bowles, D. 1983. The effects of sediment transport on grain-size distributions. In preparation.
- McMahon, E. et al. 1974. A survey of great blue heron rookeries on the Oregon coast: a student-originated studies project. Charleston: Ore. Inst. Mar. Biol. 143 pp.
- Misitano, D.A. 1977. Species composition and relative abundance of larval and post-larval fishes in the Columbia River Estuary. 1973. *Fish. Bull.* 74:218-222.
- Moore, C.R.; Hickson, R.E. 1939. The lower Columbia River. *Milit. Eng.* 31:19-23.
- Morse, B.A.; Gross, M.G.; Barnes, C.A. 1968. Movement of seabed drifters near the Columbia River. *WWI, Proc. A.S.C.E., J. Waterways and Harbors Div.* 94:93-103.
- National Marine Consultants. 1961a. Oceanographic study for the Columbia River entrance. Santa Barbara, CA. 15 pp., 4 tables, 23 figures.
- National Marine Consultants. 1961b. Wave statistics for three deep water stations along the Oregon-Washington coast. Santa Barbara, CA. 17 pp., tables, figures.

- National Marine Consultants. 1961c. Wave statistics of twelve most severe storms selecting three selected stations off the coast of Washington and Oregon, during the period 1950-60. Santa Barbara, CA. 10 pp., tables, addenda, errata.
- National Oceanic and Atmospheric Administration. 1980. The relationship between the upper limit of coastal wetlands and tidal datums along the Pacific coast. Rockville, MD: National Ocean Survey. 37 pp.
- Neal, V.T. 1965. A calculation of flushing time and pollution distribution for the Columbia River Estuary. Ph.D. thesis. Corvallis: Oregon State University. 83 pp.
- Neal, V.T. 1972. Physical aspects of the Columbia River and its Estuary. Pruter, A.T.; Alverson, D.L. eds. The Columbia River Estuary and adjacent ocean waters, pp. 19-40. Seattle: University of Washington Press.
- Nelson, E.R. 1949. Columbia River Basin flood. Mon. Weather Rev. 77(1):1-10.
- Nelson, J.L.; Perkins, R.W.; Haushild, W.L. 1966. Determination of Columbia River flow times downstream from Pasco, Washington, using radioactive tracers introduced by the Hanford reactors. Wat. Res. 2(1):31-39.
- Nittrouer, C.A. 1977. Continental shelf sedimentation - a bibliography. Appendix A-11, U.S. Army Engineers WES Tech. Rep. D-77-30.
- Nittrouer, C.A. 1978. The process of detrital sediment accumulation in a continental shelf environment: an examination of the Washington shelf. Ph.D. thesis. Seattle: University of Washington. 243 pp.
- Norberg, J.R. 1980. Black sand occurrences in the Columbia River estuary and vicinity. Tech. Assistance Report. Spokane: U.S. Bureau of Mines, Western Field Operations Center.
- Northwest Cartography, Inc. 1983. Final report to Columbia River Estuary Data Development Program. Unpublished report. Astoria, OR.
- O'Brien, M.P. 1951. Wave measurements at the Columbia River light vessel 1933-36. Trans. Am. Geophys. Un. 32(6):875-877.
- O'Brien, M. P. 1952. Salinity Currents in Estuaries. Trans. Am. Geophys. Un. 33:520-522.
- O'Brien, M.P. 1971. Field and laboratory studies navigation channels of the Columbia River Estuary. Hyd. Eng. Lab., Rep. HEL-24-4. Berkeley: University of California. 35 pp.
- Ocean Engineering Programs School of Engineering, Oregon State University, Corvallis, Oregon. 1975. Physical characteristics of the Youngs Bay estuarine environs. Submitted to ALUMAX Pacific Aluminum Corporation. 149 pp.

- Officer, C.B. 1976. Physical oceanography of estuaries (and associated coastal waters). New York: Wiley-Interscience. 465 pp.
- Officer, C.B. 1980. Discussion of the turbidity maximum in partially mixed estuaries. *Estuarine Coastal Marine Science* 10:239-246.
- Officer, C.B. 1981. Dynamics of mixing in estuaries. *Est. Coast. Shelf Sci.* 12:525-533.
- Oregon Historical Society. 1980. Columbia's gateway, a history of the Columbia River Estuary to 1920. Vancouver, WA: Pacific Northwest River Basins Commission.
- Orem, H.M. 1968. Discharge in the lower Columbia River basin, 1928-65. Circular 550. Washington, D. C.: U. S. Geological Survey. 24 pp.
- Parke, M.E. 1980. M2, S2, K1 models of the global ocean tide on an elastic earth. *Mar. Geol.*:379-408.
- Paulsen, C.G. 1949. Floods of May-June 1948 in the Columbia River basin. Water Supply Paper 1080. Washington, D. C.: U.S. Geological Survey. 476 pp.
- Peterson, C.; Scheidegger, K.; Komar, P. 1982. Sand-dispersal patterns in an active-margin estuary of the northwestern United States as indicated by sand composition, texture, and bedforms. *Mar. Geol.* 50:77-96.
- Phillips, O.M. 1980. The dynamics of the upper ocean. Cambridge: Cambridge University Press. 336 pp.
- Pruter, A.T.; Alverson, D.L. eds. 1972. The Columbia River Estuary and adjacent ocean waters - bioenvironmental studies. Seattle: University of Washington Press. 868 pp.
- Rattray, M. Jr.; Dworski, J.G. 1980. Comparison of methods of analysis of the transverse and vertical circulation contributions to the longitudinal advective salt flux in estuary. *Est. Coast. Mar. Sci.* 11:515-536.
- Robe, R.Q. 1968. Salt flux in and classification of the Columbia River Estuary during high and low discharge. Unpublished ms. Seattle: University of Washington.
- Roberson, J.A.; Copp, H.D.; Naik, B. 1980. Mathematical modeling of circulation in Baker Bay. R.L. Albrook Hyd. Lab. Tech Rep. HY-4/80. Washington State University. 102 pp.
- Roy, E.H.; Creager, J.S.; Walter, S.R.; Borgeld, J.C. 1979. An investigation to determine the bedload and suspended sediment transport over the outer tidal delta and monitor the sedimentary environment of sites E and D near the mouth of the Columbia River. Final report, December 1979. Portland: Department of the Army, Corps of Engineers, Portland District.

- Roy, E.H.; Creager, J.S.; Gelfenbaum, G.R.; Sherwood C.R.; Stewart, R.J. 1982. An investigation to determine sedimentary environments near the entrance to the Columbia River Estuary. Final Report, June 1982. Portland: Department of the Army, Corps of Engineers, Portland District.
- Rubin, D.M.; McCulloch, D.S. 1980. Single and superimposed bedforms: a synthesis of San Francisco Bay and flume observations. *Sed. Geology* 26:207-231.
- Runge, E.J. Jr. 1966. Continental shelf sediments, Columbia River to Cape Blanco, Oregon. Ph.D. thesis. Corvallis: Oregon State University.
- Scheffer, T.H. 1925. Notes on the breeding of beavers. *J. Mammal.* 6:129-130.
- Scheidegger, K.F.; Kulm, L.D.; Runge, E.J. 1971. Sediment source sand dispersal patterns of Oregon continental shelf sands. *J. Sed. Pet.* 41:1112-1120.
- Schubel, J.R.; Wilson, R.E.; Okubo, A. 1978. Vertical transport of suspended sediment in upper Chesapeake Bay. Kjerfve, B. ed. *Estuarine transport processes*. Belle W. Baruch Library in Marine Science Number 7. Columbia: University of South Carolina Press. 331 pp.
- Schuster, R.L. 1981. Effects of the eruption on civil works and operations in the Pacific Northwest. Lipman, P.W.; Mullineaux, D.R. eds. *The 1980 eruption of Mt. St. Helens, Washington*. U.S.G.S. Prof. Paper 1250.
- Scwidorski, E.W. 1980. Ocean tides, part II: a hydrodynamical interpolation model. *Mar. Geol.* 3:219-256.
- Seaman, M.H. ed. 1977. *Columbia River Estuary: Inventory of physical, biological and cultural characteristics*. Astoria, OR: Col. Riv. Est. Study Taskforce. 302 pp.
- Senate Document 49. 1881. 46th Congress, 3rd Session. 8 pp.
- Senate Document 57. 1917. 65th Congress, 1st Session. 5 pp.
- Shalowitz, A.L. 1964. *Shore and sea boundaries, vol. II*. Washington, D. C.: U.S. Coast and Geodetic Survey and Government Printing Office. 749 pp.
- Shepard, F.P. 1954. Nomenclature based on sand-silt-clay ratios. *J. Sed. Pet.* 24:151-158.
- Sherwood, C.R.; Creager, J.S.; Roy, E.H.; Gelfenbaum, G.; Dempsey, T. 1984. *Sedimentary processes and environments in the Columbia River Estuary*. Astoria, OR: Columbia River Estuary Data Development Program.

- Shields, A. 1936. Application of similarity principles and turbulence research to bedload movement (trans. by W. P. Ott and J. C. Van Uchelen). U.S. Dept. of Agriculture Soil Conservation Service, Coop. Laboratory, California Institute of Technology.
- Simmons, A.B. 1966. Field experience in estuaries. Ippin, A.T. ed. estuarine and coastline hydrodynamics, pp. 673-690. New York: McGraw-Hill.
- Simmons, H.B.; Hermann, F.A. Jr. 1972. Effects of man-made works on the hydraulic, salinity, and shoaling regimes of estuaries. G.S.A. Memoir 133:555-570.
- Simons, D.B.; Richardson, E.V.; Nordin, C.F. 1965. Sedimentary structures generated by flow in alluvial channels. Society of Economic Paleontologists and Mineralogists Spec. Publ. 12:34-52.
- Sims, C.W. 1970. Juvenile salmon and steelhead in the Columbia River Estuary. Proc. NW Est. Coastal Zone Symp., pp. 80-86. Portland, OR: U.S. Dept. Interior, Bur. Sport Fish. Wildl.
- Sims, C.W. 1974. Food of chum salmon fry in brackish and freshwater areas of the Columbia River Estuary. Unpubl. rep., NOAA, Natl. Mar. Fish. Serv., NW Alaska Fish. Cntr., Seattle, WA. 15 pp.
- Smith, J.D. 1970. Stability of a sand bed subjected to a shear flow of low froude number. J. Geophys. Res. 75:5928-5940.
- Smith, J.D. 1977. Modeling of sediment transport on continental shelves. The Sea, v. 6. New York: Wiley-Interscience.
- Smith, J.D.; Hopkins, T.S. 1972. Sediment transport on the continental shelf off of Washington and Oregon in light of recent lowest measurements. Swift, D.J.P.; Duane, D.B.; Pilkey, O.H. eds. Shelf sediment transport: processes and patterns, Chap. 7. Stroudsburg, PA: Dowden, Hutchinson and Ross.
- Smith, J.D.; McLean, S.R. 1977. Spatially averaged flow over a wavy surface. J. Geophys. Res. 82:1735-1746.
- Snyder, G.R.; McConnell, J.R. 1973. Frequency and duration of flow reversal in the lower Columbia River, April 1968 - March 1970. Fish. Bul. 71:312-315.
- Sternberg, R.W.; Creager, J.S.; Glassley, W.; Johnson, J. 1977. Aquatic disposal field investigations, Columbia River disposal site, Oregon. Appendix A: Investigation of the hydraulic regime and physical nature of bottom sedimentation. Final Report, December 1977. Vicksburg: U.S. Army Engineer Waterways Experiment Station.
- Sternberg, R.W.; McManus, D.A. 1972. Implications of sediment dispersal from long-term, bottom current measurements on the continental shelf of Washington. Swift, D.J.P.; Duane, D.B.; Pilkey, O.H. eds. Shelf sediment transport: processes and patterns. Stroudsburg, PA: Dowden, Hutchinson and Ross.

- Stevens, H.H. Jr.; Hubbell, D.W.; Glenn, J.L. 1973. Model for sediment transport through an estuary cross section. 21st Annual Hydraulics Division Specialty Conference, Bozeman, Montana State University. A.S.C.E.
- Sundborg, A. 1956. The river klara-lven: a study of fluvial processes. *Geografiska Annaler* 38:126-316.
- Sundborg, A. 1967. Some aspects on fluvial sediments and fluvial morphology. *Geografiska Annaler* 49A (2-4):333-343.
- Suring, L.H.; Vohs, P.A. Jr. 1979. Habitat use by Columbian white-tailed deer. *J. Wildl. Mgmt.* 43:610-619.
- Tabor, J.E. 1974. Productivity, survival, and population status of river otter in western Oregon. M.S. thesis. Corvallis: Ore. State Univ. 62 pp.
- Tabor, J.E. 1976a. Vertebrate wildlife of the Skipanon River site. Montague-Bierly and Assoc. Natural resource base and physical characteristics of the proposed offshore oil platform fabrication site. pp. 23-63. Portland, OR.
- Tabor, J.E. 1976b. Inventory of riparian habitats and associated wildlife along the Columbia and Snake Rivers. vol. 11A and 11B, lower Columbia River. Rep. to U.S. Army Corps Engineers. North Pacific Division. Corvallis: Coop. Wildl. Fish. Unit, Ore. State Univ. 861 pp.
- Thomas, D.W. 1983. Changes in Columbia River Estuary habitat types over the past century. Astoria: Columbia River Estuary Data Development Program.
- Thompson, K.; Snow, D. 1974. Fish and wildlife resources. Oregon coastal zone. Salem: Ore. Coastal Conserv. Dev. Comm. 114 pp.
- Thompson, R.O.; Hamon, R.Y.; Hamon, B.V. 1980. Wave setup of harbor water levels. *J. Geophys. Res.* 85:1151-52.
- Towell, D.E. 1974. Winter food habits of river otters in western Oregon. *J. Wildl. Mgmt.* 38:107-111.
- Townsend, C.K.; Hull, W.V. 1981. Circulatory survey, Columbia River Estuary, OR. OPR-N805-AR-81. 9 pp.
- Twenhofel, W.H. 1946. Mineralogical and physical composition of sands of the Oregon coast from Coos Bay to the mouth of the Columbia River. Oregon Department Geol. and Min. Ind. Bull. 30. 64 pp.
- Uncles, R.J.; Jordan, M.D. 1980. A one-dimensional representation of residual currents in the Severn Estuary and associated observations. *Est. Coast. Mar. Sci.* 10.
- U.S. Army Engineers. 1875. Report of Chief of Engineers, Appendix GG, pp. 730-759.

- U.S. Army Engineers. 1903. Report of the Board of Engineers, Appendix XX of Annual Report, Chief of Engineers, U.S. Army. Part 3, Vol. 3.
- U.S. Army Engineers. 1933. Mouth of Columbia River current survey, 1932-1933. Report No. MCR 100/5.288. Portland, OR.
- U.S. Army Engineers. 1960. 1959 current measurement program, Columbia River at mouth, Oregon and Washington, Vol. IV. Corps of Engineers, Portland, OR. 320 pp.
- U.S. Army Engineers, Board of Engineers. 1903. Report of Board of Engineers on project improvement of mouth of Columbia River, App XXV, Report of Chief of Engineers, Vol. XI, Pt. 3, pp. 2271-2318. Appendix, 47 plates. Washington, D. C.
- U.S. Army Engineers, Chief of Engineers. 1884. Report of the Chief of Engineers, Appendix QQ13, Gauging Waters of the Columbia River and principal tributaries, pp. 2290-2293. Washington, D. C.
- U.S. Army Engineers, Portland District. 1949. Columbia River and tributaries below Yakima River, Report on flood of May-June 1948. Portland, OR. 87 pp., plates.
- U.S. Army Engineers, Waterways Experiment Station. 1954. Bibliography on tidal hydraulics. Report #2 of Committee on Tidal Hydraulics. Vicksburg, MI.
- U.S. Army Engineers, Waterways Experiment Station 1955. Bibliography on tidal hydraulics. Supplement #1 to Report #2 of Committee on Tidal Hydraulics. Vicksburg, MI.
- U.S. Army Engineers, Waterways Experiment Station. 1957. Bibliography on Tidal Hydraulics. Supplement #2 to Report #2 of Committee on Tidal Hydraulics. Vicksburg, MI.
- U.S. Army Corps of Engineers Portland District. 1975. Columbia and lower Willamette River maintenance and completion of the 40-foot navigation channel downstream of Vancouver, Washington, and Portland, Oregon - environmental impact statement. Portland, OR. 77 pp.
- U.S. Army Corps of Engineers Portland District. 1976. Lower Columbia River bank protection project, Oregon and Washington - final environmental impact statement. Supplement. Portland, OR. 170 pp.
- U.S. Army Engineers, Waterways Experiment Station. 1959. Bibliography on tidal hydraulics. Supplement #3 to Report #2 of Committee on Tidal Hydraulics. Vicksburg, MI.
- U.S. Coast and Geodetic Survey. 1952. Manual of harmonic constant reductions. Special Publication No. 260, U.S. Government Printing Office.

- U.S. Fish and Wildlife Service. 1977. Columbian white-tailed deer recovery plan. U.S. Fish Wildlife Serv., Columbian White-tailed Deer Recovery Team.
- U.S. Geological Survey. 1958. Compilation of records of surface waters of the United States through 1950, Part 14: Pacific Slope basins in Oregon and Lower Columbia River basin. Water Supply Paper 1318. Washington, D. C.
- U.S. Geological Survey. 1963. Compilation of records of surface waters of the United States October 1950 to September 1960, Part 14: Pacific Slope basins in Oregon and lower Columbia River basin. Water Supply Paper 1738. Washington, D. C.
- U.S. Geological Survey. 1964. Magnitude and frequency of floods, Pt. 14: Pacific Slope basins in Oregon and lower Columbia River basin. Water Supply Paper 1689. Washington, D. C.
- U.S. Navy Hydrographic Office. 1960. Inshore survey results, Columbia River approaches. H. O. Misc. 15359-21S. Washington, D. C. 181 pp.
- Van Straaten, L.M.; Kuenen, J.U.; Kuenen, Ph. H. 1958. Tidal action as a cause for clay accumulation. J. Sed. Pet. 28:406-413.
- Van Winkle, W. 1914a. Quality of the surface waters of Washington. U.S. Geological Survey Water Supply Paper 339.
- Van Winkle, W. 1914b. Quality of the surface waters of Oregon. U.S. Geological Survey Water Supply Paper 363.
- Vincent, C.E. 1979. The interaction of wind-generated sea waves with tidal currents. J. Phys. Oceanogr. 9:748-755.
- Walker, P.H.; Woodyer, D.D.; Hutka, J. 1974. Particle size measurements by Coulter counter of very small deposits and low suspended sediment concentrations in streams. J. Sed. Pet. 44:673-679.
- Walter, S.R.; Roy, E.H.; Creager, J.S.; Borgeld, J.C. 1979. An investigation to determine the bedload and suspended load transport over the outer tidal delta and monitor the sedimentary environment of sites A, E, and D near the mouth of the Columbia River. Annual Report, March 1979. Portland: Department of the Army Corps of Engineers, Portland District.
- Wang, S.C.; Leidersdorf, C.; Butcher, C. 1979. Columbia River entrance, deep-draft vessel motion study, Final Report - Phase 1, Tetra Tech Report # TC-3925. 125 pp, Appendices.
- Washington Department of Game. 1975. Marine shoreline fauna of Washington: A status survey. Coastal Zone Environ. Studies Rep. 1. Olympia, WA. 594 pp.

- Webster, I.; Juhasz, T. 1980. Columbia River Estuary study, circulation and hydrography, current studies 1980. Dobrocky Seatech, Ltd. 25 pp.
- Werner, F.; Hickey, B.M. 1983. The role of a longshore pressure gradient in Pacific Northwest coastal dynamics. J. Phys. Oceanogr. 13:395-410.
- Werschkal, D.; McMahon, E.; Leitschuh, M.; English, S.; Skibinski, C.; Williamson, G. 1977. Observations on the reproductive ecology of the great blue heron (Ardea herodias) in western Oregon. Murrelet 58:7-12.
- Westerheim, S.J. 1955. Migrations of starry flounder (Platichthys stellatus) tagged in the Columbia River. Ore. Fish Comm. Res. Briefs 6:33-37.
- Whetten, J.T. 1966. Sediments from the lower Columbia River and origin of graywacke. Science 152:1057-1058.
- Whetten, J.T.; Kelley, J.C.; Hanson, L.G. 1969. Characteristics of Columbia River sediment and sediment transport. J. Sed. Pet. 39:1149-1166.
- White, S.M. 1967. The mineralogy and geochemistry of the sediments on the continental shelf off the Washington-Oregon coast. Ph.D. thesis. Seattle: University of Washington.
- White, S.M. 1970. Mineralogy and geochemistry of continental shelf sediments off the Washington-Oregon coast. J. Sed. Pet. 40:38-54.
- Wilkes, C. 1846. Statement on survey of the mouth of the Columbia River by the United States Exploring Expedition. XXIX Congress, 1st Session, Senate Document #475. 10 pp.
- Williams, C.F. 1933. Mouth of Columbia River current survey 1932-33. War Dept., Office of District Engineer, Portland, OR. Part I, 45 pp., Part II, 35 plates (oversize).
- Williams, L.G. 1964. Possible relationships between plankton-diatom species numbers and water-quality estimates. Ecology 45:809-823.
- Williams, L.G. 1972. Plankton diatom species biomasses and the quality of American rivers and the Great Lakes. Ecology 53:1038-1050.
- Woodward-Clyde Consultants. 1978. Inventory assessment of post-propagation terrestrial resources on dredged material. Clairain, E.J. ed. Habitat development field investigations, Miller Sands marsh and upland habitat development site, Columbia River, Oregon, Appendix C. Tech. Rep. D-77-38, Dredged Material Res. Prog. U.S. Army Corps Engineers Waterways Exp. Sta., Vicksburg, MI.